







Faculty of Pharmaceutical, Biomedical and Veterinary Sciences  
Department of Pharmaceutical Sciences

**Identification of contaminants of emerging concern and their biotransformation products by ion-mobility high-resolution mass spectrometry based screening approaches**

PhD thesis

submitted for the degree of Doctor of Pharmaceutical Sciences

at the University of Antwerp to be defended by

Lidia BELOVA

Promotors:

Prof. Dr. Adrian Covaci

Prof. Dr. Alexander L. N. van Nuijs

Antwerp, 2024

## Disclaimer

The author allows to consult and copy parts of this work for personal use. Further reproduction or transmission in any form or by any means without the prior permission of the author is forbidden.

## **Members of the jury**

### **Promotors**

Prof. dr. Adrian Covaci  
University of Antwerp, Department of Pharmaceutical Sciences  
Toxicological Centre, Antwerp, Belgium

Prof. dr. Alexander L.N. van Nuijs  
University of Antwerp, Department of Pharmaceutical Sciences  
Toxicological Centre, Antwerp, Belgium

### **Internal jury members**

Prof. dr. Nina Hermans  
University of Antwerp, Department of Pharmaceutical Sciences  
Natural Products and Food Research and Analysis – Pharmaceutical Technology  
(NatuRA-PT), Antwerp, Belgium

Prof. Dr. Karolien De Wael  
University of Antwerp, Department of Bioscience Engineering  
NANOlab Center of Excellence, Antwerp, Belgium

### **External jury members**

Prof. dr. Tim Causon  
University of Natural Resources and Life Sciences, Department of Chemistry  
Institute of Analytical Chemistry, Vienna, Austria

Prof. dr. Eppe Gauthier  
University of Liege, Department of Chemistry  
Inorganic Analytical Chemistry Laboratory, Liege, Belgium



# Table of Contents

<b>List of Abbreviations</b> .....	<b>7</b>
<b>Chapter 1: General Introduction</b> .....	<b>13</b>
1.1 Legacy contaminant classes and Contaminants of Emerging Concern.....	15
1.2 Suspect and non-target screening approaches .....	20
1.3 Ion-mobility as an additional separation dimension .....	24
1.3.1 Drift-tube ion-mobility spectrometry (DTIM) .....	26
1.3.2 Travelling-wave ion-mobility spectrometry (TWIMS) .....	28
1.3.3 Trapped ion-mobility spectrometry (TIMS).....	30
1.3.4 Ion-mobility in environmental screening studies.....	32
1.4 Recent developments in semi-quantification approaches .....	33
<b>Chapter 2: Objectives and Outline</b> .....	<b>37</b>
<b>Chapter 3: Ion-mobility for the identification of contaminants of emerging concern.</b>	<b>43</b>
3.1 Ion Mobility-High-Resolution Mass Spectrometry (IM-HRMS) for the Analysis of Contaminants of Emerging Concern (CECs) .....	45
3.1.1 Introduction.....	45
3.1.2 Materials and Methods .....	46
3.1.2.1 Chemicals.....	46
3.1.2.2 DTIMS conditions .....	46
3.1.2.3 Mobility measurements and calculation of CCS values .....	47
3.1.2.4 Analysis of spiked urine samples.....	48
3.1.3 Results and Discussion .....	48
3.1.3.1 Reproducibility of <sup>DT</sup> CCS <sub>N2</sub> values of QA compounds .....	48
3.1.3.2 <sup>DT</sup> CCS <sub>N2</sub> values of contaminants of emerging concern and their metabolites .....	50
3.1.3.3 Comparison with literature <sup>DT</sup> CCS <sub>N2</sub> and <sup>TW</sup> CCS <sub>N2</sub> values .....	55
3.1.3.4 Application of the <sup>DT</sup> CCS <sub>N2</sub> Database to Human Urine Samples .....	56

3.1.4	Conclusions.....	57
	Supplementary Information – Chapter 3.1 .....	59
3.2	Comparison of <sup>DT</sup> CCS <sub>N2</sub> values with experimental <sup>TW</sup> CCS <sub>N2</sub> values and <i>in-silico</i> predicted data .....	75
3.2.1	Introduction.....	75
3.2.2	Materials and Methods .....	76
3.2.2.1	Selection of standards .....	76
3.2.2.2	DTIMS measurements .....	77
3.2.2.3	TWIMS measurements (VION) .....	77
3.2.2.4	TWIMS measurements (Synapt).....	78
3.2.2.5	Quality assurance measures.....	78
3.2.2.6	CCS predictions - Artificial Neural Network (ANN) based prediction model .....	79
3.2.2.7	CCS predictions - Multivariate Adaptive Regression Splines (MARS) based prediction model .....	79
3.2.3	Results and Discussion.....	80
3.2.3.1	Quality control and quality assurance results .....	80
3.2.3.2	Selection of reference CCS values for further comparisons.....	81
3.2.3.3	Comparison of experimental <sup>TW</sup> CCS <sub>N2</sub> and <sup>DT</sup> CCS <sub>N2</sub> values.....	81
3.2.3.4	Comparison of predicted CCS and experimental <sup>DT</sup> CCS <sub>N2</sub> values.....	86
3.2.3.5	Comparison of predicted CCS and experimental <sup>DT</sup> CCS <sub>N2</sub> values.....	90
3.2.4	Conclusions.....	91
	Supplementary Information – Chapter 3.2.....	93
3.3	Comparison of CCS calculations and resolving power between DTIM and TIMS .....	103
3.3.1	Introduction.....	103
3.3.2	Materials and Methods .....	104
3.3.2.1	Selection of standards .....	104
3.3.2.2	DTIMS measurements .....	104
3.3.2.3	TIMS measurements.....	104

3.3.2.4 <sup>DT</sup> CCS <sub>N2</sub> calculations and assessment of resolving power .....	105
3.3.2.5 <sup>TIMS</sup> CCS <sub>N2</sub> calculations.....	106
3.3.2.6 Comparison of CCS <sub>N2</sub> datasets and data visualization.....	106
3.3.3 Results and Discussion .....	106
3.3.3.1 Comparison of <sup>DT</sup> CCS <sub>N2</sub> and <sup>TIMS</sup> CCS <sub>N2</sub> values .....	107
3.3.3.2 Differences in resolving power between TIMS and DTIM.....	110
3.3.4 Conclusions.....	113
Supplementary Information – Chapter 3.3 .....	114
<b>Chapter 4: Identification of known and emerging contaminants in indoor dust .....</b>	<b>125</b>
4.1 Identification and semi-quantification of quaternary ammonium compounds in indoor dust using IM derived CCS- <i>m/z</i> trendlines as an additional identification parameter.....	127
4.1.1 Introduction.....	127
4.1.2 Materials and Methods .....	130
4.1.2.1 Chemicals.....	130
4.1.2.2 Sample collection .....	130
4.1.2.3 Sample preparation .....	131
4.1.2.4 Instrumental analysis .....	131
4.1.2.5 Target screening - data analysis .....	132
4.1.2.6 Suspect screening - data analysis.....	133
4.1.2.7 Semi-quantification .....	134
4.1.2.8 Quality control.....	135
4.1.2.9 Exposure assessment .....	136
4.1.3 Results and Discussion .....	136
4.1.3.1 Method development and quality control results .....	136
4.1.3.2 Target screening and semi-quantification.....	139
4.1.3.3 Health risk assessment .....	142
4.1.3.4 Suspect screening results .....	143
4.1.3.5 IM-MS analysis .....	148
4.1.4 Conclusions.....	152

Supplementary Information – Chapter 4.1.....	153
4.2 Identification and semi-quantification of contaminants of emerging concern in indoor dust samples using IM derived CCS-m/z trendlines as an additional identification parameter.....	169
4.2.1 Introduction.....	169
4.2.2 Materials and Methods.....	170
4.2.2.1 Chemicals.....	170
4.2.2.2 Sample collection.....	170
4.2.2.3 Sample preparation.....	170
4.2.2.4 Instrumental analysis.....	171
4.2.2.5 Quality control and data analysis.....	172
4.2.2.6 Semi-quantification approach.....	173
4.2.2.7 Statistical analysis.....	174
4.2.2.8 Exposure assessment.....	174
4.2.3 Results and Discussion.....	175
4.2.3.1 Quality control and quality assurance results.....	175
4.2.3.2 Suspect screening results - identified compounds.....	176
4.2.3.3 <sup>DT</sup> CCS <sub>N2</sub> values as additional identification parameter for suspect CECs....	184
4.2.3.4 Semi-quantification results.....	187
4.2.3.5 Statistical comparison.....	190
4.2.3.6 Risk assessment based on semi-quantified concentrations.....	190
4.2.4 Conclusions.....	192
Supplementary Information – Chapter 4.2.....	194
<b>Chapter 5: Suspect screening of contaminants of emerging concern and their metabolites in human urine.....</b>	<b>221</b>
5.1 Introduction.....	223
5.2 Materials and Methods.....	225
5.2.1 Chemicals.....	225
5.2.2 Sample selection.....	225
5.2.3 Sample preparation.....	226

5.2.4	Instrumental analysis .....	226
5.2.5	Quality control.....	227
5.2.6	Data analysis.....	228
5.2.6.1	Data processing .....	228
5.2.6.2	Statistical analysis.....	230
5.3	Results and Discussion .....	231
5.3.1	Quality control results .....	231
5.3.2	Suspect screening results .....	232
5.3.3	Comparison with literature .....	237
5.3.4	Statistical analysis.....	239
5.4	Conclusions .....	241
	Supplementary Information – Chapter 5 .....	243

**Chapter 6: In vitro biotransformation products of prioritized emerging contaminants .....** **251**

6.1	Introduction .....	253
6.2	Materials and Methods.....	254
6.2.1	Materials and Methods .....	254
6.2.2	<i>In vitro</i> metabolism assay.....	255
6.2.3	Quality control of <i>in vitro</i> metabolization assays.....	256
6.2.4	Selection of human urine samples .....	257
6.2.5	Preparation of human urine samples.....	257
6.2.6	Instrumental analysis .....	258
6.2.7	Data processing and interpretation .....	258
6.3	Results and Discussion .....	260
6.3.1	Quality control results for <i>in vitro</i> metabolism assay .....	260
6.3.2	Identification of <i>in vitro</i> metabolites.....	261
6.3.2.1	C <sub>12</sub> -BAC - Phase I.....	261
6.3.2.2	C <sub>16</sub> -ATMAC - Phase I .....	263
6.3.2.3	C <sub>10</sub> -DDAC - Phase I .....	264

6.3.2.4 Phase II incubations .....	268
6.3.3 IM-MS analysis of the annotated metabolites .....	268
6.3.4 Confirmation of <i>in vitro</i> annotated metabolites in human urine samples.	271
6.4 Conclusions .....	274
Supplementary Information – Chapter 6.....	275
<b>Chapter 7: General discussion and future perspectives.....</b>	<b>299</b>
7.1 General discussion .....	301
7.2 Future perspectives.....	313
<b>Summary .....</b>	<b>317</b>
<b>Samenvatting .....</b>	<b>321</b>
<b>References.....</b>	<b>327</b>
<b>Curriculum Vitae .....</b>	<b>357</b>
<b>Acknowledgments .....</b>	<b>367</b>

## List of Abbreviations

3OH-TPHP	3-Hydroxyphenyl diphenyl phosphate
5OH-EHDPHP	5-hydroxy-2-ethylhexyl diphenyl phosphate
5OH-MEHA	Mono(2-ethyl-5-hydroxyhexyl) adipate
6OH-MPHP	6-Hydroxy monopropylheptyl phthalate
ACN	Acetonitrile
ADI	Acceptable Daily Intake
AME	Absolute mass error
ANN	Artificial neural networks
APEs	Absolute percent errors
APs	Alternative plasticizers
ATEC	Acetyl triethyl citrate
ATMACs	Alkyl trimethylammonium compounds
BACs	Benzyl alkyldimethyl ammonium compounds
BBzP	Butylbenzyl phthalate
BCEP	Bis(2-chloroethyl) phosphate
BCIPP	Bis(2-chloropropyl) hydrogen phosphate
BFRs	Brominated flame retardants
BPM	Bisphenol M
BPP	Bisphenol P
BPs	Bisphenols
bw	body weight
CAS	Chemical Abstracts Service
CCS	Collision cross section
CECs	Contaminants of Emerging Concern
CID	Collision-induced dissociation
CL	Confidence level
DDA	Data-dependent acquisition
DDACs	Dialkyl dimethylammonium compounds
DEET	Diethyltoluamide
DEHP	Di(2-ethylhexyl) phthalate
DF	Detection frequency
DIA	Data-independent acquisition
DiBP	Diisobutyl phthalate
DIDP	Diisodecyl phthalate
DINCH	Diisononyl cyclohexane 1,2-dicarboxylic acid
DINP	Diisononyl phthalate
DnBP	Di-n-butyl phthalate

DPP	Diphenyl phthalate
DTIM	Drift-tube ion-mobility
EDI	Estimated Daily Intake
EFSA	European Food Safety Authority
EL	Exposure load
EPA	Environmental Protection Agency
ESI	Electrospray ionization
EtOAc	Ethyl acetate
FbF	Find by Formula
FC	Fold change
FLEHS	Flemish Environment and Health Study
FRs	Flame retardants
GC	Gas chromatography
HBCD	Hexabromocyclododecane
HQ	Hazard Quotient
HRdm	High-resolution demultiplexing
HRMS	High-resolution mass spectrometry
IM-MS	Ion-mobility mass spectrometry
IQR	Interquartile ranges
IS	Internal standard
LC	Liquid chromatography
<i>m/z</i>	mass-to-charge ratio
MARS	Multiple Adaptive Regression Splines
MeOH	Methanol
MFE	Molecular feature extraction
MS	Mass spectrometry
NORMAN	Network of reference laboratories, research centers and related organizations for monitoring of emerging environmental substances
NTS	Non-target screening
OPFRs	Organophosphate flame retardants
PB	Procedural blank
PBDEs	Polybrominated diphenyl ethers
PCPs	Personal care products
PFAS	Per- and polyfluoroalkyl substances
PFCAs	Perfluoroalkyl carboxylic acids
PFSAs	Perfluoroalkyl sulfonic acids
PHs	Phthalates
POPs	Persistent organic pollutants
PVC	Polyvinyl chloride

QA	Quality assurance
QACs	Quaternary ammonium compounds
QC	Quality control
QQQ	Triple-quadrupole
QTOF-MS	Quadrupole time-of-flight mass spectrometer
REACH	Regulation on the Registration, Evaluation, Authorization and Restriction of Chemicals
R <sub>f</sub>	Response factor
RSD	Relative standard deviation
RT	Retention time
SPE	Solid-phase extraction
SSA	Suspect screening analysis
SST	System Suitability Test
TAP	Triamyl phosphate
TBOEP	Tris(2-butoxyethyl) phosphate
TBP	Tributyl phosphate
TCEP	Tris(2-chloroethyl) phosphate
TCP	Tricresyl phosphate
TDBPP	Tris(2,3-dibromopropyl)phosphate
TDCIPP	Tris(1,3-dichloro-2-propyl) phosphate
THTM	Tri-n-hexyl trimellitate
TIMS	Trapped ion-mobility spectrometry
TOF	Time-of-flight
TOTM	Tris(2-ethylhexyl) trimellitate
TPHP	Triphenyl phosphate
TWIMS	Travelling-wave ion-mobility spectrometry
USA	United States of America
WWTP	Wastewater treatment plants

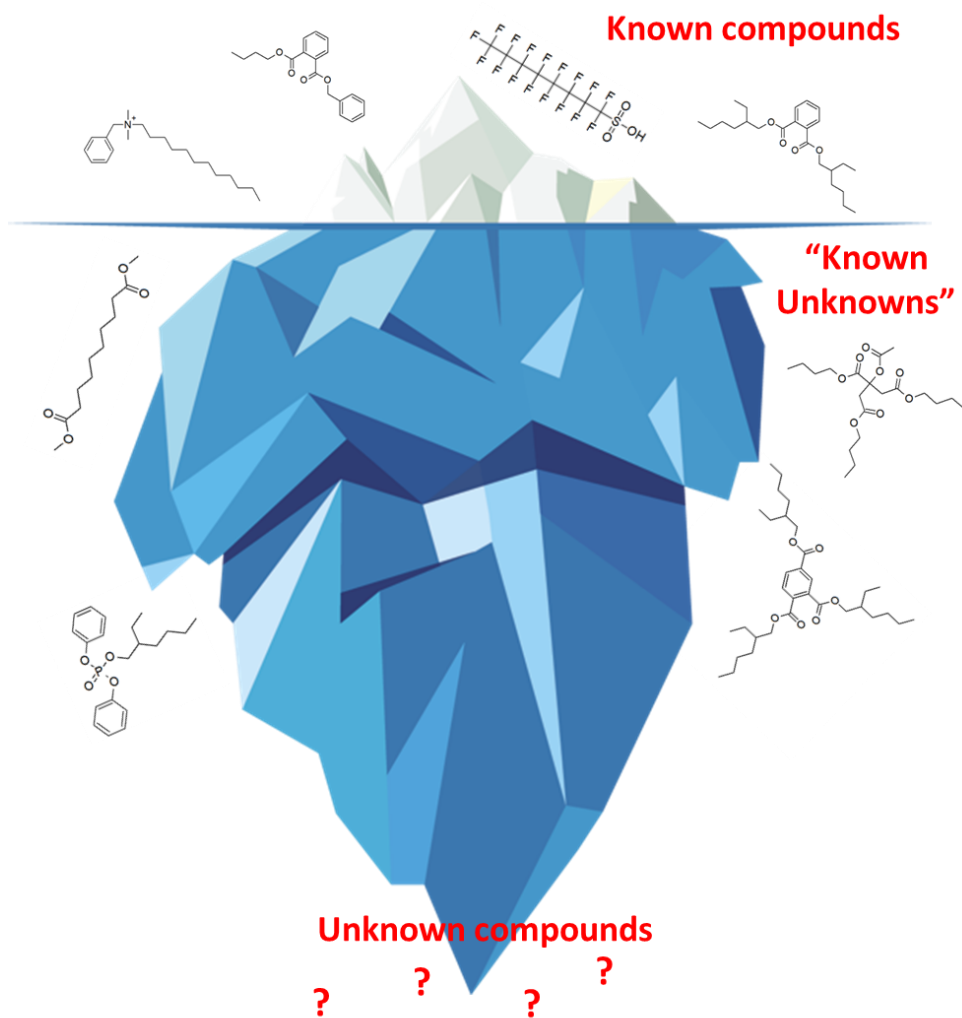


“As crude a weapon as the cave man’s club, the chemical barrage has been hurled against the fabric of life.”

*Rachel Carson, 'The Silent Spring', 1962*



# Chapter 1: General Introduction





Pollution and climate change represent the two main current threats to human health resulting from anthropogenic influences on planet earth. It is estimated that pollution is responsible for approximately 9 million deaths annually, more than 70% of which can be related to non-communicable diseases (Landrigan et al., 2018). Sources of pollution include ambient air pollution, e.g. through airborne particulate resulting from the burning of fossil fuels, soil and water pollution and chemical pollution. Latter gained first broad attention following the release of 'Silent Spring' in 1962, a book by Rachel Carson which for the first time linked the increased use and release of industrial chemicals with negative environmental and health effects (Carson, 1962). Since then, the number of new industrial chemicals introduced has been rising steadily, ultimately resulting in almost 20 million new entities in the Chemical Abstracts Service (CAS) registry in 2021 (Arp et al., 2023). This development is inevitably connected to increasing contamination of the environment with these chemicals and ultimately human exposure to environmental contaminants.

The investigation of latter has become a well-established research area in environmental chemistry, commonly summarized as the exposomics field (Wild, 2005). It focuses not exclusively on known contaminants, which often cover only the 'tip of the iceberg' of chemicals to which humans can be exposed. The greater analytical challenge is posed by so-called 'known unknowns' and 'unknown unknowns' describing compounds for which data on their identity and occurrence are scarce or fully unavailable, respectively, requiring constant development of analytical methodologies to address these challenges.

This thesis is embedded in the exposomics research field presenting novel mass spectrometric approaches and their applications for the identification of environmental contaminants in environmental and human matrices.

## 1.1 Legacy contaminant classes and Contaminants of Emerging Concern

The increasing chemical pollution reflects itself in the high number of contaminant classes reported and investigated to date. The most prevalent classes include organic pollutants, e.g., phthalates and alternative plasticizers, flame retardants, pharmaceuticals, pesticides, personal care products, per- and poly-fluoroalkyl substances (PFAS), naturally occurring compounds such as pathogens, cyanotoxins, mycotoxins or toxic elements including lead, cadmium, mercury and arsenic among others (Wang et al., 2024).

The most common organic pollutants, which will be the main focus of this thesis, are industrial chemicals which are (accidentally or intentionally) released into the environment, e.g. through wastewater treatment plants (WWTP) discharges, direct

release from industrial production sites, improper waste management, landfill leachate or agricultural activities (Eggen et al., 2010; Nguyen et al., 2023; Parida et al., 2021). Despite a slight decrease in industrial chemicals' production observed since 2004, the production volume remains on a very high level with more than 250 million tons produced in the European Union in 2022 (Eurostat, 2023) showing great potential for high-volume release into the environment and ultimately a high risk for human exposure to these chemicals. Several classes of organic contaminants (as listed above) to which humans are exposed are well-described in literature. A selection of these is discussed more in detail here, and example structures of selected classes of contaminants are summarized in **Figure 1.2.1**.

Plasticizers are chemicals added to plastic materials to increase their durability, flexibility and elasticity. Esters of phthalic acid are the most commonly used class with di(2-ethylhexyl) phthalate (DEHP) being the best known and studied phthalate homologue. Other examples include di-n-butyl phthalate (DnBP), diisobutyl phthalate (DiBP) and butylbenzyl phthalate (BBzP) and can be summarized as 'legacy phthalates' (Christia et al., 2019). Their main application is the production of polyvinyl chloride (PVC) where the added phthalate content can reach up to 40% wt% (Chiellini et al., 2013). Since phthalates are not bound to the plastic material they are added to, leachate is possible facilitating environmental contamination and ultimately human exposure. Contamination with phthalates has been reported for various environmental matrices, including indoor air and dust, food, drinking water and soil (Net et al., 2015). Several toxic effects have been described for phthalates including reproductive toxicity and endocrine disrupting properties. In human epidemiological studies, phthalate exposure was associated with reduced sperm quality, malformations of the testes and reduced testicular testosterone production (Koch and Calafat, 2009; Swan, 2008). Given these effects, several phthalate homologues (including DEHP, BBzP, DiBP and DnBP) were classified as toxic to reproduction (Repr. 1B) and added to Annex XVII of the Regulation on the registration, evaluation, authorization and restriction of chemicals (REACH) which includes a list of restricted substances. This limits their use in all articles containing plasticized material to a maximum of 0.1% (REACH, 2020).

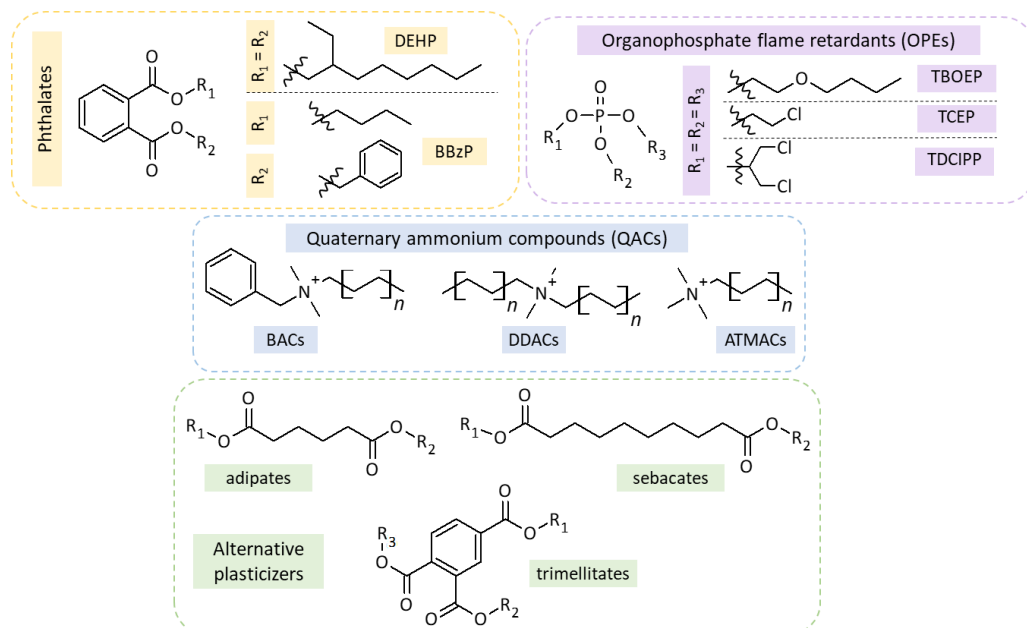


**Figure 1.2.1:** Molecular structures of relevant classes of environmental contaminants. For phthalates, structures of the legacy phthalates di(2-ethylhexyl) phthalate (DEHP) and butylbenzyl phthalate (BBzP) are shown as examples. For organophosphate flame retardants (OPEs), commonly occurring homologues are shown as examples (tris(2-butoxyethyl) phosphate (TBOEP), tris(2-chloroethyl) phosphate (TCEP), tris(1,3-dichloro-2-propyl) phosphate (TDCIPP)). For quaternary ammonium compounds (QACs), three commonly occurring classes are shown: alkyl trimethylammonium compounds (ATMACs), benzyl alkyldimethyl ammonium compounds (BACs) and dialkyl dimethylammonium compounds (DDACs). Previously reported QACs in indoor dust included even numbered chain lengths with  $n = 8-18$ ,  $n = 6-18$  and  $n = 8-18$  for ATMACs, BACs and DDACs, respectively (Zheng et al., 2020). For alternative plasticizers, examples of commonly occurring backbones corresponding to the classes of adipates, sebacates and trimellitates, which can be substituted with varying hydrocarbon side chains, are shown.

Another important group of environmental contaminants are flame retardants (FRs) which are added to or incorporated in various materials (additive vs. reactive FRs) to reduce flammability and the risk of fire. Similar to plasticizers, additive FRs can leach from the material they are added to resulting in environmental contamination (Hou et al., 2016). In the early 2000s, brominated flame retardants (BFRs) were the most commonly used representatives of this class including, e.g., hexabromocyclododecane (HBCD) or polybrominated diphenyl ethers (PBDEs). Yet, during their wide application, high bioaccumulation and persistency were observed for these compounds leading to their enrichment in the environment as well as human and animal tissues (Lyche et al., 2015). This led to the inclusion of PBDEs, HBCD and hexabromobiphenyl to the Stockholm Convention characterizing them as persistent organic pollutants (POPs) and heavily restricting their use in the European Union (Sharkey et al., 2020).

Thirdly, personal care products (PCPs) can be viewed as an example for a broad classification of environmental contaminants summarizing substances released from

products used for personal hygiene, cleaning, beautification, skin care etc. Under this collective term, several compound classes have been reported including parabens, benzophenones, antibacterial agents, such as triclosan and triclocarban, or UV-filters. The global production of PCPs has been estimated at over 10.000 t/year (Wilkinson et al., 2017). Similar to phthalates, endocrine disrupting properties have been described for other PCPs such as parabens and several UV-filters (Mao et al., 2022; Nowak et al., 2018) leading to negative influences on the human hormonal system after extensive exposure. Latter is facilitated by limited regulations on PCPs industrial use and their high-release into the environment. Their occurrence has been described for numerous environmental matrices including surface and drinking water, indoor dust, soil and sludge (Biel-Maeso et al., 2019; Shi et al., 2021; Wang et al., 2021).

A subclass of PCPs which gained increased attention in recent years, are quaternary ammonium compounds (QACs). These include high-volume production compounds carrying at least one positively charged quaternary nitrogen atom substituted with at least one hydrophobic hydrocarbon side chain (Hora et al., 2020). The main classes of QACs used (**Figure 1.2.1**) include alkyl trimethylammonium compounds (ATMACs), benzyl alkyldimethyl-ammonium compounds (BACs) and dialkyl dimethylammonium compounds (DDACs; in some studies abbreviated as DADMAC). The described structural characteristics result in surface active, amphiphilic properties allowing to use QACs as antimicrobials in cleaning and disinfecting products. These applications led to a vastly increased QAC use during the COVID-19 pandemic resulting in substantial releases of these chemicals in the environment facilitating ubiquitous human exposure. In 2020, Zheng et al. presented a study on QAC concentrations in indoor dust samples collected in the United States of America (USA). For most compounds investigated, a significant increase in concentration was observed when comparing dust samples collected before and during the COVID-19 pandemic (Zheng et al., 2020). These findings were followed by first reports of QACs in human blood and breast milk in 2021 and 2022, respectively, indicating increasing relevance of this class for potential human exposure (Zheng et al., 2021; Zheng et al., 2022). This is further supported by several toxic effects described for QACs. These include skin irritation, disrupted cholesterol homeostasis and mitochondrial function which were observed in animal studies (Anderson et al., 2016; Herron et al., 2016; Larsen et al., 2012). Human exposure to QAC-containing disinfectants has been associated with an increased risk of asthma (Gonzalez et al., 2014). Nevertheless, data on the occurrence of QACs in European indoor environments is scarce limiting the estimation of potential human exposure to this emerging class of chemicals.

The gradual phase out of contaminants, such as legacy phthalates or BFRs for which negative effects on the environment and/or human health have been proven,

introduces an urgent need for replacement chemicals which can fulfill the same needs in the corresponding industrial applications. For example, the restrictions introduced for DEHP, BBzP, DiBP and DnBP have been accompanied by the introduction of so-called alternative plasticizers (APs). These include phthalates for which solely the ester groups were modified (e.g., diisononyl phthalate (DINP) or diisodecyl phthalate (DIDP)) but also compounds with other chemical backbones, such as adipates, citrates, trimellitates, sebacates or cyclohexane dicarboxylic acid esters, whereby the carboxy groups are always esterified with varying substituents (Christia et al., 2019). Similarly, organophosphate flame retardants (OPFRs) are widely applied as a replacement for the highly restricted BFRs. These compounds have a phosphate backbone carrying three (most commonly identical) substituents. Examples for commonly applied OPFRs include tris(2-butoxyethyl) phosphate (TBOEP), triphenyl phosphate (TPHP), tris(2-chloroethyl) phosphate (TCEP), tris(1,3-dichloro-2-propyl) phosphate (TDCIPP) and others.

Even though these alternatives have been assumed to cause fewer toxicological risks than the restricted compounds they phased out, first indications of toxic effects have been reported for both APs and OPFRs. For OPFRs, strong hemolytic effects, aquatic and inhalation toxicity have been described. Halogenated OPFRs have been reported to have reproductive toxicity, be toxic to aquatic organisms and potentially carcinogenic (Van der Veen and de Boer, 2012). For DINP, epidemiological data suggests negative effects on fertility and reproduction in males even though larger cohort studies are needed to confirm this. Toxicological data available for non-phthalate APs suggests that they are less toxic than legacy phthalates (Bui et al., 2016). However, for these new alternatives, available toxicological and epidemiological data is scarce and a clear need for further assessment of their occurrence and effects in human and environmental matrices has been addressed in literature (Qadeer et al., 2024).

The described high variety and constantly changing structural characteristics of environmental contaminants pose a great analytical challenge for the exposomics field. To summarize these emerging compounds, the term 'Contaminants of Emerging Concern' (CECs) has been established. It describes classes of contaminants for which data on their occurrence, environmental fate, bioavailability and toxicity are limited (Sauve and Desrosiers, 2014). These can include contaminants whose structures are well described, e.g. above described APs and OPFRs, but for which other data is lacking. On the other hand, fully new contaminants keep emerging in recent years, whose structures still have to be characterized. For example, the class of OPFRs was recently expanded by the characterization of eleven new homologues in house dust not previously described in environmental samples (Wang et al., 2020a). These fast developments require a constant adjustment of analytical methodologies which go beyond commonly applied quantitative targeted methods.

## 1.2 Suspect and non-target screening approaches

The assessment of the occurrence of legacy contaminants and CECs in environmental and human matrices is most commonly based on the application of quantitative targeted methods. Thereby, a set of preselected analytes, for which reference standards are available, can be analyzed applying liquid or gas chromatography (LC/GC) coupled to triple-quadrupole mass spectrometry (QQQ-MS) (Heffernan et al., 2016). If validated, these highly sensitive and selective methods provide quantitative data on contaminant concentrations in the matrix of interest. This data are crucial for reliable biomonitoring and exposure risk assessment (Bastiaensen et al., 2021b) and are commonly applied within large (governmentally funded) biomonitoring studies, such as the Flemish Environment and Health Study (FLEHS). Nevertheless, targeted methods are limited to the compounds for which they were developed and validated not allowing any assessment of CECs' concentrations.

The fast increase in chemical pollution and constant reports of new contaminants or contaminant classes, facilitate the advancement of suspect and non-target screening analysis methods (SSA/NTS) in recent years. As shown in **Figure 1.2.2**, these developments are reflected in a constant increase in the number of manuscripts published since 2000 and carrying either 'suspect screening' or 'non-target screening' in the title or abstract.

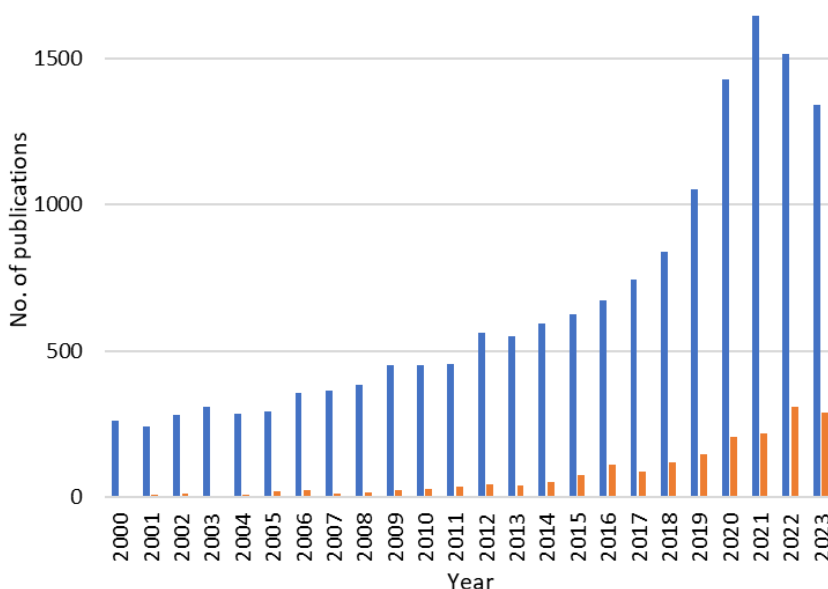


**Figure 1.2.2:** Number of publications carrying the term 'suspect screening' (blue) or 'non-target screening' (orange) in the title or abstract. The numbers were retrieved through a Web of Science search applying the following search queries: 'TI=(suspect screening) OR AB=(suspect screening)' and 'TI=(non-target screening) OR AB=(non-target screening)'

Within most SSA and NTS methods, LC or GC separation is coupled to high-resolution mass spectrometry (HRMS). In contrast to QQQ-MS based targeted methods which acquire data only for an *a priori* selected set of analytes, HRMS provides full scan mass spectrometric data potentially allowing the detection of all analytes which can be covered by the applied sample preparation and instrumental methods. Often, the acquisition of fragmentation spectra is included to increase the amount of information available for structure elucidation. Here, a distinction can be made between so-called data-dependent and data-independent (DDA/DIA) acquisition. Within DDA methods, a fraction of possible precursor ions is selected based on abundance, a predefined list of ions of interest or other considerations. DIA methods allow the fragmentation of all ions within one analysis cycle vastly increasing the amount of available fragmentation data. However, DIA datasets require more complex post-acquisition data processing to allow the assignment of fragment ions to the corresponding precursors (Renaud et al., 2017).

The analysis of environmental and human samples by SSA or NTS approaches provides complex multi-dimensional raw data files requiring complex data processing approaches prior to the actual identification of CECs or their metabolites. The data processing steps commonly included within most HRMS based screening studies are summarized in **Figure 1.2.3**.

After optional data pre-processing such as mass re-calibration or noise removal, peak picking is performed aiming at extracting separate signals from the raw data files. Each extracted signal represents a certain mass-to-charge ( $m/z$ ) ratio showing an, ideally gaussian, peak in the retention time (RT) dimension (Lennon et al., 2024). The number of signals can reach up to ten thousands per sample, especially in complex human matrices (Huber et al., 2022b).

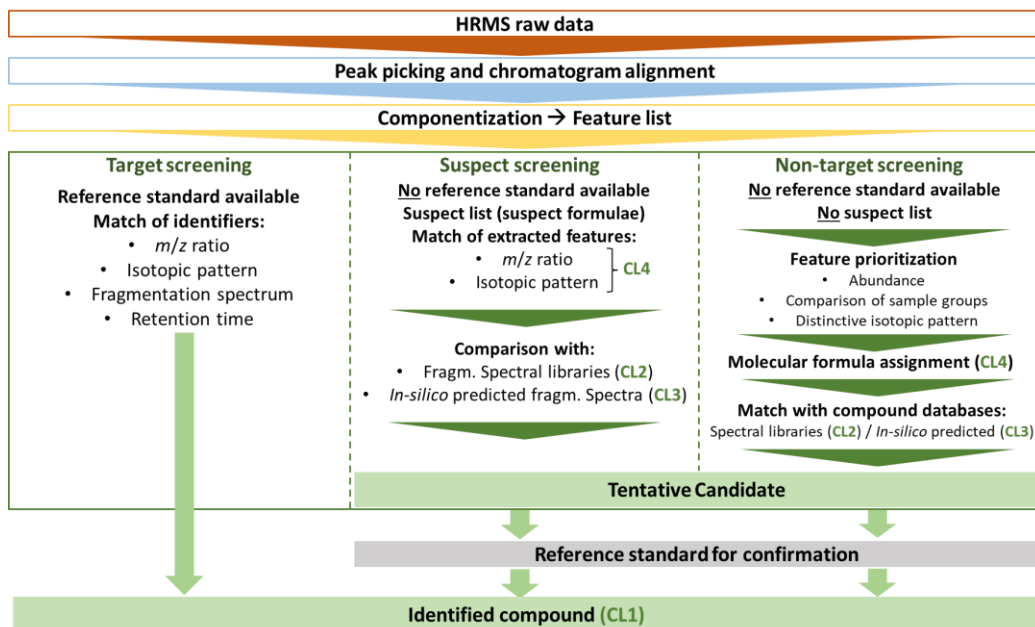


**Figure 1.2.3:** Summary of data processing workflows for target, suspect and non-target screening studies. The figure was adjusted from Celma et al., 2021. Cut-off values used for each indicated parameter are selected based on the individual research question and instrument used. CL: Confidence level. Further information on the indicated CL can be found in **Figure 1.2.3**.

Secondly, extracted chromatographic peaks are aligned between samples allowing to correct for small retention time shifts throughout the analysis sequence. Gap-filling algorithms can be applied to re-evaluate samples showing missing values for certain signals (Müller et al., 2020). Thirdly, extracted peaks are clustered into so-called features which is based on the fact that  $m/z$  ratios can be grouped into isotopic patterns and different adducts. Ultimately, each component represents a potential compound present in the sample (Schymanski et al., 2015). Therefore, the final and most crucial data analysis step aims at the assignment of possible compounds. Here, the distinction can be made between targeted, suspect and non-target screening (**Figure 1.2.3**). To allow a harmonized reporting of the identification confidence with which compounds can be identified, Schymanski et al. proposed a five level system which will be discussed in detail below and is summarized in **Figure 1.2.4** (Schymanski et al., 2014).

In target screening, compound assignment is based on a set of available reference standards. If all identifiers (i.e., RT,  $m/z$  ratio and isotopic pattern, fragmentation spectrum) can be matched between the reference standard and experimental data, confidence level (CL) 1 can be assigned (Bořík et al., 2023). Even though targeted screening is greatly limited by the availability of reference standards, CL1 is the highest achievable identification confidence which is also reached by quantitative QQQ-MS methods.

Suspect screening is based on matching extracted features with a list, commonly referred to as a 'suspect list', containing compounds suspected to be present in the samples. The compilation of the suspect list is driven by the study design and the CEC classes of interest. It can contain formulae of known compounds or *in-silico* predicted data for novel CECs or CEC metabolites (Taha et al., 2022). Compound matching is based on the exact  $m/z$  ratio of the formulae of suspect compounds (and the resulting isotopic pattern). Additionally, fragmentation spectra can be included in the identification process. If, within suspect compound annotation, all mass-spectrometric identifiers ( $m/z$  ratio, isotopic pattern, fragmentation spectrum) can be matched with a spectral library or contain characteristic evidence, allowing the assignment of a single possible candidate, excluding all others, CL2 is assigned. This is the highest possible confidence level that can be reached in screening studies for compounds for which no reference standard is available. If fragmentation spectra were acquired and provide structural information for which, however, no reference spectral library entity is available, a tentative candidate is assigned at CL3. For further confirmation of CL3 assignments, fragmentation data is often compared with *in-silico* predicted spectra (Chao et al., 2020). CL3 is also used if available data does not allow an unequivocal distinguishment between several possible candidates or structural isomers with the same molecular formula. Features for which no fragmentation spectrum is available allowing only the match of a molecular formula and the corresponding isotopic pattern are reported at CL4. Lastly, CL5 is assigned to signals for which only a single  $m/z$  ratio is known and information on the isotopic pattern or possible other adducts is missing (Celma et al., 2020; Schymanski et al., 2014). For candidates assigned CL4 or 5, very little structural information is available usually not allowing further data interpretations.

While suspect screening can ease data processing by narrowing the focus on a predefined selection of analytes, it is limited to the compounds included in the suspect lists leaving all other compounds present in the sample undetected. To close this gap, non-target screening can be applied analyzing signals without any *a priori* selection of candidate compounds. From the extracted feature list, features can be prioritized based on various considerations. These can include the selection of features based on abundance or on differences in abundance observed between groups of samples, the observation of characteristic isotopic patterns suggesting, e.g., the presence of halogens or the detection of characteristic fragments or neutral losses in the fragmentation spectra (Léon et al., 2019; Zweigle et al., 2022). For the prioritized features, molecular formulae can be predicted and matched with large open-source compound databases such as PubChem (Kim et al., 2023). From potential candidates, most probable compounds are selected based on available mass spectrometric data and expert's assessment whereby CL of identification are assigned following the same considerations as described above.

		Data requirements	
CL1	<b>Confirmed structure</b> by reference standard	MS, MS <sup>2</sup> , RT, Reference standard	CCS ≤ 2%
CL2	<b>Probable structure</b> a) library spectrum match b) diagnostic evidence	a) MS, MS <sup>2</sup> , Library MS <sup>2</sup> b) MS, MS <sup>2</sup> , characteristic MS <sup>2</sup>	CCS <sub>library</sub> ≤ 2% CCS <sub>predicted</sub>
CL3	<b>Tentative structure</b> Substructure, isomers, class	MS, MS <sup>2</sup> , experimental MS <sup>2</sup>	CCS <sub>predicted</sub> CCS- <i>m/z</i> trendlines
CL4	<b>Molecular formula</b>	MS, isotope/adduct	CCS
CL5	<b>Exact mass</b>	MS	CCS

**Figure 1.2.4:** Confidence levels (CL) used for the communication of identification confidence for compounds identified through target, suspect or non-target screening. The implementation of collision cross section (CCS) values is discussed in **chapter 1.3.4**. The figure was adjusted from Schymanski et al., 2014 and Celma et al., 2020.

Given the young age of the research fields of SSA and NTS and the large differences observed in study design and data interpretation, the harmonization of workflows has been a major focus within the research community in recent years. Recently, the Network of reference laboratories, research centers and related organizations for monitoring of emerging environmental substances (NORMAN) has proposed a set of guidelines for SSA and NTS studies in the field of environmental analyses (Hollender et al., 2023). Additionally, the implementation of suitable quality assurance and quality control measures (QA/QC) plays a crucial role to allow the assessment of data quality. Harmonized guidelines for QA/QC measures for suspect and non-target screening studies have been proposed, recommending the use of standardized terminology, implementation of isotopically labelled internal standards to monitor analyte losses through sample preparation and the reliability of data processing workflows, assessment of instrumental performance and others (Caballero-Casero et al., 2021a). Nevertheless, both sets of guidelines are still far from a wide application and the harmonization of SSA and NTS between different laboratories and working groups is limited. The scheme of confidence levels proposed by Schymanski et al. remains the only widely implemented and accepted guideline. Therefore, a detailed reporting of all parameters applied for data acquisition, processing, interpretation and reporting remains crucial. A detailed and critical assessment of these parameters plays a central role in the interpretation of study results and their relevance in an environmental context.

### 1.3 Ion-mobility as an additional separation dimension

Ion-mobility spectrometry (IMS) measures the drift of ions through an (inert) buffer gas under the influence of an electric field. It was first described in 1898 (Zeleny, 1898),

even before the first introduction of mass spectrometry in 1912 (Thompson, 1912). Already in the early development stages, IMS was coupled to a mass spectrometer, providing an additional separation dimension (Cohen and Karasek, 1970). For this coupling, the abbreviations IMS-MS or IM-MS are commonly used. In the early development stages, applications of IM-MS were limited to in-house developed instrumentation in an academic setting (Wu et al., 1998). In 2006, the first commercially available IM-MS instrument, the Synapt IM time-of-flight MS, was introduced by Waters (Pringle et al., 2007). Since then, several instruments from different vendors were introduced incorporating different principles of ions' mobility measurement.

Generally, IMS measures an ion's mobility through a buffer gas under the influence of a weak electric field. Under ideal measurement conditions, an analyte's mobility ( $K$ ) is defined as the ratio between the ion's apparent drift velocity ( $v_d = L/t_d$ , where  $L$  is the length of the drift tube and  $t_d$  is the drift time) and the applied electric field ( $E$ , [ $V\ m^{-1}$ ]), as displayed in **equation 1.3.1**.

$$K = \frac{v_d}{E} \quad (1.3.1)$$

When  $K$  is normalized to standard conditions, the reduced mobility ( $K_0$ ) can be calculated as follows (**equation 1.3.2**) where  $p$  and  $T$  are the experimental pressure and temperature, respectively, and  $p_0$  and  $T_0$  are standardized pressure (760 Torr = 101.325 Pa) and temperature (273.15 K), respectively (Gabelica et al., 2019):

$$K_0 = K \cdot \frac{p}{p_0} \cdot \frac{T_0}{T} \quad (1.3.2)$$

For drift-tube ion-mobility measurements (DTIM, **chapter 1.3.1**) where a uniform low electric field is applied, a collision cross section ( $\Omega$ ) value describing the rotationally averaged surface of an ion can be calculated from the reduced mobility (**equation 1.3.3**). This is based on a modified version of the fundamental zero field limit equation, commonly referred to as the Mason-Schamp equation (Mason and Schamp Jr, 1958; Revercomb and Mason, 1975):

$$\Omega = \frac{1}{K_0} \cdot \frac{(18\pi)^{1/2}}{16} \cdot \frac{ze}{(k_b T)^{1/2}} \cdot \left[ \frac{1}{m_i} + \frac{1}{m_b} \right]^{1/2} \cdot \frac{1}{N} \quad (1.3.3)$$

Here,  $k_b$  is the Boltzman constant,  $z$  is the charge state,  $m_i$  is the mass of the ion,  $m_b$  is the mass of the drift gas and  $N$  is the number of gas molecules per unit volume. To ensure a transparent and harmonized reporting of calculated collision cross section (CCS) values, latter are reported indicating the instrumental set-up and buffer gas used for mobility

measurements (Gabelica et al., 2019). For example,  ${}^{\text{DT}}\text{CCS}_{\text{N}_2}$  described a CCS value calculated based on DTIM measurements with nitrogen as the buffer gas.

The separation dimension provided by IMS and the calculation of CCS values which can serve as an additional identification parameter can be of great added value within suspect and non-target screening studies. Additionally, gas phase separations can allow to distinguish between isomeric or isobaric structures which often cannot be separated by liquid chromatographic methods.

### 1.3.1 Drift-tube ion-mobility spectrometry (DTIM)

DTIM separates ions based on their mobility through a drift-tube filled with the buffer gas under the influence of a low uniform electric field. In 2014, Agilent Technologies introduced a commercially available DTIM quadrupole time-of-flight mass spectrometer (6560 DTIM-QTOF) whose configuration is displayed in **Figure 1.3.1**.

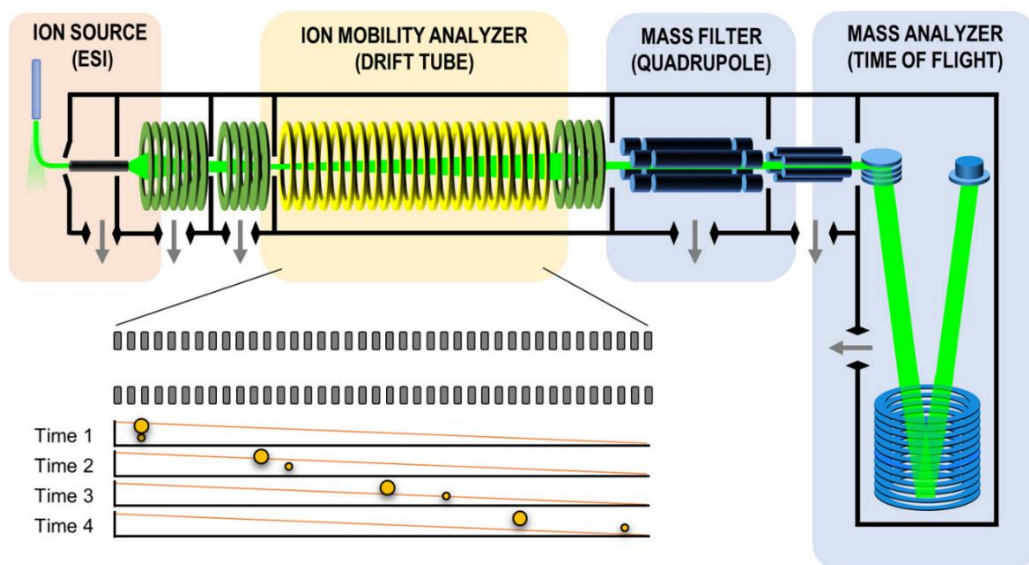


**Figure 1.3.1:** Schematic overview of an Agilent drift-tube ion-mobility quadrupole time-of-flight mass spectrometer (6560 DTIM-QTOF). Reproduced from (May and McLean, 2015) with permission from J. May, J. McLean and the American Chemical Society.

The constant ion stream coming from the electrospray ionization source (ESI) is accumulated in the trapping funnel located in front of the drift tube. Ion packages are released into the drift-tube filled with the buffer gas (most commonly nitrogen) at a pressure of approx. 3.95 Torr. After separation in the drift tube, ions can be fragmented in the collision cell located behind the quadrupole mass analyzer. Lastly, masses of ions and fragments are measured in the TOF mass analyzer. Thereby, the length of one DTIM analysis cycle is commonly set to 50-60 ms. This allows DTIM measurements to fit

perfectly on the time scale between chromatographic separation (in seconds) and TOF mass analysis (in  $\mu\text{s}$ ).

DTIM is the only instrumental set-up allowing the direct measurement of the ion's drift time and subsequent calculation of the  $^{\text{DT}}\text{CCS}_{\text{N}_2}$  value applying a primary method. However, the drift time measured by the DTIM instrumental set-up (**Figure 1.3.1**) reflects the total time ( $t_A$ ) needed for the ion to travel from the entrance of the drift tube to the detector. This time is composed of the 'real' drift time ( $t_d$ ) and  $t_{\text{fix}}$ , describing the time within which an ion passes from the exit of the drift-tube to the detector. To obtain  $t_d$ , needed for  $^{\text{DT}}\text{CCS}_{\text{N}_2}$  calculation, mobility measurements have to be conducted applying varying electric fields ( $E$ ). Then, the obtained total drift time is plotted as a function of  $1/E$ . Through extrapolation of  $1/E$  to zero,  $t_{\text{fix}}$  and subsequently  $t_d$  can be obtained from which  $^{\text{DT}}\text{CCS}_{\text{N}_2}$  calculations are possible (**equation 1.3.3**). This approach is commonly referred to as the 'stepped-field method' of calibration (Stow et al., 2017).

However, a measurement of an ion's mobility at varying electric fields is impractical, especially when IM-MS is coupled to chromatographic methods requiring IM separations on a milliseconds time scale. To address this problem, a so-called 'single-field' calibration method has been introduced. It is based on the measurement of mobilities of calibrant ions for which reference  $^{\text{DT}}\text{CCS}_{\text{N}_2}$  (acquired using the stepped-field method) are established. Thereby, calibrant ions must be analyzed under the exact same instrumental conditions as the analytes for which  $^{\text{DT}}\text{CCS}_{\text{N}_2}$  value are calculated. From the data obtained for calibrant ions, a calibration curve can be composed by plotting the total drift time ( $t_A$ ) against the reference  $^{\text{DT}}\text{CCS}_{\text{N}_2}$  value, whose slope and intercept can be used to calculate the  $^{\text{DT}}\text{CCS}_{\text{N}_2}$  value of analyte ions applying **equation 1.3.4** (Stow et al., 2017):

$$t_A = \frac{\beta}{z} \cdot \left[ \frac{1}{m_i} + \frac{1}{m_b} \right]^{1/2} \cdot \text{CCS} + t_{\text{fix}} \quad (1.3.4)$$

Here,  $\beta$  and  $t_{\text{fix}}$  are the slope and intercept obtained from the calibration curve, respectively,  $t_A$  and CCS are the total drift time and CCS value of the analyte ion, respectively,  $z$  is the charge state,  $m_i$  is the mass of the ion and  $m_b$  is the mass of the drift gas.

The described calibration methods point out that a CCS value is no physical constant but a calculated, empirical value influenced by numerous uncertainty factors. Stepped-field calibration relies on a precise measurement of experimental parameters including temperature, field strength and buffer gas pressure. Reference  $^{\text{DT}}\text{CCS}_{\text{N}_2}$  values used for single-field calibrations were acquired on a reference DTIM system where measurement accuracies of experimental parameters were improved. Nevertheless, single-field calibration is influenced by the uncertainty of the underlying reference  $^{\text{DT}}\text{CCS}_{\text{N}_2}$  values and the uncertainty of the experimental total drift times ( $t_A$ ) of calibrant and analyte ions. A previous study accessed overall measurement uncertainties for

stepped and single-field based calculations estimating expanded uncertainties in ranges of 2.7 to 4.6% ( $k = 2$ ) and 4.7 to 9.1% ( $k = 2$ ), respectively (Causon and Hann, 2020). The consideration of these uncertainties is of great importance when interpreting experimental DTIM data.

With the described commercially available DTIM system, a mobility resolution, defined as the ratio between drift time and peak width at half-maximum, of approx. 60 can be reached (Ewing et al., 2016). This resolving power might not be sufficient, especially if DTIM analyses aim at separating isomeric mixtures. Additionally, since ion trapping is needed prior to mobility analyses, ion utilization is vastly decreased due to space charge effects and ion heating in the trapping funnel (Causon et al., 2019b). To increase DTIM resolving power and ion utilization, the multiplexed acquisition mode has been developed. In contrast to the classical DTIM acquisition where one ion pulse per cycle is released into the drift tube, multiplexed acquisition allows multiple ion pulses per cycle which are modulated based on a 3-bit or 4-bit pseudorandom binary sequence. This way, trap filling times can be decreased which increases ion utilization and sensitivity leading to signal increase up to 9-fold reported for multiplexed analyses (May et al., 2020). Data files acquired in multiplexed mode require post-acquisition demultiplexing to deconvolute drift spectra into single signals (Prost et al., 2014). Recently, an additional post-processing step, referred to as high-resolution demultiplexing (HRdm), was introduced which can improve mobility resolution for a predefined set of features, thereby reaching a resolving power of up to 250 (May et al., 2020).

### 1.3.2 Travelling-wave ion-mobility spectrometry (TWIMS)

The first commercially available IM-MS instrument - the Synapt IM time-of-flight MS, introduced in 2009 - incorporated a travelling-wave ion-mobility (TWIMS) separation set-up. Since then, several new models have been developed including the Synapt G2 and VION systems. **Figure 1.3.2** shows a schematic overview of the Synapt G2 IM-MS instrument. It can be viewed as the 2<sup>nd</sup> generation of the Synapt series, whose main improvement was the introduction of a helium cell in front of the mobility cell allowing to increase nitrogen buffer gas pressures leading to improved resolution power (Giles et al., 2011). Further instrumental advancements were achieved through the release of the VION TWIMS system in 2015. Thereby, main developments included vastly improved ion optics and the incorporation of the QuanTof™ 2 technology leading to an increased dynamic range (Waters, 2013).

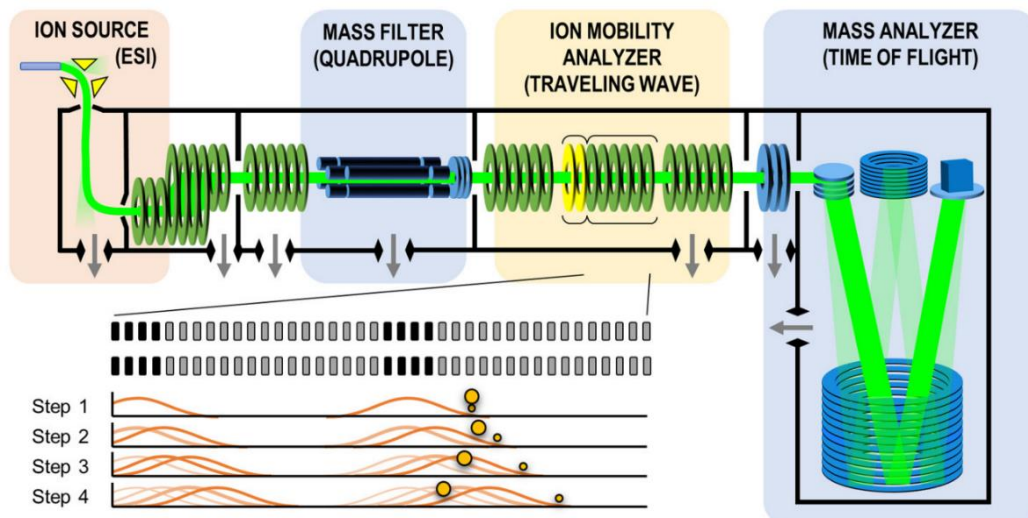


**Figure 1.3.2:** Schematic overview of a Waters travelling wave ion-mobility quadrupole time-of-flight mass spectrometer (Synapt G2). Reproduced from (May and McLean, 2015) with permission from J. May, J. McLean and the American Chemical Society.

Similar to DTIM, the TWIMS mobility cell consists of a stacked series of ring electrodes and is filled with the buffer gas (nitrogen). However, in the case of TWIMS the applied electrical field is not uniform: Voltages applied to ring electrodes are raised periodically whereby potential maxima move along the drift cell. This creates 'travelling waves' which lead to the naming of this technique. Analyte ions 'surf' these waves. Compact ions (with small CCS values) undergo less collisions with the buffer gas, whereby larger ions are more likely to topple over the wave tops due to increased collisions with the buffer gas. The height and velocity of the travelling wave and the gas pressure influence the separation capabilities. Additionally to the voltages creating the travelling waves, a radio frequency (RF) voltage is applied to ensure radial ion confinement (Gray et al., 2016).

Due to the non-uniform electric field,  $^{TW}CCS_{N_2}$  values cannot be directly derived from the measured ion mobilities. Therefore, TWIMS relies on the availability of calibrant ions for which DTIM derived reference  $^{DT}CCS_{N_2}$  values are available. Given that calibrant ions are analyzed under the exact same as the analytes of interest, their measured total drift times ( $t_A$ ) and reference  $^{DT}CCS_{N_2}$  values can be used for  $^{TW}CCS_{N_2}$  calculations based on the following equations (Ruotolo et al., 2008). To obtain the 'real' drift time ( $t'_d$ ) from the measured total drift times ( $t_A$ ), latter have to be corrected according to **equation 1.3.5**:

$$t'_D = t_A - \frac{C\sqrt{m/z}}{1000} \quad (1.3.5)$$

Here,  $m/z$  corresponds to the  $m/z$  ratio of the calibrant ion, and  $C$  is an instrument-specific constant which can be derived from the Enhanced Duty Cycle (EDC) delay coefficient. Next, reference  $^{DT}CCS_{N_2}$  values of calibrants ( $\Omega_{ref}$ ) are corrected for their charge state ( $z$ ) and reduced mass ( $\mu$ ), according to **equation 1.3.6**:

$$\Omega' = \frac{\Omega_{ref}\sqrt{\mu}}{z} \quad (1.3.6)$$

$\Omega'$  corresponds to the corrected  $^{DT}CCS_{N_2}$  value. The reduced mass ( $\mu$ ) is defined as  $\mu = (m_i m_b)/(m_i + m_b)$ , whereby  $m_i$  is the mass of the ion and  $m_b$  is the mass of the drift gas. Through plotting of  $\ln \Omega'$  as a function of  $\ln t'_d$  constants  $A$  and  $B$ , referred to as 'fit-determined constant' and 'exponential factor', can be determined (**equation 1.3.7**):

$$\ln \Omega' = B \cdot \ln t'_d + \ln A \quad (1.3.7)$$

Lastly, the constants retrieved from the linear correlation (**equation 1.3.7**) can be used to calculate  $^{TW}CCS_{N_2}$  values ( $\Omega_{analyte}$ ) of ions of interest (**equation 1.3.8**):

$$\Omega_{analyte} = A \cdot t'_d{}^B \cdot \frac{z}{\sqrt{\mu_{analyte}}} \quad (1.3.8)$$

For TWIMS measurement, various sets of contaminants have been introduced (Bush et al., 2010; Campuzano et al., 2012; Ruotolo et al., 2008). Within their implementation, structural similarity between the applied calibrants and analytes of interest was observed to be of high importance for a reliable calibration (Bush et al., 2010).

### 1.3.3 Trapped ion-mobility spectrometry (TIMS)

A third commonly applied IM-MS instrumental set-up is trapped ion-mobility spectrometry (TIMS). In contrast to DTIMS, where an electric field is applied to allow mobility through a static gas, within TIMS the buffer gas flow and driving force induced by the applied electric field show opposite directions. This provides the possibility of ion trapping.

In 2016, Bruker Daltonics introduced the first commercially available TIMS time-of-flight MS which since then gained high popularity in various research fields. **Figure 1.3.3** shows a schematic image of the TIMS funnel and tunnel assemblies located right behind the ionization source.

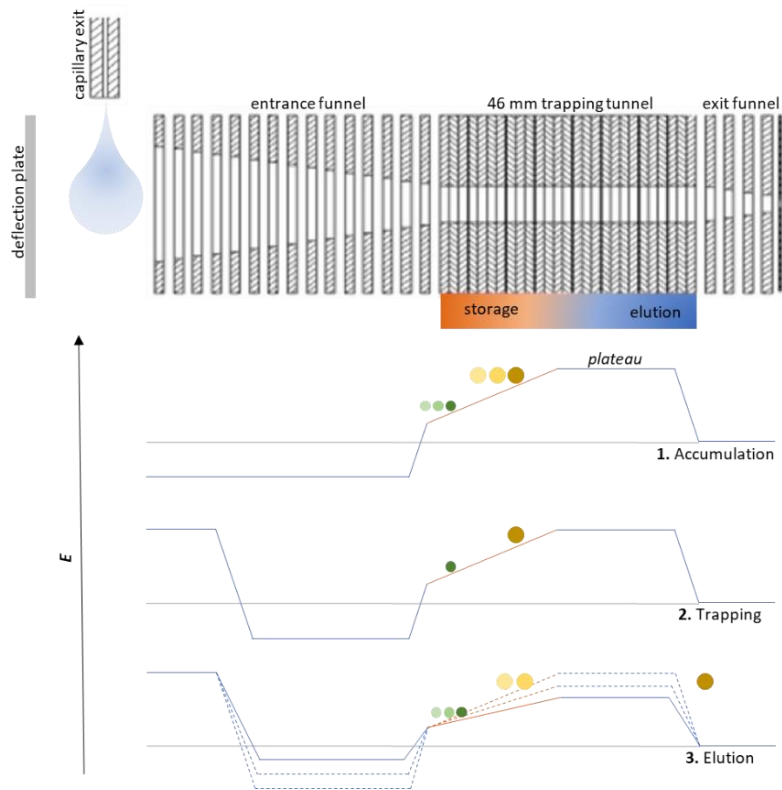


**Figure 1.3.3:** Schematic overview of a TIMS system. The electric field gradient applied during the three steps of an analysis cycle (accumulation, trapping and elution) is plotted. Yellow and green circles represent low and high mobility ions, respectively. The figure was adapted from Silveira et al. (Silveira et al., 2017).

Similar to the funnel assemblies described for TWIMS instruments, an RF voltage is applied to ensure ion confinement. The actual TIMS analysis can be divided in three steps (ion accumulation, trapping, and elution) and is driven by superimposed direct current (DC) potentials applied to the tunnel and funnel electrodes. These voltages create a so-called electric field gradient (EFG; plotted in **Figure 1.3.3**) describing the field strength as a function of location within the trapping tunnel (Silveira et al., 2017).

During the first step of the TIMS analysis cycle, a potential with opposite polarity to the ions' charge is applied to the deflection plate pulsing ions into the trapping tunnel. Ions enter the trapping funnel up to a position at which an equilibrium between the ion's drift velocity through the buffer gas and the velocity of the gas itself is reached. At this equilibrium, the net force on the ion is zero resulting in ions being trapped at the corresponding position in the trapping funnel (Michelmann et al., 2014). This corresponds to the second step of the analysis cycle (trapping). During this step, whose duration is commonly set to a few milliseconds, the ion stream coming from the ionization source is stopped by applying an attracting potential to the deflection plate.

Thirdly, ions are eluted from the trapping tunnel through decrease of the EFG profile. This happens at a rate which can be set in the acquisition method. Ions with lower mobilities elute first since their trapping position was further up the trapping funnel where the applied electric field is stronger. For ions with higher mobilities, a weaker electric field is needed resulting in their trapping closer to the tunnel's entrance and their later elution. This results in an elution order which is opposite to DTIM and TWIMS measurements (Feuerstein et al., 2022a).

It has been shown that TIMS resolving power is dependent on gas velocity (which, in turn, depends on pressure) and the ramping time, i.e., the time set for the decrease of the EFG profile. Since gas pressure and, thus, velocity is commonly kept constant during routine analyses, the EFG ramp times set within the acquisition method influence the achievable resolving power (Ridgeway et al., 2018). In routine applications resolving power of approx. 200 can be reached for single charged ions. This shows the main advantage of the TIMS technology as it can provide great resolving capacities with a relatively small drift length.

Similar to TWIMS, TIMS measurements do not allow to directly derive an ion's reduced mobility ( $K_0$ ) from which the  $^{TIMS}CCS_{N_2}$  value can be calculated. Therefore, the use of external calibrants is needed to determine the analyte's  $K_0$  and subsequent, it's  $^{TIMS}CCS_{N_2}$  value applying **equation 1.3.9** (Chai et al., 2018):

$$K_0 = a + \frac{b}{V_m} \quad (1.3.9)$$

Here,  $a$  and  $b$  are constants empirically derived from the calibration curve obtained from calibrant ions.  $V_m$  is the voltage applied at the time of the analyte's elution from the trapping tunnel. Also for TIMS, structural similarities between calibrant and analyte ions have been reported to be advantageous for reliable  $^{TIMS}CCS_{N_2}$  value calculations (Feuerstein et al., 2022b).

#### 1.3.4 Ion-mobility in environmental screening studies

In early stages of IM-MS application, the main focus was laid on the analysis of endogenous compounds (e.g., lipids, glycans, peptides or small endogenous metabolites) in the scope of different omics-based studies such as metabolomics, lipidomics, proteomics etc. (Hines et al., 2016; Lietz et al., 2014; Struwe et al., 2016). At the beginning of this PhD project, very little data were available covering the implementation of IM-MS in studies on known and emerging environmental contaminants and their metabolites. Alongside the findings presented here, other studies assessed the added value of IM-MS for CEC annotations. Several advantages have been reported such as increased quality for DIA fragmentation spectra through drift-time alignment of parent and fragmentation

ions and increased sensitivity through separation of interfering matrix components in the drift time dimension (Celma et al., 2021; Menger et al., 2022).

The main focus though was laid on the utilization of CCS values as an additional identification parameter within compound annotation facilitated by the early implementation of CCS values in the well-established scheme used for the reporting of identification confidence introduced by Schymanski et al (Schymanski et al., 2014; Celma et al., 2020). Several databases containing reference CCS<sub>N2</sub> values for xenobiotics have been reported and studies aiming at consolidating CCS databases have been conducted (Celma et al., 2020; Picache et al., 2019; Zheng et al., 2017). However, the coverage of these database remains limited, especially for newly discovered CECs or their metabolites. To fill this gap, several machine learning based prediction models have been introduced aiming to provide CCS values for which no reference standards and/or reference CCS value is available (Bijlsma et al., 2017; Celma et al., 2022; Zhang et al., 2023).

Profiting from the described advantages provided by IM-MS, this technique has facilitated the identification of CECs in environmental and human samples. For example, spectral noise removal through drift time alignment and class-specific CCS-*m/z* trendlines were used for the characterization of known and emerging per- and polyfluoroalkyl substances (PFAS) in surface water (Kirkwood-Donelson et al., 2023). Another study utilized an in-house CCS database containing both, predicted and experimental, CCS values for the characterization of organophosphate flame retardants in indoor dust (Mullin et al., 2020).

However, the number of studies implementing IM-MS for the screening of CECs remains small. Additionally, it has to be mentioned that CCS values are an empirical calculated parameter with various factors adding to its uncertainty (Causon and Hann, 2020). Therefore, many questions about the possibilities and limitation of IM-MS in environmental studies remain, several of which will be addressed in this thesis.

#### 1.4 Recent developments in semi-quantification approaches

One of the main limitations of SSA and NTS studies is that the results provided are qualitative and thus not allowing any conclusions on the concentrations of the identified CECs or their metabolites. This vastly hampers compound prioritization or the assessment of human exposure. This gap is addressed by an increasing number of applications of semi-quantification strategies which allow concentration estimations of compounds for which no reference standard is available. Thereby, three main approaches have been characterized (Malm et al., 2021). All three approaches are based on available reference standards from which a calibrant for the quantification of suspect compounds is chosen.

The first principle of calibration selection is the choice of a structurally similar compound. If the number of calibrants and suspects is reasonable and structural differences are clear, structural similarity can be assessed manually. Alternatively, online tools are available allowing to calculate structural similarity scores (based on elemental composition, number and position of functional groups, etc.) which can then be used for calibrant selection (Aalizadeh et al., 2019). The approach of choosing a structurally similar compound is often applied for transformation products (TPs) of CECs, e.g. formed through environmental degradation or metabolization (Bletsou et al., 2015). For TPs, the parent (non-transformed) compound is then chosen as calibrant.

The second approach is based on the selection of calibrants eluting closely to the suspect of interest. Thereby, the underlying assumption is that a close elution in reversed phase chromatography is accompanied by similar response factors and ionization efficiencies between calibrant and suspect (Pieke et al., 2017). It also has to be taken into account that the RT is strongly influenced by the applied chromatographic conditions. For example, small changes in the pH of the mobile phases can change the RT limiting the comparability of results within this approach.

For both approaches, the suspects' concentration ( $c_{\text{suspect}}$ ) is then calculated based on the following equation (Malm et al., 2021):

$$c_{\text{suspect}} = \frac{\text{Rel. } A_{\text{suspect}}}{R_f} \quad (1.4.1)$$

Here, Rel.  $A_{\text{suspect}}$  is the area of the suspect compound (relative to the internal standard, IS) and  $R_f$  is the response factor (i.e., slope) obtained from the calibration curve of the chosen calibrant. Latter is constructed by injection of the calibrant at varying concentrations covering a concentration range which is expected to be observed in the samples of interest. The choice of IS for semi-quantification is decided based on the same consideration as applied for the selection of calibrant compounds.

Lastly, for the structures assigned to suspect compounds, the ionization efficiency (IE) can be predicted. Therefore, machine learning based models have been developed in the past (Liigand et al., 2020; Panagopoulos Abrahamsson et al., 2020). From the predicted IE, a response factor is derived and used for concentration calculation in the same way as described above. This approach allows automated quantification for large numbers of suspects without having to invest time in the selection of calibrants. However, IE prediction models always show biases towards the compound types they were trained on. Also, these models currently only allow IE predictions for protonated, deprotonated and  $[M^+]$  ions.

Ultimately, semi-quantified concentrations can be used for further compound prioritization, exposure assessment, comparison with targeted study results of known contaminants and other purposes. It has to be noted, however, that these results have to be interpreted with care as they do not derive from validated methods. The reliability of such semi-quantification approaches still has to be assessed in a large scale allowing the estimation of quantification errors.



# Chapter 2: Objectives and Outline



Environmental pollution with industrial chemicals remains a major threat to human health. A rising release of chemicals into the environment leads to increasing human exposure to legacy contaminants, but also to CECs for which data on their occurrence and biotransformation is scarce. In recent years, SSA and NTS methods have evolved as valuable tools to identify CECs, most of which are overlooked by commonly applied targeted methods. A vast development is also observed for new instrumental techniques reflected in the introduction of ion-mobility MS providing an additional separation dimension for HRMS-based screening studies.

The two main foci of the presented PhD thesis were:

- 1) Implementation of drift-tube ion-mobility spectrometry in SSA methods for identification of environmental contaminants and their biotransformation products (**chapters 3, 4 and 6**)
- 2) The application of SSA and NTS methods for identification of CECs in indoor dust and human urine as well as evaluation of the added value of these methodologies (**chapters 4 to 6**)

SSA and NTS methods can reveal the presence of novel CECs throughout complex analytical workflows commonly applied for holistic screening. This includes the analysis of contaminants in environmental samples relevant for human exposure, human matrices and the characterization of potential biomarkers for internal exposure. In this thesis, SSA and NTS methodologies were applied within each of the described steps. SSA and NTS can benefit from the implementation of IM-MS which allows to measure ions' mobilities from which the calculated CCS values can serve as an additional identification parameter. Given the fact that IM-MS application in environmental analyses is still scarce, the compilation of reference CCS databases and the assessment of their reproducibility in instruments with different mobility measurement principles were also addressed.

In summary, this thesis aimed to answer the following research questions:

- What are the reference  $^{DT}CCS_{N_2}$  values of most relevant CEC classes? How can  $^{DT}CCS_{N_2}$  databases for environmental contaminants and their metabolites be built and compiled in a reproducible manner? (**Chapter 3**)
- Are  $CCS_{N_2}$  reproducible between different instrumental set-ups and prediction models? Which factors contribute to  $CCS_{N_2}$  biases between experimental and predicted values? (**Chapter 3**)
- How can SSA and NTS facilitate the annotation of emerging contaminant classes in indoor dust samples? Can identified CECs be prioritized based on semi-quantified concentrations and can these values be used for estimations of human exposure and potential health risks? (**Chapter 4**)

- Can IM-MS derived reference  $^{DT}CCS_{N_2}$  values improve the identification confidence for CECs in indoor dust samples? (**Chapter 4**)
- How can SSA methods be employed to identify metabolites of CECs in human urine which are overlooked in current biomonitoring campaigns? (**Chapter 5**)
- What are the *in vitro* biotransformation products of prioritized CECs? Which influence do biotransformation reactions have on  $^{DT}CCS_{N_2}$  values of the metabolites and how can this information be used for compound identification? (**Chapter 6**)

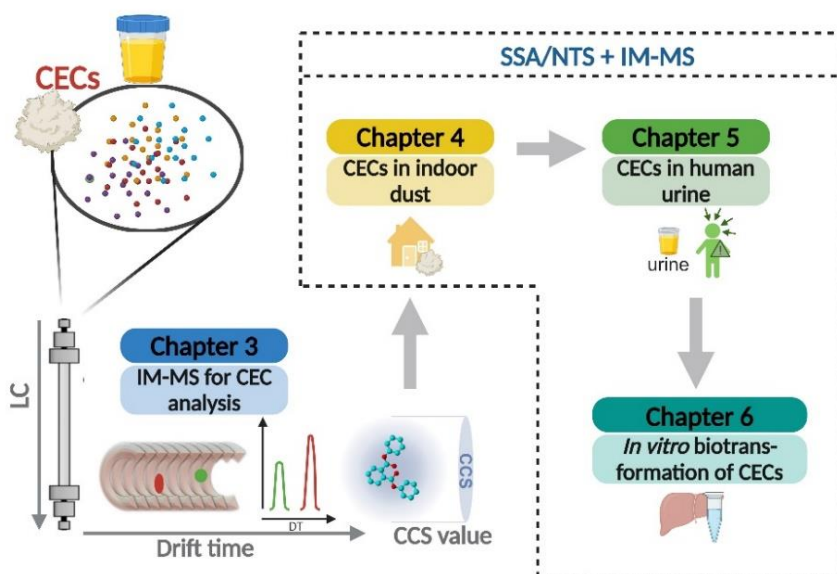


**Figure 2.1:** Schematic overview of the outline of this thesis.

**Figure 2.1** provides a schematic overview of the outline of the presented thesis.

**Chapter 3** focuses on the acquisition of reference  $^{DT}CCS_{N_2}$  values for CECs and their metabolites and the comparability of these data between different instrumental set-ups and prediction models. In **3.1**, an extensive  $^{DT}CCS_{N_2}$  database is compiled containing  $^{DT}CCS_{N_2}$  values for more than 140 contaminants and their metabolites, whereby for 113 compounds reference values are reported for the first time. In chapters **3.2** and **3.3**, DTIM derived  $^{DT}CCS_{N_2}$  values are compared with datapoints derived from TWIMS and TIMS instruments, respectively, facilitating database transfer within future applications. Additionally, experimental  $^{DT}CCS_{N_2}$  values are compared with predicted data from different prediction models aiming to assess their reliability in  $^{DT}CCS_{N_2}$  value prediction for compounds for which no reference data are available.

**Chapter 4** describes the application of SSA for the identification of CECs in indoor dust samples collected in Flanders. The investigated sample set included various indoor

environments, including private and public buildings, as well as university public spaces. In **chapter 4.1**, dust samples are screened for quaternary ammonium compounds (QACs), an emerging contaminant class which gained increased attention due to high concentrations detected in environmental and human samples during the COVID-19 pandemic. **Chapter 4.2** describes a general screening of indoor dust samples for various CEC classes. Within both approaches the detection of known contaminants was accompanied by the identification of numerous novel individual CECs and CEC classes. For both, **chapters 4.1** and **4.2**, CCS-*m/z* trendlines characterized within **chapter 3.1** were used as an additional identification parameter for assigned novel CECs which increased identification confidence. Additionally, identified CECs were semi-quantified to estimate potential human exposure through dust ingestion.

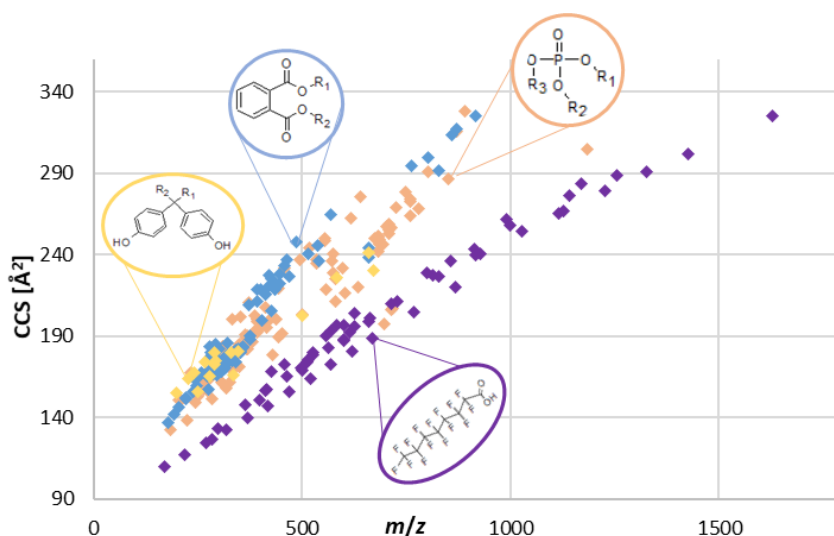
**Chapter 5** focused on the analysis of human urine samples from Flemish adolescents collected in the scope of the 4th cycle of the Flemish Environment and Health Study (FLEHS IV). Applied SSA aimed at identifying CEC metabolites which were not included in the targeted methods applied within the FLEHS IV study. This approach characterized the high variability of CEC metabolites currently not covered by applied biomonitoring campaigns.

Lastly, **chapter 6** investigated the use of SSA and NTS in combination with IM-MS for the characterization of *in vitro* biotransformation products. Therefore, three QACs with the highest semi-quantified concentrations in indoor dust samples (**chapter 4.1**) were subjected to *in vitro* biotransformation using human liver microsomes. This approach allowed the identification of more than 20 biotransformation products, four of which were described for the first time. Again, IM-MS derived <sup>DT</sup>CCS<sub>N2</sub> values obtained for assigned metabolites increased identification confidence. Eight metabolites were confirmed *in vivo* through their detection in human urine samples, thereby facilitating the selection of most suitable biomarkers for future biomonitoring studies.

The results obtained within this thesis are critically discussed in **chapter 7**, framing them in a wider research context. Remaining research gaps are identified allowing to formulate future research perspectives.



# Chapter 3: Ion-mobility for the identification of contaminants of emerging concern



This chapter is based on the following publications:

Belova, L., Caballero-Casero, N., van Nuijs, A.L.N., Covaci, A. Ion Mobility-High-Resolution Mass Spectrometry (IM-HRMS) for the Analysis of Contaminants of Emerging Concern (CECs): Database Compilation and Application to Urine Samples. *Analytical Chemistry*. **2021**. 93(16): 6428-6436.

Belova, L., Celma, A., Van Haesendonck, G., Lemière, F., Sancho, J.V., Covaci, A., van Nuijs, A.L.N., Bijlsma, L. Revealing the differences in collision cross section values of small organic molecules acquired by different instrumental designs and prediction models. *Analytica Chimica Acta*. **2022**. 1229: 340361.

Belova, L., Caballero-Casero, N., Ballesteros, A., Poma, G., van Nuijs, A.L.N., Covaci, A. Trapped and drift-tube ion-mobility spectrometry for the analysis of environmental contaminants: Comparability of collision cross section values and resolving power. *Rapid Communications in Mass Spectrometry*. **2024**. 38(21): e9901.



### 3.1 Ion Mobility-High-Resolution Mass Spectrometry (IM-HRMS) for the Analysis of Contaminants of Emerging Concern (CECs)

#### 3.1.1 Introduction

Within most IM-HRMS based suspect and non-target screening studies of known and emerging environmental contaminants, the final aim is the identification of CECs through matching experimental identifiers (MS/MS spectra and CCS values) with reference library values. This allows the potential identification of novel CECs with high identification confidence for which no reference standards are available (Celma et al., 2020; Schymanski et al., 2014). Even though in recent years high emphasis is put on the expansion of MS/MS spectral libraries, a further harmonization, the inclusion of emerging and recently discovered compounds, as well as the implementation of uniform QA/QC measures, are still required (Oberacher et al., 2020). These actions are especially needed to increase the harmonization of MS/MS spectra between different mass spectrometric instrumentation and laboratories, which at the moment poses a major challenge within non-target and suspect screening (Oberacher et al., 2020). Even if matching MS/MS spectra are available, very low concentrations of CECs in biological samples and coeluting matrix components can hamper MS/MS spectra acquisition and compromise their quality by producing low abundant fragment spectra which are difficult to interpret (Guo et al., 2020). Furthermore, generic liquid chromatography methods commonly used within suspect and non-target screening show limited separation capabilities for structurally similar, isobaric or isomeric compounds leaving potential new CECs undetected and emphasizing the need for additional separation space (Pourchet et al., 2020).

Given the limitations still present in the coverage of current MS/MS libraries and the added separation space provided by IM, the importance of the CCS values as an additional identifier is rising. However, for the use of IM-MS data for compound identification, the availability of extensive databases containing CCS values of the compounds of interest is essential. Within their compilation, the implementation of suitable QA/QC measures is crucial to monitor data quality since limitations in the inter-laboratory reproducibility of CCS values, often acquired on different instrumental setups, have been observed in the past (Hinnenkamp et al., 2018). In the scope of the compilation of a harmonized CCS database, the Unified CCS Compendium, a QA/QC guideline for the reporting of CCS databases has been introduced. It includes the acquisition of CCS values for a set of QC compounds to compare these with established references values allowing the inter-comparison of CCS deviations between different databases (Picache et al., 2019).

In the past, available CCS databases mainly focused on endogenous compounds, such as peptides (Lietz et al., 2014), glycans (Struwe et al., 2016), lipids (Hines et al., 2016) and steroids (Hernandez-Mesa et al., 2018) reflecting that omics-based studies in

different fields, such as metabolomics (Lacalle-Bergeron et al., 2020; Luo et al., 2020), lipidomics (George et al., 2020; Hines et al., 2016), plantomics (Wang et al., 2020b) or proteomics (Nys et al., 2020) have been the predominant recent application of IM-MS. Yet, interest in the use of IM-MS for the analysis of CECs is rising. Few studies on the characterization of PFAS (Ahmed et al., 2019; Dodds et al., 2020; Yukioka et al., 2020) or OPFRs (Mullin et al., 2020) using IM-MS have been reported and few databases containing CCS values of xenobiotics have been introduced in the past (Celma et al., 2020; Zheng et al., 2017). Nevertheless, a comprehensive database covering a broad range of CECs from different classes is still lacking. Therefore, this chapter introduces an innovative database containing  $^{DT}CCS_{N_2}$  values of more than 140 CECs (including PFAS, OPs, bisphenols, (alternative) plasticizers and other chemicals) and their metabolites analyzed using DTIMS in positive and negative polarity modes. The acquisition of  $^{DT}CCS_{N_2}$  values followed the QC guidelines proposed by Picache et al. which allow to monitor data reproducibility within database transfer and data submission to the Unified CCS Compendium for further use by the scientific community (Picache et al., 2019). As a proof of concept, human urine spiked with a range of CECs was analyzed to investigate the influence of matrix effects on the reproducibility of  $^{DT}CCS_{N_2}$  values.

### 3.1.2 Materials and Methods

#### 3.1.2.1 Chemicals

All organic solvents used in this study were of LC-grade. Methanol (MeOH), acetonitrile (ACN) and formic acid (FA) were purchased from Biosolve BV (Valkenswaard, the Netherlands) ( $\geq 99.9\%$ ). A PURELAB Flexsystem was used to obtain ultrapure water (18.2 M $\Omega$  cm, Milli-Q, Millipore). Ammonium acetate was purchased from Sigma-Aldrich (eluent additive for LC-MS). The sources from which reference standards of the compound classes included in the  $^{DT}CCS_{N_2}$  database were acquired are summarized in **Table SI-3.1.1**.

Except for PFAS, individual solutions of all standards were prepared in methanol at a concentration of 1 ng/ $\mu$ L. Native PFAS were available as a mixture at a concentration of 200 pg/ $\mu$ L in methanol.

#### 3.1.2.2 DTIMS conditions

Within this study, all measurements were conducted using an Agilent 6560 drift tube ion-mobility quadrupole time-of-flight mass spectrometer (DTIM-QTOF MS; Agilent Technologies, Santa Clara, USA). For both positive and negative polarity modes, the ESI source was operated using a gas temperature and sheath gas temperature of 300 °C and 350 °C, respectively. The gas and sheath gas flow were set to 9 L/min and 11 L/min,

respectively. The nebulizer pressure was 35 psig and voltages of 3500 V (capillary voltage), 1000 V (nozzle voltage) and 320 V (fragmentor voltage) were applied.

IM-MS measurements were conducted using high-purity nitrogen (99.999%) as the drift gas. The gas pressure in the drift tube was maintained at 3.95 Torr resulting in a 0.1 - 0.15 Torr pressure difference in comparison to the funnel trap to ensure drift gas purity. The drift tube settings were based on the parameters proposed by (Stow et al., 2017) and are summarized in **Table SI-3.1.2**.

### 3.1.2.3 Mobility measurements and calculation of CCS values

All standards, except perfluoroalkyl carboxylic and sulfonic acids (PFCA and PFSA, respectively) which were only available as a mixture, were directly injected as separate solutions using the Agilent 1290 Infinity II UPLC connected to the DTIM-QTOF (injection volume 2  $\mu$ L). The mobile phases consisted of water with 2 mM ammonium acetate (A) and methanol (B) for the negative ionization mode. For positive ionization, 0.1% formic acid was added to both mobile phases. These generic conditions provided sufficient ionization for all compounds reported in this database. For direct injections of standards, the mobile phase consisted of 50:50 (v/v) A/B at a flow rate of 0.2 mL/min. The liquid chromatography method applied for the analysis of PFAS mixtures is summarized in **Table SI-3.1.3**.

Single field calibration was used for all  $^{DT}CCS_{N_2}$  measurements. This approach has been validated in several studies in the past (Mordehai et al., 2015; Nichols et al., 2018) and allows the calculation of  $^{DT}CCS_{N_2}$  values based on a set of reference ions with known  $m/z$  and  $^{DT}CCS_{N_2}$  values, which have to be analyzed under the exact same conditions as the compounds of interest. The ESI low concentration tune mix (Agilent Technologies, Santa Clara, USA) was used as a reference standard and, to ensure instrument stability, was analyzed after every five standards by introducing the mix through the calibrant delivery system of the instrument.

The guidelines for QC of single field  $^{DT}CCS_{N_2}$  measurements proposed by Picache et al. provide a QA compound list whose  $^{DT}CCS_{N_2}$  values have been acquired with a DTIMS Reference System having the lowest measurement uncertainty to date (Picache et al., 2019; Stow et al., 2017). From this list, at least 5 compounds must be analyzed within every batch. Thereby, the average absolute percent error of experimental  $^{DT}CCS_{N_2}$  values must be  $\leq 0.5\%$ . The percent error for individual compounds should not exceed 1%. The calculation of the percent error is carried out using **equation 3.1.1**:

$$\text{percent error} = \text{ABS} \left( \frac{(\text{CCS}_{\text{experimental}} - \text{CCS}_{\text{QA}})}{\text{CCS}_{\text{QA}}} \cdot 100 \right) \quad (3.1.1)$$

Five QA compounds were injected within every analysis batch. The experimental  $^{DT}CCS_{N_2}$  values of QA compounds were used to ensure reproducible measurement conditions and assess the inter-day repeatability of the measurements conducted within this study.

Within every run, reference mass solution was constantly introduced into the ion source using a separate isocratic pump and an additional nebulizer assembly. Prior to any data analysis, this step allowed a recalibration of the raw data using the IM-MS Data File Reprocessing Utility (Version B.08.00, Agilent Technologies) to ensure high mass accuracy.

After recalibration, the data files were demultiplexed using the PNNL PreProcessor (version 2020.03.23), based on the assumption that true signals are present in each segment of the PRS corresponding to a pulse. These signals were searched for and extracted based on a Hadamard Transform algorithm (Prost et al., 2014). Subsequently,  $^{DT}CCS_{N_2}$  values were calculated from the demultiplexed data applying the single field calibration algorithm within the Agilent IM-MS Browser (version B.08). The average  $^{DT}CCS_{N_2}$  value obtained from five injections as well as the (relative) standard deviation were exported into the  $^{DT}CCS_{N_2}$  database.

#### 3.1.2.4 Analysis of spiked urine samples

A “dilute-and-shoot” approach was used for the preparation of (spiked) urine samples (Deventer et al., 2014). In brief, 1 mL of pooled urine consisting of urine from five healthy volunteers was spiked with a set of OPFR and AP metabolites (Table SI-3.1.7 and SI-3.1.8) at two concentration levels (i.e. 20 ng/mL and 50 ng/mL in urine). After a 1:5 dilution with methanol and centrifugation (5 min at 10000 rpm) the supernatant was frozen overnight. Finally, samples were filtered through a 0.25  $\mu$ m centrifugal filter and injected into the LC-IM-HRMS. Water was used as a blank sample and spiked following the same procedure. All samples, including blank urine and water samples, were prepared in triplicate.

All samples were analyzed applying the chromatographic conditions previously developed by (Bastiaensen et al., 2018). OPFR metabolites were analyzed in both ionization polarities, whilst AP metabolites were only analyzed in negative polarity since for all AP metabolites  $^{DT}CCS_{N_2}$  values for  $[M-H]^-$  ions were available. The ionization and IM-MS conditions remained the same as described above.

### 3.1.3 Results and Discussion

#### 3.1.3.1 Reproducibility of $^{DT}CCS_{N_2}$ values of QA compounds

To ensure high accuracy and monitor the reproducibility of  $^{DT}CCS_{N_2}$  values, the analysis of QA compounds was implemented in the database compilation workflow. The selection of QA compounds was based on the QA compound list proposed by (Picache et

al., 2019). The reference  $^{DT}CCS_{N_2}$  values of these compounds were previously determined by (Stow et al., 2017) using a reference DTIMS system which provided highly reproducible instrumental conditions.

Creatinine, L-cystine, cortisol and glucose were used as QA compounds in positive ionization mode, pyridoxal phosphate, L-histidine and uric acid in negative ionization mode and L-phenylalanine and L-tyrosine in both modes, respectively. The  $^{DT}CCS_{N_2}$  values of the compounds included in the database were acquired within four analysis batches in positive ionization mode and five analysis batches in negative ionization mode on different days, respectively. Within every analysis batch, each QA compound was analyzed four times thereby fully implementing all QA guidelines proposed by (Picache et al., 2019).

**Table 3.1.1** shows the average experimental  $^{DT}CCS_{N_2}$  values acquired throughout all sample batches. The average  $^{DT}CCS_{N_2}$  values of each individual sample batch can be found in **Table SI-3.1.4**. Considering all experimental  $^{DT}CCS_{N_2}$  values of QA compounds, the average percent error in comparison to the literature values is 0.12% in positive ionization mode and 0.08% in negative ionization mode, respectively. The mean percent error of individual compounds ranges between 0.01% and 0.82% (**Table SI-3.1.4**). The experimental  $^{DT}CCS_{N_2}$  values show that the requirements of the QA guidelines provided by Picache et al. are met in all sample batches: In both ionization polarities, the average percent error does not exceed 0.50%. Also, none of the individual compounds showed a percent error > 1% in any of the analyses (see **Table SI-3.1.4**).

Furthermore, the observed relative standard deviations (RSD) confirm the findings of Stow et al. who had observed an average interlaboratory RSD of  $0.38 \pm 0.19\%$  for three laboratories and all compounds ( $n = 65$ ) investigated in the study (Stow et al., 2017).

The acquired data shows that the DTIMS system used in this study is highly capable to acquire reproducible and accurate  $^{DT}CCS_{N_2}$  values that will be applicable in further studies and laboratories.

**Table 3.1.1:** Comparison between experimental  $^{DT}CCS_{N_2}$  values ( $CCS_{exp.}$ ) and literature  $^{DT}CCS_{N_2}$  values ( $CCS_{lit.}$ ) acquired by Stow et al., 2017 for QA compounds throughout all sample batches.

QA compound	Adduct Ion	Theoretical $m/z$	$CCS_{exp.} \pm SD$ [ $\text{\AA}^2$ ]	%RSD	$n$	$CCS_{lit.}$ [ $\text{\AA}^2$ ]	%Error
Creatinine	[M+H] <sup>+</sup>	114.0662	123.09 ± 0.26	0.21	16	122.98	0.09
Glucose	[M+Na] <sup>+</sup>	203.0526	147.03 ± 0.21	0.15	16	146.94	0.06
Cortisol	[M+H] <sup>+</sup>	363.2166	188.91 ± 0.58	0.31	16	188.34	0.30
	[M+Na] <sup>+</sup>	385.1985	212.43 ± 0.21	0.10	16	212.79	0.17
L-Phenylalanine	[M+H] <sup>+</sup>	166.0863	140.46 ± 0.25	0.18	16	140.30	0.12
	[M-H] <sup>-</sup>	164.0717	139.93 ± 0.37	0.26	20	139.94	0.01
L-Cystine	[M+H] <sup>+</sup>	241.0311	149.39 ± 0.10	0.07	16	149.48	0.06
	[M+Na] <sup>+</sup>	263.0131	151.35 ± 0.19	0.13	16	151.43	0.06
L-Tyrosine	[M+H] <sup>+</sup>	182.0812	145.68 ± 0.22	0.15	16	145.58	0.07
	[M-H] <sup>-</sup>	180.0666	144.43 ± 0.38	0.26	20	144.42	0.01
Pyridoxal-phosphate	[M-H] <sup>-</sup>	246.0173	149.42 ± 0.06	0.04	20	149.35	0.04
L-Histidine	[M-H] <sup>-</sup>	154.0622	128.55 ± 0.07	0.05	20	128.83	0.21
Uric acid	[M-H] <sup>-</sup>	167.0211	125.69 ± 0.14	0.11	20	125.55	0.11
<b>Average ESI+</b>							<b>0.12</b>
<b>Average ESI-</b>							<b>0.08</b>

### 3.1.3.2 $^{DT}CCS_{N_2}$ values of contaminants of emerging concern and their metabolites

After demonstrating that the DTIMS system used in this study can acquire  $^{DT}CCS_{N_2}$  values accurately reproducing reference  $^{DT}CCS_{N_2}$  values,  $^{DT}CCS_{N_2}$  values were calculated for more than 140 CECs from various classes based on the acquired DTIMS data. The investigated classes included bisphenols (BPs,  $n=12$ ), triazoles ( $n=5$ ), thiazoles ( $n=4$ ), OPFRs ( $n=22$ ) and their metabolites ( $n=15$ ), APs ( $n=15$ ) and their metabolites ( $n=29$ ), PFAS ( $n=33$ ) and other chemicals ( $n=13$ ). Each compound was injected five consecutive times in both ionization polarities and the average  $^{DT}CCS_{N_2}$  value of each observed ion was included in the database. Thereby, the data was searched for several ions including [M+H]<sup>+</sup>, [M+Na]<sup>+</sup>, [2M+H]<sup>+</sup>, [2M+Na]<sup>+</sup>, [M-H]<sup>-</sup>, [2M-H]<sup>-</sup> and [2M-H-CO<sub>2</sub>]<sup>-</sup> for compounds containing a carboxylic group. This approach followed the goal to provide multiple identification points for each analyte.

The final database contained 311 ions which can be found in **Table SI-3.1.5**.  $^{DT}CCS_{N_2}$  values ranged from 109.53  $\text{\AA}^2$  ([M-H-CO<sub>2</sub>]<sup>-</sup> for perfluoro-*n*-butanoic acid) and 348.02  $\text{\AA}^2$  ([2M+Na]<sup>+</sup> of butyryl-*n*-trihexyl citrate). The observed  $m/z$  ratios ranged from  $m/z$  118.0411 ([M-H]<sup>-</sup> of benzotriazole) and  $m/z$  1626.8891 ([2M-H]<sup>-</sup> of perfluoro-*n*-hexadecanoic acid). The average RSD of all  $^{DT}CCS_{N_2}$  measurements was 0.05% whereby RSDs for individual ions ranged from <0.01% to 0.73%. Comparing the experimental and theoretical  $m/z$  values led to an overall average mass error of

1.70 ppm. Except for four ions (**Table SI-3.1.5**), none of the individual measurements exceeded a mass error of 5 ppm. These results show a high repeatability of the  $^{DT}CCS_{N_2}$  measurements and are consistent with the average RSDs observed in previous studies (Tejada-Casado et al., 2018).

For 105 out of the 148 compounds, more than one ion was observed (see **Figure SI-3.1.1**). Moreover, 37 compounds were detected in both ionization polarities. These results show that the compiled database provides comprehensive information to be applied under various experimental conditions.

Several previous studies have investigated the correlation of  $m/z$  ratios and  $^{DT}CCS_{N_2}$  values of different compound classes (Hernandez-Mesa et al., 2018; Mullin et al., 2020; Tejada-Casado et al., 2018; Zheng et al., 2018). The observed trendlines can give further information on the elemental composition and shape of the molecular ions, and can serve as an additional confirmation of a correct data acquisition and interpretation workflow. For example, for several compounds investigated in this study,  $[M+H]^+$  or  $[M-H]^-$  adducts were detected which, however, showed drift times identical to the drift times of the corresponding  $[2M+H]^+$  and  $[2M-H]^-$  adducts, respectively. This indicates a post-drift tube formation of monomer ions from the corresponding dimers (Chouinard et al., 2017) which will be then assigned with an incorrect drift time and thereof  $^{DT}CCS_{N_2}$  value. Prior to erroneously submitting the resulting incorrect  $^{DT}CCS_{N_2}$  values to the database, plots of  $^{DT}CCS_{N_2}$  values as a function of the  $m/z$  ratios can reveal such effects.

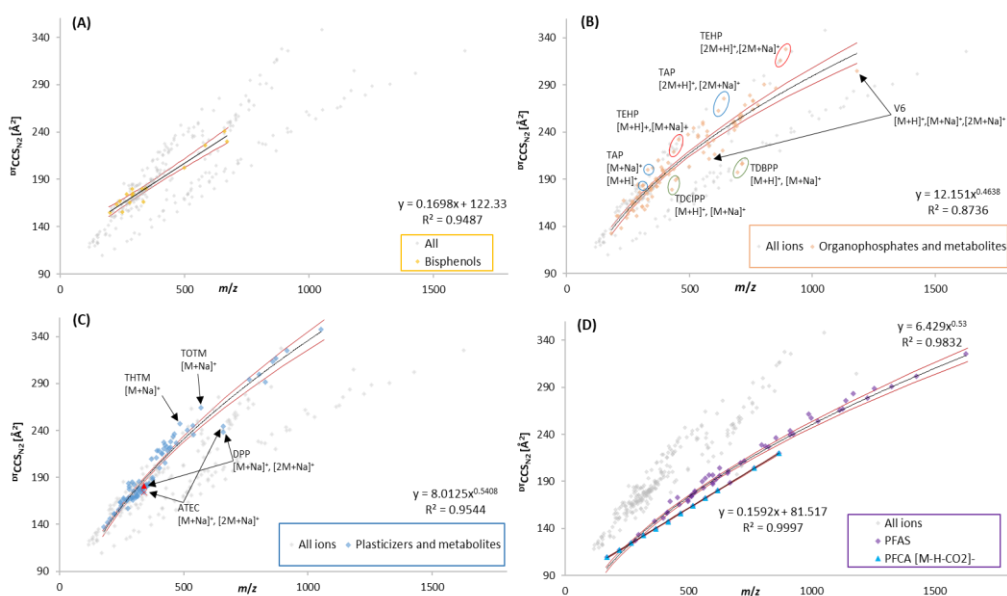


**Figure 3.1.1:** Depiction of  $^{DTCCSN_2}$  vs.  $m/z$  for the four main compound classes investigated in this chapter, including (A) bisphenols (BPs,  $n = 12$ ), (B) organophosphorus flame retardants and metabolites ( $n = 37$ ), (C) plasticizers and metabolites ( $n = 38$ ) and (D) PFAS ( $n = 32$ ). Compounds with deviations from the trendlines are indicated: tris(2-ethylhexyl) phosphate (TEHP), triamyl phosphate (TAP), tris(1,3-dichloro-2-propyl) phosphate (TDCIPP), tris(2,3-dibromopropyl) phosphate (TDBPP) and 2,2-bis(chloromethyl)-trimethylene bis(bis(2-chloroethyl)-phosphate) (V6) for OPs and tri-*n*-hexyl trimellitate (THTM), tris(2-ethylhexyl) trimellitate (TOTM), diphenyl phthalate (DPP) and acetyl triethyl citrate (ATEC) for plasticizers. For comparison, all acquired  $^{DTCCSN_2}$  values are displayed in grey. The 95% confidence intervals of the regression lines are indicated with red lines.

**Figure 3.1.1** shows the plots of  $m/z$  ratios and  $^{DTCCSN_2}$  values acquired for the four largest compound groups investigated in this study (BPs, plasticizers and their metabolites, OPFRs and their metabolites, PFAS). Generally,  $^{DTCCSN_2}$  and  $m/z$  show a non-linear correlation, especially if wide  $m/z$  ranges are considered (May et al., 2014; Tao et al., 2007). However, when evaluating narrower  $m/z$  ranges a linear dependence can provide a better fit (Dodds et al., 2020; Hernandez-Mesa et al., 2018).

Bisphenols (**Figure 3.1.1-A**) were best fitted applying a linear model resulting in a correlation coefficient ( $R^2$ ) of 0.949. This is consistent with the good linear correlation observed between  $^{DTCCSN_2}$  and  $m/z$  in previous studies (Regueiro et al., 2017). The  $^{DTCCSN_2}$  values of BPs, OPFRs and plasticizers cluster in similar areas of the  $^{DTCCSN_2}$  plot. This may be explained by a similar elemental composition of these compound classes, as well as similar molecular shapes. The relationships between  $^{DTCCSN_2}$  and  $m/z$  values for OPFRs and their metabolites (**Figure 3.1.1-B**) were best fitted applying a power regression model. Still, they showed the lowest correlation coefficient ( $R^2 = 0.874$ ), which is consistent with the highest variability in molecular shapes and elemental compositions

of this class. As an example, halogenated OPFRs, such as TDCIPP, TDBPP and V6, show clearly divergent trends and lower  $^{DT}CCS_{N_2}$  values in comparison to non-halogenated OPFRs with similar  $m/z$  ratios. Previous studies investigating  $CCS-m/z$  trends of halogen-containing compounds observed similar effects (Esquenazi et al., 2011; Mullin et al., 2020). These were assumed to derive from the higher molecular weight of halogens (F, Cl, Br) in comparison to atoms commonly present in the investigated compound classes (i.e. C, H, O, N, P and S), which results in a lower atom count and thereof in a more compact molecular shape and higher mass density (see **Table SI-3.1.5**). In contrast, TEHP and triamyl phosphate (TAP) show variations from the proposed trend towards increased  $^{DT}CCS_{N_2}$  values. Similar effects were observed for the other non-halogenated alkyl OPFRs and can be described by a separate trendline (**Figure SI-3.1.2**) showing a better fit ( $R^2 = 0.983$ ) and a higher slope in comparison to the trendline in **Figure 3.1.1-B**. These effects are assumed to be caused by the larger, less compact molecular shapes of alkyl OPFRs as observed for other unbranched alkyl compounds previously (May et al., 2014).

Additionally,  $^{DT}CCS_{N_2}$  values of common isomers of OPFRs and two isomeric metabolites are reported and compared for the first time. The  $^{DT}CCS_{N_2}$  values acquired for three isomers of tricresyl phosphate (TCP), two isomers of tributyl phosphate (TBP) and the hydroxylated metabolites 3OH-TPhP and 4OH-TPhP are given in **Table 3.1.2**. Based on the observed low RSDs (range 0.03% to 0.14%) which indicate the high repeatability of the acquired values, the reported data will allow isomer identification. This will also be demonstrated for the isomeric metabolites in urine samples (see below). In previous studies, the separation between the isomers of TCP and TBP was achieved when gas chromatography was used (Lee et al., 2020; Van den Eede et al., 2012). However, most biomonitoring methods apply liquid chromatography and lack a distinction between the different isomers of TCP, therefore reporting total TCP concentrations (Bastiaensen et al., 2019; Christia et al., 2018) or investigating only one of the TBP isomers (Ding et al., 2016). Yet, within the endocrine-disrupting effects reported for TCPs, different modes of actions have been recently reported for the three isomers, indicating a growing need for a distinction between them (Ji et al., 2020). The reported data will serve as a valuable tool to achieve this distinction in future studies.

**Table 3.1.2:**  $^{DT}CCS_{N_2}$  values of isomeric organophosphorus flame retardants and two of their metabolites.

Compound	Abbreviation	<i>m/z</i>	Ion	$^{DT}CCS_{N_2}$ ( $\pm$ SD) [ $\text{\AA}^2$ ]	RSD [%]
Triisobutyl phosphate	TiBP	267.1720	[M+H] <sup>+</sup>	165.44 (0.23)	0.14
		289.1539	[M+Na] <sup>+</sup>	183.19 (0.08)	0.04
		533.3367	[2M+H] <sup>+</sup>	234.54 (0.09)	0.04
		555.3186	[2M+Na] <sup>+</sup>	248.38 (0.12)	0.05
Tri- <i>n</i> -butyl phosphate	TnBP	267.1720	[M+H] <sup>+</sup>	166.73 (0.06)	0.03
		289.1539	[M+Na] <sup>+</sup>	184.54 (0.10)	0.05
		533.3367	[2M+H] <sup>+</sup>	236.49 (0.09)	0.04
		555.3186	[2M+Na] <sup>+</sup>	250.03 (0.12)	0.05
Tri- <i>m</i> -tolyl phosphate	TMTP	369.1250	[M+H] <sup>+</sup>	188.56 (0.10)	0.06
		391.1070	[M+Na] <sup>+</sup>	198.56 (0.12)	0.06
		759.2247	[2M+Na] <sup>+</sup>	272.51 (0.16)	0.06
Tri- <i>o</i> -tolyl phosphate	TOTP	369.1250	[M+H] <sup>+</sup>	182.39 (0.08)	0.04
		391.1070	[M+Na] <sup>+</sup>	192.43 (0.16)	0.08
		759.2247	[2M+Na] <sup>+</sup>	263.75 (0.20)	0.08
Tri- <i>p</i> -tolyl phosphate	TPTP	369.1250	[M+H] <sup>+</sup>	190.02 (0.06)	0.03
		391.1070	[M+Na] <sup>+</sup>	200.02 (0.08)	0.04
		759.2247	[2M+Na] <sup>+</sup>	273.74 (0.13)	0.05
3-Hydroxyphenyl diphenyl phosphate	3OH-TPHP*	341.0584	[M-H] <sup>-</sup>	180.46 (0.10)	0.06
4-Hydroxyphenyl diphenyl phosphate	4OH-TPHP*	341.0584	[M-H] <sup>-</sup>	181.90 (0.05)	0.03

\*compounds were also detected in ESI+, the data can be found in **Table SI-3.1.5**.

The  $^{DT}CCS_{N_2}$  values acquired for plasticizers were also well fitted using a power model (see **Figure 3.1.1-C**) showing a correlation coefficient of  $R^2 = 0.948$ . To improve the overview, several compound classes (i.e. phthalates, terephthalates, adipates and their metabolites, respectively, as well as trimellitates, citrates and a derivative of azelate) were included in the plot of plasticizers. However, only four compounds showed clear deviations from the trendline. These included tri-*n*-hexyl trimellitate (THTM) and tris(2-ethylhexyl) trimellitate (TOTM) which showed a shift towards higher  $^{DT}CCS_{N_2}$  values, as well as diphenyl phthalate (DPP) and acetyl triethyl citrate (ATEC) shifting towards lower  $^{DT}CCS_{N_2}$ . THTM and TOTM are the only two trimellitates investigated in this study. They consist of a trimellitic acid backbone which is fully esterified resulting in a large size molecule and thereof decreased ion mobility and increased  $^{DT}CCS_{N_2}$  value. In contrast, DPP was the only aryl phthalate ester investigated. Similar to the effects observed for OP aryl triesters, the compact phenyl residues lead to a smaller molecular size in comparison with the other (alkyl) phthalates. Comparable effects were observed for ATEC which in contrast to the other citrates investigated (i.e. butyryl trihexyl citrate and tributyl acetyl citrate) showed the most compact sidechains. However, this cannot fully explain the observed shifts as the described substituents of DPP and ATEC did not have a visible

influence on the  $^{DT}CCS_{N_2}$  values of the monomer ions. Molecular modeling studies are needed to further investigate possible conformational changes or intramolecular interactions between monomer and dimer ions of ATEC and DPP. To our knowledge, it is the first time that  $^{DT}CCS_{N_2}$  values for a high variety of plasticizer classes and their most important metabolites are reported. Due to the low mass range investigated here, the coelution of interfering matrix components is a common problem leading to a high number of false positives (Crowell et al., 2013; Gerona et al., 2018) and the reported data can serve as an additional identification tool to reach higher levels of certainty within compound identification.

The PFAS investigated in this study included a set of PFCAs and PFSAs as well as a selection of emerging PFAS, such as three fluorotelomer sulfonic acids (FTSA), *N*-alkylated perfluorooctanesulfonamides and others (**Table SI-3.1.5**). The high number of  $CF_2$  moieties incorporated in these compounds leads to increased molecular masses and thereof decreased  $^{DT}CCS_{N_2}$  values in relation to the  $m/z$  ratios. This results in a lower slope of the observed trendline (see **Figure 3.1.1-D**) allowing a clear distinction between PFAS and the other compound classes investigated in this study. Even though the investigated emerging PFAS varied in molecular composition (e.g. *N*-alkyl or chlorinated derivatives), no characteristic deviations from the calculated dependence were observed leading to a high correlation coefficient of  $R^2 = 0.979$ . The different trendlines observed for individual PFAS subclasses have been discussed in detail previously (Ahmed et al., 2019; Dodds et al., 2020) and therefore were not further characterized here. However, in order to show high (interlaboratory) reproducibility of the acquired data as well as the characteristic linear correlation between  $^{DT}CCS_{N_2}$  and  $m/z$  values of PFCA, **Figure 3.1.1-D** additionally shows the linear trendline of the  $[M-H-CO_2]^-$  ions of PFCAs of different chain lengths. The high linear correlation ( $R^2 = 0.999$ ) is in line with the observations from a previous study (Dodds et al., 2020). In addition,  $^{DT}CCS_{N_2}$  values of twelve emerging PFAS and the  $[M-H]^-$  ions of two PFCAs are reported for the first time.

Overall, the  $^{DT}CCS_{N_2}$  database compiled within this study yielded 113 compounds for which  $^{DT}CCS_{N_2}$  values were described for the first time, presenting a breakthrough towards a wide application of DTIMS for CECs analysis.

### 3.1.3.3 Comparison with literature $^{DT}CCS_{N_2}$ and $^{TW}CCS_{N_2}$ values

To evaluate the accuracy of the  $^{DT}CCS_{N_2}$  values included in the database and their 'between-laboratory' reproducibility, our data was compared with  $^{DT}CCS_{N_2}$  and  $^{TW}CCS_{N_2}$  values available in the literature. Several  $^{DT}CCS_{N_2}$  and  $^{TW}CCS_{N_2}$  databases were searched for reference values of the compounds described in this study (Celma et al., 2020; Dodds et al., 2020; Hines et al., 2017b; Mullin et al., 2020; Nichols et al., 2018; Picache et al.,

2019; Tejada-Casado et al., 2018; Zheng et al., 2017). Only a limited number of literature values are available, (partly) covering only two compound classes investigated in this study, i.e. PFAS (Dodds et al., 2020) and OPFRs (Mullin et al., 2020), and providing a reference  $^{DT}CCS_{N_2}$  for DEHP (Nichols et al., 2018). In the cited studies, CCS values for PFAS and DEHP were acquired using DTIMS, whereas OPFRs were analyzed using TWIMS, respectively. **Table SI-3.1.6** shows a comparison of literature IM-MS data with the  $^{DT}CCS_{N_2}$  values acquired in the presented dataset.

For  $^{TW}CCS_{N_2}$  values for OPFRs, the absolute percent errors (APE) ranged from 0.13% (for TCIPP) and 2.85% (for TPHP), with an average APE of 1.03%.  $^{DT}CCS_{N_2}$  values for PFAS showed an APE of 0.28%. Thereby, the highest absolute percent error with 1.15% was observed for the  $[M-H-CO_2]^-$  ion of perfluoro-*n*-butanoic acid (PFBA) and the lowest of 0.02% corresponded to the  $[M-H]^-$  ion of perfluoro-*n*-undecanoic acid (PFUDA). Similar values were observed for the comparison of  $^{DT}CCS_{N_2}$  values of DEHP (APE of 0.57% for  $[M+H]^+$  and 0.26% for  $[M+Na]^+$ , respectively). The low average percent error observed for the comparison of DTIMS data is in agreement with values reported in previous studies investigating inter-laboratory reproducibility  $^{DT}CCS_{N_2}$  values (Picache et al., 2019; Stow et al., 2017). The high percent error observed for PFBA most probably results from its low *m/z* (*m/z* 168.9894) which leads to an increased percent error, while the absolute deviation in  $^{DT}CCS_{N_2}$  is comparable with other PFAS compounds ( $\Delta^{DT}CCS_{N_2} = -1.27 \text{ \AA}^2$ ).

When comparing TWIMS data of OPFRs with the  $^{DT}CCS_{N_2}$  values of our database, the different calibration and acquisition principles of these techniques, which might lead to increased deviations have to be considered: Unlike DTIMS, a constantly varying electrical field used in TWIMS makes it impossible to directly derive the CCS value of a compound from its reduced mobility (*K<sub>0</sub>*). Therefore, a set of calibration standards with known CCS values derived from drift tube measurements is needed. Consequently, deviations of up to 6.2% between TWIMS and DTIMS data have been observed previously (Hinnenkamp et al., 2018). The mentioned differences between these two techniques are also assumed to cause the increased average error observed here. Hence, when applying the database introduced here for TWIMS measurements, an in-depth evaluation of the measurement deviations and, if necessary, the use of higher tolerance windows within suspect screening methods are advised.

#### 3.1.3.4 Application of the $^{DT}CCS_{N_2}$ Database to Human Urine Samples

To evaluate the applicability of the  $^{DT}CCS_{N_2}$  database to human urine samples, pooled urine samples were spiked with a set of 15 AP and 15 OPFR metabolites at two concentration levels (20 ng/mL and 50 ng/mL in urine). The selection of the latter was based on concentration levels used for method validation and observed in human urine

in previous studies on AP and OPFR metabolites (Bastiaensen et al., 2018; Been et al., 2019).

After sample preparation (which included a dilution with a factor of 5) and analysis, 13 out of 15 OPFR metabolites were detected in spiked urine samples and their average  $^{DT}CCS_{N_2}$  and mass errors were calculated (see **Table SI-3.1.7**). For all detected OPFR metabolites, the APEs of  $^{DT}CCS_{N_2}$  values observed in urine (in comparison to database values) were <1% ranging from 0.02% to 0.74% and showing an average of 0.12% for the higher and 0.15% for the lower concentration level, respectively. Bis(2-chloropropyl) hydrogen phosphate (BCIPP) and bis(2-chloroethyl) phosphate (BCEP) were not detected at either of the concentration levels. This can be explained by their lower instrumental response and recovery observed in previous studies. For BCIPP, Bastiaensen et al. reported the highest detection limit within a study validating a method for the analysis of 14 OPFR metabolites in urine. In the same study, BCEP had to be excluded from validation due to low recovery in sample preparation (Bastiaensen et al., 2018).

For AP metabolites, 11 out of their 15 metabolites were detected at both concentration levels (**Table SI-3.1.8**). Mono(2-ethyl-5-carboxypentyl) terephthalate (5-cx-MEPTP) was only detected at 50 ng/mL. The observed APEs ranged from <0.01% to 0.42% showing an average percent error of 0.09% for the lower and 0.10% for the higher concentration level, respectively. These similar results indicate that the repeatability of  $^{DT}CCS_{N_2}$  in human samples is not influenced by the concentration level. However, for a few AP metabolites an optimized chromatographic approach or adjusted sample preparation approach, including a solid-phase extraction step as used in targeted analysis of AP metabolites (Been et al., 2019), are needed to detect them at these concentration levels.

### 3.1.4 Conclusions

The described study introduced a comprehensive database of  $^{DT}CCS_{N_2}$  values of 148 CECs and their metabolites including bisphenols, alternative plasticizers, organophosphate flame retardants, perfluoroalkyl chemicals, and others.  $^{DT}CCS_{N_2}$  values of a total of 311 ions were included, whereby the  $^{DT}CCS_{N_2}$  values for 113 compounds are reported for the first time. For 105 compounds, more than one ion is reported. Moreover, the  $^{DT}CCS_{N_2}$  values of several isomeric CECs and their metabolites are reported showing the ability of DTIM to distinguish between isomers. Comprehensive quality assurance guidelines were implemented within database compilation allowing to assess data quality and facilitate database transfer. The reliability and reproducibility of the compiled database were investigated by analyzing pooled human urine spiked with 30 AP and OPFR metabolites at two concentration levels. For all investigated metabolites, the  $^{DT}CCS_{N_2}$  values measured in urine showed a percent error of <1% in comparison to database values indicating that mobility measurements are not influenced by the sample matrix. These results show that the provided database can be of great value for enhanced

identification of CECs in environmental and human matrices, which can advance future suspect screening studies on CECs.

## Supplementary Information – Chapter 3.1

**Table SI-3.1.1:** Compound classes included in the <sup>DTCCS</sup>N<sub>2</sub> database including the sources from which reference standards were purchased.

<b>Compound/compound class investigated in this chapter</b>	<b>Company</b>
Bisphenols (except for bisphenol B)	Sigma Aldrich Chemie GmbH (Steinheim, Germany)
Bisphenol B (BPB)	Tokyo Chemical Industry Co., LTD (Tokyo, Japan)
Benzotriazoles	Sigma Aldrich Chemie GmbH (Steinheim, Germany) Alfa Aesar (Kandel, Germany)
Benzothiazoles	Sigma Aldrich Chemie GmbH (Steinheim, Germany)
Organophosphates	Chiron AS (Trondheim, Norway) AccuStandard (New Heaven, CT, USA) TCI Europe (Zwijndrecht, Belgium)
Organophosphate metabolites	Sigma Aldrich Chemie GmbH (Steinheim, Germany) Provided by Dr. V. N. Belov (Max Planck Institute, Göttingen, Germany)
Plasticizers	AccuStandard (New Heaven, CT, USA)
Plasticizer metabolites	SynChem Inc. (Elk Grove Village, IL, USA) BASF (Ludwigshafen, Germany) Cambridge Isotope Laboratories (Tewksbury, MA, USA) Provided by Dr. V. N. Belov (Max Planck Institute, Göttingen, Germany)
Per- and polyfluoroalkyl substances	Wellington Laboratories (Guelph, Canada)
Other chemicals	Sigma Aldrich Chemie GmbH (Steinheim, Germany) Wellington Laboratories (Guelph, Canada)

**Table SI-3.1.2:** Drift Tube settings applied for all IM-MS measurements in positive (ESI+) and negative (ESI) ionization modes.

	ESI+	ESI-
Drift Tube Entrance [V]	1574	-1574
Drift Tube Exit [V]	224	-224
Rear Funnel Entrance [V]	217.5	-217.5
Rear Funnel Exit [V]	45	-45
Trap Funnel RF [V]	120	120
Acquisition mode	4-bit multiplexing	4-bit multiplexing
Trap Fill Time [ $\mu$ s]	3000	3000
Trap Release Time [ $\mu$ s]	250	250
Max. Drift Time [ms]	60	60
IM Transient Rate [transients/frame]	16	16
Frame Rate [frame/sec]	1	1

**Table SI-3.1.3:** Chromatographic method used for the acquisition of PFAS data. Settings for the Agilent Jet Stream ESI source, as well as the applied DTIMS conditions, were identical to the parameters used for the other compound classes.

Column:	InfinityLab Poroshell 120 EC-C18; 2.1x50 mm, 1.8 $\mu$ m particle size		
Temperature:	40 °C		
Injection volume:	2 $\mu$ L		
Flow rate:	0.25 mL/min		
Mobile phases:	(A) H <sub>2</sub> O + 2 mM ammonium acetate (B) MeOH		
Gradient	Time [min]	(A) [%]	(B) [%]
	0	70	30
	1.5	70	30
	6	30	70
	8	15	85
	10	5	95
	12	1	99
	13	1	99
	14	70	30
	20	70	30

**Table SI-3.1.4:** Detailed report of the comparison between experimental  $^{DT}CCS_{N_2}$  values ( $CCS_{exp.}$ ) and literature CCS values ( $CCS_{lit.}$ ) acquired by Stow et al. for QA compounds. For each of the sample batches acquired data is reported separately.

QA compound	Molecular formula	Batch nr.	Adduct	<i>m/z</i> values	$CCS_{exp.}$ (SD) [ $\text{\AA}^2$ ]	%RSD	$CCS_{lit.}$ [ $\text{\AA}^2$ ]	%Error
Creatinine	$C_4H_7N_3O$	1.	$[M+H]^+$	114.0662	122.99 (0.06)	0.05	122.98	0.01
		2.	$[M+H]^+$		123.49 (0.07)	0.06		0.41
		3.	$[M+H]^+$		122.81 (0.02)	0.02		0.14
		4.	$[M+H]^+$		123.05 (0.02)	0.01		0.06
Glucose	$C_6H_{12}O_6$	1.	$[M+Na]^+$	203.0526	147.17 (0.04)	0.03	146.94	0.15
		2.	$[M+Na]^+$		147.23 (0.10)	0.07		0.20
		3.	$[M+Na]^+$		146.95 (0.15)	0.10		0.01
		4.	$[M+Na]^+$		146.75 (0.07)	0.05		0.13
Cortisol	$C_{21}H_{30}O_5$	1.	$[M+H]^+$	363.2166	188.49 (0.05)	0.03	188.34	0.08
			$[M+Na]^+$	385.1985	212.16 (0.14)	0.07		212.79
		2.	$[M+H]^+$		189.88 (0.07)	0.04	0.82	
			$[M+Na]^+$		212.56 (0.11)	0.05	0.11	
		3.	$[M+H]^+$		188.57 (0.02)	0.01	0.12	
			$[M+Na]^+$		212.55 (0.16)	0.08	0.11	
		4.	$[M+H]^+$		188.71 (0.02)	0.01	0.20	
			$[M+Na]^+$		212.43 (0.12)	0.06	0.17	
L-Phenylalanine	$C_9H_{11}NO_2$	1.	$[M+H]^+$	166.0863	140.44 (0.03)	0.02	140.3	0.10
			$[M+H]^+$		140.85 (0.09)	0.07		0.39
			$[M+H]^+$		140.33 (0.03)	0.02		0.02
			$[M+H]^+$		140.23 (0.05)	0.03		0.05
		2.	$[M-H]^-$	164.0717	140.63 (0.03)	0.02	139.94	0.49
			$[M-H]^-$		139.81 (0.04)	0.03		0.09
			$[M-H]^-$		139.70 (0.11)	0.08		0.17
			$[M-H]^-$		139.82 (0.02)	0.01		0.09
			$[M-H]^-$		139.71 (0.10)	0.07		0.17
			$[M-H]^-$					
L-Cystine	$C_6H_{12}N_2O_4S_2$	1.	$[M+H]^+$	241.0311	149.50 (0.02)	0.01	149.48	0.01
			$[M+Na]^+$	263.0131	151.36 (0.11)	0.07		151.43
		2.	$[M+H]^+$		149.26 (0.03)	0.02	0.15	
			$[M+Na]^+$		151.60 (0.03)	0.02	0.22	
		3.	$[M+H]^+$		149.45 (0.05)	0.04	0.02	
			$[M+Na]^+$		151.32 (0.13)	0.08	0.04	
		4.	$[M+H]^+$		149.36 (0.05)	0.03	0.08	
			$[M+Na]^+$		151.12 (0.06)	0.03	0.09	
L-Tyrosine	$C_9H_{11}NO_3$	1.	$[M+H]^+$	182.0812	145.68 (0.04)	0.03	145.58	0.07
			$[M+H]^+$		146.03 (0.08)	0.05		0.31
			$[M+H]^+$		145.50 (0.02)	0.01		0.05
			$[M+H]^+$		145.53 (0.02)	0.01		0.04
		2.	$[M-H]^-$	180.0666	145.16 (0.03)	0.02	144.42	0.51
			$[M-H]^-$		144.31 (0.07)	0.05		0.08
			$[M-H]^-$		144.20 (0.09)	0.06		0.16
			$[M-H]^-$		144.29 (0.04)	0.02		0.09
			$[M-H]^-$		144.20 (0.02)	0.01		0.15
			$[M-H]^-$					
Pyridoxalphosphate	$C_8H_{10}NO_6P$	1.	$[M-H]^-$	246.0173	149.37 (0.04)	0.03	149.35	0.02
		2.	$[M-H]^-$		149.42 (0.05)	0.03		0.05
		3.	$[M-H]^-$		149.36 (0.04)	0.02		0.01
		4.	$[M-H]^-$		149.50 (0.05)	0.03		0.10

		5.	[M-H] <sup>-</sup>		149.43 (0.04)	0.03		0.05
L-Histidine	C <sub>6</sub> H <sub>9</sub> N <sub>3</sub> O <sub>2</sub>	1.	[M-H] <sup>-</sup>	154.0622	128.60 (0.04)	0.03	128.83	0.18
		2.	[M-H] <sup>-</sup>		128.53 (0.03)	0.03		0.23
		3.	[M-H] <sup>-</sup>		128.50 (0.10)	0.08		0.26
		4.	[M-H] <sup>-</sup>		128.58 (0.03)	0.02		0.19
		5.	[M-H] <sup>-</sup>		128.56 (0.08)	0.06		0.21
Uric acid	C <sub>5</sub> H <sub>4</sub> N <sub>4</sub> O <sub>3</sub>	1.	[M-H] <sup>-</sup>	167.0211	125.82 (0.27)	0.21	125.55	0.21
		2.	[M-H] <sup>-</sup>		125.61 (0.07)	0.05		0.05
		3.	[M-H] <sup>-</sup>		125.66 (0.05)	0.04		0.09
		4.	[M-H] <sup>-</sup>		125.63 (0.04)	0.03		0.06
		5.	[M-H] <sup>-</sup>		125.72 (0.09)	0.07		0.13

**Table SI-3.1.5:** Summary of the <sup>DT</sup>CCS<sub>N2</sub> database compiled within this chapter. The compound name, abbreviation, molecular formula, mass-to-charge ratio (*m/z*), adduct species, average observed <sup>DT</sup>CCS<sub>N2</sub> values, standard deviation (SD), relative standard deviation (RSD) and average observed mass error (AME) are reported for all detected ions.

Compound name	Abbreviation	Molecular formula	<i>m/z</i>	Ion	<sup>DT</sup> CCS <sub>N2</sub> (±SD) [Å <sup>2</sup> ]	RSD [%]	AME [ppm]
Bisphenol A	BPA	C <sub>15</sub> H <sub>16</sub> O <sub>2</sub>	227.1078	[M-H] <sup>-</sup>	163.50 (0.01)	0.01	2.53
Bisphenol AF*	BPAF	C <sub>15</sub> H <sub>10</sub> F <sub>6</sub> O <sub>2</sub>	335.0512	[M-H] <sup>-</sup>	166.06 (0.03)	0.02	3.47
			671.1097	[2M-H] <sup>-</sup>	230.13 (0.09)	0.04	0.17
Bisphenol AP*	BPAP	C <sub>20</sub> H <sub>18</sub> O <sub>2</sub>	289.1234	[M-H] <sup>-</sup>	179.95 (0.04)	0.02	1.99
Bisphenol B*	BPB	C <sub>16</sub> H <sub>18</sub> O <sub>2</sub>	241.1234	[M-H] <sup>-</sup>	167.17 (0.05)	0.03	0.56
Bisphenol C*	BPC	C <sub>14</sub> H <sub>10</sub> Cl <sub>2</sub> O <sub>2</sub>	278.9985	[M-H] <sup>-</sup>	165.30 (0.04)	0.02	2.06
Bisphenol P*	BPP	C <sub>24</sub> H <sub>26</sub> O <sub>2</sub>	345.1860	[M-H] <sup>-</sup>	180.64 (0.03)	0.01	1.26
Bisphenol Z*	BPZ	C <sub>18</sub> H <sub>20</sub> O <sub>2</sub>	267.1390	[M-H] <sup>-</sup>	174.21 (0.03)	0.02	0.65
Bisphenol F*	BPF	C <sub>13</sub> H <sub>12</sub> O <sub>2</sub>	199.0764	[M-H] <sup>-</sup>	155.05 (0.05)	0.03	0.28
Bisphenol S*	BPS	C <sub>12</sub> H <sub>10</sub> O <sub>4</sub> S	249.0227	[M-H] <sup>-</sup>	155.49 (0.03)	0.02	1.38
			499.0527	[2M-H] <sup>-</sup>	202.35 (0.05)	0.03	1.33
Benzotriazole*	BTR	C <sub>6</sub> H <sub>5</sub> N <sub>3</sub>	120.0556 <sup>1</sup>	[M+H] <sup>+</sup>	122.42 (0.03)	0.03	8.14
			118.0411	[M-H] <sup>-</sup>	118.30 (0.02)	0.02	1.60
4-Methylbenzotriazole*	4-Me-BTR	C <sub>7</sub> H <sub>7</sub> N <sub>3</sub>	134.0713 <sup>1</sup>	[M+H] <sup>+</sup>	126.79 (0.04)	0.03	5.79
			132.0567	[M-H] <sup>-</sup>	123.70 (0.07)	0.05	3.12
5-methyl-1H-benzotriazole*	5-Me-BTR	C <sub>7</sub> H <sub>7</sub> N <sub>3</sub>	132.0567	[M-H] <sup>-</sup>	124.64 (0.02)	0.01	1.18
5,6-Dimethylbenzotriazole*	5,6-diMe-BTR	C <sub>8</sub> H <sub>9</sub> N <sub>3</sub>	148.0869	[M+H] <sup>+</sup>	131.25 (0.02)	0.01	0.52
			146.0724	[M-H] <sup>-</sup>	130.84 (0.11)	0.08	2.04
5-Chlorobenzotriazole*	5Cl-BTR	C <sub>6</sub> H <sub>4</sub> ClN <sub>3</sub>	154.0167	[M+H] <sup>+</sup>	131.88 (0.03)	0.03	1.63
			152.0021	[M-H] <sup>-</sup>	122.49 (0.04)	0.03	1.45
Benzothiazole*	BTH	C <sub>7</sub> H <sub>5</sub> NS	158.0035	[M+Na] <sup>+</sup>	134.70 (0.36)	0.27	3.05
2-Hydroxybenzothiazole*	2OH-BTH	C <sub>7</sub> H <sub>5</sub> NOS	150.0019	[M-H] <sup>-</sup>	123.75 (0.02)	0.02	1.81
2-Aminobenzothiazole*	2NH <sub>2</sub> -BTH	C <sub>7</sub> H <sub>6</sub> N <sub>2</sub> S	151.0324	[M+H] <sup>+</sup>	128.60 (0.03)	0.02	3.01
			149.0179	[M-H] <sup>-</sup>	122.71 (0.07)	0.05	1.70
2-(Methylthio)benzothiazole*	2-MeSBTH	C <sub>8</sub> H <sub>7</sub> NS <sub>2</sub>	182.0093	[M+H] <sup>+</sup>	131.32 (0.06)	0.05	3.54
Tris(2-butoxyethyl)phosphate	TBOEP	C <sub>18</sub> H <sub>39</sub> O <sub>7</sub> P	399.2506	[M+H] <sup>+</sup>	194.44 (0.18)	0.09	1.33
			421.2326	[M+Na] <sup>+</sup>	199.36 (0.11)	0.06	0.50
Tri-iso-butyl phosphate*	TiBP	C <sub>12</sub> H <sub>27</sub> O <sub>4</sub> P	267.1720	[M+H] <sup>+</sup>	165.44 (0.23)	0.14	0.61
			289.1539	[M+Na] <sup>+</sup>	183.19 (0.08)	0.04	3.65
			533.3367	[2M+H] <sup>+</sup>	234.54 (0.09)	0.04	0.44

			555.3186	[2M+Na] <sup>+</sup>	248.38 (0.12)	0.05	0.85
Tri-n-butyl phosphate*	TnBP	C <sub>12</sub> H <sub>27</sub> O <sub>4</sub> P	267.1720	[M+H] <sup>+</sup>	166.73 (0.06)	0.03	2.44
			289.1539	[M+Na] <sup>+</sup>	184.54 (0.10)	0.05	3.72
			533.3367	[2M+H] <sup>+</sup>	236.49 (0.09)	0.04	0.88
			555.3186	[2M+Na] <sup>+</sup>	250.03 (0.12)	0.05	0.74
Triphenyl phosphate	TPhP	C <sub>18</sub> H <sub>15</sub> O <sub>4</sub> P	327.0781	[M+H] <sup>+</sup>	174.74 (0.03)	0.01	2.47
			349.0600	[M+Na] <sup>+</sup>	184.96 (0.06)	0.03	1.97
			675.1308	[2M+Na] <sup>+</sup>	249.80 (0.06)	0.03	1.94
Tris(2-ethylhexyl) phosphate*	TEHP	C <sub>24</sub> H <sub>51</sub> O <sub>4</sub> P	435.3598	[M+H] <sup>+</sup>	219.15 (0.13)	0.06	1.30
			457.3417	[M+Na] <sup>+</sup>	231.80 (0.12)	0.05	1.56
			869.7123	[2M+H] <sup>+</sup>	315.91 (0.47)	0.15	2.10
			891.6942	[2M+Na] <sup>+</sup>	327.65 (0.19)	0.06	0.41
Triethyl phosphate*	TEP	C <sub>6</sub> H <sub>15</sub> O <sub>4</sub> P	183.0781	[M+H] <sup>+</sup>	132.63 (0.06)	0.05	1.55
			205.0600	[M+Na] <sup>+</sup>	150.93 (0.11)	0.07	0.22
			387.1308	[2M+Na] <sup>+</sup>	192.65 (0.22)	0.11	1.16
Tri-m-tolyl phosphate*	TMTP	C <sub>21</sub> H <sub>21</sub> O <sub>4</sub> P	369.1250	[M+H] <sup>+</sup>	188.56 (0.10)	0.06	0.93
			391.1070	[M+Na] <sup>+</sup>	198.56 (0.12)	0.06	1.08
			759.2247	[2M+Na] <sup>+</sup>	272.51 (0.16)	0.06	0.29
Tri-o-tolyl phosphate*	TOTP	C <sub>21</sub> H <sub>21</sub> O <sub>4</sub> P	369.1250	[M+H] <sup>+</sup>	182.39 (0.08)	0.04	1.31
			391.1070	[M+Na] <sup>+</sup>	192.43 (0.16)	0.08	0.73
			759.2247	[2M+Na] <sup>+</sup>	263.75 (0.20)	0.08	0.82
Tri-p-tolyl phosphate	TPTP	C <sub>21</sub> H <sub>21</sub> O <sub>4</sub> P	369.1250	[M+H] <sup>+</sup>	190.02 (0.06)	0.03	1.41
			391.1070	[M+Na] <sup>+</sup>	200.02 (0.08)	0.04	1.65
			759.2247	[2M+Na] <sup>+</sup>	273.74 (0.13)	0.05	0.51
Triamyl phosphate*	TAP	C <sub>15</sub> H <sub>33</sub> O <sub>4</sub> P	309.2189	[M+H] <sup>+</sup>	183.21 (0.05)	0.03	1.50
			331.2009	[M+Na] <sup>+</sup>	199.96 (0.09)	0.05	2.13
			617.4306	[2M+H] <sup>+</sup>	262.51 (0.35)	0.13	0.58
			639.4125	[2M+Na] <sup>+</sup>	275.71 (0.08)	0.03	0.68
Tris(2-chloroethyl) phosphate	TCEP	C <sub>6</sub> H <sub>12</sub> Cl <sub>3</sub> O <sub>4</sub> P	284.9612	[M+H] <sup>+</sup>	151.31 (0.05)	0.03	1.46
			306.9431	[M+Na] <sup>+</sup>	161.39 (0.08)	0.05	2.14
Tris(2-chloroiso-propyl) phosphate	TCIPP	C <sub>9</sub> H <sub>18</sub> Cl <sub>3</sub> O <sub>4</sub> P	327.0081	[M+H] <sup>+</sup>	161.66 (0.10)	0.06	0.87
			348.9900	[M+Na] <sup>+</sup>	171.33 (0.05)	0.03	1.28
Tris(2,3-dibromo-propyl) phosphate*	TDBPP	C <sub>9</sub> H <sub>15</sub> Br <sub>6</sub> O <sub>4</sub> P	692.5881	[M+H] <sup>+</sup>	197.25 (0.20)	0.10	1.06
			714.5700	[M+Na] <sup>+</sup>	206.37 (0.78)	0.38	1.82
			716.5680	[M+Na] <sup>+</sup>	206.90 (0.07)	0.03	0.75
Tris(1,3-dichloro-2-propyl) phosphate	TDCIPP	C <sub>9</sub> H <sub>15</sub> Cl <sub>6</sub> O <sub>4</sub> P	428.8912	[M+H] <sup>+</sup>	178.56 (0.02)	0.01	2.97
			450.8731	[M+Na] <sup>+</sup>	191.22 (0.06)	0.03	3.26
Tris(tert-butyl-phenyl) phosphate*	TTBPP	C <sub>30</sub> H <sub>39</sub> O <sub>4</sub> P	495.2659	[M+H] <sup>+</sup>	237.14 (0.17)	0.07	1.24
			517.2478	[M+Na] <sup>+</sup>	243.95 (0.10)	0.04	2.18
Resorcinol bis (diphenyl phosphate)*	RDP	C <sub>30</sub> H <sub>24</sub> O <sub>8</sub> P <sub>2</sub>	575.1019	[M+H] <sup>+</sup>	228.77 (0.06)	0.02	1.22
			597.0839	[M+Na] <sup>+</sup>	231.58 (0.03)	0.01	1.27
Bisphenol A bis (diphenyl phosphate)*	BDP	C <sub>39</sub> H <sub>34</sub> O <sub>8</sub> P <sub>2</sub>	693.1802	[M+H] <sup>+</sup>	246.33 (0.16)	0.06	0.41
			715.1621	[M+Na] <sup>+</sup>	256.61 (0.12)	0.05	0.29
Isodecyl diphenyl phosphate	iDPP	C <sub>22</sub> H <sub>31</sub> O <sub>4</sub> P	391.2033	[M+H] <sup>+</sup>	200.20 (0.09)	0.05	0.95
			413.1852	[M+Na] <sup>+</sup>	207.30 (0.03)	0.01	1.73
			803.3812	[2M+Na] <sup>+</sup>	290.51 (0.05)	0.02	0.91
2-Ethylhexyl diphenyl phosphate	EHDPHP	C <sub>20</sub> H <sub>27</sub> O <sub>4</sub> P	385.1539	[M+Na] <sup>+</sup>	202.70 (0.05)	0.02	3.75
			725.3367	[2M+H] <sup>+</sup>	269.03 (0.17)	0.06	4.48
			747.3186	[2M+Na] <sup>+</sup>	278.58 (0.08)	0.03	3.28
Antiblaze V6	V6	C <sub>13</sub> H <sub>24</sub> Cl <sub>6</sub> O <sub>8</sub> P <sub>2</sub>	580,9150	[M+H] <sup>+</sup>	211.37 (0.04)	0.02	2.73

			602,8970 1182,8047	[M+Na] <sup>+</sup> [2M+Na] <sup>+</sup>	216.57 (0.08) 304.65 (0.16)	0.04 0.05	2.93 2.32
Bis(3,5,5-trimethylhexyl) phosphate*		C <sub>18</sub> H <sub>39</sub> O <sub>4</sub> P	351.2659 373.2478	[M+H] <sup>+</sup> [M+Na] <sup>+</sup>	202.09 (0.05) 210.41 (0.09)	0.03 0.04	5.14 3.66
Diphenylcresyl phosphate	CDPHP	C <sub>19</sub> H <sub>17</sub> O <sub>4</sub> P	341.0937 363.0757 681.1802 703.1621	[M+H] <sup>+</sup> [M+Na] <sup>+</sup> [2M+H] <sup>+</sup> [2M+Na] <sup>+</sup>	180.48 (0.02) 190.53 (0.05) 250.72 (0.42) 257.29 (0.04)	0.01 0.03 0.17 0.02	3.45 3.35 4.16 2.66
Di-o-cresyl phosphate*	DOCP	C <sub>14</sub> H <sub>15</sub> O <sub>4</sub> P	279.0781 301.0600 557.1489 579.1308	[M+H] <sup>+</sup> [M+Na] <sup>+</sup> [2M+H] <sup>+</sup> [2M+Na] <sup>+</sup>	163.59 (0.07) 169.40 (0.07) 218.36 (0.35) 225.36 (0.15)	0.04 0.04 0.16 0.07	2.94 2.19 3.55 2.28
Di-n-butyl phosphate*	DnBP	C <sub>8</sub> H <sub>19</sub> PO <sub>4</sub>	233.0913 209.0948	[M+Na] <sup>+</sup> [M-H] <sup>-</sup>	167.54 (0.04) 150.89 (0.02)	0.02 0.01	1.40 3.92
Diphenyl hydrogen phosphate*	DPhP	C <sub>12</sub> H <sub>11</sub> O <sub>4</sub> P	251.0468 273.0287 249.0322	[M+H] <sup>+</sup> [M+Na] <sup>+</sup> [M-H] <sup>-</sup>	157.41 (0.07) 164.38 (0.15) 152.82 (0.02)	0.04 0.09 0.01	2.37 0.87 1.22
Bis(2-chloropropyl) hydrogen phosphate*	BCIPP	C <sub>6</sub> H <sub>13</sub> Cl <sub>2</sub> O <sub>4</sub> P	272.9821 498.9784	[M+Na] <sup>+</sup> [2M-H] <sup>-</sup>	156.45 (0.02) 203.44 (0.11)	0.01 0.05	0.77 1.41
Bis(2-chloroethyl) phosphate*	BCEP	C <sub>4</sub> H <sub>9</sub> Cl <sub>2</sub> O <sub>4</sub> P	222.9688 244.9508 442.9158	[M+H] <sup>+</sup> [M+Na] <sup>+</sup> [2M-H] <sup>-</sup>	138.08 (0.08) 149.04 (0.09) 189.12 (0.14)	0.06 0.06 0.07	0.78 2.09 0.68
Bis(1,3-dichloro-2-propyl) phosphate*	BDCIPP	C <sub>6</sub> H <sub>11</sub> Cl <sub>4</sub> O <sub>4</sub> P	318.9222 316.9076 634.8225	[M+H] <sup>+</sup> [M-H] <sup>-</sup> [2M-H] <sup>-</sup>	178.72 (0.04) 157.71 (0.01) 220.13 (0.10)	0.02 0.01 0.05	1.56 0.90 1.13
Bis(1-chloro-2-propyl)-1-hydroxy-2-propyl-phosphate*	BCIPHIPP	C <sub>9</sub> H <sub>19</sub> Cl <sub>2</sub> O <sub>5</sub> P	309.0420 331.0239	[M+H] <sup>+</sup> [M+Na] <sup>+</sup>	160.61 (0.03) 168.89 (0.03)	0.02 0.02	0.49 3.84
2-ethylhexyl phenyl phosphate*	EHPHP	C <sub>14</sub> H <sub>23</sub> O <sub>4</sub> P	309.1226 573.2741 285.1261 571.2595	[M+Na] <sup>+</sup> [2M+H] <sup>+</sup> [M-H] <sup>-</sup> [2M-H] <sup>-</sup>	183.41 (0.28) 240.74 (0.09) 170.46 (0.03) 236.38 (0.03)	0.15 0.04 0.02 0.01	0.91 2.52 3.21 1.41
Bis(2-butoxyethyl) phosphate*	BBOEP	C <sub>12</sub> H <sub>27</sub> O <sub>6</sub> P	299.1618 321.1437 297.1472	[M+H] <sup>+</sup> [M+Na] <sup>+</sup> [M-H] <sup>-</sup>	171.77 (0.04) 175.66 (0.04) 175.92 (0.02)	0.02 0.02 0.01	1.15 1.81 1.79
5-Hydroxy-2-ethylhexyl diphenyl phosphate*	5OH-EHDPHP	C <sub>20</sub> H <sub>27</sub> O <sub>5</sub> P	379.1669 401.1488 779.3084	[M+H] <sup>+</sup> [M+Na] <sup>+</sup> [2M+Na] <sup>+</sup>	186.66 (0.06) 194.97 (0.06) 268.40 (0.08)	0.03 0.03 0.03	3.44 3.69 2.62
3-Hydroxyphenyl diphenyl phosphate*	3OH-TPHP	C <sub>18</sub> H <sub>15</sub> O <sub>5</sub> P	343.0730 365.0549 685.1387 707.1206 341.0584 683.1241	[M+H] <sup>+</sup> [M+Na] <sup>+</sup> [2M+H] <sup>+</sup> [2M+Na] <sup>+</sup> [M-H] <sup>-</sup> [2M-H] <sup>-</sup>	180.35 (0.01) 189.06 (0.07) 246.58 (0.21) 252.85 (0.09) 180.46 (0.10) 241.97 (0.05)	0.01 0.04 0.09 0.04 0.06 0.02	4.09 4.11 4.73 3.14 2.87 1.55
Bis(2-butoxyethyl) 2-hydroxyethyl phosphate*	BBOEHEP	C <sub>18</sub> H <sub>15</sub> O <sub>5</sub> P	343.1880 365.1700 707.3507	[M+H] <sup>+</sup> [M+Na] <sup>+</sup> [2M+Na] <sup>+</sup>	179.27 (0.01) 182.29 (0.03) 259.02 (0.08)	0.01 0.02 0.03	4.36 1.16 1.59
Bis(2-butoxyethyl)	3OH-TBOEP	C <sub>18</sub> H <sub>39</sub> O <sub>8</sub> P	415.2456 437.2275 851.4658	[M+H] <sup>+</sup> [M+Na] <sup>+</sup> [2M+Na] <sup>+</sup>	195.45 (0.04) 200.38 (0.05) 286.24 (0.10)	0.02 0.02 0.03	3.19 3.24 2.61

3'-hydroxy-2-butoxyethyl phosphate*							
4-Hydroxyphenyl diphenyl phosphate*	4OH-TPHP	C <sub>18</sub> H <sub>15</sub> O <sub>5</sub> P	341.0584	[M-H] <sup>-</sup>	181.90 (0.05)	0.03	2.97
			683.1241	[2M-H] <sup>-</sup>	251.30 (0.24)	0.09	3.48
			343.0730	[M+H] <sup>+</sup>	178.12 (0.01)	0.01	3.77
			365.0549	[M+Na] <sup>+</sup>	188.50 (0.04)	0.02	0.26
			685.1387	[2M+H] <sup>+</sup>	248.96 (0.08)	0.03	0.59
			707.1206	[2M+Na] <sup>+</sup>	254.81 (0.03)	0.01	0.20
4-Hydroxyphenyl phenyl phosphate*	4OH-PhP	C <sub>12</sub> H <sub>11</sub> O <sub>5</sub> P	267.0417	[M+H] <sup>+</sup>	162.44 (0.02)	0.01	1.51
			289.0236	[M+Na] <sup>+</sup>	169.02 (0.11)	0.07	0.63
			265.0271	[M-H] <sup>-</sup>	157.56 (0.07)	0.04	0.78
Di(2-ethylhexyl) phthalate	DEHP	C <sub>24</sub> H <sub>38</sub> O <sub>4</sub>	391.2843	[M+H] <sup>+</sup>	211.00 (0.08)	0.04	0.88
			413.2662	[M+Na] <sup>+</sup>	215.33 (0.05)	0.02	1.76
			803.5432	[2M+Na] <sup>+</sup>	299.81 (0.12)	0.04	0.60
Diisononyl phthalate*	DiNP	C <sub>26</sub> H <sub>42</sub> O <sub>4</sub>	419.3156	[M+H] <sup>+</sup>	220.60 (0.10)	0.05	1.11
			441.2975	[M+Na] <sup>+</sup>	220.94 (0.09)	0.04	1.20
			859.6058	[2M+Na] <sup>+</sup>	313.44 (0.39)	0.12	0.90
Diisodecyl phthalate*	DiDP	C <sub>28</sub> H <sub>46</sub> O <sub>4</sub>	447.3469	[M+H] <sup>+</sup>	227.85 (0.11)	0.05	1.91
			469.3288	[M+Na] <sup>+</sup>	226.42 (0.11)	0.05	1.64
			915.6684	[2M+Na] <sup>+</sup>	325.43 (0.35)	0.11	0.57
Diphenyl phthalate*	DPP	C <sub>20</sub> H <sub>14</sub> O <sub>4</sub>	341.0784	[M+H] <sup>+</sup>	181.27 (0.04)	0.02	1.72
			659.1676	[M+Na] <sup>+</sup>	238.24 (0.05)	0.02	0.92
Diisononyl hexahydrophthalate <sup>2,*</sup>	DINCH	C <sub>26</sub> H <sub>48</sub> O <sub>4</sub>	425.3625	[M+H] <sup>+</sup>	224.82 (0.37)	0.17	0.85
			447.3445	[M+Na] <sup>+</sup>	222.03 (0.12)	0.05	1.16
			871.6997	[2M+Na] <sup>+</sup>	316.74 (0.38)	0.12	0.81
Mono(2-ethylhexyl) phthalate*	MEHP	C <sub>16</sub> H <sub>22</sub> O <sub>4</sub>	301.1410	[M+Na] <sup>+</sup>	182.27 (0.04)	0.02	2.20
			277.1445	[M-H] <sup>-</sup>	168.91 (0.06)	0.03	1.21
Monoisobutyl phthalate*	MiBP	C <sub>12</sub> H <sub>14</sub> O <sub>4</sub>	245.0784	[M+Na] <sup>+</sup>	163.43 (0.06)	0.03	1.69
			221.0819	[M-H] <sup>-</sup>	151.83 (0.05)	0.03	1.18
Mono-n-butyl phthalate*	MnBP	C <sub>12</sub> H <sub>14</sub> O <sub>4</sub>	245.0784	[M+Na] <sup>+</sup>	163.94 (0.03)	0.02	1.77
			221.0819	[M-H] <sup>-</sup>	151.11 (0.04)	0.03	0.76
Mono(2-cyclohexyl) phthalate*	MCHP	C <sub>24</sub> H <sub>16</sub> O <sub>4</sub>	247.0976	[M-H] <sup>-</sup>	159.72 (0.07)	0.04	1.25
Monoethyl phthalate*	MEP	C <sub>10</sub> H <sub>10</sub> O <sub>4</sub>	193.0506	[M-H] <sup>-</sup>	141.67 (0.04)	0.03	0.52
Monomethyl phthalate*	MMP	C <sub>9</sub> H <sub>8</sub> O <sub>4</sub>	203.0315	[M+Na] <sup>+</sup>	146.13 (0.12)	0.09	2.87
			179.0350	[M-H] <sup>-</sup>	137.01 (0.06)	0.04	0.42
6-Hydroxy monopropylheptyl phthalate*	6OH-MPHP	C <sub>18</sub> H <sub>26</sub> O <sub>5</sub>	345.1672	[M+Na] <sup>+</sup>	181.90 (0.07)	0.04	1.33
			321.1707	[M-H] <sup>-</sup>	178.62 (0.03)	0.02	0.91
Mono-2-(propyl-6-oxoheptyl) phthalate*	6-oxo-MPHP	C <sub>18</sub> H <sub>24</sub> O <sub>5</sub>	343.1516	[M+Na] <sup>+</sup>	180.20 (0.07)	0.04	0.26
			319.1551	[M-H] <sup>-</sup>	177.70 (0.05)	0.03	2.74
Mono(2-propyl-6-carboxyhexyl) phthalate*	6-cx-MPHxP	C <sub>18</sub> H <sub>24</sub> O <sub>6</sub>	359.1465	[M+Na] <sup>+</sup>	183.65 (0.06)	0.03	0.38
			335.1500	[M-H] <sup>-</sup>	179.64 (0.02)	0.01	0.31
Mono(2-ethyl-5-hydroxyhexyl) phthalate*	5OH-MEHP	C <sub>16</sub> H <sub>22</sub> O <sub>5</sub>	317.1359	[M+Na] <sup>+</sup>	172.92 (0.05)	0.03	0.88
			293.1394	[M-H] <sup>-</sup>	168.99 (0.03)	0.02	0.72
Mono(2-ethyl-5-oxohexyl)phthalate*	5-oxo-MEHP	C <sub>16</sub> H <sub>20</sub> O <sub>5</sub>	315.1203	[M+Na] <sup>+</sup>	170.18 (0.03)	0.02	1.91
			291.1238	[M-H] <sup>-</sup>	168.35 (0.03)	0.02	1.28

Mono-(3-carboxypropyl) phthalate*	3-cx-MCPP	C <sub>12</sub> H <sub>12</sub> O <sub>6</sub>	275.0526	[M+Na] <sup>+</sup>	156.95 (0.09)	0.05	3.13
Mono-(2-ethyl-5-carboxypentyl) phthalate*	5-cx-MEPP	C <sub>16</sub> H <sub>20</sub> O <sub>6</sub>	331.1152 307.1187	[M+Na] <sup>+</sup> [M-H] <sup>-</sup>	174.45 (0.07) 169.87 (0.06)	0.04 0.03	1.19 0.56
Mono-hydroxyisononyl phthalate*	7OH-MiNP	C <sub>17</sub> H <sub>24</sub> O <sub>5</sub>	331.1516 307.1551	[M+Na] <sup>+</sup> [M-H] <sup>-</sup>	176.60 (0.02) 172.50 (0.03)	0.01 0.02	1.23 2.68
Mono-carboxyisononyl phthalate*	7-cx-MiNP	C <sub>18</sub> H <sub>24</sub> O <sub>6</sub>	359.1465 335.1500	[M+Na] <sup>+</sup> [M-H] <sup>-</sup>	182.64 (0.10) 177.47 (0.04)	0.06 0.02	0.59 1.17
Mono-isononyl-cyclohexane-1,2-dicarboxylate*	cis-MINCH	C <sub>17</sub> H <sub>30</sub> O <sub>4</sub>	321.2036 297.2071	[M+Na] <sup>+</sup> [M-H] <sup>-</sup>	185.87 (0.05) 175.48 (0.03)	0.03 0.02	1.06 1.43
Cyclohexane-1,2-dicarboxylic mono carboxyisooctyl ester*	cis-cx-MINCH	C <sub>17</sub> H <sub>28</sub> O <sub>6</sub>	351.1778 327.1813	[M+Na] <sup>+</sup> [M-H] <sup>-</sup>	179.93 (0.06) 176.73 (0.02)	0.03 0.01	0.44 0.90
Cyclohexane-1,2-dicarboxylic mono hydroxyisononyl ester*	cis-OH-MINCH	C <sub>17</sub> H <sub>30</sub> O <sub>5</sub>	337.1985 313.2020	[M+Na] <sup>+</sup> [M-H] <sup>-</sup>	178.57 (0.08) 175.32 (0.02)	0.05 0.01	0.41 0.79
Mono(2-ethylhexyl) terephthalate*	MEHTP	C <sub>16</sub> H <sub>22</sub> O <sub>4</sub>	277.1445	[M-H] <sup>-</sup>	183.54 (0.03)	0.02	1.86
Mono(2-ethyl-5-hydroxyhexyl) terephthalate*	5OH-MEHTP	C <sub>16</sub> H <sub>22</sub> O <sub>5</sub>	293.1394	[M-H] <sup>-</sup>	185.08 (0.09)	0.05	1.90
Mono(2-ethyl-5-carboxypentyl) terephthalate*	5-cx-MEPTP	C <sub>16</sub> H <sub>20</sub> O <sub>6</sub>	307.1187	[M-H] <sup>-</sup>	168.42 (0.05)	0.03	0.63
Di(2-ethylhexyl) adipate*	DEHA	C <sub>22</sub> H <sub>42</sub> O <sub>4</sub>	371.3156 393.2975 763.6058	[M+H] <sup>+</sup> [M+Na] <sup>+</sup> [2M+Na] <sup>+</sup>	209.38 (0.03) 218.46 (0.07) 294.67 (0.03)	0.01 0.03 0.01	3.00 2.36 3.01
Diisobutyl adipate*	DIBA	C <sub>14</sub> H <sub>26</sub> O <sub>4</sub>	259.1904 281.1723 539.3554	[M+H] <sup>+</sup> [M+Na] <sup>+</sup> [2M+Na] <sup>+</sup>	167.82 (0.13) 180.16 (0.04) 235.89 (0.12)	0.08 0.02 0.05	1.82 1.80 0.34
Di(2-ethylhexyl) terephthalate*	DEHT	C <sub>24</sub> H <sub>38</sub> O <sub>4</sub>	413.2662	[M+Na] <sup>+</sup>	215.81 (0.12)	0.05	1.08
Isooctyl-2-phenoxyethyl-terephthalate*	IOPhEt	C <sub>24</sub> H <sub>30</sub> O <sub>5</sub>	399.2166 421.1985	[M+H] <sup>+</sup> [M+Na] <sup>+</sup>	218.61 (0.09) 227.37 (0.09)	0.04 0.04	0.40 0.57
Mono(2-ethyl-5-oxohexyl) adipate*	5-oxo-MEHA	C <sub>14</sub> H <sub>24</sub> O <sub>5</sub>	295.1516 271.1551	[M+Na] <sup>+</sup> [M-H] <sup>-</sup>	165.91 (0.05) 165.29 (0.05)	0.03 0.03	0.50 0.38
Mono(2-ethylhexyl) adipate*	MEHA	C <sub>14</sub> H <sub>26</sub> O <sub>4</sub>	281.1723 257.1758	[M+Na] <sup>+</sup> [M-H] <sup>-</sup>	177.32 (0.11) 166.76 (0.03)	0.06 0.02	0.69 1.59
Mono(2-ethyl-5-hydroxyhexyl) adipate*	5OH-MEHA	C <sub>14</sub> H <sub>26</sub> O <sub>5</sub>	297.1672 273.1708	[M+Na] <sup>+</sup> [M-H] <sup>-</sup>	168.70 (0.03) 165.79 (0.04)	0.02 0.02	0.30 2.75
Mono(2-ethyl-5-carboxypentyl) adipate*	5-cx-MEPA	C <sub>14</sub> H <sub>24</sub> O <sub>6</sub>	311.1465 287.1500	[M+Na] <sup>+</sup> [M-H] <sup>-</sup>	170.01 (0.05) 167.03 (0.03)	0.03 0.02	4.16 0.23
Tris(2-ethylhexyl) trimellitate*	TOTM	C <sub>33</sub> H <sub>54</sub> O <sub>6</sub>	569.3813	[M+Na] <sup>+</sup>	264.41 (0.39)	0.15	2.06

2,4-Di-(2-ethylhexyl) trimellitate*	2,4-DEHTM	C <sub>25</sub> H <sub>38</sub> O <sub>6</sub>	435.2741	[M+H] <sup>+</sup>	218.39 (0.07)	0.03	1.44
			457.2561	[M+Na] <sup>+</sup>	233.33 (0.12)	0.05	1.28
			433.2596	[M-H] <sup>-</sup>	222.86 (0.04)	0.02	2.99
Mono-1-(2-ethyl-5-carboxyhexyl) trimellitate*		C <sub>17</sub> H <sub>20</sub> O <sub>8</sub>	375.1050	[M+Na] <sup>+</sup>	187.56 (0.09)	0.05	0.69
			351.1085	[M-H] <sup>-</sup>	180.56 (0.03)	0.02	2.96
Mono-1-[2(carboxymethyl)hexyl] trimellitate*		C <sub>17</sub> H <sub>20</sub> O <sub>8</sub>	375.1050	[M+Na] <sup>+</sup>	189.84 (0.05)	0.03	0.40
			351.1085	[M-H] <sup>-</sup>	182.23 (0.10)	0.05	3.25
Mono-1-(2-ethyl-5-oxo-hexyl) trimellitate*		C <sub>17</sub> H <sub>20</sub> O <sub>7</sub>	335.1136	[M-H] <sup>-</sup>	178.84 (0.01)	0.01	1.70
Dibutylsebacate*	DBS	C <sub>18</sub> H <sub>34</sub> O <sub>4</sub>	315.2530	[M+H] <sup>+</sup>	183.89 (0.02)	0.01	1.19
			337.2349	[M+Na] <sup>+</sup>	193.48 (0.03)	0.02	1.46
Dimethylsebacate*	DMS	C <sub>12</sub> H <sub>22</sub> O <sub>4</sub>	253.1410	[M+Na] <sup>+</sup>	159.71 (0.04)	0.02	1.63
Butyryl trihexyl citrate*	BTHC	C <sub>28</sub> H <sub>50</sub> O <sub>8</sub>	515.3578	[M+H] <sup>+</sup>	240.45 (0.18)	0.07	1.21
			537.3398	[M+Na] <sup>+</sup>	245.25 (0.07)	0.03	1.20
			105.6904	[2M+Na] <sup>+</sup>	348.02 (0.20)	0.06	0.37
Tributyl acetylcitrate*	ATBC	C <sub>20</sub> H <sub>34</sub> O <sub>8</sub>	403.2326	[M+H] <sup>+</sup>	199.82 (0.23)	0.12	1.60
			425.2146	[M+Na] <sup>+</sup>	205.77 (0.06)	0.03	0.72
			827.4400	[2M+Na] <sup>+</sup>	291.52 (0.14)	0.05	0.64
Acetyltriethyl citrate*	ATEC	C <sub>14</sub> H <sub>22</sub> O <sub>8</sub>	341.1207	[M+Na] <sup>+</sup>	174.36 (0.06)	0.03	2.60
			659.2522	[2M+Na] <sup>+</sup>	244.35 (0.24)	0.10	0.62
Tri-n-hexyl-trimellitate*	THTM	C <sub>27</sub> H <sub>42</sub> O <sub>6</sub>	463.3054	[M+H] <sup>+</sup>	236.57 (0.26)	0.11	0.49
			485.2874	[M+Na] <sup>+</sup>	247.49 (0.39)	0.16	1.41
Dimethyl azelate*	DMA	C <sub>11</sub> H <sub>20</sub> O <sub>4</sub>	239.1254	[M+Na] <sup>+</sup>	155.54 (0.03)	0.02	2.16
Atrazine		C <sub>8</sub> H <sub>14</sub> ClN <sub>5</sub>	216.1010	[M+H] <sup>+</sup>	149.53 (0.01)	0.01	1.72
Diazinon*		C <sub>12</sub> H <sub>21</sub> N <sub>2</sub> O <sub>3</sub> PS	305.1083	[M+H] <sup>+</sup>	173.15 (0.05)	0.03	0.09
			327.0903	[M+Na] <sup>+</sup>	177.72 (0.06)	0.03	1.93
p-Nitrophenol*		C <sub>6</sub> H <sub>5</sub> NO <sub>3</sub>	138,0197	[M-H] <sup>-</sup>	119.78 (0.03)	0.03	3,38
3,5,6-Trichloro-2-pyridinol*	TCPy	C <sub>5</sub> H <sub>2</sub> Cl <sub>3</sub> NO	197,9275	[M+H] <sup>+</sup>	130.45 (0.04)	0.03	0,54
3-Phenoxybenzoic acid*	3-PBA	C <sub>13</sub> H <sub>10</sub> O <sub>3</sub>	213,0557	[M-H] <sup>-</sup>	155.84 (0.07)	0.04	0,30
3,5-ditert-butyl-4-hydroxy-benzaldehyde*		C <sub>15</sub> H <sub>22</sub> O <sub>2</sub>	235.1693	[M+H] <sup>+</sup>	165.21 (0.04)	0.02	4.69
			257.1512 <sup>2</sup>	[M+Na] <sup>+</sup>	185.31 (0.10)	0.06	6.70
Dipropylene glycol dibenzoate*		C <sub>20</sub> H <sub>22</sub> O <sub>5</sub>	365.1359	[M+Na] <sup>+</sup>	186.32 (1.35)	0.73	3.50
4-((4-isopropoxyphenyl) sulfonyl) phenol*	D-8	C <sub>15</sub> H <sub>16</sub> O <sub>4</sub> S	291.0697	[M-H] <sup>-</sup>	174.81 (0.02)	0.01	4.69
			583.1466	[2M-H] <sup>-</sup>	226.14 (0.08)	0.03	0.85
4-(4-hydroxy-3-prop-2-enylphenyl)sulfonyl-2-prop-2-enylphenol*	TGSA	C <sub>18</sub> H <sub>18</sub> O <sub>4</sub> S	329.0853	[M-H] <sup>-</sup>	180.00 (0.15)	0.08	0.96
			659.1779	[2M-H] <sup>-</sup>	240.99 (0.05)	0.02	0.33
4-((4-(Benzyloxy)phenyl)-sulfonyl) phenol*	BPS-MAE	C <sub>15</sub> H <sub>14</sub> O <sub>4</sub> S	289.0540	[M-H] <sup>-</sup>	172.68 (0.02)	0.01	1.40
4-Nonylphenol*		C <sub>15</sub> H <sub>24</sub> O	219.1754	[M-H] <sup>-</sup>	161.07 (0.07)	0.05	1.13
4-t-Octylphenol*		C <sub>14</sub> H <sub>22</sub> O	205.1598	[M-H] <sup>-</sup>	156.73 (0.04)	0.02	0.46
4-n-Octylphenol*		C <sub>14</sub> H <sub>22</sub> O	205.1598	[M-H] <sup>-</sup>	160.03 (0.04)	0.02	0.81

Triclosan*	TCS	C <sub>12</sub> H <sub>7</sub> Cl <sub>3</sub> O <sub>2</sub>	286.9439	[M-H] <sup>-</sup>	158.94 (0.09)	0.06	1.14
Perfluoro-n-butanoic acid	PFBA	C <sub>4</sub> HF <sub>7</sub> O <sub>2</sub>	168.9894	[M-H-CO <sub>2</sub> ] <sup>-</sup>	109.53 (0.10)	0.09	0.60
Perfluoropentanoic acid	PFPeA	C <sub>5</sub> HF <sub>9</sub> O <sub>2</sub>	218.9862	[M-H-CO <sub>2</sub> ] <sup>-</sup>	116.78 (0.06)	0.05	2.85
			526.9593	[2M-H] <sup>-</sup>	179.96 (0.10)	0.05	1.04
Perfluoro-n-hexanoic acid	PFHxA	C <sub>6</sub> HF <sub>11</sub> O <sub>2</sub>	268.9830	[M-H-CO <sub>2</sub> ] <sup>-</sup>	124.47 (0.03)	0.04	4.03
			626.9529	[2M-H] <sup>-</sup>	195.94 (0.07)	0.03	0.25
Perfluoro-n-heptanoic acid	PFHpA	C <sub>7</sub> HF <sub>13</sub> O <sub>2</sub>	362.9696	[M-H] <sup>-</sup>	147.61 (0.14)	0.10	1.34
			318.9798	[M-H-CO <sub>2</sub> ] <sup>-</sup>	132.30 (0.07)	0.06	2.99
			726.9465	[2M-H] <sup>-</sup>	211.59 (0.15)	0.07	0.53
Perfluoro-n-octanoic acid	PFOA	C <sub>8</sub> HF <sub>15</sub> O <sub>2</sub>	412.9664	[M-H] <sup>-</sup>	156.37 (0.09)	0.06	1.90
			368.9766	[M-H-CO <sub>2</sub> ] <sup>-</sup>	139.44 (0.07)	0.05	2.18
			826.9401	[2M-H] <sup>-</sup>	226.58 (0.08)	0.04	0.30
Perfluoro-n-nonanoic acid	PFNA	C <sub>9</sub> HF <sub>17</sub> O <sub>2</sub>	462.9632	[M-H] <sup>-</sup>	165.06 (0.11)	0.07	0.90
			418.9734	[M-H-CO <sub>2</sub> ] <sup>-</sup>	147.05 (0.04)	0.03	4.10
			926.9337	[2M-H] <sup>-</sup>	240.71 (0.15)	0.06	0.12
Perfluoro-n-decanoic acid	PFDA	C <sub>10</sub> HF <sub>19</sub> O <sub>2</sub>	512.9600	[M-H] <sup>-</sup>	174.29 (0.08)	0.05	4.34
			468.9702	[M-H-CO <sub>2</sub> ] <sup>-</sup>	155.63 (0.07)	0.05	4.11
			102.9273	[2M-H] <sup>-</sup>	254.24 (0.14)	0.05	0.52
Perfluoro-n-undecanoic acid	PFUDA	C <sub>11</sub> HF <sub>21</sub> O <sub>2</sub>	562.9568	[M-H] <sup>-</sup>	182.86 (0.06)	0.03	0.61
			518.9670	[M-H-CO <sub>2</sub> ] <sup>-</sup>	163.84 (0.08)	0.05	3.19
			1126.9209	[2M-H] <sup>-</sup>	266.81 (0.12)	0.04	0.21
Perfluoro-n-dodecanoic acid	PFDoA	C <sub>12</sub> HF <sub>23</sub> O <sub>2</sub>	612.9536	[M-H] <sup>-</sup>	192.16 (0.09)	0.05	1.69
			568.9638	[M-H-CO <sub>2</sub> ] <sup>-</sup>	172.25 (0.08)	0.05	0.99
			1226.9145	[2M-H] <sup>-</sup>	278.80 (0.19)	0.07	0.48
Perfluoro-n-tridecanoic acid	PFTrDA	C <sub>13</sub> HF <sub>25</sub> O <sub>2</sub>	662.9504	[M-H] <sup>-</sup>	201.05 (0.04)	0.02	4.38
			618.9606	[M-H-CO <sub>2</sub> ] <sup>-</sup>	180.30 (0.04)	0.02	0.29
			1326.9081	[2M-H] <sup>-</sup>	290.64 (0.06)	0.02	0.45
Perfluoro-n-tetradecanoic acid	PFTeDA	C <sub>14</sub> HF <sub>27</sub> O <sub>2</sub>	712.9472	[M-H] <sup>-</sup>	209.91 (0.06)	0.03	0.40
			668.95739	[M-H-CO <sub>2</sub> ] <sup>-</sup>	188.43 (0.05)	0.03	1.28
			1426.9017	[2M-H] <sup>-</sup>	302.02 (0.14)	0.05	0.66
Perfluoro-n-hexadecanoic acid	PFHxDA	C <sub>16</sub> HF <sub>31</sub> O <sub>2</sub>	812.9409	[M-H] <sup>-</sup>	227.34 (0.05)	0.02	0.82
			1626.8891	[M-H-CO <sub>2</sub> ] <sup>-</sup>	204.50 (0.08)	0.04	0.29
			768.9511	[2M-H] <sup>-</sup>	325.43 (0.18)	0.06	0.27
Perfluoro-n-octadecanoic acid*	PFODA	C <sub>18</sub> HF <sub>35</sub> O <sub>2</sub>	912.9345	[M-H] <sup>-</sup>	243.53 (0.05)	0.02	2.67
			868.9447	[M-H-CO <sub>2</sub> ] <sup>-</sup>	220.15 (0.05)	0.02	3.73
Perfluorobutane-sulfonic acid	PFBS	C <sub>4</sub> HF <sub>9</sub> O <sub>3</sub> S	298.9430	[M-H] <sup>-</sup>	133.28 (0.03)	0.02	0.74
Perfluorohexane-sulfonic acid	PFHxS	C <sub>6</sub> HF <sub>13</sub> O <sub>3</sub> S	598.8933	[2M-H] <sup>-</sup>	196.88 (0.14)	0.07	1.07
			398.9366	[M-H] <sup>-</sup>	150.81 (0.06)	0.04	2.27
Perfluorooctyl-sulfonic acid	PFOS	C <sub>8</sub> HF <sub>17</sub> O <sub>3</sub> S	798.8805	[2M-H] <sup>-</sup>	228.66 (0.10)	0.04	0.77
			498.9302	[M-H] <sup>-</sup>	168.89 (0.07)	0.04	0.75
Perfluorodecane sulfonic acid	PFDS	C <sub>10</sub> HF <sub>21</sub> O <sub>3</sub> S	998.8677	[2M-H] <sup>-</sup>	257.72 (0.12)	0.05	1.24
			598.9238	[M-H] <sup>-</sup>	186.91 (0.07)	0.04	2.10
Sodium 1H,1H,2H,2H-perfluorooctane sulfonate	6:2 FTS	C <sub>8</sub> H <sub>5</sub> F <sub>13</sub> O <sub>3</sub> S	426.9679	[M-H] <sup>-</sup>	168.47 (0.06)	0.04	0.56
			854.9431	[2M-H] <sup>-</sup>	236.24 (0.11)	0.05	2.28
8:2 Fluorotelomer sulfonic acid	8:2 FTS	C <sub>10</sub> H <sub>5</sub> F <sub>17</sub> O <sub>3</sub> S	526.9617	[M-H] <sup>-</sup>	186.39 (0.07)	0.04	3.14
			1054.9307	[2M-H] <sup>-</sup>	263.38 (0.25)	0.10	0.39
1H,1H,2H,2H-Perfluoro-	10:2 FTS	C <sub>12</sub> H <sub>5</sub> F <sub>21</sub> O <sub>3</sub> S	626.9551	[M-H] <sup>-</sup>	204.21 (0.03)	0.02	1.51
			1254.9175	[2M-H] <sup>-</sup>	288.72 (0.09)	0.03	1.04

dodecanesulfonic acid							
6:2 chlorinated polyfluorinated ether sulfonate	F-53B	C <sub>8</sub> ClF <sub>16</sub> O <sub>4</sub> S	530.89558	[M-H] <sup>-</sup>	170.98 (0.01)	0.01	3.65
8:2 Fluorotelomer unsaturated carboxylate*	8:2 FTUCA	C <sub>10</sub> H <sub>2</sub> F <sub>16</sub> O <sub>2</sub>	456.9727 914.9526	[M-H] <sup>-</sup> [2M-H] <sup>-</sup>	172.63 (0.04) 239.96 (0.09)	0.02 0.04	1.08 0.51
10:2 Fluorotelomer unsaturated carboxylate*	10:2 FTUCA	C <sub>12</sub> H <sub>2</sub> F <sub>20</sub> O <sub>2</sub>	556.9663 1114.9398	[M-H] <sup>-</sup> [2M-H] <sup>-</sup>	189.84 (0.04) 265.53 (0.08)	0.02 0.03	0.43 0.30
8:2 Fluorotelomer phosphate diester*	8:2 diPAP	C <sub>20</sub> H <sub>9</sub> F <sub>34</sub> O <sub>4</sub> P	988.9623	[M-H] <sup>-</sup>	261.61 (0.06)	0.02	0.58
Perfluorodecyl-phosphonic acid*	PFDPA	C <sub>10</sub> H <sub>2</sub> F <sub>21</sub> O <sub>3</sub> P	598.9333	[M-H] <sup>-</sup>	188.25 (0.01)	0.01	0.74
8-Chloroperfluoro-octylphosphonic acid*	Cl-PFOPA	C <sub>8</sub> H <sub>2</sub> ClF <sub>16</sub> O <sub>3</sub> P	514.9102	[M-H] <sup>-</sup>	175.27 (0.01)	0.01	0.34
6-Chloroperfluoro-hexyl-phosphonic acid*	Cl-PFHxPA	C <sub>6</sub> H <sub>2</sub> ClF <sub>12</sub> O <sub>3</sub> P	414.9166	[M-H] <sup>-</sup>	157.41 (0.01)	0.01	1.33
Hexafluoropropylene oxide dimer acid*	HFPO-DA	C <sub>6</sub> HF <sub>11</sub> O <sub>3</sub>	284.9779 658.9427	[M-H-CO <sub>2</sub> ] <sup>-</sup> [2M-H] <sup>-</sup>	126.89 (0.09) 198.61 (0.09)	0.07 0.05	1.33 1.14
Perfluorooctane sulfonamide*	FOSA	C <sub>8</sub> H <sub>2</sub> F <sub>17</sub> NO <sub>2</sub> S	497.9462	[M-H] <sup>-</sup>	170.13 (0.02)	0.01	0.93
N-ethylperfluorooctane sulfonamide*	N-EtFOSA	C <sub>10</sub> H <sub>6</sub> F <sub>17</sub> NO <sub>2</sub> S	525.9775	[M-H] <sup>-</sup>	178.42 (0.03)	0.01	3.69
N-ethylperfluorooctane sulfonamido acetic acid	N-EtFOSAA	C <sub>12</sub> H <sub>8</sub> F <sub>17</sub> NO <sub>4</sub> S	583.9830 1168.9732	[M-H] <sup>-</sup> [2M-H] <sup>-</sup>	196.81 (0.06) 283.56 (0.06)	0.03 0.02	1.64 0.28
N-Methylperfluorooctane sulfonamide*	N-MeFOSA	C <sub>9</sub> H <sub>4</sub> F <sub>17</sub> NO <sub>2</sub> S	511.9619	[M-H] <sup>-</sup>	173.97 (0.03)	0.02	1.08
N-methylperfluorooctane sulfonamido acetic acid	N-MeFOSAA	C <sub>11</sub> H <sub>6</sub> F <sub>17</sub> NO <sub>4</sub> S	569.9673 1140.9419	[M-H] <sup>-</sup> [2M-H] <sup>-</sup>	193.17 (0.03) 275.84 (0.10)	0.02 0.04	2.40 0.28

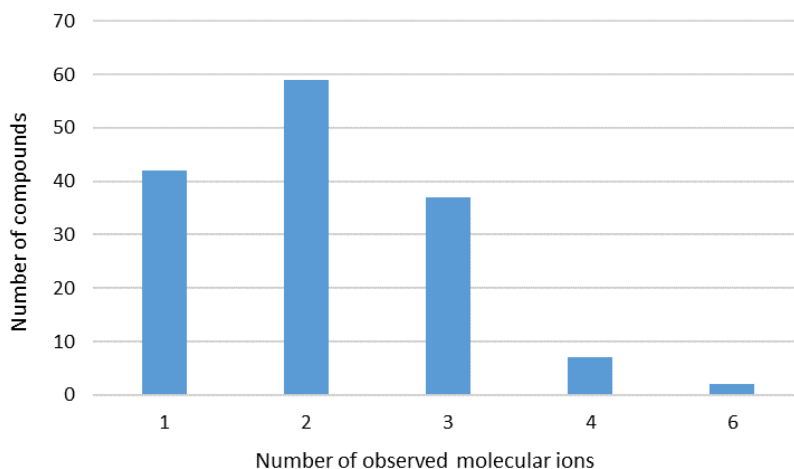


**Figure SI-3.1.1:** Number of observed ions for the studied compounds included in the  $^{DT}CCS_{N_2}$  database.

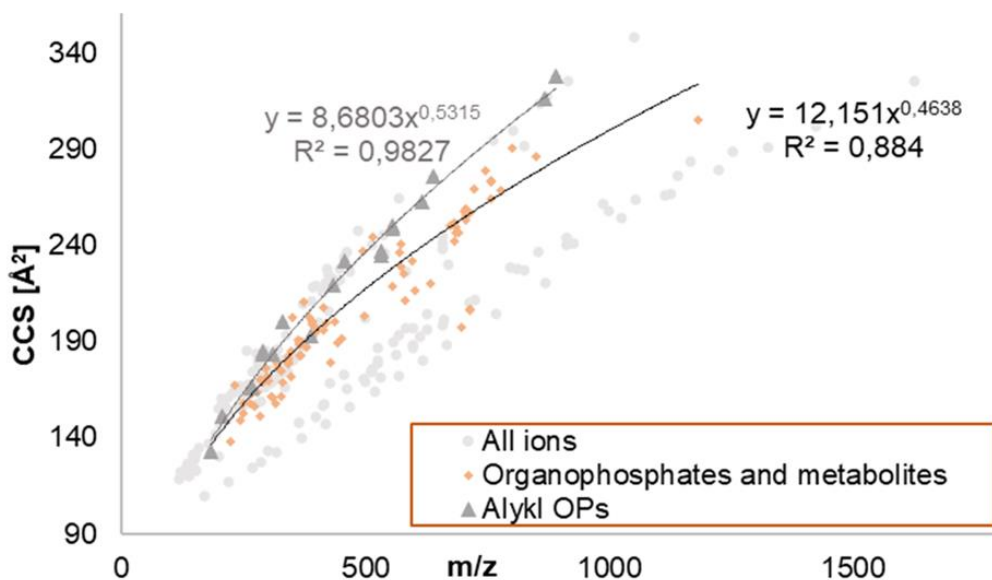


**Figure SI-3.1.2:** Depiction of  $^{DT}CCS_{N_2}$  vs.  $m/z$  for organophosphates (OPs) and metabolites. The trendline calculated for all OPs and their metabolites ( $n = 37$ ) is indicated. The subclass of alkyl OPs is marked separately with the corresponding trendline indicated in grey. For comparison, all acquired  $^{DT}CCS_{N_2}$  values are also displayed in gray.

**Table SI-3.1.6:** Comparison of experimentally determined  $^{DT}CCS_{N_2}$  values ( $^{DT}CCS_{N_2exp.}$ ) and data available from literature ( $CCS_{N_2lit.}$ ). For each compound, the absolute percentage of error was calculated.  $^{DT}CCS_{N_2}$  derived from (Dodds et al., 2020) for PFAS and (Nichols et al., 2018) for di(2-ethylhexyl) phthalate.  $^{TW}CCS_{N_2}$  for OPFRs derived from (Mullin et al., 2020).

Compound name	<i>m/z</i>	Ion	$^{DT}CCS_{N_2exp.}$ ( $\pm SD$ ) [ $\text{\AA}^2$ ]	$CCS_{N_2lit.}$ [ $\text{\AA}^2$ ]	Error [%]
tris(2-butoxyethyl) phosphate (TBOEP)	399.2506	[M+H] <sup>+</sup>	196.44 (0.18)	198.34	0.96
triphenyl phosphate (TPhP)	327.0781	[M+H] <sup>+</sup>	174.74 (0.03)	169.9	2.85
Tri-p-tolyl phosphate (TTP)	369.1250	[M+H] <sup>+</sup>	190.02 (0.06)	187.0	1.62
2-Ethylhexyl diphenyl phosphate (EHDPHP)	385.1539	[M+Na] <sup>+</sup>	202.70 (0.05)	201.6	0.55
Isodecyl diphenyl phosphate (iDPP)	391.2033	[M+H] <sup>+</sup>	200.20 (0.09)	202.4	1.08
Diphenylcresyl phosphate (CDPHP)	341.0937	[M+H] <sup>+</sup>	180.48 (0.02)	177.1	1.92
Antiblaze V6	580.9150	[M+H] <sup>+</sup>	211.37 (0.04)	212.1	0.34
tris(2-chloroethyl) phosphate (TCEP)	284.9612	[M+H] <sup>+</sup>	151.31 (0.05)	150.4	0.59
Tris(2-chloroisopropyl)-phosphate (TCIPP)	327.0081	[M+H] <sup>+</sup>	161.66 (0.10)	161.9	0.13
tris(1,3-dichloro-2-propyl)phosphate (TDCIPP)	428.8912	[M+H] <sup>+</sup>	178.56 (0.02)	176.5	1.19
Perfluoro-n-butanoic acid (PFBA)	168.9894	[M-H-CO <sub>2</sub> ] <sup>-</sup>	109.53 (0.10)	110.8	1.15
Perfluoro-n-pentanoic acid (PFPeA)	218.9862	[M-H-CO <sub>2</sub> ] <sup>-</sup>	116.78 (0.06)	117.4	0.53
Perfluoro-n-hexanoic acid (PFHxA)	268.9830	[M-H-CO <sub>2</sub> ] <sup>-</sup>	124.47 (0.03)	125.1	0.50
Perfluoro-n-heptanoic acid (PFHpA)	318.9798	[M-H-CO <sub>2</sub> ] <sup>-</sup>	132.30 (0.07)	132.4	0.08
Perfluoro-n-octanoic acid (PFOA)	368.9766	[M-H-CO <sub>2</sub> ] <sup>-</sup>	139.44 (0.07)	139.5	0.04
Perfluoro-n-nonanoic acid (PFNA)	462.9632	[M-H] <sup>-</sup>	165.06 (0.11)	165.2	0.08
	418.9734	[M-H-CO <sub>2</sub> ] <sup>-</sup>	147.05 (0.04)	147.0	0.04
Perfluoro-n-decanoic acid (PFDA)	512.9600	[M-H] <sup>-</sup>	174.29 (0.08)	174.2	0.05
	468.9702	[M-H-CO <sub>2</sub> ] <sup>-</sup>	155.63 (0.07)	155.3	0.21
Perfluoro-n-undecanoic acid (PFUdA)	562.9568	[M-H] <sup>-</sup>	182.86 (0.06)	182.9	0.02
	518.9670	[M-H-CO <sub>2</sub> ] <sup>-</sup>	163.84 (0.08)	163.4	0.27
Perfluoro-n-dodecanoic acid (PFDoA)	612.9536	[M-H] <sup>-</sup>	192.16 (0.09)	191.4	0.40
	568.9638	[M-H-CO <sub>2</sub> ] <sup>-</sup>	172.25 (0.08)	171.5	0.44
Perfluoro-n-tridecanoic acid (PFTrDA)	662.9504	[M-H] <sup>-</sup>	201.05 (0.04)	200.8	0.13
	618.9606	[M-H-CO <sub>2</sub> ] <sup>-</sup>	180.30 (0.04)	179.6	0.39
Perfluoro-n-tetradecanoic acid (PFTeDA)	712.9472	[M-H] <sup>-</sup>	209.91 (0.06)	209.2	0.34
	668.9574	[M-H-CO <sub>2</sub> ] <sup>-</sup>	188.43 (0.05)	187.6	0.44
Perfluoro-n-hexadecanoic acid (PFHxDA)	812.9409	[M-H] <sup>-</sup>	227.34 (0.05)	226.1	0.55
	768.9511	[M-H-CO <sub>2</sub> ] <sup>-</sup>	204.50 (0.08)	203.7	0.39
Perfluorobutanesulfonic acid (PFBS)	298.9430	[M-H] <sup>-</sup>	133.28 (0.03)	133.6	0.24
Perfluorohexanesulfonic acid (PFHxS)	398.9366	[M-H] <sup>-</sup>	150.81 (0.06)	150.5	0.20
Perfluorooctylsulfonic acid (PFOS)	498.9302	[M-H] <sup>-</sup>	168.89 (0.07)	168.3	0.35
Perfluorodecane sulfonic acid (PFDS)	598.9238	[M-H] <sup>-</sup>	186.91 (0.07)	186.2	0.38
Sodium 1H,1H,2H,2H-perfluorooctane sulfonate (6:2 FTS)	426.9679	[M-H] <sup>-</sup>	168.47 (0.06)	168.1	0.22
8:2 Fluorotelomer sulfonic acid (8:2 FTS)	526.9617	[M-H] <sup>-</sup>	186.39 (0.07)	185.8	0.32

1H,1H,2H,2H-Perfluoro-dodecanesulfonic acid (10:2 FTS)	626.9551	[M-H] <sup>-</sup>	204.21 (0.03)	203.6	0.30
6:2 chlorinated polyfluorinated ether sulfonate (F-53B)	530.8956	[M-H] <sup>-</sup>	170.98 (0.01)	170.2	0.46
N-ethylperfluorooctane sulfonamido acetic acid (N-EtFOSAA)	583.9830	[M-H] <sup>-</sup>	196.81 (0.06)	196.3	0.26
N-methylperfluorooctane sulfonamido acetic acid (N-MeFOSAA)	569.9673	[M-H] <sup>-</sup>	193.17 (0.03)	192.7	0.24
Di(2-ethylhexyl) phthalate	391.2843	[M+H] <sup>+</sup>	211.00 (0.08)	212.2	0.57
	413.2662	[M+Na] <sup>+</sup>	215.33 (0.05)	215.9	0.26

**Table SI-3.1.7:**  $^{DT}CCS_{N_2}$  values of 15 organophosphate metabolites acquired in spiked human urine. Pooled urine spiked at two concentration levels (20 ng/mL and 50 ng/mL in urine) was analysed in triplicate. Average measured  $m/z$  ratios and  $^{DT}CCS_{N_2}$  values are reported. Also, the calculated mass error and absolute percent error of the experimental  $^{DT}CCS_{N_2}$  values in comparison with database values are given. Bis(2-chloropropyl) hydrogen phosphate and bis(2-chloroethyl) phosphate were spiked in urine but not detected after sample preparation. Therefore, no data is reported for these compounds. n.d. = not detected

Concentration level		20 ng/mL				50 ng/mL			
Compound	Ion	Exp. $m/z$	$\Delta m/z$ [ppm]	$^{DT}CCS_{N_2}$ [Å <sup>2</sup> ]	$\Delta^{DT}CCS_{N_2}$ [%]	Exp. $m/z$	$\Delta m/z$ [ppm]	$^{DT}CCS_{N_2}$ [Å <sup>2</sup> ]	$\Delta^{DT}CCS_{N_2}$ [%]
Di-n-butyl phosphate	[M-H] <sup>-</sup>	209.0937	5.36	150.70	0.13	209.0936	5.38	150.79	0.07
Diphenyl hydrogen phosphate	[M-H] <sup>-</sup>	249.0314	3.31	152.93	0.03	249.0315	2.91	152.96	0.01
4-Hydroxyphenyl phenyl phosphate	[M-H] <sup>-</sup>	265.0256	5.75	157.79	0.15	265.0261	3.86	157.63	0.04
Bis(2-chloropropyl) hydrogen phosphate	n.d.	n.d.		n.d.		n.d.		n.d.	
Bis(2-chloroethyl) phosphate	n.d.	n.d.		n.d.		n.d.		n.d.	
Bis(1,3-dichloro-2-propyl) phosphate	[M-H] <sup>-</sup>	n.d.		n.d.		301.9038	2.95	157.80	0.03
Bis(1-chloro-2-propyl) 1-hydroxy-2-propyl phosphate	[M+H] <sup>+</sup> [M+Na] <sup>+</sup>	n.d. n.d.		n.d. n.d.		309.0418 331.0247	0.57 2.36	160.80 168.92	0.12 0.02
tris(2-chloroethyl) phosphate	[M+H] <sup>+</sup>	284.9627	5.35	151.48	0.12	284.9613	0.44	151.62	0.20
Bis(2-butoxyethyl) phosphate	[M+H] <sup>+</sup> [M+Na] <sup>+</sup>	299.1623 n.d.	1.75	171.34	0.25	299.1616 321.1436	0.59 0.37	171.69 175.99	0.05 0.19
bis(2-butoxyethyl) 2-hydroxyethyl phosphate	[M+H] <sup>+</sup> [M+Na] <sup>+</sup>	343.1890 365.1703	2.87 0.94	179.29 182.04	0.01 0.14	343.1884 365.1703	1.12 0.94	179.48 182.29	0.12 0.03
2-ethylhexyl phenyl phosphate	[M-H] <sup>-</sup>	285.1254	2.54	170.21	0.15	285.1252	3.24	170.08	0.22
5-Hydroxy 2-ethylhexyl diphenyl phosphate	[M+H] <sup>+</sup> [M+Na] <sup>+</sup>	379.1676 401.1501	1.91 3.20	186.59 193.52	0.04 0.74	379.1664 401.1489	1.26 0.20	186.88 193.61	0.12 0.70
Bis(2-butoxyethyl) 3'-hydroxy-2-butoxyethyl phosphate	[M+H] <sup>+</sup> [M+Na] <sup>+</sup>	415.2468 437.2282	2.95 1.56	195.36 199.70	0.04 0.34	415.2465 437.2272	2.23 0.73	195.79 200.16	0.18 0.11
3-Hydroxyphenyl phenyl phosphate	[M-H] <sup>-</sup>	341.0567	5.05	180.44	0.01	341.0570	4.18	180.46	0.01
4-Hydroxyphenyl phenyl phosphate	[M-H] <sup>-</sup>	341.0569	4.47	182.04	0.02	341.0573	3.30	182.06	0.03
<b>Average</b>					<b>0.15</b>				
						<b>0.12</b>			

**Table SI-3.1.8:**  $^{DT}CCS_{N_2}$  values of 15 alternative plasticizers metabolites acquired in spiked human urine. Pooled urine spiked at two concentration levels (20 ng/mL and 50 ng/mL in urine) were analysed in triplicate. Average measured  $m/z$  ratios and  $^{DT}CCS_{N_2}$  values are reported. The calculated mass error and absolute percent error of the experimental  $^{DT}CCS_{N_2}$  values in comparison with database values are given. Mono-hydroxy-isononyl phthalate, mono-carboxy-isononyl phthalate and mono(2-ethyl-5-carboxypentyl) adipate were spiked in urine but not detected after sample preparation. Therefore, no data is reported for these compounds. In all cases, data for the deprotonated ion ( $[M-H]^-$ ) is reported. n.d. = not detected

Concentration level	20 ng/mL				50 ng/mL			
Compound	Exp. $m/z$	$\Delta m/z$ [ppm]	$^{DT}CCS_{N_2}$ [ $\text{\AA}^2$ ]	$\Delta^{DT}CCS_{N_2}$ [abs%]	Exp. $m/z$	$\Delta m/z$ [ppm]	$^{DT}CCS_{N_2}$ [ $\text{\AA}^2$ ]	$\Delta^{DT}CCS_{N_2}$ [abs%]
Mono(2-ethylhexyl) terephthalate	277.1446	0.38	183.55	0.01	277.1450	1.98	183.61	0.04
Mono(2-ethyl-5-hydroxyhexyl) terephthalate	293.1405	3.44	185.22	0.08	293.1403	3.06	185.31	0.12
Mono(2-ethylhexyl) adipate	257.1765	2.87	166.62	0.09	257.1760	0.75	166.69	0.05
Mono(2-ethyl-5-hydroxyhexyl) adipate	273.1718	4.29	165.79	<0.01	273.1713	2.18	165.75	0.02
Mono(2-ethyl-5-oxohexyl) adipate	271.1624	2.62	165.17	0.07	271.1556	1.79	165.09	0.12
Mono-isononyl-cyclo-hexane-1,2-dicarboxylate	297.2071	0.16	174.82	0.38	297.2072	0.99	174.75	0.42
Cyclohexane-1,2-dicarboxylic mono carboxyisooctyl ester	327.1813	0.28	176.50	0.13	327.1811	0.58	176.61	0.07
Cyclohexane-1,2-dicarboxylic mono hydroxyisononyl ester	313.2026	2.32	175.22	0.06	313.2021	0.09	175.26	0.03
6-Hydroxy mono-propylheptyl phthalate	321.1714	2.13	178.73	0.06	321.1719	2.02	178.63	<0.01
Mono-2-(propyl-6-oxoheptyl)-phthalate	319.1551	0.19	177.77	0.04	321.1713	1.08	177.83	0.08
Mono(2-propyl-6-carboxyhexyl)phthalate	335.1513	4.71	179.80	0.09	335.1551	3.37	179.83	0.10
Mono(2-ethyl-5-carboxypentyl) terephthalate	n.d.	n.d.	n.d.	n.d.	307.1201	4.39	168.61	0.11
Monohydroxy isononyl phthalate	n.d.	n.d.	n.d.	n.d.	n.d.	n.d.	n.d.	n.d.
Monocarboxy isononyl phthalate	n.d.	n.d.	n.d.	n.d.	n.d.	n.d.	n.d.	n.d.
Mono(2-ethyl-5-carboxypentyl) adipate	n.d.	n.d.	n.d.	n.d.	n.d.	n.d.	n.d.	n.d.
	<b>Average 0.09</b>				<b>0.10</b>			

## 3.2 Comparison of $^{DT}CCS_{N_2}$ values with experimental $^{TW}CCS_{N_2}$ values and *in-silico* predicted data

### 3.2.1 Introduction

Ion mobility spectrometry has demonstrated to be a powerful additional technique for compound identification within target, suspect and non-target screening studies on CECs and in various other research fields (Causon et al., 2019a; George et al., 2020; Lacalle-Bergeron et al., 2020; Mullin et al., 2020). The implementation of IMS in suspect and non-target screening studies is commonly based on matching CCS values of signals of interest against CCS values of reference standards, scientific literature or open-source libraries (Hernandez-Mesa et al., 2018; Hines et al., 2017a; Zheng et al., 2017), including several online platforms which contain curated CCS datasets from various sources (Picache et al., 2019; Ross et al., 2020; Zhou et al., 2016). Moreover, the inclusion of ion mobility data in widely adopted confidence levels for identification of small molecules in environmental studies, including a cut-off value of 2% for the deviation between experimental and reference CCS values, has been proposed recently (Celma et al., 2020).

Nevertheless, CCS values remain an estimated empirical value which is influenced by the instrumental design and the applied calibration approach adding uncertainty to its inter-laboratory application. The uncertainty of IM-MS measurements has been assessed in detail previously (Causon and Hann, 2020; Stow et al., 2017). Several studies have investigated the inter-laboratory and inter-instrumental reproducibility of CCS measurements (Hinnenkamp et al., 2018; Righetti et al., 2020; Stow et al., 2017). Stow et al. reported an RSD of 0.29% for stepped-field measurements of  $^{DT}CCS_{N_2}$  values in three different laboratories of which all applied DTIMS (Stow et al., 2017). Hinnenkamp et al. compared CCS values acquired using TWIMS and DTIMS instruments for a set of 124 compounds and reported absolute errors of < 1% for 66%; between 1-2% for 27% and >2% for 7% of the proton adducts of the investigated compounds (Hinnenkamp et al., 2018). The latter findings indicate higher deviations if CCS values are transferred between different instrumental set-ups pointing out the need of further inter-comparison studies, especially within the field of environmental contaminants.

Despite the numerous available databases mentioned above, the use of CCS values as an additional identification parameter is often limited by the unavailability of reference CCS values, especially for novel CEC classes. This data gap can in theory be filled through the *in-silico* prediction of CCS values. Various prediction tools for different compound classes are available in the literature (Bijlsma et al., 2017; Colby et al., 2019; Mollerup et al., 2018; Zhou et al., 2016; Zhou et al., 2017b; Zhou et al., 2017c). These tools are based on experimental CCS values and apply different prediction models

including machine-learning algorithms (Zhou et al., 2016) such as artificial neural networks (ANN) (Bijlsma et al., 2017) or Multiple Adaptive Regression Splines (MARS) (Celma et al., 2022). Prediction tools have demonstrated good prediction accuracies making them a valuable addition for suspect and non-target screening studies (Bijlsma et al., 2019; Fabregat-Safont et al., 2021). However, extensive studies on the comparison of experimental  $^{DT}CCS_{N_2}$  values of CECs with *in-silico* predicted data are lacking not allowing to assess the utility of the *in-silico* prediction models for the annotation of CECs within suspect and non-target screening studies.

Based on a set of 56 CECs and their metabolites, this chapter aimed to further investigate the reproducibility of CCS values acquired on DTIMS and two TWIMS instruments applying different calibration approaches and evaluating factors potentially causing deviations. This work also included the investigation of CCS values for deprotonated ion which were not present in the above mentioned  $^{DT}CCS_{N_2}$  and  $^{TW}CCS_{N_2}$  comparison (Hinnenkamp et al., 2018). Furthermore, DTIMS derived CCS values were compared with predicted values employing two prediction models built with TWIMS derived data, namely an ANN based prediction tool and a MARS prediction model previously developed by (Bijlsma et al., 2017) and (Celma et al., 2022), respectively. Finally, the study also aimed to estimate cut-off values for database transfer from one instrumental design to another and the applicability of TWIMS-based prediction models for DTIMS measurements. This chapter adds to the detailed recommendations for the reporting of experimental IMS measurements published by (Gabelica et al., 2019) and it proposes the minimum and most relevant parameters to be reported for open-access databases of predicted CCS values. These recommendations will further contribute to a more uniform reporting of IM-MS data and will allow potential users to critically review and assess comparability with their own data. The presented results are expected to serve as a valuable additional guideline for the implementation of IM-MS in future studies on small molecule identifications.

## 3.2.2 Materials and Methods

### 3.2.2.1 Selection of standards

A set of 56 compounds, including five compound classes: triazoles, OPFRs, plasticizers and metabolites of the latter two, were selected for this comparison study. The selection of compounds was based on the following considerations: i) inclusion of various compound classes, incl. metabolites, ii) availability of ions in both ionization polarities, and iii) availability of reference standards, shared between laboratories. The selected compounds including their name, abbreviation, molecular formula, structure, SMILES, monoisotopic mass, InChi and InChiKey are summarized in **Table SI-3.2.1**. The

sources from which the reference standards were acquired can be found in Supplementary Information of **chapter 3.1 (Table SI-3.1.1)**.

### 3.2.2.2 DTIMS measurements

The  $^{DT}CCS_{N_2}$  values of the compounds included in this study were reported in **chapter 3.1.3** and are summarized in **Table SI-3.1.5**. **Chapter 3.1.2** includes a detailed description of the method used for the acquisition of  $^{DT}CCS_{N_2}$  values. In brief, all  $^{DT}CCS_{N_2}$  values were acquired on an Agilent 6560 DTIM-QTOF applying the single-field calibration method. For CCS calibration, the ESI low-concentration tune mix (Agilent Technologies, Santa Clara, USA) was used. The reference  $^{DT}CCS_{N_2}$  values of the tune mix ions were acquired by Stow et al. on a reference DTIMS system and are summarized in **Tables SI-3.2.2** and **SI-3.2.3** for positive and negative polarity, respectively. Each standard was introduced in the DTIMS-QTOF by direct injection at 1 ng/ $\mu$ L. For each standard, five measurements were conducted. The average  $^{DT}CCS_{N_2}$  value and (relative) standard deviations were reported (**Table SI-3.1.5**).

### 3.2.2.3 TWIMS measurements (VION)

The first set of  $^{TW}CCS_{N_2}$  values was acquired on a VION IMS-QTOF mass spectrometer (Waters, Milford, MA, USA), equipped with an electrospray ionization (ESI) interface operating in positive and negative ionization modes. The ionization source was operated applying the following voltages: capillary voltage of 0.8 kV; cone voltage 40 V with desolvation temperature set to 550 °C, and the source temperature to 120 °C. Nitrogen (N<sub>2</sub>) was used as the drying gas and nebulizing gas. The cone gas flow was 250 L/h and desolvation gas flow of 1000 L/h. MS data were acquired in HDMS<sup>E</sup> mode, over the range  $m/z$  50-1000, with N<sub>2</sub> as the drift gas, an IMS wave velocity of 250 m s<sup>-1</sup> and wave height ramp of 20-50 V. Leucine enkephalin ( $m/z$  556.2766 and  $m/z$  554.2620) was used for mass correction in positive and negative ionization modes, respectively. Two independent scans with different collision energies were acquired during the run: a collision energy of 6 eV for low energy and a ramp of 28-56 eV for high energy. A scan time of 0.3 s was set in both LE and HE functions. Nitrogen (purity  $\geq$  99.999%) was used as collision-induced dissociation (CID) gas. All data were examined using an in-house built accurate mass screening workflow within the UNIFI platform (version 1.9.4) from Waters Corporation. More details about the methodology followed can be found elsewhere (Celma et al., 2020).

### 3.2.2.4 TWIMS measurements (Synapt)

The second set of TWIMS derived  $^{TW}CCS_{N_2}$  values was acquired on a Synapt G2 HD mass spectrometer (Waters, Milford, MA, USA) equipped with a nano-electrospray ionization source. The ionization source was operated applying the following voltages: capillary voltage 2.5 kV, extraction cone 5 V; sample cone 35 V; trap collision energy 4.0 V; transfer collision energy 4.0 V; trap DC bias 35 V. The wave velocity was set to 1000 m/s at a constant wave height of 40 V. The gas pressures within the instrument were set as follows: desolvation gas flow 35 L/h (at a temperature of 150 °C); trap gas flow 0.4 mL/min; IMS gas flow 90 mL/min; helium cell gas flow 180 mL/min. For sample infusion, in-house pulled and gold-coated borosilicate capillaries were used.

For the positive ionization mode, calibration compounds proposed by Campuzano et al. were used to calculate  $^{TW}CCS_{N_2}$  values (Campuzano et al., 2012). For the negative ionization mode, poly-DL-alanine was chosen for CCS calibration based on the data published by (Bush et al., 2012). The molecular formulae, CAS numbers,  $m/z$  ratios and reference CCS values of the calibrants and QA compounds are summarized in **Table SI-3.2.4**.

Solutions of the calibration compounds were prepared in water/methanol (50/50; v/v) containing 0.1% formic acid at concentrations between 0.12 ng/ $\mu$ L and 0.61 ng/ $\mu$ L ( $10^{-6}$  M). Solutions of analytes and QA compounds were prepared at 1ng/ $\mu$ L in water/acetonitrile (50/50; v/v) containing 0.1% formic acid. To all infused solutions (both calibrants and analytes) leucine-enkephalin was spiked prior to infusion at a concentration of 5 ng/ $\mu$ L to be used as a lock-mass for mass calibration within data analysis. For the measurement of  $^{TW}CCS_{N_2}$  values, all analytes were infused in triplicate. The instrument was operated using the MassLynx software (version 4.1 SCN 781). After recalibration based on the added lock-mass of leucine-enkephalin, extracted ion mobilograms for each calibrant were obtained to allow establishing individual drift time values. The latter were then used to obtain the calibration curves for positive and negative ionization modes (**Figure SI-3.2.1**) that enable the calculation of  $^{TW}CCS_{N_2}$  values. The detailed workflow for  $^{TW}CCS_{N_2}$  calculations has been described in detail in previous studies (Hinnenkamp et al., 2018; Ruotolo et al., 2008).

### 3.2.2.5 Quality assurance measures

Within each instrumental design used in this study, QA measures were implemented. For DTIMS, the acquisition of  $^{DT}CCS_{N_2}$  values of nine QA compounds was conducted within each analytical batch. For these QA compounds reference  $^{DT}CCS_{N_2}$  values acquired on a reference DTIMS system were available (Stow et al., 2017). The QA measures and results of the DTIMS measurements have been described in detail in **chapter 3.1.3**.

For  $^{TW}CCS_{N_2}$  on the VION system, a set of nine QA compounds included in the System Suitability Test (SST) mix provided by the manufacturer was used to evaluate the accuracy and performance of the instrument as well as to ensure the repeatability of the measurements. The molecular formulae and reference CCS values of the Vion QA compounds are summarized in **Table SI-3.2.5**.

Terfenadine, sulfaguanidine, sulfadimethoxine and caffeine were used as QA compounds for measurements on the Synapt G2 system in positive and sulfaguanidine and sulfadimethoxine in negative ionization mode, respectively. The selection of QA compounds was based on the compounds included in the SST mix used for the TWIMS measurements on the Waters VION instrument and aimed to serve as a QA measure for measurement reproducibility between the two TWIMS set-ups used in this study. Reference CCS values of the QA compounds were provided by the manufacturer (**Table SI-3.2.4**).

#### 3.2.2.6 CCS predictions - Artificial Neural Network (ANN) based prediction model

ANN predictions of CCS values were made using Alyuda NeuroIntelligence 2.2 (Cupertino, CA) by applying a predictor previously developed and optimized (Bijlsma et al., 2017). Briefly, eight relevant molecular descriptors of the selected compounds were obtained from an Online Chemical Database ([www.ochem.eu](http://www.ochem.eu)) (Sushko et al., 2011). The ANN predictor, trained by means of a database of empirical  $^{TW}CCS_{N_2}$  values for 205 protonated small molecules, consisted of a neural network structured in three layers with 8-2-8-1 distribution. The relative error of CCS prediction was within 6% for the 95<sup>th</sup> percentile of all values for protonated ions and 8.7% for sodium adducts. Further details on the methodology can be found elsewhere (Bijlsma et al., 2017).

#### 3.2.2.7 CCS predictions - Multivariate Adaptive Regression Splines (MARS) based prediction model

CCS predictions using Multivariate Adaptive Regression Splines were performed as follows: the statistical model was trained with empirical  $^{TW}CCS_{N_2}$  values of a total number of 470 protonated ions and a set of 7 molecular descriptors obtained from the Online Chemical Database ([www.ochem.eu](http://www.ochem.eu)) (Sushko et al., 2011). The optimized model yielded an accuracy of 4.0% and 5.9% for the 95<sup>th</sup> percentile of predicted CCS values of protonated and deprotonated ions, respectively. Moreover, an additional and unique model was developed for predicting CCS values of sodium adducts obtaining an accuracy of 5.3% (95<sup>th</sup> percentile). More details of these prediction models can be found elsewhere (Celma et al., 2022).

### 3.2.3 Results and Discussion

#### 3.2.3.1 Quality control and quality assurance results

**Figure SI-3.2.2** summarizes the QA approaches implemented in the DTIMS and TWIMS measurements. This approach used within DTIMS measurements allowed the comparison with reference values obtained using the same instrumental design leading to low percent errors (PE) (all < 0.2%, see **chapter 3.1.3**). This confirmed the repeatability and accuracy of the DTIMS system used in this study.

Within the acquisition of  $^{TW}CCS_{N_2}$  values on the TWIMS VION system, the analysis of an SST mixture containing nine compounds was included (**Table SI-3.2.5**). For these compounds, reference CCS values were provided by the instruments' manufacturer. As it is the case for other reference CCS values used for TWIMS measurements (Bush et al., 2012; Campuzano et al., 2012), the provided CCS values were derived from DTIMS based measurements conducted on a modified Synapt G2 instrument. The VION instrument performance was satisfactory based on a 2% threshold for the deviation between expected and empirical CCS values.

The selection of suitable QA compounds for  $^{TW}CCS_{N_2}$  measurements on the Synapt instrument aimed to show an overlap with the SST compounds used on the VION system to investigate the reproducibility between the two TWIMS set-ups. Nevertheless, the QA approaches of both TWIMS systems must be viewed critically as in both cases experimental  $^{TW}CCS_{N_2}$  values are compared with DTIMS data. Thus, this approach represents rather a comparison of measurements between the different TWIMS set-ups than a fully independent QA approach.

The results of the Synapt G2 QA measurements are summarized in **Table SI-3.2.6**. Average APEs of 1.42% and 0.60% were observed for measurements in positive and negative ionization polarities, respectively. Both values fall within the 2% cut-off for the evaluation of SST measurements on the VION system and indicate a good reproducibility between the two TWIMS set-ups. Nevertheless, two QA compounds (sulfaguanidine and caffeine) showed deviations slightly above 2% in positive mode. These deviations must be interpreted critically as they do not indicate a poor instrumental performance, but rather a deviation between experimental TWIMS derived CCS values and the DTIMS based reference values. This will further be investigated in this study. The observed APEs can also be caused by the low CCS values observed for these compounds ( $CCS < 150 \text{ \AA}^2$ ) whereby even small deviations in measured  $t_A$  lead to high percent errors.

### 3.2.3.2 Selection of reference CCS values for further comparisons

The comparison of experimental DTIMS and TWIMS derived CCS values was based on a set of 56 standards including five compound classes: triazoles, OPFRs, plasticizers and metabolites of the latter two. Data on proton and sodium adducts, as well as deprotonated ions were included. In general, the comparison between sets of CCS values is commonly conducted through reporting the observed (absolute) percent errors (Hinnenkamp et al., 2018; Plante et al., 2019; Righetti et al., 2020). When applying this approach for the present study, the question about which set of CCS values to use as the reference set arose. Since none of the datasets was acquired with DTIMS stepped-field calibration, none of the datasets can be viewed as a calibrant-independent reference. To validate the two prediction models applied in this study, predicted CCS values have already been compared with the corresponding experimental TWIMS datasets (Bijlsma et al., 2017; Celma et al., 2022). Therefore, the use of the  $^{TW}CCS_{N_2}$  dataset as reference would reproduce this approach and exclude the available  $^{DT}CCS_{N_2}$  values from the comparison. Additionally, the choice of the reference dataset should allow the comparison of observed deviations between the different datasets. Therefore,  $^{DT}CCS_{N_2}$  values were used as reference for all calculations included in this study. Even though these values were acquired using the single-field calibration approach and thus required calibrants, the influence of the selected calibrants on the reproducibility of measurements was expected to be lower than for TWIMS calculations (Bush et al., 2012; Stow et al., 2017). Ultimately, the following equation (3.2.1) was applied for the calculation of percent errors between DTIMS and TWIMS derived or predicted CCS values:

$$\text{Error [\%]} = \left( \frac{CCS_{TWIMS/pred} - CCS_{DTIMS}}{CCS_{DTIMS}} \right) \cdot 100 \quad (3.2.1)$$

### 3.2.3.3 Comparison of experimental $^{TW}CCS_{N_2}$ and $^{DT}CCS_{N_2}$ values

For the 56 compounds, 108  $^{DT}CCS_{N_2}$  values were included in the DTIMS reference database as several of the compounds were detected both as proton and sodium adducts and/or in both ionization polarities. A total of 29  $[M+H]^+$  ions, 46  $[M+Na]^+$  ions and 33  $[M-H]^-$  ions were observed as reported in **chapter 3.1 (Table SI-3.1.5)**. The acquisition of  $^{TW}CCS_{N_2}$  values on the TWIMS VION instrument allowed the detection of a total of 94 ions which corresponded to 50 compounds available for the comparison (**Table SI-3.2.7**). Thus, six compounds were not detectable on the TWIMS VION set-up which was assumed to be caused by differences in ionization source parameters and geometries leading to differences in ionization efficiencies. The 94 detected ions included 22  $[M+H]^+$  ions and

40  $[M+Na]^+$  ions, as well as 32  $[M-H]^-$  ions. Measurements on the Synapt G2 system yielded a total of 97  $^{TW}CCS_{N_2}$  values which corresponded to 54 compounds detected (**Table SI-3.2.7**). Two compounds, tris(2-ethylhexyl) trimellitate and bisphenol A bis(diphenyl phosphate), were not detected on the Synapt G2 and VION instruments. Hence, for a total of 50 compounds, at least one CCS value was available from each of the instrumental set-ups. Within the 97 ions detected on the Synapt G2 system, 23  $[M+H]^+$ , 41  $[M+Na]^+$  and 33  $[M-H]^-$  ions were included.

As displayed in **Figure SI-3.2.3**, 83% and 82% of all included ions showed APEs  $< 2\%$  for the comparison of DTIMS data with the VION and Synapt systems, respectively. For protonated adducts, 64% (VION) and 57% (Synapt) of the observed ions had APEs  $< 2\%$ . For the sodium adducts, the observed percentages of ions with APEs  $< 2\%$  were 83% and 93% for the VION and Synapt systems, respectively. Deprotonated ions showed the lowest APEs within the comparison between TWIMS and DTIM systems. For both VION and Synapt G2 systems, only one  $[M-H]^-$  ion showed an APE  $> 2\%$  resulting in 97% of  $[M-H]^-$  ions with APEs  $< 2\%$ .

For a more detailed comparison, linear correlations between experimental DTIMS and TWIMS datasets were investigated. **Figure SI-3.2.4** shows the correlations observed between  $^{DT}CCS_{N_2}$  and  $^{TW}CCS_{N_2}$  values acquired on the VION (**Figure SI-3.2.4-A**) and Synapt (**Figure SI-3.2.4-B**) systems.

For both TWIMS systems, high correlation coefficients ( $R^2$ ) were observed indicating a good linear correlation between  $^{DT}CCS_{N_2}$  and  $^{TW}CCS_{N_2}$  datasets. However, the  $R^2$  of 0.9889 observed for VION data was slightly lower than for Synapt data ( $R^2 = 0.9929$ ). Based on a visual inspection of the linear plots, the higher correlation coefficient observed for Synapt data is assumed to be mainly caused by the lower deviations from the trendline observed for CCS values of plasticizer metabolites in comparison with VION derived data. Additionally, interpolated regression lines indicate that  $^{TW}CCS_{N_2}$  datasets can be correlated to  $^{DT}CCS_{N_2}$  datasets with a slope close to 1 (0.9999 for Vion and 1.0180 for Synapt). This indicates that deviations between  $^{DT}CCS_{N_2}$  and  $^{TW}CCS_{N_2}$  are negligible, and data can be well compared. In order to investigate CCS deviations more in detail and distinguish between ionization polarities and ion species, combined violin and box plots of the observed percent errors were created for each dataset (**Figure 3.2.1**).

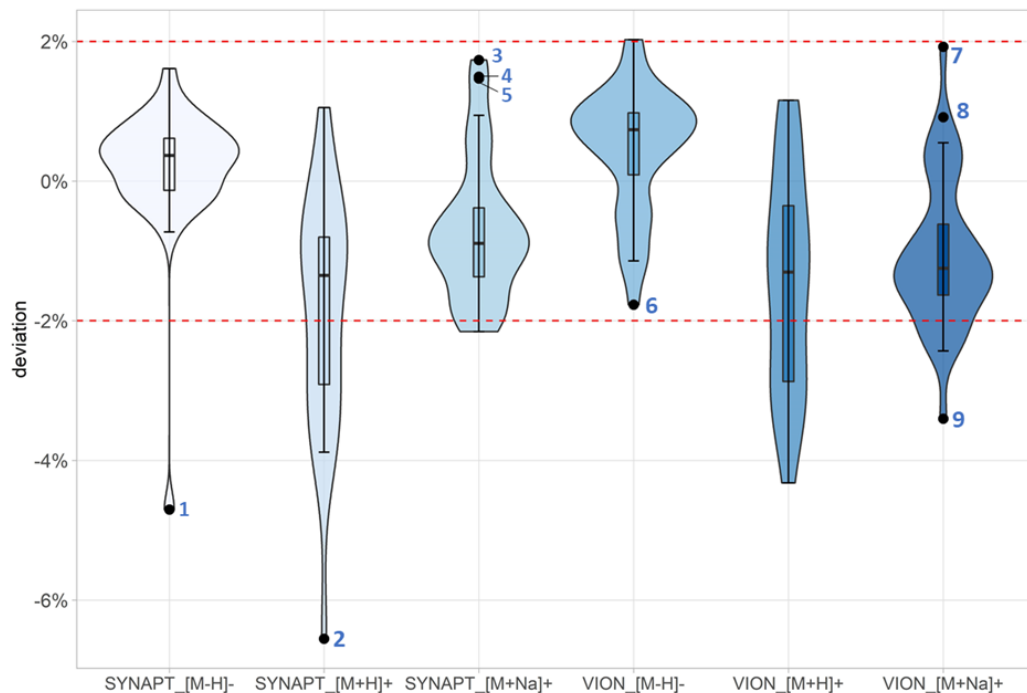


**Figure 3.2.1:** Combined box and violin plots of the error distributions observed when comparing  $^{DT}CCSN_2$  values with experimental  $^{TW}CCSN_2$  values *i.e.*, Synapt and Vion acquired in either positive or negative ionization mode. A distinction is made between proton and sodium adducts. The outliers observed for each dataset are numbered as follows: 1: BTR, 2: 5Cl-BTR, 3: DIDP, 4: DINCH, 5: DIDP, 6: pOH-TPHP, 7: EHDPPH, 8: MiBP, 9: TDCIPP. The full names of the mentioned compounds can be found in **Table SI-3.2.1**. A deviation of +/- 2% is indicated with a red dashed line.

**Figure 3.2.1** shows the combined violin and boxplots of error distributions observed for experimental TWIMS data acquired in either negative or positive ionization mode. Additionally, bar charts in **Figures SI-3.2.5** and **SI-3.2.6** summarize the percent errors observed for each ion of each individual compound on the Synapt-G2 and VION systems, respectively.

A threshold of 2% for the use of reference CCS values for compound identification was proposed, within a recent study (Celma et al., 2020). To evaluate the applicability of this threshold for databases acquired with different instrumental designs, all APEs observed in this study were compared to this cut-off value.

For  $[M+H]^+$ , both the Synapt G2 and VION systems show comparable error distributions with mean values of -1.9% and -1.4% and interquartile ranges (IQR) of 2.1% and 2.5%, respectively. The negative mean values indicate a clear off-set between DTIM and TWIMS derived data as most  $^{TW}CCSN_2$  values of proton adducts were lower than the corresponding  $^{DT}CCSN_2$  values. Except for the VION derived  $^{TW}CCSN_2$  value of TDCIPP with a deviation of -2.84%, all other deviating  $^{TW}CCSN_2$  values of  $[M+H]^+$  ions belonged either to the group of triazoles or organophosphate flame retardants (and metabolites) carrying at least two phenyl moieties. Triazoles represent the class with the lowest  $m/z$  values

( $m/z$  118 – 154) investigated in the study. Low  $m/z$  values result in lower CCS values for which even small absolute deviations can lead to high percentual errors. As it was previously observed for DPP (**chapter 3.1.3**), aromatic substitutes are assumed to lead to more compact ions resulting in lower  $^{DT}CCS_{N_2}$  values. The observed deviations of TWIMS data lead to the assumption that this effect has a higher influence within DTIMS measurements, indicating differing molecular conformations of the described compounds between TWIMS and DTIMS systems.

Interestingly, the error distributions observed for  $[M+Na]^+$  show a smaller spread in comparison to the protonated ions. The deviations calculated for  $[M+Na]^+$  showed mean values of -0.7% and -1.0% and IQRs of 1.0% and 1.0% for the Synapt and VION systems, respectively. A study by Hinnenkamp et al. reported slightly higher percent errors for sodium adducts in comparison to protonated ions: 87% of the included  $[M+Na]^+$  ions showed APEs < 2% while this percentage was 93% for  $[M+H]^+$  (Hinnenkamp et al., 2018). This was assumed to be caused by the fact that sodium adducts were not included in the ions used as calibrants for TWIMS measurements. However, these observations were not reproduced in this study which might be caused by different compound classes or sample sizes included in the two studies. Again, a negative off-set between  $^{TW}CCS_{N_2}$  and  $^{DT}CCS_{N_2}$  values was observed, as most  $^{TW}CCS_{N_2}$  values of  $[M+Na]^+$  ions were lower than the corresponding DTIMS values (**Figures SI-3.2.5 and SI-3.2.6**). From the VION derived  $^{TW}CCS_{N_2}$  values of  $[M+Na]^+$  ions, for seven values an APE > 2% was observed. Again, four of the seven values belonged to OPFRs and their metabolites carrying phenyl moieties. From the Synapt derived  $^{TW}CCS_{N_2}$  values of  $[M+Na]^+$  ions, three values showed an APE > 2%. All of these deviating values overlapped with the deviating VION derived values and included two OPFRs carrying phenyl moieties (triphenyl phosphate and diphenylcresyl phosphate). Except for mono-(3-carboxypropyl) phthalate (PE of -2.2%), all remaining deviating  $^{TW}CCS_{N_2}$  values of  $[M+Na]^+$  ions belong to the group of halogenated OPFRs and metabolites. Here, an influence of the applied calibrants is assumed. While the calibrants used for DTIMS measurements included several halogenated compounds (**Tables SI-3.2.2 and SI-3.2.3**), this was not the case for neither the Synapt nor the VION calibrations possibly leading to the observed high deviations for halogenated compounds. The latter was confirmed by the fact that the  $^{TW}CCS_{N_2}$  values of the  $[M+H]^+$  ion of 5-chlorobenzotriazole showed the highest deviation of all  $[M+H]^+$  ions for both the VION and Synapt systems (outlier nr. 2 in **Figure 3.2.1**). However, further investigations are needed to confirm these effects for larger sample sizes and wider  $m/z$  ranges.

Within the Synapt dataset of  $[M+Na]^+$  ions, three outliers (nr. 3-5 in **Figure 3.2.1**) with higher  $^{TW}CCS_{N_2}$  values in comparison to the corresponding  $^{DT}CCS_{N_2}$  values were identified. These values derived from DIDP, DINP and diisononyl cyclohexane 1,2-dicarboxylic acid (DINCH). For two of these compounds (DIDP and DINCH), the  $^{DT}CCS_{N_2}$  values of sodium adducts were lower than the corresponding values of protonated adducts which was in contrast to the trend observed for most other compounds included

in the  $^{DT}CCS_{N_2}$  database described in **chapter 3.1.3**. This observation was not reproduced for the Synapt derived  $^{TW}CCS_{N_2}$  values leading to the assumption of different ion conformations being observed between the TWIMS and DTIM systems due to slight differences in ionization processes. Alternatively, the fact that the used DIDP and DINCH standards represented mixtures of isomers could also lead to the described observation.

For the dataset acquired in negative ionization polarity, the observed deviations show a lower spread compared to the positive ionization mode. This reflects in the low IQRs of 0.7% and 0.9% for Synapt and VION datasets, respectively. Within the Synapt G2 dataset, all APEs of negatively charged ions were < 2%, except for the outlier indicated in **Figure 3.2.1** (outlier nr. 1,  $[M-H]^-$  ion of benzotriazole). For the VION dataset, one out of 32  $^{TW}CCS_{N_2}$  values of  $[M-H]^-$  ions showed an APE of > 2% ( $[M-H]^-$  ion of 2,4-di-(2-ethylhexyl) trimellitate). These observations indicate a high reproducibility of  $CCS_{N_2}$  values of  $[M-H]^-$  ions between different instrumental set-ups. The observed high reproducibility might be due to the fact that OPFRs and their metabolites (for which high deviations were observed in positive ionization polarity) were not included, since these compounds were not detected in negative ionization polarity. Additionally, an opposite trend in comparison to data obtained in positive ionization polarity was observed: both datasets showed a positive median error indicating a positive off-set between TWIMS and DTIM data. The included compound classes which differed between the datasets might have an influence on these effects.

Good correlations were observed between DTIM and TWIMS derived CCS values. Nevertheless, a few compounds showed high deviations of up to -4.3% and -6.6%. Several potential factors which might cause the high deviations could be identified and must be considered when interpreting the quality and reliability of the presented dataset. Firstly, an influence of the compound class can be assumed as most of the highly deviating values derived from a particular class (OPFRs and their metabolites carrying at least two phenyl substituents). These effects might be traced back to differences in ion conformations between DTIM and TWIMS systems for certain classes. Secondly, an effect of the applied calibration approach on CCS deviations is considered possible. Several previous studies have characterized the influence of the calibrants applied for TWIMS measurements and addressed the advantage of a match in compound class and charge state between calibrants and analytes. However, most of these studies focused on proteomic and lipidomic applications, which means that only a limited amount of studies including small molecules applications can be found (Bush et al., 2010; Gelb et al., 2014; Hines et al., 2016). Recently, a study assessed the influence of different calibration approaches on TWIMS measurements of steroids evaluating and comparing the observed bias. Additionally, a new set of reference DTIM derived CCS values for TWIMS calibration was proposed whose implementation improved the reproducibility of CCS measurements on different instrumental set-ups (Feuerstein et al., 2022b). These observations highlight the need of similar evaluations of different calibration approaches for the analysis of CECs

and a potential implementation of the newly proposed sets of reference CCS values. A critical manual evaluation of the calibration approaches applied for the compilation of TWIMS derived databases thus remains crucial before database implementation for different instrumental designs and/or calibration approaches. Lastly, the described limitations confirm that CCS values represent empirical measurements which are influenced by several factors and do not allow the establishment of a 'true CCS value'. It is recommended to assess potential deviations based on a subset of reference standards of the class of interest prior to applying a database acquired with a different instrumental design. Subsequently, the cut-off value of 2% which has been proposed previously might need to be adjusted for databases deriving from different instrumental designs or different calibration approaches (Celma et al., 2020).

#### 3.2.3.4 Comparison of predicted CCS and experimental $^{DT}CCS_{N_2}$ values

The experimental  $^{DT}CCS_{N_2}$  values were compared with predicted datasets which derived from two different prediction models, namely an ANN and a MARS based model (Bijlsma et al., 2017; Celma et al., 2022). Both models were built using experimental TWIMS derived CCS values. To the best of our knowledge, this is the first study investigating the capabilities of these models in predicting CCS values for DTIM measurements.

During the development of the ANN based prediction model, an APE < 6% was observed for 95% of the protonated ions when comparing predicted with experimental  $^{TW}CCS_{N_2}$  values. To be able to compare these observations, the same threshold (6%) was applied to assess the deviations of ANN based predicted CCS values (further referred to as  $CCS_{ANN}$ ) of  $[M+H]^+$  ions presented here. A 6% threshold was also used to assess deviations of  $[M-H]^-$  ions, even though it must be noted that the ANN based model was built using  $[M+H]^+$  data, but not evaluated for  $[M-H]^-$  ions within its development. For  $[M+Na]^+$  ions, an APE of 8.7% was reported for the 95<sup>th</sup> percentile confidence interval (Bijlsma et al., 2017). This higher value is caused by the fact that the ANN based prediction model has been developed without the inclusion of  $[M+Na]^+$  ions in the training, validation and blind datasets. On the contrary to the  $[M-H]^-$  ions,  $[M+Na]^+$  data has been evaluated within its development. Hence, a threshold of 8.7% was applied for  $[M+Na]^+$  ions as higher APEs can be assumed for this ion species.

**Figure 3.2.2** shows the combined violin and boxplots of the error distributions observed for predicted CCS values differentiating between prediction models and ion species. Datapoints for individual compounds can be found in **Table SI-3.2.8**. For the linear correlation between  $^{DT}CCS_{N_2}$  and  $CCS_{ANN}$  values, a correlation coefficient of  $R^2 = 0.9305$  and a slope of 0.9753 were observed (see **Figure SI-3.2.7-A**). For  $[M+H]^+$  ions, the ANN based model showed a median APE of -1.8% and an IQR of 1.6%. Due to the small IQR (in comparison to other ion species) which influences the upper and lower fence (defined as the  $Q_3/Q_1 \pm 1.5 \times IQR$ ), several outliers were observed (see **Figure 3.2.2**).

Similar to the comparison of experimental  $^{DT}CCS_{N_2}$  and  $^{TW}CCS_{N_2}$  values, all observed outliers belonged to either OPs (and metabolites) with at least two aromatic moieties or low-mass (halogenated) triazoles. Nevertheless, most of the observed outliers fall within the threshold of  $\pm 6\%$  resulting in 93.1% of the  $CCS_{ANN}$  values showing an APE  $< 6\%$ . Comparable results were obtained for  $CCS_{ANN}$  values of  $[M-H]^-$  ions of which 93.9% showed APEs  $< 6\%$  with only two values exceeding this threshold ( $CCS_{ANN}$  of mono(2-ethylhexyl) terephthalate and mono(2-ethyl-5-hydroxyhexyl) terephthalate). Therefore, for  $[M-H]^-$  and  $[M+H]^+$ , it can be concluded that the ANN based prediction model can successfully be applied for DTIM measurements of small molecules structurally similar to the compound classes investigated here. Again, the deviations observed for some classes point out the necessity of evaluating the applicability of the model based on a subset of reference standards.

$CCS_{ANN}$  values of  $[M+Na]^+$  ions show the highest APE with a median value of -3.7% and an IQR of 6.8%. From the 46  $[M+Na]^+$  ions included in the comparison, 80.4 % showed an APE below the applied threshold ( $< 8.7\%$ ). Similar to the conclusions made within the development of the ANN based model, a higher cut-off value is recommended when applying the model for the prediction of  $[M+Na]^+$  ions within DTIM measurements (see below).

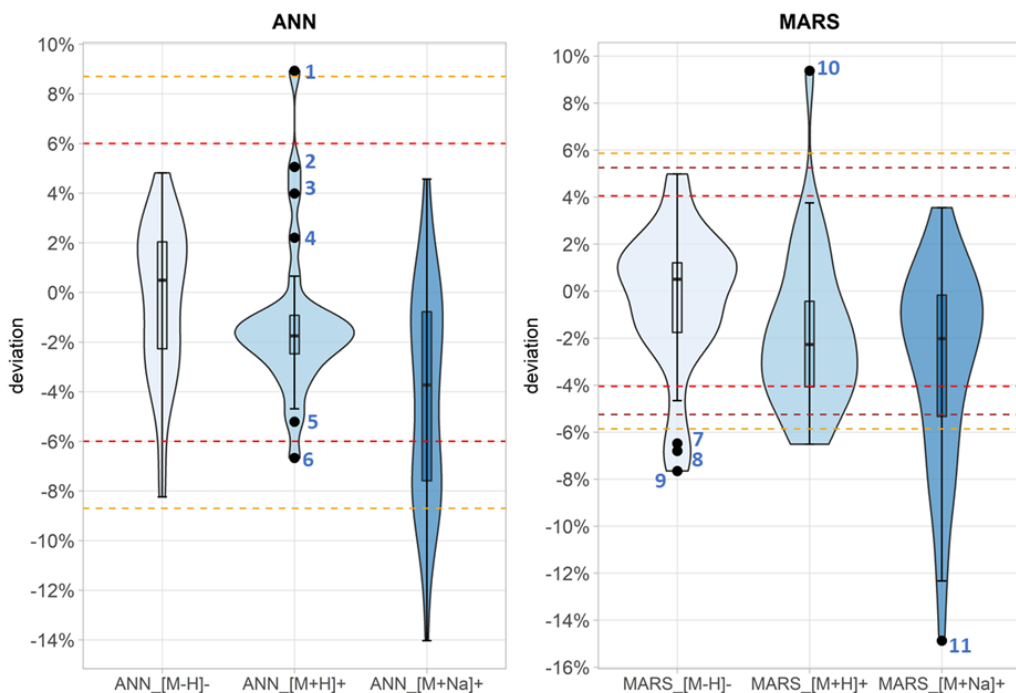


**Figure 3.2.2:** Combined violin and boxplots of the error distributions observed when comparing  ${}^{\text{DT}}\text{CCS}_{\text{N}_2}$  values with predicted CCS values deriving from Artificial Neural Network (ANN) and Multivariate Adaptive Regression Splines (MARS) based models. For data in positive ionization polarity, a distinction between proton and sodium adducts is made. The outliers observed for each dataset are numbered as follows: 1: Fyroflex BDP, 2: 5OH-EHDPPH, 3: Fyroflex RDP, 4: TOTP, 5: 4OH-PhP, 6: 5Cl-BTR, 7: 2,4-DEHTM, 8: MEHTP, 9: 5OH-MEHTP, 10: Fyroflex BDP, 11: TOTM. The full names of the mentioned compounds can be found in **Table SI-3.2.1**. The thresholds applied for the comparisons are indicated with dashed lines. These thresholds are based considering the 95<sup>th</sup> confidence interval of each model. For the ANN based model, thresholds of 6% ( $[\text{M}+\text{H}]^+$  and  $[\text{M}-\text{H}]^-$  ions; red dashed line) and 8.7% ( $[\text{M}+\text{Na}]^+$ ; orange dashed line) were applied. MARS based data was compared based on thresholds of 4.1% (red dashed line), 5.9% (orange dashed line) and 5.3% (brown dashed line) for  $[\text{M}+\text{H}]^+$ ,  $[\text{M}+\text{Na}]^+$  and  $[\text{M}-\text{H}]^-$  ions, respectively.

In contrast to the ANN based prediction model, the MARS based model was validated for all ion species included here (*i.e.*,  $[\text{M}+\text{H}]^+$ ,  $[\text{M}+\text{Na}]^+$  and  $[\text{M}-\text{H}]^-$  ions). This allowed the reporting of APEs observed for the 95<sup>th</sup> percentile of the datapoints for each ion species separately (Celma et al., 2022). In detail, these APEs corresponded to 4.1%, 5.9% and 5.3% for  $[\text{M}+\text{H}]^+$ ,  $[\text{M}-\text{H}]^-$  and  $[\text{M}+\text{Na}]^+$  ions, respectively, which will be used as thresholds to access the deviations presented in this study.

From the CCS values predicted for  $[\text{M}+\text{H}]^+$  ions applying the MARS based model (further referred to as  $\text{CCS}_{\text{MARS}}$ ), 71.9% showed an APE < 4.0%. This corresponds to 9 out of 32  $\text{CCS}_{\text{MARS}}$  values for  $[\text{M}+\text{H}]^+$  ions showing an APE above the applied threshold. Two of these deviating  $\text{CCS}_{\text{MARS}}$  values were also observed as deviating  $\text{CCS}_{\text{ANN}}$  values, namely BDP ( $\text{CCS}_{\text{MARS}}$  with a deviation of 9.38%) and 5Cl-BTR ( $\text{CCS}_{\text{MARS}}$  with a deviation of -6.52%). Additionally, the  $\text{CCS}_{\text{MARS}}$  values of DIDP, DINP and DINCH showed APEs > 4.0%. The same assumptions as described about the causes of these deviations can be applied here.

For the  $[M+Na]^+$  ions, 73.9% of which showed an APE <5.3%, a median deviation of -2.3% and an IQR of 5.2% were observed. This indicates higher (i.e., closer to zero) median values and a smaller IQR than observed for  $CCS_{ANN}$  values of sodium adducts. Within the development of the MARS based model, a separate model was developed for the prediction of CCS values of  $[M+Na]^+$  ions. Thereby, experimental values of  $[M+Na]^+$  adducts were included in the training dataset to account for the higher volume and particularities derived from the allocation of the sodium ion within the molecular structure influencing the shape and size of ions (Bijlsma et al., 2017). The lower APEs observed for  $CCS_{MARS}$  values of sodium adducts confirm the added value of the described approach indicating that the MARS based model is more suitable for a reliable prediction of CCS values for this ion species. Nevertheless, the APEs reported here still show higher deviations than observed for the comparison with experimental TWIMS based values (Celma et al., 2022) indicating that additional factors influence the accuracy of the prediction.

For  $CCS_{MARS}$  values of  $[M-H]^-$  ions, a median deviation of 0.5% and an IQR of 3.0% were observed. 90.0% of the  $CCS_{MARS}$  values of  $[M-H]^-$  ions showed an APE < 5.9%. This corresponds to 3 out of 30  $CCS_{MARS}$  values with an APE >5.9% which are indicated as outliers in **Figure 3.2.2**. Two of the corresponding compounds (MEHTP and 5-HO-MEHTP) had also shown high deviations within their ANN based predicted values. Based on the low number of terephthalates and metabolites included in the dataset, it cannot be stated whether particular structural characteristics or other factors cause the observed high deviations. The same applies to the high deviation observed for the  $CCS_{MARS}$  value of the  $[M-H]^-$  ion of 2,4-DEHTM (-6.48%).

**Table 3.2.1:** The 95<sup>th</sup> percentiles observed for the absolute percent errors (APEs) between experimental  $^{DT}CCS_{N_2}$  values and predicted CCS values. The latter were predicted applying Artificial Neural Network (ANN) and Multivariate Adaptive Regression Splines (MARS) based models.

Ion species	95 <sup>th</sup> percentile of observed APEs	
	ANN	MARS
$[M+H]^+$	6.08%	6.38%
$[M+Na]^+$	10.29%	11.13%
$[M-H]^-$	5.70%	6.66%

The percentages of ions showing an APE below the applied thresholds are summarized in **Table SI-3.2.9**. Additionally, the 95<sup>th</sup> percentiles of the absolute percent errors observed for each ion species were calculated (**Table 3.2.1**). This aimed at estimating thresholds recommended for future applications of the ANN and MARS based models for DTIMS measurements. From the observed 95<sup>th</sup> percentiles the conclusion might be drawn that the ANN based model provides better results for DTIMS predictions, as all reported values are lower in comparison to the MARS based model. However, in contrast to the 95<sup>th</sup> percentiles which were reported within the development of the

prediction models (Bijlsma et al., 2017; Celma et al., 2022) the values reported in this study are based on a smaller sample size. Thus, after grouping the observed APEs by size, the reported 95<sup>th</sup> percentile is strongly influenced by the data points determining the 95% cut-off. Due to the small percentage range and sample size investigated, even slight deviations of these values towards higher APEs can have strong effects on the calculated percentiles. Especially for  $[M+Na]^+$  ions, this approach does not reflect the added advantages of the MARS based model described above, thus not allowing the direct use of the 95<sup>th</sup> percentiles as proposed thresholds. Nevertheless, the 95<sup>th</sup> percentiles reported reflect deviations between experimental  $^{DT}CCS_{N_2}$  values and predicted data which are comparable to the observations reported within the development of the prediction models, thus indicating their applicability for DTIMS measurements. It is recommended to use the reported 95<sup>th</sup> percentiles in combination with an assessment of possible deviations for the compound class of interest to estimate applicable thresholds. The MARS based model is recommended for the prediction of  $[M+Na]^+$  ions (Celma et al., 2022).

### 3.2.3.5 Comparison of predicted CCS and experimental $^{DT}CCS_{N_2}$ values

The acquisition of CCS values represents a measurement of empirical values rather than an absolute and constant physical property. Therefore, a detailed reporting of experimental settings, as well as applied QA measures is crucial to estimate the influence of these parameters on IMS-MS measurements and their reproducibility using other instrumental designs. Parameters recommended to be reported for experimental CCS values have been discussed in detail by (Gabelica et al., 2019) and include mainly mobility device hardware parameters, used drift gas and calibrants or QC compounds. The observed deviations between  $^{DT}CCS_{N_2}$  and  $^{TW}CCS_{N_2}$  values described for some of the compound classes investigated in the presented study confirm the necessity of a unified reporting of experimental parameters to trace back possible causes for such findings. Adding to these recommendations, this study proposes a set of parameters recommended to be reported for CCS prediction models in order to highlight their usefulness for other instrumental designs (**Table 3.2.2**).

**Table 3.2.2:** Recommended parameters for the reporting of CCS prediction models.

Parameter	Recommended information to report
General	General aim of the development. For which compound classes is the model being developed? Which experimental datasets will be used for the development?
Prediction model	Characteristics of applied prediction model; settings and descriptors used for training of the model
Training set	Detailed information on the identity of compounds used for training of the model; ion species included in the training set; detailed description of experimental parameters used for the acquisition of experimental CCS values used for training of the model
Validation results	Description of results obtained after validating the developed model; description of validation dataset and detailed reporting of results for each ion species. Which thresholds should be applied in future applications of the prediction model?
Inter-lab validation	Evaluation of prediction performance of the model for the particular instrument in use. Study of accuracy of prediction for a small set of molecules to support the decisions on suspect substances.

### 3.2.4 Conclusions

A dataset containing 106 DTIMS derived  ${}^{\text{DT}}\text{CCS}_{\text{N}_2}$  values including  $[\text{M}+\text{H}]^+$ ,  $[\text{M}+\text{Na}]^+$  and  $[\text{M}-\text{H}]^-$  ions was compared with both experimental (TWIMS derived)  ${}^{\text{TW}}\text{CCS}_{\text{N}_2}$  values and predicted CCS values.  ${}^{\text{TW}}\text{CCS}_{\text{N}_2}$  values were acquired on a VION and Synapt G2 system showing absolute errors  $< 2\%$  for 83% and 82% of the values, respectively, indicating a good reproducibility between different instrumental designs. Moreover, good linear correlations were observed for both systems resulting in correlation coefficients of  $R^2 = 0.9889$  (VION) and  $R^2 = 0.9929$  (Synapt). Nevertheless, deviations of up to  $-6.55\%$  were observed for a few compounds, most of which belonged to the class of OPFRs and their metabolites carrying at least two phenyl substituents. Additionally, the applied calibration approaches could not be excluded as a potential cause for the observed deviations. These findings point out that potential biases of experimental databases built on data acquired by a different instrumental set-up, need to be evaluated prior to its implementation.

With regards to CCS prediction models, the 95<sup>th</sup> percentiles of deviations reported for  $[\text{M}+\text{H}]^+$  and  $[\text{M}-\text{H}]^-$  ions between experimental  ${}^{\text{DT}}\text{CCS}_{\text{N}_2}$  values and predicted data were comparable to the values reported within the development of the ANN and

MARS based models, indicating their applicability for DTIMS measurements. These percentiles can be used to establish thresholds to be applied in future DTIMS based studies. However, different parameters such as the aim and compound class for which the model is developed should be considered prior to its applications.

## Supplementary Information – Chapter 3.2

**Table SI-3.2.1:** Compounds included in this chapter. For each compound the name, abbreviation, molecular formula, structure, SMILES, monoisotopic mass, InChi and InChiKey are included. (The table can be openly assessed in the Supporting Information of online version of the corresponding article (Table S1): <https://doi.org/10.1016/j.aca.2022.340361>)

**Table SI-3.2.2:** Reference CCS values published by Stow et al. (2017) for compounds included in the ESI low-concentration tune mix (Agilent Technologies, Santa Clara, USA) for positive ionization mode.

Compound	Formula	$m/z$ [M+H] <sup>+</sup>	<sup>DT</sup> CCS <sub>N2</sub> [Å <sup>2</sup> ] for [M+H] <sup>+</sup>
Betaine	C <sub>5</sub> H <sub>11</sub> NO <sub>2</sub>	118.0863	121.30
Hexamethoxyphosphazine	C <sub>6</sub> H <sub>18</sub> N <sub>3</sub> O <sub>6</sub> P <sub>3</sub>	322.0481	153.73
Hexakis(2,2-difluoroethoxy)-phosphazine	C <sub>12</sub> H <sub>18</sub> F <sub>12</sub> N <sub>3</sub> O <sub>6</sub> P <sub>3</sub>	622.0290	202.96
Hexakis(1H, 1H, 3H-tetrafluoropropoxy)phosphazine	C <sub>18</sub> H <sub>18</sub> F <sub>24</sub> N <sub>3</sub> O <sub>6</sub> P <sub>3</sub>	922.0098	243.64
Hexakis(1H, 1H, 4H-hexafluorobutyloxy)phosphazine	C <sub>24</sub> H <sub>18</sub> F <sub>36</sub> N <sub>3</sub> O <sub>6</sub> P <sub>3</sub>	1221.9906	282.20
Hexakis(1H, 1H, 5H-octafluoropentoxy)phosphazine	C <sub>30</sub> H <sub>18</sub> F <sub>48</sub> N <sub>3</sub> O <sub>6</sub> P <sub>3</sub>	1521.9715	316.96

**Table SI-3.2.3:** Reference CCS values published by Stow et al. (2017) for compounds included in the ESI low-concentration tune mix (Agilent Technologies, Santa Clara, USA) for negative ionization mode.

Compound	Formula	$m/z$	Ion	<sup>DT</sup> CCS <sub>N2</sub> [Å <sup>2</sup> ]
Tris(trifluoromethyl)-1, 3, 5-triazine	C <sub>6</sub> F <sub>9</sub> N <sub>3</sub>	118.0863	[M+OH] <sup>-</sup>	121.30
Tris(heptafluoropropyl)-1, 3, 5-triazine	C <sub>12</sub> F <sub>21</sub> N <sub>3</sub>	322.0481	[M+OH] <sup>-</sup>	153.73
Hexakis(1H, 1H, 3H-tetrafluoropropoxy)phosphazine	C <sub>18</sub> H <sub>18</sub> F <sub>24</sub> N <sub>3</sub> O <sub>6</sub> P <sub>3</sub>	622.0290	[M+C <sub>2</sub> HF <sub>3</sub> O <sub>2</sub> -H] <sup>-</sup>	202.96
Hexakis(1H, 1H, 4H-hexafluorobutyloxy)phosphazine	C <sub>24</sub> H <sub>18</sub> F <sub>36</sub> N <sub>3</sub> O <sub>6</sub> P <sub>3</sub>	922.0098	[M+C <sub>2</sub> HF <sub>3</sub> O <sub>2</sub> -H] <sup>-</sup>	243.64
Hexakis(1H, 1H, 5H-octafluoropentoxy)phosphazine	C <sub>30</sub> H <sub>18</sub> F <sub>48</sub> N <sub>3</sub> O <sub>6</sub> P <sub>3</sub>	1521.9715	[M+C <sub>2</sub> HF <sub>3</sub> O <sub>2</sub> -H] <sup>-</sup>	316.96

**Table SI-3.2.4:** Calibration and QA compounds selected for the measurements of  $^{TW}CCS_{N_2}$  values (Synapt G2). The reported reference CCS values are based on Campuzano et al. (2012) (for calibrants) and on values provided by the instruments' manufacturer (for QA compounds). For calibrants, the measured drift times (DT) which were used to obtain the calibration curves are indicated.

Type	Name	Formula	Monoisotopic mass	$m/z$ ratio	Adduct	Ref. CCS [ $\text{\AA}^2$ ]	Measured DT [ms]	CAS number
Calibrant - ESI+	N-Ethylaniline	$C_8H_{11}N$	121.0891	122.0964	$[M+H]^+$	124.50	2.55	103-69-5
	Acetaminophen	$C_8H_9NO_2$	151.0633	152.0706	$[M+H]^+$	130.40	2.77	103-90-2
	Alprenolol	$C_{15}H_{23}NO_2$	249.1729	250.1802	$[M+H]^+$	157.50	4.23	13655-52-2
	Ondansetron	$C_{18}H_{19}N_3O$	293.1528	294.1601	$[M+H]^+$	172.70	4.94	99614-02-5
	Clozapine N-oxide	$C_{18}H_{19}ClN_4O$	342.1247	343.1320	$[M+H]^+$	180.60	5.53	34233-69-7
	Colchicine	$C_{22}H_{25}NO_6$	399.1682	400.1755	$[M+H]^+$	196.20	6.40	64-86-8
	Verapamil	$C_{27}H_{38}N_2O_4$	454.2832	455.2904	$[M+H]^+$	210.00	7.32	52-53-9
	Reserpine	$C_{33}H_{40}N_2O_9$	608.2734	609.2807	$[M+H]^+$	254.30	10.20	50-55-5
Calibrant - ESI-	H-(Ala) <sub>3</sub> -OH	$C_9H_{17}N_3O_4$	231.1219	230.1146	$[M-H]^-$	155.2	3.69	56-41-7
	H-(Ala) <sub>4</sub> -OH	$C_{12}H_{22}N_4O_5$	302.1590	301.1517	$[M-H]^-$	169.0	4.39	56-41-7
	H-(Ala) <sub>5</sub> -OH	$C_{15}H_{27}N_5O_6$	373.1961	372.1889	$[M-H]^-$	183.1	5.37	56-41-7
	H-(Ala) <sub>6</sub> -OH	$C_{18}H_{32}N_6O_7$	444.2332	443.2260	$[M-H]^-$	198.1	6.29	56-41-7
	H-(Ala) <sub>7</sub> -OH	$C_{21}H_{37}N_7O_8$	515.2704	514.2631	$[M-H]^-$	211.4	7.27	56-41-7
	H-(Ala) <sub>8</sub> -OH	$C_{24}H_{42}N_8O_9$	586.3075	585.3002	$[M-H]^-$	224.6	8.19	56-41-7
	H-(Ala) <sub>9</sub> -OH	$C_{27}H_{47}N_9O_{10}$	657.3446	656.3373	$[M-H]^-$	238.6	9.28	56-41-7
	H-(Ala) <sub>10</sub> -OH	$C_{30}H_{52}N_{10}O_{11}$	728.3817	727.3744	$[M-H]^-$	251.9	10.25	56-41-7
QA compounds	Terfenadine	$C_{32}H_{41}NO_2$	471.3137	472.3210	$[M+H]^+$	228.70		50679-08-8
	Sulfaguanidine	$C_7H_{10}N_4O_2S$	214.0524	215.0597	$[M+H]^+$	146.80		57-67-0
	Sulfaguanidine	$C_7H_{10}N_4O_2S$	214.0524	213.0452	$[M-H]^-$	145.20		57-67-0
	Sulfadimethoxine	$C_{12}H_{14}N_4O_4S$	310.0736	311.0809	$[M+H]^+$	168.40		122-11-2
	Sulfadimethoxine	$C_{12}H_{14}N_4O_4S$	310.0736	309.0663	$[M-H]^-$	170.10		122-11-2
	Caffeine	$C_8H_{10}N_4O_2$	194.0804	195.0877	$[M+H]^+$	138.20		58-08-2

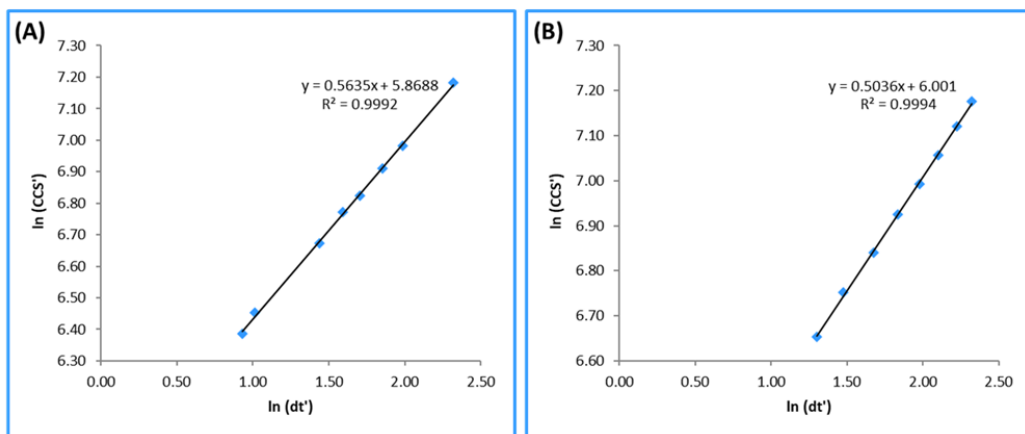


**Figure SI-3.2.1:** Calibration curves derived from the data obtained for calibration compounds (Table SI-3.2.3) and used for the calculation of TWIMS derived CCS values (Synapt G2). Calibration curves were obtained in positive (A) and negative (B) ionization modes. Calculations of TWIMS derived CCS values were based on Hinnenkamp et al. (2018).

**Table SI-3.2.5:** SST compounds selected for the measurements of  $^{TW}CCS_{N_2}$  values (Vion IMS QTOF). The reported reference CCS values are based on values provided by the instruments' manufacturer.

Name	Formula	Adduct	$m/z$ ratio	Ref. CCS [ $\text{\AA}^2$ ]
Acetaminophen	$C_8H_9NO_2$	-H	150.0651	131.5
		+H	152.0706	130.4
Caffeine*	$C_8H_{10}N_4O_2$	+H	195.0877	138.2
Leucine Enkephalin	$C_{28}H_{37}N_5O_7$	-H	554.2620	225.4
		+H	556.2766	229.8
Reserpine	$C_{33}H_{40}N_2O_9$	-H	607.2661	265.2
		+H	609.2807	252.3
Sulfadimeth- oxine	$C_{12}H_{14}N_4O_4S$	-H	309.0663	170.1
		+H	311.0809	168.4
Sulfaguanidine	$C_7H_{10}N_4O_2S$	-H	213.0452	145.2
		+H	215.0597	146.8
Terfenadine*	$C_{32}H_{41}NO_2$	+H	472.3210	228.7
Val-tyr-val	$C_{19}H_{29}N_3O_5$	-H	378.2034	192.5
		+H	380.2180	191.7
Verapamil*	$C_{27}H_{38}N_2O_4$	+H	455.2904	208.8

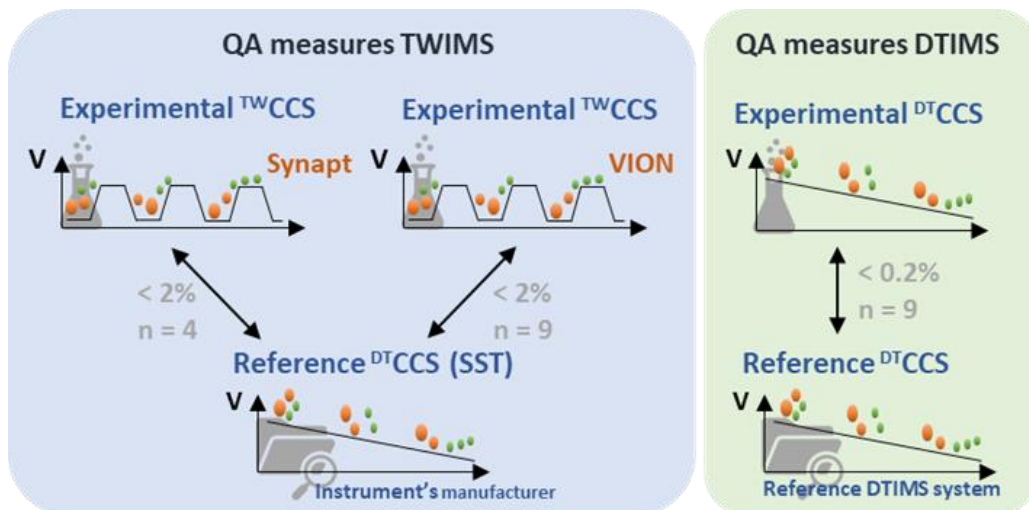


**Figure SI-3.2.2:** Schematic overview of the QA measures implemented in TWIMS (blue) and DTIMS (green) measurements. SST: system suitability test mixture.

**Table SI-3.2.6:** Results for QA compounds acquired on the Synapt G2 instrument. The average CCS values of three consecutive measurements are reported. The reference CCS values are based on values provided by the instruments' manufacturer.

Name	Formula	Adduct	$m/z$ ratio	Ref. CCS [ $\text{\AA}^2$ ]	$\bar{x}$ CCS <sub>exp.</sub> [ $\text{\AA}^2$ ]	APE [%]
Caffeine	$\text{C}_8\text{H}_{10}\text{N}_4\text{O}_2$	+H	195.0877	138.2	134.88	2.40
Sulfadimethoxine	$\text{C}_{12}\text{H}_{14}\text{N}_4\text{O}_4\text{S}$	-H	309.0663	170.1	169.76	0.20
		+H	311.0809	168.4	167.26	0.68
Sulfaguanidine	$\text{C}_7\text{H}_{10}\text{N}_4\text{O}_2\text{S}$	-H	213.0452	145.2	143.75	1.00
		+H	215.0597	146.8	143.24	2.43
Terfenadine	$\text{C}_{32}\text{H}_{41}\text{NO}_2$	+H	472.3210	228.7	229.12	0.18
					Average POS	1.42
					Average NEG	0.60

**Table SI-3.2.7:** Experimental  $\text{TWCCS}_{\text{N}_2}$  values acquired on the Synapt-G2 and VION instruments. (The table can be openly assessed in the Supporting Information of online version of the corresponding article (Table S7): <https://doi.org/10.1016/j.aca.2022.340361>)

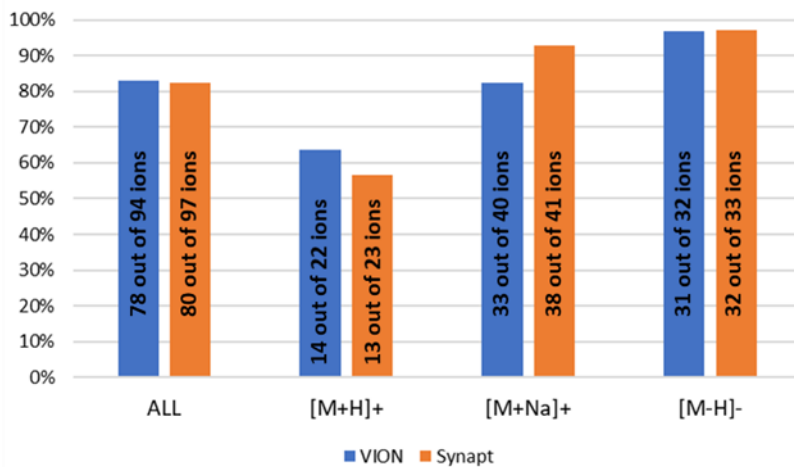


**Figure SI-3.2.3:** Percentage of ions showing absolute percent errors <2% for the comparison between <sup>14</sup>C<sub>CS</sub><sub>N<sub>2</sub> and <sup>13</sup>C<sub>CS</sub><sub>N<sub>2</sub> values. For VION and Synapt systems the calculations displayed as “ALL” are based on a total of 94 and 97 ions included in the comparison, respectively. A total of 22 and 23 [M+H]<sup>+</sup> ions as well as 40 and 41 [M+Na]<sup>+</sup> ions were included for the VION and Synapt systems, respectively. The calculations for deprotonated ions are based on a total of 32 (VION) and 33 (Synapt) ions.</sub></sub>

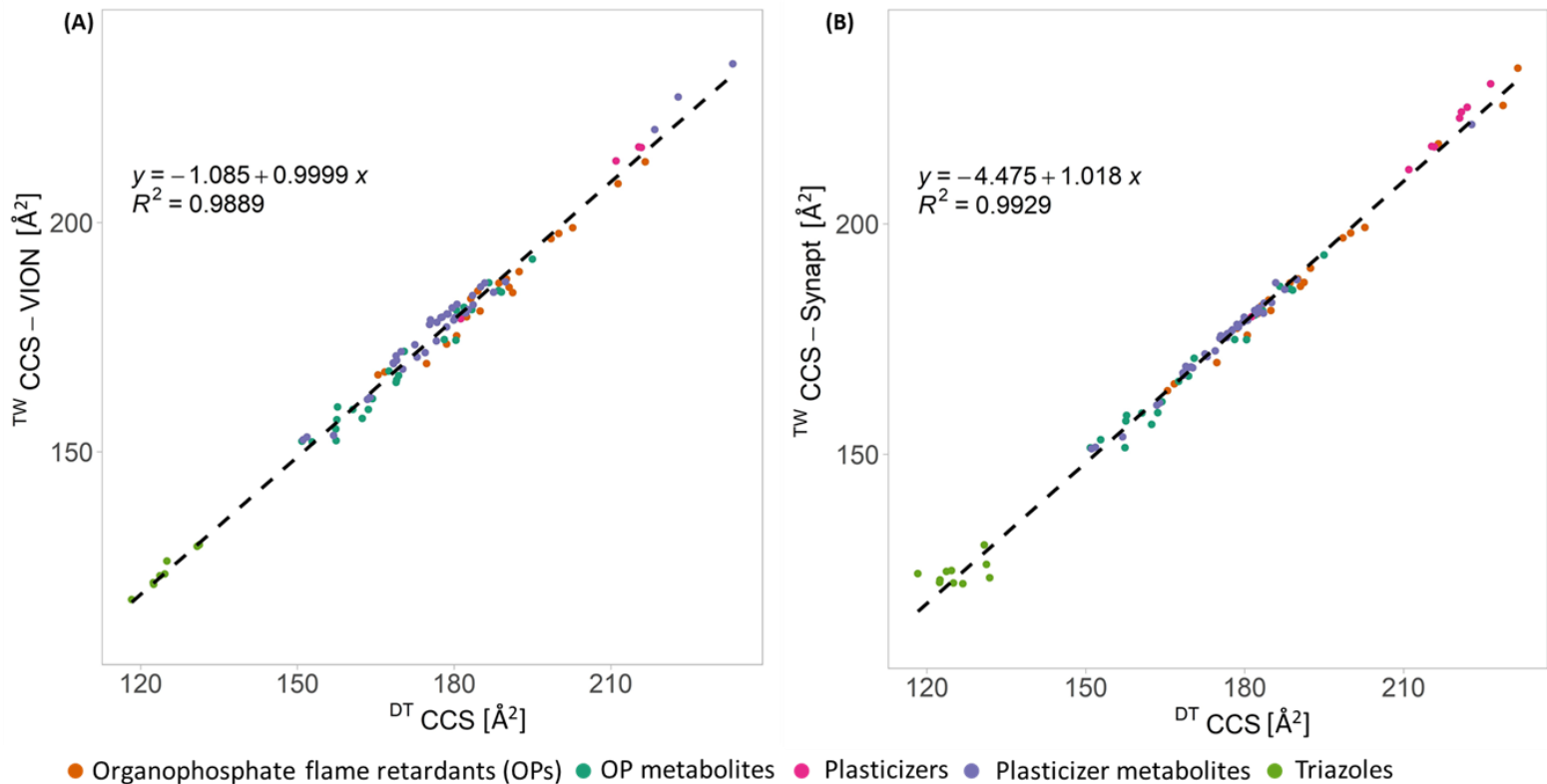


**Figure SI-3.2.4:** Linear correlations observed between DTIMS and TWIMS derived CCS values. Latter were measured on a VION (A) and Synapt (B) system. For each regression line the equation and correlation coefficient ( $R^2$ ) are indicated.

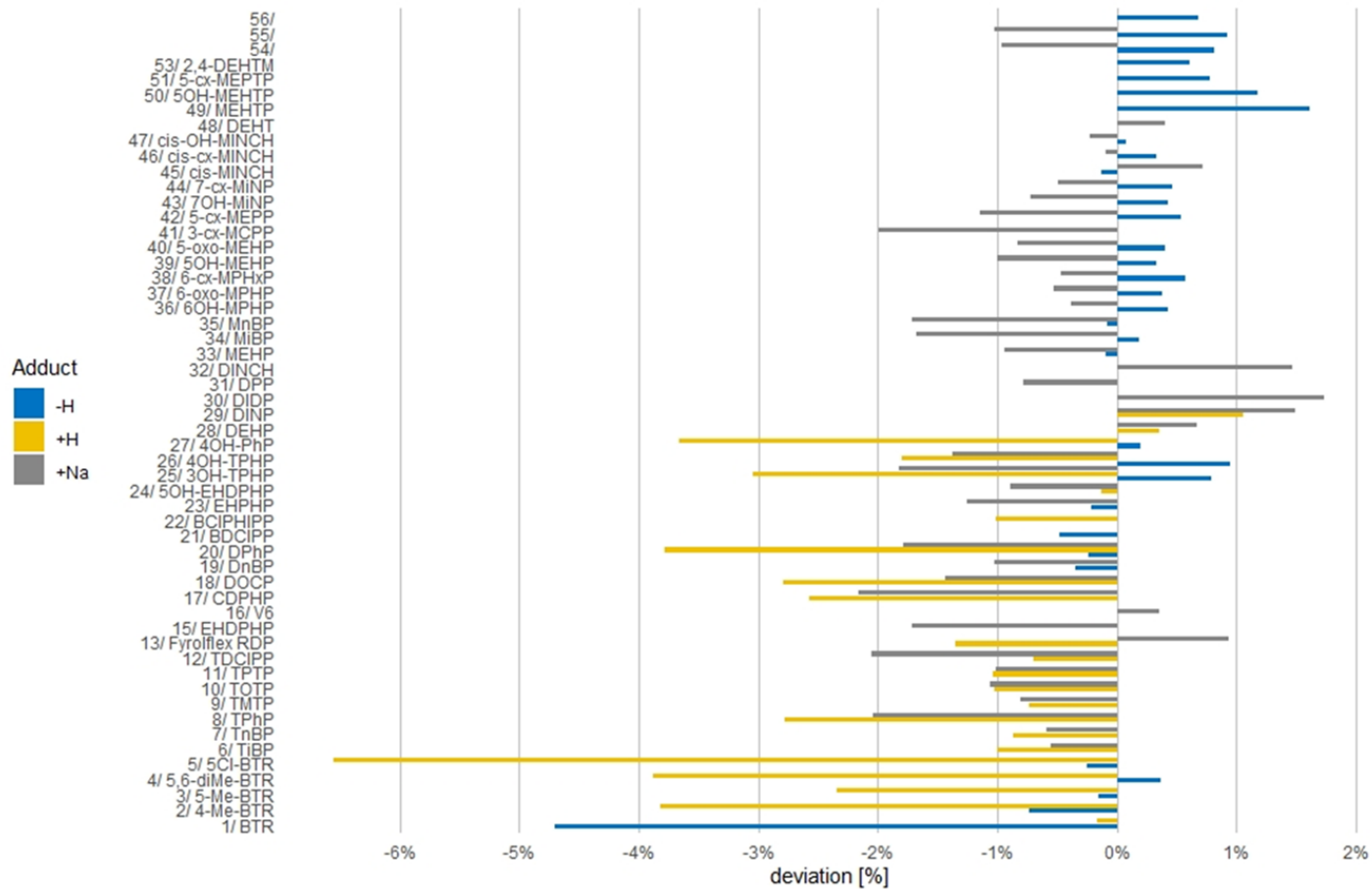


**Figure SI-3.2.5:** Percent errors observed between DTIMS and TWIMS derived CCS values. Latter were acquired on a Synapt-G2 instrument. All compounds which were detectable on both instruments are included in the figure.

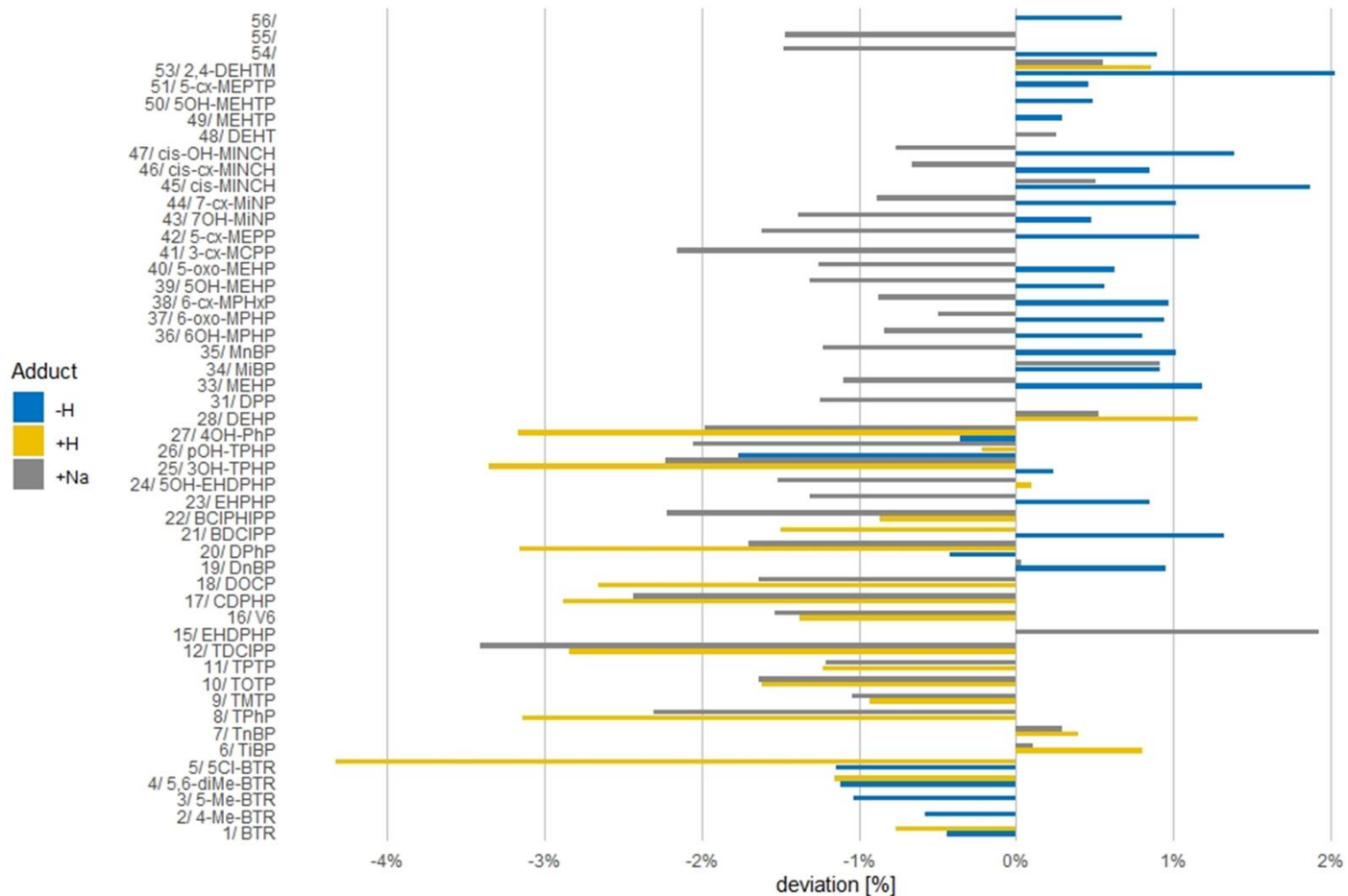


**Figure SI-3.2.6:** Percent errors observed between DTIMS and TWIMS derived CCS values. Latter were acquired on a VION instrument. All compounds which were detectable on both instruments are included in the figure.

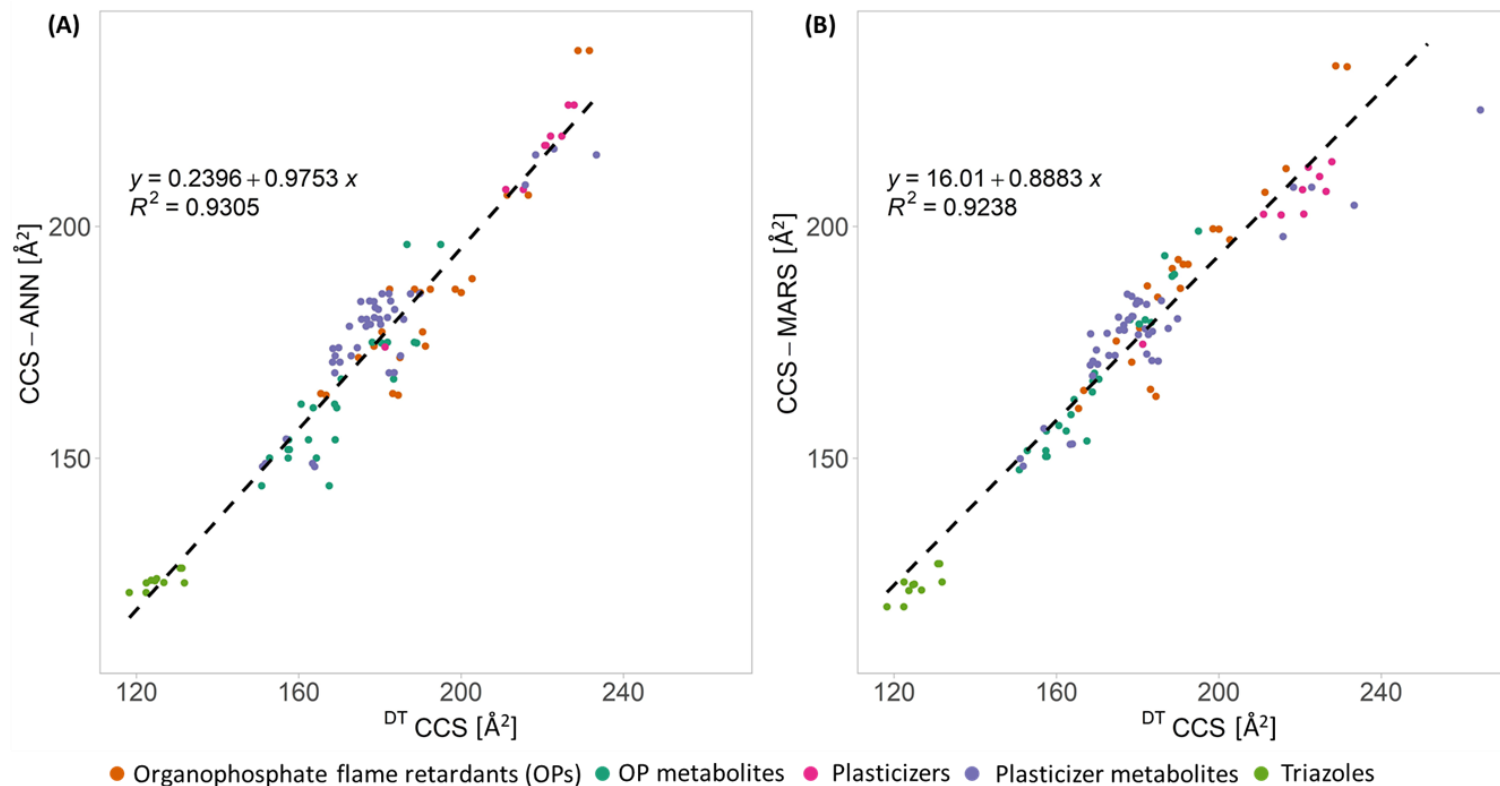


**Figure SI-3.2.7:** Linear correlations observed between DTIMS derived and predicted CCS values. Latter were predicted using an Artificial Neural Network (ANN, (A)) and a Multivariate Adaptive Regression Splines (MARS, (B)) based model. For each regression line, the equation and correlation coefficient ( $R^2$ ) are indicated.

**Table SI-3.2.8:** Predicted CCS values derived from an Artificial Neural Network (ANN) and a Multivariate Adaptive Regression Splines (MARS) based model. (The table can be openly assessed in the Supporting Information of online version of the corresponding article (Table S8): <https://doi.org/10.1016/j.aca.2022.340361>)

**Table SI-3.2.9:** Summary of absolute percent errors (APE) observed for the comparison of DTIM and predicted CCS values. Latter were predicted applying Artificial Neural Network (ANN) and Multivariate Adaptive Regression Splines (MARS) based models. ANN derived values of [M+H]<sup>+</sup> and [M-H]<sup>-</sup> ions were compared based on a 6% threshold. For ANN derived values of [M+Na]<sup>+</sup> ions a threshold of 8.7% reported within the development of the model<sup>36</sup> was applied. (\*) MARS based values were also compared with threshold reported within the development of the model. These corresponded to 4.05%, 5.86% and 5.25% for the 95th percentile of [M+H]<sup>+</sup>, [M+Na]<sup>+</sup> and [M-H]<sup>-</sup> ions, respectively.

Ion species	ANN		MARS	
	APE < 6% [%]	APE < 8.7% [%]	APE < 6% [%]	APE < X* [%]
[M+H] <sup>+</sup>	93.1 %	n.a.	87.5 %	71.9 %
[M+Na] <sup>+</sup>	58.7 %	80.4 %	78.3 %	73.9 %
[M-H] <sup>-</sup>	93.9 %	n.a.	90.0 %	90.0 %

### 3.3 Comparison of CCS calculations and resolving power between DTIM and TIMS

#### 3.3.1 Introduction

As discussed in **chapter 3.2.1**, the assessment of the reproducibility of  $CCS_{N_2}$  values acquired on different instrumental set-ups plays a crucial role for inter-laboratory database transfer. The intercomparability of TWIMS and DTIM derived  $CCS_{N_2}$  values was addressed in **chapter 3.2**. A third commonly used instrumental setup is the trapped ion-mobility spectrometry (TIMS). Thereby, the buffer gas flow and applied electric field show opposed directions allowing ion trapping. Through a stepwise decrease of the potential barrier, ions are gradually released from the trap whereby the transit time of an ion correlates with its inversed mobility ( $1/K_0$ ) (Michelmann et al., 2014). This leads to IM measurements with increased resolution ( $> 100$ ) within relative small trapping space. Similar to TWIMS and single-field DTIM measurement, from the TIMS derived reduced mobilities  $^{TIMS}CCS_{N_2}$  values can be calculated based on the implementation of CCS calibrants. Here, the question of  $CCS_{N_2}$  reproducibility between DTIM and TIMS has to be addressed to estimate the reliability of database transfer between these two systems.

A recent study has compared  $CCS_{N_2}$  values of steroids acquired with three commonly used instrument types (DTIM, TWIMS and TIMS). A high interlaboratory reproducibility was reported with 95% of the included CCS values showed deviations of  $\pm 1\%$  or  $\pm 2\%$  when comparing TWIMS or TIMS derived  $CCS_{N_2}$  values to  $^{DT}CCS_{N_2}$ , respectively, indicating good reproducibility for this compound class. However, when comparing  $CCS_{N_2}$  values of different compound classes, previous studies on DTIM and TWIMS instrumentation reported percentages of CCS values with deviations  $< 2\%$  that ranged between 82 and 93%, depending on the applied calibration approach and analyzed classes of compounds (Feuerstein et al., 2022a). However, a comparison of  $CCS_{N_2}$  values for CECs derived from the three commonly used instrumental set-ups is lacking even though differences in CCS are assumed between different compound classes, as shown in **chapter 3.2**.

In this subchapter, TIMS derived  $CCS_{N_2}$  values ( $^{TIMS}CCS_{N_2}$ ) for 48 environmental contaminants covering the classes of BPs, APs and OPFRs, were calculated. The latter class of CECs showed the highest deviations between the DTIMS and TWIMS derived  $CCS_{N_2}$  values (**chapter 3.2**), adding relevance to the acquisition of their  $^{TIMS}CCS_{N_2}$  values. Lastly, the presented work assessed the increased resolution capacities of TIMS by comparing the separation of BPs isomers achieved on DTIMS and TIMS instruments. The presented data is expected to further improve the assessment of CCS database transfer and to reveal potential deviations in TIMS and DTIMS derived  $CCS_{N_2}$  values relevant within the interpretation of  $CCS_{N_2}$  database matching.

## 3.3.2 Materials and Methods

### 3.3.2.1 Selection of standards

A total of 48 standards were selected for the comparison of  $\text{CCS}_{\text{N}_2}$  values. These included 20 OPFRs, 8 PHs and APs and 20 BPs (**Table S-3.3.1**). For the vast majority of compounds, DTIMS derived  $^{\text{DT}}\text{CCS}_{\text{N}_2}$  values were available as reported in **chapter 3.1**. The class of OPFRs was selected since for these compounds high deviations were previously reported between their  $^{\text{DT}}\text{CCS}_{\text{N}_2}$  and  $^{\text{TW}}\text{CCS}_{\text{N}_2}$  (**chapter 3.2**). The selection of this compound group thus aimed at assessing whether the described trends will be reproduced for  $^{\text{TIMS}}\text{CCS}_{\text{N}_2}$  values. BPs were selected since within this class, two pairs of isomers, that are difficult to separate by LC, were available allowing to assess the differences in resolution power. The sources from which reference standards of the compounds included in this study were purchased, are included in **Table SI-3.3.2**. For all compounds, except for a sub-selection of BPs which were only available as mixture (1 ng/ $\mu\text{L}$  in methanol), individual solutions were prepared in methanol at a concentration of 1 ng/ $\mu\text{L}$ .

### 3.3.2.2 DTIMS measurements

Most DTIM derived  $^{\text{DT}}\text{CCS}_{\text{N}_2}$  values used here were acquired in the scope of **chapter 3.1** where the applied instrumental settings, acquisition method parameters and QC guidelines were described in detail. For the new set of reference  $^{\text{DT}}\text{CCS}_{\text{N}_2}$  values reported for a sub-selection of BPs (marked with (\*)) in **Table SI-3.3.1**), the same acquisition method was used. In brief, an Agilent 6560 DTIM-QTOF (Agilent Technologies, Santa Clara, USA) was used for all DTIM measurements implementing the well-established single-field calibration approach for  $^{\text{DT}}\text{CCS}_{\text{N}_2}$  calculations. The latter was based on the ESI low-concentration tune mix (Agilent Technologies, Santa Clara, USA) for which reference  $^{\text{DT}}\text{CCS}_{\text{N}_2}$  values were established on a reference DTIM system (Stow et al., 2017). All reported  $^{\text{DT}}\text{CCS}_{\text{N}_2}$  values were based on the direct injection of 1 ng/ $\mu\text{L}$  solutions for which five measurements were conducted. Obtained average  $^{\text{DT}}\text{CCS}_{\text{N}_2}$  values and (relative) standard deviations are reported in **Table SI-3.3.1**.

### 3.3.2.3 TIMS measurements

TIMS data was acquired using a hybrid ion mobility quadrupole/TOFMS (TimsTOF) coupled to an ELUTE UHPLC system and equipped with an electrospray ionization (ESI) source (Bruker Daltonics, Bremen, Germany). It was operated using the Compass otofControl software, version 6.2 (Bruker Daltonics, Bremen, Germany). For all measurements, ion source parameters were set to 500 V, 4.5 kV, 4.0 bar, 10 L/min and 220 °C for the End Plate Offset, Capillary voltage, Nebulizer pressure, Drying gas flow and temperature, respectively. Above mentioned standard solutions were injected directly

(injection volume: 4  $\mu$ L) in triplicate with a total run time of 1.5 min. Thereby, mobile phases consisted of (A) ultrapure water (obtained through a Elix<sup>®</sup> Essential 3 water purification system from Merck Millipore, Madrid, Spain) and (B) methanol (Fisher Scientific, LCMS grade) to both of which 0.1% formic acid or 5 mM ammonium acetate (both from Sigma Aldrich, St Louis, MO, USA) were added for positive or negative polarity, respectively. A total of four methods for the TIMS settings were applied which are summarized in **Table SI-3.3.3**. Methods POS-1 and NEG-1 were used for the acquisition of reference <sup>TIMS</sup>CCS<sub>N2</sub> values, in positive and negative polarity, respectively, aimed for the comparison with DTIMS derived data (**chapter 3.3.3.1**). Methods NEG-2 and NEG-3 covered smaller mobility windows allowing to assess improved TIMS resolution (**chapter 3.3.3.2**).

TOF mass calibration was conducted using a 10 mM sodium formate (50:50, v/v water:isopropyl alcohol) solution applying the high-performance calibration mode. Additionally, a 1:1 (v/v) mixture of the mass calibration solution and the ESI low-concentration tune mix (Agilent Technologies, Santa Clara, USA) was infused at the end of each standard injection to allow for internal mass and CCS calibration.

#### 3.3.2.4 <sup>DT</sup>CCS<sub>N2</sub> calculations and assessment of resolving power

Calculations of <sup>DT</sup>CCS<sub>N2</sub> values from DTIMS data were described in detail in chapter 3.1. In brief, raw data files were recalibrated using the IM-MS Reprocessing Tool (Version B.10.0; Agilent Technologies, Santa Clara, USA). Then, datafiles were demultiplexed using the PNNL PreProcessor (version 2020.03.23) including the smoothing function (moving average of 3). Features were extracted through the IM-MS Browser software (Version B.10.0; Agilent Technologies, Santa Clara, USA) using the 'Find Features' algorithm, set to 'chromatographic' and an ion intensity  $\geq 500$  counts. The obtained <sup>DT</sup>CCS<sub>N2</sub> values, averaged over five injections, were submitted to the <sup>DT</sup>CCS<sub>N2</sub> database.

Resolution observed for DTIMS derived mobilograms was estimated through the calculation of the ratio between drift time and peak width at half-maximum, as described previously (Ewing et al., 2016). The drift time was retrieved from the feature finding approach described above. Peak width at half-maximum was obtained manually after extracting the mobilograms of the corresponding feature. To further improve the resolution for BPs isomers, a selection of datafiles was processed by applying the HRdm tool (v 2.0) with default processing settings (Agilent Technologies, Santa Clara, USA) (May et al., 2020).

### 3.3.2.5 <sup>TIMS</sup>CCS<sub>N2</sub> calculations

All TIMS data was processed using the Compass DataAnalysis software (version 5.3). For each datafile, internal mass calibration was performed using the calibration mixture infused at the end of each injection and applying the HPC mode. For internal <sup>TIMS</sup>CCS<sub>N2</sub> calibration, calibrant ion mobilograms were extracted (mass window  $\pm 0.01$  Da) and <sup>TIMS</sup>CCS<sub>N2</sub> calculations were recalibrated applying the internal recalibration algorithm. Then, mobilograms of  $m/z$  values of each expected ion species were extracted (mass window  $\pm 0.01$  Da). Using the 'Find Compounds in Mobilogram' algorithm, compounds were extracted from the mobilograms and for each compound, <sup>TIMS</sup>CCS<sub>N2</sub> values were calculated. As previously discussed in detail, the resolving power of TIMS measurements is dependent on gas velocity, scan rate and length of the electric field gradient plateau (Michelmann et al., 2014). The calculated resolution was provided by the 'Find Compounds in Mobilogram' algorithm of the data processing software. Each mobilogram was manually investigated to ensure sufficient peak height ( $S/N > 5$ ) and shape. Average <sup>TIMS</sup>CCS<sub>N2</sub> values from triplicate injections were exported for CCS<sub>N2</sub> comparison. For mobility measurements conducted to assess improved TIMS resolution (**chapter 3.3.3.2**), the observed mobility windows were narrowed not allowing the inclusion of all calibrant ions. Therefore, for these measurements, <sup>TIMS</sup>CCS<sub>N2</sub> calculations could not be performed.

### 3.3.2.6 Comparison of CCS<sub>N2</sub> datasets and data visualization

To assess differences between DTIMS and TIMS derived CCS<sub>N2</sub> values, percent deviations between <sup>TIMS</sup>CCS<sub>N2</sub> and <sup>DT</sup>CCS<sub>N2</sub> values were calculated whereby DTIMS derived values were used as reference. For data visualization and statistical testing of correlation coefficients (t-test;  $p < 0.05$ ), Microsoft Excel (version 2302) and R language (4.3.2) combined with RStudio (version 2024.04.1) were used.

## 3.3.3 Results and Discussion

To assess the inter-platform reproducibility of CCS<sub>N2</sub> values for CECs, TIMS and DTIM based CCS<sub>N2</sub> values were acquired for a total of 48 compounds from four CEC classes. These resulted in a total of 80 CCS<sub>N2</sub> values available for the comparison. By assessing the deviations between <sup>TIMS</sup>CCS<sub>N2</sub> and <sup>DT</sup>CCS<sub>N2</sub> values, the reproducibility of CCS<sub>N2</sub> values on different instrumental setups could be further assessed adding to previous comparison studies (Feuerstein et al., 2022a; Hinnenkamp et al., 2018). Additionally, sets of isomers available within the class of BPs, were used to compare the resolving power between DTIM and TIMS systems. These observations were expected to serve as a valuable additional insight facilitating database transfer within future IM-based studies on the screening and identification of CECs.

### 3.3.3.1 Comparison of $^{DT}CCS_{N_2}$ and $^{TIMS}CCS_{N_2}$ values

Prior to addressing the intercomparability of DTIM and TIMS derived  $CCS_{N_2}$  values, the precision of both datasets was assessed. RSDs obtained for  $^{DT}CCS_{N_2}$  values were reported within **chapter 3.1**, and were based on five injections for each compound. Additionally, the presented study introduces a new set of reference  $^{DT}CCS_{N_2}$  values reported for a set of BPs (marked with (\*) in **Table SI-3.3.1**). Within their acquisition, four QC compounds (pyridoxal phosphate, L-histidine, L-phenylalanine and L-tyrosine) were included for which reference  $^{DT}CCS_{N_2}$  values were reported previously (Stow et al., 2017) to follow the QC guidelines proposed by Picache et al. The results obtained for the QC compounds are summarized in **Table SI-3.3.4**. Average observed errors did not exceed 0.5% and none of the individual datapoints exceeded an error of 1%, thereby meeting the QC guidelines and confirming the reliability and quality of the additional reference  $^{DT}CCS_{N_2}$  values.

Overall, for  $^{DT}CCS_{N_2}$  values included here, an average RSD of  $0.06 \pm 0.05\%$  (**Table SI-3.3.1**) with a range of 0.01 - 0.38 % was measured indicating very good reproducibility.  $^{TIMS}CCS_{N_2}$  values showed an average RSD of  $0.12 \pm 0.05\%$  ranging between 0.01 - 0.39 %, for triplicate injections. This indicates slightly higher inter-injection deviations for TIMS measurements. The above mentioned internal  $^{TIMS}CCS_{N_2}$  calibration approach required a manual adjustment of the selection of peak apex for calibrant signals if incorrectly assigned by the software. This step can introduce an additional bias and results in slightly different calibration settings for each TIMS-generated datafile, while within the DTIMS single-field calibration approach, a uniform set of calibrant settings can be applied throughout a complete sample batch.

Based on a linear regression plot, correlations between  $^{DT}CCS_{N_2}$  and  $^{TIMS}CCS_{N_2}$  datasets and occurrence of potential systematic offsets were assessed. As displayed in **Figure SI-3.3.1**, the two datasets showed a strong linear relationship reflected in a correlation coefficient of  $R^2 = 0.998$ . However, the observed slope and intercept, showing values of  $> 1.04$  and  $< 9.4 \text{ \AA}^2$ , respectively, indicated a systematic offset between DTIMS and TIMS derived data. This can be further characterized through the assessment of the relationship between calculated bias ( $^{DT}CCS_{N_2}$  set as reference) and the corresponding  $^{TIMS}CCS_{N_2}$  values, as represented in **Figure 3.3.1** and **Figure SI-3.3.2**, whereby the latter makes a distinction between different ion species.

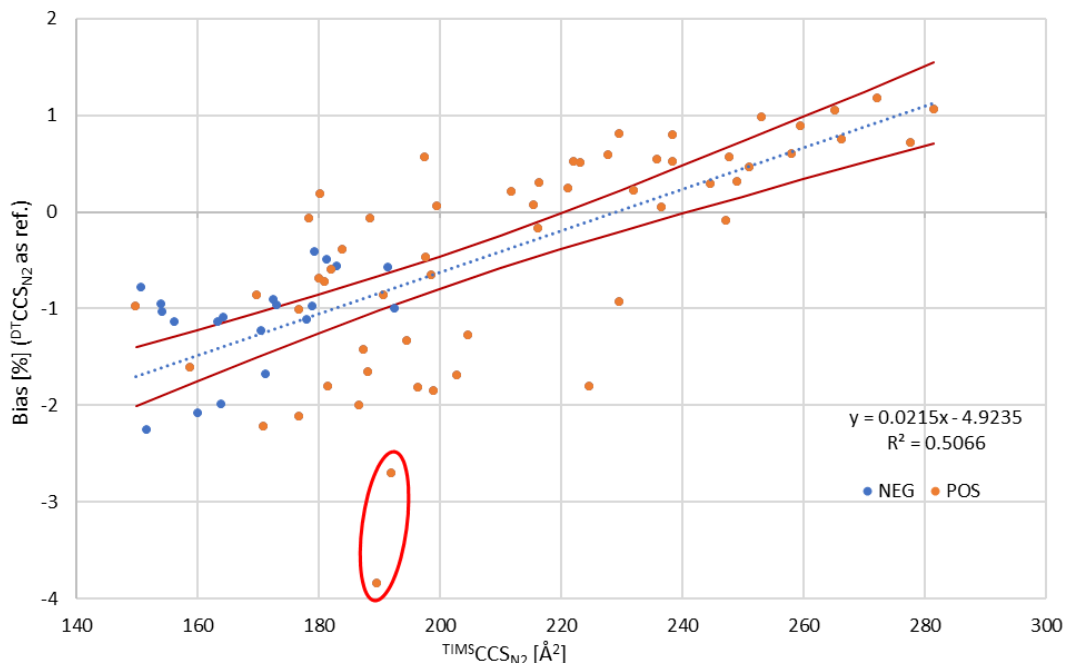


**Figure 3.3.1:** Percent bias (with  ${}^{\text{DTCCSN}_2}$  set as reference) as a function of corresponding  ${}^{\text{TIMSCCSN}_2}$  values. Datapoints obtained in positive and negative ionization polarity are represented in orange and blue, respectively. For the whole dataset, correlation was described applying a linear model, represented by a blue dotted trendline for which the obtained function and correlation coefficient ( $R^2$ ) are indicated. The 95% confidence interval of the regression line is indicated with red lines. Datapoints for which the highest bias were observed (discussed in the text) are marked in red.

Observed percent errors ranged between -3.84 % and 1.17 % with an average APE of  $0.96 \pm 0.70$  %. For 91.3 % of the datapoints, observed APEs were  $< 2$  %. More in detail, **Figure SI-3.3.3** shows the deviations observed between  ${}^{\text{DTCCSN}_2}$  and  ${}^{\text{TIMSCCSN}_2}$  values distinguishing between protonated, deprotonated ions and sodium adducts. For both plots (**Figures 3.3.1** and **SI-3.3.3**), similar trendlines describing the calculated bias were observed. Median errors and interquartile ranges of -1.0 % and 0.3 %, -0.4 % and 1.7 %, -0.5 % and 1.6 % were observed for  $[\text{M}-\text{H}]^-$ ,  $[\text{M}+\text{H}]^+$  and  $[\text{M}+\text{Na}]^+$  ions, respectively. This does not suggest differing trends between ion species and confirms the offset towards lower  ${}^{\text{TIMSCCSN}_2}$  values (compared to DTIMS) already observed in **Figure 3.3.1**. Described results show a good reproducibility of  ${}^{\text{DTCCSN}_2}$  values by TIMS indicating that the above mentioned cut-off value of 2% is applicable for most compounds included here. Nevertheless, a clear trend visible within **Figure 3.3.1** cannot be neglected: observed bias positively correlated ( $p < 0.01$ ) with  ${}^{\text{TIMSCCSN}_2}$  values resulting in a correlation coefficient of  $R^2 = 0.502$ . Previous studies described an influence of measurement settings, e.g. high ramp times or wide mobility windows, on observed errors (Feuerstein et al., 2022a), even though the concrete relationship between applied settings and potential bias is still unknown. The presented dataset indicates such

systematic offsets suggesting that wide mobility windows can influence the data obtained for calibrant signals and the derived calibration constants.

For a sub-selection of OPs included in the presented comparison study, previously published TWIMS derived  $^{TW}CCS_{N_2}$  values were available (**chapter 3.2**). Even though this only included 19 datapoints (compounds marked with (#) in **Table SI-3.3.1**), the comparison of their biases with data obtained for TIMS measurements can give a first indication of the suitability of both systems to reproduce reference  $^{DT}CCS_{N_2}$  values. As displayed in **Figure SI-3.3.4**, the TIMS derived dataset showed a higher number of datapoints falling within a  $\pm 2\%$  window as only three datapoints showed an APE  $> 2\%$ . This suggests that the applied TIMS approach is best capable to reproduce the DTIM data for the investigated compounds which, as already hypothesized by Feuerstein et al., might be caused by the fact that both systems are calibrated with the same calibrants and corresponding reference values.

Interestingly, compounds showing the highest percent errors overlapped between TWIMS and TIMS data. For example,  $CCS_{N_2}$  values of cresyl diphenyl phosphate and triphenyl phosphate, both belonging to the class of OPFRs carrying aromatic substituents, showed APEs  $> 2\%$  for both datasets. As described in **chapter 3.2**, high deviations between TWIMS and DTIMS derived  $CCS_{N_2}$  values have been reported for these compounds which seem to be reproduced by TIMS. However, further studies including bigger datasets are needed to confirm and further characterize these trends.

Within **Figure 3.3.1**, two datapoints (marked in red) clearly deviated from the overall dataset showing a bias of up to  $-3.84\%$ . Both of these points derived from tris(2,3-dibromopropyl)phosphate (TDBPP). The TIMS mobilograms extracted for (theoretical)  $m/z$  ratios of 696.5840 (second most abundant isotopologue of the  $[M+H]^+$  ion) and 716.5680 (third most abundant isotope of  $[M+Na]^+$  ion) are displayed in **Figure SI-3.3.5**. The mentioned  $m/z$  ratios were selected since for these reference  $^{DT}CCS_{N_2}$  values were reported previously (**chapter 3.1**). For the sodium adduct, one peak was observed allowing a calculation of a single  $^{TIMS}CCS_{N_2}$  values. For the proton adduct, however, three peak apex were observed within a reduced mobility range of 0.91-0.96  $Vs/cm^2$ , as well as a later peak at approx. 1.0  $Vs/cm^2$ . This observation was consistent between the three replicates and resulted in three  $^{TIMS}CCS_{N_2}$  values of 189.66, 191.90 and 194.62  $\text{\AA}^2$  for the three peak apex, respectively. To assess the reproducibility of these observations by DTIM, mobilograms obtained for TDBPP in the scope of  $^{DT}CCS_{N_2}$  database compilation were investigated (**Figure SI-3.3.6**). Similarly, the DTIM derived mobilogram showed a peak for the  $[M+H]^+$  ion whose drift time matched the peak of the sodium adduct. It is assumed that within both systems, a formation of protonated ions from sodium adducts is possible leading to two peaks with similar drift times. The wider peak observed for the proton adduct within the DTIMS derived mobilograms suggests multiple underlying peaks which could not be further separated, even when high-resolution demultiplexing

was applied. These observations might indicate different protomers even though the structure of TDBPP does not allow to distinguish three different protonation sides. Alternatively, the observed signals might derive from isomeric impurities of the reference standard. For transparency and to assess whether this observation can be reproduced on other IM set-ups, all three obtained  $^{TIMS}CCS_{N_2}$  values were considered here. Similar observations were made for tris(1,3-dichloro-2-propyl)phosphate (TCIPP) also resulting in three reported  $^{TIMS}CCS_{N_2}$  values. These were the only two compounds showing multiple peaks for proton adducts indicating that the presence of multiple halogen atoms might contribute to the varying gaseous ion formation.

In conclusion, the presented comparison revealed a generally good reproducibility of DTIM derived  $CCS_{N_2}$  values with TIMS derived  $CCS_{N_2}$  values since 91.3 % of datapoints showed APEs < 2%. The observation of bias > 2 %, however, still indicates potential for false negative annotations if a 2 % cut-off is implemented without further evaluations of potential biases introduced by the investigated compound class or the calibration approach. Also, observed trends within the calculated bias suggested an influence of the instrumental settings on deviations between experimental and reference sets of  $CCS_{N_2}$  values. Such trends should be assessed, especially if wide ranges of measured (reduced) mobilities are applied, which can be necessary for general screening applications requiring the detectability of wide  $m/z$  ranges.

In accordance to previous inter-platform  $CCS_{N_2}$  comparisons, the presented data emphasize several factors influencing  $CCS_{N_2}$  calculations (Feuerstein et al., 2022a; Feuerstein et al., 2022b). Since characterization of sources of bias and estimation of the resulting uncertainty remain areas of intense research, the proposal of compound class independent cut-off values for  $CCS_{N_2}$  database transfer is not considered possible here. Especially when  $CCS_{N_2}$  values are used to distinguish between isomers, results should be interpreted with care since uncertainty in  $CCS_{N_2}$  calculations and, as presented here, inter-platform  $CCS_{N_2}$  deviations are expected to be greater than  $CCS_{N_2}$  differences between isomers. Further improvement of IM resolving power, further harmonization of calibration approaches, and possible implementation of reference materials should be considered to overcome the described limitations.

### 3.3.3.2 Differences in resolving power between TIMS and DTIM

Within the class of bisphenols, two sets of isomers were available to assess the resolving power of the TIMS system. These included 1) *ortho,ortho*-bisphenol A (*o,o*-BPA) and *ortho,para*-bisphenol A (*o,p*-BPA) which differed by the position of one of the hydroxy groups, and 2) bisphenol M and P (BPM/BPP) differing by the conformation at the middle aromatic moiety. The potential separation of BPA isomers can be of high relevance since differences in toxicity are assumed for the different homologues. Also, a coelution within the LC dimension has been reported for *o,o*-BPA and *o,p*-BPA previously (Li et al., 2022). The two BPA isomers were injected both individually and as a mixture

applying the initial methods used for the compilation of the TIMS and DTIMS databases (see **Table SI-3.3.2-NEG1** and **chapter 3.1**). The obtained TIMS mobilograms are displayed in **Figure SI-3.3.7**. The applied acquisition method, including a wide window of monitored reduced mobilities, allowed a nearly baseline separation of the two BPA isomers, not requiring further method optimization. The TIMS resolution reported by the data processing software corresponded to 88 and 98 for *o,o*-BPA and *o,p*-BPA injected as individual standards, respectively. Within the injection of the mixture, slightly lower resolution was obtained, corresponding to 76 and 77 for the two compounds, respectively. In **chapter 3.3.3.1**, reference  $^{TIMS}CCS_{N_2}$  values of  $150.73 \pm 0.27 \text{ \AA}^2$  (RSD: 0.18%) and  $154.22 \pm 0.10 \text{ \AA}^2$  (RSD: 0.06%) were calculated for *o,o*-BPA and *o,p*-BPA, respectively. This corresponds to a  $\Delta CCS$  of 2.3% between these two compounds. The observed standard deviations in combination with the resolving power of the TIMS setup indicates that the applied acquisition method allows an unequivocal separation and distinction of the BPA isomers.

The same individual and mixed standards of the BPA isomers were also analyzed using the DTIMS system applying the acquisition method described in **chapter 3.1**. **Figure SI-3.3.8** (blue line) displays the obtained mobilograms for which a resolution of 52 and 46 was estimated for *o,o*-BPA and *p,p*-BPA, respectively. For these two isomers,  $^{DT}CCS_{N_2}$  values of  $151.90 \pm 0.06 \text{ \AA}^2$  (RSD: 0.04%) and  $155.96 \pm 0.04 \text{ \AA}^2$  (RSD: 0.02%), respectively, which corresponds to a  $\Delta CCS$  of 2.6%. The application the high-resolution demultiplexing tool (mobilogram with orange dotted line in **Figure SI-3.3.8**) increased the resolution to 176 and 124 for *o,o*-BPA and *p,p*-BPA, respectively, allowing a baseline separation of these compounds. Despite the low RSDs indicated above for  $^{DT}CCS_{N_2}$  calculations which clearly fall within the observed  $\Delta CCS$  window, the described post-processing step can vastly improve isomer resolution easing their distinguishment.

For both, TIMS and DTIM, systems, the main BPA isomer (*para,para*-bisphenol A; *p,p*-BPA) baseline separated from *o,o*-BPA/*o,p*-BPA applying the acquisition methods used for database compilation. Thereby, a  $\Delta CCS$  of 3.7% and 4.6% (between *o,p*-BPA and *p,p*-BPA) was observed within the TIMS and DTIM systems, respectively. Given this good separation achieved without any further postprocessing or modifications of the acquisition settings, *p,p*-BPA was not considered in the assessment of resolving power described here.

The increased resolving power which can be achieved through the adjustment of the trapping window and ramp time within TIMS was also demonstrated for the second set of BP isomers consisting of BPM and BPP. Within the acquisition of reference  $^{TIMS}CCS_{N_2}$  values (**chapter 3.3.3.1**), both isomers were injected as separate solutions, and  $^{TIMS}CCS_{N_2}$  values of  $178.87 \pm 0.02 \text{ \AA}^2$  (RSD: 0.01 %) and  $181.40 \pm 0.07 \text{ \AA}^2$  (RSD: 0.04 %) were obtained for BPP and BPM, respectively, corresponding to a  $\Delta CCS$  of 1.4 %. However, when the isomers were injected as a mixture, the method applied for database acquisition led to a poor separation of the two isomers (**Figure 3.3.2-A**).

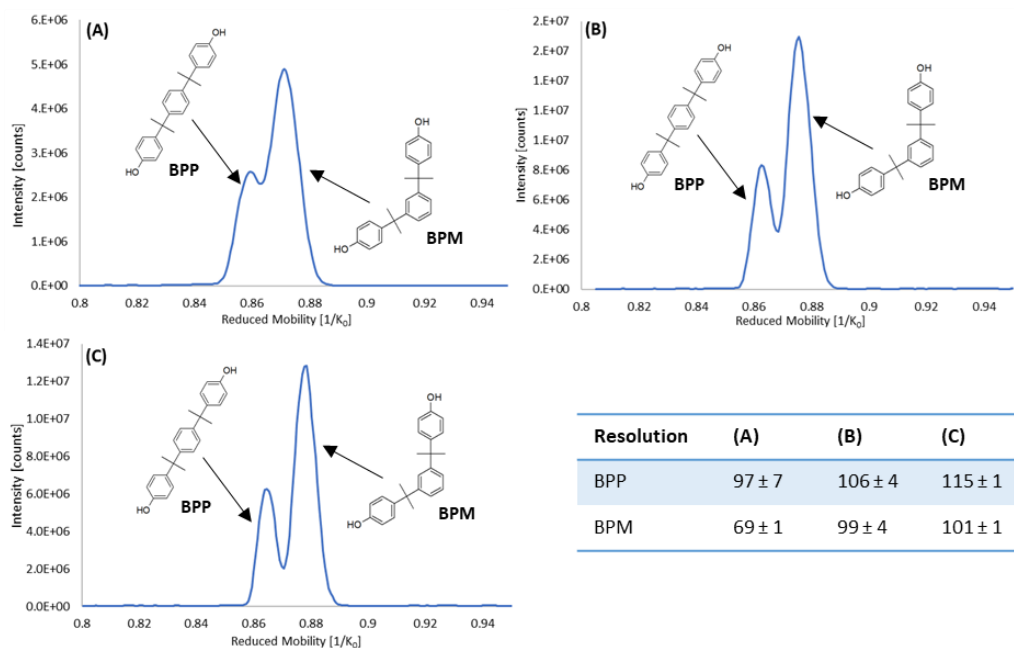


**Figure 3.3.2:** Extracted TIMS mobilograms of bisphenol P (BPP) and bisphenol M (BPM) injected as a mixture. Mobilograms (A), (B) and (C) were acquired using the acquisition methods NEG-1, NEG-2 and NEG-3 listed in **Table SI-3.3.3**, decreasing the monitored reduced mobility window and increasing ramp time. The observed changes in resolution are displayed in the table in the lower right corner. The (theoretical)  $m/z$  ratio of 345.1860 of the deprotonated ion was extracted applying a mass window of  $\pm 0.01$  Da. Average resolution (and standard deviation) obtained from triplicate injections are indicated.

As described previously (Silveira et al., 2014), the adjustment of the measured mobility windows to narrower values or the increase of ramp time can improve TIMS resolving power. Therefore, the same isomer mixture was analysed applying methods NEG-2 and NEG-3 (**Table SI-3.3.3**) whereby the mobility window was narrowed to 0.8 - 1.0 Vs/cm<sup>2</sup> with ramp times set to 400 and 650 ms, respectively. The obtained mobilograms are represented in **Figure 3.3.2-B** and **3.3.2-C**, respectively, whereby a constant improvement of resolving power was observed. Latter resulted in a resolution of up to 116. These results characterize the relationship between TIMS resolving capacity and applied trapping settings. Even though the adjusted acquisition methods did not allow the calculation of <sup>TIMS</sup>CCS<sub>N<sub>2</sub></sub> values since the narrow windows did not cover sufficient calibrant ions, the presented approach can be used for specific applications wherein an increased resolution is required, showing also the high flexibility of the TIMS set-up. Nevertheless, it has to be noted that adjustment of trapping settings to higher ramp times and/or narrower reduced mobility windows decreases acquisition speed and excludes all analytes showing mobilities outside the selected window, respectively. This reduces the coverage of detectable analytes which has to be considered in method selection, especially in a non-targeted or suspect screening setting.

When analysing the mixture of BPM and BPP isomers with the initial DTIM method, only one peak was observed in the mobilogram, indicating the failure to detect the presence of two compounds (**Figure SI-3.3.9**). For this peak, a resolution of 46 was calculated. Again, the application of the high-resolution demultiplexing tool improved the resolving power significantly revealing two peaks (**Figure SI-3.3.9**, dotted line) whereby a resolution of 157 and 170 was estimated for BPP and BPM, respectively. This observation also indicates the high relevance of the application of post-processing resolution improvement in DTIM if underlying isomers are assumed.

### 3.3.4 Conclusions

Within the presented study, TIMS and DTIM derived  $CCS_{N_2}$  values were compared for a set of 48 environmental contaminants. A good reproducibility was observed between the two MS systems resulting in an average absolute percent error of  $0.96 \pm 0.70$  % between  $^{TIMS}CCS_{N_2}$  and  $^{DT}CCS_{N_2}$  values. Nevertheless, 9 % of the included datapoints exceeded an APE of 2% indicating that a general application of a 2% cut-off within database transfer can still lead to false negative identifications. The presented  $^{TIMS}CCS_{N_2}$  dataset also indicated a potential influence of TIMS acquisition settings on  $CCS_{N_2}$  reproducibility pointing out the relevance of their detailed reporting within database publication. Lastly, the resolving power of both IM systems was compared based on two sets of bisphenol isomers. For TIMS measurements, the adjustment of ramp times and monitored mobility windows allowed to achieve a resolution  $> 115$ . For DTIM, high resolving power ( $> 160$ ) was only achievable when the recently introduced high-resolution postprocessing tool was applied (May et al., 2020). These results are expected to ease database transfer between IM set-ups and selection of suitable data acquisition and post-processing workflows within future environmental screening studies.

## Supplementary Information – Chapter 3.3

**Table SI-3.3.1:** Reference  $^{13}\text{C}$ CCS<sub>N<sub>2</sub> and  $^{12}\text{C}$ CCS<sub>N<sub>2</sub> values included in the comparison study.  $^{12}\text{C}$ CCS<sub>N<sub>2</sub> values of compounds marked with (\*) were reported within **chapter 3.3** while the remaining DTIM data was introduced in **chapter 3.1**. For datapoints marked with (#),  $^{12}\text{C}$ CCS<sub>N<sub>2</sub> were available reported **chapter 3.2**. Average  $^{12}\text{C}$ CCS<sub>N<sub>2</sub> and  $^{13}\text{C}$ CCS<sub>N<sub>2</sub> are based on five and three injections, respectively. For each CCS value, the standard and relative standard deviations (SD/RSD) are indicated.</sub></sub></sub></sub></sub></sub>

Compound name	Abbreviation	Molecular formula	<i>m/z</i>	Ion	$^{13}\text{C}$ CCS <sub>N<sub>2</sub></sub> (±SD) [Å <sup>2</sup> ]	RSD [%]
4-((4-(Benzyloxy)phenyl)sulfonyl) phenol	BPS-MAE	C <sub>15</sub> H <sub>14</sub> O <sub>4</sub> S	289.0540	[M-H] <sup>-</sup>	170.55 (0.12)	0.07
4-((4-Isopropoxy-phenyl)sulfonyl) phenol	D-8	C <sub>15</sub> H <sub>16</sub> O <sub>4</sub> S	291.0697	[M-H] <sup>-</sup>	173.12 (0.07)	0.04
4-(4-hydroxy-3-prop-2-enylphe-nyl)sulfonyl-2-prop-2-enyl phenol	TGSA	C <sub>18</sub> H <sub>18</sub> O <sub>4</sub> S	329.0853	[M-H] <sup>-</sup>	179.25 (0.07)	0.04
Bisphenol A	BPA	C <sub>15</sub> H <sub>16</sub> O <sub>2</sub>	227.1078	[M-H] <sup>-</sup>	160.09 (0.14)	0.09
<i>ortho, ortho</i> -Bisphenol A	<i>o,o</i> -BPA	C <sub>15</sub> H <sub>16</sub> O <sub>2</sub>	227.1078	[M-H] <sup>-</sup>	150.73 (0.27)	0.18
<i>ortho, para</i> -Bisphenol A	<i>o,p</i> -BPA	C <sub>15</sub> H <sub>16</sub> O <sub>2</sub>	227.1078	[M-H] <sup>-</sup>	154.22 (0.10)	0.06
Bisphenol AF	BPAF	C <sub>15</sub> H <sub>10</sub> F <sub>6</sub> O <sub>2</sub>	335.0512	[M-H] <sup>-</sup>	164.24 (0.15)	0.09
Bisphenol AP	BPAP	C <sub>20</sub> H <sub>18</sub> O <sub>2</sub>	289.1234	[M-H] <sup>-</sup>	177.94 (0.11)	0.06
Bisphenol B	BPB	C <sub>16</sub> H <sub>18</sub> O <sub>2</sub>	241.1234	[M-H] <sup>-</sup>	163.85 (0.22)	0.13
Bisphenol C	BPC	C <sub>14</sub> H <sub>10</sub> Cl <sub>2</sub> O <sub>2</sub>	278.9985	[M-H] <sup>-</sup>	163.41 (0.12)	0.07
Bisphenol E	BPE	C <sub>14</sub> H <sub>14</sub> O <sub>2</sub>	213.0916	[M-H] <sup>-</sup>	156.09 (0.19)	0.12
Bisphenol M	BPM	C <sub>24</sub> H <sub>26</sub> O <sub>2</sub>	345.1860	[M-H] <sup>-</sup>	181.40 (0.07)	0.04
Bisphenol P	BPP	C <sub>24</sub> H <sub>26</sub> O <sub>2</sub>	345.1860	[M-H] <sup>-</sup>	178.87 (0.02)	0.01
Bisphenol Z	BPZ	C <sub>18</sub> H <sub>20</sub> O <sub>2</sub>	267.1390	[M-H] <sup>-</sup>	171.28 (0.13)	0.07
Bisphenol F	BPF	C <sub>13</sub> H <sub>12</sub> O <sub>2</sub>	199.0764	[M-H] <sup>-</sup>	151.55 (0.18)	0.12
Bisphenol S	BPS	C <sub>12</sub> H <sub>10</sub> O <sub>4</sub> S	249.0227	[M-H] <sup>-</sup>	154.01 (0.11)	0.07
Tetrabromobisphenol A	TBBPA	C <sub>15</sub> H <sub>12</sub> Br <sub>4</sub> O <sub>2</sub>	542.7453	[M-H] <sup>-</sup>	191.49 (0.13)	0.07
4,4'-Methylenebis(2,6-dimethylphenol)	TMBPF	C <sub>17</sub> H <sub>20</sub> O <sub>2</sub>	255.1385	[M-H] <sup>-</sup>	172.49 (0.24)	0.14
Tetrachlorobisphenol A	TeCBPA	C <sub>15</sub> H <sub>12</sub> Cl <sub>4</sub> O <sub>2</sub>	362.9513	[M-H] <sup>-</sup>	182.92 (0.11)	0.06
Bisphenol FL	BispFL	C <sub>25</sub> H <sub>18</sub> O <sub>2</sub>	349.1229	[M-H] <sup>-</sup>	192.61 (0.11)	0.06
2-Ethylhexyl diphenyl phosphate	EHDPPH	C <sub>20</sub> H <sub>27</sub> O <sub>4</sub> P	385.1539 725.3367 747.3186	[M+Na] <sup>+</sup> [2M+H] <sup>+</sup> [2M+Na] <sup>+</sup>	198.94 (0.36) 272.19 (0.32) 281.53 (0.39)	0.18 0.12 0.14
Antiblaze V6 <sup>#</sup>	V6	C <sub>13</sub> H <sub>24</sub> Cl <sub>6</sub> O <sub>8</sub> P <sub>2</sub>	580.9150 602.8970	[M+H] <sup>+</sup> [M+Na] <sup>+</sup>	211.82 (0.42) 216.21 (0.19)	0.20 0.09
Bisphenol A bis (diphenyl phosphate)	BDP	C <sub>39</sub> H <sub>34</sub> O <sub>8</sub> P <sub>2</sub>	693.1802 715.1621	[M+H] <sup>+</sup> [M+Na] <sup>+</sup>	247.74 (0.34) 258.14 (0.35)	0.14 0.14
Diphenylcresyl phosphate <sup>#</sup>	CDPHP	C <sub>19</sub> H <sub>17</sub> O <sub>4</sub> P	341.0937 363.0757 681.1802 703.1621	[M+H] <sup>+</sup> [M+Na] <sup>+</sup> [2M+H] <sup>+</sup> [2M+Na] <sup>+</sup>	176.66 (0.25) 186.71 (0.28) 253.17 (0.99) 259.57 (0.47)	0.14 0.15 0.39 0.18
Isodecyl diphenyl phosphate	iDPP	C <sub>22</sub> H <sub>31</sub> O <sub>4</sub> P	413.1852	[M+Na] <sup>+</sup>	204.65 (0.37)	0.18
Resorcinol bis (diphenyl phosphate)	RDP	C <sub>30</sub> H <sub>24</sub> O <sub>8</sub> P <sub>2</sub>	575.1019 597.0839	[M+H] <sup>+</sup> [M+Na] <sup>+</sup>	224.63 (0.34) 232.08 (0.26)	0.15 0.11
Triamyl phosphate	TAP	C <sub>15</sub> H <sub>33</sub> O <sub>4</sub> P	331.2009 617.4306	[M+Na] <sup>+</sup> [2M+H] <sup>+</sup>	198.66 (0.29) 265.26 (0.63)	0.15 0.24

			639.4125	[2M+Na] <sup>+</sup>	277.66 (0.41)	0.15
Triethyl phosphate	TEP	C <sub>6</sub> H <sub>15</sub> O <sub>4</sub> P	n.d.			
Tri-iso-butyl phosphate <sup>#</sup>	TiBP	C <sub>12</sub> H <sub>27</sub> O <sub>4</sub> P	289.1539	[M+Na] <sup>+</sup>	182.10 (0.56)	0.31
			533.3367	[2M+H] <sup>+</sup>	235.81 (0.52)	0.22
			555.3186	[2M+Na] <sup>+</sup>	249.16 (0.38)	0.15
Tri-m-tolyl phosphate <sup>#</sup>	TMTP	C <sub>21</sub> H <sub>21</sub> O <sub>4</sub> P	369.1250	[M+H] <sup>+</sup>	188.43 (0.37)	0.20
			391.1070	[M+Na] <sup>+</sup>	197.63 (0.45)	0.23
Tri-n-butyl phosphate <sup>#</sup>	TnBP	C <sub>12</sub> H <sub>27</sub> O <sub>4</sub> P	289.1539	[M+Na] <sup>+</sup>	183.83 (0.01)	0.00
			533.3367	[2M+H] <sup>+</sup>	238.37 (0.35)	0.15
			555.3186	[2M+Na] <sup>+</sup>	251.17 (0.11)	0.05
Tri-o-tolyl phosphate <sup>#</sup>	TOTP	C <sub>21</sub> H <sub>21</sub> O <sub>4</sub> P	369.1250	[M+H] <sup>+</sup>	181.06 (0.40)	0.22
			391.1070	[M+Na] <sup>+</sup>	190.76 (0.26)	0.14
Triphenyl phosphate <sup>#</sup>	TPhP	C <sub>18</sub> H <sub>15</sub> O <sub>4</sub> P	327.0781	[M+H] <sup>+</sup>	170.85 (0.22)	0.13
			349.0600	[M+Na] <sup>+</sup>	181.61 (0.29)	0.16
Tri-p-tolyl phosphate <sup>#</sup>	TPTP	C <sub>21</sub> H <sub>21</sub> O <sub>4</sub> P	369.1250	[M+H] <sup>+</sup>	187.30 (0.30)	0.16
			391.1070	[M+Na] <sup>+</sup>	196.39 (0.29)	0.15
Tris(1,3-dichloro-2-propyl) phosphate <sup>#</sup>	TDCIPP	C <sub>9</sub> H <sub>15</sub> Cl <sub>6</sub> O <sub>4</sub> P	428.8912	[M+H] <sup>+</sup>	176.76 (0.03)	0.02
			428.8912	[M+H] <sup>+</sup>	178.44 (0.32)	0.18
			428.8912	[M+H] <sup>+</sup>	180.17 (0.19)	0.10
			450.8731	[M+Na] <sup>+</sup>	188.05 (0.06)	0.03
Tris(2,3-dibromo-propyl) phosphate	TDBPP	C <sub>9</sub> H <sub>15</sub> Br <sub>6</sub> O <sub>4</sub> P	692.5881	[M+H] <sup>+</sup>	189.66 (0.34)	0.18
			692.5881	[M+H] <sup>+</sup>	191.90 (0.31)	0.16
			692.5881	[M+H] <sup>+</sup>	194.62 (0.32)	0.16
			714.5700	[M+Na] <sup>+</sup>	202.89 (0.49)	0.24
			716.5680	[M+Na] <sup>+</sup>	202.39 (0.23)	0.11
Tris(2-butoxyethyl) phosphate	TBOEP	C <sub>18</sub> H <sub>39</sub> O <sub>7</sub> P	399.2506	[M+H] <sup>+</sup>	197.55 (0.19)	0.10
			421.2326	[M+Na] <sup>+</sup>	199.48 (0.03)	0.01
Tris(2-chloroethyl) phosphate	TCEP	C <sub>6</sub> H <sub>12</sub> Cl <sub>3</sub> O <sub>4</sub> P	284.9612	[M+H] <sup>+</sup>	149.84 (0.06)	0.04
			306.9431	[M+Na] <sup>+</sup>	158.78 (0.17)	0.11
Tris(2-chloroiso-propyl) phosphate	TCIPP	C <sub>9</sub> H <sub>18</sub> Cl <sub>3</sub> O <sub>4</sub> P	348.9900	[M+Na] <sup>+</sup>	169.89 (0.18)	0.11
Tris(2-ethylhexyl) phosphate	TEHP	C <sub>24</sub> H <sub>51</sub> O <sub>4</sub> P	457.3417	[M+Na] <sup>+</sup>	229.64 (0.23)	0.10
Tris(tert-butyl-phenyl) phosphate	TTBPP	C <sub>30</sub> H <sub>39</sub> O <sub>4</sub> P	495.2659	[M+H] <sup>+</sup>	238.35 (0.23)	0.10
			517.2478	[M+Na] <sup>+</sup>	244.64 (0.16)	0.07
Di(2-ethylhexyl) phthalate <sup>#</sup>	DEHP	C <sub>24</sub> H <sub>38</sub> O <sub>4</sub>	413.2662	[M+Na] <sup>+</sup>	215.48 (0.56)	0.26
Di(2-ethylhexyl) terephthalate	DEHT	C <sub>24</sub> H <sub>38</sub> O <sub>4</sub>	413.2662	[M+Na] <sup>+</sup>	216.46 (0.06)	0.03
Diisodecyl phthalate	DiDP	C <sub>28</sub> H <sub>46</sub> O <sub>4</sub>	447.3469	[M+H] <sup>+</sup>	229.69 (0.20)	0.09
			469.3288	[M+Na] <sup>+</sup>	227.75 (0.39)	0.17
Diisononyl hexahydrophthalate	DINCH	C <sub>26</sub> H <sub>48</sub> O <sub>4</sub>	447.3445	[M+Na] <sup>+</sup>	223.15 (0.06)	0.03
Diisononyl phthalate	DINP	C <sub>26</sub> H <sub>42</sub> O <sub>4</sub>	419.3156	[M+H] <sup>+</sup>	221.15 (0.35)	0.16
			441.2975	[M+Na] <sup>+</sup>	222.08 (0.40)	0.18
Diphenyl phthalate <sup>#</sup>	DPP	C <sub>20</sub> H <sub>14</sub> O <sub>4</sub>	341.0784	[M+Na] <sup>+</sup>	180.02 (0.19)	0.10
Tri-n-hexyl-trimellitate	THTM	C <sub>27</sub> H <sub>42</sub> O <sub>6</sub>	463.3054	[M+H] <sup>+</sup>	236.67 (0.21)	0.09
			485.2874	[M+Na] <sup>+</sup>	247.25 (0.20)	0.08
Tris(2-ethylhexyl) trimellitate	TOTM	C <sub>33</sub> H <sub>54</sub> O <sub>6</sub>	569.3813	[M+Na] <sup>+</sup>	266.38 (0.14)	0.05

Compound name	Abbreviation	Molecular formula	<i>m/z</i>	Ion	<sup>D1</sup> CCS <sub>N2</sub> (±SD) [Å <sup>2</sup> ]	RSD [%]
<i>ortho, ortho</i> -Bisphenol A*	o,o-BPA	C <sub>15</sub> H <sub>16</sub> O <sub>2</sub>	227.1078	[M-H] <sup>-</sup>	151.90 (0.06)	0.04
<i>ortho, para</i> -Bisphenol A*	o,p-BPA	C <sub>15</sub> H <sub>16</sub> O <sub>2</sub>	227.1078	[M-H] <sup>-</sup>	155.96 (0.04)	0.02
Bisphenol E	BPE	C <sub>14</sub> H <sub>14</sub> O <sub>2</sub>	213.0916	[M-H] <sup>-</sup>	158.10 (0.01)	0.01
Bisphenol M	BPM	C <sub>24</sub> H <sub>26</sub> O <sub>2</sub>	345.1860	[M-H] <sup>-</sup>	182.26 (0.02)	0.01
Tetrabromobisphenol A	TBBPA	C <sub>15</sub> H <sub>12</sub> Br <sub>4</sub> O <sub>2</sub>	542.7453	[M-H] <sup>-</sup>	192.43 (0.29)	0.15
4,4'-Methylenebis(2,6-dimethylphenol)	TMBPF	C <sub>17</sub> H <sub>20</sub> O <sub>2</sub>	255.1385	[M-H] <sup>-</sup>	174.20 (0.02)	0.01
Tetrachlorobisphenol A	TeCBPA	C <sub>15</sub> H <sub>12</sub> Cl <sub>4</sub> O <sub>2</sub>	362.9513	[M-H] <sup>-</sup>	184.07 (0.03)	0.02

**Table SI-3.3.2:** Compound classes included in this study and the sources from which the corresponding reference standards were purchased.

Investigated compound/compound class	Source from which reference standards were obtained
Bisphenols	Sigma Aldrich Chemie GmbH (Steinheim, Germany) Toronto Research Chemicals (Toronto, Canada)
Organophosphate flame retardants	Chiron AS (Trondheim, Norway) AccuStandard (New Heaven, CT, USA) TCI Europe (Zwijndrecht, Belgium)
Plasticizers	AccuStandard (New Heaven, CT, USA)

**Table SI-3.3.3:** Summary of methods used for the acquisition of TIMS data. ICC: Ion Charge Control.

Method	POS-1	POS-2	NEG-1	NEG-2	NEG-3
ICC [counts]	$2.5 \cdot 10^6$				
Mass range [ $m/z$ ]	100 - 1300	100 - 950	100 -1050	100 -800	100 - 800
Reduced mobility window [ $Vs/cm^2$ ]	0.45 - 1.43	0.70 - 1.25	0.50 - 1.30	0.80 - 1.00	0.8 - 1.00
Accumulation time [ms]	10	10	10	10	10
Ramp time [ms]	300	300	300	400	650
Funnel 1 RF [Vpp]	300	300	200	200	200
Funnel 2 RF [Vpp]	200	200	400	400	400
Multipole RF [Vpp]	60	60	300	300	300
Collision RF [Vpp]	450	450	600	600	600

**Table SI-3.3.4:** Experimental data obtained for QC compounds implemented within the acquisition of DTIMS derived reference  $^{DT}CCS_{N_2}$  values. For each compound, the obtained reference  $^{DT}CCS_{N_2}$  value (average of triplicate injection) and (relative) standard deviations are indicated (SD/RSD). The observed average mass error and percent error in comparison with literature  $^{DT}CCS_{N_2}$  values (obtained from Picache et al., 2019) are given.

QC compound	Theor. $m/z$	Exp. $^{DT}CCS_{N_2} \pm SD [Å^2]$	RSD [%]	$\bar{x}$ mass error [ppm]	Lit. $^{DT}CCS_{N_2} [Å^2]$	Error [%]
Pyridoxalphosphate	246.0173	$149.48 \pm 0.02$	0.01	1.62	149.35	0.09
L-Histidine	154.0622	$128.48 \pm 0.02$	0.01	0.01	128.83	0.27
L-Phenylalanine	164.0717	$139.74 \pm 0.08$	0.05	1.20	139.94	0.15
L-Tyrosine	180.0666	$144.19 \pm 0.04$	0.03	0.40	144.42	0.16

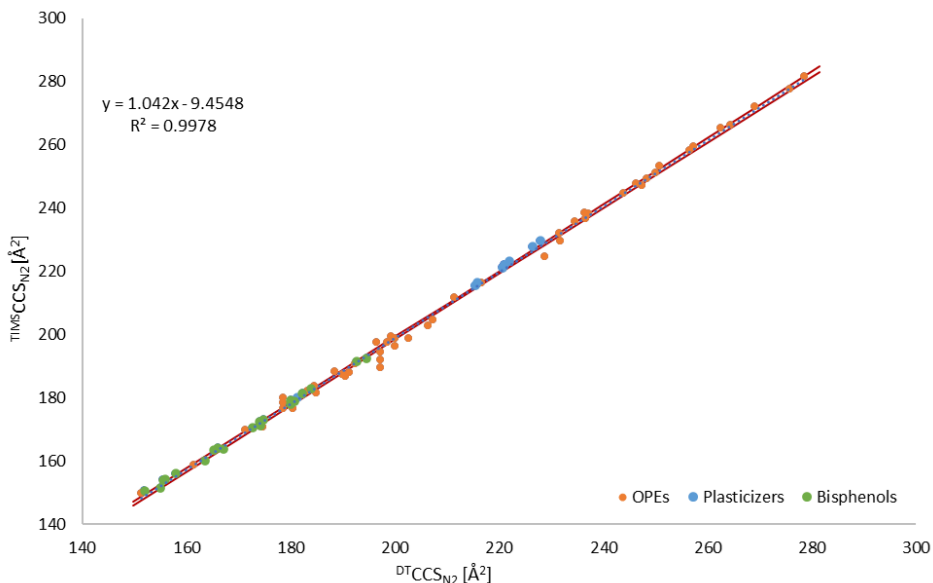


**Figure SI-3.3.1:** Linear regression model describing the relationship between  $DTCCSN_2$  and  $TIM^5CCSN_2$  values. The three compound classes are indicated in orange, blue and green for organophosphate flame retardants (OPEs), plasticizers and bisphenols, respectively. The 95% confidence interval of the regression line is indicated with red lines.

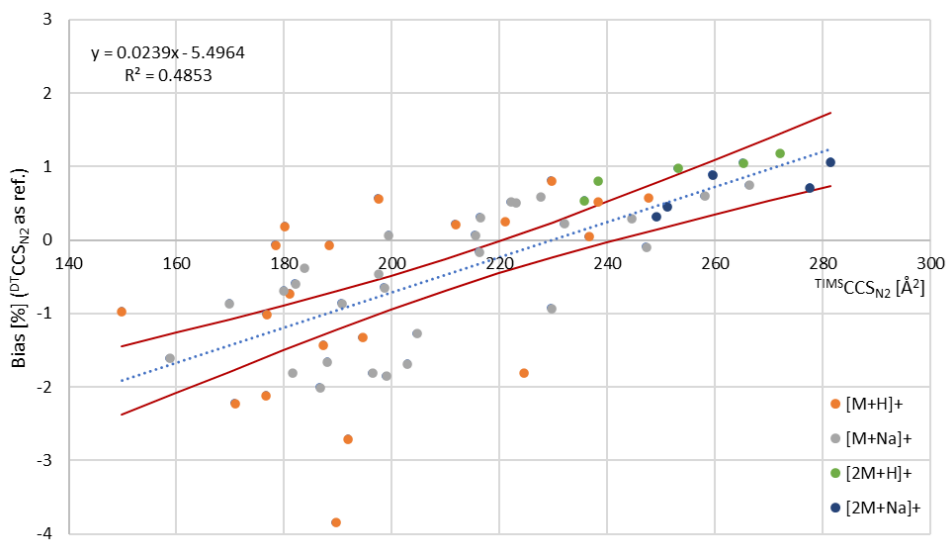


**Figure SI-3.3.2:** Percent bias (with  $DTCCSN_2$  set as reference) as a function of corresponding  $TIM^5CCSN_2$  values. Datapoints obtained in positive ionization polarity are included and a distinction between  $[M+H]^+$  (orange),  $[M+Na]^+$  (grey),  $[2M+H]^+$  (green) and  $[2M+Na]^+$  (blue) is made. The complete dataset was described using a linear model with the trendline represented by the blue dotted line. The equation and correlation coefficient of the obtained trendline are indicated. The 95% confidence interval of the regression line is indicated with red lines.

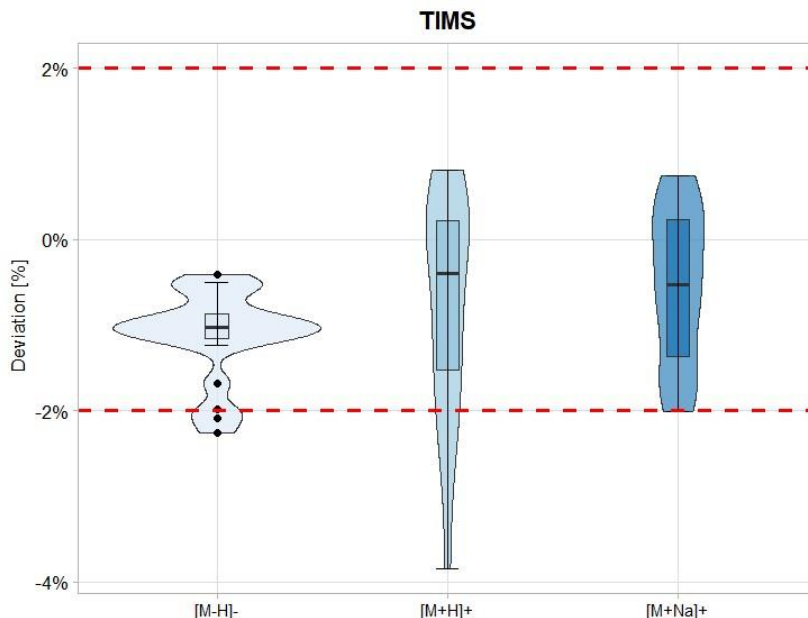


**Figure SI-3.3.3:** Combined violin and boxplots of percent deviations observed when comparing  ${}^{\text{TMS}}\text{CCS}_{\text{N}_2}$  and  ${}^{\text{DT}}\text{CCS}_{\text{N}_2}$  values (latter set as reference). For data in positive ionization polarity, a distinction between proton and sodium adducts is made. The threshold of  $\pm 2\%$ , commonly applied for database transfer (Celma et al., 2020), is indicated with a red dashed line.

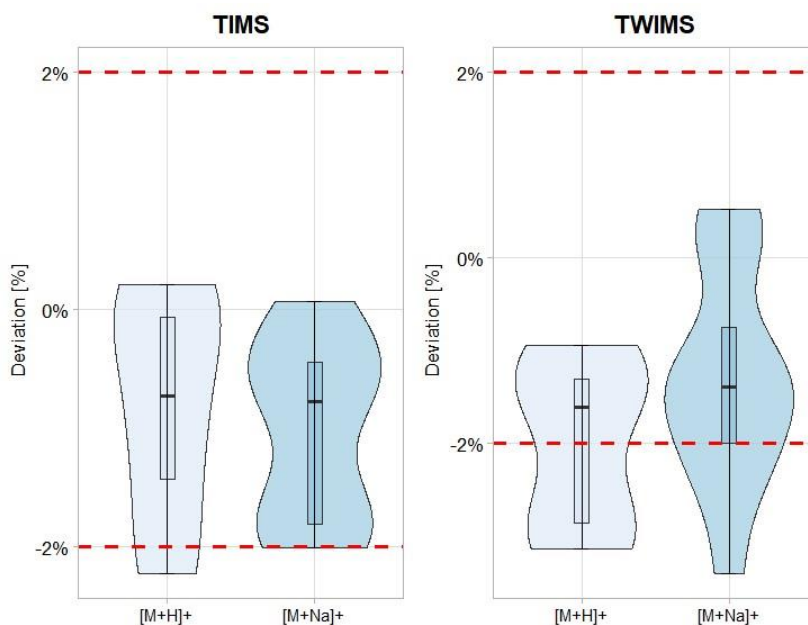


**Figure SI-3.3.4:** Combined violin and boxplots of percent deviations observed when comparing  ${}^{\text{TMS}}\text{CCS}_{\text{N}_2}$  and  ${}^{\text{TW}}\text{CCS}_{\text{N}_2}$  with  ${}^{\text{DT}}\text{CCS}_{\text{N}_2}$  values (latter set as reference). Only datapoints for which both, TWIMS and TMS derived data were available are included resulting in a total of 19 datapoints. A distinction between proton and sodium adducts is made. The threshold of  $\pm 2\%$ , commonly applied for database transfer (Celma et al., 2020), is indicated with a red dashed line.

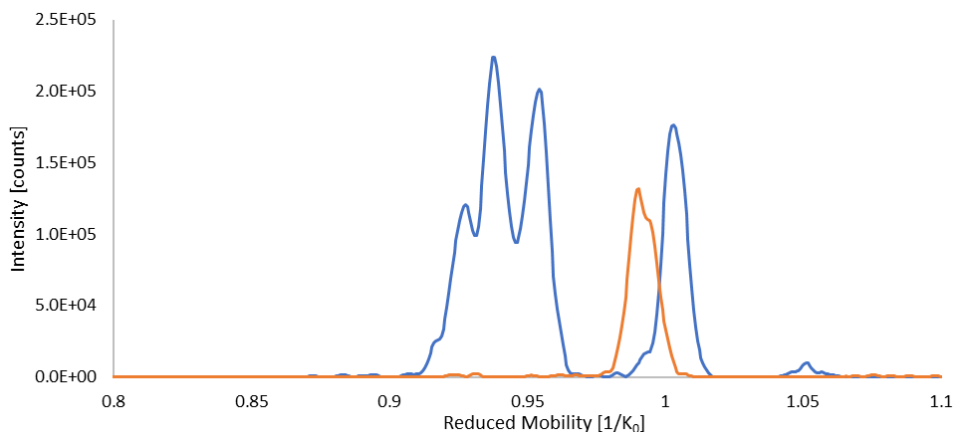


**Figure SI-3.3.5:** Extracted TIMS mobiligram for the proton and sodium adducts of tris(2,3-dibromopropyl)phosphate (TDBPP). The (theoretical)  $m/z$  ratios of 696.5840 (blue; second most abundant isotopologue of  $[M+H]^+$  ion) and 716.5680 (orange; third most abundant isotope of  $[M+Na]^+$  ion) were extracted applying a mass window of  $\pm 0.01$  Da. Mobiligrams were zoomed in covering a window in which peaks of the extracted  $m/z$  ratios occurred.

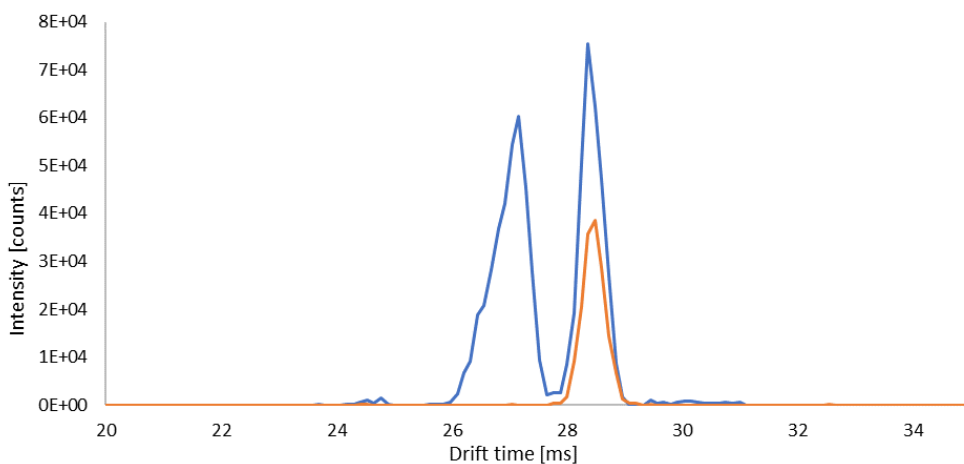


**Figure SI-3.3.6:** Extracted DTIM mobiligram for the proton and sodium adducts of tris(2,3-dibromopropyl)phosphate (TDBPP). The (theoretical)  $m/z$  ratios of 696.5840 (blue; second most abundant isotopologue of  $[M+H]^+$  ion) and 716.5680 (orange; third most abundant isotope of  $[M+Na]^+$  ion) were extracted applying a mass window of  $\pm 0.01$  Da. Instrumental settings used for the acquisition of DTIM data have been reported previously<sup>1</sup>. Mobiligrams were zoomed in covering a window in which peaks of the extracted  $m/z$  ratios occurred.

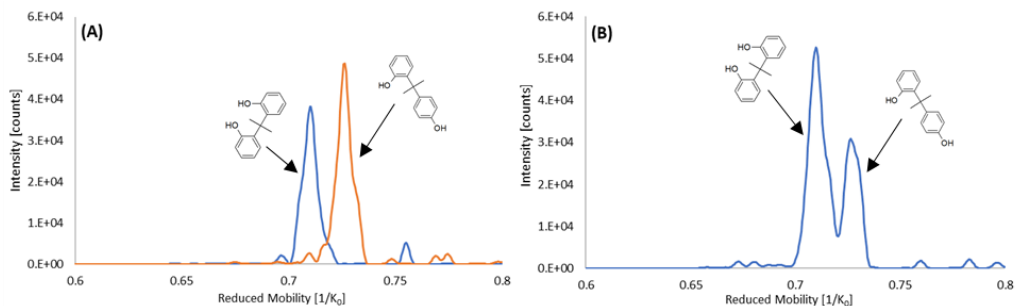


**Figure SI-3.3.7:** Extracted TIMS mobilograms of *ortho,ortho*-bisphenol A (o,o-BPA, displayed in blue in plot (A)) and *ortho,para*-bisphenol A (o,p-BPA, displayed in orange in plot (A)). Both compounds were injected as individual solutions (A) and as a mixture (B). The (theoretical)  $m/z$  ratio of 227.1078 of the deprotonated ion was extracted applying a mass window of  $\pm 0.01$  Da.

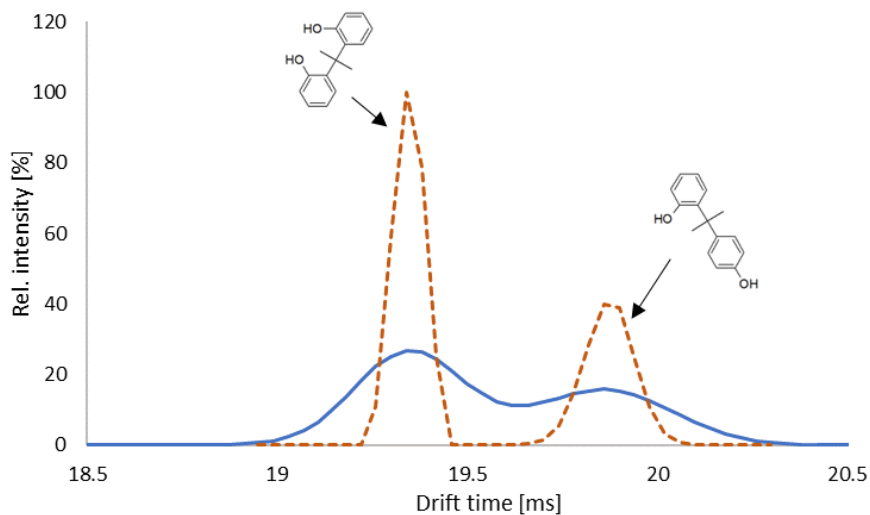


**Figure SI-3.3.8:** Extracted DTIM mobilograms of *ortho,ortho*-bisphenol A and *ortho,para*-bisphenol A. Both compounds were injected as a mixture. The (theoretical)  $m/z$  ratio of 227.1078 of the deprotonated ion was extracted applying a mass window of  $\pm 0.01$  Da. The mobilograms displayed in blue were acquired using the initial method used for <sup>DT</sup>CCS<sub>N2</sub> database compilation. To acquire the mobilogram displayed in orange dashed line, data were post-processed applying the high-resolution data demultiplexing tool.

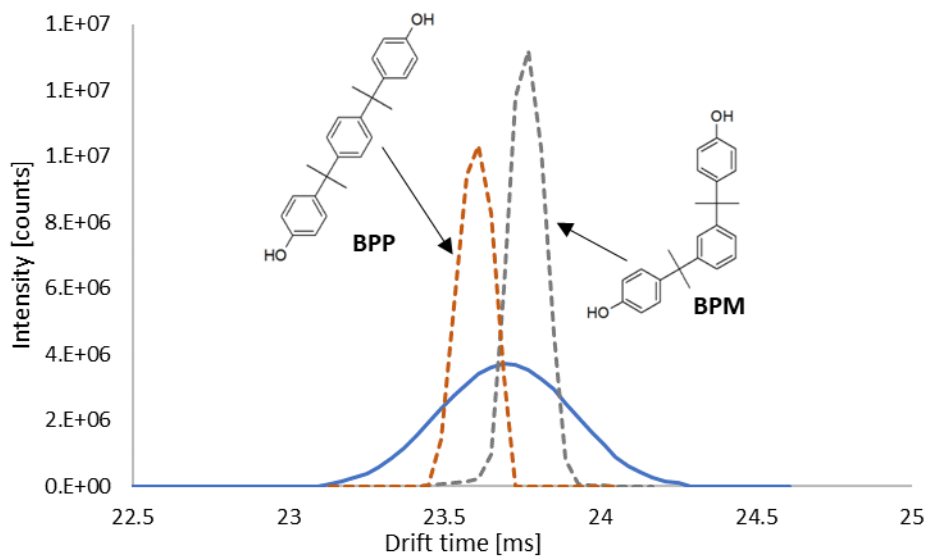
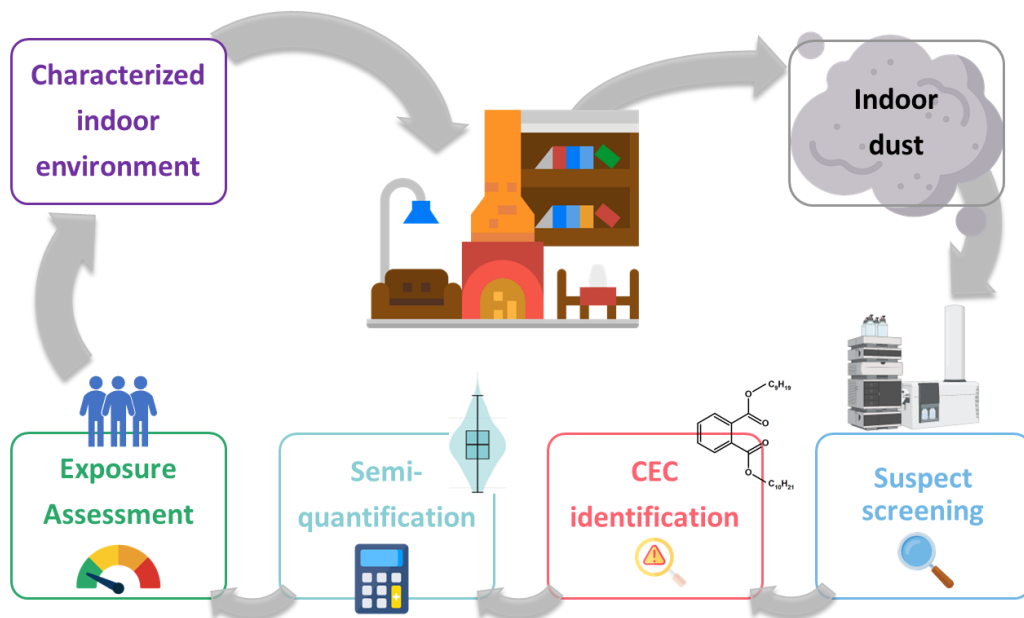


**Figure SI-3.3.9:** Extracted DTIM mobilograms of bisphenol P and bisphenol M. Both compounds were injected as a mixture. The mobilograms displayed in blue were acquired using the initial method used for  $^{DT}CCS_{N_2}$  database compilation, as described by Belova et al., 2021. To acquire the mobilograms displayed in orange and grey dashed lines, data were post-processed by applying the high-resolution data demultiplexing tool.





# Chapter 4: Identification of known and emerging contaminants in indoor dust



This chapter is based on the following publications:

Belova, L., Poma, G., Roggeman, M., Jeong, Y., Kim, D.-H., Berghmans, P., Peters, J., Salamova, A., van Nuijs, A.L.N., Covaci, A. Identification and characterization of quaternary ammonium compounds in Flemish indoor dust by ion-mobility high-resolution mass spectrometry. *Environment International*. **2023**. 177: 108021.

Belova, L., Roggeman, M., den Ouden, F., Cleys, P., Ait Bamai, Y., Yin, S., Zhao, Y., Bombeke, J., Peters, J., Berghmans, P., Gys, C., van Nuijs, A.L.N., Poma, G., Covaci, A. Identification, semi-quantification and risk assessment of contaminants of emerging concern in Flemish indoor dust through high-resolution mass spectrometry. *Environmental Pollution*. **2024**. 345: 123475.



## 4.1 Identification and semi-quantification of quaternary ammonium compounds in indoor dust using IM derived CCS-*m/z* trendlines as an additional identification parameter

### 4.1.1 Introduction

Quaternary ammonium compounds (QACs) are a group of compounds which consist of a quaternary ammonium cation substituted with one or more hydrophobic hydrocarbon side chains and three or less shorter side chains, leading to amphiphilic properties. QACs have many applications as surfactants, in cleaning products, softeners and personal care products. Alkyl trimethylammonium compounds (ATMACs), benzyl alkyldimethyl ammonium compounds (BACs) and dialkyl dimethylammonium compounds (DDACs; in some studies abbreviated as DADMAC) are the most frequently used QAC classes (**Figure 4.1.1**). Following their wide applications, QACs have been detected in various environmental matrices, such as surface sediments (Li and Brownawell, 2009; Pintado-Herrera et al., 2017), wastewater (Pati and Arnold, 2020; Wieck et al., 2018), sludge (Godfrey et al., 2022; Östman et al., 2017), surface water (Köppe et al., 2023), indoor dust (Zheng et al., 2020) and food (Bertuzzi and Pietri, 2014; Xian et al., 2016).

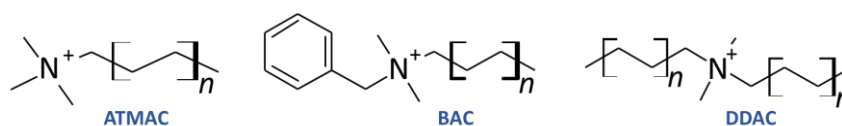


**Figure 4.1.1:** Structures of most commonly used quaternary ammonium compound (QAC) classes: alkyl trimethylammonium compounds (ATMACs), benzyl alkyldimethyl ammonium compounds (BACs) and dialkyl dimethylammonium compounds (DDACs). Previously reported QACs in indoor dust included even numbered chain lengths with  $n = 8-18$ ,  $n = 6-18$  and  $n = 8-18$  for ATMACs, BACs and DDACs, respectively (Zheng et al., 2020).

Antimicrobial activities have been described for QACs as these can interact with the phospholipid membranes of viruses, bacteria and other pathogens (Gilbert and Moore, 2005). This leads to membrane disruption and ultimately to cell lysis (Schrank et al., 2020). Due to these properties, QACs are widely applied in disinfecting agents, hand sanitizers, soaps and disinfecting hand wipes. During the COVID-19 pandemic, caused by the SARS coronavirus 2 (SARS-CoV-2), significantly higher concentrations of various QACs were measured in indoor dust (Zheng et al., 2020) and human blood samples (Zheng et al., 2021) collected in the USA compared to samples collected before the COVID-19 pandemic. This suggests a substantial increase in the use of products containing QACs and therefore also in the potential risk of increased human exposure to these chemicals.

This opened a big research gap since data on the occurrence of QACs in European microenvironments is lacking.

Oral ingestion, (dust) inhalation and dermal absorption (e.g., through contact with disinfected surfaces) have been identified as possible human exposure routes to QACs (Li et al., 2020). Furthermore, these chemicals have recently been detected in breast milk samples indicating a potential exposure of nursing infants (Zheng et al., 2022). Another exposure source can be assumed through the intake of contaminated foods as QACs have been detected in dry and liquid milk samples as well as various sorts of vegetables (Bertuzzi and Pietri, 2014; Xian et al., 2016).

Following the detection of QACs in various foods, an Acceptable Daily Intake (ADI) of 0.1 mg/kg body weight (bw) per day has been established by the European Food Safety Authority (EFSA) (EFSA, 2014a). The given ADI applies (separately) for both DDACs and BACs covering (even numbered) chain lengths of C<sub>8</sub>-C<sub>12</sub> and C<sub>8</sub>-C<sub>18</sub>, respectively.

The need of reliable data on human exposure to QACs is supported by numerous toxic effects described for this compound class. Within *in vitro* models, BACs were identified as potent inhibitors of the cholesterol biosynthesis in both human and mouse cells (Herron et al., 2016). Exposure of mice to mixtures of QACs with doses up to 480 mg/kg bw/day ( $\Sigma$ QAC) lead to various effects including immune cell dysfunction, birth defects and decreased fertility (Abdelhamid et al., 2020; Hrubec et al., 2017; Melin et al., 2014).

In humans, the exposure to QACs has been associated with several hypersensitivity reactions such as inflammation, contact dermatitis and ocular hypersensitivity, supported by multiple case reports from humans exposed to QACs (Oropeza et al., 2011; Peyneau et al., 2022; Purohit et al., 2000). However, these observations derived from single case studies or from occupational studies in which QAC exposure was assessed through questionnaires and not through objective quantitative measurements (LaKind and Goodman, 2019) hampering the linkage of these results to internal QAC levels. Lastly, a study on human blood samples collected from 43 volunteers in the US reported QACs with a detection frequency (DF) of 80%, identifying an association between QAC concentrations and a decrease in mitochondrial function as well as an increase in inflammatory cytokines (Hrubec et al., 2021). The assessment of correlations between toxic effects in animal studies and toxicity observed in humans following (potentially chronic) QAC exposure, is thus hampered by the unavailability of data on biotransformation of these compounds, which is crucial for the design of biomonitoring studies. This data gap will be addressed in **chapter 6**.

Within most available studies, the analysis of QACs in environmental samples was performed by applying quantitative methods based on liquid chromatography coupled to tandem mass spectrometry (Slimani et al., 2017; Zheng et al., 2020). While

this targeted approach allows the unequivocal identification and quantification of a limited number of analytes of interest, QACs not included in the target list remain undetected. On the contrary, SSA and NTS would allow a simultaneous detection and identification of a higher number of QACs. For example, SSA was applied for the identification of various cationic surfactants in wastewater samples based on an extensive suspect list which, besides a large set of (emerging) environmental contaminants contained two suspect lists derived from the NORMAN suspect list exchange (S7 EAWAGSURF (410 compounds) and S23 EIUBASURF (1154 compounds) focusing specifically on surface active substances (Alygizakis et al., 2021). Yet, the application of suspect screening approaches for a comprehensive characterization of QACs present in indoor dust samples has not been performed before.

Similarly, the implementation of IM-MS in suspect screening studies on QACs is limited even though it can provide valuable additional information for compound annotation. Only one previous study provided reference  $^{TW}CCS_{N_2}$  values for a set of QACs (Song et al., 2022). This allowed a first investigation of the correlations between CCS and  $m/z$  values, referred to as 'CCS- $m/z$  trendlines', for this compound class. In **chapter 3.1**, CCS- $m/z$  trendlines have already been characterized for other classes of environmental contaminants, such as PFAS or APs. These trendlines are hypothesized to facilitate compound identification by matching a suspected compound from the class with the defined trendline for the class of contaminants.

This chapter presents the first comprehensive target and suspect screening analysis of QACs in indoor dust samples collected in Belgium. Even though this approach cannot account for QAC exposure through, for example, consumption of contaminated food or direct contact with QAC containing product, indoor dust was identified as a matrix relevant for human exposure to various contaminants (Christia et al., 2021b; Zheng et al., 2020). The target screening included the unequivocal identification and semi-quantification of 21 QACs (belonging to ATMAC, BAC and DDAC classes) for which reference standards were available. Additionally, a suspect list containing > 350 formulae of known and predicted QACs was used to identify QACs not included in the targeted approach. To further improve compound annotation, reference  $^{DT}CCS_{N_2}$  values of the 21 available QAC standards were acquired based on applying the method described in **chapter 3.1** to characterize CCS- $m/z$  trendlines for each of the investigated QAC classes. These allowed the comparison of  $^{DT}CCS_{N_2}$  values acquired for the suspect QACs with the previously established CCS- $m/z$  trendlines to increase identification confidence.

## 4.1.2 Materials and Methods

### 4.1.2.1 Chemicals

All solvents used in this study were of ULC/MS purity. Methanol (MeOH), acetonitrile (ACN), isopropanol and formic acid (99%, used as mobile phase modifier) were purchased from Biosolve BV (Valkenswaard, the Netherlands). Ultrapure water (18.2 M $\Omega$  cm, Milli-Q, Millipore) was obtained using a PURELAB Flexsystem. Ammonium acetate which was used as a mobile phase additive, was purchased from Sigma Aldrich (Missouri, USA). Twenty-one individual standards of QACs were purchased from Sigma Aldrich Chemie GmbH (Steinheim, Germany) and are summarized in **Table SI-4.1.1**. Three labelled QAC standards (*D*<sub>7</sub>-C<sub>12</sub>-BAC, *D*<sub>7</sub>-C<sub>14</sub>-BAC and *D*<sub>9</sub>-C<sub>10</sub>-ATMAC) were obtained from Toronto Research Chemicals (Toronto, Canada) and used as internal standards (IS). Cortisol, creatinine, L-phenylalanine, which were used as QC compounds within IM-MS measurements, were purchased from Sigma Aldrich Chemie GmbH (Steinheim, Germany).

Stock solutions of QACs were prepared in methanol at a concentration of 1 mg/mL. Working solutions at the desired concentrations were obtained through further dilution of the stock solution with methanol.

### 4.1.2.2 Sample collection

Dust samples were collected in January and February 2022 at 40 locations spread throughout Flanders, Belgium. The locations included private dwellings (n = 24) and public locations (n = 16) such as offices, university auditoriums, and sport halls. At three locations (corresponding to one sport hall and two campuses with several auditoriums under the same address), more than one sample was collected resulting in a total of 46 dust samples included in this study. For each sampling site, information about the type (public vs. private) and age of the sampled building, the location (urban vs. rural) and the time passed since the last cleaning was obtained through a questionnaire (**Table SI-4.1.2**).

The sample collection approach was based on previously described methods (Christia et al., 2021b; Harrad et al., 2008). An area of 1 m<sup>2</sup> (in case of carpet flooring) or 4 m<sup>2</sup> (in case of hard flooring) was vacuumed for 1 min/m<sup>2</sup>. The head of the vacuum cleaner was equipped with a nylon bag filter (pore size: 25  $\mu$ m) which allowed the dust collection. At 8 locations, field blanks were collected by gritting of sodium sulphate on a previously vacuumed floor and collecting latter in the same way as the dust samples. Samples were stored at room temperature in Falcon tubes prior to analysis.

#### 4.1.2.3 Sample preparation

All dust samples were homogenized through mixing and sieved using a mesh size of 500  $\mu\text{m}$  (Christia et al., 2021b). Dust aliquots of 20 mg were weighed and spiked with 12 ng of each of the three labelled IS (final concentration in extract: 50  $\text{pg}/\mu\text{L}$ ). Samples were directly extracted twice with 3 mL of MeOH. The direct extraction included vortexing for 1 min and consecutive sonication for 1h. The extracts were pooled and evaporated to dryness under a gentle nitrogen stream. After reconstitution in 240  $\mu\text{L}$  MeOH:H<sub>2</sub>O (9:1; v/v) and vortexing for 1 min, samples were filtered using centrifugal filters (0.2  $\mu\text{m}$  pore size; VWR, Leuven, Belgium) and analyzed applying the methods described below. Within sample preparation, four procedural blanks spiked with IS and four QC (see **chapter 4.1.2.8**) samples were included and treated applying the same approach as for the actual samples.

#### 4.1.2.4 Instrumental analysis

All measurements were conducted on an Agilent 6560 ion-mobility quadrupole time-of-flight high-resolution mass spectrometer coupled to an Agilent 1290 Infinity II UPLC system (Agilent Technologies, Santa Clara, USA). The instrument was equipped with a Dual Jet Stream ESI source. For all measurements, the MassHunter Data Acquisition software (version B.09.00, Agilent Technologies) was used. Chromatographic separation was achieved by applying a method modified from an approach described by Li and Brownawell (Li and Brownawell, 2009). A Phenomenex LUNA C18 column (150 mm x 2 mm; 3  $\mu\text{m}$  particle size) was used. A quaternary pump allowed the implementation of a ternary gradient using the following three mobile phases: (A) ACN:H<sub>2</sub>O 80:20 (v/v) + 0.1% acetic acid; (B) ACN:H<sub>2</sub>O 95:5 (v/v) + 5 mM ammonium acetate; (C) isopropanol + 0.1% formic acid. The detailed chromatographic conditions and gradient are summarized in **Table SI-4.1.3**.

Data was acquired in positive ionization mode only. The following ion source settings were used: gas temperature and flow were set to 300 °C and 11 L/min, respectively. For the sheath gas, the temperature and flow were 300 °C and 12 L/min, respectively. The nebulizer pressure was set to 30 psig. Voltages of 3000 V, 500 V and 300 V were applied for the capillary cap, nozzle and fragmentor, respectively. Within the QTOF only approach, data dependent acquisition (referred to as 'Auto MS/MS' by the instruments' manufacturer) was used whereby, per scan, 4 precursor ions were automatically selected for fragmentation at 10, 20 and 40 eV. Thereby, mass ranges and scan rates were set to  $m/z$  100-1500 – 4 spectra/sec and  $m/z$  50-1500 – 8 spectra/sec for MS and MS/MS, respectively. The IM-MS settings are summarized in **Table SI-4.1.4**. Even though the IM-MS data was acquired in alternating frames mode including all-ions

fragmentation, a discussion of the IM-MS fragmentation spectra is not included here as further optimization of the fragmentation parameters is necessary which is subject of an ongoing study. Therefore, for compound identification through suspect screening, fragmentation spectra acquired in QTOF only mode were used. These allowed a clear assignment of fragments to the corresponding parent ion which was not possible for all IM-MS derived data files given high noise levels in lower  $m/z$  ranges. The suspect screening analysis suggested the presence of isomers for some of the detected suspects. Therefore, a sub-selection of 20 samples was reinjected in 4-bit multiplexing IM-MS mode (**Table SI-4.1.4**). The LC conditions and ion source settings were identical between IM-MS and QTOF only measurements. Within each of the IM-MS acquisition sequences, data for the tune mix ions included in the ESI low-concentration tune mix (Agilent Technologies, Santa Clara) was acquired under the exact same conditions as for the rest of the sequence. The acquired calibrant data was used for single-field calibration and consecutive calculation of  $^{DT}CCS_{N_2}$  values for each of the suspects.

#### 4.1.2.5 Target screening - data analysis

The raw data files obtained using the QTOF only acquisition approach were screened in a targeted manner for the 21 QACs available as reference standards using the 'Find By Formula' algorithm of the MassHunter Qualitative Analysis software (version B.07.00). Thereby, mass and retention time (RT) cut-offs of 5 ppm and 0.2 min were applied, respectively. If all molecular identifiers of a detected compound, including the  $m/z$  ratio, isotopic pattern, RT and fragmentation spectrum, unequivocally matched the corresponding reference standard, confidence level (CL) 1 was assigned following the system introduced by Schymanski et al. (Schymanski et al., 2014). However, this system does not allow to reflect the detection of a compound for which the  $m/z$  ratio, isotopic pattern, and RT match the reference standard, but no fragmentation spectrum is available. Such compound detection is considered to have a higher identification confidence than a CL3 assignment since reference data from a reference standard is available. At the same time, the assignment of CL1 is not justified as the set of experimental data is not complete. Since the existing subdivision of CL2 does not reflect the described case, a third subdivision of CL2, namely the assignment of CL2C, was proposed as described in **chapter 5**. Following this proposal, targeted matches for which no fragmentation spectrum was available were assigned with CL2C. The peaks of all targeted compounds were integrated applying the Agile 2 integrator implemented in the 'Find By Formula' algorithm.

#### 4.1.2.6 Suspect screening - data analysis

Additionally to the target screening, a suspect screening was performed using the data files acquired in QTOF only mode. A suspect list containing > 350 entities was created including QACs from the three investigated classes (ATMACs, BACs and DDACs; **Table SI-4.1.5**). Homologues with varying lengths of the hydrocarbon side chain(s) were included (both even and uneven numbers of carbon atoms). Targeted QACs, covered within the approach described in **chapter 4.1.2.5**, were also included as their detection served as a positive control within the suspect screening workflow. The suspect list also contained (positively charged) quaternary ammonium surfactants from other classes, such as derivatives of piperidinium, pyridinium, imidazolium and others. These were expected to also be detectable by the described data analysis approach which focused specifically on the detection of the  $[M^+]$  ion.

Raw data files were preprocessed using the Agilent MassHunter Profinder software (version 10.0). Chromatographic alignment, peak picking and recursive feature extraction were performed applying the batch recursive feature extraction algorithm for small molecules. Thereby, the following settings were applied: The RT was restricted to a range from 1.0 to 20.5 min. The minimum peak height was set to 500 counts. Compounds were aligned with mass and RT tolerances of 15 ppm and 0.2 min, respectively. Post-processing filters were restricted to an absolute height of 5000 counts and a molecular feature extraction (MFE) score of 70. The extracted features were exported as a compound exchange file (.cef) for further processing using the Mass Profiler Professional software (version 15.1). A fold change analysis was performed which retained features showing a fold change (FC) of 5 or higher compared to their intensities in the procedural blanks. If a compound was detected in a field blank sample at a signal intensity which exceeded the 5-fold signal intensity detected in the procedural blanks, the signal intensity observed in the dust sample collected at the same location was manually investigated. This aimed at verifying that the intensity observed in the dust sample exceeds the 5-fold intensity of the field blank sample. The remaining filtered features were matched against the developed suspect list using the IDBrowser software (version 10.0) and applying a mass tolerance cut-off of 10 ppm and an overall matching score of at least 70. Only  $[M^+]$  ions were considered.

All obtained matches were manually investigated to evaluate the peak shape, isotopic pattern and the availability and quality of fragmentation spectra. If no reference fragmentation spectra or characteristic fragments were available, experimental data was compared to a predicted fragmentation spectrum obtained using the MS Fragmenter software (ACD/Labs, version 2022.1.1). To each confirmed compound, an identification

CL was assigned following the workflow proposed by Schymanski et al. (Schymanski et al., 2014).

All IM-MS datafiles were recalibrated using the Agilent IM-MS Reprocessor (v10.00). For all identified suspects, the  $^{DT}CCS_{N_2}$  values were calculated from the single pulse datafiles applying the single-field calibration approach and the IM feature extraction algorithm of the Agilent IM-MS Browser (v10.0). Datafiles acquired in 4bit multiplexing mode, were demultiplexed using the PNNL Preprocessor (v 2022.02.17) (Prost et al., 2014). After feature extraction following the same workflow as for the single pulse data, a Feature list was compiled containing the features corresponding to compounds for which the presence of multiple isomers was assumed. The feature list was used for a consecutive data processing step using the recently introduced Agilent high resolution demultiplexing (HRdm) tool (v 2.0) with default processing settings, which allows an improved resolution in the IM dimension through a post-acquisition deconvolution step (May et al., 2020).

#### 4.1.2.7 Semi-quantification

For semi-quantification, calibration curves of the targeted QACs (**Table SI-4.1.1**) were prepared in methanol. The calibration curve of each QAC consisted of eight points covering a concentration range of 0.5 pg/ $\mu$ L to 100 pg/ $\mu$ L, resulting in a total of 21 calibration curves available for semi-quantification. All three IS were added to the calibration curves at the same concentration as in the dust extracts (final concentration in extract/calibration curve: 50 pg/ $\mu$ L). For each calibration point, the peak area relative to the IS was calculated for each of the targeted QACs. Since not all targeted QACs had a labelled IS, the used IS were selected based on structural similarity (for ATMACs and BACs) or similarity in RT (for DDACs). The assignment of an IS to the corresponding target QAC is summarized in **Table SI-4.1.6**. Calibration curves were fitted using a linear model (no weighing) and the response factor ( $R_f$ ) was obtained through calculation of the slope.

For each targeted QAC detected in the dust samples, the ratio between the peak areas of the compound and corresponding IS was used for semi-quantification of the concentration in the extract ( $c_{QAC}$  in **equation 4.1.1**). This was based on **equation 4.1.1** which included the response factor  $R_f$  and the peak area of the QAC of interest ( $A_{QAC}$ ) (relative to the peak area of the IS ( $A_{IS}$ )) detected in the dust samples (Malm et al., 2021):

$$c_{QAC} [\text{pg}/\mu\text{L}] = \frac{A_{QAC}/A_{IS}}{R_f} \quad (4.1.1)$$

All compounds identified through suspect screening were semi-quantified using the same approach. A calibration curve to be used for the semi-quantification was chosen based on structural similarity (Malm et al., 2021). When a compound was detected in the PBs, the average concentration calculated for the PBs was subtracted from the concentrations semi-quantified in the dust samples. If a compound was detected in a field blank sample at a signal intensity which exceeded the 5-fold signal intensity detected in the PBs, the signal intensity observed in the dust sample collected at the same location was manually investigated. This aimed at verifying that the intensity observed in the dust sample exceeds the 5-fold intensity of the field blank sample.

#### 4.1.2.8 Quality control

Four quality control (QC) samples were included in the analysis batch. These consisted of 50 mg of pre-cleaned sodium sulfate. Sodium sulfate was cleaned by sonicating it in hexane twice for 30 min. After cleaning, the sodium sulfate was placed in the oven overnight at 130°C to dry. Prior to sample preparation, the QC samples were spiked with all target QACs and IS listed in **Table SI-4.1.1** (except for C<sub>20</sub>-ATMAC as this standard was delivered with a major delay) and treated in the same way as the actual dust samples. The spiking concentration was 50 pg/μL (final concentration in extract) for both, the IS and targeted compounds. The injections of the four QC samples were evenly spread throughout the sample sequence. The concentrations of all targeted QACs in the QC samples were semi-quantified applying the approach described in **chapter 4.1.2.7** to estimate accuracy. Additionally, the QC samples were used to monitor mass accuracy, RT and signal stability throughout the sample sequence. The calibration curves obtained for the targeted QACs were investigated closely to access the correlation coefficients and linear range for each of the analytes.

To monitor the reproducibility of the CCS calculations within the IM-MS measurements, the QC approach described in **chapter 3.1** was implemented with slight modifications. This included a triplicate injection of three QC compounds (cortisol, creatinine, L-phenylalanine) within the IM-MS acquisition sequence. For these compounds, reference CCS values were previously established (Stow et al., 2017). A comparison of the data obtained within the presented study with the reference values allowed the estimation of the reliability of the reported CCS values both for the targeted and suspect QACs. Accuracy of measurements was considered acceptable if the APEs between experimental and reference CCS values did not exceed 1%.

#### 4.1.2.9 Exposure assessment

Summed median semi-quantitative concentrations acquired for the three groups of targeted QACs were used to estimate the human exposure based on the inadvertent ingestion of dust. For this assessment, the sample dataset was divided in “homes” and “public spaces”, based on the sample collection location, to better represent the different exposure scenarios. The estimated daily intake (EDI) (mg/kg body weight (bw)/day) was calculated following the general approach reported by McGrath et al. and displayed in **equation 4.1.2** (McGrath et al., 2022):

$$\text{EDI [ mg/kg bw/day]} = \frac{\text{Concentration} \times \text{Ingestion} \times \text{Fraction}}{\text{Body weight}} \quad (4.1.2)$$

*Concentration* refers to concentrations of semi-quantified QACs in dust. *Ingestion* refers to dust ingestion rates of 20 and 60 mg/day and of 50 and 100 mg/day for adults and toddlers in the 50<sup>th</sup> and 95<sup>th</sup> percentile exposure scenario, respectively (EPA, 2017), *fraction* refers to the fraction of time spent at home (0.69 for adults and 0.91 for toddlers) or in public spaces (0.18 for adults) (Klepeis et al., 2001; Poma et al., 2020), and *body weight* refers to a fixed body mass of 70 kg for adults and 12 kg for toddlers. Bioaccessibility was assumed to be 100% for each compound, to provide a conservative estimate of internal exposure (Christia et al., 2021a).

The potential risk of non-carcinogenic effects (Hazard Quotient, HQ) per QAC class was then calculated by dividing the EDI by the reference values established by the EFSA, which set an ADI of 0.1 mg/kg bw/day for both DDACs and BACs (EFSA, 2014a). This ADI value was also used to evaluate EDIs obtained for ATMACs, as no separate ADI was available for this group. HQ values equal to or greater than 1 indicate a potential exposure risk for the target population (EPA, 2024).

### 4.1.3 Results and Discussion

#### 4.1.3.1 Method development and quality control results

Due to the high hydrophobicity of (long chain) QACs, the chromatographic separation of these compounds has proven to be challenging due to carry over effects and instrument blank contamination (Manier et al., 2008). Li and Brownawell addressed this problem by implementing a separate chromatographic method for the analysis of DDACs, the most hydrophobic of the three QAC classes, in sediment samples using mobile phases with high elution power (Li and Brownawell, 2009). This approach resulted in a duplicate injection of the samples. The method presented by Li and Brownawell was used as a starting point for the chromatographic method developed in this study. Thereby, the

goal of combining the analysis of all QAC classes was followed. A quaternary pump was used allowing the development of a tertiary gradient with the mobile phases listed in **chapter 4.1.2.4** and **Table SI-4.1.3**. In the final stage of the gradient, the mobile phase composition reached 50% isopropanol ensuring an efficient elution of the long-chain DDACs. Additionally, the presented chromatographic method provided satisfying peak shapes for all analytes and allowed their spread over a wide RT range (3-17 min; **Figure 4.1.2**). Despite the high eluting strength in the final stage of the gradient, 10 out of 21 targeted QACs were detected in solvent blanks injected between samples, albeit at low signal abundances, which were consistent throughout the sample sequence. Since none of the blanks exceeded the abundances observed for the lowest calibration point (0.5 pg/ $\mu$ L), these slight carry over effects were considered negligible.

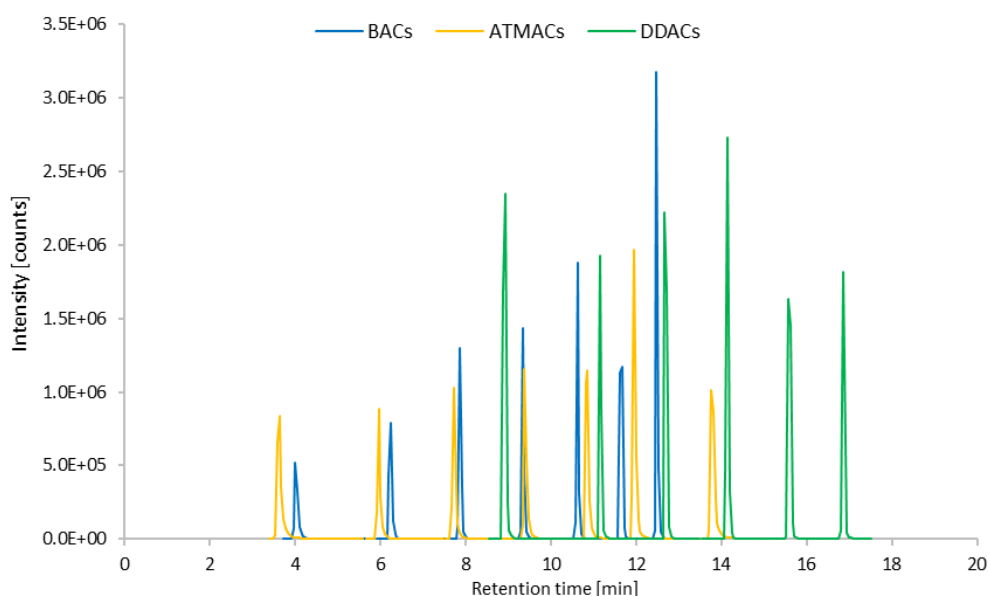


**Figure 4.1.2:** Total ion chromatogram obtained for a quality control sample containing all QACs listed in **Table SI-4.1.1** at a concentration of 0.05 ng/ $\mu$ L in methanol. Peaks of alkyltrimethylammonium compounds (ATMACs), benzylalkyldimethylammonium compounds (BACs) and dialkyldimethylammonium compounds (DDACs) are represented in yellow, blue and green, respectively. Chain lengths (with even numbers of carbons) of C<sub>8</sub>-C<sub>22</sub> (excluding C<sub>20</sub>-ATMAC), C<sub>6</sub>-C<sub>18</sub> and C<sub>8</sub>-C<sub>18</sub> are included for ATMACs, BACs and DDACs, respectively.

Furthermore, reference fragmentation spectra of all available standards were acquired to identify characteristic fragments for each QAC group. An example of a fragmentation spectrum for each class is shown in **Figures SI-4.1.1** to **SI-4.1.3**. For ATMACs, the loss of the hydrocarbon side chain was observed resulting in a characteristic common fragment with the formula [C<sub>3</sub>H<sub>10</sub>N]<sup>+</sup> (theoretical *m/z* 60.0808). For DDACs, both the loss of one and two hydrocarbon side chains was observed. The latter resulted in a

characteristic common fragment corresponding to  $[C_3H_8N]^+$  (theoretical  $m/z$  58.0651). This is in line with fragmentation patterns described for DDACs in previous studies (Ruan et al., 2014; Wegh et al., 2017). BACs showed the loss of a fragment corresponding to the benzyl group ( $[C_7H_7]^+$ ; theoretical  $m/z$  91.0542) (Pati and Arnold, 2020). Similar to DDACs, a fragment with the formula  $[C_3H_8N]^+$  (theoretical  $m/z$  58.0651) was observed for BACs as well.

All targeted QACs were semi-quantified in the QC samples. The obtained average accuracies of each targeted QAC in the four QC samples are summarized in **Figure SI-4.1.4**. Averaged over all targeted QACs, an accuracy of  $104.9 \pm 11.3\%$  was observed. Accuracies of individual compounds ranged between 86.1 and 125.7%. Except for the average accuracy obtained for C16-ATMAC and C8:C8-DDAC, all other values fell within the range of  $100\% \pm 20\%$ .

It has to be noted that within the presented semi-quantification workflow several factors, which need to be considered within the interpretation of results, were suspected to potentially negatively influence the accuracy. Firstly, the applied Auto MS/MS acquisition mode, necessary for the acquisition of fragmentation spectra, leads to an increased cycle time and thus to a decreased number of datapoints available for peak integration (approx. 4-5 data points at a peak width of 0.15-0.2 min). In turn, this can lead to an over- or underestimation of analyte concentrations, depending on whether the “real” peak apex is covered by a datapoint for both the IS and the targeted analyte. Secondly, labelled IS were not available for all target compounds which means that a perfect compensation of possible matrix effects or for different mobile phase compositions depending on the time point of the chromatogram cannot be guaranteed. Lastly, for most targeted QACs, the lowest peak areas observed in the samples were below the peak areas observed for the lowest calibration point. As latter showed peaks clearly above noise levels, the lowest calibration point cannot be viewed as the quantification limit. Therefore, an extrapolation of the calibration curve below the lowest calibration point was needed in some cases. For four DDACs and one ATMAC, the two or three highest calibration points had to be excluded from the calibration curve as they fell outside the linear range suggesting detector saturation (**Table SI-4.1.7**). Ultimately, correlation coefficients ( $R^2$ )  $> 0.990$  and response factors ranging between 14.5 and 48.7 were obtained for all calibration curves (**Table SI-4.1.7**). This, in combination with the described good accuracies, justified the application of the presented semi-quantification approach.

The average absolute mass errors (AMEs) and RTs and their standard deviations (SDs) obtained in the QC samples for the targeted QACs are summarized in **Table SI-4.1.8**. The low SDs obtained for the RTs (all  $< 0.04$  min) indicate their high reproducibility and

stability throughout the sample sequence. None of the targeted QACs showed an average AME > 2 ppm indicating the high mass accuracy of the measurements.

**Table SI-4.1.9** shows the experimental  $^{DT}CCS_{N_2}$  values obtained for the QC compounds in triplicate within the IM-MS acquisition sequence. The  $^{DT}CCS_{N_2}$  values were compared with reported literature values (Stow et al., 2017). The obtained APEs ranged between 0.06% and 0.34%. Thus, none of the APEs exceeded the set cut-off value of 1% (Picache et al., 2019) indicating the reproducibility and reliability of the IM-MS measurements and  $^{DT}CCS_{N_2}$  calculations.

#### 4.1.3.2 Target screening and semi-quantification

Within the target screening approach, 21 QACs, available as reference standards, were screened for and semi-quantified in the Flemish indoor dust samples. A compound was considered as detected if the observed  $m/z$  ratio, isotopic pattern, RT and fragmentation spectrum unequivocally matched the corresponding reference standard, including characteristic fragments described in **chapter 4.1.3.1**. If no fragmentation spectrum was acquired but the remaining identifiers still matched the reference standard, CL 2C was assigned, as described in **chapter 4.1.2.5** and introduced in **chapter 5**.

All 21 targeted QACs were detected in at least two dust samples, corresponding to a minimum detection frequency (DF) of 4.3%. Out of the 21 targeted QACs, 15 compounds showed DFs > 90%. All targeted QACs were semi-quantified according to the approach described in **chapter 4.1.2.7**. A summary of the detected QACs and their semi-quantified concentrations is given in **Table 4.1.1**.

**Table 4.1.1:** Summary of alkyl trimethylammonium compounds (ATMACs), benzyl alkyldimethyl ammonium compounds (BACs) and dialkyl dimethylammonium compounds (DDACs) detected in indoor dust samples. For each of the homologues, the total detection frequency (DF<sub>total</sub>), the detection frequency at confidence level 1 or 2 (DF<sub>CL1</sub>/DF<sub>CL2c</sub>), the semi-quantified minimum, maximum and median concentrations and the relative contribution to the total (% contr total) quaternary ammonium compound (QAC) concentration as well as to the corresponding QAC class (% contr class) are given. The median was calculated based on the lower bound approach whereby a concentration corresponding to zero was assigned if a compound was not detected. The reported minimum concentration represents the lowest quantified concentrations (thus, excluding samples in which the compound was not detected).

Compound	DF <sub>total</sub> (DF <sub>CL1</sub> /DF <sub>CL2c</sub> ) [%]	Median [µg/g]	Min [µg/g]	Max [µg/g]	% contr total	% contr class
C8-ATMAC	28.3 (0/28.3)	0.00	6.91E-04	0.01	0.0	0.0
C10-ATMAC	97.8 (32.6/65.2)	0.02	2.01E-03	1.90	0.2	0.83
C12-ATMAC	100 (82.6/17.4)	0.09	1.96E-02	6.72	1.1	4.0
C14-ATMAC	76.1 (56.5/19.6)	0.08	3.55E-02	1.55	0.9	3.2
C16-ATMAC	100 (97.8/2.2)	1.08	2.06E-02	3.40	10.4	37.7
C18-ATMAC	100 (78.3/21.3)	0.31	6.36E-02	1.97	2.7	9.8
C20-ATMAC	84.8 (34.8/50.0)	0.18	4.61E-02	2.94	1.5	5.3
C22-ATMAC	100 (95.7/4.3)	1.45	5.91E-02	7.28	10.8	39.2
<b>ΣATMAC</b>		<b>4.46</b>	<b>0.30</b>	<b>15.50</b>	<b>27.5</b>	
C6-BAC	4.3 (0/4.3)	0.00	7.09E-03	0.06	0.0	0.0
C8-BAC	19.6 (0/19.6)	0.00	3.42E-03	0.06	0.0	0.0
C10-BAC	93.5 (23.9/69.6)	0.01	1.74E-03	2.54	0.1	0.3
C12-BAC	100 (100/0)	2.99	5.41E-01	28.41	26.8	58.7
C14-BAC	100 (95.7/4.3)	1.64	2.65E-01	20.44	13.5	29.5
C16-BAC	100 (63.0/37.0)	0.29	2.11E-02	18.75	2.2	4.9
C18-BAC	100 (82.6/17.4)	0.44	5.93E-02	13.61	3.1	6.7
<b>ΣBAC</b>		<b>5.83</b>	<b>1.01</b>	<b>70.61</b>	<b>45.7</b>	
C8-DDAC	84.8 (21.7/63.1)	0.01	1.05E-03	0.90	0.1	0.4
C10-DDAC	100 (100/0)	1.86	1.87E-01	9.52	15.6	58.2
C12-DDAC	95.7 (0/95.7)	0.01	1.93E-03	0.07	0.1	0.3
C14-DDAC	100 (6.5/93.5)	0.02	3.18E-03	0.14	0.1	0.4
C16-DDAC	100 (100/0)	0.97	9.69E-02	20.60	5.4	20.0
C18-DDAC	97.8 (97.8/0)	1.12	1.78E-01	32.23	5.6	20.8
<b>ΣDDAC</b>		<b>3.41</b>	<b>0.88</b>	<b>55.72</b>	<b>26.8</b>	
<b>ΣQAC</b>		<b>14.73</b>	<b>2.80</b>	<b>103.70</b>		

The median concentrations of individual QACs presented here ranged between 0.00 and 2.99 µg/g. The three compounds with the highest median concentrations of 2.99, 1.86 and 1.64 µg/g were C12-BAC, C<sub>10</sub>-DDAC, and C<sub>14</sub>-BAC, respectively, which corresponded to 26.8, 15.6 and 13.5% of the total QACs detected. With the exception of C<sub>10</sub>-DDAC, contributions of shorter chain QACs (C<sub>10</sub> or lower) to the summed QAC concentration were negligible (< 0.5 %).

For the class of ATMACs, the C<sub>16</sub> and C<sub>22</sub> homologues showed the highest median concentrations contributing 37.7 and 39.2% to the ΣATMAC content. For BACs, the C<sub>12</sub>

and C<sub>14</sub> homologues contributed 58.7 and 29.5% to the  $\Sigma$ BAC concentration, respectively, while the other BAC homologues showed lower percent contributions with values  $\leq 7\%$ . Within the class of DDACs, the C<sub>10</sub> and C<sub>18</sub> homologues showed the highest median concentrations corresponding to 58.2 and 20.8% of the  $\Sigma$ DDAC concentration.

The high DFs observed for most QACs confirm their ubiquitous occurrence in the indoor environment. To the best of our knowledge, only one study has reported the presence of QACs in indoor dust samples from Indiana, USA (Zheng et al., 2020), while the present study is the first one to characterize the occurrence of QACs in European dust.

In comparison with the study of Zheng et al. which reported median  $\Sigma$ QAC concentrations of 36.3 and 58.9  $\mu\text{g/g}$  for US indoor dust samples collected before and during the COVID-19 pandemic, respectively (Zheng et al., 2020), lower median concentrations were observed in the present study. The reported median  $\Sigma$ QAC concentration, as well as most of the median concentrations of individual QACs, show lower values than reported by Zheng et al. even in pre-pandemic samples. These differences might be explained by different legislation in the US and European Union regarding the use of QACs in disinfecting products. In the early stages of the COVID-19 pandemic, the US Environmental Protection Agency (EPA) published a list containing 430 products recommended as disinfectants against SARS-CoV-2 (*List N: Disinfectants for Use Against SARS-CoV-2*) (EPA, 2020). Of these products, 216 contained QACs, resulting in their wide application (Hora et al., 2020). Within the European Union, the Biocidal Products Regulation ((EU) No 528/2012 (BPR)) regulates the authorization of active ingredients in biocidal products (including products for human hygiene) before these can be made available on the market. This regulation requires separate approvals for every active substance/product-type combination. Currently, C<sub>10</sub>:C<sub>10</sub>-DDAC (CAS: 7173-51-5) is approved for the use in products for human hygiene which might explain its high contribution to the  $\Sigma$ DDAC concentration. The approvals of several other QACs (C<sub>12</sub>- to C<sub>18</sub>-BACs, C<sub>12</sub>- to C<sub>14</sub>-BACs and others) for the same product type are currently under evaluation. Furthermore, the current approval of C<sub>10</sub>-DDAC (CAS: 7173-51-5) and C<sub>8</sub>- to C<sub>18</sub>-BAC (CAS: 61789-18-2) in wood preservatives can provide another possible exposure source. C<sub>10</sub>-DDAC and several BACs are currently under evaluation for an approval in construction material preservatives. Nevertheless, the generally stricter regulations in force in the EU suggest less extensive applications of QACs contributing to lower concentrations in the indoor environment. The numerous approvals currently under evaluation for additional substance/product-type combinations suggest an increased use of QACs in the future.

Despite the described differences in the legislation, various similarities in the patterns of most abundant QAC homologues and the percental contributions of each QAC

class to the  $\Sigma$ QAC concentration were observed. This suggests similar patterns in the potential sources contributing to the QAC contamination such as cleaning and disinfecting products. The patterns observed for the three main QAC classes are compared with the data of Zheng et al. in **Figure SI-4.1.5**. Similar to the results presented here, Zheng et al. identified C<sub>12</sub>- and C<sub>14</sub>-BACs as the most abundant QACs. Additionally, C<sub>10</sub>-DDAC was identified as the most abundant DDAC homologue. Interestingly, the present study identified C<sub>22</sub>-ATMAC, which was not included in the study of Zheng et al., as an important ATMAC homologue showing a median concentration of 1.45  $\mu\text{g/g}$ , which corresponded to 10.8% of the  $\Sigma$ QAC concentration.

#### 4.1.3.3 Health risk assessment

The EDI values calculated for the three groups of targeted QACs are reported in **Table 4.1.2**. The calculated EDIs ranged from 0.24E-07 to 3.96E-05, lower than those calculated in indoor dust samples collected in the USA before and during the COVID-19 pandemic (up to 6.15E-04) (Zheng et al., 2020). The corresponding HQs ranged between 2.24E-06 and 3.96E-04, with the highest values determined for toddlers in the worst-case exposure scenario. These results suggest that the target population has a low exposure to QACs compared to the risk threshold and should not suffer adverse health effects via dust ingestion. However, this approach does not take other exposure routes and sources into consideration and does not account for QACs which might be overlooked by traditional targeted screening studies.

**Table 4.1.2:** EDI values (mg/kg bw/day) and HQs calculated from the median concentrations of semi-quantified QACs in the indoor dust samples collected from homes and public spaces according to the 50<sup>th</sup> and 95<sup>th</sup> percentile exposure scenarios. ADI values (mg/kg bw/day) are from EFSA, 2014.

Compound	ADI mg/kg bw/day	HOMES				HOMES				PUBLIC SPACES			
		EDI	HQ	EDI	HQ	EDI	HQ	EDI	HQ	EDI	HQ	EDI	HQ
		50th p. adult	50th p. toddler	95th p. adult	95th p. toddler	50th p. adult	95th p. adult	50th p. adult	95th p. adult				
Sum	1.00	9.53	9.53	1.83	1.83	2.86	2.86	3.66	3.66	2.33	2.33	7.00	7.00
ATMAC	E-01	E-07	E-06	E-05	E-04	E-06	E-05	E-05	E-04	E-07	E-06	E-07	E-06
SumBAC	1.00	1.03	1.03	1.98	1.98	3.09	3.09	3.96	3.96	3.00	3.00	8.99	8.99
	E-01	E-06	E-05	E-05	E-04	E-06	E-05	E-05	E-04	E-07	E-06	E-07	E-06
Sum	1.00	7.68	7.68	1.48	1.48	2.30	2.30	2.95	2.95	2.24	2.24	6.71	6.71
DDAC	E-01	E-07	E-06	E-05	E-04	E-06	E-05	E-05	E-04	E-07	E-06	E-07	E-06

#### 4.1.3.4 Suspect screening results

In addition to the target screening, all indoor dust samples were analyzed by applying a suspect screening workflow. After data pre-treatment and feature extraction, the obtained dataset was matched against a suspect list summarized in **Table SI-4.1.5** and described in **chapter 4.1.2.6**.

All obtained matches (n = 66) were manually investigated to confirm the assignment of a formula, identify a false positive detection or an identification at a low CL (CL4). To each confirmed compound, a CL of identification was assigned following the workflow proposed by Schymanski et al. (Schymanski et al., 2014). Compounds were identified with CL3 if a fragmentation spectrum was available and contained characteristic fragments confirming the proposed assignment. As discussed in **chapter 4.1.3.1**, the investigated QAC classes show characteristic fragmentation patterns easing compound identification. Thus, available characteristic fragmentation spectra can be considered as diagnostic evidence increasing the confidence in the assignments. Nevertheless, the presence of branched side chains, leading to various isomers, cannot unequivocally be excluded impeding the assignment of CL2. To samples for which no fragmentation spectrum of the compound of interest was available, CL4 was assigned. These were excluded from further discussion and interpretation given the low identification confidence. All compounds identified applying the described workflow are summarized in **Table 4.1.3**.

**Table 4.1.3:** Summary of suspect dimethyl ethyl alkyl ammonium compounds (DEACs), dialkyl dimethylammonium compounds (DDACs) and benzyl alkyldimethyl ammonium compounds (BACs) detected with the suspect screening approach. For each compound the average absolute mass error (AME), the detection frequency with confidence level 3 (DF CL3) and the total detection frequency (DF total= DF CL3 + DF CL4) as well as the semi-quantified median, minimum and maximum concentrations are given. The median was calculated based on the lower bound approach whereby a concentration corresponding to zero was assigned if a compound was not detected. The reported minimum concentration represents the lowest quantified concentrations (thus, excluding samples in which the compound was not detected).

Compound	Formula	$\bar{x}$ AME [ppm]	DF CL3 [%]	DF total [%]	Median [ $\mu\text{g/g}$ ]	Min [ $\mu\text{g/g}$ ]	Max [ $\mu\text{g/g}$ ]
C2:C12-DEAC	C <sub>16</sub> H <sub>36</sub> N <sup>+</sup>	0.99	69.6	100	0.08	3.72E-03	3.13
C2:C14-DEAC	C <sub>18</sub> H <sub>40</sub> N <sup>+</sup>	0.88	52.2	100	0.03	1.41E-03	1.66
C2:C16-DEAC	C <sub>20</sub> H <sub>44</sub> N <sup>+</sup>	0.91	15.2	34.8	0.00	1.06E-02	2.31
C2:C18-DEAC	C <sub>22</sub> H <sub>48</sub> N <sup>+</sup>	1.11	2.2	4.4	0.00	3.43E-02	0.49
C8:C10-DDAC	C <sub>20</sub> H <sub>44</sub> N <sup>+</sup>	0.94	4.35	93.5	0.02	5.88E-03	2.57
C14:C16/ C12:C18-DDAC	C <sub>32</sub> H <sub>68</sub> N <sup>+</sup>	0.85	26.1	100	0.04	7.79E-03	0.87
DDAC	C <sub>33</sub> H <sub>70</sub> N <sup>+</sup>	0.91	n.a.*	95.7	0.01	1.89E-03	0.28
C15:C18/ C16:C17-DDAC	C <sub>35</sub> H <sub>74</sub> N <sup>+</sup>	0.98	26.1	97.8	0.03	5.20E-03	0.61
C16:C18-DDAC	C <sub>36</sub> H <sub>76</sub> N <sup>+</sup>	0.82	100	100	1.71	2.55E-01	24.90
C18:20-DDAC	C <sub>40</sub> H <sub>84</sub> N <sup>+</sup>	1.31	4.3	100	0.01	8.65E-04	0.67
C11-BAC	C <sub>20</sub> H <sub>36</sub> N <sup>+</sup>	2.95	2.2	45.7	3.89E-03	5.99E-04	0.16
C13-BAC	C <sub>22</sub> H <sub>40</sub> N <sup>+</sup>	2.68	2.2	52.2	1.28E-03	1.16E-03	0.51
C20-BAC	C <sub>29</sub> H <sub>54</sub> N <sup>+</sup>	1.31	2.2	58.7	1.07E-03	5.83E-04	0.05
1-Hexadecyl- pyridinium	C <sub>21</sub> H <sub>38</sub> N <sup>+</sup>	3.14	4.3	56.5	0.00	2.14E-03	3.48
Benzethonium	C <sub>27</sub> H <sub>42</sub> NO <sub>2</sub> <sup>+</sup>	2.12	10.9	26.1	0.00	6.04E-03	0.44
Choline	C <sub>5</sub> H <sub>14</sub> NO <sup>+</sup>	3.44	71.7 <sup>#</sup>	100	0.06	1.22E-02	0.31
Tetraethyl- ammonium	C <sub>8</sub> H <sub>20</sub> N <sup>+</sup>	2.5	2.2	2.2	0.04	n.a.	n.a.

\*Fragmentation spectra were acquired in 10.9% of the samples but showed low abundances and inconsistent fragmentation patterns not allowing an assignment of assumed chain lengths.

<sup>#</sup>Fragmentation spectra were matched with a library spectrum excluding other potential isomers and justifying the assignment of CL2.

All identified compounds were semi-quantified using the calibration curves acquired with the target screening approach. For each suspect, a calibration curve of a targeted compound from a similar class and with a close RT was selected and used for quantification (**Table SI-4.1.10**). The obtained semi-quantified concentrations are listed in **Table 4.1.3**.

A total of 17 compounds were detected through the suspect screening approach, 16 of which were assigned with CL3 while one compound had to be reported at CL4 due to low abundant and inconsistent fragmentation patterns. Suspect compounds included

a homologue series of dimethyl ethyl alkyl ammonium compounds (DEACs), including side chains of 12, 14, 16 and 18 carbon atoms. The identity of the DEACs was confirmed by the observations of three characteristic fragments with the formulae  $[C_4H_{12}N]^+$  (theoretical  $m/z$ : 74.0964),  $[C_4H_{10}N]^+$  (theoretical  $m/z$ : 72.0808) and  $[C_3H_8N]^+$  ( $m/z$  58.0651) (**Figure SI-4.1.6**). The latter fragment was also observed in the fragmentation patterns of DDACs, suggesting that both classes contain two methyl groups. Therefore, the presence of one ethyl group could be concluded from the observed fragments with  $m/z$  74.0964 and 72.0808. For each of the four DEAC homologues, a neutral loss of the side chain with the corresponding number of carbons (C12, C14, C16 or C18) was observed. Total DFs and median concentrations of DEACs ranged between 4.4 and 100%, and between 0.00 and 0.08  $\mu\text{g/g}$ , respectively. The highest maximum concentration of 3.13  $\mu\text{g/g}$  was observed for C2:C12-DEAC. To the best of our knowledge, this is the first report of DEACs in indoor dust samples. For this QAC group, applications in liquid detergent, dishwashers, cosmetics and other products have been reported (Kim et al., 2023) which might explain the high DFs of this homologue series.

Three DDACs with mixed chain lengths were identified. These included C8:C10-, C16:C18- and C18:C20-DDACs. A typical MS/MS spectrum of one of these homologues (C16:C18-DDAC) is shown in **Figure SI-4.1.7**. Again, the fragment ion with the formula  $[C_3H_8N]^+$  ( $m/z$  58.0651), which was identified as characteristic for DDACs, confirmed the assignment of these homologues to the class of DDACs. The presence of two hydrocarbon chains with different chain lengths was confirmed by the presence of two fragments each of which corresponds to the neutral loss of one side chain. This allowed the calculation of their number of carbons. For C8:C10- and C18:C20-DDACs, maximum concentrations of 2.57 and 0.67  $\mu\text{g/g}$  were observed, respectively. These values are evidently lower than the concentrations observed for the most abundant targeted QACs. This suggests that these two QACs are of lower relevance for a potential estimation of human exposure to QACs and might derive from impurities within the higher abundant QACs or from other minor sources.

On the other hand, the maximum concentration of 24.9  $\mu\text{g/g}$ , calculated for C16:C18-DDAC is comparable with the values obtained for the most abundant targeted DDACs. This shows that the applied approach allowed the identification and quantification of an additional major QAC homologue which, based on its high DF and median concentration, might be of interest for further quantitative studies. These findings also indicate that a focus solely on DDACs with two chains of equal length can lead to an underestimation of the total human exposure to QACs.

For two DDAC homologues, whose assignment to this class was again confirmed by the characteristic fragment with  $m/z$  58.0651, the lengths of the hydrocarbon side chains could not be determined unequivocally. As shown in the MS/MS spectrum in

**Figure SI-4.1.8**, four fragment ions corresponding to neutral losses of hydrocarbon side chains with four different lengths were observed. A similar observation was previously reported by Ruan et al. who suggested the coelution of two DDACs with varying chain lengths (Ruan et al., 2014). Therefore, these two homologues are reported with two possible combinations of chain lengths, and a summed concentration is given. C14:C16/C12:C18-DDAC and C15:C18/C16:C17-DDAC show total DFs and maximum concentrations of 100 and 97.8%, 0.87 and 0.61 µg/g, respectively. Similar to the results obtained for DEACs, these concentrations are clearly lower than observed for the most abundant DDACs. As the described suspects were assumed to be present as mixtures of isomers, they were further investigated in the IM-MS datafiles acquired in 4bit multiplexing mode (**chapter 4.1.3.5**).

Lastly, a DDAC with the formula C<sub>33</sub>H<sub>70</sub>N<sup>+</sup> was detected in 95.7% of the samples with 10.9% of the samples providing fragmentation spectra. These allowed the assignment to the class of DDACs through the observation of the characteristic fragment with *m/z* 58.0651. However, the remaining fragments showed low abundances and inconsistencies between the samples not allowing assumptions about the lengths of the hydrocarbon side chains. This compound was further investigated within the IM-MS measurements to obtain more structural information from the experimental <sup>DTCCS</sup>N<sub>2</sub> values.

Within the class of BACs, three homologues (C11-, C13- and C20-BAC) were identified which, for the samples assigned with CL3, were all confirmed through the observation of the characteristic fragments corresponding to benzyl [C<sub>7</sub>H<sub>7</sub>]<sup>+</sup> (*m/z* 91.0542) and to the loss of the hydrocarbon side chain (**Figure SI-4.1.9**). The low median concentrations observed for these homologues (≤ 0.01 µg/g) indicate that they have a minor contribution to the ΣBAC concentration in the samples. Nevertheless, these findings indicate a high structural variability within this class and show that the chain lengths of the occurring BACs go beyond the homologues covered within the target screening.

Lastly, four compounds not belonging to the three QAC classes covered within the target screening were detected. 1-Hexadecylpyridinium was detected in 56.5% of the samples, whereby two samples provided MS/MS spectra, corresponding to a DF of 4.3% at CL3. The latter allowed the identification of the compound through a characteristic fragment (**Figure SI-4.1.10**) with the formula [C<sub>5</sub>H<sub>6</sub>N]<sup>+</sup> (*m/z* 80.0495), which confirmed the pyridinium backbone, and the corresponding neutral loss of a C16 hydrocarbon side chain. Benzethonium was detected in a total of 26.1% of the samples whereby 10.9% of the samples provided a MS/MS spectrum. The latter was compared with a predicted MS/MS spectrum which matched three fragments confirming a benzyl moiety and a quaternary ammonium cation (**Figure SI-4.1.11**). Both benzethonium and 1-

hexadecylpyridinium are used as disinfecting agents and as antibacterial and antimicrobial products (Kim et al., 2023; Sreevidya et al., 2018) suggesting similar sources for these compounds, as for the other detected QACs.

Furthermore, choline and tetramethylammonium were detected in 100 and 2.2% of the samples, respectively. The latter DF corresponded to the detection of tetramethylammonium in one sample in which the obtained fragmentation spectrum was matched against predicted data resulting in the assignment of CL3. Due to the low DF and quantified concentration (0.04 µg/g), this compound was considered of minor importance with a very limited contribution to the summed QAC concentrations. On the other hand, choline was detected in all samples. For 71.7% of the samples, fragmentation spectra were obtained and matched with the corresponding mzCloud entity excluding potential isomers and justifying the assignment of CL2.

From the obtained results, it can be concluded that the applied method allowed the identification of a high number of additional QACs from various classes and a comprehensive characterization of the occurrence of cationic surfactants in indoor dust. These compounds would have likely been overlooked if only target analysis was applied. The use of characteristic fragments and RT trends for compound identification, characterized within the target screening approach, increased the identification confidence. Nevertheless, the implementation of an additional identification parameter would provide supplementary structural information for each suspect increasing the confidence of CL3 assignments. This can be achieved by the implementation of IM-MS derived CCS values in compound assignment (**chapter 4.1.3.5**). Additionally, increased utilization of suspect list matches can be achieved through improved coverage and quality of fragmentation spectra which would decrease the amount of matches assigned with CL4.

The provided semi-quantified concentrations of the newly identified QACs have to be interpreted with caution given the limitations described in **chapter 4.1.3.1**. Nevertheless, the applied quantification approach was considered acceptable given the structural similarities between the targeted and suspect compounds. The reported concentrations provide a valuable indication of occurrence and levels of QACs in dust, to be further used for the prioritization of the suspects in monitoring studies. For example, the applied approach provides the first report of C16:C18-DDAC in indoor dust samples at concentrations comparable with the values obtained for the most abundant targeted QACs. This clearly highlights the need to include this compound in future monitoring campaigns to estimate a representative total QAC human exposure.

#### 4.1.3.5 IM-MS analysis

To provide reference  $^{DT}CCS_{N_2}$  values to establish CCS- $m/z$  trendlines for QACs and compare the latter with other classes of environmental contaminants, reference  $^{DT}CCS_{N_2}$  values of all available targeted QACs were acquired from all calibration points ( $n = 8$ ), thus covering a concentration range between 0.5  $\mu\text{g}/\mu\text{L}$  and 100  $\mu\text{g}/\mu\text{L}$ . The obtained  $^{DT}CCS_{N_2}$  values and (relative) standard deviations are summarized in **Table SI-4.1.11**. For BACs, DDACs and ATMACs,  $^{DT}CCS_{N_2}$  values ranged between 157.58 and 215.92  $\text{\AA}^2$ , 187.96 and 265.52  $\text{\AA}^2$ , and 150.70 and 215.11  $\text{\AA}^2$ , respectively. The average standard deviation (SD) and average relative standard deviation (RSD) of 0.33  $\text{\AA}^2$  and 0.16%, respectively, indicate a high reproducibility of the measurements and show that the acquisition of the  $^{DT}CCS_{N_2}$  value was independent of the analyte's concentration.

For seven compounds (C8- to C16-BAC, C10-DDAC, and C16-ATMAC), literature travelling wave IM-MS derived  $^{TW}CCS_{N_2}$  values were available from the study of Song et al. (Song et al., 2022). The study of Hines et al. provided additional literature  $^{TW}CCS_{N_2}$  values for three BAC homologues (Hines et al., 2017b). The dataset presented here was compared with the available literature values. For the comparison with the dataset of Song et al., observed absolute percent errors (APEs) ranged between 1.4% and 3.7% with an average of 2.4%, whereby the highest APE (3.7%) was observed for C16-BAC. Interestingly, APEs of BACs increased with increasing chain lengths indicating potential differences in the correlation trends of  $^{TW}CCS_{N_2}$  values and  $m/z$  ratios. The comparison with the  $^{TW}CCS_{N_2}$  values derived from Hines et al. lead to slightly lower APEs with an average of 1.5%. Generally, the observed APEs are consistent with deviations between  $^{DT}CCS_{N_2}$  and  $^{TW}CCS_{N_2}$  values observed in previous studies (Hinnenkamp et al., 2018) and described in **chapter 3.2**.

From the acquired  $^{DT}CCS_{N_2}$  values, CCS- $m/z$  trendlines were plotted for every QAC class describing the relationship between the  $^{DT}CCS_{N_2}$  value and  $m/z$  ratio. For all three QAC classes, this relationship was best described using a power fit model resulting in correlation coefficients ( $R^2$ ) > 0.99 (**Figure 4.1.3**). The obtained CCS- $m/z$  trendlines were compared with the dataset described in **chapter 3.1** containing more than 300  $^{DT}CCS_{N_2}$  values of 148 environmental contaminants and their metabolites. Within this dataset, CCS- $m/z$  trendlines were characterized for various classes of contaminants, such as organophosphate flame retardants (PFRs), plasticizers and PFAS. The trendlines of DDACs and ATMACs are clearly clustered above the other contaminant classes included in the dataset (**Figure 4.1.3**). This is likely caused by the linear structure of these compounds which, in combination with a molecular formula not containing any heavy hetero atoms, leads to increased CCS values. The BAC trendline clusters slightly below the other two QAC classes showing the influence of the benzyl group which causes a more compact

structure and decreased CCS values. Due to the characteristic positions of the CCS- $m/z$  trendlines of QACs in comparison to other contaminant classes and the good fit of the calculated trendlines, they showed to be a valuable tool for the confirmation of the assigned suspect compounds. Given the low RSDs observed for the presented reference  ${}^{\text{DT}}\text{CCS}_{\text{N}_2}$  values and the QC measures implemented in their acquisition, the presented dataset can also be used in future studies on QACs in order to increase identification confidence of homologues for which no reference standard is available.

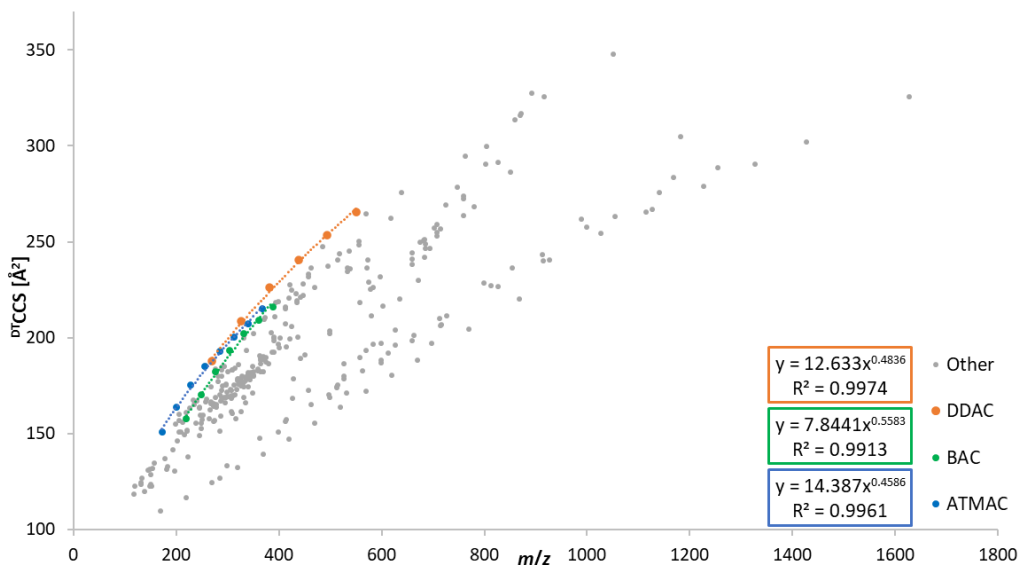


**Figure 4.1.3:** Plot of  ${}^{\text{DT}}\text{CCS}_{\text{N}_2}$  values vs  $m/z$  ratios for the three quaternary ammonium compound (QAC) classes of alkyl trimethyl ammonium compounds (ATMACs; blue), benzyl alkyl ammonium compounds (BACs; green) and dimethyl dialkyl ammonium compounds (DDACs; orange). For each class, the CCS- $m/z$  relationship was fitted using a power model resulting in three trendlines. For each of the trendlines, the equation and correlation coefficient are indicated. The QAC data was compared to the dataset described in **chapter 3.1** (grey) containing 311  ${}^{\text{DT}}\text{CCS}_{\text{N}_2}$  values of 148 environmental contaminants and their metabolites.

For all targeted and suspect QACs,  ${}^{\text{DT}}\text{CCS}_{\text{N}_2}$  values were acquired following the workflow described in **chapter 4.1.2.4**.  ${}^{\text{DT}}\text{CCS}_{\text{N}_2}$  values obtained for the targeted QACs were compared to the reference values, and obtained deviations did not exceed 2% (data not shown). **Table 4.1.4** reports the average  ${}^{\text{DT}}\text{CCS}_{\text{N}_2}$  values acquired throughout all samples for suspect QACs detected applying the suspect screening workflow. The obtained average  ${}^{\text{DT}}\text{CCS}_{\text{N}_2}$  values were plotted against the corresponding  $m/z$  ratios together with the data obtained for reference  ${}^{\text{DT}}\text{CCS}_{\text{N}_2}$  values of targeted QACs to compare the positioning of suspect QACs' datapoints with the previously established trendlines (**Figure 4.1.4**). The  ${}^{\text{DT}}\text{CCS}_{\text{N}_2}$  values acquired for suspect DDACs (nr. 5-10 in **Table 4.1.4**) aligned with the trendline calculated for the targeted DDACs. The same applies for the suspect BACs (nr. 11-13 in **Table 4.1.4**) which aligned with the BAC trendline. The

$^{DT}CCS_{N_2}$  values of two of the DEACs (C2:C16- and C2:C18-DEAC) are clustered slightly below the DDAC trendline. This is likely due to the slight differences in structures of these two groups. Therefore, the DEACs can be viewed as a separate class and well fitted ( $R^2 = 0.9996$ ) by an additional regression line applying a power model (**Figure SI-4.1.12**). Interestingly, the  $^{DT}CCS_{N_2}$  value obtained for 1-Hexadecylpyridinium well fitted with the BACs' trendline. This can be viewed as an additional confirmation of the aromatic moiety included in the proposed compound assignment. On the other hand, the  $^{DT}CCS_{N_2}$  value of benzethonium deviated from all QAC trendlines, confirming the clearly different, more compact structure of the assigned compound. In conclusion, the clear fit of the  $^{DT}CCS_{N_2}$  values or  $CCS-m/z$  trendlines (in the case of DEACs) of suspect QACs with the data obtained from targeted QACs is a valuable additional confirmation of the compound assignment. It also has to be pointed out that the  $^{DT}CCS_{N_2}$  value was available in every sample independently on whether or not fragmentation spectra were acquired with sufficient quality (within the QTOF only approach) providing additional identification confidence to the complete sample set.

**Table 4.1.4:** Experimental  $^{DT}CCS_{N_2}$  values and their (relative) standard deviations ((R)SD) measured for all suspect compounds identified within the suspect screening approach. The total detection frequency ( $DF_{total}$ ) derives from the data obtained with the suspect screening approach. The corresponding absolute number of samples (n) which was used to calculate average  $^{DT}CCS_{N_2}$  values, SD and RSD is given.

Nr.	Compound	Formula	$DF_{total}$ [%]	$\bar{x}^{DT}CCS_{N_2}$ exp. [ $\text{\AA}^2$ ]	SD [ $\text{\AA}^2$ ]	RSD [%]	n
1	C2:C12-DDAC	$C_{16}H_{36}N^+$	100	177.94	0.73	0.41	46
2	C2:C14-DDAC	$C_{18}H_{40}N^+$	100	187.23	0.55	0.29	46
3	C2:C16-DDAC	$C_{20}H_{44}N^+$	34.8	195.26	0.73	0.37	16
4	C2:C18-DDAC	$C_{22}H_{48}N^+$	4.4	203.14	0.59	0.29	2
5	C8:C10-DDAC	$C_{20}H_{44}N^+$	93.5	197.21	0.66	0.34	43
6	C14:C16/C12:C18-DDAC	$C_{32}H_{68}N^+$	100	246.42	0.89	0.36	46
7	C13:C18-DDAC	$C_{33}H_{70}N^+$	95.7	249.75	1.12	0.45	44
8	C15:C18/C16:C17-DDAC	$C_{35}H_{74}N^+$	97.8	256.24	0.97	0.38	45
9	C16:C18-DDAC	$C_{36}H_{76}N^+$	100	259.73	0.80	0.31	46
10	C18:20-DDAC	$C_{40}H_{84}N^+$	100	271.94	1.40	0.51	46
11	C11-BAC	$C_{20}H_{36}N^+$	45.7	187.06	0.75	0.40	21
12	C13-BAC	$C_{22}H_{40}N^+$	52.2	196.63	0.63	0.32	24
13	C20-BAC	$C_{29}H_{54}N^+$	58.7	222.53	0.80	0.36	27
14	1-Hexadecylpyridinium	$C_{21}H_{38}N^+$	56.5	192.06	0.71	0.37	26
15	Benzethonium	$C_{27}H_{42}NO_2^+$	26.1	207.66	0.56	0.27	12
16	Choline	$C_5H_{14}NO^+$	100	116.91	0.38	0.32	46
17	Tetraethylammonium	$C_8H_{20}N^+$	2.2	134.74	n.a.	n.a.	1
				<b>Average</b>	<b>0.77</b>	<b>0.36</b>	

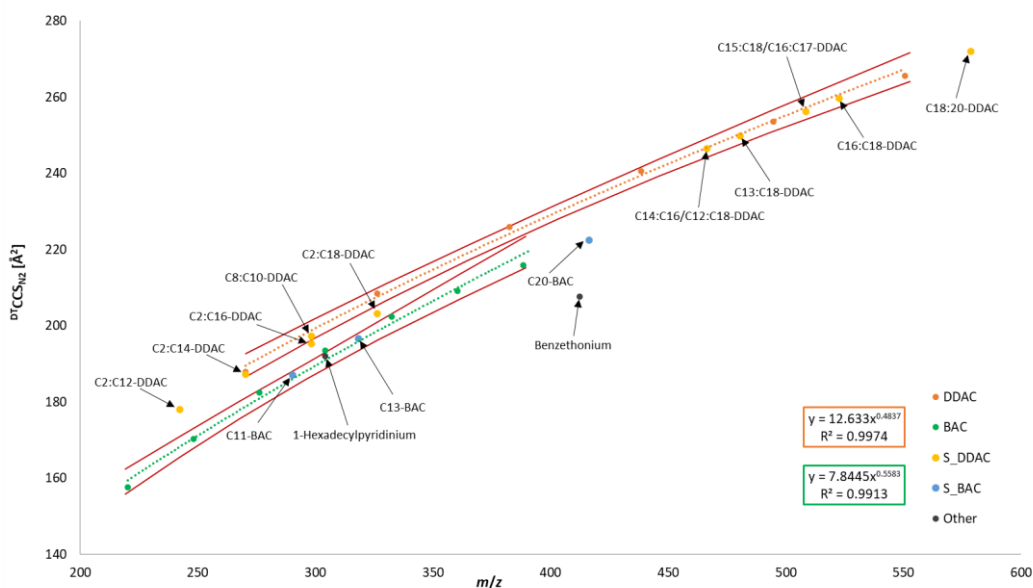


**Figure 4.1.4:** Plot of  $^{DT}CCS_{N_2}$  values vs  $m/z$  ratios for the quaternary ammonium compound (QAC) classes of benzyl alkyl ammonium compounds (BACs; green) and dialkyl dimethyl ammonium compounds (DDACs; orange). For each class, the CCS- $m/z$  relationship was fitted using a power model resulting in two trendlines for which the 95% confidence interval is indicated with red lines. For each of the trendlines, the equation and correlation coefficient are indicated. The CCS- $m/z$  datapoints of all compounds identified within the suspect screening approach are indicated with the assigned compound. Thereby, suspect DDACs (S\_DDAC), suspect BACs (S\_BAC) and other suspects are given in yellow, blue and black, respectively.

As described in **chapter 4.1.3.3**, the fragmentation spectra obtained for two suspects C14:C16/C12:C18-DDAC and C15:C18/C16:C17-DDAC within the suspect screening data analysis described above, had suggested the presence of isomers. In order to confirm this hypothesis, the IM-MS datafiles acquired in 4bit multiplexing mode for a sub-selection of 20 samples and processed using the recently introduced HRdm tool (May et al., 2020) were searched for the signals obtained for the suspects of interest (C14:C16/C12:C18-, C15:C18/C16:C17-DDAC). In 5 out of 20 samples (for each, C14:C16/C12:C18-, C15:C18/C16:C17-DDAC), two peaks were observed in the drift time dimension which were extracted as separate features by the feature extraction algorithm. An exemplary mobilogram obtained for C14:C16/C12:C18-DDAC in one of the samples in which a distinguishment of isomers was possible, is shown in **Figure SI-4.1.13**. In nine and seven additional files (for C14:C16/C12:C18- and C15:C18/C16:C17-DDAC, respectively) the peak shapes suggested the presence of a second isomer as clear peak shoulders were observed. These observations confirm the presence of isomers and point out the improved resolution capacities of the 4bit multiplexing acquisition mode and the consecutive HRdm processing.

#### 4.1.4 Conclusions

QACs were characterized and semi-quantified in 46 indoor dust samples collected in Belgium, applying target and suspect screening approaches. All 21 targeted QACs were detected in at least two dust samples with DFs ranging between 4.3 and 100%. C12-BAC, C10:C10-DDAC and C14-BAC were identified as the major targeted QACs contributing each with 26.8, 15.6 and 13.5% to the summed QAC concentrations, respectively. The most abundant QACs matched the patterns observed in indoor dust collected in the US even though clearly lower QAC concentrations were observed in European samples. From the semi-quantified concentrations of targeted compounds, Estimated Daily Intakes (EDI) and corresponding Hazard quotients (HQ) were calculated. These results suggested a low exposure of the targeted population to QACs compared to the risk threshold. Nevertheless, this approach does not account for other exposure sources or QACs which are overlooked by targeted approaches.

The suspect screening approach allowed the identification of 13 additional QACs and four other (positively charged) surfactants. Dimethyl ethyl ammonium compounds (DEACs) were identified as an additional class of QACs covering (even numbered) side chain lengths of C12 to C18. C16:C18-DDACs was identified as an additional major QAC homologue with a semi-quantified maximum concentration of 24.90  $\mu\text{g/g}$ . This pointed out the importance of semi-quantitative suspect screening approaches to allow a complete characterization of the most abundant QAC homologues. Reference  $^{\text{DT}}\text{CCS}_{\text{N}_2}$  values of all targeted QACs were reported and used to characterize  $\text{CCS-}m/z$  trendlines for each class. Experimental  $^{\text{DT}}\text{CCS}_{\text{N}_2}$  values of suspect QACs were compared with the obtained trendlines. Suspect BACs and DDACs aligned well with the trendlines of the corresponding target QAC class. This evidence provides additional identification confidence. The newly characterized class of DEACs was described by a separate trendline which showed slight deviations from the trendline of DDACs confirming the structural differences between these classes. The presented use of IM-MS derived data as an additional identification parameter highlights the added value of this technique. In conclusion, the high DFs and high concentrations of several QACs in the indoor environment raise the need for further studies on the human exposure to these compounds.

## Supplementary Information – Chapter 4.1

**Table SI-4.1.1:** Summary of compounds which were available as reference standards. All compounds were purchased as salts. The CAS number, formula and molecular weight ( $MW_{\text{salt}}$ ) of the corresponding salt is indicated. Additionally, the formula of the raw QAC ( $[M^+]$  ion) and the corresponding  $m/z$  value of the  $[M^+]$  ion which were used for data analysis, is indicated.

Class	Name	Abbreviation	CAS number	Formula [salt]	$MW_{\text{salt}}$ [g/mol]	Formula $[M^+]$	$m/z$ $[M^+]$
BAC	Benzyltrimethylammonium chloride	C6-BAC	22559-57-5	$C_{15}H_{26}ClN$	255.82	$[C_{15}H_{26}N]^+$	220.2060
	Benzyltrimethyloctylammonium chloride	C8-BAC	959-55-7	$C_{17}H_{30}ClN$	283.90	$[C_{17}H_{30}N]^+$	248.2373
	Benzyltrimethyldecylammonium chloride	C10-BAC	63449-41-2	$C_{19}H_{34}ClN$	311.90	$[C_{19}H_{34}N]^+$	276.2686
	Benzyltrimethyl dodecylammonium chloride	C12-BAC	139-07-1	$C_{21}H_{38}ClN$	340.00	$[C_{21}H_{38}N]^+$	304.2999
	Benzyltrimethyl tetradecylammonium chloride dihydrate	C14-BAC	147228-81-7	$C_{23}H_{46}ClNO_2$	404.10	$[C_{23}H_{42}N]^+$	332.3312
	Benzyltrimethyl hexadecylammonium chloride	C16-BAC	122-18-9	$C_{25}H_{46}ClN$	396.10	$[C_{25}H_{46}N]^+$	360.3625
	Stearyltrimethylbenzylammonium chloride	C18-BAC	122-19-0	$C_{27}H_{50}ClN$	424.10	$[C_{27}H_{50}N]^+$	388.3938
DDAC	Dimethyldioctylammonium chloride	C8:C8-DDAC	5538-94-3	$C_{18}H_{40}ClN$	306.00	$[C_{18}H_{40}N]^+$	270.3155
	Didecyltrimethylammonium bromide	C10:C10-DDAC	2390-68-3	$C_{22}H_{48}BrN$	406.50	$[C_{22}H_{48}N]^+$	326.3781
	Didodecyltrimethylammonium bromide	C12:C12-DDAC	3282-73-3	$C_{26}H_{56}BrN$	462.60	$[C_{26}H_{56}N]^+$	382.4407
	Dimethylditetradecylammonium bromide	C14:C14-DDAC	68105-02-2	$C_{30}H_{64}BrN$	518.70	$[C_{30}H_{64}N]^+$	438.5033
	Dihexadecyltrimethylammonium bromide	C16:C16-DDAC	70755-47-4	$C_{34}H_{72}BrN$	574.80	$[C_{34}H_{72}N]^+$	494.5659
	Dimethyldioctadecylammonium bromide	C18:C18-DDAC	3700-67-2	$C_{38}H_{80}BrN$	631.00	$[C_{38}H_{80}N]^+$	550.6285
ATMAC	Trimethyloctylammonium chloride	C8-ATMAC	10108-86-8	$C_{11}H_{26}ClN$	207.78	$[C_{11}H_{26}N]^+$	172.2060
	Decyltrimethylammonium bromide	C10-ATMAC	2082-84-0	$C_{13}H_{30}BrN$	280.29	$[C_{13}H_{30}N]^+$	200.2373
	Dodecyltrimethylammonium chloride	C12-ATMAC	112-00-5	$C_{15}H_{34}ClN$	263.89	$[C_{15}H_{34}N]^+$	228.2686
	Trimethyltetradecylammonium chloride	C14-ATMAC	4574-04-3	$C_{17}H_{38}ClN$	291.90	$[C_{17}H_{38}N]^+$	256.2999
	Hexadecyltrimethylammonium chloride	C16-ATMAC	112-02-7	$C_{19}H_{42}ClN$	320.00	$[C_{19}H_{42}N]^+$	284.3312
	Trimethyloctadecylammonium chloride	C18-ATMAC	112-03-8	$C_{21}H_{46}ClN$	348.00	$[C_{21}H_{46}N]^+$	312.3625
	Eicosyltrimethylammonium bromide	C20-ATMAC	7342-61-2	$C_{23}H_{50}BrN$	420.60	$[C_{23}H_{50}N]^+$	340.3938
	Docosyltrimethylammonium chloride	C22-ATMAC	17301-53-0	$C_{25}H_{54}ClN$	404.20	$[C_{25}H_{54}N]^+$	368.4251

**Table SI-4.1.2:** Summary of information about the housing type, location, construction year and days passed since the last cleaning for the indoor dust samples investigated in **chapters 4.1** and **4.2**.

<b>Sample name</b>	<b>Housing type</b>	<b>Field blank?</b>	<b>Location</b>	<b>Construction year</b>	<b>Days since last cleaning</b>
VPO.01	Private		rural	NA	NA
VPO.02	Public		urban	1980	5
VPO.03	Public	Yes	urban	1980	5
VPO.04	Private		urban	NA	1
VPO.05	Private		urban	NA	7
VPO.06	Private		urban	1958	> 1 week
VPO.07	Private		rural	1988	4
VPO.08	Private		rural	1933	3
VPO.09	Private		rural	1998	7
VPO.10	Private	Yes	rural	2005	2
VPO.11	Private		rural	2005	2
VPO.12	Private		urban	1991	4
VPO.13	Private		rural	2003	8
VPO.14	Private		urban	2005	14
VPO.15	Private	Yes	rural	1986	6
VPO.16	Private		rural	1986	6
VPO.17	Private		rural	1915	10
VPO.18	Private		urban	1902	21
VPO.19	Public		urban	2007	3
VPO.20	Private		urban	2011	7
VPO.21	Private		rural	2005	7
VPO.22	Private	Yes	rural	2009	6
VPO.23	Private		rural	2009	6
VPO.24	Private		rural	2011	6
VPO.25	Public		urban	2015	3
VPO.26	Public		urban	2015	3
VPO.27	Public		urban	NA	NA
VPO.28	Public		urban	NA	NA
VPO.29	Public	Yes	urban	NA	NA
VPO.30	Private		rural	2007	6
VPO.31	Public	Yes	urban	NA	NA
VPO.32	Public		urban	NA	NA
VPO.33	Public		urban	NA	NA
VPO.34	Public		urban	NA	NA
VPO.35	Public		urban	NA	NA
VPO.36	Public		urban	NA	NA
VPO.37	Public	Yes	urban	NA	NA
VPO.38	Private		urban	1958	7
VPO.39	Private		rural	2012	4
VPO.40	Private		urban	2015	2
VPO.41	Private		urban	2017	7
VPO.42	Private		urban	2007	5

VPO.43	Public		urban	NA	NA
VPO.44	Public		urban	NA	NA
VPO.45	Public		rural	2019	6
VPO.46	Public		rural	2019	1
VPO.47	Public		rural	1985	12
VPO.48	Public		rural	NA	7
VPO.49	Public		rural	1998	NA
VPO.50	Private		rural	2000	2
VPO.51	Public		urban	2009	7
VPO.52	Public		rural	NA	NA
VPO.53	Private		rural	1990	2
VPO.54	Public	Yes	rural	NA	NA

**Table SI-4.1.3:** Mobile phases and gradient used for the analysis of quaternary ammonium compounds in indoor dust samples.

<b>Mobile phases</b>	(A) 80:20 water/acetonitrile (v/v) + 0.1 % acetic acid (B) 95:5 acetonitrile/water (v/v) + 5 mM ammonium acetate (C) Isopropanol + 0.1 % formic acid			
<b>Gradient</b>	<b>Time [min]</b>	<b>A [%]</b>	<b>B [%]</b>	<b>C [%]</b>
	0	95	5	0
	5	50	50	0
	10	5	75	20
	15	0	50	50
	18	0	50	50
	20	95	5	0
24	95	5	0	
<b>Column temperature</b>	40°C			
<b>Flow rate</b>	0.3 mL/min			

**Table SI-4.1.4:** Drift tube ion-mobility mass spectrometry (IM-MS) settings applied for the IM-MS measurements.

Single Pulse	Drift Tube Entrance [V]	1574
	Drift Tube Exit [V]	224
	Rear Funnel Entrance [V]	217.5
	Rear Funnel Exit [V]	45
	Trap Funnel RF [V]	120
	Acquisition mode	Alternating Frames. Frame 2 with ramped collision energies [Drift time 0 ms: 15 eV; Drift time 25 ms: 25 eV; Drift time 59 ms: 60 eV]
	Trap Fill Time [ $\mu$ s]	20 000
	Trap Release Time [ $\mu$ s]	150
	Max. Drift Time [ms]	60
	IM Transient Rate [transients/frame]	19
	Frame Rate [frame/sec]	0.8
4-bit multiplexing	Drift Tube Entrance [V]	1574
	Drift Tube Exit [V]	224
	Rear Funnel Entrance [V]	217.5
	Rear Funnel Exit [V]	45
	Trap Funnel RF [V]	120
	Acquisition mode	4bit multiplexing
	Trap Fill Time [ $\mu$ s]	3000
	Trap Release Time [ $\mu$ s]	150
	Max. Drift Time [ms]	60
	IM Transient Rate [transients/frame]	16
	Frame Rate [frame/sec]	1

**Table SI-4.1.5:** Suspect list used for the suspect screening analysis of quaternary ammonium compounds and other cationic surfactants in indoor dust samples. *(The table can be openly assessed in the Supporting Information of online version of the corresponding article (Table S4): <https://doi.org/10.1016/j.envint.2023.108021>)*

**Table SI-4.1.6:** Assignment of internal standards used for the semi-quantification for each of the targeted quaternary ammonium compounds (QAC). The full names of each targeted QAC can be found in **Table SI-4.1.1**.

<b>Target QAC</b>	<b>Assigned internal standard</b>
C6-BAC	<i>D</i> <sub>7</sub> -C12-BAC
C8-BAC	<i>D</i> <sub>7</sub> -C12-BAC
C10-BAC	<i>D</i> <sub>7</sub> -C12-BAC
C12-BAC	<i>D</i> <sub>7</sub> -C12-BAC
C14-BAC	<i>D</i> <sub>7</sub> -C14-BAC
C16-BAC	<i>D</i> <sub>7</sub> -C14-BAC
C18-BAC	<i>D</i> <sub>7</sub> -C14-BAC
C8:C8-DDAC	<i>D</i> <sub>7</sub> -C14-BAC
C10:C10-DDAC	<i>D</i> <sub>7</sub> -C14-BAC
C12:C12-DDAC	<i>D</i> <sub>7</sub> -C14-BAC
C14:C14-DDAC	<i>D</i> <sub>7</sub> -C14-BAC
C16:C16-DDAC	<i>D</i> <sub>7</sub> -C14-BAC
C18:C18-DDAC	<i>D</i> <sub>7</sub> -C14-BAC
C8-ATMAC	<i>D</i> <sub>9</sub> -C10-ATMAC
C10-ATMAC	<i>D</i> <sub>9</sub> -C10-ATMAC
C12-ATMAC	<i>D</i> <sub>9</sub> -C10-ATMAC
C14-ATMAC	<i>D</i> <sub>9</sub> -C10-ATMAC
C16-ATMAC	<i>D</i> <sub>9</sub> -C10-ATMAC
C18-ATMAC	<i>D</i> <sub>9</sub> -C10-ATMAC
C22-ATMAC	<i>D</i> <sub>9</sub> -C10-ATMAC

**Table SI-4.1.7:** Summary of the calibration parameters obtained from the calibration curves of each of the targeted alkyltrimethylammonium compounds (ATMACs), benzylalkyldimethylammonium compounds (BACs) and dialkyldimethylammonium compounds (DDACs). For each compound, the calibration range, the response factor and the correlation coefficient are given.

Target QAC	Lowest calibration point [pg/ $\mu$ L]	Highest calibration point [pg/ $\mu$ L]	Response factor $R_f$	Correlation coefficient $R^2$
C6-BAC	0.5	100	14.5	0.997
C8-BAC	0.5	100	18.0	0.994
C10-BAC	0.5	100	21.7	0.996
C12-BAC	0.5	100	23.3	0.997
C14-BAC	0.5	100	22.9	0.995
C16-BAC	0.5	100	24.8	0.991
C18-BAC	0.5	100	35.9	0.995
C8:C8-DDAC	0.5	50	45.2	0.998
C10:C10-DDAC	0.5	50	30.5	0.998
C12:C12-DDAC	0.5	50	48.7	0.999
C14:C14-DDAC	0.5	50	44.8	0.998
C16:C16-DDAC	0.5	100	36.8	0.991
C18:C18-DDAC	0.5	100	31.9	0.999
C8-ATMAC	0.5	100	33.5	0.999
C10-ATMAC	0.5	100	23.2	0.999
C12-ATMAC	0.5	100	26.1	0.999
C14-ATMAC	0.5	100	29.6	0.999
C16-ATMAC	0.5	83	36.6	0.999
C18-ATMAC	0.5	100	43.2	0.993
C20-ATMAC	0.5	100	33.8	0.993
C22-ATMAC	0.5	100	33.4	0.998

**Table SI-4.1.8:** Average retention times (RT) and average absolute mass errors (AME) obtained for the targeted alkyltrimethylammonium compounds (ATMACs), benzylalkyldimethylammonium compounds (BACs) and dialkyldimethylammonium compounds (DDACs) in the QC samples (n = 4). For both, the standard deviation (SD) is given.

Target QAC	Average RT [min]	SD <sub>RT</sub> [min]	Average AME [ppm]	SD <sub>AME</sub> [ppm]
C6-BAC	4.03	0.02	0.39	0.24
C8-BAC	6.24	0.02	1.11	0.20
C10-BAC	7.86	0.01	0.26	0.26
C12-BAC	9.73	0.10	0.82	0.43
C14-BAC	10.62	0.01	0.76	0.42
C16-BAC	11.65	0.02	0.85	0.87
C18-BAC	12.48	0.03	0.55	0.53
C8:C8-DDAC	8.90	0.01	0.42	0.22
C10:C10-DDAC	11.16	0.02	0.45	0.28
C12:C12-DDAC	12.69	0.03	1.43	1.95
C14:C14-DDAC	14.15	0.03	0.55	0.66
C16:C16-DDAC	15.59	0.03	0.86	0.37
C18:C18-DDAC	16.87	0.03	1.05	0.17
C8-ATMAC	3.62	0.02	0.39	0.30
C10-ATMAC	5.96	0.01	0.33	0.21
C12-ATMAC	7.72	0.02	0.33	0.10
C14-ATMAC	9.39	0.03	0.63	0.42
C16-ATMAC	10.85	0.01	1.05	0.78
C18-ATMAC	11.95	0.01	1.11	0.64
C22-ATMAC	13.78	0.03	0.78	0.34

**Table SI-4.1.9:** Experimental CCS values (<sup>DT</sup>CCS<sub>expN<sub>2</sub></sub>) obtained for the QC compounds within IM-MS measurements. The <sup>DT</sup>CCS<sub>expN<sub>2</sub></sub> were obtained through triplicate measurements. The standard deviation (SD) and relative standard deviation (RSD) are given. <sup>DT</sup>CCS<sub>expN<sub>2</sub></sub> were compared with literature reference values (<sup>DT</sup>CCS<sub>litN<sub>2</sub></sub>) and absolute percent errors (APEs) were calculated.

QA compound	Adduct	Theoretical m/z	<sup>DT</sup> CCS <sub>expN<sub>2</sub></sub> ± SD [Å <sup>2</sup> ]	RSD [%]	<sup>DT</sup> CCS <sub>litN<sub>2</sub></sub> [Å <sup>2</sup> ]	APE [%]
Cortisol	[M + H] <sup>+</sup>	363.2166	188.78 ± 0.07	0.04	188.34	0.23
	[M + Na] <sup>+</sup>	385.1985	212.07 ± 0.20	0.09	212.79	0.34
Creatinine	[M + H] <sup>+</sup>	166.0863	122.91 ± 0.33	0.27	122.98	0.06
L-phenyl-alanine	[M + H] <sup>+</sup>	182.0812	139.94 ± 0.10	0.07	140.30	0.25

**Table SI-4.1.10:** Summary of targeted QACs and IS used for the semi-quantification of suspects identified within the suspect screening approach.

Suspect QAC				Targeted QAC used for semi-quantification			Assigned IS
Nr.	Name	Formula	RT [min]	Name	Formula	RT [min]	Name
1	C2:C12-DDAC	[C <sub>16</sub> H <sub>36</sub> N] <sup>+</sup>	8.12	C8-DDAC	[C <sub>18</sub> H <sub>40</sub> N] <sup>+</sup>	8.90	D-C14-BAC
2	C2:C14-DDAC	[C <sub>18</sub> H <sub>40</sub> N] <sup>+</sup>	9.72	C8-DDAC	[C <sub>18</sub> H <sub>40</sub> N] <sup>+</sup>	8.90	D <sub>7</sub> -C14-BAC
3	C2:C16-DDAC	[C <sub>20</sub> H <sub>44</sub> N] <sup>+</sup>	11.05	C10-DDAC	[C <sub>22</sub> H <sub>48</sub> N] <sup>+</sup>	11.16	D <sub>7</sub> -C14-BAC
4	C2:C18-DDAC	[C <sub>22</sub> H <sub>48</sub> N] <sup>+</sup>	12.05	C12-DDAC	[C <sub>26</sub> H <sub>56</sub> N] <sup>+</sup>	12.69	D <sub>7</sub> -C14-BAC
5	C8:C10-DDAC	[C <sub>20</sub> H <sub>44</sub> N] <sup>+</sup>	10.16	C10-DDAC	[C <sub>22</sub> H <sub>48</sub> N] <sup>+</sup>	11.16	D <sub>7</sub> -C14-BAC
6	C14:C16/ C18:C12-DDAC	[C <sub>32</sub> H <sub>68</sub> N] <sup>+</sup>	14.88	C14-DDAC	[C <sub>30</sub> H <sub>64</sub> N] <sup>+</sup>	14.15	D <sub>7</sub> -C14-BAC
7	C18:C13-DDAC	[C <sub>33</sub> H <sub>70</sub> N] <sup>+</sup>	15.25	C16-DDAC	[C <sub>34</sub> H <sub>72</sub> N] <sup>+</sup>	15.59	D <sub>7</sub> -C14-BAC
8	C15:C18/ C16:C17-DDAC	[C <sub>35</sub> H <sub>74</sub> N] <sup>+</sup>	15.93	C16-DDAC	[C <sub>34</sub> H <sub>72</sub> N] <sup>+</sup>	15.59	D <sub>7</sub> -C14-BAC
9	C16:C18-DDAC	[C <sub>36</sub> H <sub>76</sub> N] <sup>+</sup>	16.25	C18-DDAC	[C <sub>36</sub> H <sub>76</sub> N] <sup>+</sup>	16.87	D <sub>7</sub> -C14-BAC
10	C18:20-DDAC	[C <sub>40</sub> H <sub>84</sub> N] <sup>+</sup>	17.40	C18-DDAC	[C <sub>36</sub> H <sub>76</sub> N] <sup>+</sup>	16.87	D <sub>7</sub> -C14-BAC
11	C11-BAC	[C <sub>20</sub> H <sub>36</sub> N] <sup>+</sup>	8.67	C12-BAC	[C <sub>21</sub> H <sub>38</sub> N] <sup>+</sup>	9.39	D <sub>7</sub> -C12-BAC
12	C13-BAC	[C <sub>22</sub> H <sub>40</sub> N] <sup>+</sup>	10.04	C12-BAC	[C <sub>21</sub> H <sub>38</sub> N] <sup>+</sup>	9.39	D <sub>7</sub> -C12-BAC
13	C20-BAC	[C <sub>29</sub> H <sub>54</sub> N] <sup>+</sup>	13.29	C18-BAC	[C <sub>27</sub> H <sub>50</sub> N] <sup>+</sup>	12.48	D <sub>7</sub> -C14-BAC
14	1-Hexadecyl-pyridinium	[C <sub>21</sub> H <sub>38</sub> N] <sup>+</sup>	11.04	C10-DDAC	[C <sub>22</sub> H <sub>48</sub> N] <sup>+</sup>	11.16	D <sub>7</sub> -C14-BAC
15	Benzethonium	[C <sub>27</sub> H <sub>42</sub> NO <sub>2</sub> ] <sup>+</sup>	9.53	C12-BAC	[C <sub>21</sub> H <sub>38</sub> N] <sup>+</sup>	9.39	D <sub>7</sub> -C12-BAC
16	Choline	[C <sub>5</sub> H <sub>14</sub> NO] <sup>+</sup>	0.92	C8-ATMAC	[C <sub>11</sub> H <sub>26</sub> N] <sup>+</sup>	3.62	D <sub>9</sub> -C10-ATMAC
17	Tetraethyl-ammonium	[C <sub>8</sub> H <sub>20</sub> N] <sup>+</sup>	0.92	C8-ATMAC	[C <sub>11</sub> H <sub>26</sub> N] <sup>+</sup>	3.62	D <sub>9</sub> -C10-ATMAC

**Table SI-4.1.11:** Summary of experimental  $^{DT}CCS_{N_2}$  values acquired for the targeted QAC. Average  $^{DT}CCS_{N_2}$  values of the eight calibration solutions (covering concentrations between 0.5 pg/ $\mu$ L and 100 pg/ $\mu$ L; n = 8) and the (relative) standard deviations are given. If available, experimental  $^{DT}CCS_{N_2}$  values were compared with literature  $^{TW}CCS_{N_2}$  values obtained from the studies of (Song et al., 2022) and (Hines et al., 2017b).

Class	Abbreviation	$m/z$ [ $M^+$ ]	$^{DT}CCS_{N_2}$ exp. [ $\text{\AA}^2$ ]	SD [ $\text{\AA}^2$ ]	RSD [%]	$^{TW}CCS_{N_2}$ lit. [ $\text{\AA}^2$ ] <sup>1</sup>	APE [%]	$^{TW}CCS_{N_2}$ lit. [ $\text{\AA}^2$ ] <sup>2</sup>	APE [%]
BAC	C6-BAC	220.2060	157.58	0.12	0.08				
	C8-BAC	248.2373	170.34	0.19	0.11	172.80	1.4		
	C10-BAC	276.2686	182.45	0.32	0.18	185.55	1.7		
	C12-BAC	304.2999	193.45	0.29	0.15	196.96	1.8	193.0	0.2
	C14-BAC	332.3312	202.32	0.27	0.13	207.60	2.6	205.7	1.7
	C16-BAC	360.3625	209.18	0.47	0.22	217.02	3.7	214.8	2.7
	C18-BAC	388.3938	215.92	0.49	0.23				
DDAC	C8:C8-DDAC	270.3155	187.96	0.52	0.28				
	C10:C10-DDAC	326.3781	208.44	0.45	0.22	213.34	2.4		
	C12:C12-DDAC	382.4407	225.99	0.51	0.23				
	C14:C14-DDAC	438.5033	240.57	0.51	0.21				
	C16:C16-DDAC	494.5659	253.51	0.45	0.18				
	C18:C18-DDAC	550.6285	265.52	0.31	0.12				
ATMAC	C8-ATMAC	172.2060	150.70	0.11	0.07				
	C10-ATMAC	200.2373	163.72	0.10	0.06				
	C12-ATMAC	228.2686	175.18	0.15	0.09				
	C14-ATMAC	256.2999	184.85	0.20	0.11				
	C16-ATMAC	284.3312	193.01	0.32	0.16	199.22	3.2		
	C18-ATMAC	312.3625	200.29	0.37	0.19				
	C20-ATMAC	340.3938	207.09	0.43	0.21				
	C22-ATMAC	368.4251	215.11	0.25	0.12				
			<b>Average</b>	<b>0.33</b>	<b>0.16</b>		<b>2.4</b>		<b>1.5</b>

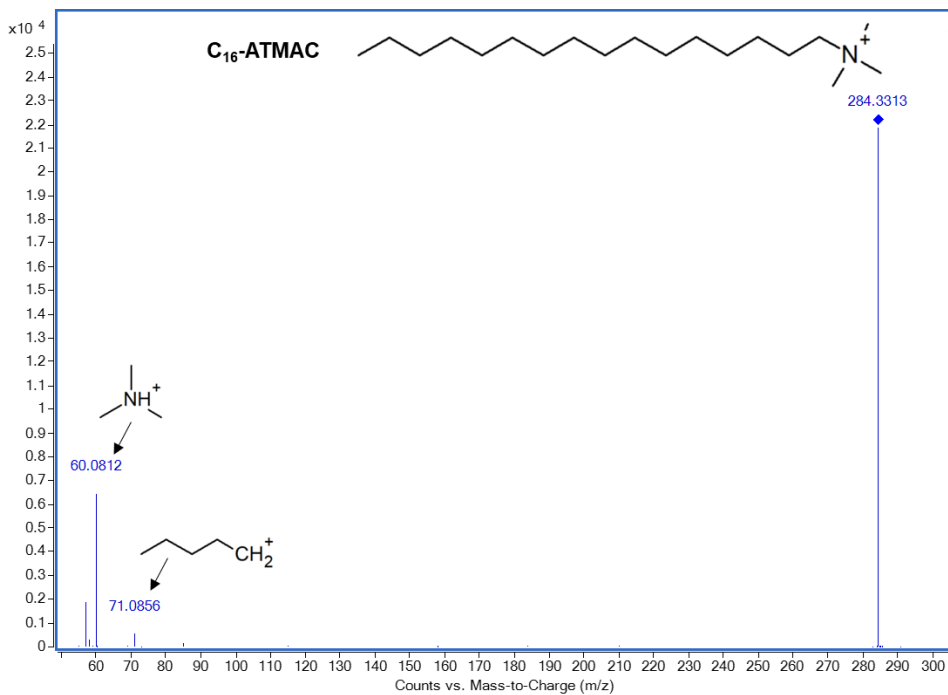


**Figure SI-4.1.1:** Fragmentation spectrum of C<sub>16</sub>-ATMAC obtained at a collision energy of 20 eV. The structure of the parent ion and the main fragments are indicated.

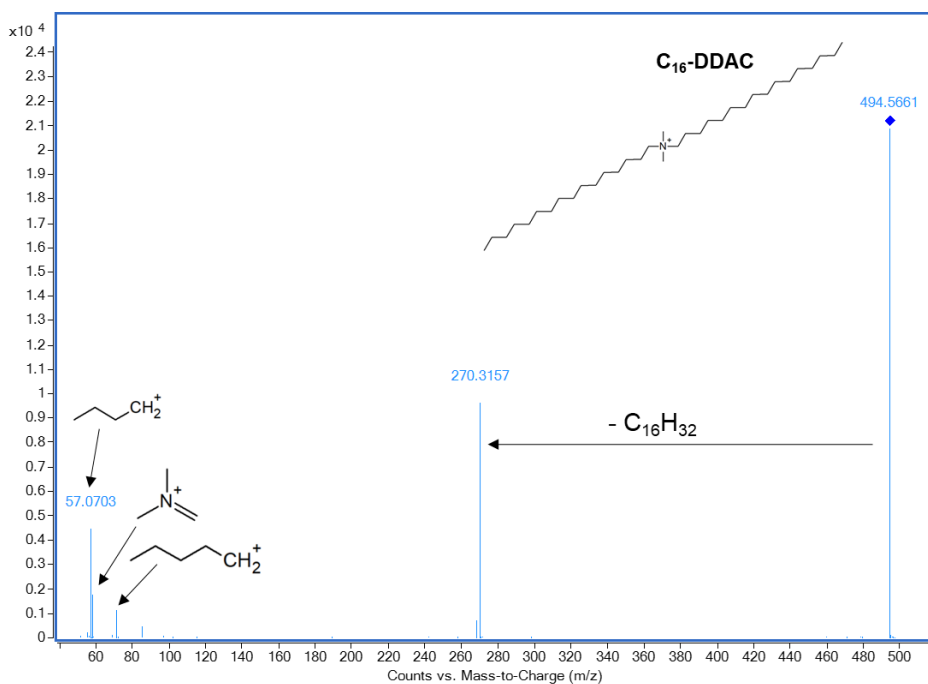


**Figure SI-4.1.2:** Fragmentation spectrum of C<sub>16</sub>-DDAC obtained at a collision energy of 20 eV. The structure of the parent ion and the main fragments are indicated.

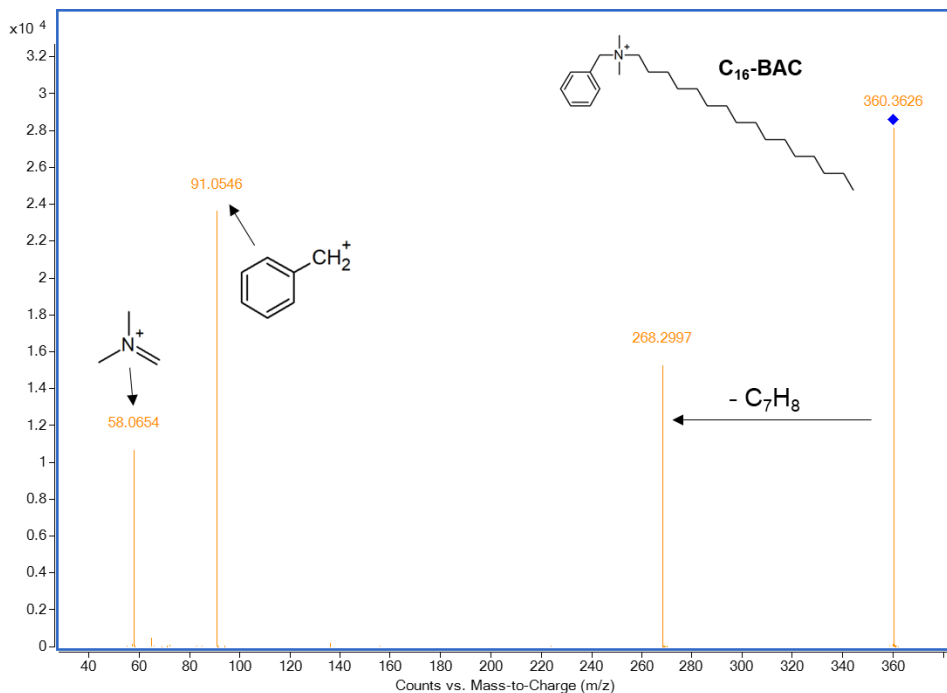


**Figure SI-4.1.3:** Fragmentation spectrum of C<sub>16</sub>-BAC obtained at a collision energy of 20 eV. The structure of the parent ion and the main fragments are indicated.

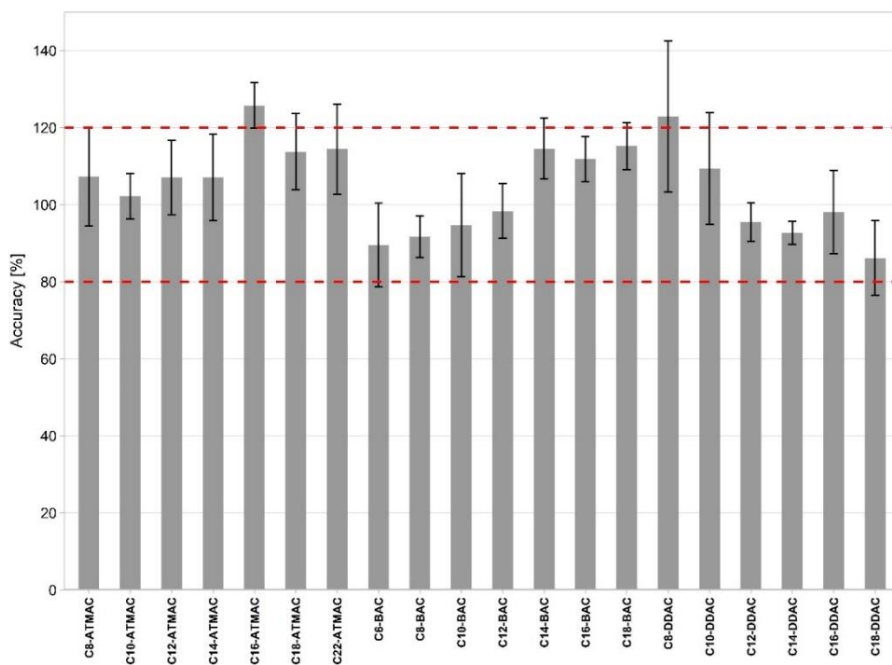


**Figure SI-4.1.4:** Average accuracies obtained for the 21 targeted quaternary ammonium compounds in quality control (QC) samples (n = 4). For each targeted QACs, the error bars indicate the standard deviation.

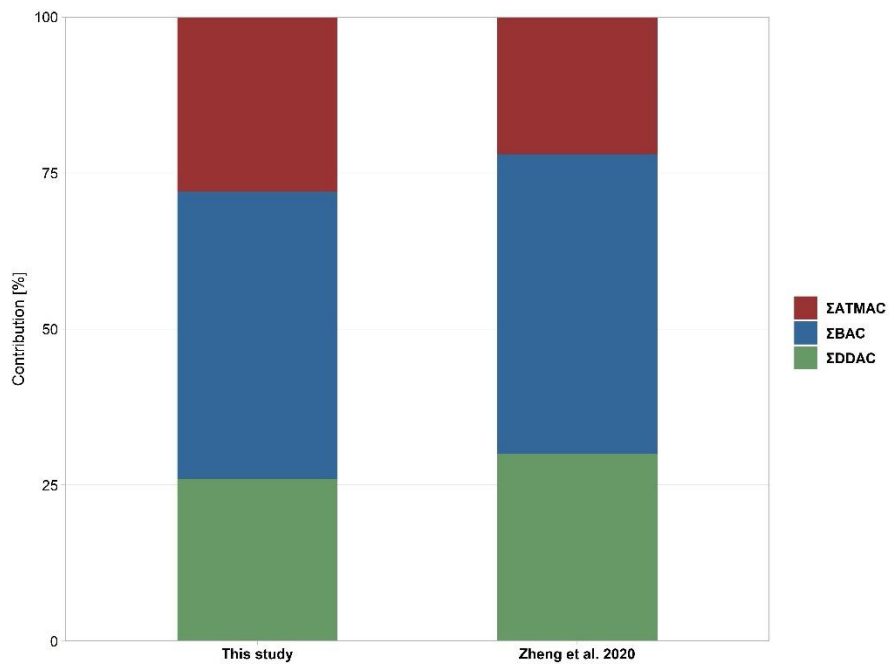


**Figure SI-4.1.5:** Comparison of the percental contribution of the three classes of quaternary ammonium compounds (QACs), alkyl trimethyl ammonium compounds (ATMACs; blue), benzyl alkyl ammonium compounds (BACs; green) and dimethyl dialkyl ammonium compounds (DDACs; orange) to the total QAC concentration between this study (left) and the data quantified by Zheng et al., 2020, in dust samples collected before the COVID-19 pandemic (Zheng et al., 2020).

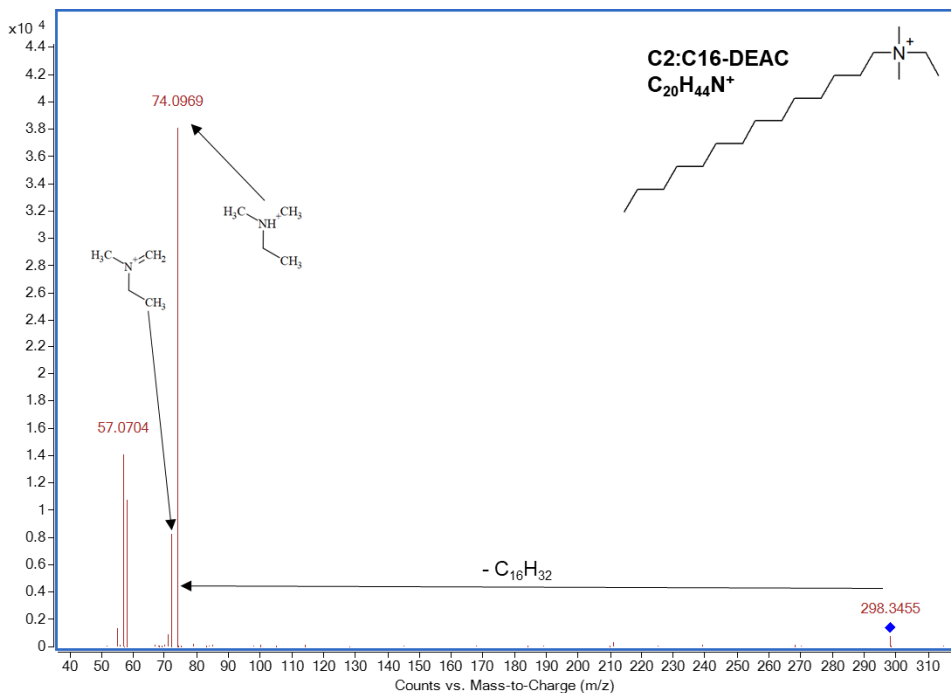


**Figure SI-4.1.6:** Fragmentation spectrum of the dimethyl ethyl ammonium compound (DEAC) C2:C16-DEAC obtained with a collision energy of 40 eV. For characteristic fragments, the proposed structure is indicated.

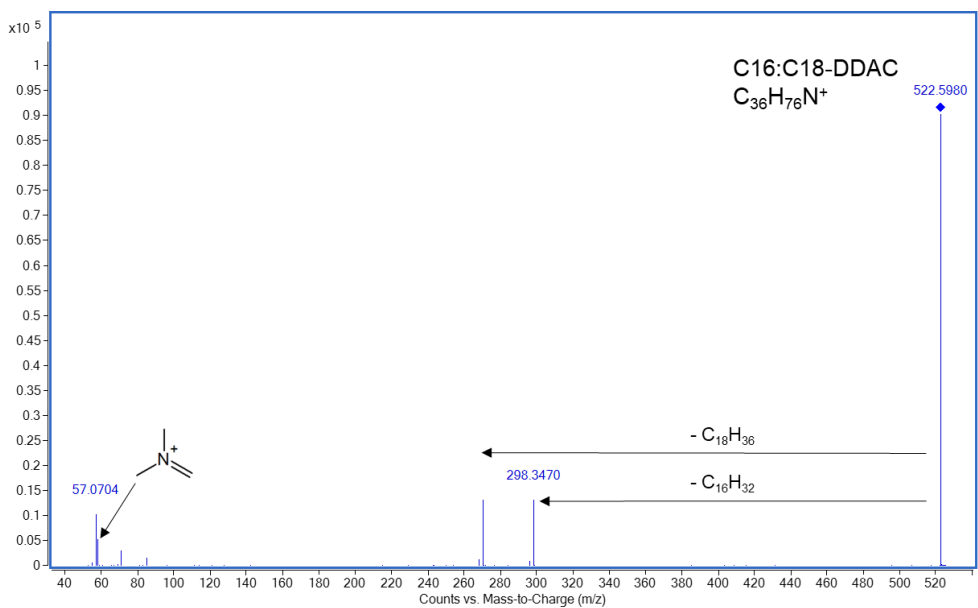


**Figure SI-4.1.7:** Fragmentation spectrum of the C16:C18-DDAC obtained with a collision energy of 40 eV. For characteristic fragments, the proposed structure or the corresponding neutral loss is indicated.

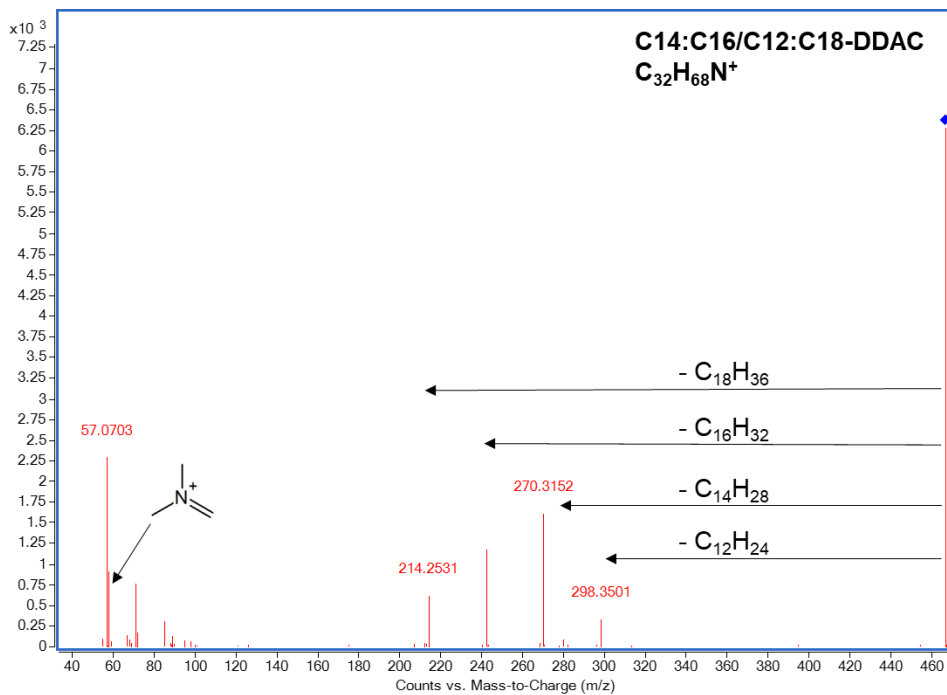


**Figure SI-4.1.8:** Fragmentation spectrum of C14:C16/C12:C18-DDAC obtained with a collision energy of 40 eV. For characteristic fragments, the proposed structure or the corresponding neutral loss is indicated.

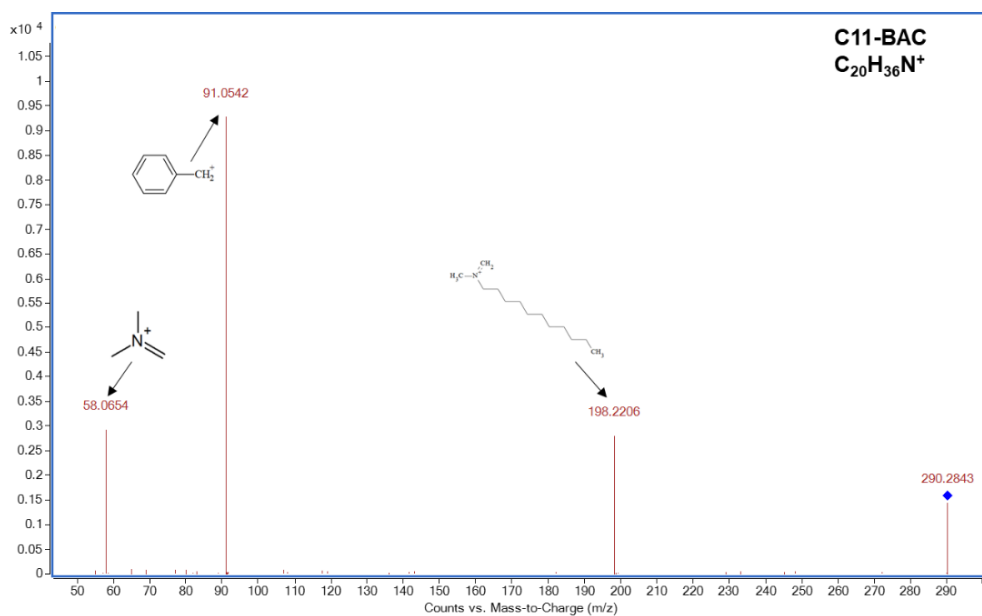


**Figure SI-4.1.9:** Fragmentation spectrum of C11-BAC obtained with a collision energy of 20 eV. For characteristic fragments, the proposed structure is indicated.

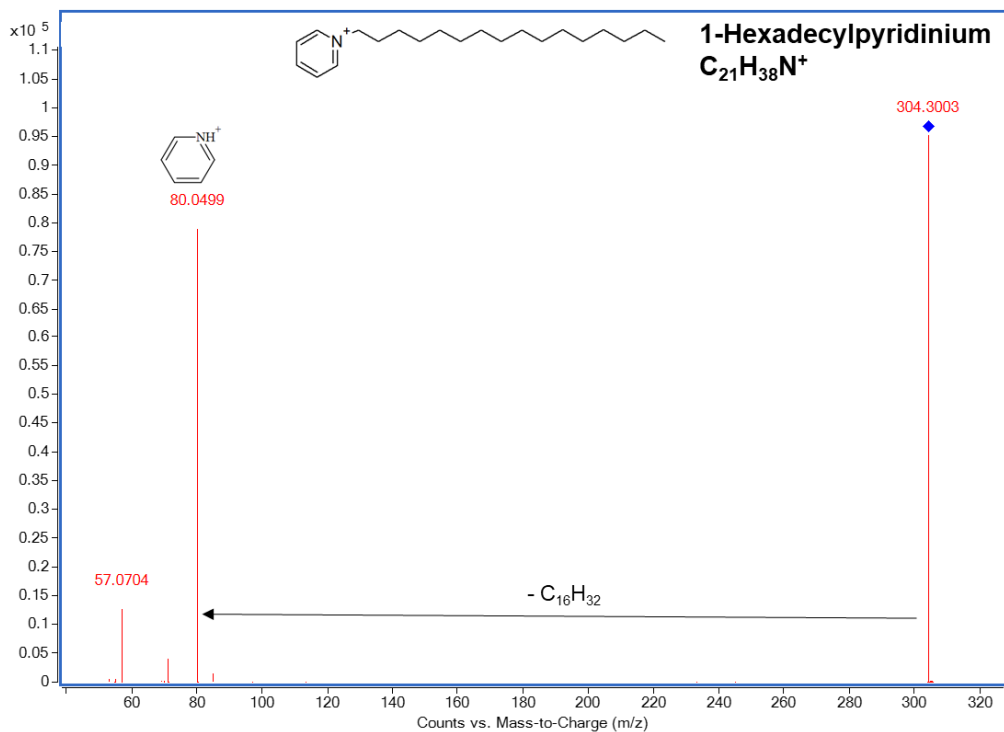


**Figure SI-4.1.10:** Fragmentation spectrum of 1-Hexadecylpyridinium obtained with a collision energy of 20 eV. For characteristic fragments, the proposed structure or the corresponding neutral loss is indicated.

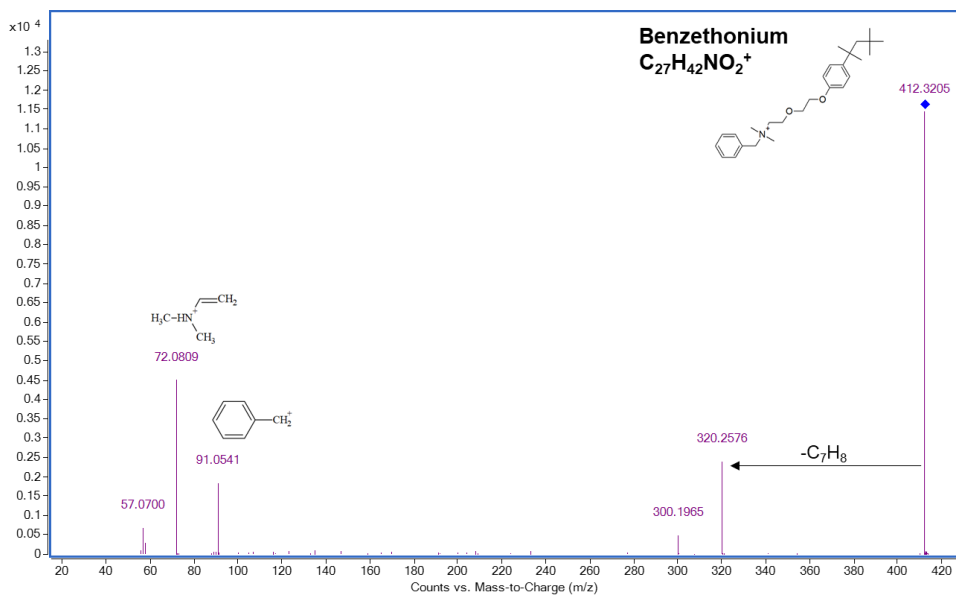


**Figure SI-4.1.11:** Figure S12: Fragmentation spectrum of Benzethonium obtained with a collision energy of 20 eV. For characteristic fragments, the proposed structure or the corresponding neutral loss is indicated.

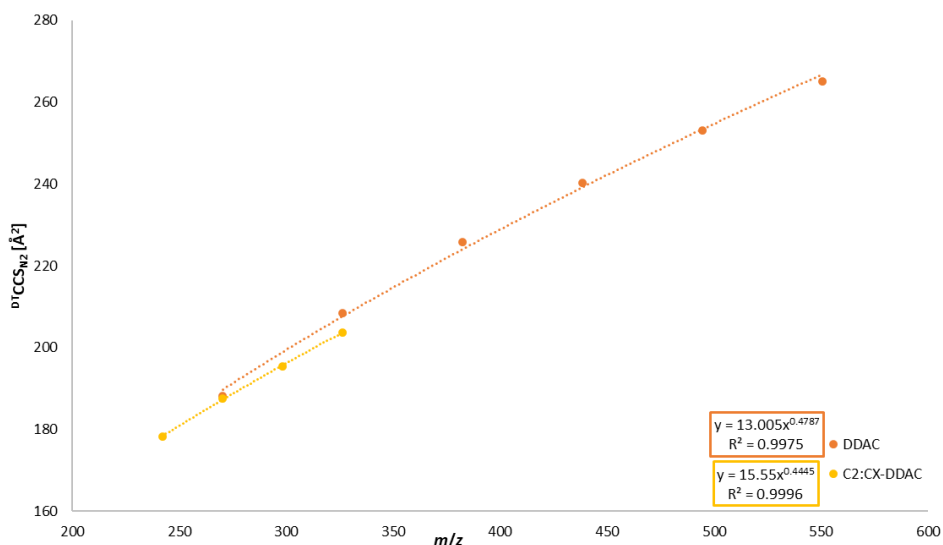


**Figure SI-4.1.12:** Plot of  $^{DT}CCS_{N_2}$  values vs  $m/z$  ratios of targeted DDACs (orange) and suspect DEACs (yellow). For both classes, the CCS- $m/z$  relationship was fitted using a power model resulting in two trendlines. For each of the trendlines, the equation and correlation coefficient are indicated.

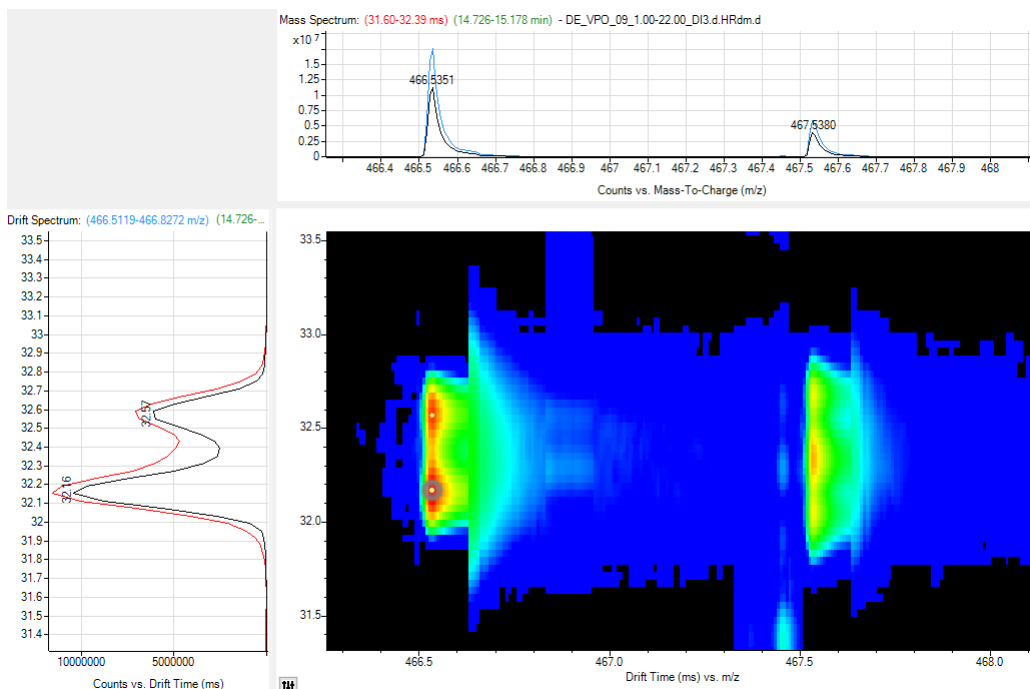


**Figure SI-4.1.13:** Mobilogram and MS spectrum obtained for C14:C16/C12:C18 dimethyl dialkyl ammonium compound (DDAC) after acquisition using 4-bit multiplexed ion-mobility spectrometry. The drift spectrum (left) shows two peaks confirming the presence of a mixture of isomers in the sample.

## 4.2 Identification and semi-quantification of contaminants of emerging concern in indoor dust samples using IM derived CCS-m/z trendlines as an additional identification parameter

### 4.2.1 Introduction

The indoor environment contributes substantially to human exposure to various environmental contaminants. For the latter, the ingestion and inhalation of, or the dermal contact with indoor dust represent major exposure routes which are especially relevant for toddlers due to crawling behaviour and frequent hand-to-mouth contact (Cui et al., 2023; Dubocq et al., 2021). In recent years, numerous studies have identified various contaminant classes in indoor dust including phthalate and alternative plasticizers, OPFRs, UV-filters, polybrominated diphenyl ethers, polycyclic aromatic hydrocarbons, among others, pointing out the suitability of this matrix to identify indoor contamination (Ao et al., 2018; Christia et al., 2021b; Dvoršćak et al., 2022; Xu and Li, 2021). Numerous of these compounds can be considered as CECs.

While quantitative results obtained through target analysis, commonly applied for contaminant analysis, are important for a thorough exposure assessment (Christia et al., 2021a) these approaches do not allow the detection of contaminants which are not *a priori* targeted. This gap is addressed through the application of SSA and NTS approaches which have been widely implemented in the exposomics field and can support the identification of novel CECs which might be overlooked with traditional targeted methods.

For example, two recent studies using an NTS approach for prioritizing and characterizing compounds based on characteristic fragmentation patterns showed the identification of 20 novel OPFRs (Wang et al., 2022; Wang et al., 2020a). Other SSA and NTS studies reported additional novel compounds from various classes including plasticizers, pharmaceuticals, and PCPs, pointing out the added value of the described approaches and the high variety of CECs present in dust (Christia et al., 2021b; Rostkowski et al., 2019; Zhang et al., 2021).

Recently, the absence of quantitative results within SSA and NTS studies was addressed by semi-quantitative approaches allowing to obtain data for suspect compounds for which reference standards are often not available. These approaches are based on the selection of calibrators similar in structure and/or retention time (RT) to the suspect compound or the prediction of ionization efficiencies for the latter (Bieber et al., 2023; Malm et al., 2021). Subsequently, the obtained semi-quantified concentrations can be used for further prioritization of the detected compounds, estimation of human exposure and other purposes further improving the usability of obtained results derived from SSA and NTS studies.

Therefore, this chapter aimed at combining the added value of SSA and semi-quantification analysing indoor dust samples by HRMS. A combination of 1) targeted and

suspect screening, 2) implementation of a semi-quantification workflow for a subset of suspect compounds, and 3) the subsequent calculations of estimated daily intakes (EDIs) allowed a comprehensive characterization of a wide range of CECs and an estimation of potential human exposure to the latter easing further compound prioritization.

## 4.2.2 Materials and Methods

### 4.2.2.1 Chemicals

Methanol (MeOH), acetonitrile (ACN), and formic acid (FA) were purchased from Biosolve BV (Valkenswaard, the Netherlands) ( $\geq 99.9\%$ ). N-hexane (Hex) and acetone were purchased from Thermo Scientific Chemicals (Geel, Belgium) (95% and 99.9% respectively). Toluene was purchased from Acros Organics (Geel, Belgium) ( $\geq 99.8\%$ ) and ethyl acetate (EtOAc) was purchased from Merck (Darmstadt, Germany) (99.8%). All organic solvents were of LC grade. Ultrapure water (18.2 M $\Omega$  cm, Milli-Q, Millipore) was obtained using a PURELAB Flexsystem (Elga Veolia, Tienen, Belgium). Ammonium acetate, which was used as an eluent additive, was purchased from Sigma-Aldrich (Bornem, Belgium). A set of 31 native standards of phthalates (PHs), alternative plasticizers (APs) and organophosphate flame retardants (PFRs) and 6 labelled PHs and PFRs were used as quality control and internal standards (IS). Their name, formula, supplier and further identifiers are summarized in Supplementary Information (**Table SI-4.2.1**). The same data are listed in **Table SI-4.2.1** for 11 reference standards purchased for the confirmation of assigned suspects. These include a selection of reference standards purchased for compounds identified with a confidence level of 2 or 3 (see **chapter 4.2.3.2**). PCPs and others were excluded from the list of standards to consider for purchase as they were considered to have a lower priority.

### 4.2.2.2 Sample collection

Here, the same set of samples was investigated as in **chapter 4.1**. Details on sample characteristics and collection can therefore be found in **chapter 4.1.2.2**.

### 4.2.2.3 Sample preparation

The sample preparation was based on an in-house developed method (Christia et al., 2021b). After homogenization through manual mixing, samples were sieved using a mesh size of 500  $\mu\text{m}$ . Sieved dust (20 mg) was weighed into pre-cleaned glass tubes. After spiking of IS (100 ng for TCEP-*D*<sub>12</sub>/TDCIPP-*D*<sub>15</sub>/TPhP-*D*<sub>15</sub>; 500 ng for DBzP-*D*<sub>4</sub>/DEHP-*D*<sub>4</sub>/DnBP-*D*<sub>4</sub>), dust samples were extracted twice with 2.5 mL of a Hex/acetone mixture (1:1; v/v) and 0.5 mL of toluene through vortexing for 1 min and sonicating for 5 min. Extracts were pooled and evaporated to near dryness under a gentle nitrogen stream (T = 36 °C) prior to reconstitution in 1 mL of hexane.

Obtained extracts were fractionated using SeP-Pak® Vac 3cc (500 mg) Florisil® solid-phase extraction (SPE) cartridges (Waters; Milford, MA, USA). These were precleaned with 3 mL MeOH, EtOAc and Hex prior to loading the extracts on the cartridges. Fractions were sequentially eluted with 8 mL Hex, 10 mL EtOAc and 6 mL MeOH corresponding to fractions A, B and C, respectively. Each fraction was evaporated to near dryness and separately reconstituted in 100 µL isoctane (fraction A) or 100 µL MeOH:H<sub>2</sub>O (9:1; v/v; fractions B and C). After filtering through centrifugal filters (pore size: 0.2 µm, VWR, Leuven, Belgium), fractions B and C were separately analysed using the approach described below, while fraction A was subject of another study. Fraction A was expected to contain nonpolar compounds more suitable for analysis with gas chromatography. Its analysis therefore fell outside the scope of this thesis.

In each batch of samples, two procedural blanks and two quality control (QC) samples were included which were spiked with IS and treated in the same way as the actual samples. Procedural blanks and QC samples consisted of pre-cleaned sodium sulphate which, in case of QC samples, was additionally spiked with a set of 31 reference standards (**Table SI-4.2.1**; final theoretical concentration in extract: 1 ng/µL).

#### 4.2.2.4 Instrumental analysis

All samples were analysed on an Agilent 6560 ion-mobility quadrupole time-of-flight high resolution mass spectrometer operating in positive polarity coupled to an Agilent Infinity II UPLC system (Agilent Technologies, Santa Clara, USA) and equipped with a Dual Jet Stream ESI source.

Chromatographic separation was achieved using an InfinityLab Poroshell 120 EC-C18 column (2.1 x 100 mm, particle size 2.7 µm) equipped with a guard column (2.1 x 5 mm) containing the same stationary phase and maintained at a temperature of 40 °C. Ultrapure water (A) and MeOH (B) were used as mobile phases (flow rate: 0.35 mL/min) to both of which 0.1% formic acid was added. The injection volume was set to 3 µL. The following gradient was applied for both ionization modes: 5% B (0 min), 50% B (0-3 min), 80% B (3-5 min), 99% B (5-16 min), 99% B (16-18 min), 5% B (18.1-21 min).

As ion source parameters, voltages of 3500 V, 1000 V, 350 V and 65 V were applied for the capillary, nozzle, fragmentor and skimmer, respectively. Gas and sheath gas temperatures were maintained at 325 °C and 350 °C, respectively, with a gas flow, sheath gas flow and nebulizer pressure of 9 L/min, 11 L/min and 35 psig, respectively.

A range of  $m/z$  100-1500 and  $m/z$  50-1500 was included for acquisition of MS and MS/MS spectra, respectively. Data was acquired using a data-dependent acquisition approach. Thereby, four precursors per acquisition cycle were automatically selected for fragmentation based on their abundance with the quadrupole isolation width set to 'narrow'. Fragmentation spectra were obtained applying collision energies of 10, 20, and 40 eV. Data were acquired in QTOFonly and ion-mobility mode. For the latter, the same settings as listed in chapter 4.1 (**Table SI-4.1.4**, single pulse mode).

Procedural blanks were injected at the beginning of the sequence (after system stabilization through injection of instrumental blanks). Remaining samples were injected once in a randomized manner with the QC samples evenly spread throughout the injection sequence. Every five samples, an instrumental blank consisting of MeOH was injected to assess potential carry-over and background contamination.

#### 4.2.2.5 Quality control and data analysis

Prior to any data processing, the mass accuracy of the raw data and stability of the chromatographic conditions were assessed by investigating the signals and RTs obtained for IS in all samples and native compounds included in the QC samples. For these investigations, the 'Find By Formula' algorithm was used (Agilent MassHunter Qualitative Analysis software version B.07.00) applying a mass tolerance of 10 ppm and an overall matching score of at least 70. For the extraction of the IS signals from raw data of the dust samples, both the proton ( $[M+H]^+$ ) and sodium ( $[M+Na]^+$ ) adducts were considered and a peak area consisting of the summed signals of both adducts was reported. For the IS and native compounds included in the QC samples, only the signals obtained for the more abundant of the two mentioned adducts was reported as the selection of the more abundant adduct of each parent compound was relevant for the semi-quantification approach described in **chapter 4.2.2.6**.

After the described QC measures, molecular features were extracted from the raw data using the 'Batch recursive feature extraction' algorithm within the MassHunter Profinder software (version B.08.00; Agilent Technologies, Santa Clara, USA). Thereby, the minimum peak height was set to 2000 counts. Ions corresponding to  $[M+H]^+$  or  $[M+Na]^+$  were included. For chromatogram alignment, tolerances were set to 0.20 min and 10 ppm for the retention time and mass tolerance, respectively. All obtained features were imported in the Mass Profiler Professional software (version 15.0, Agilent Technologies) and further filtered using a fold change analysis which only retained features showing at least a 5-fold intensity difference between samples and procedural blanks. Filtered features were matched against a previously developed suspect list using the MassHunter ID Browser (version 10.0). Thereby, a mass tolerance of 7 ppm, an isotope abundance score of 80 and an overall matching score of at least 75 were set. The applied suspect list was based on an in-house suspect list developed within a previous study (Christia et al., 2021b). Additionally, a list of compounds associated with plastic packaging was added to further expand the coverage of the group of plastic related chemicals (Groh et al., 2019). Lastly, a list was included containing new OPFRs and triazine UV filters recently discovered in indoor dust and soil samples from South China (Du et al., 2022; Gong et al., 2022; Wang et al., 2020a) to potentially confirm the occurrence of these compounds in European dust samples. Ultimately, the final version of the suspect list contained > 4300 entities.

All annotated compounds which fulfilled the matching criteria described above, were manually investigated to confirm compound annotation and avoid the report of false positive detections. Thereby, the mass accuracy, the match between theoretical and experimental isotopic pattern and, if available, the fragmentation spectra were investigated. This aimed at assigning a CL of identification based on the scheme introduced by Schymanski et al. (Schymanski et al., 2014). CL1 was assigned if all experimental data (RT,  $m/z$ , isotopic pattern and fragmentation spectrum) of a feature unequivocally matched data of an available reference standard following the same criteria as mentioned above. CL2A or CL2B were assigned if available experimental fragmentation spectra could be matched with library data (e.g., derived from open-source libraries such as MassBank or mzcloud (date of last access: 01/11/2023)) or provided diagnostic evidence, respectively, and allowed the assignment of a single possible compound structure (Celma et al., 2020). As described in **chapter 5**, CL2 was expanded by the addition of CL2C which was assigned if no fragmentation spectrum was available but the remaining data ( $m/z$ , RT and isotopic pattern) unequivocally matched the reference standard (RT difference < 0.2 min, mass error < 7 ppm). If, based on the available experimental data (incl. a fragmentation spectrum), a tentative candidate could be proposed but no match with a library spectrum was possible and other possible candidates could not be excluded, CL3 was assigned. Within this study, only compounds which were assigned with CL3 or better in at least one of the investigated samples were reported.

#### 4.2.2.6 Semi-quantification approach

A similar approach as described in **chapter 4.1.2.7** was used for semi-quantification. A sub-selection of the reference standards included in the QC samples (**Table SI-4.2.1**) were used as calibrators to prepare calibration curves to be used for semi-quantification of the compounds identified through the described SSA approach (**chapter 4.2.2.5**). The calibrator used for semi-quantification of the corresponding suspect was selected aiming to have the highest possible similarity in structure and retention time between calibrator and suspect. The same approach was used to assign an IS to each of the calibrators. For each calibrator, a calibration curve was prepared covering eight calibration points with a concentration range of 0.01 to 2 ng/ $\mu$ L. To each calibration point, the same selection and concentration of IS as used for the dust samples were added. To account for possible matrix effects, the relative peak area (ratio peak areas calibrator/analyte and the IS) was used for semi-quantification of the corresponding suspect in the dust extract. To obtain the peak areas of calibrators and IS, the 'Find By Formula' algorithm with the settings described in **chapter 4.2.2.5** was used. Thereby, for each of the calibrators and IS only the more abundant adduct (thus,  $[M+H]^+$  or  $[M+Na]^+$ ) was considered as stable ratios of both adducts between calibrants and samples could not be guaranteed.

From the relative areas obtained for each calibration point, the response factor (corresponding to the slope of the calibration curve) was calculated. Through division of the relative area of the suspect of interest ( $A_{\text{Suspect}}/A_{\text{IS}}$ ) by the response factor ( $R_f$ ) of the assigned calibrant, the concentration of the suspect ( $c_{\text{Susp.}}$ ) in the corresponding dust extract was obtained as displayed in the following formula (Malm et al., 2021):

$$c_{\text{Susp.}} [\text{ng}/\mu\text{L}] = \frac{A_{\text{Suspect}}/A_{\text{IS}}}{R_f} \quad (4.1.1)$$

From this data, the concentration in the dust (in  $\mu\text{g}/\text{g}$ ) was calculated. For CECs, very low signal intensities were obtained for the IS in the MeOH fractions obtained through SPE (**chapter 4.2.2.3**) which suggested that most of the IS eluted in the previous (EtOAc) fraction. Therefore, semi-quantification of the analytes detected in the MeOH fraction was not possible as no suitable IS was available in that fraction.

#### 4.2.2.7 Statistical analysis

Semi-quantified concentrations (**chapter 4.2.2.6**) were compared applying a Mann-Whitney U Test between different sample categories after grouping based on housing type (private homes vs. public buildings), location of sample collection (urban vs. rural areas), age of the building (< 20 years vs. > 20 years) and time passed since last cleaning (< 5 days vs. > 5 days). Information for the latter two categories was only available for 32 and 34 of the 46 samples, respectively, so that parts of the dataset were not included in the statistical comparisons for these two categories.

The concentrations were compared only for compounds with a detection frequency (DF) of 50% or higher. As a similar distribution of values cannot be guaranteed in all sample groups, the described testing was based on the comparison of mean n ranks. A difference between groups was considered significant if the obtained (2-tailed) p-value was < 0.05. For each sample grouping, the obtained p-values, means, 25th, 50th and 75th percentiles are reported. All statistical testing was conducted using the SPSS software (version 28.0.0.0).

#### 4.2.2.8 Exposure assessment

From semi-quantified concentrations (**chapter 4.2.2.6**), human exposure was assessed based in the same approach and equation as described in **chapter 4.1.2.9**.

Then, the potential risk of non-carcinogenic effects (Hazard Quotient, HQ) per individual compound was calculated by dividing the EDI by the relative oral reference dose factor ( $RfD$ ,  $\text{mg}/\text{kg bw}/\text{d}$ ), if available. When the  $RfD$  was not available, such as the case for most semi-quantified compounds, the reference dose value of the calibrant used

for semi-quantification was chosen as the most suitable proxy. HQ values equal to or greater than 1 indicate a potential exposure risk for the target population.

## 4.2.3 Results and Discussion

### 4.2.3.1 Quality control and quality assurance results

Prior to any data processing and analysis, the QC results were investigated by assessing the peak areas obtained for the native compounds and IS in the QC samples and for the IS in the dust samples. These results are summarized in **Tables SI-4.2.2** (QC samples) and **SI-4.2.3** (dust samples), whereby in both cases a distinction was made between the EtOAc and MeOH fractions.

Except for 2,2-bis(chloromethyl)-1,3-propanediyl bis(bis(2-chloroethyl) phosphate) (V6; belonging to the class of OPFRs), all native QC compounds and IS were detected with a DF of 100% in the EtOAc fractions of the QC samples meeting the data extraction criteria listed in **chapter 4.2.2.5**. This indicates the suitability of the sample preparation approach for the included compound classes and the utilization of the same data processing settings for the dust samples. For both fractions, all observed average AMEs and RSDs of RTs were below 7 ppm and 0.4%, respectively, showing satisfying mass accuracy and chromatographic stability of the method. In the MeOH fraction of the QC samples, 45% (14 out of 31) of the native QC compounds were detectable with DFs ranging between 33 and 100% indicating that suspect analytes from similar compound classes as the QC compounds were more likely to be detected in the EtOAc fraction. Additionally, some QC compounds were detected in both fractions indicating an incomplete elution with EtOAc. However, in all these cases, the signal observed in the MeOH fraction was at least one order of magnitude lower compared to the EtOAc fraction, confirming that the latter fraction is expected to contain compounds structurally similar to the set of QC analytes.

In the EtOAc fraction of the dust samples (**Table SI-4.2.3**), all six IS were detected with DFs of 100% and stable RTs (RSDs < 0.2%) indicating no major analyte losses during sample preparation. Similar to the results obtained for the native QC compounds in the MeOH fractions, only one of the IS showed a DF of 100% within that fraction, suggesting that most IS eluted in the EtOAc fraction. Given the suspect screening approach of this chapter, which aimed at covering a broad range of potential analytes rather than ensuring optimal conditions for a limited number of compounds, a complete separation of all compounds between the two fractions was outside the scope of the study and the presented QC results were considered acceptable.

#### 4.2.3.2 Suspect screening results - identified compounds

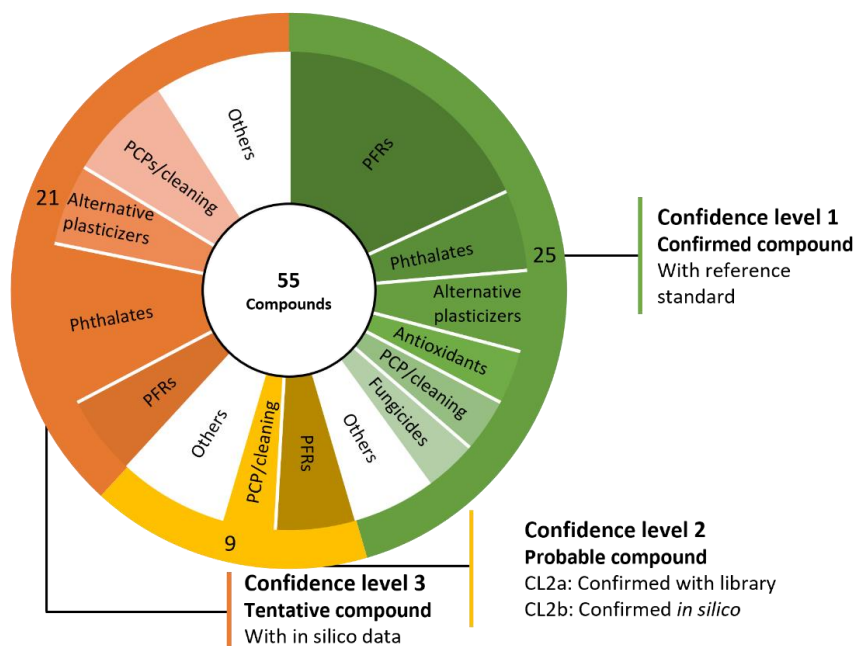


**Figure 4.2.1:** Compounds detected in the dust with confidence level 1-3 and the subcategories they belong to. With PFR: phosphate flame retardant; PCP: personal care products.

Based on the workflow described in **chapter 4.2.2.5**, a total of 55 compounds were identified (total of both, EtOAc and MeOH fractions), whereby only compounds identified with CL3 or better are reported here. CL1 or 2 were assigned if compounds could unequivocally be confirmed by matching all identifiers ( $m/z$ , RT, isotopic pattern, and fragmentation spectrum) to one of the QC standards (**Table SI-4.2.1**) or if the obtained fragmentation spectrum could be matched with library data allowing to assign only one possible candidate. Subsequently, based on the list of compounds assigned with CL2 or 3, 11 reference standards were purchased after the suspect screening analysis to confirm the most relevant suspects. Consequently, for eight compounds which were initially identified at CL2 or CL3, this allowed the assignment of CL1. For one compound, comparison with a reference standard improved the assigned CL from 3 to 2C resulting in the final summaries of identified compounds listed in **Tables 4.2.1** (CL1 and CL2,  $n = 34$ ) and **SI-4.2.4** (CL3,  $n = 21$ ). For only one compound, the comparison with the reference standard led to the identification of a false positive showing the reliability of the applied identification workflow. To each of the identified compounds, a compound class was assigned allowing the identification of the major contaminant classes as shown in **Figure 4.2.1**.

**Table 4.2.1:** Compounds identified with confidence level (CL) 1 and 2 in at least one of the indoor dust samples. CL2C represents a sub-division of the initial scheme of levels of identification confidence (Schymanski et al., 2014) which is explained in chapter 5. For each compound the detection frequency (DF) at a certain CL, the total DF and the fraction in which the compound was detected, is indicated. With PHs: phthalates, APs: alternative plasticizers, OPFRs: organophosphate flame retardant, AOX: synthetic antioxidants, PCPs: Personal care products, CPs: Cleaning products.

Name	Formula	DF (CL) [%]	DF <sub>total</sub> [%]	Class	Fraction
Diisodecyl phthalate (DIDP)	C <sub>28</sub> H <sub>26</sub> O <sub>4</sub>	97.8 (1)	97.8	PHs	EtOAc
Diethylhexyl phthalate (DEHP)	C <sub>24</sub> H <sub>38</sub> O <sub>4</sub>	91.3 (1)	91.3	PHs	EtOAc
Diisononylphthalate (DINP)	C <sub>26</sub> H <sub>42</sub> O <sub>4</sub>	100 (1)	100	PHs	EtOAc
Diethylhexyl adipate (DEHA)	C <sub>22</sub> H <sub>42</sub> O <sub>4</sub>	95.7 (1) 4.3 (2C)	100	APs	EtOAc
Acetyltributyl citrate (ATBC)	C <sub>20</sub> H <sub>34</sub> O <sub>8</sub>	100 (1)	100	APs	EtOAc
Tris(2-ethylhexyl) trimellitate (TOTM)	C <sub>33</sub> H <sub>54</sub> O <sub>6</sub>	2.2 (1) 97.8 (2C)	100	APs	EtOAc
2-Ethylhexyl diphenyl phosphate (EHDPHP)	C <sub>20</sub> H <sub>27</sub> O <sub>4</sub> P	84.8 (1) 10.9 (2C)	95.7	PFRs	EtOAc
Tri-p-tolyl phosphate (TPTP)	C <sub>21</sub> H <sub>21</sub> O <sub>4</sub> P	63.0 (1) 21.7 (2C)	84.8	PFRs	EtOAc
Tris(2-butoxyethyl) phosphate (TBOEP)	C <sub>18</sub> H <sub>39</sub> O <sub>7</sub> P	87.0 (1) 13.0 (2C)	100	PFRs	EtOAc
Triphenyl phosphate (TPHP)	C <sub>18</sub> H <sub>15</sub> O <sub>4</sub> P	87.0 (1) 13.0 (2C)	100	PFRs	EtOAc
Tris(1-chloro-2-propyl) phosphate (TCIPP)	C <sub>9</sub> H <sub>18</sub> Cl <sub>3</sub> O <sub>4</sub> P	65.2 (1) 28.3 (2C)	93.5	PFRs	EtOAc
Tris(1,3-dichloro-2-Propyl)phosphate (TDCIPP)	C <sub>9</sub> H <sub>15</sub> Cl <sub>6</sub> O <sub>4</sub> P	2.2 (1) 10.9 (2C)	13.1	PFRs	EtOAc
Tris(2-chloroethyl) phosphate (TCEP)	C <sub>6</sub> H <sub>12</sub> Cl <sub>3</sub> O <sub>4</sub> P	8.7 (1) 80.4 (2C)	89.1	PFRs	EtOAc
Tris(2-ethylhexyl) phosphate (TEHP)	C <sub>24</sub> H <sub>51</sub> O <sub>4</sub> P	17.4 (1) 69.6 (2C)	87.0	PFRs	EtOAc
Resorcinol bis(diphenyl phosphate) (RDP)	C <sub>30</sub> H <sub>24</sub> O <sub>8</sub> P <sub>2</sub>	2.2 (1) 89.1 (2C)	91.3	PFRs	EtOAc
Bisphenol A bis(diphenyl phosphate) (BDP)	C <sub>39</sub> H <sub>34</sub> O <sub>8</sub> P <sub>2</sub>	10.9 (1) 73.9 (2C)	84.8	PFRs	EtOAc
Diphenylcresyl phosphate (CDPHP)	C <sub>19</sub> H <sub>17</sub> O <sub>4</sub> P	89.1 (2C)	89.1	PFRs	EtOAc
Tributylphosphate (TBP)	C <sub>12</sub> H <sub>27</sub> O <sub>4</sub> P	52.2 (2C)	52.2	PFRs	EtOAc
Bis(2,4-di-tert-butylphenyl)penta-	C <sub>33</sub> H <sub>50</sub> O <sub>8</sub> P <sub>2</sub>	23.9 (2) 65.2 (4)	89.1	PFRs	EtOAc

erythritol diphosphate (BDTPDP)					
N,N'-hexamethylene bis (3,5-di-t-butyl-4-hydroxy-hydrocinnam-amide) (AO1098)	C <sub>40</sub> H <sub>64</sub> N <sub>2</sub> O <sub>4</sub>	2.2 (1) 26.0 (2C)	28.2	AOX	MeOH
N-1,3-dimethylbutyl-N-phenyl-p-phenylenediamine (6PPD)*	C <sub>18</sub> H <sub>24</sub> N <sub>2</sub>	45.7 (1) 17.4 (2C)	63.1	AOX	EtOAc
N-(2-ethoxyphenyl)-N-(2-ethylphenyl) oxamide*	C <sub>18</sub> H <sub>20</sub> N <sub>2</sub> O <sub>3</sub>	10.9 (1) 21.7 (2C)	32.6	UV filters	EtOAc
Bemotrizinol*	C <sub>38</sub> H <sub>49</sub> N <sub>3</sub> O <sub>5</sub>	4.3 (1) 6.6 (2C)	10.9	UV filters	MeOH
Octabenzene*	C <sub>21</sub> H <sub>26</sub> O <sub>3</sub>	4.3 (1) 45.7 (2C)	50.0	PCPs/ CPs	MeOH
Diethyltoluamide (DEET)*	C <sub>12</sub> H <sub>17</sub> NO	23.9 (1) 54.3 (2C)	78.2	PCPs/bio- cide	MeOH
Bumetrizole <sup>1</sup>	C <sub>17</sub> H <sub>18</sub> ClN <sub>3</sub> O	34.8 (2C)	34.8	UV filters	EtOAc
Carbendazim*	C <sub>9</sub> H <sub>9</sub> N <sub>3</sub> O <sub>2</sub>	10.9 (1) 54.3 (2C)	65.2	Fungicides	MeOH
Propiconazole*	C <sub>15</sub> H <sub>17</sub> Cl <sub>2</sub> N <sub>3</sub> O <sub>2</sub>	10.9 (1) 65.2 (2C)	76.1	Fungicides	EtOAc
Triphenylphosphine oxide*	C <sub>18</sub> H <sub>15</sub> OP	37.0 (1) 58.7 (2C)	95.7	Other	MeOH
Paracetamol	C <sub>8</sub> H <sub>9</sub> NO <sub>2</sub>	10.9 (2A)	10.9	Pharma- ceuticals	EtOAc
N,N-bis(2-hydroxyethyl)-dodecanamide	C <sub>16</sub> H <sub>33</sub> NO <sub>3</sub>	82.6 (2A) 15.2 (4)	97.8	PCPs	MeOH
1,3-diphenylguanidine	C <sub>13</sub> H <sub>13</sub> N <sub>3</sub>	80.4 (2A) 17.4 (4)	97.8	Other	MeOH
1,3-di-o-tolylguanidine	C <sub>15</sub> H <sub>17</sub> N <sub>3</sub>	2.2 (2A) 30.4 (4)	32.6	Other	MeOH
Triethylene glycol bis(2-ethylhexanoate)	C <sub>22</sub> H <sub>42</sub> O <sub>6</sub>	71.7 (2A) 23.9 (4)	95.6	Other	EtOAc

Most identified compounds belonged to the OPFRs, with 13 compounds assigned with CL1 or 2, and 3 compounds assigned with CL3. In total, ten OPFRs were unequivocally confirmed with a reference standard by matching all identifiers and thus resulting in CL1. Except for tris(1,3-dichloro-2-propyl)phosphate, all PFRs identified with CL1 showed DFs > 80%. Three OPFRs, [4-[2-(4-diphenoxy-phosphoryloxyphenyl)-propan-2-yl]phenyl] diphenyl phosphate, diphenylcresyl phosphate and tributyl phosphate, were detected with a DF of 84.8%, 89.1% and 52.2%, respectively, and were assigned with CL2C as no fragmentation spectra could be obtained. These findings of known PFRs in indoor dust at high DFs confirm their ubiquitous occurrence in the indoor environment which was

reported and quantified in numerous previous studies from Europe, the US and Asian countries (Esplugas et al., 2022; Hoang et al., 2023; Lee et al., 2020; Tang et al., 2020; Xu et al., 2016; Zhou et al., 2017a).

Besides these well studied PFRs, three novel compounds were identified. As first, bis(2,4-di-tert-butylphenyl)pentaerythritol diphosphate (BDTPDP) was detected with CL2 and a DF of 89.1%. This novel PFR was first reported by Liu and Mabury in indoor dust from Toronto (Canada) (Liu and Mabury, 2019), who suggested that its occurrence in indoor dust originates from the oxidation of the antioxidant (AOX) bis(2,4-di-tert-butylphenyl) pentaerythritol diphosphite (AO626). This finding identified organophosphate antioxidants as a potential source of PFR contamination in dust. Wang et al. confirmed the occurrence of BDTPDP in dust collected from North China and provided a reference MS/MS spectrum for this compound which was matched with the data obtained in this study, allowing the assignment of CL2 and confirming the occurrence of this novel PFR also in European indoor environments (Wang et al., 2020a).

Furthermore, two novel PFRs were identified for the first time in indoor dust. These included didecyl butoxyethoxyethyl phosphate (DDeBEEP) and bis(butoxyethyl) butyl phosphate (BBEBP) which were detected with DFs of 4.4% and 45.7%, respectively. The fragmentation spectra obtained for DDeBEEP (**Figure 4.2.2**) partially matched spectra reported by Wang et al. for compounds carrying a butoxyethoxyethyl moiety (Wang et al., 2020a).

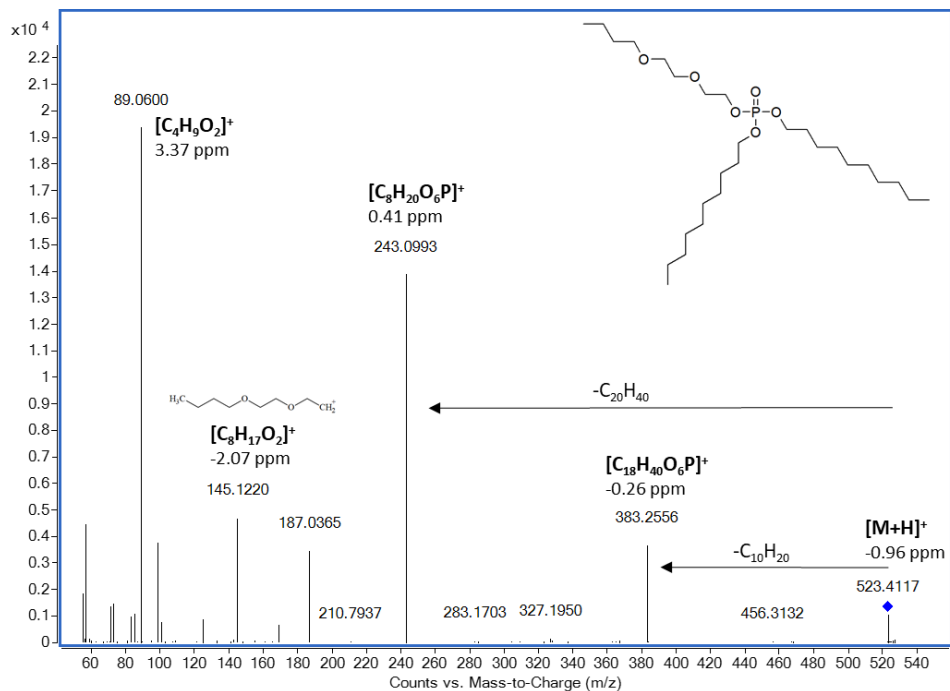


**Figure 4.2.2:** Example of a fragmentation spectrum obtained for didecyl butoxyethoxyethyl phosphate (DDeBEEP) at a collision energy of 20 eV. The proposed formula and the main neutral losses and fragments are indicated.

Additionally, neutral losses corresponding to the loss of one and two hydrocarbon side chains with ten carbons were observed. Lastly, a fragment confirming the presence of a phosphate group was observed ([H<sub>4</sub>PO<sub>4</sub>]<sup>+</sup>; theoretical *m/z* 98.9842). Based on the available data, it could not be unequivocally determined whether the hydrocarbon side chains are branched or linear. This, combined with the absence of reference spectra, led to the assignment of DDeBEEP at CL3 (**Table SI-4.2.4**).

The fragmentation spectrum obtained for BBEP (**Figure 4.2.3**) partially matched with the reference spectrum obtained for TBOEP confirming both the presence of a phosphate group and at least one butoxyethyl moiety. Again, observed neutral losses indicated the presence of a butyl and two butoxyethoxy substituents leading to the proposal of the structure indicated in **Figure 4.2.3** at CL3.

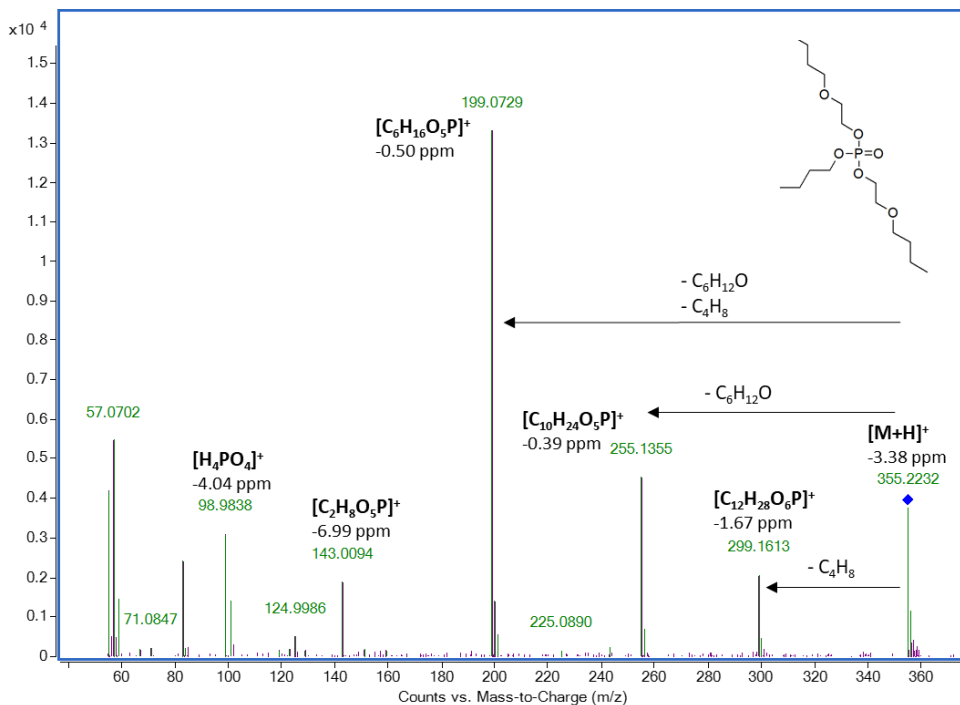


**Figure 4.2.3:** Example of a fragmentation spectrum obtained for bis(butoxyethyl) butyl phosphate (BBEPP) at a collision energy of 10 eV. The proposed formula and the main neutral losses and fragments are indicated.

The second largest group of identified compounds were plastic additives, including PHs and APs. Three and six phthalates were assigned with CL1 and CL3, respectively. DEHP, DIDP and DINP were all assigned with CL1 through matching with a reference standard and were all detected with a DF > 90%. These results are in line with previous studies which identified these phthalates as the major phthalate homologues worldwide (Bu et al., 2020; Zhu et al., 2023). Likewise for the novel PFRs, the described suspect screening approach allowed the identification of the novel phthalate homologue decyl nonyl phthalate (DeNoP) detected with a DF of 93.5%. **Figure 4.2.4** shows an example of a fragmentation spectrum obtained for DeNoP in one of the dust samples.

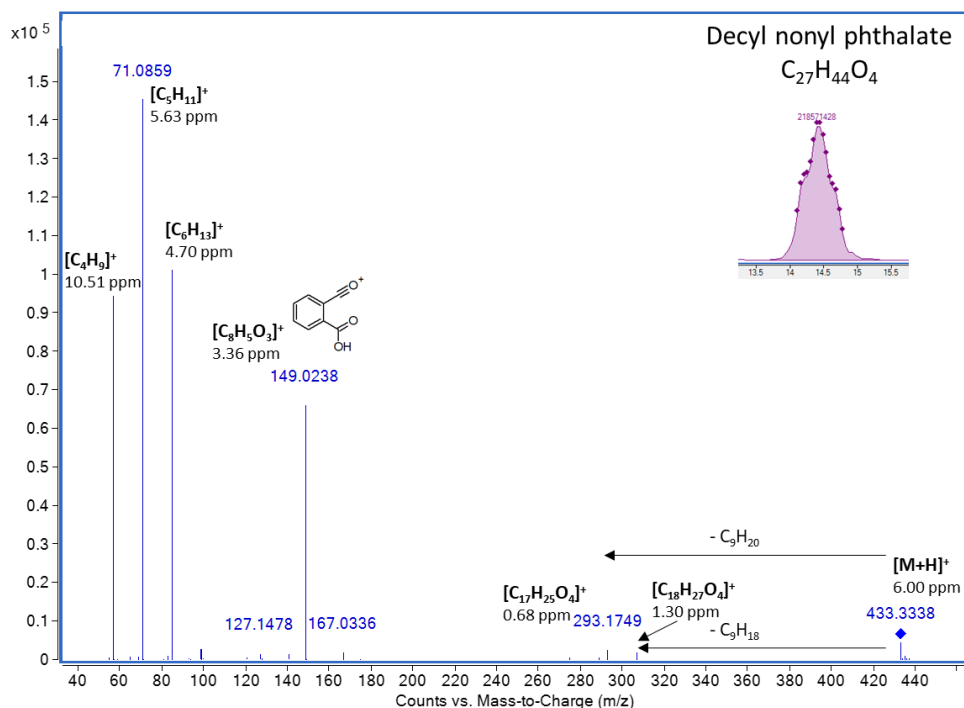


**Figure 4.2.4:** Example of a fragmentation spectrum obtained for decyl nonyl phthalate (DeNoP) in one of the indoor dust samples at a collision energy of 10 eV. The proposed formula and the main neutral losses and fragments are indicated.

The different and partially uneven numbered substituents were proposed based on the observation of neutral losses corresponding to hydrocarbon side chains with nine and ten carbon atoms. Thereby, the observed wide peak (**Figure 4.2.4**) suggested the coelution of numerous isomers indicating branched side chains. The phthalate backbone was confirmed through the characteristic fragment for phthalate esters with a (theoretical)  $m/z$  value of 149.0233 (Jeilani et al., 2011). A reference standard was purchased whereby decyl nonyl phthalate was available with linear side chains (CAS 96507-76-5). Between the linear reference standard and the (assumably) branched DeNoP detected in the samples, a RT difference of 1.05 min was observed which is assumed to be caused by the very slow increase in the percentage of the stronger (organic) eluent within the applied gradient (**chapter 4.2.2.4**) allowing a separation between branched and linear compounds. Nevertheless, clear similarities were observed between the fragmentation spectra obtained in the dust samples and the reference standards (**Figure 4.2.4/SI-4.2.1**).

A previous study reported compounds with the same molecular formula as DeNoP (C<sub>27</sub>H<sub>44</sub>O<sub>4</sub>) in indoor dust samples to which phthalate esters were assigned (Christia et al., 2021b). However, no further experimental evidence was provided hampering a more confident compound identification. The results presented here allow a more in-depth characterization of a potentially novel and highly abundant phthalate

(**chapter 4.2.3.4**). Following a similar approach as described for DeNoP, two more phthalates with different and partially uneven numbered substituents were identified. These included decyl undecyl (DeUnP) and undecyl dodecyl phthalate (UnDoP), detected with DFs of 82.6% and 4.3%, respectively, at CL3. Similar to DeNoP, the lengths of the side chains were confirmed through the observation of corresponding neutral losses in both cases (**Figure SI-4.2.2 and SI-4.2.3**) while the phthalate backbone was confirmed through the characteristic fragment with  $m/z$  149.0233.

Lastly, dioctyl phthalate (DOP) was detected with a DF of 56.5%. Again, the phthalate backbone was confirmed through the fragment with  $m/z$  149.0233 (thereby excluding a trimellitate as potential candidate structure) and no fragments suggesting side chains with different numbers of carbons were observed. The compound assigned as dioctyl phthalate (RT = 13.2 min) eluted 0.7 min later than DEHP (RT = 13.2 min) suggesting linear side chains leading to higher retention. However, this observation was not considered sufficient to exclude all possible branched isomers leading to the assignment of CL3.

The reported PHs show a high structural variability of PH homologues present in dust. This is of high concern indication potential human exposure to mixtures of homologues, especially considering the high signal abundances observed for several of the PHs (**chapter 4.2.3.4**). However, the available mass spectrometric data did not allow to reach an identification confidence level better than 3 and the annotation of the phthalate backbone was based solely on the observation of one characteristic fragment. This indicates a need of additional identifiers to confirm compound annotation. These can be obtained through calculation of DTIM derived  $^{DT}CCS_{N_2}$  values which is discussed in **chapter 4.2.3.3**.

Apart from the described phthalate plasticizers, three known alternative plasticizers, (DEHA, acetyltributyl citrate and tris(2-ethylhexyl) trimellitate) were detected with CL1 and a DF of 100% indicating the simultaneous occurrence of legacy phthalate and alternative plastic additives. Three additional adipate homologues were identified at CL3 (**Table SI-4.2.4**). There, an adipate backbone was assigned based on the observation of characteristic fragments which matched the reference spectrum obtained for DEHA included in the QC samples. The assigned possible side chains should be interpreted cautiously as they could not unequivocally be confirmed through the available fragmentation data.

After a first data analysis cycle, a sub selection of compounds identified at CL3 was made for which reference standards were purchased to increase identification confidence and provide an alternative approach for semi-quantification (**chapter 4.2.3.4**). This allowed to assign eight additional compounds with CL1 (marked with an \* in **Table 4.2.1**). For example, these included the three biocides, diethyltoluamide (DEET), carbendazim and propiconazole, all of which were detected with DFs > 60% and have already been described in previous indoor dust studies (Béranger et al., 2019; Ouyang et

al., 2017; Rostkowski et al., 2019). Furthermore, three UV filters have been assigned with CL1/2C, some of which have also been introduced in previous studies on indoor dust (Carpinteiro et al., 2010). Similarly, a recent study characterized the worldwide occurrence of 1,3-diphenylguanidine and 1,3-di-o-tolylguanidine in indoor dust based on a sample set collected in 11 countries (Li and Kannan, 2023). Both compounds were also detected in the present study, covering an additional geographical location as the abovementioned study did not include samples from Belgium and the only European datapoints derived from Greece and Romania. These findings confirm the occurrence of the mentioned compound classes in the indoor environment and provide an extra datapoint for the estimation of the geographical range of their occurrence.

Further, three antistatic agents were detected (N,N-bis(2-hydroxyethyl)-dodecanamide (CL2), N,N-bis(2-hydroxyethyl) oleamide and N-(2-hydroxyethyl) octadecanamide (both CL3) all of which carried at least one hydroxyethyl moiety (confirmed through the observation of both a characteristic neutral loss and fragment). These compounds thus only differed by the length of and presence of double bonds in the conjugated fatty acid chain. Even though the applied identification workflow cannot unequivocally exclude the presence of branched side chains or determine the position of the double bond assumed in some of the reported compounds, these results confirm high structural variabilities in classes of CECs. Additionally, one of the assigned antistatics (N,N-bis(2-hydroxyethyl)oleamide) is a potential source for the detected oleamide (CL3; DF 21.8%) which might be formed as a degradation product.

Lastly, two synthetic antioxidants (AOX) were identified at CL1 through matching with reference standards. These included N,N'-hexamethylene bis (3,5-di-t-butyl-4-hydroxy-hydrocinnam-amide) (AO 1098), which was detected with a total DF of 28.2%. The observed DF is in agreement with a previous report of AO 1098 in indoor dust samples collected in Toronto, Canada (DF = 33%) (Liu and Mabury, 2020). The other AOX was N-1,3-dimethylbutyl-N-phenyl-p-phenylenediamine (6PPD) showing a total DF of 63.1%. Again, this is in line with a previous study which reported 6PPD in South-Chinese houses near an E-waste dismantling site (DF = 56%) (Huang et al., 2021). In this Chinese location, the main transformation product of 6PPD, 6PPD-Quinone, was detected in 6 of the 18 houses, which was not confirmed here.

#### 4.2.3.3 $^{DT}CCS_{N_2}$ values as additional identification parameter for suspect CECs

To obtain an additional identification parameter through calculation of  $^{DT}CCS_{N_2}$  values, EtOAc fractions were analysed in IM-MS mode as described in **chapter 4.2.2.4**. For compounds assigned at CL1, experimental  $^{DT}CCS_{N_2}$  values were compared with the reference database reported in **chapter 3.1**. Observed percent errors ranged between -1.51 % and 0.98 % with an average absolute percent error of 0.44 %. Interestingly, DIDP

showed the two highest percent errors (-1.51 % and 0.98 % for proton and sodium adduct, respectively). This PH is assumed to be present as a technical mixture of several isomers with numerous possible branches in the hydrocarbon side chains. This can have an influence on the gaseous shape of the ion and ultimately on its  $^{DT}CCS_{N_2}$  value resulting in the observed deviations. For all other compounds, absolute percent errors were  $< 1\%$  indicating a good intra-laboratory matrix independent reproducibility of  $^{DT}CCS_{N_2}$  calculations.

For suspect compounds (CL3), the main focus was laid on adding identification confidence to phthalate annotations since for this class an extensive homologue series with partially high abundances was observed (**chapter 4.2.3.1**).  $^{DT}CCS_{N_2}$  values obtained for PHs are summarized in **Table 4.2.2**, while data for the other compounds from the EtOAc fraction is given in **Table SI-4.2.5**.

**Table 4.2.2:**  $^{DT}CCS_{N_2}$  values obtained for all suspect compounds detected in the EtOAc fraction. Additional identifiers and confidence levels of each compounds are summarized in **Tables 4.2.1** and **SI-4.2.4**. The reported average  $^{DT}CCS_{N_2}$  values are based on the indicated number of samples (n). For each data point, the (relative) standard deviation is given (SD/RSD). If reference  $^{DT}CCS_{N_2}$  values were available (**chapter 3.1**), experimental average  $^{DT}CCS_{N_2}$  values were compared through calculation of percent deviations between the two datapoints [ $\Delta CCS$ ].

Name	DF total [%]	Class	$\bar{x}^{DT}CCS_{N_2}$ [ $\text{\AA}^2$ ]	STDEV [ $\text{\AA}^2$ ]	RSD [%]	n	$\Delta CCS$ [%]
Diisodecyl phthalate (DIDP)	97.8	PHs	[M+H] <sup>+</sup> : 224.42 [M+Na] <sup>+</sup> : 228.63	2.59 1.24	1.15 0.54	45	-1.51 0.98
Diethylhexyl phthalate (DEHP)	91.3	PHs	[M+H] <sup>+</sup> : 211.60 [M+Na] <sup>+</sup> : 217.34	0.47 0.74	0.22 0.34	42	0.28 0.93
Diisononylphthalate (DINP)	100	PHs	[M+H] <sup>+</sup> : 220.71 [M+Na] <sup>+</sup> : 222.77	1.50 0.96	0.68 0.43	46	0.05 0.83
Decyl nonyl phthalate (DeNoP)	93.5	PHs	[M+H] <sup>+</sup> : 224.71 [M+Na] <sup>+</sup> : 224.97	0.57 0.96	0.25 0.43	43	n.a.
Diheptyl phthalate (DHP)	89.2	PHs	[M+H] <sup>+</sup> : 207.72 [M+Na] <sup>+</sup> : 210.25	0.55 0.57	0.26 0.27	41	n.a.
Diocetyl phthalate (DOP)	56.5	PHs	[M+H] <sup>+</sup> : 215.03 [M+Na] <sup>+</sup> : 216.43	0.59 1.00	0.28 0.46	26	n.a.
Diundecyl phthalate (DiUnP)	45.6	PHs	[M+H] <sup>+</sup> : 234.37 [M+Na] <sup>+</sup> : 232.16	0.62 0.83	0.26 0.36	21	n.a.
Undecyl dodecyl phthalate (UnDoP)	4.3	PHs	[M+H] <sup>+</sup> : 238.00 [M+Na] <sup>+</sup> : 236.30	n.a. n.a.	n.a. n.a.	2	n.a.
Decyl undecyl phthalate (DeUnP)	78.3	PHs	[M+H] <sup>+</sup> : 231.34 [M+Na] <sup>+</sup> : 229.86	0.78 0.94	0.34 0.41	36	n.a.

$^{DT}CCS_{N_2}$  values of PHs were plotted as a function of corresponding  $m/z$  ratios (**Figure 4.2.5**). For the four phthalates for which reference standards were available (DEHP, DINP, DIDP, DPP), the reference  $^{DT}CCS_{N_2}$  values reported in **chapter 3.1** were used.

For suspect phthalates assigned at CL3, the obtained average  $^{DT}CCS_{N2}$  values (**Table 4.2.2**) were plotted. All data points were well described applying a power model leading to a correlation coefficient of  $R^2 = 0.9200$ . When only one of the two adducts was included in the regression modelling, correlation coefficients further improved. For example, for proton adducts (blue trendline in **Figure 4.2.5**), a correlation coefficient of  $R^2 = 0.9883$  was calculated. The observed correlations serve as an additional confirmation of the assignment of all included compounds to the class of phthalates. For comparison purposes, the reference  $^{DT}CCS_{N2}$  value available for diphenyl phthalate ( $[M+Na]^+$  adducts) was added to **Figure 4.2.5** clearly indicating a trend towards  $^{DT}CCS_{N2}$  value caused by the more compact aromatic substituents.

Examined in more detail, the positioning of  $^{DT}CCS_{N2}$  values of single suspect compounds along the  $m/z$ -CCS trendline clearly corresponded to the side chain lengths assigned. For example,  $^{DT}CCS_{N2}$  values obtained for the proton and sodium adducts of DeNoP ( $C_9$ - $C_{10}$  side chains), represented by green dots in **Figure 4.2.5**, cluster between the datapoints of reference  $^{DT}CCS_{N2}$  values of DINP and DIDP with  $C_9$ - $C_9$  and  $C_{10}$ - $C_{10}$  side chains, respectively. Overall,  $^{DT}CCS_{N2}$  values increased with increasing length of assigned side chains resulting in the highest values calculated for UnDoP. Furthermore, in **chapter 3.1**, a characteristic observation was described for  $^{DT}CCS_{N2}$  values of PHs with longer side chains ( $C_9$  and higher). In contrast to most other investigated CECs for which  $^{DT}CCS_{N2}$  values increased with increasing  $m/z$  ratios, this trend was not reproduced by the data obtained for proton and sodium adducts of PHs. For the  $[M+Na]^+$  adducts (with higher  $m/z$  ratios than proton adducts)  $^{DT}CCS_{N2}$  values with similar or even lower values than corresponding datapoints of  $[M+H]^+$  adducts were observed. This trend was reproduced by all suspect PHs with side chain lengths higher than  $C_9$  suggesting more compact ion gaseous structures for these adducts.

Interestingly, the experimental  $^{DT}CCS_{N2}$  value obtained for the proton adduct of DOP, for which linear side chains were assumed, was 1.9 % higher than the values obtained for (the isomer) DEHP. This can be viewed as a confirmation of the less compact linear side chains proposed for DOP. This difference was less prone for sodium adducts ( $\Delta CCS$ : 0.5 %) which is assumed to be caused by the more compact ion structures described for sodium adducts above.

The described observations confirm the assignments of suspect phthalates described in **chapter 4.2.3.2**, showing additional identifiers provided by IM-MS. It has to be noted that the current schemes of identification confidence reporting do not allow to fully reflect the additional identification information provided by IM-MS. Despite the conclusions described here, suspect phthalates still have to be assigned CL3 (Celma et al., 2020) since the presence of different (branched) side chains cannot be excluded.

Therefore, a detailed communication of all data leading to the assignment of CLs should be included and considered for the interpretation of the CLs.

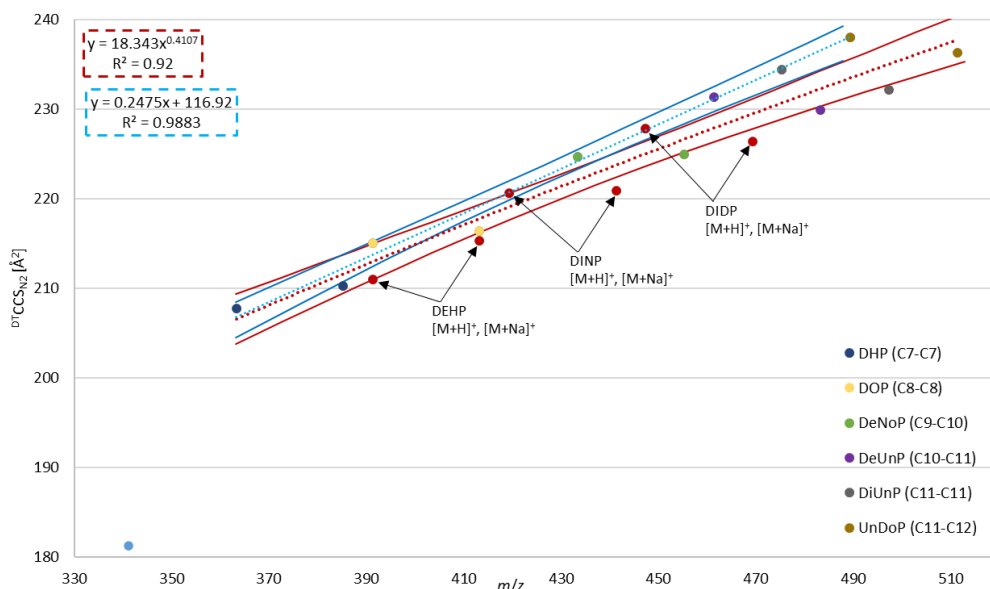


**Figure 4.2.5:**  ${}^{\text{DTCCSN}}_2$  values of reference and suspect phthalates as a function of corresponding  $m/z$  ratios. The red dotted trendline describes the correlation (based on a power model) for the complete dataset (excluding diphenyl phthalate) while for the blue dotted line only proton adducts were included. 95% confidence intervals are given for both trendlines in the corresponding colour. For diphenyl phthalate, the  ${}^{\text{DTCCSN}}_2$  value of the sodium adduct is included while for all other compounds both proton and sodium adduct, are plotted. Proton and sodium adducts can be distinguished based on the difference in  $m/z$  ratio. DEHP: Di(2-ethylhexyl) phthalate; DINP: Diisononyl phthalate; DIDP: Diisodecyl phthalate; DHP: Diheptyl phthalate; DOP: Dioctyl phthalate; DeNoP: Decyl nonyl phthalate; DeUnP: Decyl undecyl phthalate; DiUnP: Diundecyl phthalate; UnDoP: Undecyl dodecyl phthalate.

#### 4.2.3.4 Semi-quantification results

Suspect compounds identified with the SSA in the EtOAc fraction were semi-quantified using the available reference standards listed in **Table SI-4.2.1**. As described in **chapter 4.2.2.6**, the semi-quantification was based on the response factors obtained from the relative areas between calibrators and assigned IS. The same IS and (most abundant) adduct were considered for both, quantified suspect and corresponding calibrator. This resulted in the minimum, maximum and median concentrations listed in **Table SI-4.2.6** whereby the latter was calculated applying the lower bound approach, thus assigning a concentration of zero for samples in which a compound was not detected. **Figure 4.2.6** shows the boxplots summarizing the semi-quantified concentrations for the PHs and OPFRs. All other compounds are summarized in **Figure SI-4.2.4**. In both cases, the boxplots include all compounds with a DF  $\geq$  45% and exclude

datapoints corresponding to non-detects. For the interpretation of these semi-quantitative data, a few limitations have to be considered as discussed in **chapter 4.1.3.1**. Additionally, even though a maximum similarity in RT of IS and calibrant/suspect was sought after, a difference in RT and the fact that the calibration curves were prepared in solvent, do not allow an optimal compensation for possible matrix effects. Lastly, an extrapolation of the calibration curve was necessary to cover the high phthalate concentration observed in some samples. Nevertheless, the reported semi-quantitative data can serve as a tool for a general estimation of dust concentrations, prioritization of compounds for future (targeted) studies and estimation of human exposure (**chapter 4.2.3.6**).

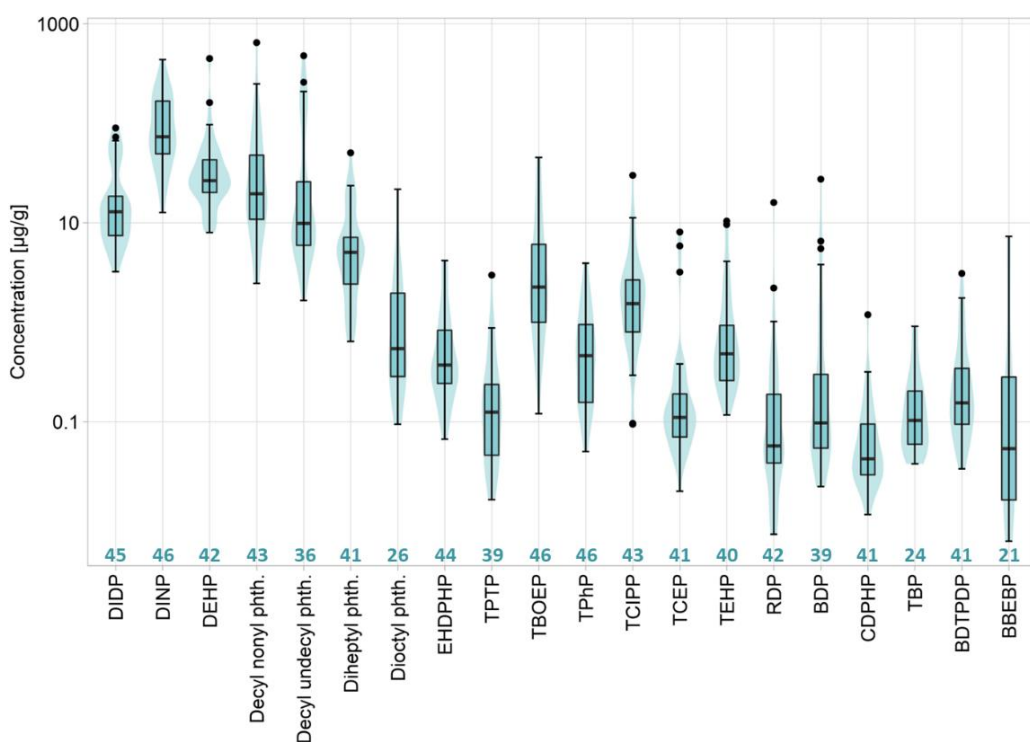


**Figure 4.2.6:** Violin plots and boxplots representing the semi-quantified concentrations obtained for phthalates and organophosphate flame retardants detected with a detection frequency  $\geq 50\%$ . The presented plots only include datapoints for which a concentration was obtained, thus excluding non-detects. Therefore, for each boxplot/compound the underlying number of datapoints (n) is indicated below the plot. The full names corresponding to each of the abbreviations can be found in **Table 4.2.1** and **Table SI-4.2.4**.

The median and maximum concentrations observed for phthalates ranged between n.d. - 73  $\mu\text{g/g}$  and 31 - 646  $\mu\text{g/g}$ , respectively, and showed a generally higher concentration range than observed for OPFRs (**Figure 4.2.6**). Interestingly, high concentrations of one particular phthalate in a sample were often accompanied by at least one other phthalate showing high concentrations in the same sample. For example,

the sample with the overall maximum concentration of DINP (437 µg/g) also showed the overall maximum concentration of DeNoP (646 µg/g) and the third highest concentrations of DIDP (67 µg/g) and DEHP (96.8 µg/g). This indicates a potential exposure to a mixture of these compounds. Also, the semi-quantified concentrations obtained for the newly identified phthalates with differing substituents such as DeNoP were in the same order of magnitude as the values observed for the legacy phthalates such as DINP and DEHP. This points out the relevance of the newly identified phthalates and suggests that targeted methods in which these phthalates are not included, may underestimate phthalate concentrations and consequently the human exposure to these compounds.

Median and maximum concentrations observed for PFRs ranged between n.d. - 2 µg/g and 1 - 51 µg/g, respectively. Similar to the observations described for phthalates, several samples showed a simultaneous occurrence of various PFRs at higher concentrations. Again, the newly identified PFRs (BDTPDP and BBEBP) showed concentrations comparable to the data obtained for some of the targeted PFR homologues.

In the EtOAc fraction, five compounds were confirmed after purchase of reference standards (**Table 4.2.1**). Therefore, for these compounds, two different quantification approaches using two different calibrators were possible. On the one hand, these compounds were quantified using the calibrators derived from the reference standards included in the QC samples (**Table SI-4.2.6**). On the other hand, calibration curves of the newly purchased standards were prepared in the same calibration ranges. For both approaches, the same IS was used. This allowed to estimate the influence of using a structurally less similar calibrator for quantification and compare these concentrations with the results obtained using a reference standard of the corresponding compound as calibrator. **Table SI-4.2.7** summarizes the minimum, maximum and median concentrations obtained using the two approaches. As described in **chapter 4.2.2.6**, the suspect's concentration is derived by the division of the suspect's (relative) signal through the response factor of the used calibrator. Therefore, the differences in quantified concentrations observed for the two approaches are proportional to the differences in the response factors of the two possible calibrants. Thereby, the response factors differed by a factor of up to 9 between the two approaches, resulting in proportional differences in semi-quantified concentrations. This indicates the high importance of similar response factors between suspect and calibrator in case no reference standard is available. Thereby, an optimal selection of calibrator can be addressed by simulative tools predicting response factors for identified suspect facilitating the selection of suitable calibrators (Malm et al., 2021).

#### 4.2.3.5 Statistical comparison

Obtained semi-quantified concentrations were compared between sample groups whereby latter were based on the type of sampled housing, the housing location, the age of the building and the time passed since the last cleaning. The obtained *p*-values and means are summarized in **Table SI-4.2.8 to SI-4.2.11** whereby the most significant differences were observed between public buildings and homes. Out of 26 compounds for which data were compared, 16 showed significantly higher ( $p < 0.05$ ) concentrations in public buildings compared to homes. These included, among others, all phthalates with a DF > 50% except for DEHP. Propiconazole was the only compound showing significantly higher concentrations in homes. These results suggest a generally higher CEC contamination in public spaces which might be caused by a higher number and variety of contamination sources. For several contaminants, significant differences were observed between rural and urban locations whereby the latter showed significantly higher concentrations in all cases. For the remaining groupings (age and time passed since the last cleaning) the number of significant differences was low, not allowing the characterization of a clear trend in the quantified concentrations.

#### 4.2.3.6 Risk assessment based on semi-quantified concentrations

The EDIs and HQs calculated from the semi-quantified concentrations are summarized in **Table SI-4.2.12**. The HQs calculated for semi-quantified suspect compounds should be interpreted with care since for those no *RfD* values were available and the *RfD* value of the calibrant used for semi-quantification was applied. For none of the compounds, HQs were > 1. As an example, **Figure 4.2.7** summarises the data obtained for PFRs for datapoints representing samples collected in private homes considering the 95<sup>th</sup> percentile exposure scenario. There, only *RfD* values which can directly be assigned to the semi-quantified compound are shown thus excluding reference values for suspect compounds for which no *RfD* value was available and estimations based on the *RfD* values of the calibrant had to be made.

### EDI PFRs - 95th% - Home

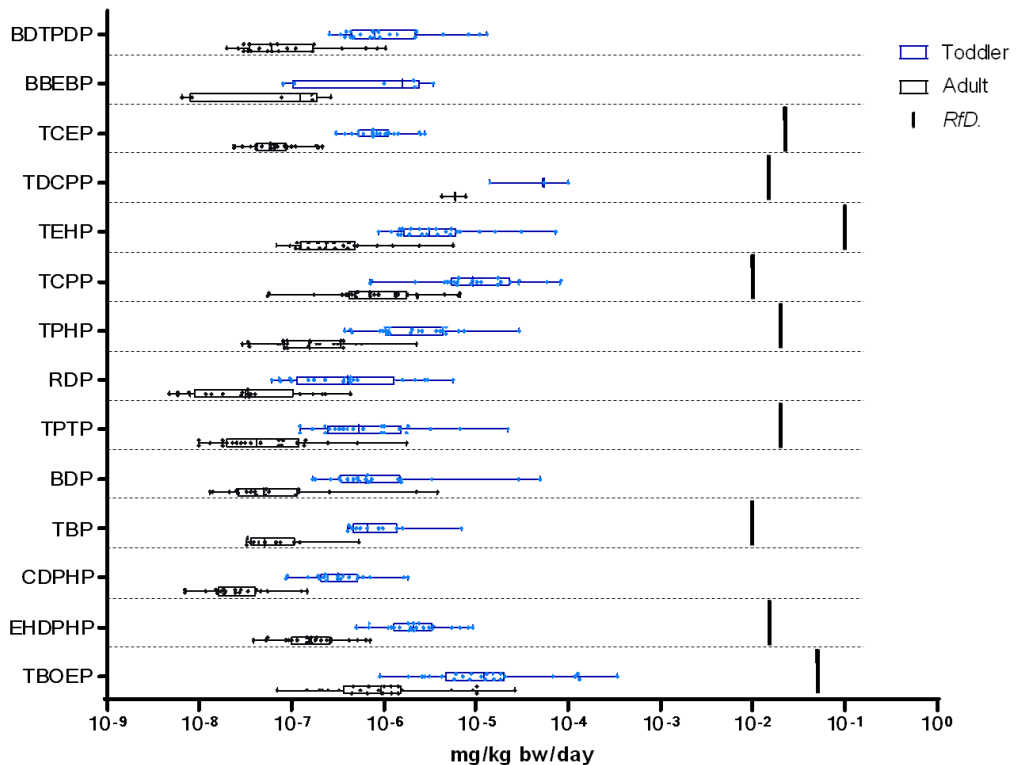


**Figure 4.2.7:** Boxplots of Estimated Daily Intakes (EDIs) obtained from the semi-quantified concentrations of organophosphate flame retardants (PFRs) for samples collected in private homes. For the calculation of EDIs, the 95<sup>th</sup> percentile exposure scenario was considered. Obtained EDIs were compared with reference dose values (*RfD*) indicated with a black line and obtained for the corresponding compound from the literature sources listed in **Table SI-4.2.12**. If no *RfD* is indicated, no datapoint for the corresponding semi-quantified compound was available.

Overall, EDIs of PFRs ranged from 1.1E-09 to 1.2E-05 mg/kg bw/day, with corresponding HQs between 2.2E-08 and 9.2 E-04. The EDIs (mg/kg bw/day) of PFRs (TBOEP, TPHP, TEHP, TCIPP, and TCEP) that can be compared with other studies from different regions and/or countries in Europe ranged from 2.0E-08 to 5.7E-05 for adults and from 1.1E-07 to 5.0E-05 for children, respectively. This indicated that EDIs of the selected PFRs in Flemish dust were within comparable ranges as reported for other European countries (Dou and Wang, 2023). However, compared to EDIs of children from studies in China and other Asian regions, median EDIs of TEHP and TCIPP in Flemish residential dust (7.80E-08 and 2.38E-07 mg/kg bw/day, respectively) are still within the range of 4.0E-08 to 2.1E-06 and 4.0E-08 to 7.8E-06 mg/kg bw/day, respectively (Dou and Wang, 2023). Thereby, the EDIs used for these comparisons were based on slightly

different body weights used for the calculations (32/80 kg and 29/63 kg for children/adults from Western and Asian countries, respectively).

Of the newly identified OPFRs, semi-quantified concentrations were only available for BDTDP and BBEBP allowing the calculation of their EDIs, which resulted in comparable values as for the legacy OPFR compounds. This highlights the potential for human exposure to these compounds and the need for further monitoring in the environment and humans.

The EDIs calculated for plasticizers ranged from  $2.14\text{E-}07$  to  $3.74\text{E-}04$  mg/kg bw/day, with corresponding HQs between  $9.53\text{E-}07$  and  $8.10\text{E-}03$ . As expected, the highest EDI and relative HQ values were calculated for the legacy phthalate DEHP, corresponding to the toddler exposure in the 50th and 95th percentile scenario. The EDIs (mg/kg bw/day) for DEHP in Flemish dust were lower for both adults and toddlers when comparing with EDIs from various studies from Asia ( $3.08\text{E-}03$  and  $6.37\text{E-}03$  mg/kg bw/day), North America ( $2.65\text{E-}03$  and  $5.84\text{E-}03$  mg/kg bw/day) and Europe ( $2.43\text{E-}03$  and  $6.74\text{E-}03$  mg/kg bw/day) (Hammel et al., 2019; Qu et al., 2022). The EDIs from alternative plasticizers DEHA and ATBC in Flanders showed lower results for both the 50th and 95th percentile scenario in toddlers and adults compared to a recent study from the USA ( $4.33\text{E-}07$  and  $3.48\text{E-}08$  mg/kg bw/day,  $1.13\text{E-}06$  and  $8.99\text{E-}08$  mg/kg bw/day for DEHA and ATBC, respectively) (Subedi et al., 2017).

Interestingly, the risk assessment of the two newly identified phthalates (i.e. decyl nonyl phthalate and decyl undecyl phthalate) showed EDI and HQ values in the same order of magnitude as DEHP (up to  $9.77\text{E-}05$  mg/kg bw/day and  $4.89\text{E-}03$ , respectively). This highlights the relevance of such novel findings and calls for further (bio)monitoring investigation of these compounds. Finally, the EDIs of the other selected compounds were calculated with up to  $1.29\text{E-}05$  mg/kg bw/day, with a corresponding max HQ of  $6.47\text{E-}04$  for triethylene glycol bis(2-ethylhexanoate).

The above-mentioned results suggest that the exposure of the target population to individual CECs is lower than the risk threshold and should thus not suffer adverse health effects through dust ingestion. However, EDI calculated from dust ingestion covers only one exposure pathway and the available RfDs are based on the current toxicological evidence. Further research to identify relevant human exposure biomarkers to assess internal exposure levels of newly identified phthalates is needed.

#### 4.2.4 Conclusions

This study investigated the occurrence of known contaminants and CECs in 46 indoor dust samples collected in Belgium. The application of a combined targeted and suspect screening approach allowed the identification of 55 contaminants, 34 of which

were assigned with a high confidence level (1 or 2). Besides the detection of a set of known and well-studied compounds such as DEHP, DEHA or TBOEP, the applied workflow lead to the identification of a set of novel phthalates. In contrast to known and well-studied PHs, these novel compounds contained side chains with differing chain lengths, e.g. decyl nonyl or decyl undecyl phthalates, both of which were detected with a DF > 80%. Additionally, two novel PFRs, not previously described in dust, were reported: DDeBEEP and BBEBP, showing a DF of 4.4% and 45.7%, respectively. These findings demonstrate the high structural variability in the classes of PHs and OPFRs, pointing out the need for potential reevaluation of compounds included in targeted quantitative methods.

For a sub-selection of the identified compounds, semi-quantitative data was acquired, showing similar concentration ranges for the novel compounds as for the traditional PHs and PFRs, while also allowing the calculation of EDIs. Through the comparison of these EDIs with available *RfDs*, HQs were obtained, which indicated no potential health risks. However, the presented approach accounts solely for the exposure through dust ingestion and does not consider other exposure routes or mixture effects through the combined exposure to various contaminants.

In conclusion, this study clearly highlights the added value of suspect screening approaches and the need for implementation of such approaches in biomonitoring studies.

## Supplementary Information – Chapter 4.2

**Table SI-4.2.1:** Summary of compounds available as reference standards and used in quality control samples, as calibrants for semi-quantification or as internal standards. APs: Alternative plasticizers; PHs: Phthalates; OPFRs: Organophosphate flame retardants; PCP/CP: Personal care products/cleaning products; AOX: Synthetic antioxidants.

Use	Name	Abbreviation	Formula	Class	InChIKey	Manufacturer
Quality control compounds / calibrants semi-quantification	Acetyltriethyl citrate	ATEC	C <sub>14</sub> H <sub>22</sub> O <sub>8</sub>	APs	WEAPVABOECTMGR-UHFFFAOYSA-N	AccuStandard (New Haven, CT, USA)
	Acetyl Tributyl citrate	ATBC	C <sub>20</sub> H <sub>34</sub> O <sub>8</sub>	APs	QZCLKYGREBVARF-UHFFFAOYSA-N	AccuStandard (New Haven, CT, USA)
	Butyryl trihexyl citrate	BTHC	C <sub>28</sub> H <sub>50</sub> O <sub>8</sub>	APs	GWVUTNGDMGTPFE-UHFFFAOYSA-N	AccuStandard (New Haven, CT, USA)
	Diisobutyl adipate	DIBA	C <sub>14</sub> H <sub>26</sub> O <sub>4</sub>	APs	RDOFJDLLWVCMRU-UHFFFAOYSA-N	AccuStandard (New Haven, CT, USA)
	Di(2-ethylhexyl) adipate	DEHA	C <sub>22</sub> H <sub>42</sub> O <sub>4</sub>	APs	SAOKZLXYCUGLFA-UHFFFAOYSA-N	AccuStandard (New Haven, CT, USA)
	Tri-n-hexyltrimellitate	THTM	C <sub>27</sub> H <sub>42</sub> O <sub>6</sub>	APs	MXHBQKVKHGQWRB-UHFFFAOYSA-N	AccuStandard (New Haven, CT, USA)
	Tris(2-ethylhexyl)trimellitate	TOTM	C <sub>33</sub> H <sub>54</sub> O <sub>6</sub>	APs	KRADHMIOFJQKEZ-UHFFFAOYSA-N	AccuStandard (New Haven, CT, USA)
	Dibutyl sebacate	DBS	C <sub>18</sub> H <sub>34</sub> O <sub>4</sub>	APs	PYGXAGIECVVIOZ-UHFFFAOYSA-N	AccuStandard (New Haven, CT, USA)
	Dimethyl phthalate	DMP	C <sub>10</sub> H <sub>10</sub> O <sub>4</sub>	PHs	NIQCNGHVCWTJSM-UHFFFAOYSA-N	AccuStandard (New Haven, CT, USA)
	Diethyl phthalate	DEP	C <sub>12</sub> H <sub>14</sub> O <sub>4</sub>	PHs	FLKPEMZONWLCSK-UHFFFAOYSA-N	AccuStandard (New Haven, CT, USA)
	Di-n-butyl phthalate	DnBP	C <sub>16</sub> H <sub>22</sub> O <sub>4</sub>	PHs	DOIRQSBPFJWKBE-UHFFFAOYSA-N	AccuStandard (New Haven, CT, USA)

Quality control compounds / calibrants semi-quantification	Diphenyl phthalate	DPHP	C <sub>20</sub> H <sub>14</sub> O <sub>4</sub>	PHs	DWNAQMUDCDVSLT-UHFFFAOYSA-N	AccuStandard (New Haven, CT, USA)
	Benzyl butyl phthalate	BBzP	C <sub>19</sub> H <sub>20</sub> O <sub>4</sub>	PHs	IRIAEXORFWYRCZ-UHFFFAOYSA-N	AccuStandard (New Haven, CT, USA)
	Di(2-ethylhexyl) phthalate	DEHP	C <sub>24</sub> H <sub>38</sub> O <sub>4</sub>	PHs	BJQHLKABXJIVAM-UHFFFAOYSA-N	AccuStandard (New Haven, CT, USA)
	Diphenylcresyl phosphate	CDPHP	C <sub>19</sub> H <sub>17</sub> O <sub>4</sub> P	OPFRs	XMNDMAQKWSQVOV-UHFFFAOYSA-N	Wellington Laboratories (Guelph, ON, Canada)
	Triethyl phosphate	TEP	C <sub>6</sub> H <sub>15</sub> O <sub>4</sub> P	OPFRs	DQWPFLDHJDLRL-UHFFFAOYSA-N	Wellington Laboratories (Guelph, ON, Canada)
	Tris(2-chloroethyl) phosphate	TCEP	C <sub>6</sub> H <sub>12</sub> Cl <sub>3</sub> O <sub>4</sub> P	OPFRs	HQUQLFOMPYWACS-UHFFFAOYSA-N	Wellington Laboratories (Guelph, ON, Canada)
	Tris(1-chloro-2-propyl) phosphate	TCIPP	C <sub>9</sub> H <sub>18</sub> Cl <sub>3</sub> O <sub>4</sub> P	OPFRs	KVMPUXDNESXNOH-UHFFFAOYSA-N	Wellington Laboratories (Guelph, ON, Canada)
	Tributyl phosphate	TBP	C <sub>12</sub> H <sub>27</sub> O <sub>4</sub> P	OPFRs	STCOOQWBFONSKY-UHFFFAOYSA-N	Wellington Laboratories (Guelph, ON, Canada)
	Tris(1,3-dichloro-2-propyl) phosphate	TDCIPP	C <sub>9</sub> H <sub>15</sub> Cl <sub>6</sub> O <sub>4</sub> P	OPFRs	ASLWPAWFJZFCKF-UHFFFAOYSA-N	Wellington Laboratories (Guelph, ON, Canada)
	Triphenyl phosphate	TPhP	C <sub>18</sub> H <sub>15</sub> O <sub>4</sub> P	OPFRs	XZZNDPSIHUTMOC-UHFFFAOYSA-N	Wellington Laboratories (Guelph, ON, Canada)
	2-Ethylhexyl diphenyl phosphate	EHDPHP	C <sub>20</sub> H <sub>27</sub> O <sub>4</sub> P	OPFRs	CGSLYBDCEGBZCG-UHFFFAOYSA-N	Wellington Laboratories (Guelph, ON, Canada)
	Tris(2-ethylhexyl) phosphate	TEHP	C <sub>24</sub> H <sub>51</sub> O <sub>4</sub> P	OPFRs	GTVWRXRDKAHEAD-UHFFFAOYSA-N	Wellington Laboratories (Guelph, ON, Canada)
	Tris(4-tert-butylphenyl) phosphate	TBuPhP	C <sub>30</sub> H <sub>39</sub> O <sub>4</sub> P	OPFRs	LORSVOJSXMHDHF-UHFFFAOYSA-N	Wellington Laboratories (Guelph, ON, Canada)
	Tris(2-butoxyethyl) phosphate	TBOEP	C <sub>18</sub> H <sub>39</sub> O <sub>7</sub> P	OPFRs	WTLBZVNBKMDVP-UHFFFAOYSA-N	Wellington Laboratories (Guelph, ON, Canada)
Tricresyl phosphate	TPtP	C <sub>21</sub> H <sub>21</sub> O <sub>4</sub> P	OPFRs	BOSMZFBHAYFUBJ-UHFFFAOYSA-N	Wellington Laboratories (Guelph, ON, Canada)	

	2,2-Bis(chloromethyl)-1,3-propanediyl bis(bis(2-chloroethyl) phosphate)	V6	C <sub>13</sub> H <sub>24</sub> Cl <sub>6</sub> O <sub>8</sub> P <sub>2</sub>	OPFRs	ZGHUDSLQAGWEY-UHFFFAOYSA-N	Wellington Laboratories (Guelph, ON, Canada)
	Tris(2,3-dibromopropyl) phosphate	TDBPP	C <sub>9</sub> H <sub>15</sub> Br <sub>6</sub> O <sub>4</sub> P	OPFRs	PQYJRMFWJJONBO-UHFFFAOYSA-N	Wellington Laboratories (Guelph, ON, Canada)
	Isodecyl diphenyl phosphate	iDPP	C <sub>22</sub> H <sub>31</sub> O <sub>4</sub> P	OPFRs	RYUJRXVZSJCHDZ-UHFFFAOYSA-N	Wellington Laboratories (Guelph, ON, Canada)
	Resorcinol bis(diphenyl phosphate)	RDP	C <sub>30</sub> H <sub>24</sub> O <sub>8</sub> P <sub>2</sub>	OPFRs	OWICEWMBIBPFAH-UHFFFAOYSA-N	Wellington Laboratories (Guelph, ON, Canada)
	Bisphenol A bisdiphenyl phosphate	BDP	C <sub>39</sub> H <sub>34</sub> O <sub>8</sub> P <sub>2</sub>	OPFRs	BQPNUOYXSVUVMY-UHFFFAOYSA-N	Wellington Laboratories (Guelph, ON, Canada)
<b>Internal standards</b>	Dibenzyl phthalate-d4	DBzP-d4	C <sub>22</sub> H <sub>14</sub> D <sub>4</sub> O <sub>4</sub>	PHs	UCVPKAZCQPRWAY-ZZRPVTOQSA-N	Sigma-Aldrich (Bornem, Belgium)
	Diethylhexyl phthalate-d4	DEHP-d4	C <sub>24</sub> H <sub>34</sub> D <sub>4</sub> O <sub>4</sub>	PHs	BJQHKLKABXJIVAM-SAQXESPHSA-N	Sigma-Aldrich (Bornem, Belgium)
	Di-n-butyl phthalate-d4	DnBP-d4	C <sub>16</sub> H <sub>18</sub> D <sub>4</sub> O <sub>4</sub>	PHs	DOIRQSBPFJWKBE-ULDPCNCHSA-N	Sigma-Aldrich (Bornem, Belgium)
	Tris(2-butoxyethyl) phosphate-d6	TBOEP-d6	C <sub>18</sub> H <sub>33</sub> D <sub>6</sub> O <sub>7</sub> P	OPFRs	n.a.	Provided by Dr. V. N. Belov (Max Planck Institute, Göttingen, Germany)
	Tris(2-chloroethyl) phosphate-d12	TCEP-d12	C <sub>6</sub> D <sub>12</sub> Cl <sub>3</sub> O <sub>4</sub> P	OPFRs	n.a.	Provided by Dr. V. N. Belov (Max Planck Institute, Göttingen, Germany)
	Triphenyl phosphate-d15	TPHP-d15	C <sub>18</sub> D <sub>15</sub> O <sub>4</sub> P	OPFRs	n.a.	Provided by Dr. V. N. Belov (Max Planck Institute, Göttingen, Germany)

Confirmation standards	2-hydroxy-4-n-octyloxybenzophenone		C <sub>21</sub> H <sub>26</sub> O <sub>3</sub>	PCPs/CPs	CPTZEZGTUFXACE-UHFFFAOYSA-N	Tokyo Chemical Industry (Zwijndrecht, Belgium)
	N-(1,3-Dimethylbutyl)-N'-phenyl-1,4-phenylenediamine	6PPD	C <sub>18</sub> H <sub>24</sub> N <sub>2</sub>	AOX	ZZMVLMMVFMGSMY-UHFFFAOYSA-N	Tokyo Chemical Industry (Zwijndrecht, Belgium)
	Butyl methoxy-dibenzoylmethane*	Avobenzone	C <sub>20</sub> H <sub>22</sub> O <sub>3</sub>	UV filters	XNEFYCZVKIDDMS-UHFFFAOYSA-N	Tokyo Chemical Industry (Zwijndrecht, Belgium)
	2-(5-Chloro-2-benzotriazolyl)-6-tert-butyl-p-cresol	Bumetrizole	C <sub>17</sub> H <sub>18</sub> ClN <sub>3</sub> O	UV filter	OCWYEMOEOGEQAN-UHFFFAOYSA-N	Tokyo Chemical Industry (Zwijndrecht, Belgium)
	Triphenylphosphine oxide	TPPO	C <sub>18</sub> H <sub>15</sub> OP	Other	FIQMHBVVRAXMOP-UHFFFAOYSA-N	Thermo Scientific Chemicals (Geel, Belgium)
	Bis-ethylhexyloxyphenol Methoxyphenyl Triazine	Bemotrizinol	C <sub>38</sub> H <sub>49</sub> N <sub>3</sub> O <sub>5</sub>	UV filters	n.a.	Tokyo Chemical Industry (Zwijndrecht, Belgium)
	N-(2-ethoxyphenyl)-N-(2-ethylphenyl) Oxamide		C <sub>18</sub> H <sub>20</sub> N <sub>2</sub> O <sub>3</sub>	UV filters	YIMHRDBSVCPJOV-UHFFFAOYSA-N	LGC standards (Augsburg, Germany)
	Diethyltoluamide	DEET	C <sub>12</sub> H <sub>17</sub> NO	PCPs	MMOXZBCLCQITDF-UHFFFAOYSA-N	Sigma Aldrich (Bornem, Belgium)
	Decyl nonyl phthalate		C <sub>27</sub> H <sub>44</sub> O <sub>4</sub>	APs	n.a.	Aaron Chemicals (San Diego, United States)
	1-[[2-(2,4-dichlorophenyl)-4-propyl-1,3-dioxolan-2-yl]methyl-1H-1,2,4-triazole	Propiconazole	C <sub>15</sub> H <sub>17</sub> Cl <sub>2</sub> N <sub>3</sub> O <sub>2</sub>	Fungicides	STJLVHWMYQXCPB-UHFFFAOYSA-N	LGC standards (Augsburg, Germany)
	Methyl 2-benzimidazolecarbamate	Carbendazim	C <sub>9</sub> H <sub>9</sub> N <sub>3</sub> O <sub>2</sub>	Fungicides	TWFZGCMQGLPBSX-UHFFFAOYSA-N	LGC standards (Augsburg, Germany)

\*Confirmation standard revealed assignment of false positive. Therefore, this compound is not included in overview of identified compounds.

**Table SI-4.2.2:** Summary of the detection frequency (DF), the average retention time (RT), average peak area (PA) and the relative standard deviations (RSDs) of the latter two as well as the average absolute mass error (AME) obtained for the native compounds and internal standards (IS) in the QC samples (n = 6). The mentioned parameters are given for the most abundant adduct which is indicated in the 2<sup>nd</sup> column.

	<b>Adduct*</b>	<b>DF [%]</b>	<b><math>\bar{x}</math> RT [min]</b>	<b>RSD<sub>RT</sub> [%]</b>	<b><math>\bar{x}</math> Peak area [cps]</b>	<b>RSD<sub>PA</sub> [%]</b>	<b><math>\bar{x}</math> AME [ppm]</b>
<b>ATEC</b>							
EtOAc fraction	[M+Na] <sup>+</sup>	100	5.36	0.09	9.67E+06	7.5	1.36
MeOH fraction	[M+Na] <sup>+</sup>	50	5.34	0.50	9.40E+03	34.5	0.70
<b>ATBC</b>							
EtOAc fraction	[M+Na] <sup>+</sup>	100	7.70	0.09	1.54E+07	10.7	1.84
MeOH fraction	[M+Na] <sup>+</sup>	100	7.69	0.10	2.83E+04	37.7	1.12
<b>BTHC</b>							
EtOAc fraction	[M+Na] <sup>+</sup>	100	13.51	0.07	1.91E+07	10.7	1.47
MeOH fraction	n.d.	n.d.	n.d.	n.d.	n.d.	n.d.	n.d.
<b>DIBA</b>							
EtOAc fraction	[M+Na] <sup>+</sup>	100	6.93	0.24	4.38E+06	14.1	4.02
MeOH fraction	n.d.	n.d.	n.d.	n.d.	n.d.	n.d.	n.d.
<b>DEHA</b>							
EtOAc fraction	[M+Na] <sup>+</sup>	100	12.65	0.08	1.69E+07	12.2	1.30
MeOH fraction	[M+Na] <sup>+</sup>	100	12.62	0.13	1.21E+05	46.8	0.41
<b>THTM</b>							
EtOAc fraction	[M+Na] <sup>+</sup>	100	14.36	0.08	1.06E+07	26.2	1.83
MeOH fraction	n.d.	n.d.	n.d.	n.d.	n.d.	n.d.	n.d.
<b>TOTM</b>							
EtOAc fraction	[M+H] <sup>+</sup>	100	17.27	0.05	9.66E+06	21.2	1.46
MeOH fraction	n.d.	n.d.	n.d.	n.d.	n.d.	n.d.	n.d.
<b>DBS</b>							
EtOAc fraction	[M+Na] <sup>+</sup>	100	9.41	0.11	1.71E+07	9.9	1.73
MeOH fraction	[M+Na] <sup>+</sup>	100	9.40	0.08	3.97E+04	32.2	2.45
<b>DMP</b>							
EtOAc fraction	[M+Na] <sup>+</sup>	100	4.55	0.10	2.75E+05	20.6	0.53
MeOH fraction	[M+Na] <sup>+</sup>	50	4.55	0.62	4.55E+03	61.1	4.89
<b>DEP</b>							
EtOAc fraction	[M+Na] <sup>+</sup>	100	5.42	0.29	1.83E+06	19.3	3.03
MeOH fraction	[M+Na] <sup>+</sup>	66.7	5.40	0.14	3.31E+04	16.3	2.34
<b>DnBP</b>							
EtOAc fraction	[M+Na] <sup>+</sup>	100	7.02	0.24	6.02E+06	6.3	3.75
MeOH fraction	[M+Na] <sup>+</sup>	100	6.95	0.80	3.00E+05	30.1	1.25
<b>DPP</b>							
EtOAc fraction	[M+Na] <sup>+</sup>	100	6.46	0.10	3.81E+06	19.0	2.23
MeOH fraction	n.d.	n.d.	n.d.	n.d.	n.d.	n.d.	n.d.
<b>BBzP</b>							
EtOAc fraction	[M+Na] <sup>+</sup>	100	6.93	0.09	5.13E+06	8.7	3.59
MeOH fraction	[M+Na] <sup>+</sup>	100	6.93	0.09	1.69E+04	83.6	2.41
<b>DEHP</b>							

EtOAc fraction	[M+Na] <sup>+</sup>	100	12.52	0.09	6.17E+06	11.9	6.30
MeOH fraction	[M+Na] <sup>+</sup>	100	12.50	0.09	4.04E+05	63.5	0.65
<b>CDPHP</b>							
EtOAc fraction	[M+H] <sup>+</sup>	100	6.85	0.21	4.22E+06	5.03	1.40
MeOH fraction	n.d.	n.d.	n.d.	n.d.	n.d.	n.d.	n.d.
<b>TEP</b>							
EtOAc fraction	[M+Na] <sup>+</sup>	100	4.32	0.38	5.24E+04	47.4	1.44
MeOH fraction	n.d.	n.d.	n.d.	n.d.	n.d.	n.d.	n.d.
<b>TCEP</b>							
EtOAc fraction	[M+H] <sup>+</sup>	100	4.79	0.09	4.46E+05	16.2	0.24
MeOH fraction	n.d.	n.d.	n.d.	n.d.	n.d.	n.d.	n.d.
<b>TCIPP</b>							
EtOAc fraction	[M+Na] <sup>+</sup>	100	5.84	0.11	1.62E+05	17.7	0.80
MeOH fraction	n.d.	n.d.	n.d.	n.d.	n.d.	n.d.	n.d.
<b>TBP</b>							
EtOAc fraction	[M+Na] <sup>+</sup>	100	6.89	0.20	8.42E+05	6.9	2.22
MeOH fraction	[M+Na] <sup>+</sup>	100	6.88	0.09	3.57E+04	44.7	2.05
<b>TDCIPP</b>							
EtOAc fraction	[M+H] <sup>+</sup>	100	6.40	0.25	3.15E+05	40.4	0.35
MeOH fraction	[M+H] <sup>+</sup>	66.7	6.40	0.11	5.57E+03	16.4	4.23
<b>TPhP</b>							
EtOAc fraction	[M+H] <sup>+</sup>	100	6.46	0.10	6.44E+06	5.9	1.66
MeOH fraction	[M+H] <sup>+</sup>	100	6.46	0.21	4.28E+03	47.4	2.08
<b>EHDPPH</b>							
EtOAc fraction	[M+Na] <sup>+</sup>	100	8.50	0.09	1.43E+06	16.3	1.94
MeOH fraction	n.d.	n.d.	n.d.	n.d.	n.d.	n.d.	n.d.
<b>TEHP</b>							
EtOAc fraction	[M+Na] <sup>+</sup>	100	14.60	0.08	1.22E+06	26.9	2.08
MeOH fraction	n.d.	n.d.	n.d.	n.d.	n.d.	n.d.	n.d.
<b>TBuPhP</b>							
EtOAc fraction	[M+H] <sup>+</sup>	100	13.22	0.08	2.85E+06	15.6	1.88
MeOH fraction	n.d.	n.d.	n.d.	n.d.	n.d.	n.d.	n.d.
<b>TBOEP</b>							
EtOAc fraction	[M+H] <sup>+</sup>	100	7.22	0.09	1.55E+06	23.7	1.90
MeOH fraction	[M+H] <sup>+</sup>	100	7.21	0.09	2.55E+05	48.4	0.36
<b>TpTP</b>							
EtOAc fraction	[M+H] <sup>+</sup>	100	7.93	0.23	4.69E+06	10.7	2.00
MeOH fraction	n.d.	n.d.	n.d.	n.d.	n.d.	n.d.	n.d.
<b>V6</b>							
EtOAc fraction	n.d.	n.d.	n.d.	n.d.	n.d.	n.d.	n.d.
MeOH fraction	[M+H] <sup>+</sup>	33.3	5.88	0.01	2.83E+04	39.6	1.13
<b>TDBPP</b>							
EtOAc fraction	[M+H] <sup>+</sup>	100	6.70	0.09	1.09E+05	20.6	1.99
MeOH fraction	n.d.	n.d.	n.d.	n.d.	n.d.	n.d.	n.d.
<b>iDPP</b>							
EtOAc fraction	[M+H] <sup>+</sup>	100	9.87	0.26	2.22E+05	18.0	0.70

MeOH fraction	n.d.	n.d.	n.d.	n.d.	n.d.	n.d.	n.d.
<b>RDP</b>							
EtOAc fraction	[M+Na] <sup>+</sup>	100	7.52	0.27	8.59E+05	19.5	0.77
MeOH fraction	n.d.	n.d.	n.d.	n.d.	n.d.	n.d.	n.d.
<b>BDP</b>							
EtOAc fraction	[M+Na] <sup>+</sup>	100	9.89	0.10	6.64E+05	22.7	0.23
MeOH fraction	n.d.	n.d.	n.d.	n.d.	n.d.	n.d.	n.d.
<b>TBOEP-d<sub>6</sub></b>							
EtOAc fraction	[M+H] <sup>+</sup>	100	7.22	0.09	1.19E+07	24.2	1.03
MeOH fraction	[M+H] <sup>+</sup>	100	7.21	0.09	2.53E+06	53.6	1.37
<b>TCEP-d<sub>12</sub></b>							
EtOAc fraction	[M+H] <sup>+</sup>	100	4.79	0.09	3.94E+06	17.1	0.92
MeOH fraction	[M+H] <sup>+</sup>	83.3	4.78	0.37	2.28E+04	113.9	6.21
<b>TPhP-d<sub>15</sub></b>							
EtOAc fraction	[M+H] <sup>+</sup>	100	6.41	0.11	9.08E+06	5.0	1.49
MeOH fraction	n.d.	n.d.	n.d.	n.d.	n.d.	n.d.	n.d.
<b>DBzP-d<sub>4</sub></b>							
EtOAc fraction	[M+Na] <sup>+</sup>	100	6.84	0.10	1.75E+07	8.3	2.24
MeOH fraction	[M+Na] <sup>+</sup>	100	6.83	0.10	5.22E+04	89.7	1.15
<b>DEHP-d<sub>4</sub></b>							
EtOAc fraction	[M+Na] <sup>+</sup>	100	12.46	0.08	2.13E+07	10.8	2.34
MeOH fraction	[M+Na] <sup>+</sup>	100	12.45	0.09	3.24E+05	89.8	0.80
<b>DnBP-d<sub>4</sub></b>							
EtOAc fraction	[M+Na] <sup>+</sup>	100	6.98	0.09	1.93E+07	8.0	2.15
MeOH fraction	[M+Na] <sup>+</sup>	83.3	6.98	0.10	7.95E+04	107.0	1.18

\*Indicates most abundant adduct observed for the corresponding compound. For this adduct only, data is provided in the consecutive columns.

**Table SI-4.2.3:** Summary of the detection frequency (DF), the retention time (RT), average peak area and their relative standard deviations (RSDs) of the latter two as well as the average absolute mass error (AME) obtained for the native compounds and internal standards in the dust samples (n = 46).

	<b>DF [%]</b>	<b><math>\bar{x}</math> RT [min]</b>	<b>RSD<sub>RT</sub> [%]</b>	<b><math>\bar{x}</math> Peak area [cps]</b>	<b>RSD<sub>Peak.area</sub> [%]</b>	<b><math>\bar{x}</math> AME [ppm]</b>
<b>TBOEP-d<sub>6</sub></b>						
EtOAc fraction	100	7.21	0.19	1.66E+07	35.7	2.95
MeOH fraction	100	7.22	0.12	5.56E+06	78.8	1.93
<b>TCEP-d<sub>12</sub></b>						
EtOAc fraction	100	4.79	0.18	4.19E+06	18.8	0.87
MeOH fraction	72.2	4.78	0.43	6.39E+04	137	2.69
<b>TPhP-d<sub>15</sub></b>						
EtOAc fraction	100	6.41	0.09	1.09E+07	14.8	2.05
MeOH fraction	n.d.	n.d.	n.d.	n.d.	n.d.	n.d.
<b>DBzP-d<sub>4</sub></b>						
EtOAc fraction	100	6.84	0.14	1.32E+07	24.5	3.14
MeOH fraction	85.2	6.84	0.13	6.31E+04	103	3.24
<b>DEHP-d<sub>4</sub></b>						
EtOAc fraction	100	12.45	0.13	2.39E+07	34.3	4.11
MeOH fraction	98.2	12.45	0.11	5.36E+05	112	1.47
<b>DnBP-d<sub>4</sub></b>						
EtOAc fraction	100	6.98	0.15	1.92E+07	22.6	2.45
MeOH fraction	63.0	6.98	0.09	1.26E+05	101	2.51

**Table SI-4.2.4:** Compounds identified with confidence level (CL) 3 in at least one of the indoor dust samples. For each compound the detection frequency (DF) at a certain CL, the total DF and the fraction in which the compound was detected, is indicated. With PHs: phthalates, APs: alternative plasticizers, PFRs: organophosphate flame retardant, AOX: synthetic antioxidants, PCPs: Personal care products, CPs: Cleaning products.

Name	Formula	DF (CL) [%]	DF total [%]	Class	Fraction
(Vinyl methyl) adipate	C <sub>9</sub> H <sub>14</sub> O <sub>4</sub>	10.9 (3) 10.9 (4)	21.8	APs	MeOH
(Vinyl hydrogen) adipate	C <sub>8</sub> H <sub>12</sub> O <sub>4</sub>	6.5 (3) 10.9 (4)	17.4	APs	MeOH
(Nonyl undecyl) adipate	C <sub>26</sub> H <sub>50</sub> O <sub>4</sub>	6.5 (3) 87 (4)	93.5	APs	MeOH
Decyl nonyl phthalate	C <sub>27</sub> H <sub>44</sub> O <sub>4</sub>	76.1 (3) 17.4 (4)	93.5	PHs	EtOAc
Diheptyl phthalate (DHP)	C <sub>22</sub> H <sub>34</sub> O <sub>4</sub>	87.0 (3) 2.2 (4)	89.2	PHs	EtOAc
Diocetyl phthalate (DOP)	C <sub>24</sub> H <sub>38</sub> O <sub>4</sub>	6.5 (3) 50.0 (4)	56.5	PHs	EtOAc
Diundecyl phthalate	C <sub>30</sub> H <sub>50</sub> O <sub>4</sub>	30.4 (3) 15.2 (4)	45.6	PHs	EtOAc
Undecyl dodecyl phthalate	C <sub>31</sub> H <sub>52</sub> O <sub>4</sub>	4.3 (3)	4.3	PHs	EtOAc
Decyl undecyl phthalate	C <sub>29</sub> H <sub>48</sub> O <sub>4</sub>	41.3 (3) 37.0 (4)	78.3	PHs	EtOAc
N-(2-hydroxyethyl) octadecanamide	C <sub>20</sub> H <sub>41</sub> NO <sub>2</sub>	95.7 (3) 4.3 (4)	100	PCPs/CPs	MeOH
Tridecylphosphate	C <sub>30</sub> H <sub>63</sub> O <sub>4</sub> P	2.2 (3)	2.2	PFRs	EtOAc
Didecyl butoxyethoxyethyl phosphate (DDeBEEP)	C <sub>28</sub> H <sub>59</sub> O <sub>6</sub> P	2.2 (3) 2.2 (4)	4.4	PFRs	EtOAc
Bis(butoxyethyl) butyl phosphate (BBEBP)	C <sub>16</sub> H <sub>35</sub> O <sub>6</sub> P	10.9 (3) 34.8 (4)	45.7	PFRs	EtOAc
N,N-bis(2-hydroxyethyl) Oleamide	C <sub>22</sub> H <sub>43</sub> NO <sub>3</sub>	8.7 (3) 69.6 (4)	78.3	PCPs/CPs	MeOH
N,N'-Ethylenebis(12-hydroxy-octadecanamide)	C <sub>38</sub> H <sub>76</sub> N <sub>2</sub> O <sub>4</sub>	13.0 (3) 84.8 (4)	97.8	Other	MeOH
N,N-ethane-1,2-diylbis hexadecan-1-amide	C <sub>34</sub> H <sub>68</sub> N <sub>2</sub> O <sub>2</sub>	43.5 (3) 56.5 (4)	100.0	Other	MeOH
N-lauroylsarcosine	C <sub>15</sub> H <sub>29</sub> NO <sub>3</sub>	8.7 (3) 6.5 (4)	15.2	PCPs/CPs	MeOH
Dibenzylamine	C <sub>14</sub> H <sub>15</sub> N	41.3 (3) 52.2 (4)	93.5	Other	EtOAc
Oleamide	C <sub>18</sub> H <sub>35</sub> NO	10.9 (3) 10.9 (4)	21.8	Other	MeOH
N,N-dicyclohexylbenzothiazole-2-sulphenamide	C <sub>19</sub> H <sub>26</sub> N <sub>2</sub> S <sub>2</sub>	2.2 (3) 2.2 (4)	4.4	Other	EtOAc

Propane-1,2-diyl dibenzoate	C <sub>17</sub> H <sub>16</sub> O <sub>4</sub>	15.2 (3) 34.8 (4)	50.0	PCPs/CPs	EtOAc
-----------------------------	--	----------------------	------	----------	-------

**Table SI-4.2.5:**  $^{DT}CCS_{N_2}$  values obtained for all suspect compounds detected in the EtOAc fraction. Additional identifiers and confidence levels of each compounds are summarized in **Tables 4.2.1** and **SI-4.2.4**. The reported average  $^{DT}CCS_{N_2}$  values are based on the indicated number of samples (n). For each data point, the (relative) standard deviation is given (SD/RSD). If reference  $^{DT}CCS_{N_2}$  values were available (chapter 3.1), experimental average  $^{DT}CCS_{N_2}$  values were compared through calculation of percent deviations between the two datapoints. Phrm.: Pharmaceuticals.

Name	DF total [%]	Class	$\bar{x}^{DT}CCS_{N_2}$ [ $\text{\AA}^2$ ]	SD [ $\text{\AA}^2$ ]	RSD [%]	$\Delta CCS$ [%]
Diethylhexyl adipate (DEHA)	100	APs	[M+H] <sup>+</sup> : 209.38 [M+Na] <sup>+</sup> : 218.46	0.61 0.77	0.29 0.35	-0.01 0.01
Acetyltributyl citrate (ATBC)	100	APs	[M+H] <sup>+</sup> : 200.17 [M+Na] <sup>+</sup> : 206.85	0.42 0.48	0.21 0.23	0.17 0.53
Tris(2-ethylhexyl) trimellitate (TOTM)	100	APs	[M+H] <sup>+</sup> : 257.16 [M+Na] <sup>+</sup> : 265.75	0.57 0.65	0.22 0.24	n.a. 0.51
2-Ethylhexyl diphenyl phosphate (EHDPHP)	95.7	OPFRs	[M+H] <sup>+</sup> : n.d. [M+Na] <sup>+</sup> : 200.99	0.46	0.23	n.a. -0.84
Tri-p-tolyl phosphate (TPTP)	84.8	OPFRs	[M+H] <sup>+</sup> : 188.92 [M+Na] <sup>+</sup> : 198.55	0.43 0.60	0.23 0.30	-0.58 -0.74
Tris(2-butoxyethyl) phosphate (TBOEP)	100	OPFRs	[M+H] <sup>+</sup> : 196.82 [M+Na] <sup>+</sup> : 200.19	0.40 0.40	0.20 0.20	0.19 0.42
Triphenyl phosphate (TPHP)	100	OPFRs	[M+H] <sup>+</sup> : 173.35 [M+Na] <sup>+</sup> : 184.26	0.54 0.46	0.31 0.25	-0.80 -0.38
Tris(1-chloro-2-propyl) phosphate (TCIPP)	93.5	OPFRs	[M+H] <sup>+</sup> : 161.98 [M+Na] <sup>+</sup> : 171.70	0.33 0.51	0.21 0.30	0.20 0.21
Tris(1,3-dichloro-2-Propyl)phosphate (TDCIPP)	13.1	OPFRs	[M+H] <sup>+</sup> : 179.44 [M+Na] <sup>+</sup> : 189.95	0.34 0.73	0.19 0.38	0.49 -0.67
Tris(2-chloroethyl) phosphate (TCEP)	89.1	OPFRs	[M+H] <sup>+</sup> : 150.83 [M+Na] <sup>+</sup> : 161.11	0.51 0.58	0.34 0.36	-0.32 -0.17
Tris(2-ethylhexyl) phosphate (TEHP)	87.0	OPFRs	[M+H] <sup>+</sup> : n.d. [M+Na] <sup>+</sup> : 231.96	0.68	0.29	n.a. 0.07
Resorcinol bis(diphenyl phosphate) (RDP)	91.3	OPFRs	[M+H] <sup>+</sup> : 229.86 [M+Na] <sup>+</sup> : 231.63	1.13 0.69	0.49 0.30	0.48 0.02
Bisphenol A bis(diphenyl phosphate) (BDP)	84.8	OPFRs	[M+H] <sup>+</sup> : 247.58 [M+Na] <sup>+</sup> : 257.03	0.80 0.61	0.32 0.24	0.51 0.16
Diphenylcresyl phosphate (CDPHP)	89.1	OPFRs	[M+H] <sup>+</sup> : 179.69 [M+Na] <sup>+</sup> : n.d.	0.49	0.27	-0.44
Tributylphosphate (TBP)	52.2	OPFRs	[M+H] <sup>+</sup> : 166.18 [M+Na] <sup>+</sup> : 185.24	0.68 0.41	0.76 0.41	-0.33* 0.38*
Bis(2,4-di-tert-butylphenyl)penta-erythritol diposphate (BDTPDP)	89.1	OPFRs	[M+H] <sup>+</sup> : 254.74 [M+Na] <sup>+</sup> : 282.81	0.55 0.81	0.22 0.29	n.a.
N-1,3-dimethylbutyl-N-phenyl-p-phenylenediamine (6PPD)	63.1	AOX	[M+H] <sup>+</sup> : 174.51 [M+Na] <sup>+</sup> : n.d.	0.88	0.50	n.a.
N-(2-ethoxyphenyl)-N-(2-ethylphenyl)	32.6	UV filters	[M+H] <sup>+</sup> : 177.56 [M+Na] <sup>+</sup> : 189.42	0.23 1.04	0.13 0.55	n.a.

Oxamide						
Bumetrizole	34.8	UV filters	[M+H] <sup>+</sup> : 177.71 [M+Na] <sup>+</sup> : n.d.	0.40	0.23	n.a.
Propiconazole	76.1	Fungicides	[M+H] <sup>+</sup> : 179.30 [M+Na] <sup>+</sup> : n.d.	0.43	0.24	n.a.
Paracetamol	10.9	Phrm.	[M+H] <sup>+</sup> : 131.42 [M+Na] <sup>+</sup> : n.d.	0.08	0.06	n.a.
Triethylene glycol bis(2-ethylhexanoate)	95.6	Other	[M+H] <sup>+</sup> : 211.10 [M+Na] <sup>+</sup> : 207.33	0.64 0.51	0.30 0.24	n.a.
Decyl nonyl phthalate	93.5	PHs	[M+H] <sup>+</sup> : 224.71 [M+Na] <sup>+</sup> : 224.97	0.57 0.96	0.25 0.43	n.a.
Diheptyl phthalate (DHP)	89.2	PHs	[M+H] <sup>+</sup> : 207.72 [M+Na] <sup>+</sup> : 210.25	0.55 0.57	0.26 0.27	n.a.
Dioctyl phthalate (DOP)	56.5	PHs	[M+H] <sup>+</sup> : 215.03 [M+Na] <sup>+</sup> : 216.43	0.59 1.00	0.28 0.46	n.a.
Diundecyl phthalate	45.6	PHs	[M+H] <sup>+</sup> : 234.37 [M+Na] <sup>+</sup> : 232.16	0.62 0.83	0.26 0.36	n.a.
Undecyl dodecyl phthalate	4.3	PHs	[M+H] <sup>+</sup> : 238.00 [M+Na] <sup>+</sup> : 236.30	n.a. n.a.	n.a. n.a.	n.a.
Decyl undecyl phthalate	78.3	PHs	[M+H] <sup>+</sup> : 231.34 [M+Na] <sup>+</sup> : 229.86	0.78 0.94	0.34 0.41	n.a.
Tridecylphosphate	2.2	OPFRs	[M+H] <sup>+</sup> : 245.46 [M+Na] <sup>+</sup> : 249.05	n.a. n.a.	n.a. n.a.	n.a.
Didecyl butoxyethoxyethyl phosphate (DDeBEEP)	4.4	OPFRs	[M+H] <sup>+</sup> : 239.89 [M+Na] <sup>+</sup> : 246.04	n.a. n.a.	n.a. n.a.	n.a.
Bis(butoxyethyl) butyl phosphate (BBEP)	45.7	OPFRs	[M+H] <sup>+</sup> : 187.24 [M+Na] <sup>+</sup> : 188.89	0.49 0.61	0.26 0.32	n.a.
Dibenzylamine	93.5	Other	[M+H] <sup>+</sup> : 148.82 [M+Na] <sup>+</sup> : n.d.	0.46	0.31	n.a.
N,N-dicyclohexylbenzothiazole-2-sulphenamide	4.4	Other	[M+H] <sup>+</sup> : 184.98 [M+Na] <sup>+</sup> : n.d.	1.09	0.59	n.a.
Propane-1,2-diyl dibenzoate	50.0	PCPs/C Ps	[M+H] <sup>+</sup> : n.d. [M+Na] <sup>+</sup> : 180.31	0.46	0.25	n.a.

\*The indicated ΔCCS are based on a comparison with reference values of tri-n-butyl phosphate. For the comparison with tri-iso-butyl phosphate ΔCCS of 0.45 % and 1.12 % were obtained for the proton and sodium adducts, respectively.

**Table SI-4.2.6:** Minimum, maximum and median semi-quantified concentrations for the suspect compounds identified in the ethyl acetate fraction (all in [µg/g]). The median was calculated based on the lower bound approach whereby a concentration corresponding to zero was assigned if a compound was not detected. Thus, the presented median is representing the complete sample set with n = 46. The reported minimum concentration represents the lowest quantified concentrations (thus, excluding samples in which the compound was not detected). For each compound, the most abundant adduct (considered for quantification), the used calibrator and internal standard are given. Full compound names and further identifiers can be found in **Tables 4.2.1, SI-4.2.1 and SI-4.2.4**. Compounds which were quantified with the matching reference standard, are marked with an asterisk (\*).

Name	DF (CL) [%]	Adduct	Calibrator	IS	Min	Max	Med.
DIDP*	97.8 (1)	[M+H] <sup>+</sup>	DIDP	DEHP-d <sub>4</sub>	3.2	89.6	12.9
DEHP*	91.3 (1)	[M+Na] <sup>+</sup>	DEHP	DEHP-d <sub>4</sub>	8.0	447.7	26.4
DINP*	100 (1)	[M+Na] <sup>+</sup>	DINP	DEHP-d <sub>4</sub>	12.7	437.0	73.1
DeNoP	76.1 (2) 17.4 (4)	[M+H] <sup>+</sup>	DEHP	DEHP-d <sub>4</sub>	2.5	645.5	18.2
DEHA	95.7 (1) 4.3 (2C)	[M+Na] <sup>+</sup>	DEHP	DEHP-d <sub>4</sub>	0.3	141.1	10.9
ATBC	100 (1)	[M+Na] <sup>+</sup>	TBP	TPHP-d <sub>15</sub>	1.3	19.9	7.7
TOTM*	2.2 (1) 97.8 (2C)	[M+H] <sup>+</sup>	TOTM	DEHP-d <sub>4</sub>	0.4	19.7	3.3
EHDPHP	84.8 (1) 10.9 (2C)	[M+Na] <sup>+</sup>	TBOEP	TBOEP-d <sub>6</sub>	0.1	4.2	0.4
TpTP*	63.0 (1) 21.7 (2C)	[M+H] <sup>+</sup>	TpTP	TBOEP-d <sub>6</sub>	0.02	3.0	0.1
TBOEP*	87.0 (1) 13.0 (2C)	[M+H] <sup>+</sup>	TBOEP	TBOEP-d <sub>6</sub>	0.1	45.2	2.3
TPHP*	87.0 (1) 13.0 (2C)	[M+H] <sup>+</sup>	TPHP	TPHP-d <sub>15</sub>	0.1	3.9	0.5
TCIPP*	65.2 (1) 28.3 (2C)	[M+Na] <sup>+</sup>	TCPP	TCEP-d <sub>12</sub>	0.1	29.9	1.5
TDCIPP*	2.2 (1) 10.9 (2C)	[M+H] <sup>+</sup>	TDCIPP	TCEP-d <sub>12</sub>	1.9	13.0	0.0
TCEP*	8.7 (1) 80.4 (2C)	[M+H] <sup>+</sup>	TCEP	TCEP-d <sub>12</sub>	0.02	8.1	0.1
TEHP*	17.4 (1) 69.6 (2C)	[M+Na] <sup>+</sup>	TEHP	TBOEP-d <sub>6</sub>	0.1	10.4	0.5
RDP*	2.2 (1) 89.1 (2C)	[M+Na] <sup>+</sup>	RDP	TBOEP-d <sub>6</sub>	0.01	15.9	0.1
BDP*	10.9 (1) 73.9 (2C)	[M+H] <sup>+</sup>	BDP	TBOEP-d <sub>6</sub>	0.02	27.4	0.1
CDPHP	89.1 (2C)	[M+H] <sup>+</sup>	TPHP	TPHP-d <sub>15</sub>	0.01	1.2	0.04
TBP*	52.2 (2C)	[M+Na] <sup>+</sup>	TBP	TBOEP-d <sub>6</sub>	0.04	0.9	0.1
BDTPDP	23.9 (2) 65.2 (4)	[M+H] <sup>+</sup>	TpTP	TBOEP-d <sub>6</sub>	0.03	3.1	0.2
6-PPD	45.7 (1) 17.4 (2C)	[M+H] <sup>+</sup>	TEP	TPHP-d <sub>15</sub>	0.1	2.7	0.6

N-(2-ethoxy-phenyl)- N-(2-ethylphenyl) Oxamide	10.9 (1) 21.7 (2C)	[M+H] <sup>+</sup>	TPHP	TPHP-d <sub>15</sub>	0.02	1.2	0.0
Bumetrizole	34.8 (2C)	[M+H] <sup>+</sup>	TBuPHP	TBOEP-d <sub>6</sub>	0.01	0.7	0.0
Propiconazole	10.9 (1) 65.2 (2C)	[M+H] <sup>+</sup>	TDCIPP	TCEP-d <sub>12</sub>	0.2	24.2	0.6
Paracetamol	10.9 (2)	[M+H] <sup>+</sup>	TEP	TPHP-d <sub>15</sub>	0.2	3.9	0.0
Triethylene glycol bis(2-ethylhexanoate)	71.7 (2) 23.9 (4)	[M+Na] <sup>+</sup>	DEHP	DEHP-d <sub>4</sub>	0.3	81.2	3.7
DHP	87.0 (3) 2.2 (4)	[M+Na] <sup>+</sup>	DEHP	DEHP-d <sub>4</sub>	0.6	50.4	5.0
Diundecyl phthalate	30.4 (3) 15.2 (4)	[M+H] <sup>+</sup>	DEHP	DEHP-d <sub>4</sub>	2.7	122.2	0.0
Undecyl dodecyl phthalate	4.3 (3)	[M+H] <sup>+</sup>	DEHP	DEHP-d <sub>4</sub>	6.4	30.7	0.0
Decyl undecyl phthalate	41.3 (3) 37.0 (4)	[M+H] <sup>+</sup>	DEHP	DEHP-d <sub>4</sub>	1.7	477.8	9.8
Tridecyl phosphate	2.2 (3)	[M+H] <sup>+</sup>	TEHP	TBOEP-d <sub>6</sub>	51.3	51.3	0.0
DDeBEEP	2.2 (3) 2.2 (4)	[M+H] <sup>+</sup>	TBOEP	TBOEP-d <sub>6</sub>	1.3	39.1	0.0
BBEBP	10.9 (3) 34.8 (4)	[M+H] <sup>+</sup>	TBOEP	TBOEP-d <sub>6</sub>	0.01	7.3	0.1
Avobenzone	4.3 (3) 32.7 (4)	[M+H] <sup>+</sup>	TPHP	TPHP-d <sub>15</sub>	0.1	3.2	0.0
Dibenzylamine	41.3 (3) 52.2 (4)	[M+H] <sup>+</sup>	TEP	TPHP-d <sub>15</sub>	0.1	8.3	0.4
N,N-dicyclohexyl- benzo- thiazole-2- sulphenamide	2.2 (3) 2.2 (4)	[M+H] <sup>+</sup>	DEHP	DEHP-d <sub>4</sub>	0.1	32.5	0.0
Propane-1,2-diyl dibenzoate	15.2 (3) 34.8 (4)	[M+Na] <sup>+</sup>	DPP	DBzP-d <sub>4</sub>	0.1	7.2	0.03

**Table SI-4.2.7:** Compounds, detected in the ethyl acetate fraction, for which a reference standard was purchased for confirmation. These were semi-quantified using both, a calibrant derived from the QC compounds or the matching reference standard for semi-quantification. For both approaches, the minimum, maximum and median concentrations and the response factor of the calibrant are indicated.

<b>Decyl nonyl phthalate</b> <b>C<sub>27</sub>H<sub>44</sub>O<sub>4</sub></b>	<b>Calibrator:</b> DEHP		<b>IS:</b> DEHP-d <sub>4</sub>	
	Response factor <i>R<sub>f(1)</sub></i>	Min [µg/g]	Max [µg/g]	Median [µg/g]
	0.20	2.5	645.5	18.2
	<b>Calibrator:</b> Decyl nonyl phthalate		<b>IS:</b> DEHP-d <sub>4</sub>	
	Response factor <i>R<sub>f(2)</sub></i>	Min [µg/g]	Max [µg/g]	Median [µg/g]
	0.49	1.0	260.5	7.9
Ratio betw. Response factors [ <i>R<sub>f(1)</sub></i> / <i>R<sub>f(2)</sub></i> ]: 0.41				
<b>N-(2-ethoxyphenyl)- N-(2-ethylphenyl) Oxamide</b> <b>C<sub>18</sub>H<sub>20</sub>N<sub>2</sub>O<sub>3</sub></b>	<b>Calibrator:</b> TPHP		<b>IS:</b> TPHP-d <sub>15</sub>	
	Response factor <i>R<sub>f(1)</sub></i>	Min [µg/g]	Max [µg/g]	Median [µg/g]
	1.36	0.02	1.2	0.0
	<b>Calibrator:</b> DEHP		<b>IS:</b> TPHP-d <sub>15</sub>	
	Response factor <i>R<sub>f(2)</sub></i>	Min [µg/g]	Max [µg/g]	Median [µg/g]
	0.57	0.1	2.9	0.0
Ratio betw. Response factors [ <i>R<sub>f(1)</sub></i> / <i>R<sub>f(2)</sub></i> ]: 2.36				
<b>N-1,3-dimethylbutyl- N-phenyl- p-phenylene diamine</b> <b>C<sub>18</sub>H<sub>24</sub>N<sub>2</sub></b>	<b>Calibrator:</b> TEP		<b>IS:</b> TPHP-d <sub>15</sub>	
	Response factor <i>R<sub>f(1)</sub></i>	Min [µg/g]	Max [µg/g]	Median [µg/g]
	0.22	0.1	2.7	0.3
	<b>Calibrator:</b> N-1,3-dimethylbutyl- N-phenyl-p-phenylenediamine		<b>IS:</b> TPHP-d <sub>15</sub>	
	Response factor <i>R<sub>f(2)</sub></i>	Min [µg/g]	Max [µg/g]	Median [µg/g]
	0.99	0.03	0.6	0.1
Ratio betw. Response factors [ <i>R<sub>f(1)</sub></i> / <i>R<sub>f(2)</sub></i> ]: 0.22				
<b>Bumetrizole</b> <b>C<sub>17</sub>H<sub>18</sub>ClN<sub>3</sub>O</b>	<b>Calibrator:</b> TBuPHP		<b>IS:</b> TBOEP-d <sub>6</sub>	
	Response factor <i>R<sub>f(1)</sub></i>	Min [µg/g]	Max [µg/g]	Median [µg/g]
	0.99	0.01	0.7	0.0
	<b>Calibrator:</b> Bumetrizole		<b>IS:</b> TBOEP-d <sub>6</sub>	
	Response factor <i>R<sub>f(2)</sub></i>	Min [µg/g]	Max [µg/g]	Median [µg/g]
	0.11	0.05	6.68	0.0
Ratio betw. Response factors [ <i>R<sub>f(1)</sub></i> / <i>R<sub>f(2)</sub></i> ]: 9.00				
<b>Propiconazole</b> <b>C<sub>15</sub>H<sub>17</sub>Cl<sub>2</sub>N<sub>3</sub>O<sub>2</sub></b>	<b>Calibrator:</b> TDCPP		<b>IS:</b> TCEP-d <sub>12</sub>	
	Response factor <i>R<sub>f(1)</sub></i>	Min [µg/g]	Max [µg/g]	Median [µg/g]
	0.47	0.2	24.2	0.4
<b>Calibrator:</b> Propiconazole		<b>IS:</b> TCEP-d <sub>12</sub>		

	Response factor $R_{f(2)}$	Min [ $\mu\text{g/g}$ ]	Max [ $\mu\text{g/g}$ ]	Median [ $\mu\text{g/g}$ ]
	1.70	0.04	6.7	0.2
Ratio betw. Response factors [ $R_{f(1)}/R_{f(2)}$ ]: 0.28				

**Table SI-4.2.8:** Results of the statistical comparison (Mann-Whitney U Test) between samples collected in public buildings and private homes. For each compound and sample group, the obtained *p*-value, the mean and the 25<sup>th</sup>, 50<sup>th</sup> and 75<sup>th</sup> percentiles are given. Compounds for which a significant difference was observed, are marked in green. . Full compound names and further identifiers can be found in **Tables 4.2.1, SI-4.2.1 and SI-4.2.4.**

Class	Compound	2-tailed <i>p</i> -value	Type	Mean	Percentile			N
					25	50	75	
Adipate	DEHA	< 0.001	Public	43.31	11.03	41.92	63.07	22
			Home	8.13	1.51	3.32	10.80	24
AOX	6-PPD	0.004	Public	0.75	0.00	0.77	1.09	22
			Home	0.26	0.00	0.15	0.31	24
Citrate	ATBC	0.001	Public	10.14	6.83	9.52	13.09	22
			Home	5.89	2.76	5.62	8.30	24
Fungicide	Propiconazole	0.003	Public	0.33	0.00	0.23	0.54	22
			Home	2.99	0.27	0.64	2.86	24
Other	Dibenzylamine	0.004	Public	0.98	0.33	0.60	1.02	22
			Home	0.37	0.15	0.30	0.44	24
Other	Triethylene glycol bis(2-ethyl-hexanoate)	< 0.001	Public	15.76	2.24	13.07	20.74	22
			Home	3.43	0.57	1.71	3.78	24
PCP	Propane-1,2-diyl dibenzoate	0.001	Public	1.44	0.00	0.56	1.99	22
			Home	0.09	0.00	0.00	0.07	24
PFRS	TBP	0.388	Public	0.12	0.00	0.05	0.16	22
			Home	0.08	0.00	0.00	0.09	24
	BDP	0.087	Public	1.77	0.05	0.13	0.93	22
			Home	0.50	0.02	0.07	0.17	24
	TpTP	0.494	Public	0.20	0.02	0.13	0.28	22
			Home	0.25	0.03	0.06	0.19	24
	TEHP	0.860	Public	1.16	0.12	0.41	1.20	22
			Home	1.04	0.21	0.40	0.79	24
	TCEP	0.895	Public	0.88	0.04	0.11	0.29	22
			Home	0.13	0.07	0.10	0.15	24
	CDPHP	0.111	Public	0.12	0.03	0.05	0.12	22
			Home	0.05	0.01	0.03	0.07	24
	BDTPDP	0.035	Public	0.39	0.12	0.20	0.36	22
			Home	0.28	0.05	0.10	0.27	24
	RDP	0.027	Public	0.96	0.04	0.09	0.30	22
			Home	0.11	0.01	0.04	0.07	24
	TCIPP	0.636	Public	3.13	0.68	1.96	2.51	22
			Home	2.44	0.66	1.21	2.91	24
EHDPHP	0.007	Public	1.12	0.29	0.49	1.66	22	
		Home	0.35	0.15	0.27	0.44	24	
TBOEP		0.024	Public	8.48	1.65	3.51	7.12	22

			Home	5.33	0.61	1.59	2.64	24
	TPhP	0.003	Public	1.05	0.34	0.70	1.64	22
			Home	0.48	0.14	0.27	0.59	24
Phthalates	DeUnP	< 0.001	Public	78.24	7.61	13.87	154.9	22
			Home	11.27	0.41	4.81	8.01	24
	DHP	0.004	Public	8.97	3.54	5.70	16.35	22
			Home	4.89	0.70	1.77	5.66	24
	DEHP	0.077	Public	54.10	20.94	30.41	55.25	22
			Home	28.57	11.29	21.35	33.03	24
	DeNoP	0.006	Public	83.22	13.88	34.54	110.3	22
			Home	16.66	5.33	12.89	20.52	24
DIDP	< 0.001	Public	32.79	14.54	17.89	51.79	22	
		Home	9.43	5.14	7.54	12.72	24	
DINP	< 0.001	Public	163.5	87.89	157.5	205.9	22	
		Home	63.22	31.69	49.34	69.68	24	
Trimellitates	TOTM	0.008	Public	5.70	2.45	4.17	7.47	22
			Home	3.43	1.27	2.07	4.17	24

**Table SI-4.2.9:** Results of the statistical comparison (Mann-Whitney U Test) between samples collected in urban and rural areas. For each compound and sample group, the obtained *p*-value, the mean and the 25<sup>th</sup>, 50<sup>th</sup> and 75<sup>th</sup> percentiles are given. Compounds for which a significant difference was observed, are marked in green.

Class	Compound	2-tailed <i>p</i> -value	Location	Mean	Percentile			N
					25	50	75	
Adipate	DEHA	< 0.001	urban	37.74	10.29	22.99	59.36	25
			rural	9.72	1.45	5.01	10.20	21
AOX	6-PPD	0.519	urban	0.52	0.00	0.29	0.79	25
			rural	0.46	0.00	0.17	0.82	21
Citrate	ATBC	0.125	urban	8.85	5.83	8.65	11.91	25
			rural	6.82	2.94	5.73	9.60	21
Fungicide	Propiconazole	0.982	urban	1.07	0.00	0.49	1.13	25
			rural	2.48	0.18	0.36	0.90	21
Other	Dibenzylamine	0.020	urban	0.64	0.33	0.56	0.83	25
			rural	0.69	0.15	0.30	0.44	21
Other	Triethylene glycol bis(2-ethylhexanoate)	0.487	urban	12.33	1.53	3.49	20.02	25
			rural	5.76	1.18	3.45	8.01	21
PCP	Propane-1,2-diyl dibenzoate	0.334	urban	0.84	0.00	0.07	1.18	25
			rural	0.61	0.00	0.00	0.25	21
PFRS	TBP	0.009	urban	0.16	0.00	0.07	0.21	25
			rural	0.03	0.00	0.00	0.05	21
	BDP	0.063	urban	0.74	0.05	0.10	0.63	25

			rural	1.56	0.00	0.05	0.17	21
	TpTP	0.683	urban	0.30	0.02	0.12	0.23	25
			rural	0.14	0.03	0.06	0.20	21
	TEHP	0.529	urban	0.78	0.23	0.48	0.85	25
			rural	1.48	0.20	0.26	1.08	21
	TCEP	0.895	urban	0.82	0.09	0.14	0.35	25
			rural	0.09	0.04	0.07	0.12	21
	CDPHP	0.140	urban	0.07	0.03	0.04	0.10	25
			rural	0.10	0.01	0.03	0.07	21
	BDTPDP	0.051	urban	0.43	0.09	0.17	0.41	25
			rural	0.22	0.04	0.12	0.21	21
	RDP	0.106	urban	0.78	0.05	0.06	0.21	25
			rural	0.21	0.01	0.04	0.17	21
	TCIPP	0.251	urban	3.53	0.73	1.90	3.58	25
			rural	1.86	0.63	1.22	2.26	21
	EHDPHP	< 0.001	urban	1.09	0.29	0.49	1.41	25
			rural	0.27	0.10	0.23	0.37	21
	TBOEP	0.343	urban	7.76	1.15	2.88	7.77	25
			rural	5.73	0.49	2.08	5.98	21
	TPhP	0.031	urban	0.91	0.33	0.54	1.35	25
			rural	0.56	0.14	0.21	0.70	21
Phthalates	DeUnP	0.255	urban	32.55	5.52	9.66	21.38	25
			rural	56.09	2.08	5.71	18.91	21
	DHP	0.001	urban	10.34	3.12	5.87	16.77	25
			rural	2.68	0.72	2.43	4.55	21
	DEHP	0.145	urban	53.21	19.43	31.12	53.75	25
			rural	25.98	11.97	21.46	32.38	21
	DeNoP	0.559	urban	34.20	9.23	20.64	55.77	25
			rural	65.52	6.78	14.76	40.07	21
	DIDP	0.056	urban	22.74	9.24	15.13	28.37	25
			rural	18.05	5.34	7.42	17.44	21
	DINP	0.018	urban	127.9	64.49	95.07	189.5	25
			rural	91.15	32.54	58.26	115.4	21
Trimel- litates	TOTM	0.022	urban	6.06	1.98	4.09	9.67	25
			rural	2.68	1.305	2.22	4.09	21

**Table SI-4.2.10:** Results of the statistical comparison (Mann-Whitney U Test) between samples collected in buildings which were <20 and >20 years old. For each compound and sample group, the obtained *p*-value, the mean and the 25<sup>th</sup>, 50<sup>th</sup> and 75<sup>th</sup> percentiles are given. Compounds for which a significant difference was observed, are marked in green.

Class	Compound	2-tailed <i>p</i> -value	Age	Mean	Percentile			N
					25	50	75	
Adipate	DEHA	0.345	< 20y	16.12	2.39	7.76	22.81	17
			> 20y	12.66	1.48	5.01	21.14	15
AOX	6-PPD	0.771	< 20y	0.36	0.00	0.25	0.73	17
			> 20y	0.44	0.00	0.20	0.40	15
Citrate	ATBC	0.748	< 20y	6.20	3.25	6.87	8.25	17
			> 20y	7.62	2.72	5.73	13.40	15
Fungicide	Propiconazole	0.306	< 20y	1.26	0.24	0.36	0.56	17
			> 20y	3.15	0.16	0.70	3.25	15
Other	Dibenzylamine	0.326	< 20y	0.99	0.16	0.42	0.82	17
			> 20y	0.35	0.17	0.29	0.45	15
Other	Triethylene glycol bis(2-ethylhexanoate)	0.610	< 20y	5.17	0.99	2.28	4.52	17
			> 20y	4.16	0.37	1.70	6.60	15
PCP	Propane-1,2-diyl dibenzoate	0.219	< 20y	0.26	0.00	0.00	0.11	17
			> 20y	1.22	0.00	0.06	1.26	15
PFRs	TBP	0.284	< 20y	0.04	0.00	0.00	0.07	17
			> 20y	0.16	0.00	0.05	0.13	15
	BDP	0.306	< 20y	0.71	0.01	0.05	0.14	17
			> 20y	0.20	0.02	0.09	0.23	15
	TpTP	0.047	< 20y	0.08	0.02	0.04	0.15	17
			> 20y	0.19	0.04	0.12	0.27	15
	TEHP	0.206	< 20y	0.39	0.21	0.33	0.64	17
			> 20y	1.65	0.19	0.39	2.14	15
	TCEP	0.092	< 20y	0.10	0.05	0.10	0.12	17
			> 20y	0.16	0.07	0.12	0.26	15
	CDPHP	0.688	< 20y	0.06	0.02	0.03	0.07	17
			> 20y	0.04	0.02	0.03	0.05	15
	BDTPDP	0.219	< 20y	0.33	0.08	0.12	0.30	17
			> 20y	0.17	0.04	0.10	0.19	15
	RDP	0.835	< 20y	0.13	0.01	0.04	0.18	17
			> 20y	0.09	0.01	0.06	0.13	15
TCIPP	0.865	< 20y	2.08	0.47	1.19	3.22	17	

	EHDPHP	0.162	> 20y	1.68	0.65	1.22	2.28	15
			< 20y	0.66	0.18	0.44	0.77	17
	TBOEP	0.637	> 20y	0.33	0.11	0.25	0.36	15
			< 20y	2.49	0.88	1.24	2.46	17
	TPhP	0.806	> 20y	7.02	0.56	2.02	9.13	15
			< 20y	0.59	0.14	0.38	0.60	17
Phthalates	DeUnP	0.115	> 20y	17.05	0.00	5.13	8.74	17
			< 20y	61.79	3.35	10.38	27.44	15
	DHP	0.865	> 20y	5.47	0.96	4.39	6.68	17
			< 20y	7.26	1.00	2.93	5.87	15
	DEHP	0.650	> 20y	24.61	16.06	21.46	30.41	17
			< 20y	34.08	10.16	31.12	38.58	15
	DeNoP	0.375	> 20y	21.84	7.05	11.14	20.19	17
			< 20y	43.28	5.97	19.58	54.47	15
	DIDP	0.336	> 20y	12.89	6.89	7.65	9.98	17
			< 20y	16.77	4.94	12.85	16.49	15
	DINP	0.558	> 20y	72.36	37.67	58.26	80.00	17
			< 20y	95.02	34.22	62.89	166.65	15
Trimellitates	TOTM	0.664	> 20y	3.41	1.31	2.04	4.41	17
			< 20y	3.69	1.41	2.22	4.41	15

**Table SI-4.2.11:** Results of the statistical comparison (Mann-Whitney U Test) between samples collected at locations in which < 5d and > 5d passed since the last cleaning. For each compound and sample group, the obtained *p*-value, the mean and the 25<sup>th</sup>, 50<sup>th</sup> and 75<sup>th</sup> percentiles are given. Compounds for which a significant difference was observed, are marked in green.

Class	Compound	2-tailed <i>p</i> -value	Last cleaning	Mean	Percentile			N
					25	50	75	
Adipate	DEHA	0.901	< 5d	18.14	1.51	7.23	29.67	13
			> 5d	14.74	1.94	7.76	21.49	21
AOX	6-PPD	0.927	< 5d	0.45	0.00	0.29	0.57	13
			> 5d	0.37	0.00	0.20	0.54	21
Citrate	ATBC	0.736	< 5d	6.53	2.94	5.73	9.37	13
			> 5d	7.39	3.10	6.87	10.45	21
Fungicide	Propiconazole	< 0.001	< 5d	2.01	0.00	0.23	0.30	13
			> 5d	2.30	0.48	0.70	2.48	21
Other	Dibenzylamine	1.000	< 5d	0.46	0.15	0.35	0.79	13
			> 5d	0.81	0.20	0.33	0.58	21
Other	Triethylene glycol bis(2-ethylhexanoate)	0.632	< 5d	5.34	1.65	2.31	4.52	13
			> 5d	5.43	0.53	1.87	6.64	21

PCP	Propane-1,2-diyl dibenzoate	0.702	< 5d	0.35	0.00	0.00	0.49	13	
			> 5d	0.80	0.00	0.00	0.16	21	
PFRS	TBP	0.893	< 5d	0.05	0.00	0.00	0.09	13	
			> 5d	0.12	0.00	0.00	0.09	21	
	BDP	0.125	< 5d	0.47	0.00	0.04	0.09	13	
			> 5d	0.68	0.03	0.09	0.34	21	
	TpTP	0.320	< 5d	0.15	0.03	0.04	0.15	13	
			> 5d	0.28	0.04	0.09	0.22	21	
	TEHP	0.512	< 5d	0.90	0.20	0.30	1.37	13	
			> 5d	0.97	0.24	0.48	0.77	21	
	TCEP	0.709	< 5d	0.53	0.05	0.11	0.12	13	
			> 5d	0.14	0.06	0.10	0.21	21	
	CDPHP	0.210	< 5d	0.04	0.02	0.03	0.05	13	
			> 5d	0.06	0.03	0.04	0.08	21	
	BDTPDP	0.020	< 5d	0.13	0.02	0.09	0.14	13	
			> 5d	0.36	0.07	0.19	0.31	21	
	RDP	0.293	< 5d	0.06	0.02	0.03	0.06	13	
			> 5d	0.15	0.01	0.06	0.29	21	
	TCIPP	0.045	< 5d	1.49	0.31	0.65	1.96	13	
			> 5d	2.55	0.84	1.51	2.76	21	
	EHDPHP	0.523	< 5d	0.55	0.10	0.40	0.57	13	
			> 5d	0.61	0.21	0.29	0.81	21	
TBOEP	0.901	< 5d	7.93	0.80	1.24	16.30	13		
		> 5d	4.32	0.66	2.02	3.10	21		
TPhP	0.221	< 5d	0.30	0.10	0.16	0.56	13		
		> 5d	0.60	0.15	0.31	0.61	21		
Phthalates	DeUnP	0.631	< 5d	33.84	0.83	5.91	45.32	13	
			> 5d	35.55	2.93	6.13	16.05	21	
	DHP	0.790	< 5d	4.85	1.23	2.93	5.96	13	
			> 5d	7.51	0.72	4.39	7.00	21	
	DEHP	0.972	< 5d	27.12	11.88	26.75	36.03	13	
			> 5d	31.74	16.60	24.26	38.19	21	
	DeNoP	0.123	< 5d	18.80	5.55	10.67	19.25	13	
			> 5d	36.15	9.37	20.17	48.19	21	
	DIDP	0.385	< 5d	13.90	5.35	8.05	12.87	13	
			> 5d	17.18	6.89	12.33	17.03	21	
	DINP	0.559	< 5d	75.08	24.46	60.91	88.69	13	
			> 5d	93.73	38.23	60.75	166.7	21	
	Trimellitates	TOTM	0.901	< 5d	4.27	1.59	2.22	4.41	13
				> 5d	3.55	1.27	2.40	4.74	21

**Table SI-4.2.12:** Median EDI values [mg/kg bw/day] and HQs calculated from the concentrations of semi-quantified compounds in the indoor dust samples collected from homes (H) and public spaces (PS) according to the 50th and 95th percentile exposure scenarios. For those compounds lacking a specific *RfD*, the reference dose value of the calibrant used for semi-quantification was chosen as the most suitable proxy (marked with \*). The indicated literature sources correspond to [1] (Völkel et al., 2002); [2] (Poma et al., 2018); [3] (EPA, 2024); [4] (Ali et al., 2012); [5] (EFSA, 2005a); [6] (EFSA, 2005b); [7] (EPA, 1992); [8] (Christia et al., 2019).

Compound	Class	<i>RfD</i> mg/kg bw/day	Residential								Public space			
			EDI		HQ		EDI		HQ		EDI		HQ	
			H 50th p. adult	H 50th p. toddler	H 95th p. adult	H 95th p. toddler	PS 50th p. adult	PS 95th p. adult						
TBOEP	PFRs	5.00E-02 <sup>[1]</sup>	3.14E-07	6.28E-06	6.03E-06	1.21E-04	9.41E-07	1.88E-05	1.21E-05	2.41E-04	1.80E-07	3.61E-06	5.41E-07	1.08E-05
EHDPPH	PFRs	1.50E-02 <sup>[2]</sup>	5.29E-08	3.53E-06	1.02E-06	6.78E-05	1.59E-07	1.06E-05	2.04E-06	1.36E-04	2.54E-08	1.69E-06	7.61E-08	5.07E-06
CDPHP	PFRs	2.00E-02* <sup>[3]</sup>	6.27E-09	3.13E-07	1.21E-07	6.03E-06	1.88E-08	9.40E-07	2.41E-07	1.21E-05	2.31E-09	1.15E-07	6.92E-09	3.46E-07
TBP	PFRs	1.00E-02 <sup>[3]</sup>	-	-	-	-	-	-	-	-	2.28E-09	2.28E-07	6.84E-09	6.84E-07
BDP	PFRs	NA	1.28E-08	-	2.45E-07	-	3.83E-08	-	4.91E-07	-	6.37E-09	-	1.91E-08	-
TPTP	PFRs	2.00E-02 <sup>[3]</sup>	1.12E-08	5.60E-07	2.15E-07	1.08E-05	3.36E-08	1.68E-06	4.30E-07	2.15E-05	6.24E-09	3.12E-07	1.87E-08	9.36E-07
RDP	PFRs	NA	7.77E-09	-	1.49E-07	-	2.33E-08	-	2.99E-07	-	4.52E-09	-	1.35E-08	-
TPHP	PFRs	2.00E-02 <sup>[3]</sup>	5.18E-08	2.59E-06	9.95E-07	4.98E-05	1.55E-07	7.76E-06	1.99E-06	9.95E-05	3.57E-08	1.79E-06	1.07E-07	5.36E-06
TCIPP	PFRs	1.00E-02 <sup>[3]</sup>	2.38E-07	2.38E-05	4.58E-06	4.58E-04	7.14E-07	7.14E-05	9.15E-06	9.15E-04	1.01E-07	1.01E-05	3.02E-07	3.02E-05
TEHP	PFRs	1.00E-01 <sup>[3]</sup>	7.80E-08	7.80E-07	1.50E-06	1.50E-05	2.34E-07	2.34E-06	3.00E-06	3.00E-05	2.09E-08	2.09E-07	6.26E-08	6.26E-07
TDCIPP	PFRs	1.50E-02 <sup>[4]</sup>	-	-	-	-	-	-	-	-	-	-	-	-
TCEP	PFRs	2.20E-02 <sup>[4]</sup>	1.97E-08	8.96E-07	3.79E-07	1.72E-05	5.91E-08	2.69E-06	7.58E-07	3.45E-05	5.66E-09	2.57E-07	1.70E-08	7.71E-07
BBEPP	Novel PFR	5.00E-02* <sup>[1]</sup>	-	-	-	-	-	-	-	-	1.09E-09	2.17E-08	3.26E-09	6.52E-08
BDTPDP	Novel PFR	2.00E-02* <sup>[3]</sup>	1.91E-08	9.57E-07	3.68E-07	1.84E-05	5.74E-08	2.87E-06	7.36E-07	3.68E-05	1.04E-08	5.22E-07	3.13E-08	1.57E-06
DEHP	PHs	2.00E-02 <sup>[3]</sup>	4.21E-06	2.10E-04	8.10E-05	4.05E-03	1.26E-05	6.31E-04	1.62E-04	8.10E-03	1.56E-06	7.82E-05	4.69E-06	2.35E-04
DIDP	PHs	1.50E-01 <sup>[5]</sup>	1.49E-06	-	2.86E-05	-	4.46E-06	-	5.71E-05	-	9.20E-07	-	2.76E-06	-
DHP	PHs	2.00E-02* <sup>[3]</sup>	3.48E-07	1.74E-05	6.70E-06	3.35E-04	1.04E-06	5.22E-05	1.34E-05	6.70E-04	2.93E-07	1.46E-05	8.79E-07	4.39E-05
DUnP	PHs	2.00E-02* <sup>[3]</sup>	-	-	-	-	-	-	-	-	2.87E-07	1.43E-05	8.60E-07	4.30E-05
DINP	PHs	1.50E-01 <sup>[6]</sup>	9.73E-06	6.48E-05	1.87E-04	1.25E-03	2.92E-05	1.95E-04	3.74E-04	2.49E-03	8.10E-06	5.40E-05	2.43E-05	1.62E-04
DeNoP	Novel PH	2.00E-02* <sup>[3]</sup>	2.54E-06	1.27E-04	4.89E-05	2.44E-03	7.62E-06	3.81E-04	9.77E-05	4.89E-03	1.78E-06	8.88E-05	5.33E-06	2.66E-04
DeUnP	Novel PH	2.00E-02* <sup>[3]</sup>	9.48E-07	4.74E-05	1.82E-05	9.11E-04	2.84E-06	1.42E-04	3.65E-05	1.82E-03	7.13E-07	3.57E-05	2.14E-06	1.07E-04
DEHA	AP	6.00E-01 <sup>[7]</sup>	6.54E-07	1.09E-06	1.26E-05	2.10E-05	1.96E-06	3.27E-06	2.51E-05	4.19E-05	2.16E-06	3.59E-06	6.47E-06	1.08E-05
ATBC	AP	2.00E-01 <sup>[8]</sup>	1.11E-06	5.54E-06	2.13E-05	1.07E-04	3.32E-06	1.66E-05	4.26E-05	2.13E-04	4.89E-07	2.45E-06	1.47E-06	7.34E-06

TOTM	AP	2.25E-01 <sup>[8]</sup>	4.07E-07	1.81E-06	7.83E-06	3.48E-05	1.22E-06	5.43E-06	1.57E-05	6.96E-05	2.14E-07	9.53E-07	6.43E-07	2.86E-06
propane-1,2-diylidibenzoate	PCP	NA	-	-	-	-	-	-	-	-	2.85E-08	-	8.56E-08	-
Bumetizole	PCP	NA	-	-	-	-	-	-	-	-	5.56E-10	-	1.67E-09	-
6-PPD	AOX	NA	2.98E-08	-	5.74E-07	-	8.95E-08	-	1.15E-06	-	3.91E-08	-	1.17E-07	-
propiconazole	Fungicide	1.50E-02* <sup>[4]</sup>	1.26E-07	8.39E-06	2.42E-06	1.61E-04	3.77E-07	2.52E-05	4.84E-06	3.23E-04	1.15E-08	7.65E-07	3.44E-08	2.29E-06
Triethylene glycol bis(2-ethyl-hexanoate)	Other	2.00E-02* <sup>[3]</sup>	3.37E-07	1.68E-05	6.47E-06	3.24E-04	1.01E-06	5.05E-05	1.29E-05	6.47E-04	6.72E-07	3.36E-05	2.02E-06	1.01E-04
Dibenzylamine	Other	NA	5.74E-08	-	1.10E-06	-	1.72E-07	-	2.21E-06	-	3.09E-08	-	9.28E-08	-

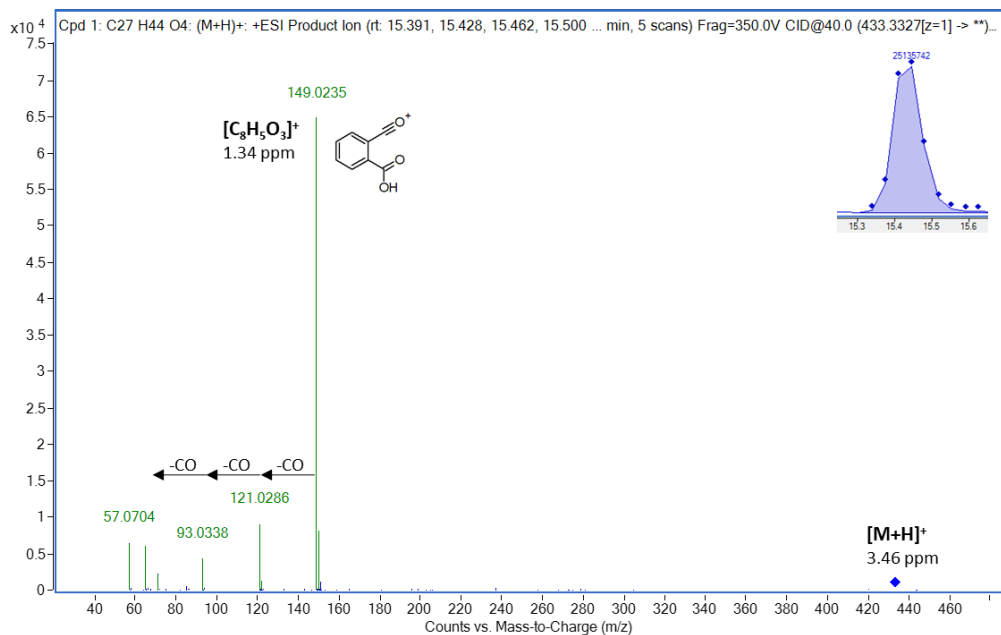


**Figure SI-4.2.1:** Example of a fragmentation spectrum obtained for decyl nonyl phthalate (DeNoP) in the reference standard at a collision energy of 40 eV. The proposed formula and the main neutral losses and fragments are indicated.

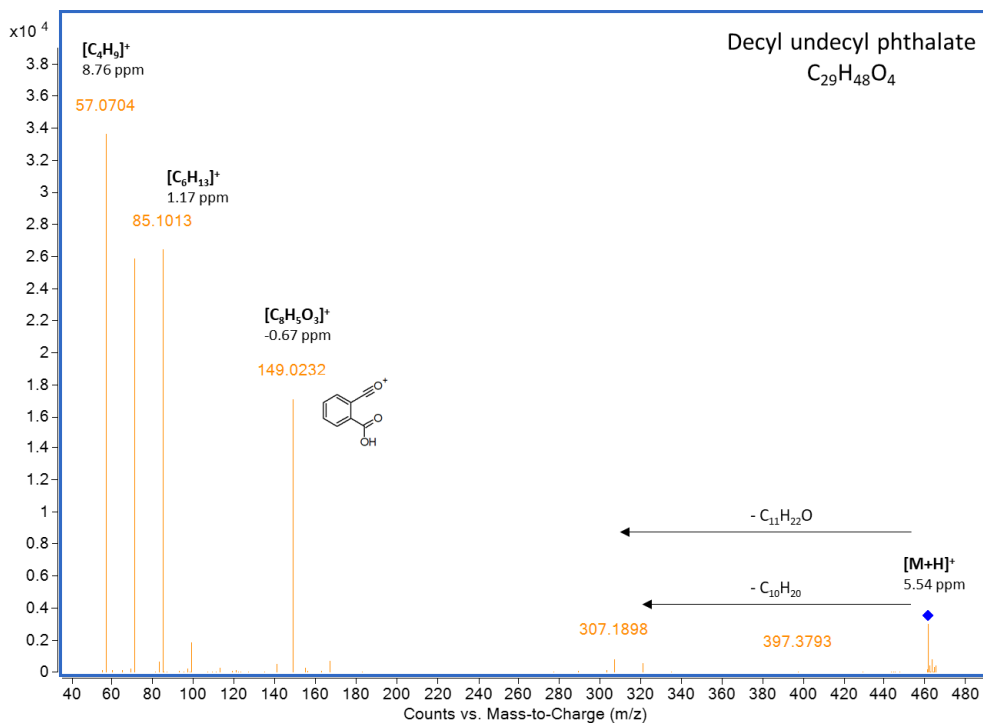


**Figure SI-4.2.2:** Example of a fragmentation spectrum obtained for decyl undecyl phthalate (DeUnPH) in one of the indoor dust samples at a collision energy of 10 eV. The proposed formula and the main neutral losses and fragments are indicated.

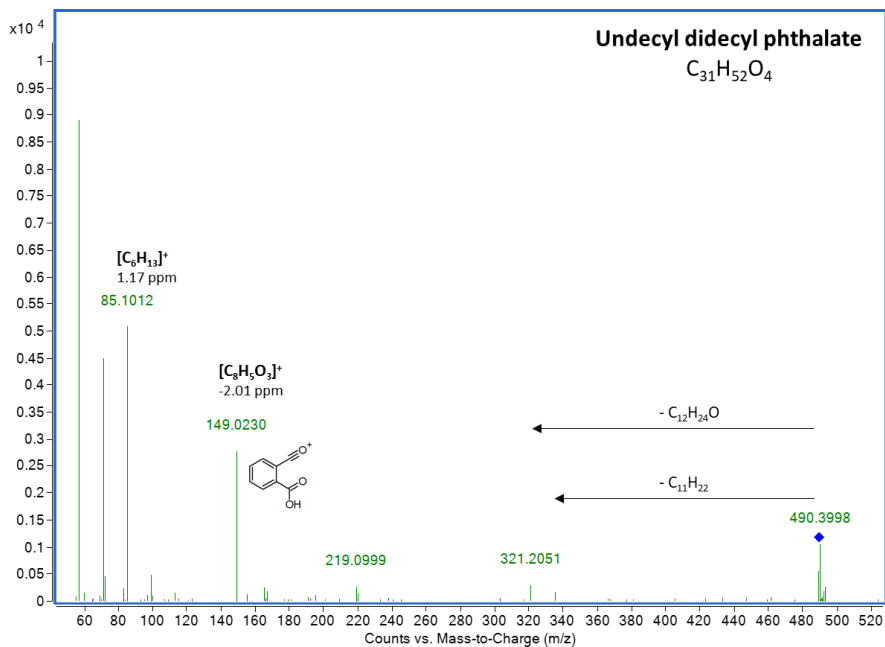


**Figure SI-4.2.3:** Example of a fragmentation spectrum obtained for undecyl didecyl phthalate in one of the indoor dust samples at a collision energy of 10 eV. The proposed formula and the main neutral losses and fragments are indicated.

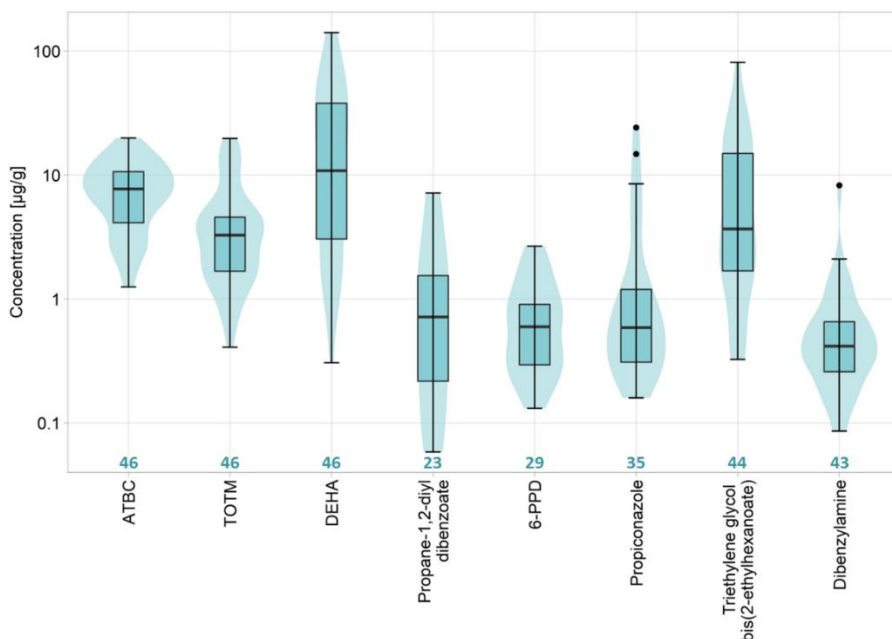
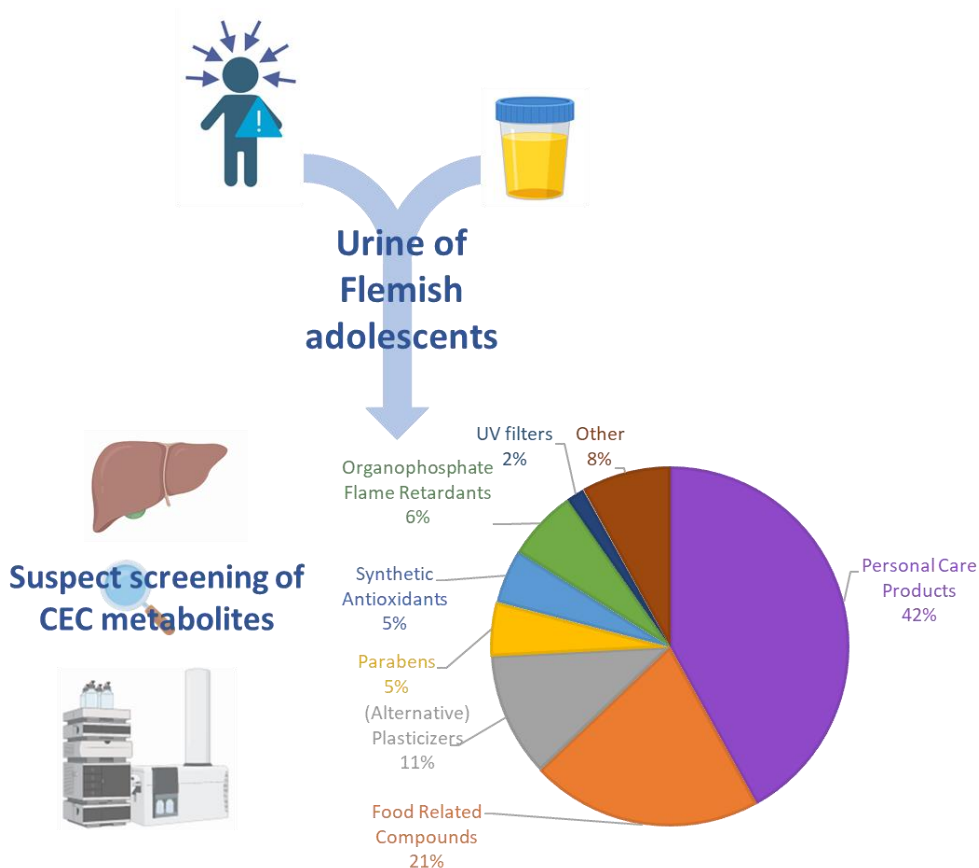


**Figure SI-4.2.4:** Violin plots and boxplots representing the semi-quantified concentrations obtained for compounds belonging to the groups of alternative plasticizers and others detected with a detection frequency  $\geq 50\%$ . The full names corresponding to each of the abbreviations can be found in **Table 4.2.1** and **Table SI-4.2.4**. The presented plots only include datapoints for which a concentration was obtained, thus excluding non-detects. Therefore, for each boxplot/compound the underlying number of datapoints (n) is indicated below the plot.



# Chapter 5: Suspect screening of contaminants of emerging concern and their metabolites in human urine



This chapter is based on the following publication:

Roggeman, M.\*, Belova, L.\*, Fernández, S.F., Kim, D.-H., Jeong, Y., Poma, G., Remy, S., Verheyen, V.J., Schoeters, G., van Nuijs, A.L.N., Covaci, A. Comprehensive suspect screening for the identification of contaminants of emerging concern in urine of Flemish adolescents by liquid chromatography high-resolution mass spectrometry. *Environmental Research*. **2024**. 214(3): 114105. (\*contributed equally)



## 5.1 Introduction

Human biomonitoring (HBM) studies, such as the 4th cycle of the Flemish Environment and Health Study (FLEHS IV, 2016–2020) (Schoeters et al., 2017) aim to assess human exposure to environmental chemicals. These studies are of high importance for the collection of quantitative data on internal exposure to known contaminants. Such chemicals can be monitored using targeted analytical approaches (Smolders et al., 2009) given that precise information about the chemical identity of the analytes and their corresponding reference standards are available. In the scope of the FLEHS IV study, several targeted studies reported biomonitoring results for known biomarkers from various classes such as phthalates, alternative plasticizers (APs), organophosphate flame retardants (OPFRs), polycyclic aromatic hydrocarbons (PAHs), and others (Bastiaensen et al., 2021a; Gys et al., 2021a; Verheyen et al., 2021).

While these studies are indispensable to obtain quantitative biomonitoring data and eventually link the data with health effects and potential exposure pathways, targeted approaches leave CECs undetected (Sauve and Desrosiers, 2014). As a result, a potential internal exposure to CECs cannot be assessed. This gap can be closed by the application of LC-HRMS based suspect screening methods. Thereby, metabolized forms of CECs can be included in the applied suspect list acknowledging that environmental contaminants are often present in human samples in a metabolized form. Thus, the inclusion of the parent compounds alone could potentially lead to a high number of false negative detects (del Mar Gómez-Ramos et al., 2011; Huntscha et al., 2014).

In addition to matching accurate-mass data, the acquired MS/MS spectra can be compared with mass spectral libraries or predicted MS/MS spectra derived from *in silico* prediction tools (Djombou-Feunang et al., 2019; Kind et al., 2018; Ruttkies et al., 2016) to further increase identification confidence. Optimally, within suspect screening studies, confidence levels of up to 2 can be reached based on the scheme proposed by Schymanski et al. if experimental MS/MS spectra can unequivocally be matched with reference data (Schymanski et al., 2014). Despite the high relevance of suspect and non-target analysis of human biological samples using HRMS, research works in this field are still limited (González-Gaya et al., 2021). For example, at the time of analyses conducted within this chapter, only 7 studies on suspect screening of contaminants in urine samples have been published so far, three of them focused on pesticides (Bonvallot et al., 2021; López-García et al., 2019; López et al., 2016), three studying different CECs (Caballero-Casero et al., 2021b; Dolios et al., 2019; Plassmann et al., 2015) and another one investigating occupational exposure to PAHs (Tang et al., 2016).

Even though the described techniques show high potential for the identification of CECs and their metabolites, several limiting factors must be considered within the

development of suspect screening approaches. Despite continuous developments and expansion of mass spectral libraries, the availability of reference MS/MS spectra of novel CECs and their metabolites is limited, hampering compound identification at high confidence levels (Oberacher et al., 2020; Stein, 2012). The analysis of complex human matrices, such as urine, blood, or serum, can be accompanied by considerable matrix effects leading to signal suppression and limiting the detection of exogenous compounds. This is especially challenging since the latter are present at low concentration levels (sub ng/mL range) and can additionally be suppressed by the presence of endogenous compounds, which normally show higher concentrations (Raposo and Barceló, 2021). These limitations indicate that an extensive optimization of each analysis step is crucial to obtain reliable suspect screening results. This issue has been addressed by a previous study conducted by Caballero-Casero et al. in which a comprehensive suspect screening approach for the detection of CECs and their metabolites in urine samples has been described (Caballero-Casero et al., 2021b).

This chapter involved additional optimization steps to the method developed by Caballero-Casero et al. The modified method was then applied to biobanked urine samples of 83 Flemish adolescents participating in the FLEHS IV (2016–2020) aiming to identify additional CECs and their metabolites not included in previous target FLEHS biomonitoring studies. A suspect list previously proposed by Caballero-Casero et al. was further expanded and finally it included >3200 CECs from several compound classes, such as traditional phthalate-based and new non-phthalate alternative plasticizers, organophosphate flame retardants, synthetic antioxidants, UV-light stabilizers, pesticides, and others (Caballero-Casero et al., 2021b). As the study of Caballero-Casero et al. had shown, most CECs were present in urine samples in a metabolized form. However, the inclusion of only the parent compounds in the suspect screening workflow would leave potential metabolites undetected. Consequently, metabolites of all parent compounds corresponding to most commonly observed metabolization reactions (Ballesteros-Gómez et al., 2015; Gys et al., 2018; Testa and Kramer, 2005), namely hydroxylation (Phase I), glucuronidation and methylation (Phase II) were predicted, which resulted in a suspect list containing >12,500 compounds. In particular, the focus of this study was on CECs and metabolites which were not included in the list of targeted analytes available from the FLEHS IV study. The obtained results revealed the complementary value of suspect screening for the analysis of human exposure to environmental contaminants by reporting a high number of CECs and their metabolites which would have remained undetected if targeted screening methods alone are applied. The reported compounds could subsequently be added to the list of targeted analytes of, among others, upcoming FLEHS cycles.

## 5.2 Materials and Methods

### 5.2.1 Chemicals

Methanol (MeOH), acetonitrile (ACN), and formic acid (FA) were purchased from Biosolve BV (Valkenswaard, the Netherlands) ( $\geq 99.9\%$ ). All organic solvents were of LC grade. A PURELAB Flexsystem was used to obtain ultrapure water (18.2 M $\Omega$  cm, Milli-Q, Millipore). Ammonium acetate was purchased from Sigma-Aldrich (eluent additive for LC-MS). A set of 30 native standards of organophosphate and alternative plasticizer metabolites was used for the optimization and the quality control of the sample preparation and the LC-HRMS. Additionally, 13 standards were purchased in order to confirm the identity of compounds assigned within the suspect screening approach. The name, formula, and further identifiers of both sets of compounds are summarized in **Table SI-5.1**. Samples were spiked with nine isotopically labelled IS which are summarized in **Table SI-5.2**. Working solutions of IS were prepared at a concentration of 300 ng/mL in MeOH.

### 5.2.2 Sample selection

The spot urine samples investigated in this study were selected from the biobanked samples stored at  $-20^{\circ}\text{C}$ . Samples were collected between September 2017 and June 2018 as part of the FLEHS IV reference biomonitoring study (2016-2020). The study was approved by the Ethical Committee of the University Hospital of Antwerp, Belgium (Belgian Registry Number: B300201732753). For the participants of the FLEHS IV reference population (428 adolescents, 14-15 years), quantitative data on the exposure to a set of known contaminants was available since the samples had already been investigated within previous targeted biomonitoring studies (Bastiaensen et al., 2021a; Gys et al., 2021a; Verheyen et al., 2021). Based on the 45 quantified chemicals studied in these targeted biomonitoring studies, Buekers et al. calculated the exposure load of a participant (Buekers et al., 2021). Participants were scored based on their exposure to each chemical as opposed to a threshold, placed at the 50<sup>th</sup> percentile (P50) of the FLEHS IV cohort. A value of 0 was assigned if the exposure was below the P50, and 1 if the concentration was above P50. This exposure load, therefore, summarizes the overall exposure above the threshold (P50) for 45 known contaminants belonging to the phthalates, APs, OPFRs, PAHs, bisphenols and others. In total 83 urine samples were selected according to the following objectives: The exposure load sum (EL) was used to select the samples for analysis with the primary objective of including high and low exposure load groups. The high exposure group consisted of 43 samples with the highest exposure load, which was ( $\geq 27$ ). The low exposure group consisted of the 39 lowest

exposure load samples ( $\leq 17$ ). The second objective for sample selection was to have a balanced distribution across sexes. Based on the first objective of the exposure load, urine samples of 47 male and 36 female participants were selected. Since this distribution was considered balanced, no further intervention was made to ensure the maximal potential of the EL. The distribution stayed balanced when considering the EL, resulting in 19 female and 20 male participants in the low exposure group, and 17 female and 27 male participants in the high exposure group. Specific gravity was measured on the selected urine samples by employing the hand refractometer (RF .5612) from EUROMEX microscopes (Holland).

### 5.2.3 Sample preparation

Glass tubes were thoroughly cleaned (rinsed with water, acetone and baked at 300 °C). Urine spot samples were collected in clean metal-free polyethylene containers; they were kept at 4°C and processed within 24 h. Samples were divided into aliquots in glass vials and kept at -20°C until analysis. A 750  $\mu$ L aliquot of urine was transferred to the precleaned tubes and centrifuged for 5 min at 3,500 rpm. Then, 500  $\mu$ L of the supernatant were transferred to a clean glass tube and spiked with the IS working solution at 30 ng/mL (final concentration in urine) and vortexed. Captiva® non-drip lipid cartridges (3 mL, Agilent Technologies, Santa Clara, USA) were used for sample clean-up. One milliliter of ACN (with 0.1% formic acid, v/v) was added to the cartridge, immediately followed by the addition of the spiked urine. The solution in the cartridge was then carefully mixed and collected by push out. The obtained eluate was stored overnight at -20 °C. Then, 500  $\mu$ L of the solution were filtered through a centrifugal nylon filter of 0.2  $\mu$ m (VWR, Leuven, Belgium) for 5 min at 3,500 rpm, to ensure filtration of solids and precipitated material. Optimization of the applied sample preparation method can be found in Supplementary Information **SI-T5.1**.

### 5.2.4 Instrumental analysis

All measurements were conducted on an Agilent 6560 QTOF-MS coupled to an Agilent Infinity II UPLC (ultra-high performance liquid chromatography; Agilent Technologies, Santa Clara, USA). The instrument was equipped with a Dual Jet Stream ESI source. For chromatographic separation, an InfinityLab Poroshell 120 EC-C18 column (3.0 x 100 mm, particle size 2.7  $\mu$ m) equipped with a guard column (3.0 x 5 mm) of the same stationary phase was used. Column temperature was maintained at 35 °C. The mobile phases consisted of ultrapure water (A) and MeOH (B). As modifiers, 0.1% FA (v/v) and 5 mM ammonium acetate were added for positive and negative ionization modes, respectively. The flow was maintained at 0.3 mL/min with an injection volume of 3  $\mu$ L.

For both ionization polarities, the following gradient was applied: 5% B - 50% B (0-3 min), 50% B - 80% B (3-5 min), 80% B - 100% B (5-16 min), 100% B - 5% B (16-16.5 min), 5% B (16.6-21 min).

The mass spectrometer was operated in 2 GHz, extended dynamic range mode. The ESI source parameters of the Agilent 6560 were based on the optimized values proposed by Caballero-Casero et al. with slight modifications (Caballero-Casero et al., 2021b): Sheath and drying gas temperatures were set to 300 °C and 250 °C, respectively, with a flow rate of 12 L/min for both. Voltages of 3000 V, 500 V, 300 V and 65 V were applied for the capillary, nozzle, fragmentor and skimmer, respectively. Nebulizer pressure was set to 35 psi.

Both MS and MS/MS spectra were acquired in a mass range ranging from  $m/z$  50 to 1500. Data dependent acquisition mode was used whereby four precursors per acquisition cycle were automatically selected for fragmentation based on their abundance. The quadrupole isolation width was set to 'narrow', and collision energies of 10, 20 and 40 eV were applied.

### 5.2.5 Quality control

The quality of the analyses was assured by several measures to obtain reliable results. Samples were prepared in batches of 20 and one batch of 3 samples, two QC samples of which one consisted of Milli-Q water spiked with native standards (**Table SI-5.1**) (30 ng/mL) and IS (**Table SI-5.2**), and one of pooled urine spiked with IS were added to each batch. Additionally, two procedural blanks (Milli-Q water) were included per batch. Each QC sample was prepared applying the same workflow as for real urine samples (**chapter 5.2.3**). Standards of native compounds (10 ng/mL) (**Table SI-5.1**) solubilized in methanol were directly injected into the LC at the beginning and end of the sequence to monitor the stability of RTs and instrument sensitivity. Pooled urine samples spiked with IS (**Table SI-5.2**) were prepared to ensure the detectability of the IS in a pooled matrix, as well as ensuring instrument sensitivity. Procedural blanks were used to monitor potential background contamination during batch preparation or analysis.

Additionally, a solvent blank (MeOH) was injected (every 5 samples) to monitor potential carryover during the sequence. All urine samples were spiked with the IS working solution to monitor potential analyte losses during sample preparation. During analysis, a reference mass solution was continuously infused to ensure automatic mass calibration. The mass calibration was based on ions with  $m/z$  121.0509 and 922.0098, as well as  $m/z$  119.0363 and 980.0164 for positive and negative ionization modes, respectively. The intensity of the reference mass ions was also monitored as an additional

indicator for potential signal suppression due to matrix effects and instrumental variation.

## 5.2.6 Data analysis

### 5.2.6.1 Data processing

First, an in-house suspect list containing chemical information (Name, molecular formula, exact monoisotopic mass, and canonical SMILES) of different classes of CECs was compiled. It was based on previously published lists deriving from Caballero-Casero et al., the NORMAN Suspect List Exchange and the European Human Biomonitoring project (HBM4EU) (Caballero-Casero et al., 2021b; Govarts et al., 2020; Meijer et al., 2021). A total number of 3221 compounds, including synthetic antioxidants, plasticizers, organophosphate flame retardants, personal care products, UV filters, food additives, and pesticides, were included. For the prediction of biotransformation products, hydroxylation (Phase I), as well as O- and N-glucuronidation and methylation (both Phase II) were selected. On the molecular level, hydroxylation, O- or N-glucuronidation and methylation correspond to the addition of oxygen (O), C<sub>6</sub>H<sub>8</sub>O<sub>6</sub> and CH<sub>2</sub> to the molecular formula of the parent compound, respectively. To predict each of the three considered metabolization reactions for each compound included in the suspect list, the corresponding amounts of C, O and/or H atoms were added to the molecular formulae through an in-house developed R script (RStudio, version 2021.09.1). At this stage, the predicted molecular formula have not been accessed on the probability of their occurrence. This step was performed after matching the suspect list as described below. Molecular formulae and exact monoisotopic masses of the generated metabolites were incorporated in the suspect list, containing > 12,500 compounds in total.

The suspect screening workflow was based on a previously developed approach with slight modifications (Caballero-Casero et al., 2021b) as displayed in **Figure 5.1**. Two HRMS datasets (one in positive and one in negative ionization polarity) were analyzed applying the same suspect screening workflow.

First, mass accuracy, isotopic pattern, and stability of RT and intensities (area and height) for IS (**Table SI-5.2**) in all samples (with the exception of solvent blanks) were checked using the 'Find By Formula' (FbF) algorithm in MassHunter Qualitative Analysis (version 10.0, Agilent Technologies, Santa Clara, USA). Similarly, the native standards (**Table SI-5.1**) were analysed in the spiked miliQ standards and the standards that were directly injected into the LC system. Then, molecular feature extraction (peak picking and deconvolution) and alignment of the batch data files were performed using the 'Batch recursive feature extraction' algorithm for small organic molecules in MassHunter Profinder (version 10.0, Agilent). The following settings were applied: i) considered ion

species:  $[M+H]^+$  and  $[M+Na]^+$  in ESI+, and  $[M-H]^-$  in ESI-; ii) a peak height above 2000 counts; iii) a mass tolerance of 20 and 25 ppm, for parent and product ions, respectively; iv) a maximal RT variation of  $\pm 0.3$  min; and v) a match score above 70. A match score has a range from 0-100 and takes into account accurate mass, isotope abundance, isotope spacing and RT.

After performing a principal component analysis to investigate the general grouping of the different sample types, features were filtered by fold change (FC) analysis applying a  $FC > 5$  between samples and procedural blanks, performed using the Mass Profiler Professional software (version 15.0, Agilent). Next, MassHunter ID Browser (version 8.0, Agilent) was used for compound annotation. The filtered molecular features were screened against the in-house suspect list. The criteria for screening were based on Caballero-Casero et al. and were as followed: i) a mass tolerance of 7 ppm for parent ions, to account for instrument deviation; ii) an isotope abundance score (measured vs predicted) of at least 80, strengthening the match of a feature to a suspected molecular formula; and iii) a match score above 75.

Finally, a manual inspection of each annotated compound in each urine sample was performed using the FBF algorithm in MassHunter Qualitative Analysis. When no fragmentation spectra were available, if only one molecular formula satisfactorily explained the MS spectra of a tentative annotation according to the abovementioned criteria (mass tolerance: 7 ppm, isotope score  $> 80$ , and match score  $> 75$ ), it was directly assigned as CL4. Otherwise, a combination of *in silico* fragmentation tools, such as ACD/MS Fragmenter (version 2019.1.3, Advanced Chemistry Development Inc., Toronto, Canada) and CFM-ID 4.0 (Wang et al., 2021), and mass spectral databases, such as mzCloud (HighChem Ltd., Bratislava, Slovakia) and MassBank (Horai et al., 2010), were used to check all fragmentation spectra of tentatively identified compounds. A fragmentation spectrum was considered as matched if at least two fragments matched the reference data at all applied collision energies or when at least three fragments matched the reference data for 2 applied collision energies. In addition, The identification of compounds was based on the confidence level system introduced by Schymanski et al. with the addition of CL 2C (Schymanski et al., 2014). CL 2C was defined as a feature for which no fragmentation spectra were available but for which the RT was within a 0.2 min window in comparison to a reference standard. A diagram of the criteria for the assignment of an identification CL is presented in **Figure 5.1**.

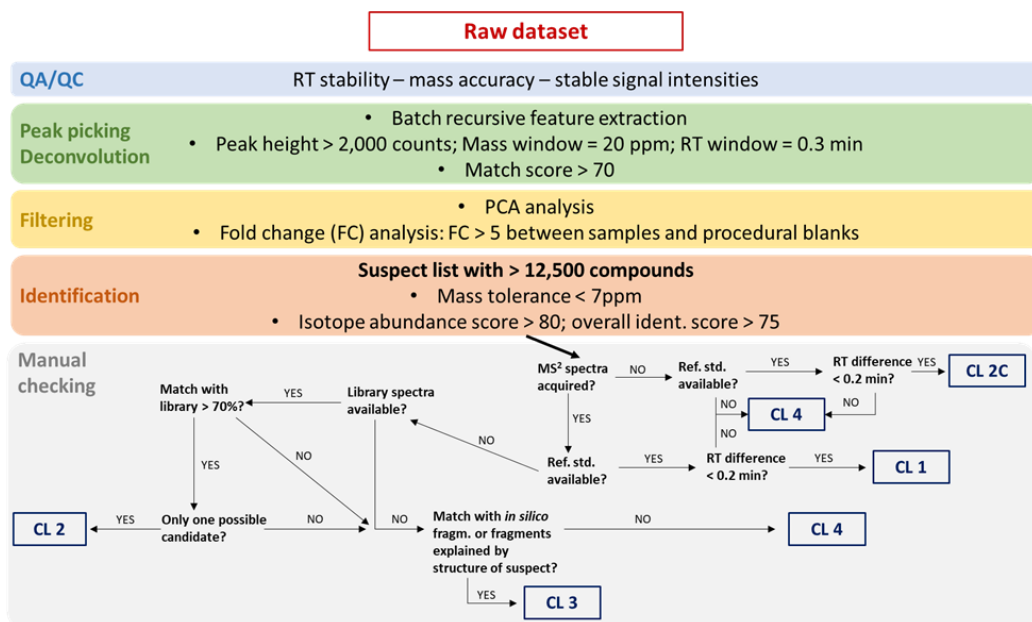


**Figure 5.1:** Diagram summarizing the different steps, cut-off values and criteria used in the suspect screening workflow for the detection and identification of CECs in human urine. CL: confidence level.

When a predicted metabolite was tentatively identified, the feasibility of its occurrence in the human body was evaluated considering its structure and the functional groups in which metabolism reactions could take place (Testa and Krämer, 2006). In addition, annotated endogenous compounds that were not classified under any CEC group were removed from the final results. If more than one isomer could be potentially assigned to a feature, and the experimental data did not allow a distinguishment, all possible isomers are reported. Ultimately, commercially available reference standards were purchased for the compounds assigned with CL 2. The standards were injected applying the same chromatographic conditions (**chapter 5.2.4**). The data obtained from the standard injection was used for the confirmation of compound assignment (CL 1) applying the same cut-offs as mentioned above. Thereby, CL 1 was assigned if all experimental data (exact mass, isotopic pattern, RT and MS/MS spectra) could be matched with the reference standards. In case, no fragmentation spectra were acquired, CL 2C was assigned to the corresponding samples.

### 5.2.6.2 Statistical analysis

For each sample, the total number of detected compounds was submitted to R (RStudio, version 2021.09.1) indicating the assigned CL of identification. From the submitted data, the number of compounds detected at CL 3 and CL 4 or better was calculated.

For all statistical analysis, an in-house R script (RStudio, version 2021.09.1) was applied. The ggplot2 package (version 3.3.5) was used for data visualization. The density plots of both the number of compounds annotated at CL 1-3 and CL 1-4, were visually investigated to ensure the normal distribution of the data. Subsequently, numbers of annotated compounds were compared between low and high exposure groups through a two-sample t-test ( $p < 0.05$ ). For the comparison between high and low exposure groups, the dataset was additionally split in two groups based on sex. The statistical analysis aimed at testing the hypothesis that the exposure to CECs is expected to be significantly higher in the high exposure load group in comparison to the low exposure load group.

## 5.3 Results and Discussion

### 5.3.1 Quality control results

All urine samples were spiked at 30 ng/mL with the mixture of labelled IS. The detectability of the IS in the samples was on average 95%, ranging from 83% for chlorpyrifos- $d_{10}$  to 100% for diphenyl phosphate- $d_{10}$  (or DPHP- $D_{10}$ ),  $^{13}C_4$ -2-(((2-ethylhexyl)oxy)carbonyl)benzoic acid (or  $^{13}C_4$ -oxo-MEHP),  $^{13}C_6$ -methyl 4-hydroxybenzoate (or  $^{13}C$ -methylparaben) and  $^{13}C_3$ -3,5,6-trichloro-2-pyridinol (or  $^{13}C$ -TCPY). Detection frequencies for each individual IS can be found in **Table SI-5.3**.

The RTs of IS in the samples were investigated to estimate the stability of the LC system. The RTs were stable with a standard deviation between 0.01 and 0.03 min. A FC analysis was applied to subtract the background features present in the samples. A feature was eliminated if it had an abundance less than 5 times higher than the average abundance of the feature in the procedural blanks. This allows the analysis of compounds such as, for example, the low molecular weight plasticizers that are present as a contamination in the blanks but show a more than 5-fold higher abundance in urine. This is caused by their presence in the indoor and laboratory environment leading to low-level contamination in the procedural blanks. For the blank control samples, the number of features that matched the suspect list is reported. For solvent blanks, the number of detected features was 175 and 135 in positive and negative ionization modes, respectively. For procedural blanks, 543 and 1011 features were detected in positive and negative ionization polarities, respectively. The high number of features detected could be caused by the low abundance cut-off in data analysis, necessary for the detection of low abundant metabolites. For standards of native compounds injected at the beginning and end of the sequence, variance stayed within expected values. All compounds were detected, RT variation was below 1%, area variation of (alternative) plasticizers was between 0.02-23.1% for 6-hydroxy monopropylheptylphthalate (6OH-MPHP) and

mono(2-ethyl-5-hydroxyhexyl) adipate (5OH-MEHA), respectively, and area variation of OPFRs was between 0.21-43.7% for 3-hydroxyphenyl diphenyl phosphate (3OH-TPHP) and 5-hydroxy-2-ethylhexyl diphenyl phosphate (5OH-EHDPHP), respectively.

Ten compounds detected in the FLESH IV target studies that had DF close to 100% (Bastiaensen et al., 2021a; Gys et al., 2021a; Verheyen et al., 2021) were selected as positive controls for the suspect screening approach (**Table SI-5.4**). The DF was between 15% for mono-carboxy isodecyl phthalate and 100% for mono-n-butyl phthalate. A lower DF was expected due to the lower sensitivity of the instrumental method, the less selective sample preparation and chromatographic method. Additionally, mentioned target studies used deconjugation steps resulting in measurements of aglycons only which can contribute to higher sensitivity. Moreover, annotation at a CL better than 4 was not feasible for most of the compounds, due to the absence of MS/MS spectra.

### 5.3.2 Suspect screening results

After method optimization and the evaluation of QA results, the samples were analyzed following the procedure described in **chapter 5.2.6**. The matching of the created suspect list against the filtered set of features resulted in a total of 1806 and 1677 hits in positive and negative ionization polarities, respectively. However, the number of the matched compounds was lower, as several compounds appeared in the reported list of hits several times at different RTs. Each compound was manually investigated aiming to assign a confidence level of identification following the considerations described in **Figure 5.1**. Here, only compounds assigned with a CL 3 or better (thus lower) in at least one sample are reported, since the assignment of CL 4 (throughout all samples) allows only a proposal of a tentative molecular formula without any additional information about the structure of the (potential) contaminant. Such tentative reporting was outside the scope of this study and would not allow the interpretation of potential adverse effects of the equivocally annotated contaminants.

Additionally, the assignment of CLs for the annotation of glucuronidated metabolites was challenging. As for all other compounds annotated at CL 3, this level was assigned to a glucuronidated metabolite if fragmentation spectra were obtained which provided additional experimental evidence for the compound's identity. Most of the glucuronidated conjugates included in the suspect list are derived from *in silico* prediction of metabolites, none of the annotated glucuronidated metabolites could be assigned with CL 2 as no library spectra were available. Furthermore, the observed fragmentation spectra only allowed the unequivocal identification of the glucuronide moiety since in most cases no fragments or only one fragment corresponding to the molecular ion of the parent compound could be assigned, not allowing to draw structural conclusions. As an

example of this limitation, the fragmentation spectrum of the glucuronidated form of mono(2-ethyl-5-hydroxyhexyl) adipate is shown in **Figure 5.2**. The structure of the glucuronide moiety is confirmed by the corresponding fragment ( $[C_6H_9O_7]^-$ ; theoretical  $m/z$  193.0354), derived from the glucuronide moiety and not from the parent compound, since the same fragments appeared in several library spectra of other known glucuronides. Only a few other characteristic fragments deriving from this moiety were observed in the mass range between  $m/z$  50 and 200, providing limited information about the structure of the parent compound. It can only be confirmed by the observed molecular ion ( $[C_{14}H_{25}O_5]^-$ ; theoretical  $m/z$  273.1707) and two losses of water. None of the fragments below  $m/z$  200 could be assigned to the parent compound. It was suspected that the fragmentation spectrum of the parent compound was suppressed by the fragments of the presumably better ionizing glucuronide moiety. The same effect was observed for most other glucuronides reported in this study and must be considered within the interpretation of the results. Nevertheless, the assignment of CL 3 was considered to be acceptable in these cases, since the observed fragments confirmed the presence of a glucuronide moiety, and the molecular ion of the parent compounds was observed.

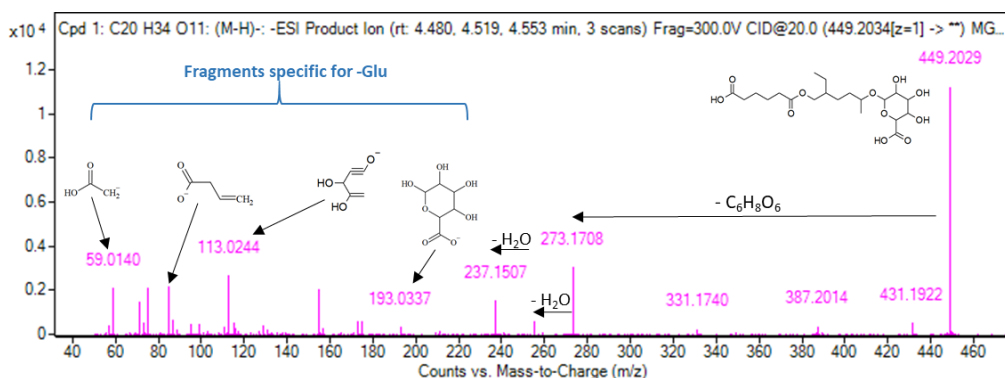


**Figure 5.2:** Example of a fragmentation spectrum of a glucuronidated metabolite. The fragmentation spectrum and the proposed structure of the glucuronide of mono(2-ethyl-5-hydroxyhexyl) are shown. For selected fragments specific for the glucuronide moiety proposed structures are indicated.

After manual investigation of all matched candidates, 63 compounds were reported with a CL 3 or better. These compounds belonged to eight different compound classes as summarized in **Figure 5.3**. These classes included PCPs (42%), food related compounds (21%), APs (11%), OPFRs (6%), synthetic antioxidants (5%), parabens (5%), UV-filters (2%) and others (8%). All the compounds that are a part of the class of food related compounds have additional uses as personal care products. The different metabolization reactions (**Figure 5.3-B**) show the high fraction of metabolites found, especially the glucuronidation metabolites. The distribution of the CLs (**Figure 5.3-C**)

shows that higher identification levels are most likely for classes of parent compounds for which, reference spectra and standards are available.

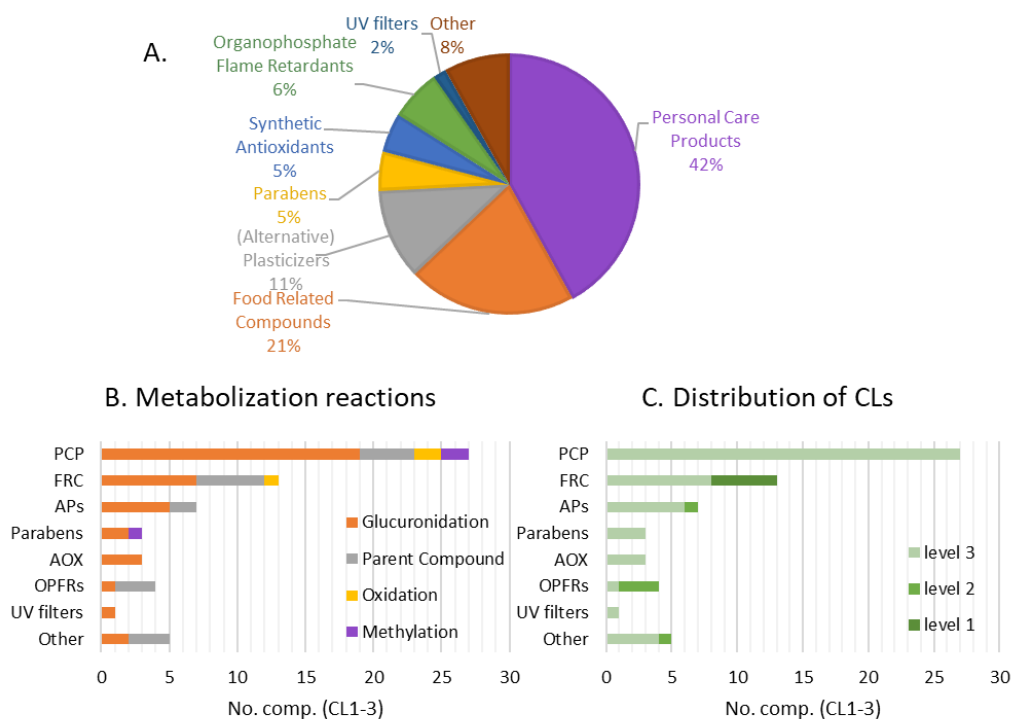


**Figure 5.3:** Overview of the compound classes which were included in the 63 compounds detected in urine samples. A) pie chart showing the distribution of the different classes. B) the distribution of the different metabolization products and the parent compounds for each class. C) distribution of the Confidence levels for each class. Abbreviations: PCP; personal care product, FRP; food related compounds, APs; (Alternative) plasticizers, AOX; Synthetic antioxidants, OPFRs; phosphate flame retardants.

After completing the suspect screening data analysis workflow, from the 63 annotated compounds, 13 compounds were assigned with CL 2. For all CL2 compounds, commercially available reference standards were purchased in order to confirm the annotations (**Table SI-5.1**). For five compounds, all experimental data (exact mass, isotopic pattern, RT and MS/MS spectra) could be matched with the reference standards using the same mass tolerance window as described above resulting in five CL1 identifications. For four compounds, no MS/MS spectra were acquired within sample analysis resulting in fewer identifiers available for compound confirmation. Therefore, level 2C was assigned (**Table 5.1**).

Ultimately, the purchase of reference standards revealed three false positive annotations: Based on the comparison with in silico predicted MS/MS spectra, three compounds (Catechol, Benzyl alcohol and 8-Hydroxyquinoline) were initially assigned

with CL2. However, the RTs observed for the corresponding reference standards did not match the samples' data which led to the removal of the mentioned compounds from the results.

All results of CL1 and CL2 assignments are summarized in **Table 5.1**, indicating their name, formula, RT, compound class, CL and DF. For each PCP, the subcategory was retrieved from the Chemical and Products Database (CPDat) (Williams et al., 2017). Of the summarized compounds (n = 10), six were assigned to the class of food components/additives, although they are also used as PCPs.

**Table 5.1:** Summary of compounds detected at confidence level 1 or 2. For each compound the name, formula, retention time (RT), detection polarity, confidence level (CL), compound class and detection frequency (DF) are indicated.

Name	Formula	RT [min]	Polarity	CL	Class	DF [%]
L-/D-Pantothenate	C <sub>9</sub> H <sub>17</sub> NO <sub>5</sub>	2.75	-	1	Food, PCP	68.7 (CL 1); 16.9 (CL 2C)
4-hydroxy-benzaldehyde	C <sub>7</sub> H <sub>6</sub> O <sub>2</sub>	4.99	-	1	Food, PCP	36.1 (CL 1); 49.4 (CL 2C)
Diphenyl hydrogen phosphate	C <sub>12</sub> H <sub>11</sub> O <sub>4</sub> P	6.02	-	2C	OPFR.met	43.4 (CL 2C)
Bis(1,3-dichloro-isopropyl) phosphate	C <sub>6</sub> H <sub>11</sub> Cl <sub>4</sub> O <sub>4</sub> P	6.56	-	2C	OPFR.met	25.3 (CL 2C)
2-ethyl hexyl phenyl phosphate	C <sub>14</sub> H <sub>23</sub> O <sub>4</sub> P	7.67	-	2C	OPFR.met	1.2 (CL 2C)
Theobromine	C <sub>7</sub> H <sub>8</sub> N <sub>4</sub> O <sub>2</sub>	3.78	+	1	Food, PCP	84.3 (CL 1)
Theophylline	C <sub>7</sub> H <sub>8</sub> N <sub>4</sub> O <sub>2</sub>	4.17	+	1	Food, PCP	61.4 (CL 1) 2.4 (CL 2C)
Phthalic anhydride	C <sub>8</sub> H <sub>4</sub> O <sub>3</sub>	4.88	+	2	Plasticizerm etabolite	6.0 (CL 2); 74.7 (CL 4)
Riboflavin	C <sub>17</sub> H <sub>20</sub> N <sub>4</sub> O <sub>6</sub>	4.92	+	1	Food, PCP	18.1 (CL 1); 39.8 (CL 2C)
Isoquinoline	C <sub>9</sub> H <sub>7</sub> N	4.99	+	2C	Food, Other	74.7 (CL 2C)

For example, theobromine, theophylline, riboflavin (or vitamin B<sub>2</sub>) and pantothenate (or vitamin B<sub>3</sub>), identified at CL1 in 84, 61, 18 and 69% of the urine samples, respectively, are more likely to originate from food (plants) (Kim et al., 2021) than from PCP exposure. This may provide an explanation for their detection in most samples. Moreover, theophylline is a prescription drug as a bronchodilator for asthma and chronic obstructive pulmonary disease (COPD) (National Institute for Health and Care Excellence [NICE], 2017). Theobromine and theophylline have been also identified in a previous suspect screening study on breast milk samples (Baduel et al., 2015). Another compound commonly present in food but as a flavoring agent, named isoquinoline, was detected

with a DF of 25% at CL 2 and 35% at CL 4. Apart from dietary intake, exposure to this compound may occur through cigarette smoke and it is also used in the chemical industry as an intermediate (National Library of Medicine USA, 2019).

Among the OPFRs investigated in this research, 2-ethyl hexyl phenyl phosphate (EHPHP), a specific metabolite of ethyl hexyl diphenyl phosphate (EHDPHP), diphenyl hydrogen phosphate (DPHP), a non-specific biomarker of EHDPHP and TPHP (Van den Eede et al., 2016), and bis(1,3-dichloro-isopropyl) phosphate (BDCIPP), a specific metabolite of tris(1,3-dichloro-isopropyl) phosphate (TDCIPP), were detected at CL 2, with DFs of 1%, 43%, and 35%, respectively. EHDPHP is an organophosphate used as a plasticizer in food-contact materials and other consumer products (Poma et al., 2017), and TDCIPP, which has been associated with reproductive, dermal and endocrine effects in humans (Meeker and Stapleton, 2010), is used in upholstered furniture and decorative materials. Human exposure to these compounds is predominantly caused by the ingestion of contaminated food and indoor dust, and to a lesser extent by dermal contact (Cequier et al., 2014; Poma et al., 2017; Poma et al., 2018). The detection of these PFR metabolites is in agreement with previous results of target studies on Flemish adolescents (Bastiaensen et al., 2021a). In addition, other PFRs and their metabolites, mainly tris-chloro-organophosphates, have also been identified in two previous suspect screening studies on urine (Dolios et al., 2019) and breast milk samples (Baduel et al., 2015), confirming the ubiquitous human exposure to this compound class.

**Table SI-5.5** summarizes the name, formula, RT, compound class, CL, and DF of the 53 compounds annotated at level 3 in the 83 urine samples. Out of the 53 compounds, 39 were PCPs, 6 alternative plasticizers, 3 antioxidants, 3 parabens, 1 UV-filter, 1 OPFR, among others. Among the potential candidates, 15 were also food components/additives. Due to the lack of libraries with reference MS/MS spectra of metabolites, most compounds with CL 3 were predicted metabolites (85%), with glucuronides being the most abundant ones (77%), followed by methylated (6%) and hydroxylated (4%) compounds. The most relevant findings and compounds annotated at CL 3 with a high DF are discussed in the following paragraphs.

Among PCPs, the most frequently detected compounds were L-/D-pyroglutamic acid (DF = 98.8% at CL3), an (uncommon) amino acid derivative that is naturally present in some plants (Wishart et al., 2022) and is also used in cosmetic products, benzyl alcohol (DF = 79.5% at CL3 and 20.5% at CL4), which is a flavoring agent also used as a solvent in the production of perfumes, naphthylamine (DF = 44.6% at CL3 and 55.4% at CL4), a urinary biomarker of exposure to amino and nitro PAHs (He et al., 2021; Niu et al., 2018; Yu et al., 2020), two metabolites of nail conditioning products, i.e. the oxidation product of 1-N-(2-methoxyethyl)-benzene-1,4-diamine (DF = 75.9 % at CL3 and 24.1% at CL4) and the glucuronide of 2-carboxyethyl acrylate (DF = 94% at CL3) (Dionisio et al., 2018), and

the glucuronide of (4Z)-hept-4-en-2-yl salicylate (DF = 18.1% at CL3 and 78.3% at CL4), normally used in fragrances. Most of these compounds have not been extensively addressed yet in HBM studies.

For parabens, the most abundant metabolites were the methylated products of butyl paraben (DF = 80.7% at CL3 and 19.3% at CL4), although no information about the methylation of parabens in the human body has been published in the literature yet. Glucuronides of benzyl paraben isomers or benzophenone-3 (both have the same molecular formula), as well as isomers of propyl paraben were also detected in more than 40% of the samples, but less than 4% could be assigned with a CL 3. Baduel et al. and Tran et al. have also identified parent compounds of these and other parabens in breast milk and human serum samples by suspect screening strategies (Baduel et al., 2015; Tran et al., 2020).

For APs, mono(2-ethylhexyl) adipate derivatives (Gluc-MEHA, 5-OH-MEHA and Gluc-5-OH-MEHA), which are metabolites of bis(2-ethylhexyl) adipate, were annotated at CL 3 with DFs between 6 – 24%, which are in line with the targeted results of the FLEHS study (Bastiaensen et al., 2021a). In addition, glucuronidated conjugates of phthalates, i.e. MEHP, MnBP, MiDP and MiNP, were found at CL 3 with DFs between 2 - 17%, although these compounds were detected in more than 30% of the samples in the targeted FLEHS study. This difference is assumed to be caused by the lower sensitivity of suspect screening approaches compared to the targeted methods (Bastiaensen et al., 2021a). Unconjugated compounds of these phthalates have been previously reported by a suspect screening study on human serum with DFs up to 90% (Gerona et al., 2018).

### 5.3.3 Comparison with literature

Several compounds identified/annotated here, such as Irganox 1135, methylated products of parabens and some glucuronides, have not been previously determined in HBM studies on urine (Bonvallot et al., 2021; González-Gaya et al., 2021; López-García et al., 2019; López et al., 2016). As an example, Plassman et al. performed a suspect screening study on CECs, which were also included in the present research, but only tentatively identified less than 10 compounds, most of them food items. The study did not report any of the compounds identified/annotated here, which may be due to the differences in the applied methodologies (Plassman et al., 2015). Other compounds, i.e. metabolites of pesticides (Bonvallot et al., 2021; González-Gaya et al., 2021; López-García et al., 2019; López et al., 2016), OPFRs (Dolios et al., 2019), and PAHs (Tang et al., 2016) have been previously identified in urine samples using other suspect and non-target strategies. However, the chemicals and metabolites found in those studies were not detected in the present study, probably because the sample preparation approach was

not optimized for these specific contaminant groups and/or since these groups were not included in the applied suspect list. In other studies, some parabens and phthalates, that were annotated here as conjugated metabolites, were identified in breast milk (Baduel et al., 2015) and serum samples (Gerona et al., 2018) as unmetabolized compounds.

Compared to a previous suspect screening approach which also aimed to identify CECs in urines of the FLEHS IV (Caballero-Casero et al., 2021b) a higher number of CECs were annotated in the present study (63 compounds compared to 45 for Caballero-Casero et al. at CL 3 or better). This is assumed to be caused by the larger suspect list and the higher number of analyzed samples (50 vs. 83). In addition, some differences were observed in the classes of annotated compounds. For example, most of the features reported in the present study were matched with PCPs (42%) and no pesticides were detected, while Caballero-Casero et al. found more frequently plasticizers (40%) than PCPs (31%), and 7% of the detected compounds were matched with pesticides and/or their metabolites (Caballero-Casero et al., 2021b). However, similar findings were observed when comparing parent compounds with metabolites, since in both studies more than 60% of the tentatively identified compounds were predicted metabolites, predominantly glucuronides. Due to the lack of native standards of glucuronide conjugates, a deconjugation step would be necessary if targeted methods are used to quantify these compounds in urine samples.

The high number of reported compounds indicates that the applied suspect screening approach is a valuable tool for the detection of unknown CECs and their metabolites. These reported compounds would remain undetected if only targeted biomonitoring approaches would have been applied. Nevertheless, the annotation of only 63 compounds at CL 3 or better using a suspect list of >12,500 entries indicates limitations of the applied workflow. Firstly, inclusion of possible metabolization products decreases false negative annotations as opposed to only using the parent compound. However, adding metabolization products based on molecular formula largely increased the entries in the suspect list making it unfeasible to include all possible metabolization reactions. In addition, it should also be noted that in this study only 3 metabolization reactions have been included in the predictions. Although these are the most frequent, other metabolization reactions, such as formation of higher oxidation states (Phase I) and sulfation (Phase II), are not negligible. Moreover, in an *in vivo* scenario metabolization products can be based on several metabolization reactions, of special mention is the combination of hydroxylation and glucuronidation. It is recommended to include these in future studies. Alternatively, predictions software can be used resulting in a higher chance of including realistic metabolites in the suspect list. However, this approach is currently not feasible with large amounts of entries. Secondly, the applied acquisition approach (DDA) fragments the 4 most abundant features at a given time, resulting in a

limit of fragmentation spectra generated. Other techniques such as iterative MS/MS expand on the number of fragmentation spectra generated but increase the analysis time by at least 3-fold (Koelmel et al., 2017). For an increase in the annotation of compounds at CL2 or better further improvements of the available reference mass spectral libraries or of the available standards are needed (Picardo et al., 2021). Furthermore, the application of novel approaches in data processing, such as in silico deconjugation methods, could allow resolving the above-described challenges within the identification of glucuronidated metabolites (Huber et al., 2022).

### 5.3.4 Statistical analysis

The numbers of assigned compounds were compared between high and low exposure groups in order to investigate whether a significant difference could be observed (Figure 5.4).

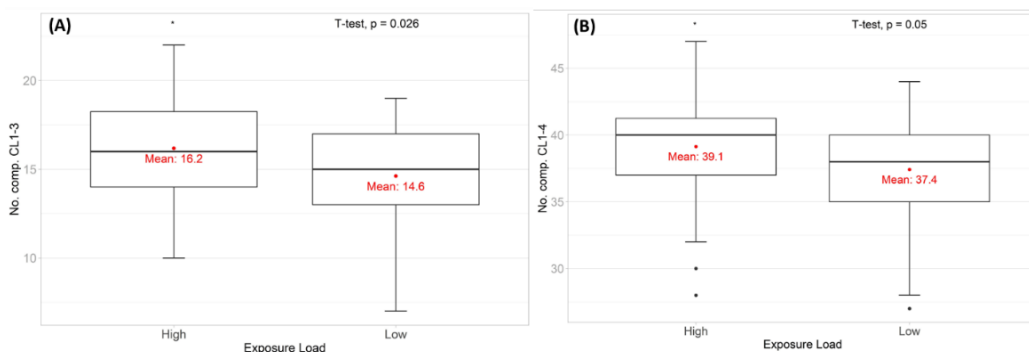


**Figure 5.4:** Boxplots representing the number of annotated compounds in the low and high exposure load groups. (A) Only compounds annotated at CL 3 or better are considered. (B) All compounds reported in this study (i.e. CL 1-4) are considered. (\*) Significant difference between mean values ( $p < 0.05$ ).

The comparison was made including only compounds assigned at CLs 1-3 as well as all compounds reported (i.e., assigned CLs 1-4). In both cases, the number of assigned compounds differed significantly ( $p < 0.05$ ) between the high and low exposure groups. When considering only compounds assigned with CLs 1-3 mean values of 16.2 and 14.6 were observed for the high and low exposure groups, respectively. To further investigate which compounds contribute to the observed significant difference, the number of detections at CL 1-3 was compared between the high and low exposure groups for each compound separately. Of the 63 reported compounds, for 41 compounds the number of detections was higher in the high exposure group. However, it should be noted that the total number of samples in the high exposure group was 44, while the low exposure group contained 39 samples. Therefore, for compounds whose DFs differed by less than five detects, the observations might be biased by the slight differences in the sample size. Therefore, only compounds which differed by at least five detects between the high and

low exposure groups (n = 13) are considered as the major contributors to the observed significant differences. Ten out of the 13 compounds belong to the class of PCPs which is in line with the fact that most compounds reported in this study belong to this group.

**Figure 5.5** shows the comparison of high and low exposure load groups divided by sex. Only compounds assigned with CL 1-3 were considered. This approach showed that the observed significant differences were caused by the significantly different numbers of detected compounds in high and low exposure load samples from female participants ( $p = 0.0038$ ). For samples from male participants, no significant differences could be observed. It is assumed that PCPs, which were the most frequently detected compound group in this study, are used more often or more extensively among females. Yet, no significant differences for neither of the sexes could be observed between high and low exposure load groups when CL 4 compounds were considered (**Figure SI-5.5**).

In conclusion, the number of detected compounds differed significantly between high and low exposure groups for samples from female participants. However, a few factors have to be considered in the interpretation of results. The size of the suspect list and the high number of included compound classes do not allow a full optimization of the sample preparation and chromatographic methods for all compounds equally. Therefore, it cannot be excluded that the applied method favored a particular compound class resulting in higher DFs and ultimately leading to the observed significant differences. In addition, when the deviation between sex is made the number of participants in the high and low exposure groups is vastly decreased.

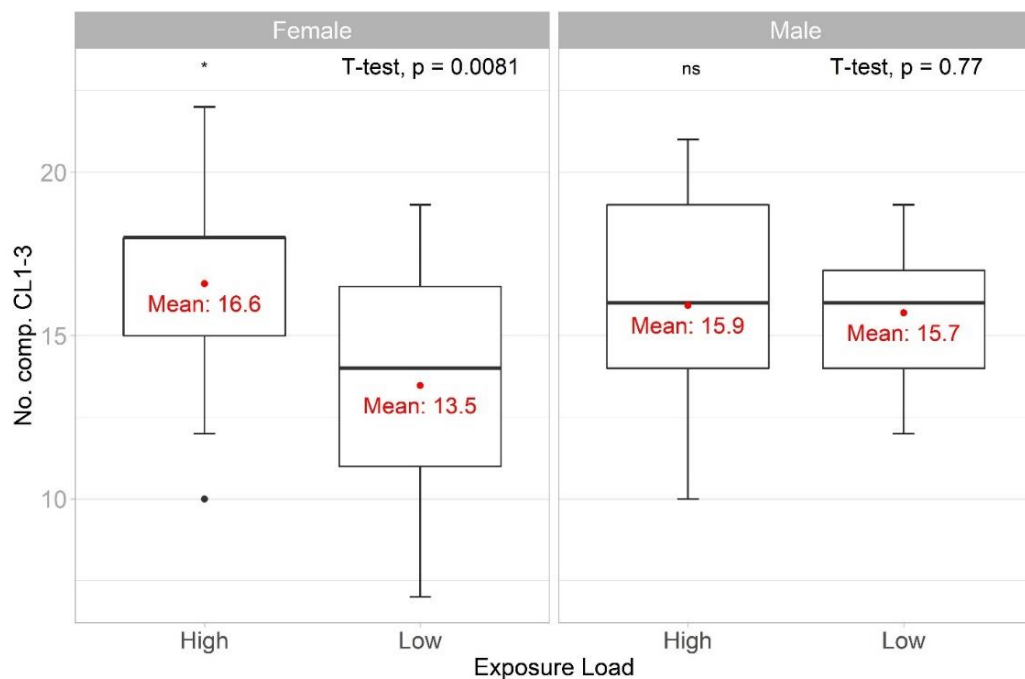


**Figure 5.5:** Boxplots representing the number of annotated compounds in the low and high exposure load groups. Each group was divided based on sex. Only compounds annotated at CL 3 or lower are considered. (\*\*) significant difference between mean values ( $p < 0.01$ ); ns: not significant.

## 5.4 Conclusions

The present study describes the analysis of 83 urine samples from Flemish adolescents by applying a suspect screening workflow and suspect list containing > 12,500 CECs and their metabolites. The screening yielded the identification of 5 compounds (CL1) and the tentative identification of 63 compounds (CL2-3) of which several have not been previously reported in urine. This clearly indicates the added value of suspect screening as a complementary tool to common targeted approaches in HBM. Due to the high number of hits (most of them unknowns) obtained using the suspect screening approach, the need for risk assessment of exposure to mixtures is evidenced. Several possibly toxic compounds that are not currently quantified in HBM programs have been tentatively identified. For example, several PCPs (e.g., benzyl alcohol) and Irganox 1135, were detected at high detection frequencies, showing a need to include them in targeted HBM studies. The comparison of the number of detected compounds between high and low exposure groups revealed a significant difference ( $p < 0.05$ ). When differentiating between sexes, this difference could only be observed between high and low exposure groups of females ( $p < 0.01$ ). In comparison with target HBM studies, this study shows that higher exposure to targeted contaminants also encompasses higher

exposure to the newly identified CECs, especially for female participants, which points towards a higher exposure of personal care product related compounds for female participants as opposed to male participants. Consequently, more investment in suspect screening as a tool to support, enhance, and complement quantitative targeted studies is necessary. Apart from suspect screening, a full non-targeted approach could be applied to expand CEC annotations.

## Supplementary Information – Chapter 5

**Table SI-5.1:** Summary of compounds used for method optimization and confirmation of compound identifications. OPFRs.met: Organophosphate flame retardant metabolites. AP.met: Alternative plasticizer metabolites. Conf.Std: Reference standard used for feature confirmation. Number codes of manufacturers correspond to the following: (1) Sigma-Aldrich (Bornem, Belgium); (2) Custom synthesized by Dr. Vladimir Belov (Max Planck Institute, Göttingen, Germany); (3) Chiron AS (Trondheim, Norway); (4) Cambridge Isotope Laboratories, Inc. (Andover, MA, USA).

Compound name	Abbr.	Formula	Class	InChIKey	Manufacturer
Di-n-butyl phosphate	DnBP	C <sub>8</sub> H <sub>19</sub> PO <sub>4</sub>	OPFR.met	JYFHYPJRHGVZDY-UHFFFAOYSA-N	(1)
Diphenyl hydrogen phosphate	DPhP	C <sub>12</sub> H <sub>11</sub> O <sub>4</sub> P	OPFR.met	ASMQGLCHMVWBQR-UHFFFAOYSA-N	(1)
Bis(2-chloropropyl) hydrogen phosphate	BCIPP	C <sub>6</sub> H <sub>13</sub> Cl <sub>2</sub> O <sub>4</sub> P	OPFR.met	UXEXPVAWQLGFAP-UHFFFAOYSA-N	(2)
Bis(2-chloroethyl) phosphate	BCEP	C <sub>4</sub> H <sub>9</sub> Cl <sub>2</sub> O <sub>4</sub> P	OPFR.met	PMGHIGLOERPWGC-UHFFFAOYSA-N	(2)
Bis(1,3-dichloro-2-propyl) phosphate	BDCIPP	C <sub>6</sub> H <sub>11</sub> Cl <sub>4</sub> O <sub>4</sub> P	OPFR.met	NNKRUBFJSSBFSS-UHFFFAOYSA-N	(2)
2-Ethylhexyl phenyl phosphate	EHPHP	C <sub>14</sub> H <sub>23</sub> O <sub>4</sub> P	OPFR.met	UGIWGFXQNPWKPR-UHFFFAOYSA-N	(2)
Bis(2-butoxyethyl) phosphate	BBOEP	C <sub>12</sub> H <sub>27</sub> O <sub>6</sub> P	OPFR.met	NNXWIPHZHATIFE-UHFFFAOYSA-N	(2)
5-Hydroxy-2-ethylhexyl diphenyl phosphate	5OH-EHDPHP	C <sub>20</sub> H <sub>27</sub> O <sub>5</sub> P	OPFR.met	PZMFWNXABLTZRN-UHFFFAOYSA-N	(2)
3-Hydroxyphenyl diphenyl phosphate	3OH-TPHP	C <sub>18</sub> H <sub>15</sub> O <sub>5</sub> P	OPFR.met	AWYVETCHVQGXMB-UHFFFAOYSA-N	(2)
Bis(2-butoxyethyl) 2-hydroxyethyl phosphate	BBOEHEP	C <sub>14</sub> H <sub>31</sub> O <sub>7</sub> P	OPFR.met	UQSRKBXTCXVEJL-UHFFFAOYSA-N	(2)
Bis(2-butoxyethyl) 3'-hydroxy-2-butoxyethyl phosphate	3OH-TBOEP	C <sub>18</sub> H <sub>39</sub> O <sub>8</sub> P	OPFR.met	ZYWDVPVGRFHQPGL-UHFFFAOYSA-N	(2)
4-Hydroxy triphenyl phosphate	4OH-TPHP	C <sub>18</sub> H <sub>15</sub> O <sub>5</sub> P	OPFR.met	NOPNBQOZUKISRP-UHFFFAOYSA-N	(2)
4-Hydroxyphenyl phenyl phosphate	4OH-PhP	C <sub>12</sub> H <sub>11</sub> O <sub>5</sub> P	OPFR.met	TUBVQVOADJADLU-UHFFFAOYSA-N	(2)
Tris(2-chloroethyl) phosphate	TCEP	C <sub>6</sub> H <sub>12</sub> Cl <sub>3</sub> O <sub>4</sub> P	OPFR.met	HQUQLFOMPYWACS-UHFFFAOYSA-N	(3)
Bis(1-chloro-2-propyl) 1-hydroxy-2-propyl phosphate	BCIPHIPP	C <sub>9</sub> H <sub>19</sub> Cl <sub>2</sub> O <sub>5</sub> P	OPFR.met	AUUWEOBTRZWTTC-UHFFFAOYSA-N	(2)
6-Hydroxy Monopropyl-heptylphthalate	6OH-MPHP	C <sub>18</sub> H <sub>26</sub> O <sub>5</sub>	AP.met	KNDRVUUMYPIFIU-UHFFFAOYSA-N	(4)

Cyclohexane-1,2-dicarboxylic mono carboxyisooctyl ester	cis-cx-MINCH	C <sub>17</sub> H <sub>28</sub> O <sub>6</sub>	AP.met	HGYNPCSGHWFMTB-KFTPUIBSA-N	(4)
Cyclohexane-1,2-dicarboxylic mono hydroxyisononyl ester	cis-OH-MINCH	C <sub>17</sub> H <sub>30</sub> O <sub>5</sub>	AP.met	WPTRTTWYMWWTQ-PFSRBDOWSA-N	(4)
Mono(2-ethyl-5-carboxypentyl) adipate	5-cx-MEHA	C <sub>14</sub> H <sub>24</sub> O <sub>6</sub>	AP.met	GSEREAHHKPORII-UHFFFAOYSA-N	(4)
Mono(2-ethyl-5-carboxypentyl)terephthalate	5-cx-MEPTP	C <sub>16</sub> H <sub>20</sub> O <sub>6</sub>	AP.met	BIQPFHSSQDGFTK-UHFFFAOYSA-N	(4)
Mono(2-ethyl-5-hydroxyhexyl) adipate	5-OH-MEHA	C <sub>14</sub> H <sub>26</sub> O <sub>5</sub>	AP.met	GUWFIYHOYMKJE-UHFFFAOYSA-N	(4)
Mono(2-ethyl-5-hydroxyhexyl) terephthalate	5-OH-MEHTP	C <sub>16</sub> H <sub>22</sub> O <sub>5</sub>	AP.met	ODRKAFOVPBFSIN-UHFFFAOYSA-N	(4)
Mono(2-ethyl-5-oxohexyl) adipate	5-oxo-MEHA	C <sub>14</sub> H <sub>24</sub> O <sub>5</sub>	AP.met	XLMWFRRVVDGMRV-UHFFFAOYSA-N	(4)
Mono(2-ethylhexyl) adipate	MEHA	C <sub>14</sub> H <sub>26</sub> O <sub>4</sub>	AP.met	MBGYSHXGENGTBP-UHFFFAOYSA-N	(4)
Mono(2-ethylhexyl) terephthalate	MEHTP	C <sub>16</sub> H <sub>22</sub> O <sub>4</sub>	AP.met	HRUJAEJKCNCOGW-UHFFFAOYSA-N	(4)
Mono(2-propyl-6-carboxyhexyl) phthalate	6-cx-MPHxP	C <sub>18</sub> H <sub>24</sub> O <sub>6</sub>	AP.met	DPQMLPCFIOCYFY-UHFFFAOYSA-N	(4)
Mono-2-(propyl-6-oxoheptyl)-phthalate	6-oxo-MPHP	C <sub>18</sub> H <sub>24</sub> O <sub>5</sub>	AP.met	NSGSMZPMFOBAFF-UHFFFAOYSA-N	(4)
Mono-carboxy-isononyl phthalate	7-cx-MiNP	C <sub>18</sub> H <sub>24</sub> O <sub>6</sub>	AP.met	IOWADRRGIUUGJH-UHFFFAOYSA-N	(4)
Mono-hydroxy-isononyl phthalate	7-OH-MiNP	C <sub>17</sub> H <sub>24</sub> O <sub>5</sub>	AP.met	RWCHSWLUPRJYEX-UHFFFAOYSA-N	(4)
Mono-isononyl-cyclohexane-1,2-dicarboxylate	MINCH	C <sub>17</sub> H <sub>30</sub> O <sub>4</sub>	AP.met	IGGVQTVKZINOGK-NOYMGPGASA-N	(4)
2-(2-Butoxyethoxy)ethyl acetate		C <sub>10</sub> H <sub>20</sub> O <sub>4</sub>	Conf.Std	VXQBJTKSVGFQOL-UHFFFAOYSA-N	(1)
D-Pantothenate		C <sub>19</sub> H <sub>17</sub> NO <sub>5</sub>	Conf.Std	GHOKWGTUJEAQD-ZETCQYMHSA-N	(1)
4-Amino-3-nitrophenol		C <sub>6</sub> H <sub>6</sub> N <sub>2</sub> O <sub>3</sub>	Conf.Std	IQXUIDYRTHQTET-UHFFFAOYSA-N	(1)
Pentyl paraben		C <sub>12</sub> H <sub>16</sub> O <sub>3</sub>	Conf.Std	ZNSSPLQZSUWFJT-UHFFFAOYSA-N	(1)
D-Pyroglutamic acid		C <sub>5</sub> H <sub>7</sub> NO <sub>3</sub>	Conf.Std	ODHCTXKNWHXJC-GSVOUGTGSA-N	(1)
4-hydroxy-benzaldehyde		C <sub>7</sub> H <sub>6</sub> O <sub>2</sub>	Conf.Std	RGHHSNMVTDWUBI-UHFFFAOYSA-N	(1)
Catechol		C <sub>6</sub> H <sub>6</sub> O <sub>2</sub>	Conf.Std	YCIMNLLNPGFGHC-UHFFFAOYSA-N	(1)

Benzyl alcohol		C <sub>7</sub> H <sub>8</sub> O	Conf.Std	WVDDGKGOMKODPV-UHFFFAOYSA-N	(1)
Theobromine		C <sub>7</sub> H <sub>8</sub> N <sub>4</sub> O <sub>2</sub>	Conf.Std	YAPQBXQYLJRXS-UHFFFAOYSA-N	(1)
Theophylline		C <sub>7</sub> H <sub>8</sub> N <sub>4</sub> O <sub>2</sub>	Conf.Std	ZFXYFBGIUFBOJW-UHFFFAOYSA-N	(1)
8-Hydroxyquinoline		C <sub>9</sub> H <sub>7</sub> NO	Conf.Std	MCJGNVYPOGVAJF-UHFFFAOYSA-N	(1)
Riboflavin		C <sub>17</sub> H <sub>20</sub> N <sub>4</sub> O <sub>6</sub>	Conf.Std	AUNGANRZJHBGPY-SCRDCRAPSA-N	(1)
Quinoline		C <sub>9</sub> H <sub>7</sub> N	Conf.Std	SMWDFEZZVXVCRB-UHFFFAOYSA-N	(1)
Isoquinoline		C <sub>9</sub> H <sub>7</sub> N	Conf.Std	AWJUIBRHMBBTKR-UHFFFAOYSA-N	(1)

**Table SI-5.2:** Summary of the isotopically labelled internal standards used in this study.

Compound name	Formula	Manufacturer
<sup>13</sup> C <sub>12</sub> -bisphenol S	[ <sup>13</sup> C] <sub>12</sub> H <sub>10</sub> O <sub>4</sub> S	CanSyn Chem. Corp. (Toronto, Canada)
Tris(2-chloroethyl) phosphate- <i>D</i> <sub>12</sub>	C <sub>6</sub> D <sub>12</sub> Cl <sub>3</sub> O <sub>4</sub> P	Custom synthesized by Dr. Vladimir Belov (Max Planck Institute, Göttingen, Germany)
Triphenyl phosphate- <i>D</i> <sub>15</sub>	C <sub>18</sub> D <sub>15</sub> O <sub>4</sub> P	Sigma-Aldrich (Bornem, Belgium)
Diphenyl phosphate- <i>D</i> <sub>10</sub>	C <sub>12</sub> D <sub>10</sub> HO <sub>4</sub> P	Sigma-Aldrich (Bornem, Belgium)
<sup>13</sup> C <sub>4</sub> -Mono(2-ethyl-5-oxohexyl) phthalate	C <sub>12</sub> [ <sup>13</sup> C] <sub>4</sub> H <sub>22</sub> O <sub>4</sub>	Cambridge Isotope Laboratories, Inc. (Andover, MA, USA)
Chlorpyrifos- <i>D</i> <sub>10</sub>	C <sub>9</sub> D <sub>10</sub> HCl <sub>3</sub> NO <sub>3</sub> PS	Sigma-Aldrich (Bornem, Belgium)
Mono-isononyl-cyclohexane-1,2-dicarboxylate- <i>D</i> <sub>2</sub>	C <sub>17</sub> D <sub>2</sub> H <sub>28</sub> O <sub>4</sub>	Cambridge Isotope Laboratories, Inc. (Andover, MA, USA)
<sup>13</sup> C <sub>6</sub> -methylparaben	[ <sup>13</sup> C] <sub>6</sub> C <sub>2</sub> H <sub>8</sub> O <sub>3</sub>	Cambridge Isotope Laboratories, Inc. (Andover, MA, USA)
<sup>13</sup> C <sub>3</sub> -3,5,6-Trichloro-2-pyridinol	[ <sup>13</sup> C] <sub>3</sub> C <sub>2</sub> H <sub>2</sub> Cl <sub>3</sub> NO	Cambridge Isotope Laboratories, Inc. (Andover, MA, USA)

**Table SI-5.3:** Detection frequencies of the isotopically labelled internal standards spiked in the urine samples.

Compound name	DF ESI+ [%]	DF ESI- [%]
<sup>13</sup> C <sub>12</sub> -bisphenol S	97.6	-
Tris(2-chloroethyl) phosphate- <i>D</i> <sub>12</sub>	-	97.1
Triphenyl phosphate- <i>D</i> <sub>15</sub>	-	95.2
Diphenyl phosphate- <i>D</i> <sub>10</sub>	100	98.8
<sup>13</sup> C <sub>4</sub> -Mono(2-ethyl-5-oxohexyl) phthalate	100	85.5
Chlorpyrifos- <i>D</i> <sub>10</sub>	-	83.1
Mono-isononyl-cyclohexane-1,2-dicarboxylate- <i>D</i> <sub>2</sub>	85.5	-
<sup>13</sup> C <sub>6</sub> -methylparaben	100	-
<sup>13</sup> C <sub>3</sub> -3,5,6-Trichloro-2-pyridinol	100	-

**Table SI-5.4:** Detection frequencies obtained within the presented chapter (DF<sub>SSA</sub>) for compounds which were included in target analysis of the FLESH IV study.

Compound name	DF [%] FLEHS targeted	Metabolite identified here	DF <sub>SSA</sub> [%]	Lowest CL
Diphenyl phosphate	99	Not conjugated	43.4	2
Mono ethyl phthalate	100	Glucuronide	31.3	4
Mono n-butyl phthalate	100	Glucuronide	100	3
Mono (2-ethyl-5-carboxypentyl) phthalate	100	Glucuronide	16.9	4
Mono (2-ethyl-5-hydroxyhexyl) phthalate	100	Not conjugated	89.2	4
Mono hydroxy isononyl phthalate	100	Glucuronide	50.6	4
Mono carboxy isodecyl phthalate	100	Not conjugated	2.4	4
Mono carboxy isodecyl phthalate	100	Glucuronide	14.5	4
Cyclohexane 1,2-dicarboxylic mono hydroxyisononyl ester	95	Glucuronide	54.2	4
Cyclohexane 1,2-dicarboxylic mono carboxyisooctyl ester	98	Glucuronide	50.6	4
2-hydroxy-naphthalene	100	Glucuronide	22.9	4
2-hydroxy-naphthalene	100	Not conjugated	18.1	4

**Table SI-5.5:** Summary of annotations which were detected in urine samples of Flemish adolescents at confidence level 3. For each annotation, the formula, retention time, polarity, detection frequency, candidate name and compound class are indicated. If more than one candidate from the suspect list could be matched to a certain formula, all possible assignments are indicated. *(The table can be openly assessed in the Supporting Information of online version of the corresponding article (Table S7 in the online version)):* <https://doi.org/10.1016/j.envres.2022.114105>

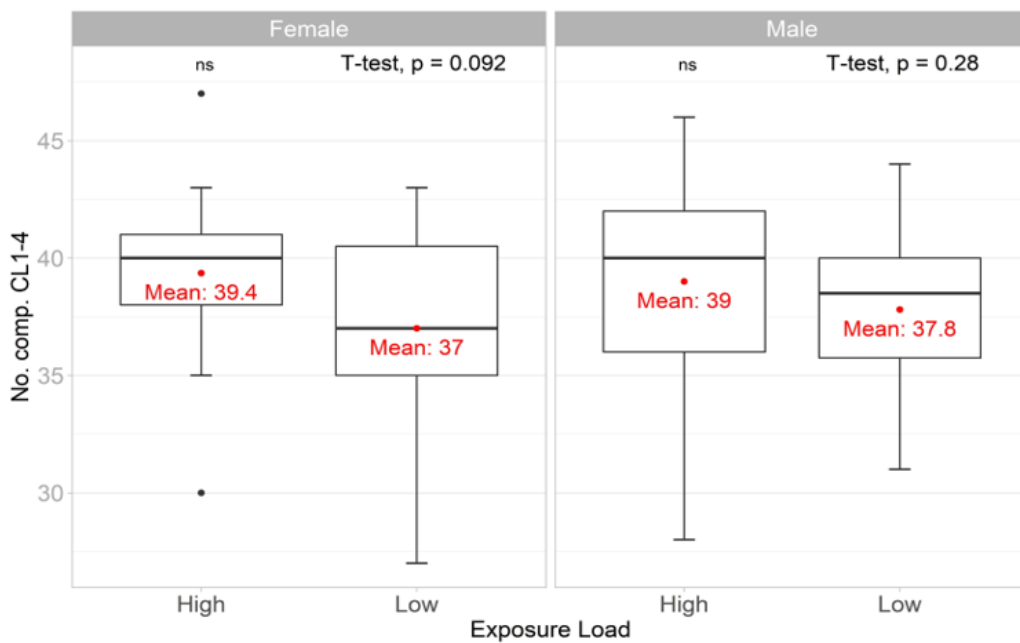


**Figure SI-5.1:** Boxplots representing the number of annotated compounds in the low and high exposure load groups. Each group was divided based on sex. Compounds annotated with CL 4 or better are considered. ns: not significant.

### **Supplementary text SI-T5.1.** Sample preparation method optimization.

Method optimization was based on a previously developed approach of Caballero-Casero et al. (Caballero-Casero et al., 2021b). To expand on this workflow, three protocols were tested:

#### **1) Dilution with acetonitrile**

Glass tubes were thoroughly cleaned, rinsed with water, acetone and baked at 400°C before usage. A 750 µL aliquot of urine was transferred to the precleaned tubes and centrifuged for 5 minutes at 3500 rpm. Then, 500 µL of the supernatant were transferred to a clean glass tube and spiked with the IS working solution at 30 ng/mL (final concentration in urine) and vortexed. One milliliter acetonitrile (with 0.1% formic acid, v/v) was added to the sample and vortexed. The solution was stored overnight at -20 °C. After thawing at room temperature, 500 µL of the solution were filtered through a centrifugal nylon filter of 0.2 µm (VWR, Leuven, Belgium). Lastly, the filtrate was transferred to a vial for injection.

#### **2) Captiva SPE cartridge**

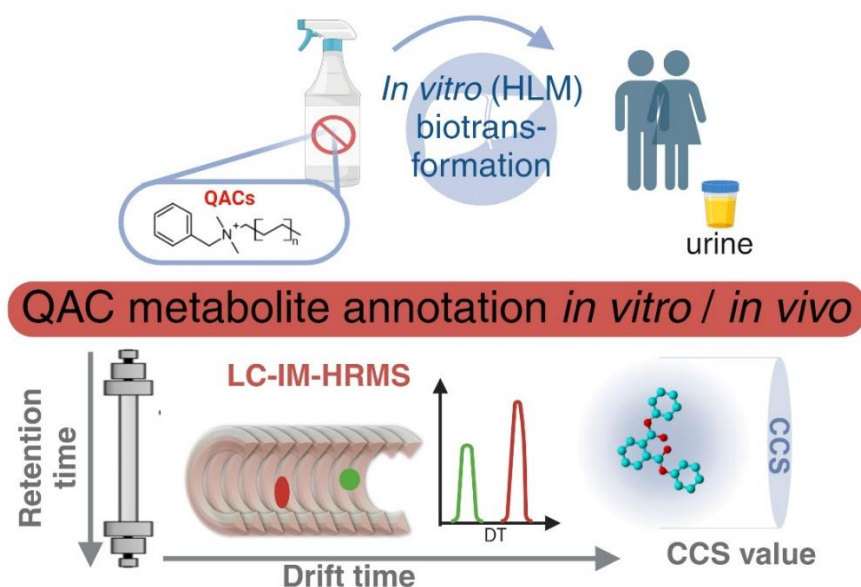
Glass tubes were thoroughly cleaned (rinsed with water, acetone and baked at 400°C before usage). A 750 µL aliquot of urine was transferred to the precleaned tubes and centrifuged for 5 minutes at 3500 rpm. Then, 500 µL of the supernatant were transferred to a clean glass tube and spiked with the IS working solution at 30 ng/mL (final concentration in urine) and vortexed. The aliquot was transferred to Captiva® cartridges (3 mL, Agilent Technologies, Santa Clara, USA). The solution in the cartridge was then carefully mixed and collected by push out. The solution was stored overnight at -20 °C. After thawing at room temperature, 500 µL of the solution were filtered through a centrifugal nylon filter of 0.2 µm (VWR, Leuven, Belgium). Lastly, the filtrate was transferred to a vial for injection.

#### **3) Captiva cartridge diluted with acetonitrile**

See **chapter 5.2.3** for the final sample preparation method applied for all urine samples.



# Chapter 6: In vitro biotransformation products of prioritized emerging contaminants



This chapter is based on the following publication:

Belova, L., Musatadi, M., Gys, C., Roggeman, M., den Ouden, F., Olivares, M., van Nuijs, A.L.N., Poma, G., Covaci, A. In vitro metabolism of quaternary ammonium compounds and confirmation in human urine by liquid chromatography ion-mobility high-resolution mass spectrometry. In press in *Environmental Science & Technology*. **2024**.



## 6.1 Introduction

Quaternary ammonium compounds (QACs) are a class of CECs recently gaining increasing attention. QACs are characterized by a quaternary ammonium cation carrying at least one long hydrocarbon side chain together with other substituents (methyl groups, benzyl groups, second hydrocarbon side chain and others). The three main classes of QACs are alkyl trimethylammonium compounds (ATMACs), benzyl alkyldimethyl ammonium compounds (BACs) and dialkyl dimethyl ammonium compounds (DDACs; in some studies abbreviated as DADMAC) (Arnold et al., 2023). The described structural characteristics lead to distinct amphiphilic properties resulting in an ubiquitous use of QACs in disinfectants, as surfactants, in cleaning and personal care products (Vereshchagin et al., 2021).

This wide usage of QACs has resulted in their release into the environment and detection in various environmental matrices. Within **chapter 4.1**, this was confirmed by the ubiquitous detection of QACs in indoor dust samples. Additionally, frequent occurrence of QACs has been reported in wastewater (Pati and Arnold, 2020; Wieck et al., 2018), surface sediments (Li and Brownawell, 2009; Pintado-Herrera et al., 2017), sludge (Godfrey et al., 2022; Östman et al., 2017) and food (Bertuzzi and Pietri, 2014; Xian et al., 2016). During the COVID-19 pandemic, the use of QACs vastly increased, resulting in their first detection in human matrices including blood (Zheng et al., 2021), urine (Li et al., 2023) and breast milk (Zheng et al., 2022), whereby high detection frequencies have been observed for all matrices. This is of high concern given the numerous toxic effects reported for QACs. In animal studies, inhalation of QAC aerosols led to pulmonary irritation and inflammation (Larsen et al., 2012). In mice, chronic exposure to a QAC mixture consisting of BACs and C<sub>10</sub>-DDAC led to decreased reproductive performance and neural tube defects (Hrubec et al., 2017; Melin et al., 2014). In humans, increased QAC exposure has been associated with decreased mitochondrial function, disruption in cholesterol homeostasis and an increased risk of asthma (Gonzalez et al., 2014; Hrubec et al., 2021).

The described toxic effects point out the need for further assessment of human exposure to QACs through biomonitoring studies. However, information on biotransformation of QACs is still scarce and only two studies on the *in vitro* biotransformation of QACs are published: Seguin et al. reported *in vitro* metabolites of C<sub>10</sub>- to C<sub>16</sub>-BACs (Seguin et al., 2019), and some of them were later confirmed and quantified in urine (Li et al., 2023). Recently, Nguyen et al. reported Phase I *in vitro* metabolites for a set of 19 QACs whereby TWIMS-HRMS was used for their annotation (Nguyen et al., 2024). However, data on higher oxidized metabolites and time trends of the *in vitro* biotransformations is still lacking. Additionally, the assessment of the

reproducibility TWIMS derived CCS values on a drift-tube ion-mobility (DTIM) system can be of great added value given that high CCS deviations have been observed between these two instrumental set-ups (**chapter 3.2**).

Therefore, this chapter aimed at confirming and expanding the IM-HRMS derived data available on the biotransformation products of QACs. For each of the three main classes, one homologue was selected for which high concentrations in indoor environments were reported within **chapter 4.1**, indicating their relevance for human exposure. HLM-derived *in vitro* metabolites were assigned based on a suspect and non-target screening approach. Additionally, drift-tube IM-HRMS derived CCS values ( $^{DT}CCS_{N_2}$ ) were acquired for each assigned metabolite. Based on the  $^{DT}CCS_{N_2}$  changes introduced following metabolism, further conclusions about the structures of QACs metabolites were drawn, adding identification confidence. Lastly, human urine samples were screened for the annotated *in vitro* metabolites, to confirm their presence in an *in vivo* setting and thereby further facilitate future human biomonitoring studies.

## 6.2 Materials and Methods

### 6.2.1 Materials and Methods

The analytical standards of C<sub>12</sub>-BAC, C<sub>16</sub>-ATMAC and C<sub>10</sub>-DDAC were purchased from Sigma Aldrich Chemie GmbH (Steinheim, Germany). Labelled compounds (*D*<sub>7</sub>-C<sub>12</sub>-BAC, *D*<sub>7</sub>-C<sub>14</sub>-BAC and *D*<sub>9</sub>-C<sub>10</sub>-ATMAC) used as internal standards (IS) were purchased from Toronto Research Chemicals (Toronto, Canada). All used solvents were of UHPLC-MS purity. Isopropanol (IPA), methanol (MeOH), acetonitrile (ACN) and formic acid (99%) were obtained from Biosolve BV (Valkenswaard, the Netherlands) while ammonium acetate (used as mobile phase modifier) was purchased from VWR (Leuven, Belgium). A PURELAB Flexsystem was applied to obtain ultrapure water (18.2 MΩ cm, Milli-Q, Millipore).

Human liver microsomes (20 mg/mL, pooled, mixed gender, n = 50) human liver cytosol (10 mg/mL, pooled mixed gender, n = 50) were purchased from Tebu-Bio (Boechout, Belgium). Phenacetin, 2,5-uridinediphosphate glucuronic acid (UDPGA), alamethicin (> 98%), dimethyl sulfoxide (DMSO), 4-nitrophenol (4-NP), adenosine-3'-phosphate 5'-phosphosulfate lithium salt hydrate (PAPS, > 60%) and nicotinamide-adenine-dinucleotide phosphate (NADPH) tetrasodium salt hydrate (> 96%) were purchased from Merck (Darmstadt, Germany). For the preparation of a 100 mM TRIS buffer, 12.1 g of Trizma base (Janssen Chimica, Beerse, Belgium) and 1.0 g MgCl<sub>2</sub> (Merck, Darmstadt, Germany) were dissolved in 1 L of ultrapure water. The pH was adjusted to 7.4 through addition of the required volume 1 M HCl solution (Merck Darmstadt, Germany).

## 6.2.2 *In vitro* metabolism assay

The applied *in vitro* metabolism assay was based on a previously developed in-house approach (den Ouden et al., 2024; Gys et al., 2018; Mortelé et al., 2018) and is schematically summarized in **Figure 6.1**.

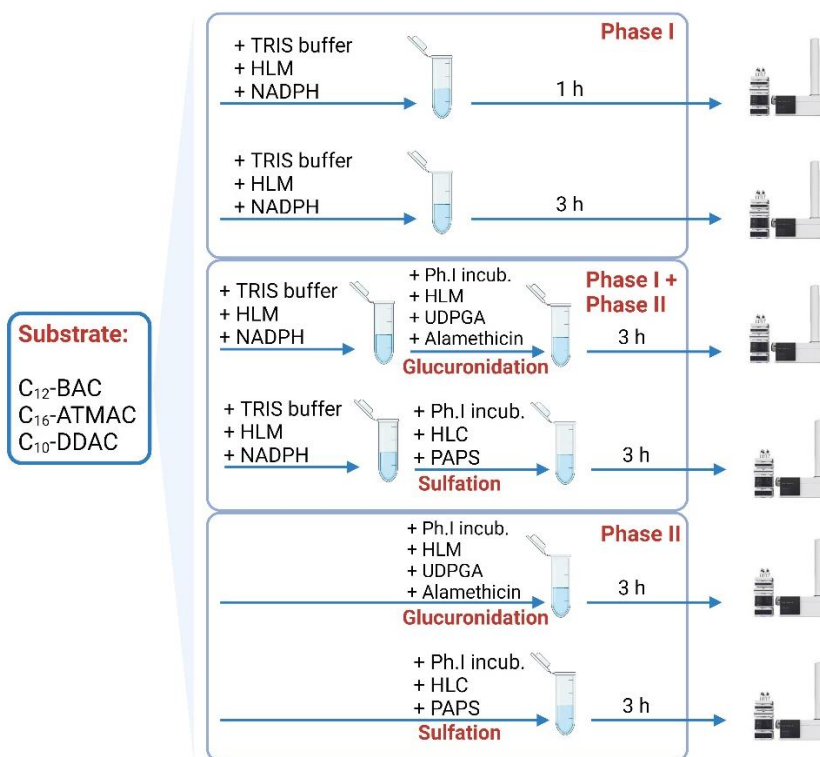


**Figure 6.1:** Schematic overview of sample preparation for human liver microsomal incubations. HLM: Human Liver Microsomes; NADPH: nicotinamide-adenine-dinucleotide phosphate; UDPGA: 2,5-uridinediphosphate glucuronic acid; PAPS: adenosine-3'-phosphate 5'-phosphosulfate lithium salt hydrate; HLC: Human Liver Cytosol.

For the Phase I metabolism assay, mixtures of 935-980  $\mu\text{L}$  (adjusted to result in a final volume of 1 mL for all samples) TRIS buffer, 10  $\mu\text{L}$  of a 0.5 mM substrate solution (in MeOH) and 25  $\mu\text{L}$  of HLMs (20 mg/mL) were prepared in 1.5 mL Eppendorf tubes and left to equilibrate for 5 min in a water bath at 37  $^{\circ}\text{C}$ . The substrate concentration was chosen based on previous in-house studies which observed reliable metabolite formations at this concentration level (den Ouden et al., 2024; Gys et al., 2018; Mortelé et al., 2018). Incubations were prepared for a total incubation time of 1 and 3 h by triplicate. After 5 min of equilibration time, NADPH solution (0.1 M in TRIS buffer, 10  $\mu\text{L}$ ) was added to start the incubation. For the 3h incubations, addition of NADPH was repeated 60 min and 120 min of incubation in a water bath at 37  $^{\circ}\text{C}$ . After either 1 h or 3 h, reactions were stopped through the addition of 250  $\mu\text{L}$  of ice-cold ACN containing 1 % formic acid

containing the above mentioned IS ( $D_7$ -C<sub>12</sub>-BAC,  $D_7$ -C<sub>14</sub>-BAC and  $D_9$ -C<sub>10</sub>-ATMAC, concentration in stopping solution: 0.2 µg/mL).

For the Phase II metabolism assay, two sample sets were included. Triplicate samples were prepared on which both Phase I and subsequent Phase II incubations were performed. Additionally, duplicate samples including only Phase II reactions were prepared. Phase I reactions were performed as described above whereby incubations were stopped after 3 h through placing the samples on ice. After centrifugation (5 min at 8000 rpm), 935 µL of the supernatants of Phase I incubation or 935 µL of fresh TRIS buffer (for Phase II reactions only) was transferred to new 1.5 mL Eppendorf tubes and 10 µL of substrate solution (0.5 mM in MeOH) as well as 25 µL of HLMs (20 mg/mL) were added to the latter. To the sample set covering glucuronidation reactions, 10 µL of an alamethicin solution (1 mg/mL in DMSO) was added (Fisher et al., 2000).

To sulfation reaction, 10 µL of human liver cytosol (HLC) was added. Subsequently, 10 µL of solutions of corresponding cofactors (PAPS (100 µM in TRIS buffer) and UDPGA (1 mM in TRIS buffer) for sulfation and glucuronidation reactions, respectively) was added after 5, 60, and 120 min. After 180 min, reactions were stopped through the addition of 250 µL of the above mentioned ice-cold ACN solution containing formic acid and IS.

After stopping the incubations, all samples were centrifuged (5 min at 8000 rpm) and 1000 µL were transferred to new 1.5 mL Eppendorf tubes. Samples were concentrated (with N<sub>2</sub>) to near dryness, reconstituted in 100 µL of MeOH:H<sub>2</sub>O (80:20; v/v), and stored at -80 °C. Directly before analysis, samples were diluted in a ratio of 1:200 (aiming to avoid saturation of the detector given the high sensitivity observed for QACs in **chapter 4.1**; for positive controls, a dilution factor of 1:10 was applied) and filtered through 0.2 µm centrifugal filters (VWR, Leuven, Belgium).

### 6.2.3 Quality control of *in vitro* metabolization assays

A separate positive control sample was included whereby the substrate was replaced by addition of 10 µL phenacetin (5 µg/mL in TRIS buffer) or 4-NP (1 mM in TRIS buffer) for Phase I and II incubations, respectively. All other incubation parameters were identical to the parameters applied for the QAC substrates with a total incubation time of 3 h. For these compounds, expected metabolites were known (den Ouden et al., 2024; Gys et al., 2018) and their detection confirmed the successful performance of the *in vitro* metabolism assay. For Phase I experiments, three sets of negative controls (for each time point) were included, within which the addition of the substrate, the cofactor (NADPH) or the HLMs was omitted. Similarly, for Phase II incubations, a sample within which no Phase II cofactor (PAPS or UDPGA) was added and a sample without the addition of

substrate was included. Negative controls served as an estimation of background contamination and as a proof that the observed metabolites did not originate from the latter or resulted from non-HLM or non-HLC mediated reactions.

#### 6.2.4 Selection of human urine samples

Aiming at confirming the *in vitro* metabolites in a human matrix, human urine samples were selected. Previously, the detection of oxidized (monohydroxy and carboxy) QAC metabolites has been described in urine proving it to be a suitable matrix for QAC exposure assessment (Li et al., 2023). Within the in-house sample repository, a total of 309 urine samples from ten healthy volunteers (sample of every urination collected on five consecutive days) was available which was collected in the scope of previous studies investigating the short-term temporal variability of urinary biomarkers of various contaminant classes (Bastiaensen et al., 2021c; Gys et al., 2021b). Ethical approval for sample collection and analysis was received from the Ethical Committee of the Antwerp University Hospital (EC Reference Number: 18/03/023, Belgian Registry Number: B300201835329). Details of the sampled cohort and sample collection were previously described by Gys et al. and Bastiaensen et al. (Bastiaensen et al., 2021c; Gys et al., 2021b). For this study, four urine samples were randomly selected from each participant and prepared as described in **chapter 6.2.5**. Additionally, two field blank samples were prepared alongside the collection of the urine samples. These blanks consisted of Milli-Q water added to polypropylene containers of the same type used for urine collection and storage. This approach allowed for the evaluation of potential contamination from the materials used throughout the analytical process, as well as from other sources.

#### 6.2.5 Preparation of human urine samples

The sample preparation protocol was based on a workflow previously described by Li et al. (Li et al., 2023) for a quantitative study on QAC metabolites in human urine, with slight modifications, and applied to four urine samples randomly selected for each of the ten participants. In brief, 250  $\mu$ L of urine was spiked with 2.5 ng of IS (for information on chemicals see **chapter 6.2.1**). Oasis WCX solid phase extraction cartridges (60 mg, 3 mL; VWR, Leuven, Belgium) were prewashed with 2 mL of MeOH and 2 mL of MilliQ water, and the samples were loaded. The cartridges were washed with 2 mL of MilliQ water, H<sub>2</sub>O:MeOH (50:50; v/v) and MeOH. Then, samples were eluted with 2.5 mL of MeOH containing 3% of formic acid. The solvent was evaporated to dryness under a nitrogen steam. Samples were reconstituted in 250  $\mu$ L MeOH:H<sub>2</sub>O (80:20; v/v) and filtered through 0.2  $\mu$ m centrifugal filter prior to instrumental analysis. Two procedural

blanks and the two field blanks mentioned above (both spiked with IS) were included to monitor background contamination.

### 6.2.6 Instrumental analysis

All samples were analyzed using an Agilent 6560 ion-mobility high-resolution quadrupole time-of-flight (QTOF) mass spectrometer coupled to an Agilent 1290 Infinity II UPLC system equipped with a quaternary pump (Agilent Technologies, Santa Clara, USA). The instrument was operated using the MassHunter Data Acquisition software (version 11.0, Agilent Technologies). The applied chromatographic method was modified from the study described in **chapter 4.1** analyzing parent QACs in indoor dust samples. The elution power of mobile phase (A) and the gradient were adjusted to facilitate the separation of more polar metabolites. This resulted in chromatographic conditions summarized in **Table SI-6.1**.

Phase I incubations and urine samples were analyzed in positive ionization mode while Phase II incubations were injected in both negative and positive ionization modes. For the initial annotation of metabolites and consequent analysis of human urine, all samples were analyzed in QTOF without using the ion-mobility separation. Data-dependent acquisition was applied in which the three most abundant precursor ions per acquisition cycle were fragmented at collision energies of 10, 20 and 40 eV, with the quadrupole set to a narrow ( $\sim 1.3$  amu) isolation window. All  $m/z$  ratios of predicted metabolites (**chapter 6.2.7**) were included as preferred for fragmentation. This ensured that they were fragmented even if they were not the most abundant signals in an acquisition cycle while still keeping the number of precursors fragmented per cycle at three, resulting in a duty cycle of 1.45 s. An  $m/z$  range of 100-1500 and 50-1500 was applied for MS and MS/MS acquisition, respectively. Additionally, all HLM incubations of QACs and pooled urine samples (pool of four urine samples per participant) were injected in 4-bit multiplexed IM mode allowing mobility separation and  $^{DT}CCS_{N_2}$  calculations. For all measurements, ion source settings and drift-tube parameters summarized in **Table SI-6.2** were applied and a calibration solution for online mass calibration was infused constantly.

### 6.2.7 Data processing and interpretation

For the three parent compounds investigated here, metabolites were predicted using the Meteor Nexus (version v.3.2.0) and BioTransformer 3.0 software. Within the Meteor Nexus software, all possible Phase I biotransformation reactions were included in the predictions while Phase II reactions were limited to glucuronidation and sulfation, since only for these biotransformation pathways the necessary cofactors were added.

The prediction method and minimum likelihood of biotransformation reactions were set to “absolute/relative reasoning” and “doubted”, respectively, applying a max. depth of 3. The predicted metabolites were exported to obtain suspect lists to be used in the suspect screening approach described below. No duplicate formulae were included even though different combinations of metabolism reactions can lead to the formation of some metabolites. The underlying reactions were interpreted from the obtained mass spectrometric data after matching of single formulae from the suspect list.

Given the better reproducibility of lower abundant fragments in QTOF only mode and the unavailability of all-ions fragmentation in multiplexed IMS mode, initial metabolite assignments were based on QTOF only data. From the raw QTOF only data, features were extracted using the “Recursive Feature Extraction” algorithm within the MassHunter Profinder software (v 10.0) applying retention time (RT) and mass tolerances of 0.3 min and 10 ppm, respectively, and retrieving features with a minimum peak height of 1000 counts. Extracted features were imported in MassHunter Mass Profiler Professional software (version 15.1). Based on a FC analysis, only features were retained showing a FC of 3 or higher between QAC incubations and negative controls. Filtered features were matched against the above described suspect lists applying a mass tolerance of 7 ppm and including  $[M^+]$  ions. All matched features were manually investigated aiming at assigning a CL of identification according to the criteria introduced by Schymanski et al. (Schymanski et al., 2014). If no fragmentation spectrum was obtained in any of the incubations, features were discarded given the low CL of 4. From obtained fragmentation spectra, possible structures of metabolites were retrieved based on the similarity of characteristic fragments to corresponding parent compounds and the observation of neutral losses. If these observations allowed the assignment of one possible structure excluding all other candidates, CL2 was assigned. If the latter was not the case, e.g. if the exact position of the metabolization reaction could not be determined, metabolites were reported with CL3. From the three available collision energies, the spectrum containing the most fragments, and thus the most structural information, was selected and reported in the results section (**chapter 6.3**).

To ensure that within the suspect screening approach no metabolites were overlooked, raw data were investigated applying a non-targeted approach. Based on the fragmentation spectra obtained for the parent compounds in **chapter 4.1** and for the metabolites identified using the suspect screening workflow, characteristic fragments were identified for each parents’ metabolites. Based on their observation within suspect screening results, their detection was also expected for metabolites not covered by suspect screening. Additionally, characteristic fragments of glucuronides and sulfates could be retrieved from literature (Fitzgerald et al., 2022; Yan et al., 2003). This resulted in a list of characteristic fragments and neutral losses given in **Table SI-6.3**. Using the

MassHunter Qualitative Analysis software (v B.07.00), these fragments and neutral losses were extracted from the MS/MS data applying a mass window of 10 ppm. All obtained peaks showing these masses in their MS/MS spectra, were manually investigated to assess whether the extracted metabolites were already reported within the suspect screening approach or whether new compounds can be identified assigning CLs as described above.

For the analysis of human urine samples, formulae of parent compounds and metabolites identified *in vitro* were directly extracted from raw data applying the 'Find by formula' algorithm with MassHunter Qualitative analysis software (version B.07.00), applying a mass window of 7 ppm and a matching score cut-off of 70. Hits were only reported if the peak area observed in urine samples showed a minimum fold change of three compared to procedural and field blank samples. For each detected peak, the obtained fragmentation spectra were assessed and compared with data obtained from HLM incubations. Only if all fragments matched between urine and HLM samples, the same CLs were assigned. If this was not the case, and thus only *m/z* ratio and RT could be matched, metabolites were reported with CL4.

Obtained IM raw data was recalibrated using the Agilent IM-MS Reprocessor (version 10.00). Data were demultiplexed using the PNNL demultiplexing tool (version 4.1) whereby one drift bin was interpolated to three and data were smoothed with a moving average of three. Features were extracted using the IM-MS Browser software (v 10.0). For each extracted feature,  $^{DT}CCS_{N_2}$  values were calculated based on the single-field approach<sup>5</sup>. From the list of identified features,  $^{DT}CCS_{N_2}$  values of the identified metabolites were extracted based on the RTs and *m/z* ratios obtained within the described suspect and non-targeted screening approaches. Average  $^{DT}CCS_{N_2}$  values obtained for triplicate samples of 1h and 3h incubations were reported.

## 6.3 Results and Discussion

### 6.3.1 Quality control results for *in vitro* metabolism assay

Phenacetin and 4-NP were used as substrates in the positive control samples in the Phase I and Phase II incubations, respectively, given their expected metabolites were known from literature (den Ouden et al., 2024; Gys et al., 2018; Hinson, 1983). For phenacetin, these included the dealkylated and monohydroxylated metabolites. Both of these metabolites were detected in all positive control samples, i.e. within the incubations of each of the three investigated QACs. The observed fragmentation spectra (**Figures SI-6.1 and SI-6.2**) matched the data reported in literature (den Ouden et al., 2024).

Similarly, both metabolites expected for 4-NP (4-NP-glucuronide and 4-NP-sulfate) were detected in all positive control samples of the glucuronidation and sulfation experiments, respectively. Again, the observed fragmentation spectra matched data reported previously (**Figures SI-6.3 and SI-6.4**).

These findings indicate a successful set-up and incubation for both Phase I and II experiments confirming that the reported QAC metabolites resulted from HLM metabolism reactions.

Except for a selection of C<sub>12</sub>-BAC, none of the reported QAC metabolites were detected in any of the negative control (NCs) samples. The C<sub>12</sub>-BAC metabolites were detected in the NC samples to which no substrate, thus no C<sub>12</sub>-BAC, was added. It is assumed to originate from a background contamination with the parent compound since no C<sub>12</sub>-BAC metabolites were detectable in NCs to which no cofactors or HLMs were added. In all cases, their abundances (relative to IS) were at least one order of magnitude lower than in the C<sub>12</sub>-BAC incubations.

### 6.3.2 Identification of *in vitro* metabolites

#### 6.3.2.1 C<sub>12</sub>-BAC - Phase I

The data obtained for the parent compound and the assigned metabolites of C<sub>12</sub>-BAC Phase I incubations are summarized in **Table SI-6.4**. The parent compound was detected in all replicates from both incubation time points with an average mass error of 2.28 ppm and 1.17 ppm for the 1 h and 3 h incubations, respectively. Thereby, the observed fragmentation spectra matched data described in chapter 4.1 displaying the loss of the benzyl moiety (neutral loss of [C<sub>7</sub>H<sub>8</sub>]) resulting in a fragment with theoretical *m/z* 212.2373 and the tropylium ion (theoretical *m/z* 91.0542) as the two characteristic fragments.

A total of 11 individual metabolites were annotated originating from five metabolism reactions. Through the suspect screening workflow described in **chapter 6.2.7**, metabolites originating from desaturation (-2H), mono- and dihydroxylation (+O/+2O) and further oxidation reactions, leading to +O, -2H and +2O, -2H metabolites, were assigned. For all annotated metabolites, average mass errors were below 3 ppm indicating high mass accuracy and reliability of formula matching. In contrast to the *in vitro* data recently published by Nguyen et al., a desaturation metabolite (-2H) was observed for C<sub>12</sub>-BAC and confirmed at confidence level 3 (CL3) through the detection of the characteristic fragmentation pattern described above (Nguyen et al., 2024). However, this metabolite was observed solely in the 1 h incubations showing a low peak area of 8.79E03 ± 1.89E03 cps, while for the IS an average peak area of 5.08E05 ± 9.97E04

cps was observed resulting in a relative abundance of 0.02. This metabolite was therefore considered to be an intermediate product indicating further oxidation.

For the metabolites derived from the other four metabolism reactions (+O/+2O/+O,-2H/+2O,-2H), the obtained fragmentation spectra are summarized in **Figure SI-6.5**. The detection of the tropylium ion indicated that the metabolism site was located on the C<sub>12</sub> hydrocarbon side chain leaving the benzyl moiety unmodified.

The obtained fragmentation spectra did not allow any conclusions regarding the position of the oxidation sites, leading to the assignment of CL3 to most metabolites. Nevertheless, for the +2O metabolite, one of the formed hydroxy groups is assumed to be present in  $\omega$ -position to allow the subsequent formation of the carboxy metabolite, which was previously reported for C<sub>12</sub>-BAC in human samples (Li et al., 2023; Seguin et al., 2019). For the +O and +O/-2H metabolites, two peaks matching the identification criteria were observed differing in retention time by 0.24 min and 0.29 min, respectively (**Table SI-6.4**). This indicates different metabolism positions within the hydrocarbon side chain leading to metabolite isomers, which are separable by the applied chromatographic method. A previous study investigating the CYP 450 based *in vitro* metabolism of BACs (Seguin et al., 2019) confirmed through comparison with reference standards that keto (+O/-2H) and dihydroxy (+2O) functional groups were present in  $\omega$ -1- and  $\omega$ -positions, suggesting that the metabolites observed here might show the same structures. In addition, the provided fragmentation data does not allow distinguishing between a carboxy or keto/hydroxy group for the M5 (**Table SI-6.4**) metabolite. Given the confirmation of a carboxy metabolite in human samples described in literature (Li et al., 2023), the carboxy metabolite is considered the most probable.

The effect of multiple isomers observed was even more prone for +2O metabolites, for which five chromatographic peaks were detected in a retention time range of 2.44-4.23 min. Through the formation of two hydroxy groups (+2O), numerous combinations of hydroxylation positions are possible leading to the observed increased number of peaks.

Except for the identification of the desaturated metabolite, the metabolism findings presented for C<sub>12</sub>-BAC reproduce the results described by Nguyen et al. (Nguyen et al., 2024). However, within the cited study, no conclusion about the time trends of the formation of C<sub>12</sub>-BAC metabolites were possible, which would provide valuable insights in further prioritization of the most prevalent metabolism pathways. Here, time trends were described for each of the observed metabolites by comparing their abundance (relative to IS *D*<sub>7</sub>-C<sub>12</sub>-BAC) between the 1 h and 3 h time points (**Figure SI-6.6**). For the parent compound, a clear decrease was observed indicating that metabolism reactions progressed throughout the whole incubation time. After 3 h, the +2O,-2H metabolite showed the highest relative abundance which increased from  $4.12 \pm 0.41$  to  $6.95 \pm 0.41$

between the 1 h and 3 h time points. The second and third most abundant metabolites in 3h incubations were +O and +O,-2H homologues (M2.1 and M4.1 in **Table SI-6.4/Figure SI-6.6**, respectively) for both of which relative abundance decreased between 1 h and 3 h time points. That outcome indicates that they might be further oxidized to form the abundant +2O,-2H homologue. Interestingly, relative abundances of the other +O metabolite (M2.2) slightly increased over time suggesting that M2.1 carries the hydroxy group in  $\omega$ -positions (to allow further oxidation), while M2.2 is oxidized at another position within the hydrocarbon side chain. All other metabolites showed lower relative abundances (< 0.9 after 3 h) indicating minor metabolic pathways. These findings are in line with a previous study which identified and quantified both monohydroxy and carboxy C<sub>12</sub>-BAC metabolites in human urine confirming their formation *in vivo* (Li et al., 2023).

#### 6.3.2.2 C<sub>16</sub>-ATMAC - Phase I

The parent compound C<sub>16</sub>-ATMAC was detected in all incubations with an average mass error of 2.21 ppm and 2.94 ppm for the 1h and 3h time points, respectively. Thereby, the fragmentation spectra showed the specific trimethyl amine fragment (theoretical *m/z* 60.0808) as described in **chapter 4.1** and shown in **Figure SI-6.7**. In the Phase I incubations, a total of six metabolites were annotated (**Table SI-6.5**) originating from the same five metabolism reactions as described for C<sub>12</sub>-BAC, corresponding to losses/addition of -2H/+O/+2O/+O,-2H/+2O,-2H. All metabolites were assigned through matching of formulae (**chapter 6.2.7**; all average mass errors < 3 ppm) and through observation of the above mentioned characteristic trimethyl amine fragment. For all metabolites, no other signals besides the mentioned fragment were observed in the fragmentation spectra, again suggesting that metabolism reactions occurred on the hydrocarbon side chain. This also did not allow to determine exact positions for the oxidation sites resulting in the assignment of CL3 for all metabolites.

A metabolite formed through desaturation was annotated for both time points which has not been previously described for C<sub>16</sub>-ATMAC (Nguyen et al., 2024). For the +O metabolite, two peaks were observed differing by 0.2 min in RT and suggesting two positional isomers. Again, one of the +O metabolites is assumed to carry a hydroxy group in  $\omega$ -position to allow further oxidation. In contrast to C<sub>12</sub>-BAC, only single peaks were observed for the +2O / +O,-2H / +2O,-2H metabolites suggesting one major isomer for each of them.

Abundances (relative to IS D<sub>9</sub>-C<sub>10</sub>-ATMAC) were compared for all metabolites between the two incubation times. Since all IS showed similar abundances and similar response factors have been previously observed for the parent compounds (**chapter 4.1**),

a comparison of relative abundances between C<sub>16</sub>-ATMAC and C<sub>12</sub>-BAC was considered reasonable, allowing first indications of possible differences in metabolism rates. As shown in **Figure SI-6.8**, average relative abundances were < 1.2 for all C<sub>16</sub>-ATMAC metabolites, while values of up to 6.95 have been observed for C<sub>12</sub>-BAC (**Figure SI-6.6**). In contrast to C<sub>12</sub>-BAC, the two +O metabolites were most abundant in 3h incubations whereby their relative abundance increased over time (**Figure SI-6.8**). The +O, -2H metabolite was most abundant within the 1 h incubations, but increased to a lower extent than the +O metabolites between the 1 h and 3 h time intervals. The remaining three metabolites (+2O/+2O,-2H/-2H) showed a constant increase over the complete incubation time with relative areas between 0.19 and 0.65 for the 3 h time points.

The relative abundance of the parent compound C<sub>16</sub>-ATMAC decreased throughout the incubation process, but was still clearly higher than observed for C<sub>12</sub>-BAC and all C<sub>16</sub>-ATMAC metabolites with values of 13.82 and 10.08 for the 1 h and 3 h time points, respectively. These findings suggest a slower metabolism of C<sub>16</sub>-ATMAC in comparison to the investigated BAC homologue. This might be attributed to the longer hydrocarbon chain length of C<sub>16</sub>-ATMAC since decreasing metabolism rates with increasing hydrocarbon chain length have been reported for HLM *in vitro* metabolism of lipids (Adas et al., 1999). The low metabolism rate is also assumed to contribute to the lower number of observed metabolites for +2O and +O,-2H modifications.

### 6.3.2.3 C<sub>10</sub>-DDAC - Phase I

The parent compound, C<sub>10</sub>-DDAC, was detected at both time points with intensities (relative to IS D<sub>7</sub>-C<sub>12</sub>-BAC) of  $6.57 \pm 0.43$  and  $4.62 \pm 0.43$  for the 1 h and 3 h incubations, respectively (**Table SI-6.6**). As described in **chapter 4.1**, the fragmentation spectrum of C<sub>10</sub>-DDAC showed two characteristic fragments: one corresponding to the [C<sub>3</sub>H<sub>8</sub>N]<sup>+</sup> ion (theoretical *m/z* 58.0651) and the other to the loss of one hydrocarbon side chain (loss of 140.1565, [C<sub>10</sub>H<sub>20</sub>]).

A total of thirteen metabolites were assigned formed by eight different metabolism reactions (**Table SI-6.6**). Thereby, three C<sub>10</sub>-DDAC metabolites are described for the first time, and a detailed discussion of observed fragmentation spectra, not included in previous investigations of DDAC metabolism (Nguyen et al., 2024), is included providing a valuable dataset for further investigations of DDAC metabolites *in vivo*. Similar to C<sub>10</sub>-DDAC, fragmentation spectra of metabolites showed the characteristic ion with *m/z* 58.0651 and neutral losses of the hydrocarbon side chains. Through prediction of formulae from the latter, a conclusion could be drawn regarding the metabolism reactions they underwent. **Table 6.1** summarizes the neutral losses and corresponding assigned formulae observed in the fragmentation spectra (**Figure SI-6.9**) of each

identified metabolite. It has to be mentioned that the observed neutral losses can be extrapolated to metabolites of other DDAC metabolites, providing a useful approach for metabolite identification. In **Figure SI-6.10**, the relative abundances of all metabolites detected for both time points are compared between the 1 h and 3 h incubations.

**Table 6.1:** Neutral losses observed in the fragmentation spectra of annotated C<sub>10</sub>-DDAC metabolites. For each neutral loss, a molecular formula was predicted indicating the modification of the corresponding side chain. If marked with a green tick, the neutral loss was observed within the spectrum of the indicated metabolite.

		Neutral losses observed in fragmentation spectra of C <sub>10</sub> -DDAC metabolites				
Metabolite	Metabolism Reaction	- C <sub>10</sub> H <sub>20</sub> - 140.1565	- C <sub>10</sub> H <sub>20</sub> O - 156.1514	- C <sub>10</sub> H <sub>20</sub> O <sub>2</sub> - 172.1463	- C <sub>10</sub> H <sub>18</sub> O - 154.1358	- C <sub>10</sub> H <sub>18</sub> O <sub>2</sub> - 170.1307
C <sub>10</sub> -DDAC-M2	Monohydroxy (+O)	✓	✓	✗	✗	✗
C <sub>10</sub> -DDAC-M3	Dihydroxy (+2O)	✗	✓	✗	✗	✗
C <sub>10</sub> -DDAC-M4	Ketone (+O, -2H)	✓	✗	✗	✓	✗
C <sub>10</sub> -DDAC-M5	Keto-hydroxy (+2O, -2H)	✗	✓	✗	✓	✗
C <sub>10</sub> -DDAC-M6	Carboxy-hydroxy (+3O, -2H)	✗	✓	✗	✗	✓
C <sub>10</sub> -DDAC-M7	Carboxy-keto (+3O, -4H)	✗	✗	✗	✓	✓
C <sub>10</sub> -DDAC-M8	Dicarboxy (+4O, -4H)	✗	✗	✗	✗	✓
C <sub>10</sub> -DDAC-M9	Trihydroxy (+3O)	✗	✓	✓	✗	✗

A tentative desaturated metabolite (C<sub>10</sub>-DDAC-M1 in **Table SI-6.6**) was detected in the 1 h incubations. Given the low relative abundance, no fragmentation spectrum could be obtained resulting in the assignment of CL4 for this metabolite. The +O metabolite (C<sub>10</sub>-DDAC-M2) was annotated through the observation of neutral losses corresponding to [C<sub>10</sub>H<sub>20</sub>] and [C<sub>10</sub>H<sub>20</sub>O] and showed a clear decrease in relative abundance between 1 h and 3 h time points indicating further oxidation over time. For the +2O metabolites, three peaks were observed indicating three positional isomers (C<sub>10</sub>-DDAC-M3.1 to M3.3). For all peaks, fragmentation spectra showed only a neutral loss of [C<sub>10</sub>H<sub>20</sub>O] (**Figure SI-6.9-B**) indicating that one hydroxy group is located on each of the hydrocarbon side chains. The metabolite C<sub>10</sub>-DDAC-M3.1 showed the highest relative

abundance which decreased over time, while relative abundances increased for C<sub>10</sub>-DDAC-M3.2 and C<sub>10</sub>-DDAC-M3.3.

The decreasing relative abundances of both C<sub>10</sub>-DDAC-M2 and C<sub>10</sub>-DDAC-M3.1 suggest that these metabolites have a hydroxy group in  $\omega$ -position allowing further oxidation to a  $\omega$ -carboxy function. The metabolite carrying a +O,-2H function (C<sub>10</sub>-DDAC-M4) was assigned based on the observation of neutral losses of [C<sub>10</sub>H<sub>20</sub>] and [C<sub>10</sub>H<sub>18</sub>O]. Given its low relative abundances and the non-detection in 3 h time points, it can be considered a minor, intermediate metabolite. Next, a +2O,-2H-metabolite (C<sub>10</sub>-DDAC-M5.1/5.2) was observed. Within a previous study, a  $\omega$ -carboxy group has been proposed for this metabolite even though no fragmentation spectrum was provided (Nguyen et al., 2024). However, this assignment was not confirmed by the fragmentation spectra observed here. In contrast, the detected neutral losses of [C<sub>10</sub>H<sub>18</sub>O] and [C<sub>10</sub>H<sub>20</sub>O] indicated a keto (or aldehyde)-hydroxy metabolite with the functional groups located on different side chains. These neutral losses were observed for both listed peaks indicating two positional isomers. While the relative abundance of C<sub>10</sub>-DDAC-M5.2 showed a slight increase over time, it decreased for C<sub>10</sub>-DDAC-M5.1, again suggesting a  $\omega$ -position for the hydroxy and/or aldehyde group.

Furthermore, a +3O,-2H-metabolite showing two peaks was annotated, in accordance with the results reported for C<sub>10</sub>-DDAC by Nguyen et al. (Nguyen et al., 2024). Again, no fragmentation spectrum was provided, pointing out the necessity for further structural information. This is particularly important given that this metabolite showed the highest relative area ( $4.03 \pm 0.58$ ) among all data points, except for the parent compound (**Figure SI-6.9**). Within the fragmentation spectrum of +3O,-2H-C<sub>10</sub>-DDAC (**Figure 6.2**), neutral losses of [C<sub>10</sub>H<sub>20</sub>O] and [C<sub>10</sub>H<sub>18</sub>O<sub>2</sub>] were observed indicating the presence of one hydroxy group and a carboxy (or keto-hydroxy) group on different side chains. The presented data is the first report of the fragmentation pattern of this metabolite, and provides a valuable insight for future developments of targeted tandem MS methods.

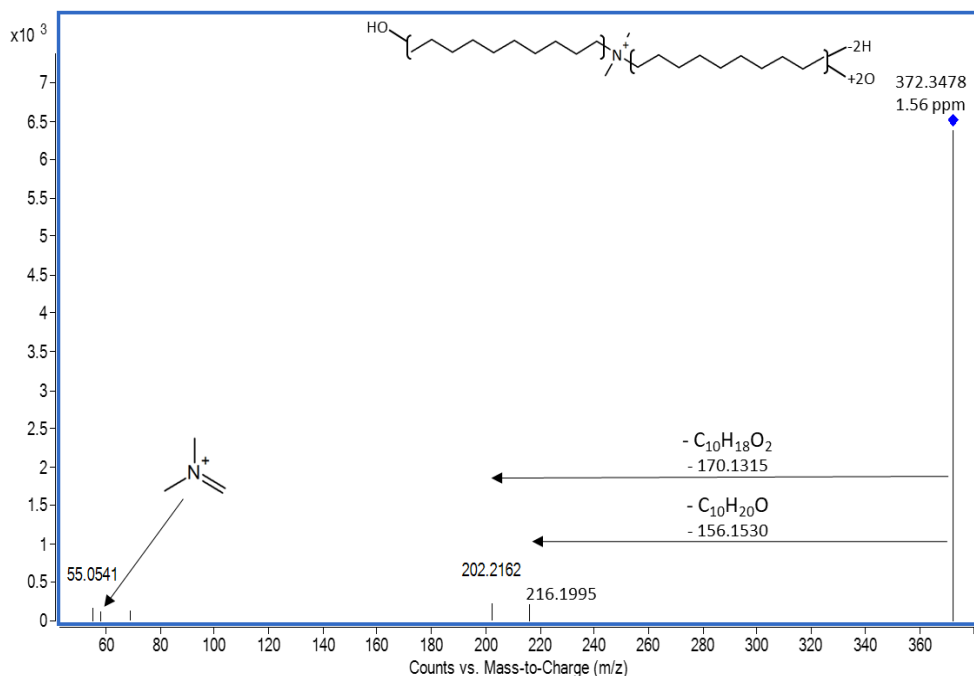


**Figure 6.2:** Fragmentation spectra obtained for the +3O,-2H-C<sub>10</sub>-DDAC metabolite at a collision energy of 20 eV. Based on the observed neutral losses, a tentative structure is proposed.

Further oxidation of the side chains was observed through the identification of +3O,-4H- and +3O,-2H-C<sub>10</sub>-DDAC metabolites. Based on the observed neutral losses (**Table 6.1/Figure SI-6.9**), they were assigned to carry a carboxy-keto and two carboxyl groups, respectively. Yet, the observed neutral losses do not allow to distinguish between a keto-hydroxy and a carboxyl group, even if the latter metabolite was suggested for other QAC homologues in previous studies (Li et al., 2023; Seguin et al., 2019). For both types of metabolites, low relative abundances (max. 0.71), slightly increasing over time, were observed. Lastly, a +3O metabolite was observed, showing two peaks at RTs of 3.74 and 3.99 min. The observed neutral losses indicated that one hydrocarbon side chain carried two hydroxy groups, while one was present on the other chain.

Ultimately, the presented data shows a stepwise, parallel oxidation of both hydrocarbon side chains of C<sub>10</sub>-DDAC. Interestingly, an oxidation of one side chain up to a carboxyl group did not occur without at least one oxidation step occurring on the other side chain. Even though *in vitro* observations cannot be directly transferred to an *in vivo* setting, the presented findings provide first valuable insights for further prioritization of relevant C<sub>10</sub>-DDAC metabolites and potential selections of mass transitions to be monitored within targeted tandem MS methods.

#### 6.3.2.4 Phase II incubations

Despite the extensive suspect and non-target screening approaches, no metabolites were annotated in either of the Phase II incubations, even though the detection of expected metabolites in the positive controls (**Figure SI-6.3 and SI-6.4**) at high abundances proved a successful incubation cycle. Also, in the samples including both, Phase I and consequent Phase II, incubations, the above described Phase I metabolites were detectable again proving successful performance. Despite the analysis in both ionization polarities, a limited detectability of potential Phase II metabolites has to be considered. The added functional groups (sulfate/glucuronide) can be deprotonated, suggesting a detection in negative polarity. However, given the positively charged nitrogen, the deprotonation would result in a zwitterion whose detectability is hampered given its (net) neutral charge. The described findings are in line with the information currently available in literature, in which no study was found describing Phase II metabolites for any of the QAC classes investigated here.

#### 6.3.3 IM-MS analysis of the annotated metabolites

In **chapters 3.1 and 4**, the added value of the extra separation dimension and possibility of CCS calculations provided by IM has been discussed in regards to the identification of CECs in environmental matrices. Thereby, IM-supported identifications are commonly based on matching of reference CCS values or CCS-*m/z* trendlines with experimental IM data. However, availability of reference CCS values for CEC metabolites and information on possible trends in CCS changes introduced by metabolism reactions are scarce. A previous study on the *in vitro* metabolization of numerous QACs reported TWIMS derived  $^{TW}CCS_{N_2}$  values for the assigned metabolites introducing first valuable insights into the  $^{TW}CCS_{N_2}$  changes following QAC metabolism (Nguyen et al., 2024), which interestingly differed from observations described for the metabolism of a set of drugs (Lanshoeft et al., 2024; Ross et al., 2020). For the latter, Lanshoeft et al. reported average changes in  $^{TW}CCS_{N_2}$  values following certain metabolism reactions. For example, hydroxylation lead to an increase in  $^{TW}CCS_{N_2}$  by  $3.8 \pm 1.4 \text{ \AA}^2$  (Lanshoeft et al., 2024). However, here and in the study of Nguyen et al., the opposite was observed; for all QACs, the introduction of a hydroxy group led to a clear decrease in  $^{DT}CCS_{N_2}$  value.

Differences of up to 5.5% were reported between the  $^{TW}CCS_{N_2}$  values of parent QACs and reference  $^{DT}CCS_{N_2}$  values included in **chapter 4.1** indicating limitations of database transfer. Additionally, the calculation of  $^{DT}CCS_{N_2}$  values for the new C<sub>10</sub>-DDAC metabolites described above can further improve IM data coverage.

Thus, the complete dataset of  $^{DT}CCS_{N_2}$  values for all metabolites annotated *in vitro* and presented in this study allows the characterization of changes introduced by

metabolism reactions and their comparison with data on other CEC metabolites available from **chapter 3.1**.  $^{DT}CCS_{N_2}$  values calculated for metabolites of C<sub>12</sub>-BAC, C<sub>16</sub>-ATMAC and C<sub>10</sub>-DDAC are summarized in **Tables SI-6.7, SI-6.8 and SI-6.9**, respectively. Thereby, average  $^{DT}CCS_{N_2}$  values for triplicate samples of each incubation time point were included. For none of the metabolites, average  $^{DT}CCS_{N_2}$  values varied more than 0.17% between the two incubation times, showing excellent intra-laboratory reproducibility. Therefore, all further discussions are based on the  $^{DT}CCS_{N_2}$  values obtained for 1h incubations.

$^{DT}CCS_{N_2}$  values of parent QACs differed from data reported in **chapter 4.1** by 0.07%, 0.10% and -0.03% for C<sub>12</sub>-BAC, C<sub>16</sub>-ATMAC and C<sub>10</sub>-DDAC, respectively, showing excellent stability of IM measurements across a two-year period. Obtained  $^{DT}CCS_{N_2}$  values of QAC metabolites were compared with the  $^{TW}CCS_{N_2}$  database published by Nguyen et al., whereby average absolute percent errors (APEs) of 0.48%, 0.84% and 1.71% were observed for metabolites of C<sub>12</sub>-BAC, C<sub>16</sub>-ATMAC and C<sub>10</sub>-DDAC, respectively, with individual deviations up to 3.37%. These observations are in line with APEs reported by Nguyen et al. for the comparison of  $^{DT}CCS_{N_2}$  and  $^{TW}CCS_{N_2}$  values for parent QACs (Nguyen et al., 2024) and indicate the increased  $CCS_{N_2}$  deviations commonly observed for comparisons of different instrumental set-ups (**chapter 4.2**).

For further assessment of changes in  $^{DT}CCS_{N_2}$  values following metabolism,  $^{DT}CCS_{N_2}$  values of all identified metabolites were plotted as a function of the  $m/z$  ratios. The obtained plots are displayed in **Figure SI-6.11** and **Figure 6.3** for C<sub>12</sub>-BAC/C<sub>16</sub>-ATMAC and C<sub>10</sub>-DDAC, respectively. For C<sub>12</sub>-BAC and C<sub>16</sub>-ATMAC very similar trends in the obtained  $^{DT}CCS_{N_2}$  values were observed following metabolism. The addition of one hydroxy group in the hydrocarbon side chain led to lower  $^{DT}CCS_{N_2}$  values suggesting much more compact gaseous ion conformations. As described by Nguyen et al., ion-dipole interactions between the positively charged nitrogen and the added oxygen are assumed to cause the described effects. This phenomenon was only observed after the addition of one hydroxy group since  $^{DT}CCS_{N_2}$  values increased for +O,-2H and +2O,-2H metabolites formed through further oxidation. Here, the  $CCS$ - $m/z$  trends followed the well described relationship of increasing  $CCS$  values with increasing molecular mass (**chapter 3.1**).

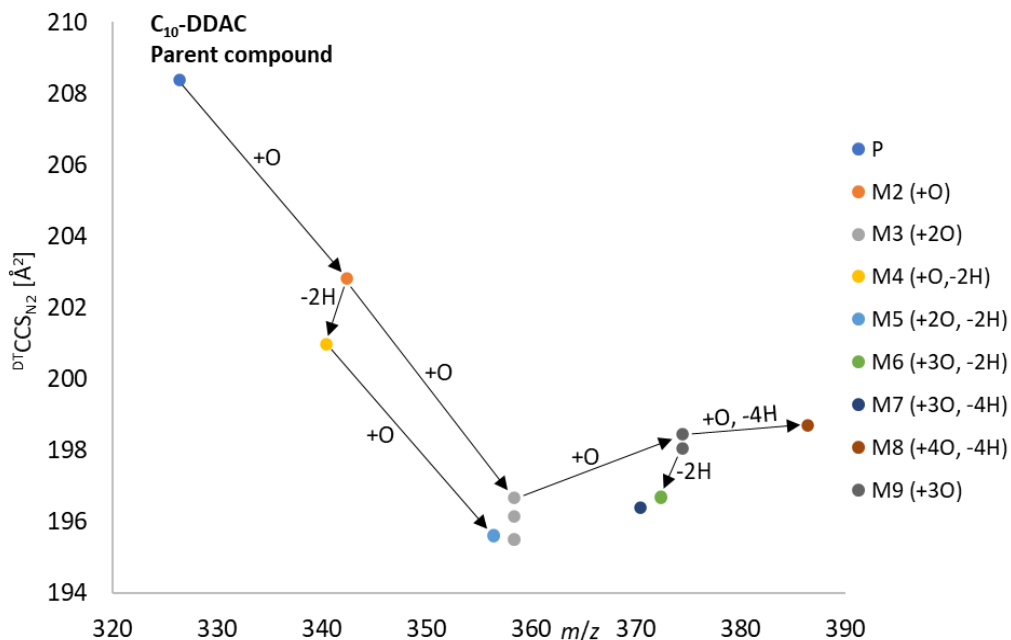


**Figure 6.3:**  $^{DT}CCS_{N_2}$  obtained for metabolites of  $C_{10}$ -DDAC as a function of the corresponding  $m/z$  ratios. The data confirming the identity of each metabolite is summarized in **Table SI-6.6**. Black arrows indicate metabolism reactions.

Next,  $^{DT}CCS_{N_2}$  values of  $C_{10}$ -DDAC metabolites covering a higher variety of oxidized forms were investigated (**Figure 6.3**). A decrease in the  $^{DT}CCS_{N_2}$  value was observed after the addition of one hydroxy group. Interestingly and in contrast to  $C_{12}$ -BAC and  $C_{16}$ -ATMAC, this trend was repeated for the dihydroxy and +2O,-2H-metabolites. This suggests that the hypothesized ion-dipole interactions can be formed between the charged nitrogen and both side chains leading to a stepwise increase in the compactness of the gaseous confirmation of metabolite ions. This also confirms that the keto (or aldehyde) and hydroxy groups of the +2O,-2H-metabolite are introduced on different side chains and no carboxyl group is present, otherwise such a stepwise folding of both side chains would not be possible. For higher oxidized metabolites (+3O; +3O, -4H, etc.), the decreasing trend is not observed, indicating that maximum ion compaction is reached after the introduction of one oxidation side on each side chain. The higher oxidized metabolites then followed the expected trend of increasing  $^{DT}CCS_{N_2}$  values with increasing  $m/z$  ratios. Only for desaturated metabolites (+3O,-2H and +3O,-4H in comparison to +3O) a slight decrease in  $^{DT}CCS_{N_2}$  was observed.

Despite the valuable information provided by the described  $^{DT}CCS_{N_2}$  trends, the importance of chromatographic separation cannot be neglected as can be demonstrated, e.g., by the data obtained for the three isomers of the  $C_{10}$ -DDAC-M3 (+2O). For these,

$^{DT}CCS_{N_2}$  values of 196.66, 196.14 and 195.50  $\text{\AA}^2$  (**Table SI-6.9**) were obtained. This corresponds to  $^{DT}CCS_{N_2}$  differences of < 0.7%. Given the low relative standard deviations observed for  $^{DT}CCS_{N_2}$  calculations and the increased resolution which can be achieved implementing the high-resolution demultiplexing step, the observed differences are considered sufficient to distinguish between isomers. However, when  $CCS_{N_2}$  values are transferred between instrumental set-ups, the observed  $\Delta CCS_{N_2}$  does not suffice to ensure isomer distinguishment given the high deviations between  $^{DT}CCS_{N_2}$  and  $^{TW}CCS_{N_2}$  described above. In these cases, the separation in the chromatographic dimension is crucial to ensure that the presence of different isomers is recognized. Here, this was achieved and RT differences of up to 0.15 min were observed between isomers.

In conclusion, the presented  $^{DT}CCS_{N_2}$  trends confirm the structures proposed based on the fragmentation spectra described in **chapter 6.3.2.3**. Their partial match with trends observed for metabolites of other CEC classes with long side chains allows the use of these observations to support future metabolite identifications. The differences between investigated QACs carrying one and two longer hydrocarbon side chains provide a valuable tool for future annotations of QAC metabolites aiming at confirming the described observations in human matrices.

#### 6.3.4 Confirmation of *in vitro* annotated metabolites in human urine samples

Human urine sample from 10 healthy participants were available from previous studies (Bastiaensen et al., 2021c; Gys et al., 2021b). From this set, four samples from each participant were randomly selected and analyzed as described in **chapters 6.2.4** and **6.2.5**. Data were screened for the parent compounds and metabolites annotated *in vitro*. In none of the samples, parent compounds were detected with signals exceeding the slight background contamination observed in procedural blanks with a fold change of at least three. A total of eight metabolites originating from six metabolism reactions were detected in urine from three out of ten participants originating from  $C_{12}$ -BAC and  $C_{10}$ -DDAC. In urine of the other seven participants, no metabolites were detectable. Interestingly, no  $C_{16}$ -ATMAC metabolites were identified. This might be attributed to lower  $C_{16}$ -ATMAC concentration reported for indoor environments (**chapter 4.1**), leading to lower human exposure, or to the lower metabolism rates described for this compound above. Detected metabolites are given in **Table 6.2** while details are summarized in **Tables SI-10** and **SI-11** for  $C_{12}$ -BAC and  $C_{10}$ -DDAC, respectively.

**Table 6.2:** Summary of C<sub>12</sub>-BAC and C<sub>10</sub>-DDAC metabolites detected in human urine samples of three out of ten participants. Detailed information for each metabolite can be found in **Tables SI-6.10** and **SI-6.11**, respectively. For each metabolite, the detection frequency (DF) in the four urine samples included for each participant, is indicated.

Compound	Proposed metabolite	Participant C (n = 4)		Participant D (n = 4)		Participant E (n = 4)	
		Detected?	DF [%]	Detected?	DF [%]	Detected?	DF [%]
C <sub>12</sub> -BAC-M2.1	(+O)	✓	100% (4/4)	✗		✗	
C <sub>12</sub> -BAC-M2.2	(+O)	✓	75% (3/4)	✗		✗	
C <sub>12</sub> -BAC-M4.1	(+O, -2H)	✓	100% (4/4)	✗		✗	
C <sub>12</sub> -BAC-M5.1	(+2O, -2H)	✓	100% (4/4)	✗		✗	
C <sub>10</sub> -DDAC-M6.1	(+3O, -2H)	✓	75% (3/4)	✗		✗	
C <sub>10</sub> -DDAC-M6.2	(+3O, -2H)	✓	75% (3/4)	✗		✗	
C <sub>10</sub> -DDAC-M7	(+3O, -4H)	✓	75% (3/4)	✗		✗	
C <sub>10</sub> -DDAC-M8	(+4O, -4H)	✓	100% (4/4)	✓	50% (2/4)	✓	50% (2/4)

For C<sub>12</sub>-BAC, the +O, +O -2H, and +2O -2H metabolites were annotated whereby all three modifications were detected in the samples of one out of ten participant. Thereby, the RTs matched between HLM incubations and urine samples ( $\Delta$ RT < 0.15 min) and all observed mass errors were <2 ppm. For all metabolites, the fragmentation spectra showed the characteristic tropylium ion and neutral loss of loss of the benzyl moiety allowing to assign CL3. Interestingly, also in urine, two peaks were observed for the +O metabolite suggesting the presence of two hydroxy metabolites. As already observed in the HLM incubations, the later eluting peak showed a higher abundance. The observed findings are in line with previous detection of oxidized BAC metabolites reported for human urine (Li et al., 2023). However, previous quantitative studies focused solely on monohydroxy and carboxy metabolites. The report of a +O -2H metabolite described here indicates the presence of another oxidized form. Its inclusion in future quantitative studies might allow a more complete exposure assessment.

For C<sub>10</sub>-DDAC, three metabolites were detected in human urine samples including +3O -2H, +3O -4H and +4O -4H. RTs matched between urine and HLM incubations ( $\Delta$ RT < 0.15 min) and low mass errors (all < 2.1 ppm) were observed. The first two metabolites were detected only in the same participant's urine, in which also the C<sub>12</sub>-BAC metabolites were found. Thereby, CL4 had to be assigned given the low abundance

which did not allow the acquisition of high-quality fragmentation spectra. The highest oxidized metabolite (+4O, -4H) was detected in three urine samples showing higher abundances thus allowing the acquisition of fragmentation spectra. As shown in **Figure 6.4**, these matched the data observed within HLM incubations: A neutral loss of  $[C_{10}H_{18}O_2]$  was observed indicating that two +2O -2H modifications (assumably carboxyl groups) are located on different hydrocarbon side chains.

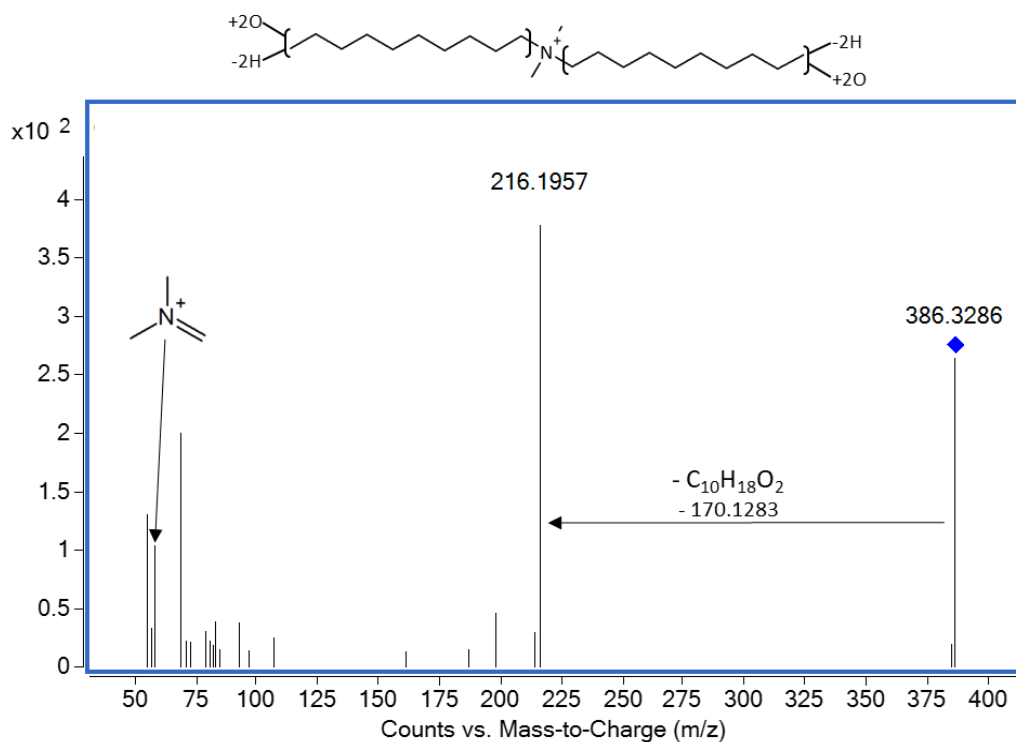


**Figure 6.4:** Fragmentation spectra obtained for the metabolite C10-DDAC-M8 (+4O, -4H) in a human urine sample obtained at a collision energy of 20 eV. The observed neutral loss and characteristic  $[C_3H_8N]^+$  ion (theoretical  $m/z$  58.0651) matched the data obtained in HLM incubations (**Figure SI-6.8**).

To the best of our knowledge, this is the first report in human urine samples for all four  $C_{10}$ -DDAC metabolites. Nguyen et al. reported lower oxidized DDAC metabolites in human feces (Nguyen et al., 2024) while, as presented here and discussed in a recent study (Li and Kannan, 2024), for higher oxidized forms a urinary excretion is expected. Nevertheless, an investigation of the metabolites annotated here in human feces samples could further expand the characterization of QAC elimination pathways. The structural differences between the detected metabolites and the available IS did not allow the use of the latter for a semi-quantitative assessment of metabolite concentrations. Additionally, the lower structural variability observed for metabolites

detected in urine in comparison to the HLM model, underlines the limited transferability of *in vitro* results to an *in vivo* setting. Nevertheless, the presented results serve as a necessary starting point for metabolite prioritization and further quantitative studies aiming at assessing human exposure to QACs. Unfortunately, no questionnaire data or similar was available for the participants investigated here not allowing to characterize particular exposure events which might have led to the detection of QAC metabolites.

For all metabolites detected in urine,  $^{DT}CCS_{N_2}$  values were calculated based on the injection of pooled urine samples (four samples pooled per participant). The obtained  $^{DT}CCS_{N_2}$  values are summarized in **Table SI-6.12** and were compared with IM data obtained for HLM incubations (**Tables SI-S7/S9**). For all metabolites,  $^{DT}CCS_{N_2}$  values matched between the two datasets with deviations ranging between 0.31 and -0.25%. This confirms the assignment of metabolite structures in human urine reproducing the  $CCS$ - $m/z$  trends described above. Furthermore,  $^{DT}CCS_{N_2}$  values serve as a valuable additional identification parameter, especially in the case of  $C_{12}$ -BAC metabolites for which no fragmentation spectra could be obtained.

## 6.4 Conclusions

In conclusion, this study characterized the hepatic oxidative metabolism pathways of  $C_{12}$ -BAC,  $C_{16}$ -ATMAC and  $C_{10}$ -DDAC providing first insights into the time trends of *in vitro* metabolism of QACs. A total of 31 metabolites were annotated whereby for  $C_{10}$ -DDAC, three metabolites are reported for the first time. The detailed report of fragmentation spectra is expected to facilitate future method development. Additionally, the report of  $^{DT}CCS_{N_2}$  for all assigned metabolites provide valuable reference data for future IM-MS studies and retrieved  $^{DT}CCS_{N_2}$  trends confirm metabolite identifications. Finally, eight metabolites were confirmed in human urine samples whereby the detection of higher oxidized  $C_{10}$ -DDAC metabolites is reported for the first time. These findings are expected to facilitate future quantitative assessments of DDAC metabolite concentrations in human matrices.

## Supplementary Information – Chapter 6

**Table SI-6.1:** Chromatographic method applied for all analyses discussed in this chapter.

<b>Mobile phases</b>	(A) ESI+: 95:5 water/acetonitrile (v/v) + 0.1 % acetic acid ESI-: 95:5 water/acetonitrile (v/v) + 5 mM ammonium acetate (B) 95:5 acetonitrile/water (v/v) + 5 mM ammonium acetate (C) Isopropanol + 0.1 % formic acid			
<b>Column</b>	Phenomenex LUNA C18 column (150 mm × 2 mm; 3 μm particle size)			
<b>Gradient</b>	<b>Time [min]</b>	<b>A [%]</b>	<b>B [%]</b>	<b>C [%]</b>
	0	95	5	0
	0.5	95	5	0
	9	50	50	0
	14	5	65	30
	17	0	55	45
	18.5	0	55	45
	20	95	5	0
	24	95	5	0
<b>Flow rate</b>	0.35 mL/min			

**Table SI-6.2:** Summary of settings applied for the ionization source and drift tube.

<b>Ion Source Settings</b>	Drying gas temperature [°C]	325	
	Drying gas flow [L/min]	11	
	Sheath gas temperature [°C]	350	
	Sheath gas flow [L/min]	12	
	Nebulizer pressure [psig]	30	
	Capillary Voltage [V]	3000	
	Nozzle Voltage [V]	500	
	Fragmentor Voltage [V]	300	
	Octopole RF [V]	750	
<b>Drift Tube Settings</b>		<b>ESI+</b>	<b>ESI-</b>
	Drift Tube Entrance Voltage [V]	1574	- 1574
	Drift Tube Exit Voltage [V]	224	- 224
	Rear Funnel Entrance Voltage [V]	217.5	- 217.5
	Rear Funnel Exit Voltage [V]	45	- 45
	Trap Funnel RF [V]	120	120
	Trap Fill Time [μs]	3000	3000
	Trap Release Time [μs]	250	250
Max. Drift Time [ms]	60	60	

**Table SI-6.3:** Characteristic fragments and neutral losses used for the non-targeted screening of metabolites. For each fragment and neutral loss, the theoretical  $m/z$  ratio and formula are indicated.

Metabolites of	Fragment	Neutral loss
C <sub>12</sub> -BAC	$m/z$ 91.0542 [C <sub>7</sub> H <sub>6</sub> ] <sup>+</sup> $m/z$ 58.0651 [C <sub>3</sub> H <sub>8</sub> N] <sup>+</sup>	$m/z$ 92.00626 [C <sub>7</sub> H <sub>8</sub> ]
C <sub>16</sub> -ATMAC	$m/z$ 60.0808 [C <sub>3</sub> H <sub>10</sub> N] <sup>+</sup> $m/z$ 58.0651 [C <sub>3</sub> H <sub>8</sub> N] <sup>+</sup>	n.a.
C <sub>10</sub> -DDAC	$m/z$ 58.0651 [C <sub>3</sub> H <sub>8</sub> N] <sup>+</sup>	All neutral losses listed in Table 6.1

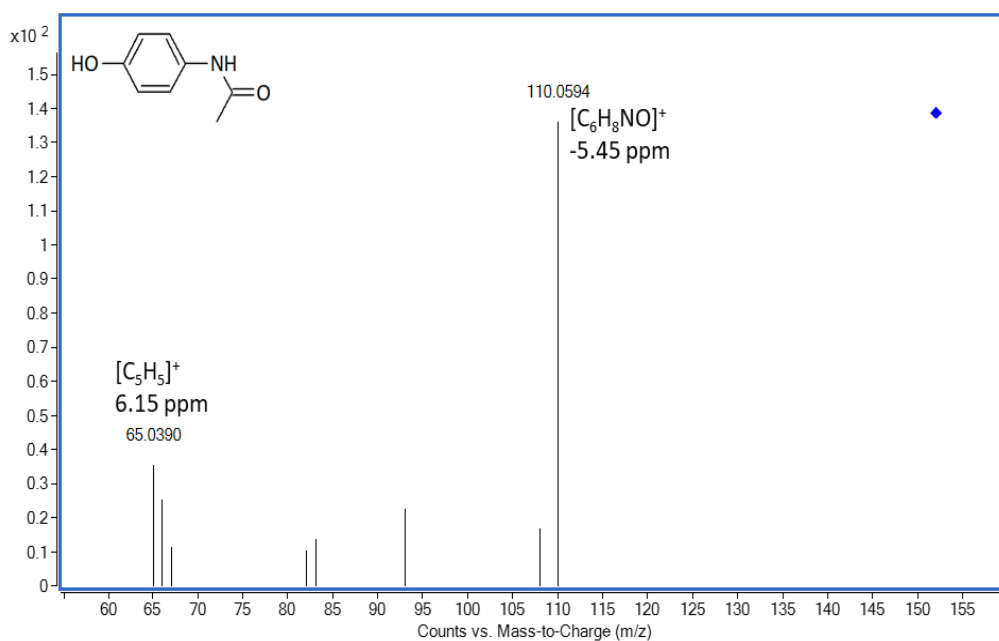


**Figure SI-6.1:** Fragmentation spectrum (collision energy: 20 eV) obtained for the dealkylated metabolite of phenacetin in the positive control (PC) samples of the Phase I incubations prepared for the three quaternary ammonium compounds investigated in this study. The structure of the metabolite as well as the formulae and observed mass errors of characteristic fragments are indicated.

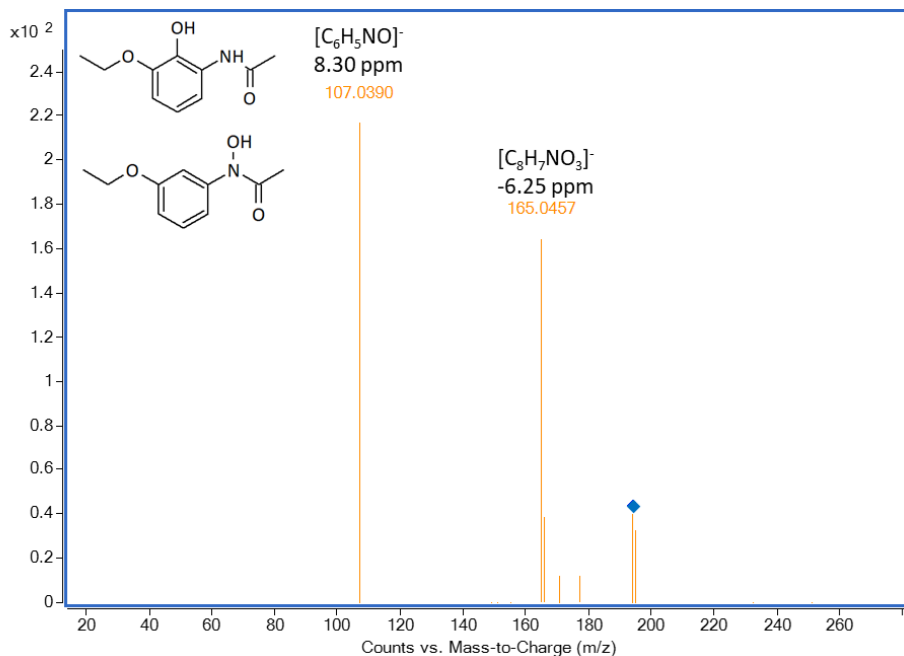


**Figure SI-6.2:** Fragmentation spectrum (collision energy: 20 eV) obtained for the hydroxylated metabolite of phenacetin in the positive control (PC) samples of the Phase I incubations prepared for the three quaternary ammonium compounds investigated in this study. Two possible structures of the metabolite are proposed based in observed fragments. Formulae and observed mass errors of characteristic fragments are indicated.

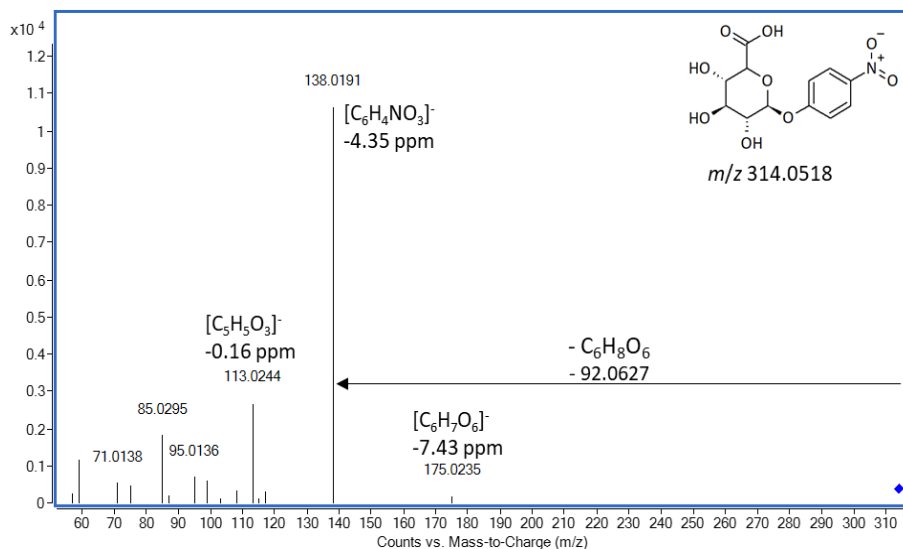


**Figure SI-6.3:** Fragmentation spectrum (collision energy: 20 eV) obtained for the 4-nitrophenol-glucuronide in the positive control (PC) samples of the Phase II incubations prepared for the three quaternary ammonium compounds investigated in this study. The structure of the metabolite as well as the formulae and observed mass errors of characteristic fragments are indicated.

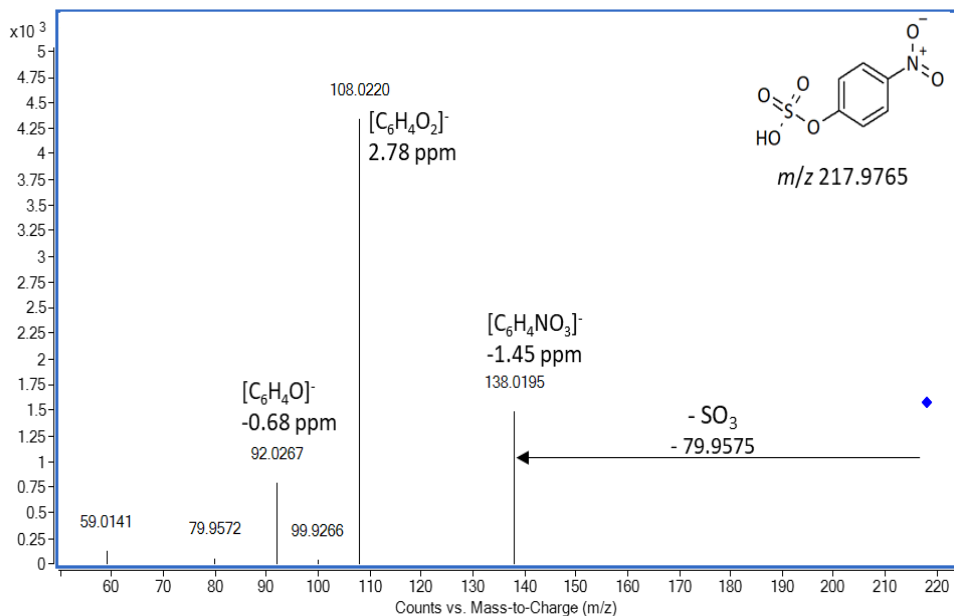


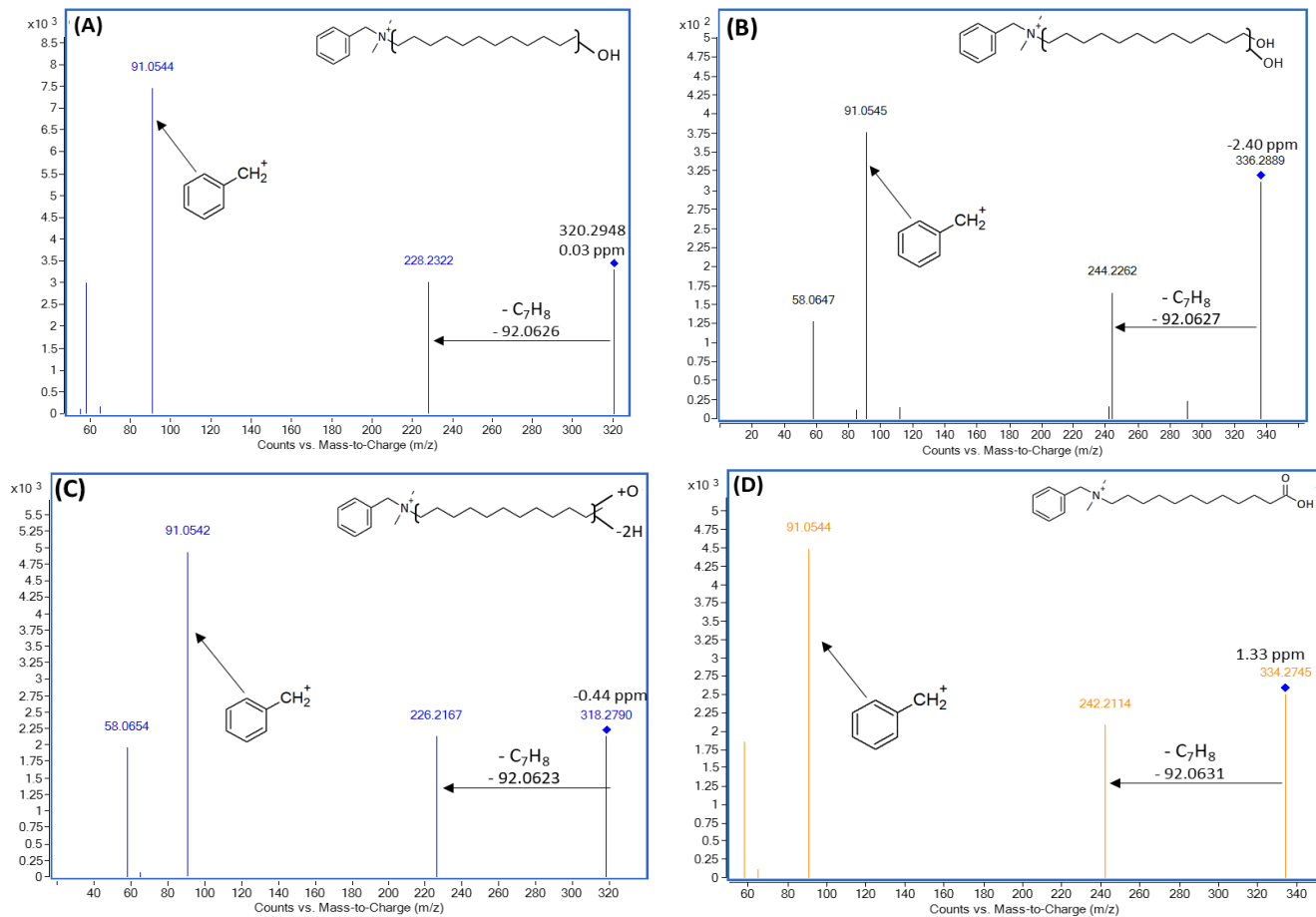
**Figure SI-6.4:** Fragmentation spectrum (collision energy: 20 eV) obtained for the 4-nitrophenol-sulfate in the positive control (PC) samples of the Phase II incubations prepared for the three quaternary ammonium compounds investigated in this study. The structure of the metabolite as well as the formulae and observed mass errors of characteristic fragments are indicated.

**Table SI-6.4:** Data obtained for benzyltrimethyl dodecylammonium (C<sub>12</sub>-BAC, parent compound) and its metabolites identified in the 1 h and 3 h incubations. For each metabolite, the formula, assigned confidence level (CL), average mass error and (triplicate analysis per time point), relative abundance and whether the metabolite was detected in negative control (NC samples) is indicated. NCS: Negative control samples without addition of substrate. \*The NC control samples refer to the NCs to which no HLMs or cofactors were added.

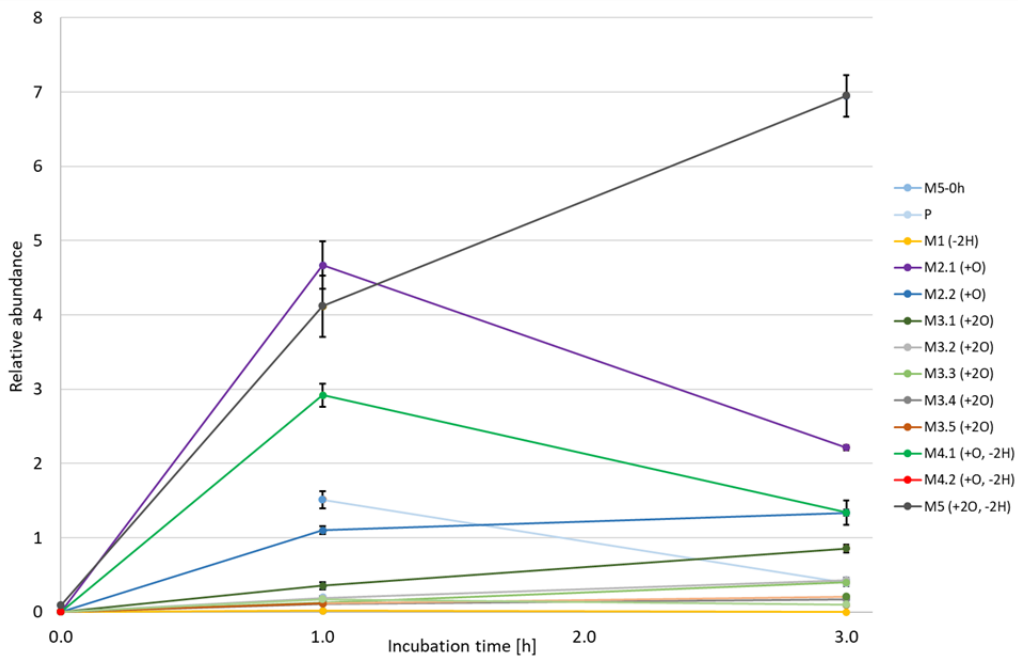
For the 0 h time point of the parent compound (interpreted as the relative abundance in the negative controls to which only the substrate and no HLMs and cofactors were added), a relative abundance of 22.61 ± 3.45 was observed.

Compound	Proposed metabolite	Formula	RT [min]	1 h incubations				3 h incubations			
				Mass error [ppm]	CL	Rel. abundance 1 h (± SD)	Detected in NC*?	Mass error [ppm]	CL	Rel. abundance 3 h (± SD)	Detected in NC*?
Benzyltrimethyl dodecylammonium (C <sub>12</sub> -BAC)	Parent	[C <sub>21</sub> H <sub>38</sub> N] <sup>+</sup>	12.95	2.28	1	1.51 ± 0.11	Yes	1.17	1	0.39 ± 0.04	Yes
C <sub>12</sub> -BAC-M1	Desaturation (-2H)	[C <sub>21</sub> H <sub>36</sub> N] <sup>+</sup>	11.90	-0.93	3	0.02 ± 0.01	No	n.d.	-	n.d.	n.a.
C <sub>12</sub> -BAC-M2.1	Monohydroxy (+O)	[C <sub>21</sub> H <sub>38</sub> NO] <sup>+</sup>	7.12	2.11	3	4.67 ± 0.32	Yes (NCS)	1.55	3	2.22 ± 0.04	Yes (NCS)
C <sub>12</sub> -BAC-M2.2	Monohydroxy (+O)	[C <sub>21</sub> H <sub>38</sub> NO] <sup>+</sup>	6.88	2.09	3	1.10 ± 0.05	Yes (NCS)	2.76	3	1.34 ± 0.16	Yes (NCS)
C <sub>12</sub> -BAC-M3.1	Dihydroxy (+2O)	[C <sub>21</sub> H <sub>38</sub> NO <sub>2</sub> ] <sup>+</sup>	4.23	0.49	3	0.36 ± 0.05	Yes (NCS)	1.74	3	0.85 ± 0.06	Yes (NCS)
C <sub>12</sub> -BAC-M3.2	Dihydroxy (+2O)	[C <sub>21</sub> H <sub>38</sub> NO <sub>2</sub> ] <sup>+</sup>	3.95	0.59	3	0.19 ± 0.02	Yes (NCS)	0.81	3	0.43 ± 0.03	Yes (NCS)
C <sub>12</sub> -BAC-M3.3	Dihydroxy (+2O)	[C <sub>21</sub> H <sub>38</sub> NO <sub>2</sub> ] <sup>+</sup>	3.56	0.35	4	0.13 ± 0.02	No	0.49	3	0.40 ± 0.02	Yes (NCS)
C <sub>12</sub> -BAC-M3.4	Dihydroxy (+2O)	[C <sub>21</sub> H <sub>38</sub> NO <sub>2</sub> ] <sup>+</sup>	2.73	0.55	4	0.11 ± 0.01	No	0.36	3	0.17 ± 0.02	No
C <sub>12</sub> -BAC-M3.5	Dihydroxy (+2O)	[C <sub>21</sub> H <sub>38</sub> NO <sub>2</sub> ] <sup>+</sup>	2.44	0.50	4	0.12 ± 0.01	No	0.47	3	0.21 ± 0.01	No

C <sub>12</sub> -BAC-M4.1	Ketone (+O, -2H)	[C <sub>21</sub> H <sub>36</sub> NO] <sup>+</sup>	7.39	2.81	3	2.92 ± 0.16	Yes (NCS)	2.40	3	1.34 ± 0.04	Yes (NCS)
C <sub>12</sub> -BAC-M4.1	Ketone (+O, -2H)	[C <sub>21</sub> H <sub>36</sub> NO] <sup>+</sup>	7.68	1.21	3	0.17 ± 0.01	No	0.34	3	0.10 ± 0.01	No
C <sub>12</sub> -BAC-M5.1	Carboxy (+2O, -2H)	[C <sub>21</sub> H <sub>36</sub> NO <sub>2</sub> ] <sup>+</sup>	6.81	2.45	3	4.12 ± 0.41	Yes (NCS)	2.47	3	6.95 ± 0.28	Yes (NCS)



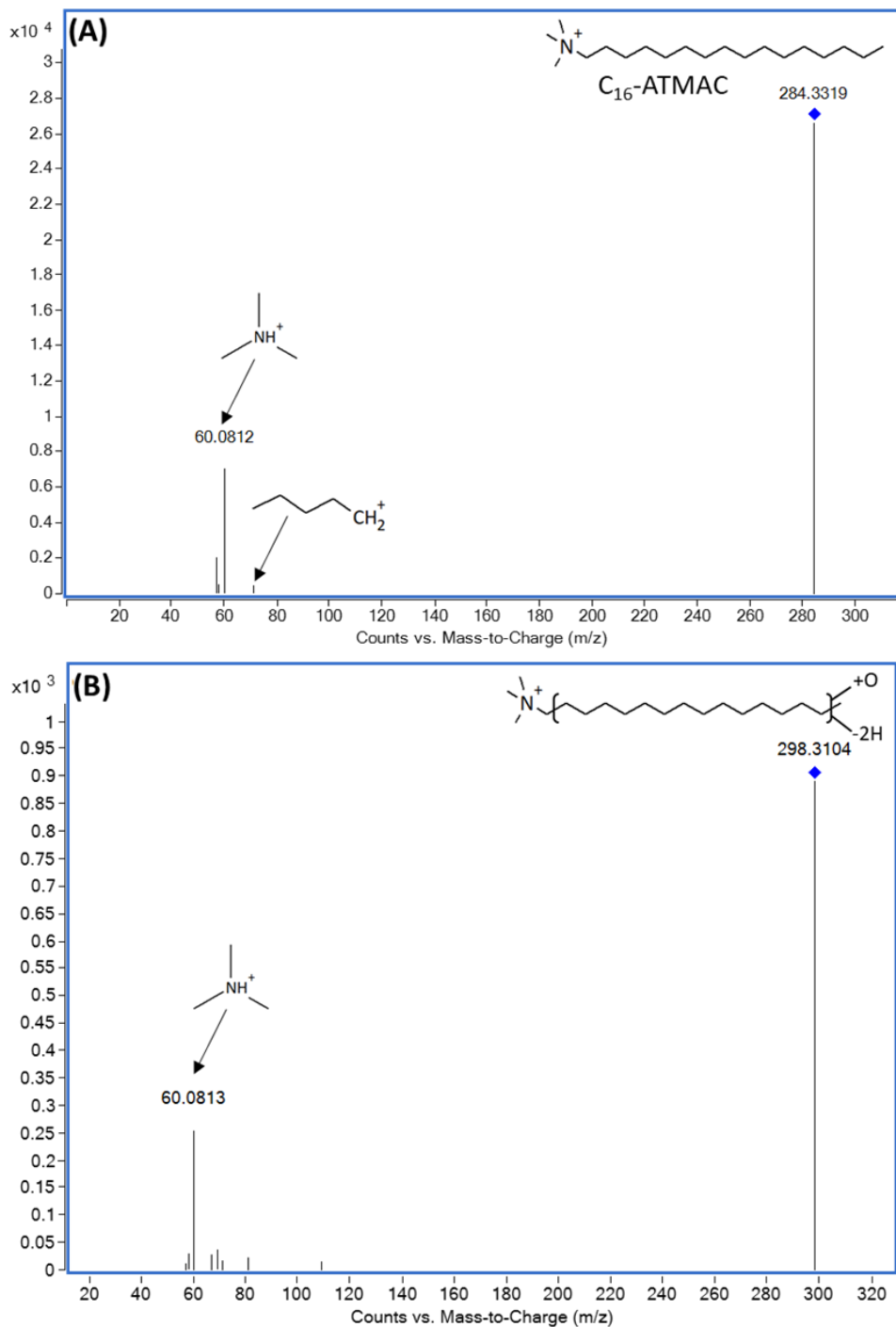
**Figure SI-6.5:** Fragmentation spectra obtained for the identified C<sub>12</sub>-BAC metabolites. These corresponded to (A) monohydroxy (+O; RT of 7.12 min; collision energy: 20 eV); (B) dihydroxy (+2O; RT of 4.23 min; collision energy: 20 eV); (C) ketone (+O, -2H; RT of 7.39 min; collision energy: 20 eV); (D) carboxy (+2O, -2H; RT of 2.45 min; collision energy: 20 eV).



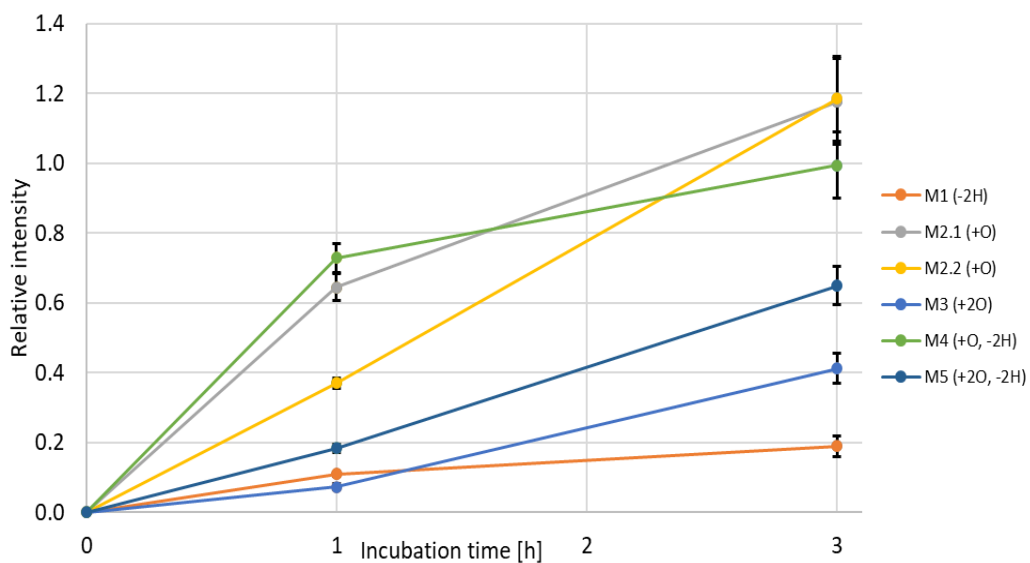
**Figure SI-6.6:** Relative abundance obtained for all C<sub>12</sub>-BAC metabolites (Table SI-6.4, relative to IS D<sub>7</sub>-C<sub>12</sub>-BAC) for 1h and 3h incubations. For each datapoint, the standard deviations (n = 3) are indicated. For metabolites, average relative abundances observed in negative control samples with no addition of the substrate were used as the 0 h time points. At 0h, M5 showed a relative abundance of 0.09 ± 0.1. For all other metabolites, values observed at 0 h were < 0.02. For the 0 h time point of the parent compound (interpreted as the relative abundance in the negative controls to which only the substrate and no HLMs and cofactors were added), a relative abundance of 22.61 ± 3.45 was observed.

**Table SI-6.5:** Data obtained for cetyltrimethylammonium (C<sub>16</sub>-ATMAC, parent compound) and its metabolites identified in the 1 h and 3 h incubations. For each metabolite, the formula, assigned confidence level (CL), average mass error and (triplicate analysis per time point), relative abundance and whether the metabolite was detected in negative control (NC samples) is indicated. \*The NC control samples refer to the NCs to which no HLMs or cofactors were added. For the 0 h time point of the parent compound (interpreted as the relative abundance in the negative controls to which only the substrate and no HLMs and cofactors were added), a relative abundance of 20.41 ± 3.79 was observed.

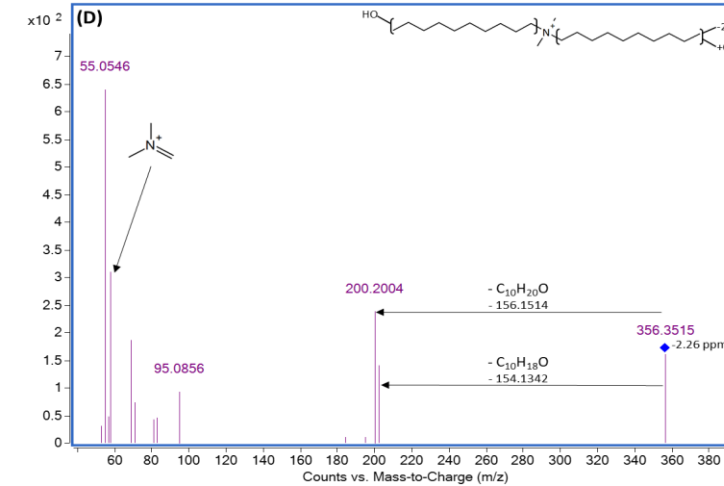
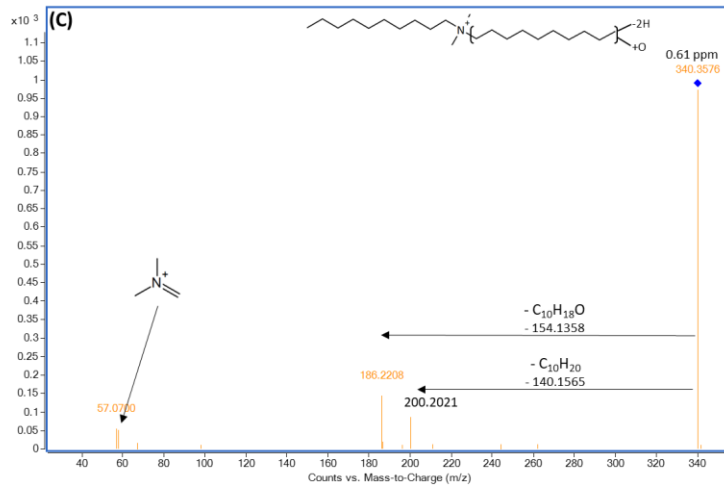
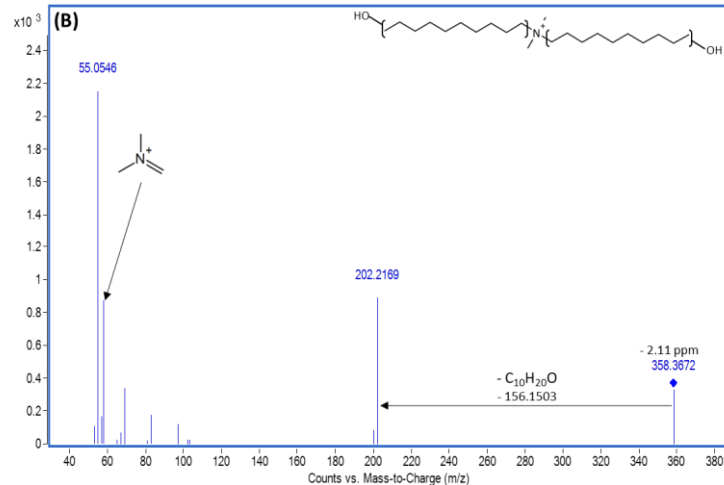
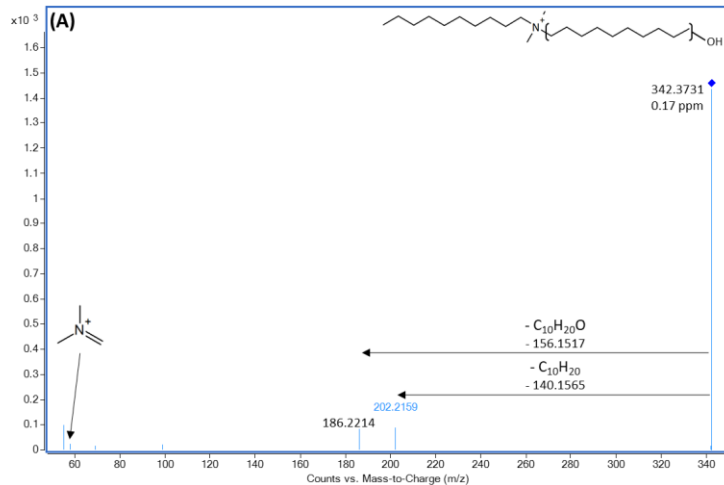
Compound	Proposed metabolite	Formula	RT [min]	1 h incubations				3 h incubations			
				Mass error [ppm]	CL	Rel. abundance 1 h (± SD)	Detected in NC*?	Mass error [ppm]	CL	Rel. abundance 3 h (± SD)	Detected in NC*?
Cetyltrimethylammonium (C <sub>16</sub> -ATMAC)	Parent	[C <sub>19</sub> H <sub>42</sub> N] <sup>+</sup>	14.53	2.21	1	13.82 ± 0.08	Yes	2.94	1	10.08 ± 2.07	Yes
C <sub>16</sub> -ATMAC-M1	Desaturation (-2H)	[C <sub>19</sub> H <sub>40</sub> N] <sup>+</sup>	13.60	1.21	3	0.11 ± 0.01	No	0.46	3	0.19 ± 0.03	No
C <sub>16</sub> -ATMAC-M2.1	Monohydroxy (+O)	[C <sub>19</sub> H <sub>42</sub> NO] <sup>+</sup>	8.98	1.45	3	0.65 ± 0.04	No	1.71	3	1.18 ± 0.12	No
C <sub>16</sub> -ATMAC-M2.2	Monohydroxy (+O)	[C <sub>19</sub> H <sub>42</sub> NO] <sup>+</sup>	8.76	0.77	3	0.37 ± 0.02	No	1.83	3	1.18 ± 0.12	No
C <sub>12</sub> -ATMAC-M3.1	Dihydroxy (+2O)	[C <sub>19</sub> H <sub>42</sub> NO <sub>2</sub> ] <sup>+</sup>	6.16	0.37	3	0.07 ± 0.01	No	1.49	3	0.41 ± 0.04	No
C <sub>12</sub> -ATMAC-M4.1	Ketone (+O, -2H)	[C <sub>19</sub> H <sub>40</sub> NO] <sup>+</sup>	9.30	2.13	3	0.73 ± 0.04	No	2.99	3	0.99 ± 0.09	No
C <sub>12</sub> -ATMAC-M5.1	Carboxy (+2O, -2H)	[C <sub>19</sub> H <sub>40</sub> NO <sub>2</sub> ] <sup>+</sup>	8.51	0.43	3	0.18 ± 0.01	No	1.81	3	0.65 ± 0.05	No



**Figure SI-6.7:** Fragmentation spectra obtained for C<sub>16</sub>-ATMAC (A) and the +O,-2H metabolite (B) at 20 eV.



**Figure SI-6.8:** Relative abundance obtained for all C<sub>16</sub>-ATMAC metabolites (Table SI-6.5, relative to IS D<sub>9</sub>-C<sub>10</sub>-ATMAC) for 1h and 3h incubations. For each datapoint, the standard deviations (n = 3) are indicated. For metabolites, average relative abundances observed in negative control samples with no addition of the substrate were used as the 0 h time points. The relative abundances of the parent compound (C<sub>16</sub>-ATMAC; Table S6) were one order of magnitude higher than for metabolites and were therefore not included in this figure. They are summarized in Table SI-6.5.



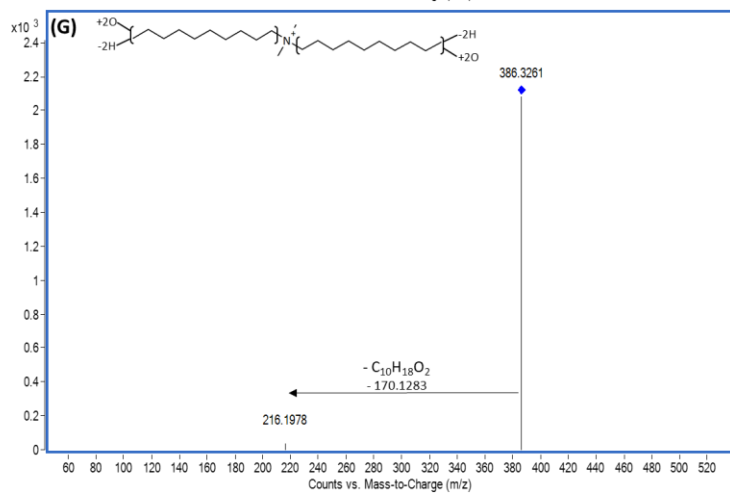
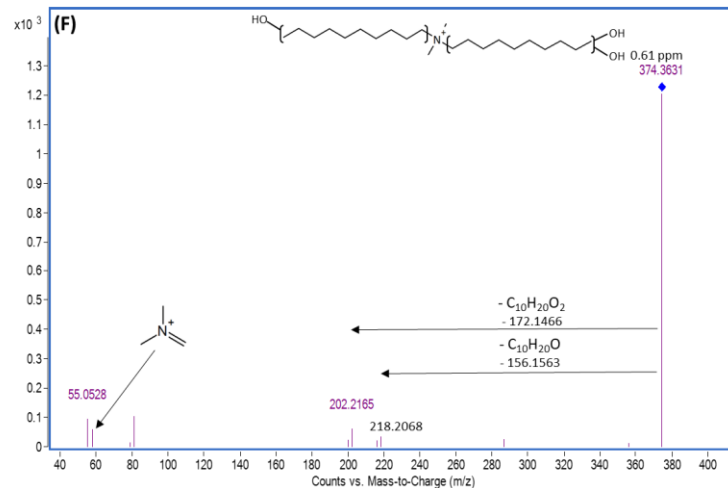
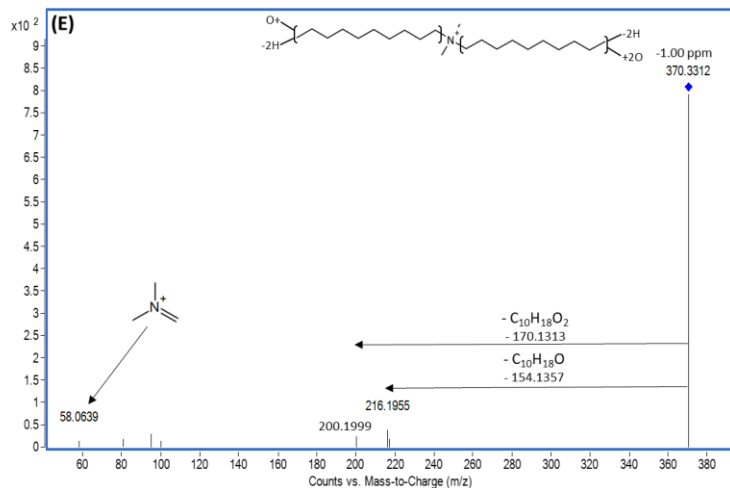


**Figure SI-6.9:** Fragmentation spectra obtained for the identified C10-DDAC metabolites. These corresponded to **(A)** monohydroxy (+O; RT 11.43 min; CE 20 eV); **(B)** dihydroxy (+2O; RT 6.28 min; CE 40 eV); **(C)** ketone (+O, -2H; RT 11.97 min; CE 20 eV); **(D)** keto-hydroxy (+2O, -2H; RT 6.79 min; CE 40 eV); **(E)** carboxy-keto (+3O, -4H; RT 6.28 min; CE 20 eV); **(F)** trihydroxy (+3O; RT 3.99 min; CE 20 eV) **(G)** dicarboxy (+4O, -4H; RT 5.88 min; CE 20 eV). In each fragmentation spectrum, the neutral losses leading to the assignment of metabolites and a proposed structure are indicated.

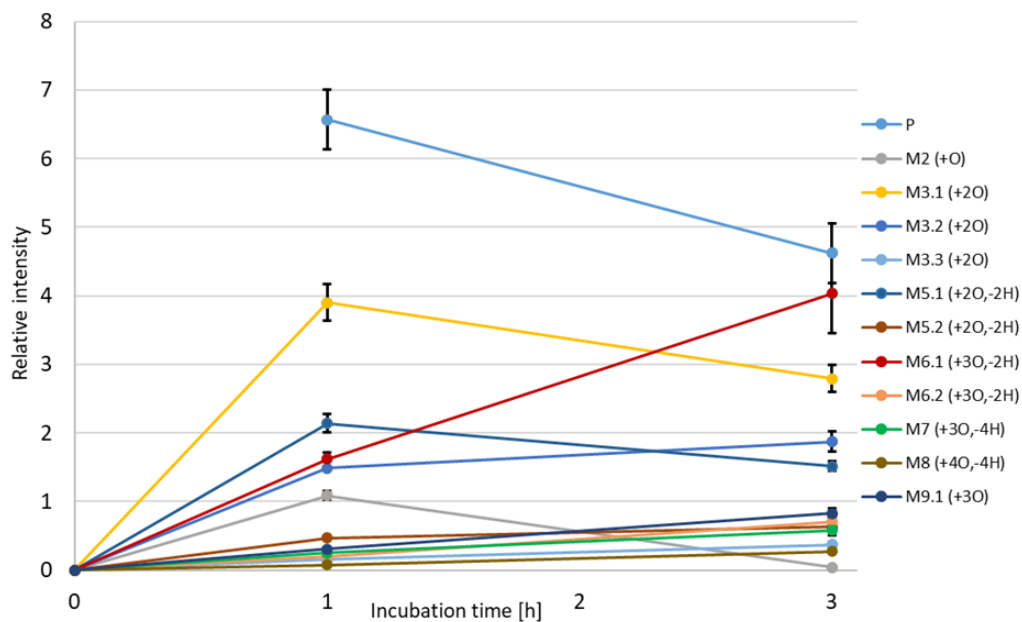


**Figure SI-6.10:** Relative abundances obtained for C<sub>10</sub>-DDAC metabolites (Table SI-6.6, relative to IS *D*<sub>7</sub>-C<sub>12</sub>-BAC) detected in both incubation time points. For each datapoint, the standard deviations (n = 3) are indicated. The assigned metabolites for each abbreviation are summarized in Table S3. Data for C<sub>10</sub>-DDAC-M4 was not included as it was only detected in one incubation time point. P: Parent compound C<sub>10</sub>-DDAC. For metabolites, average relative abundances observed in negative control samples with no addition of the substrate were used as the 0 h time points. For the 0 h time point of the parent compound (interpreted as the relative abundance in the negative controls to which only the substrate and no HLMs and cofactors were added), a relative abundance of 39.45 ± 8.71 was observed.

**Table SI-6.6:** Data obtained for didecyldimethylammonium (C<sub>10</sub>-DDAC, parent compound) and its metabolites identified in the 1 h and 3 h incubations. For each metabolite, the formula, assigned confidence level (CL), average mass error and (triplicate analysis per time point), relative abundance and whether the metabolite was detected in negative control (NC samples) is indicated. \*The NC control samples refer to the NCs to which no HLMs or cofactors were added. For the 0 h time point of the parent compound (interpreted as the relative abundance in the negative controls to which only the substrate and no HLMs and cofactors were added), a relative abundance of 39.45 ± 8.71 was observed.

Compound	Proposed metabolite	Formula	RT [min]	1 h incubations				3 h incubations			
				Mass error [ppm]	CL	Rel. abundance 1 h (± SD)	Detected in NC*?	Mass error [ppm]	CL	Rel. abundance 3 h (± SD)	Detected in NC*?
Didecyldimethylammonium (C <sub>10</sub> -DDAC)	Parent	[C <sub>22</sub> H <sub>48</sub> N] <sup>+</sup>	14.85	3.43	1	6.57 ± 0.43	Yes	2.61	1	4.62 ± 0.43	Yes
C <sub>10</sub> -DDAC-M1	Desaturation (-2H)	[C <sub>22</sub> H <sub>46</sub> N] <sup>+</sup>	14.28	2.90	4	0.03 ± 0.01	No	n.d.		n.d.	n.d.
C <sub>10</sub> -DDAC-M2	Monohydroxy (+O)	[C <sub>22</sub> H <sub>48</sub> NO] <sup>+</sup>	11.43	1.20	3	1.09 ± 0.01	No	1.81	3	0.04 ± 0.01	No
C <sub>10</sub> -DDAC-M3.1	Dihydroxy (+2O)	[C <sub>22</sub> H <sub>48</sub> NO <sub>2</sub> ] <sup>+</sup>	6.28	3.19	3	3.90 ± 0.26	No	1.56	3	2.79 ± 0.20	No
C <sub>10</sub> -DDAC-M3.2	Dihydroxy (+2O)	[C <sub>22</sub> H <sub>48</sub> NO <sub>2</sub> ] <sup>+</sup>	6.13	2.16	3	1.49 ± 0.02	No	1.88	3	1.87 ± 0.15	No
C <sub>10</sub> -DDAC-M3.3	Dihydroxy (+2O)	[C <sub>22</sub> H <sub>48</sub> NO <sub>2</sub> ] <sup>+</sup>	5.99	1.76	3	0.15 ± 0.01	No	1.09	3	0.37 ± 0.03	No
C <sub>10</sub> -DDAC-M4	Ketone (+O, -2H)	[C <sub>22</sub> H <sub>46</sub> NO] <sup>+</sup>	11.98	1.14	3	0.45 ± 0.07	No	n.d.		n.d.	n.d.
C <sub>10</sub> -DDAC-M5.1	Keto-hydroxy (+2O, -2H)	[C <sub>22</sub> H <sub>46</sub> NO <sub>2</sub> ] <sup>+</sup>	6.49	3.12	3	2.14 ± 0.13	No	2.18	3	1.52 ± 0.07	No
C <sub>10</sub> -DDAC-M5.2	Keto-hydroxy (+2O, -2H)	[C <sub>22</sub> H <sub>46</sub> NO <sub>2</sub> ] <sup>+</sup>	6.31	1.49	3	0.47 ± 0.02	No	0.73	3	0.63 ± 0.05	No
C <sub>10</sub> -DDAC-M6.1	Carboxy-hydroxy (+3O, -2H)	[C <sub>22</sub> H <sub>46</sub> NO <sub>3</sub> ] <sup>+</sup>	6.10	2.49	3	1.62 ± 0.09	No	2.33	3	4.03 ± 0.58	No
C <sub>10</sub> -DDAC-M6.2	Carboxy-hydroxy (+3O, -2H)	[C <sub>22</sub> H <sub>46</sub> NO <sub>3</sub> ] <sup>+</sup>	5.92	1.61	3	0.20 ± 0.04	No	0.21	3	0.71 ± 0.07	No
C <sub>10</sub> -DDAC-M7	Carboxy-keto	[C <sub>22</sub> H <sub>44</sub> NO <sub>3</sub> ] <sup>+</sup>	6.28	1.30	3	0.25 ± 0.03	No	0.39	3	0.58 ± 0.07	No

	(+3O, -4H)										
C <sub>10</sub> -DDAC-M8	Dicarboxy (+4O, -4H)	[C <sub>22</sub> H <sub>44</sub> NO <sub>4</sub> ] <sup>+</sup>	5.88	0.51	3	0.07 ± 0.01	No	0.26	3	0.27 ± 0.03	No
C <sub>10</sub> -DDACM9.1	Trihydroxy (+3O)	[C <sub>22</sub> H <sub>48</sub> NO <sub>3</sub> ] <sup>+</sup>	3.99	0.42	3	0.31 ± 0.01	No	0.90	3	0.83 ± 0.07	No
C <sub>10</sub> -DDAC-M9.2	Trihydroxy (+3O)	[C <sub>22</sub> H <sub>48</sub> NO <sub>3</sub> ] <sup>+</sup>	3.74	n.d.		n.d.	n.d.	0.67	4	0.29 ± 0.03	No

**Table SI-6.7:**  $^{DT}CCS_{N_2}$  values calculated for C12-BAC metabolites. The average  $^{DT}CCS_{N_2}$  value of triplicate samples, together with its (relative) standard deviation (SD/RSD), is given for each incubation time point. The  $^{DT}CCS_{N_2}$  values are compared with reference data available from literature. The reference  $^{DT}CCS_{N_2}$  value of the parent compound (C12-BAC) was retrieved from **chapter 4.1**, while all other  $^{TW}CCS_{N_2}$  values (for metabolites) were taken from Nguyen et al., 2024 (dataset based on calibration with poly alanine).

Compound	Proposed metabolite	Ref. $CCS_{N_2}$ [ $\text{\AA}^2$ ]	1 h incubations				3 h incubations			
			$^{DT}CCS_{N_2}$ [ $\text{\AA}^2$ ]	SD [ $\text{\AA}^2$ ]	RSD [%]	$\Delta CCS$ [%]	$^{DT}CCS_{N_2}$ [ $\text{\AA}^2$ ]	SD [ $\text{\AA}^2$ ]	RSD [%]	$\Delta CCS$ [%]
Benzyldimethyldodecylammonium (C <sub>12</sub> -BAC)	Parent	193.45	193.58	0.12	0.06	0.07	193.26	0.08	0.04	-0.10
C <sub>12</sub> -BAC-M1	Desaturation (-2H)		n.d.	n.d.	n.d.	n.d.	n.d.	n.d.	n.d.	n.d.
C <sub>12</sub> -BAC-M2.1	Monohydroxy(+O)	187.07	185.56	0.10	0.05	-0.81	185.31	0.06	0.03	-0.94
C <sub>12</sub> -BAC-M2.2	Monohydroxy(+O)	187.07	184.73	0.07	0.04	-1.25	184.51	0.01	0.01	-1.37
C <sub>12</sub> -BAC-M3.1	Dihydroxy (+2O)	186.49	187.43	0.13	0.07	0.50	187.17	0.07	0.04	0.36
C <sub>12</sub> -BAC-M3.2	Dihydroxy (+2O)	186.49	187.27	0.10	0.05	0.42	187.04	0.08	0.04	0.29
C <sub>12</sub> -BAC-M3.3	Dihydroxy (+2O)	186.49	186.92	0.36	0.19	0.23	186.83	0.12	0.07	0.18
C <sub>12</sub> -BAC-M3.4	Dihydroxy (+2O)	186.49	186.51	0.21	0.11	0.01	186.25	0.06	0.03	-0.13
C <sub>12</sub> -BAC-M3.5	Dihydroxy (+2O)	186.49	186.97	0.17	0.09	0.26	186.56	0.05	0.03	0.04
C <sub>12</sub> -BAC-M4.1	Ketone (+O, -2H)	182.22	182.93	0.05	0.03	0.39	182.75	0.09	0.05	0.29
C <sub>12</sub> -BAC-M4.1	Ketone (+O, -2H)	182.22	182.42	0.13	0.07	0.11	182.19	0.04	0.02	-0.02
C <sub>12</sub> -BAC-M5.1	Carboxy (+2O, -2H)	185.63	187.08	0.16	0.09	0.78	186.79	0.09	0.05	0.62

**Table SI-6.8:**  $^{DT}CCS_{N_2}$  values calculated for C10-ATMAC metabolites. The average  $^{DT}CCS_{N_2}$  value of triplicate samples, together with its (relative) standard deviation (SD/RSD), is given for each incubation time point. The  $^{DT}CCS_{N_2}$  values are compared with reference data available from literature. The reference  $^{DT}CCS_{N_2}$  value of the parent compound (C10-ATMAC) was retrieved from **chapter 4.1**, while all other  $^{TW}CCS_{N_2}$  values (for metabolites) were taken from Nguyen et al., 2024 (dataset based on calibration with poly alanine).

Compound	Proposed metabolite	Ref. $CCS_{N_2}$ [ $\text{\AA}^2$ ]	1 h incubations				3 h incubations			
			$^{DT}CCS_{N_2}$ [ $\text{\AA}^2$ ]	SD [ $\text{\AA}^2$ ]	RSD [%]	$\Delta CCS$ [%]	$^{DT}CCS_{N_2}$ [ $\text{\AA}^2$ ]	SD [ $\text{\AA}^2$ ]	RSD [%]	$\Delta CCS$ [%]
C <sub>16</sub> -ATMAC	Parent	193.01	193.21	0.03	0.02	0.10	193.20	0.07	0.04	0.10
C <sub>16</sub> -ATMAC-M1	Desaturation (-2H)	n.a.	186.69	0.05	0.03		186.78	0.03	0.02	
C <sub>16</sub> -ATMAC-M2.1	Monohydroxy (+O)	183.81	184.63	0.06	0.03	0.44	184.60	0.04	0.02	0.43
C <sub>16</sub> -ATMAC-M2.2	Monohydroxy (+O)	183.81	183.63	0.08	0.04	-0.10	183.64	0.03	0.01	-0.09
C <sub>12</sub> -ATMAC-M3.1	Dihydroxy (+2O)	183.96	185.99	0.06	0.03	1.10	186.00	0.12	0.07	1.11
C <sub>12</sub> -ATMAC-M4.1	Ketone (+O, -2H)	n.a.	181.72	0.05	0.03		181.64	0.03	0.01	
C <sub>12</sub> -ATMAC-M5.1	Carboxy (+2O, -2H)	182.08	185.61	0.05	0.03	1.94	185.49	0.06	0.03	1.87

**Table SI-6.9:**  $^{DT}CCS_{N_2}$  values calculated for C10-DDAC metabolites. The average  $^{DT}CCS_{N_2}$  value of triplicate samples, together with its (relative) standard deviation (SD/RSD), is given for each incubation time point. The  $^{DT}CCS_{N_2}$  values are compared with reference data available from literature. The reference  $^{DT}CCS_{N_2}$  value of the parent compound (C10-DDAC) was retrieved from **chapter 4.1**, while all other  $^{TW}CCS_{N_2}$  values (for metabolites) were taken from Nguyen et al., 2024 (dataset based on calibration with poly alanine).

Compound	Proposed metabolite	Ref. $CCS_{N_2}$ [Å <sup>2</sup> ]	1 h incubations				3 h incubations			
			$^{DT}CCS_{N_2}$ [Å <sup>2</sup> ]	SD [Å <sup>2</sup> ]	RSD [%]	$\Delta CCS$ [%]	$^{DT}CCS_{N_2}$ [Å <sup>2</sup> ]	SD [Å <sup>2</sup> ]	RSD [%]	$\Delta CCS$ [%]
C10-DDAC	Parent	208.44	208.39	0.04	0.02	-0.03	208.43	0.017	0.01	0.00
C10-DDAC-M1	Desaturation (-2H)	n.a.	205.73	0.21	0.10		n.d.	n.d.	n.d.	n.d.
C10-DDAC-M2	Monohydroxy (+O)	200.38	202.81	0.08	0.04	1.21	202.88	0.18	0.09	1.25
C10-DDAC-M3.1	Dihydroxy (+2O)	202.32	196.66	0.04	0.02	-2.80	196.65	0.01	0.00	-2.81
C10-DDAC-M3.2	Dihydroxy (+2O)	202.32	196.14	0.04	0.02	-3.06	196.10	0.07	0.04	-3.08
C10-DDAC-M3.3	Dihydroxy (+2O)	202.32	195.50	0.15	0.08	-3.37	195.50	0.10	0.05	-3.37
C10-DDAC-M4	Ketone (+O, -2H)	200.76	200.97	0.03	0.01	0.10	200.82	0.59	0.29	0.03
C10-DDAC-M5.1	Keto-hydroxy (+2O, -2H)	198.67	195.63	0.02	0.01	-1.53	195.66	0.03	0.02	-1.52
C10-DDAC-M5.2	Keto-hydroxy (+2O, -2H)	198.67	195.58	0.07	0.04	-1.56	195.61	0.05	0.03	-1.54
C10-DDAC-M6.1	Carboxy-hydroxy (+3O, -2H)	198.46	196.70	0.04	0.02	-0.89	196.77	0.03	0.02	-0.85
C10-DDAC-M6.2	Carboxy-hydroxy (+3O, -2H)	198.46	196.66	0.07	0.03	-0.91	196.69	0.04	0.02	-0.89
C10-DDAC-M7	Carboxy-keto (+3O, -4H)	n.a.	196.39	0.06	0.03		196.38	0.07	0.03	
C10-DDAC-M8	Dicarboxy (+4O, -4H)	n.a.	198.71	0.15	0.08		198.61	0.09	0.04	
C10-DDAC-M9.1	Trihydroxy (+3O)	n.a.	198.44	0.12	0.06		198.51	0.03	0.01	
C10-DDAC-M9.2	Trihydroxy (+3O)	n.a.	198.04	0.38	0.19		197.97	0.10	0.05	

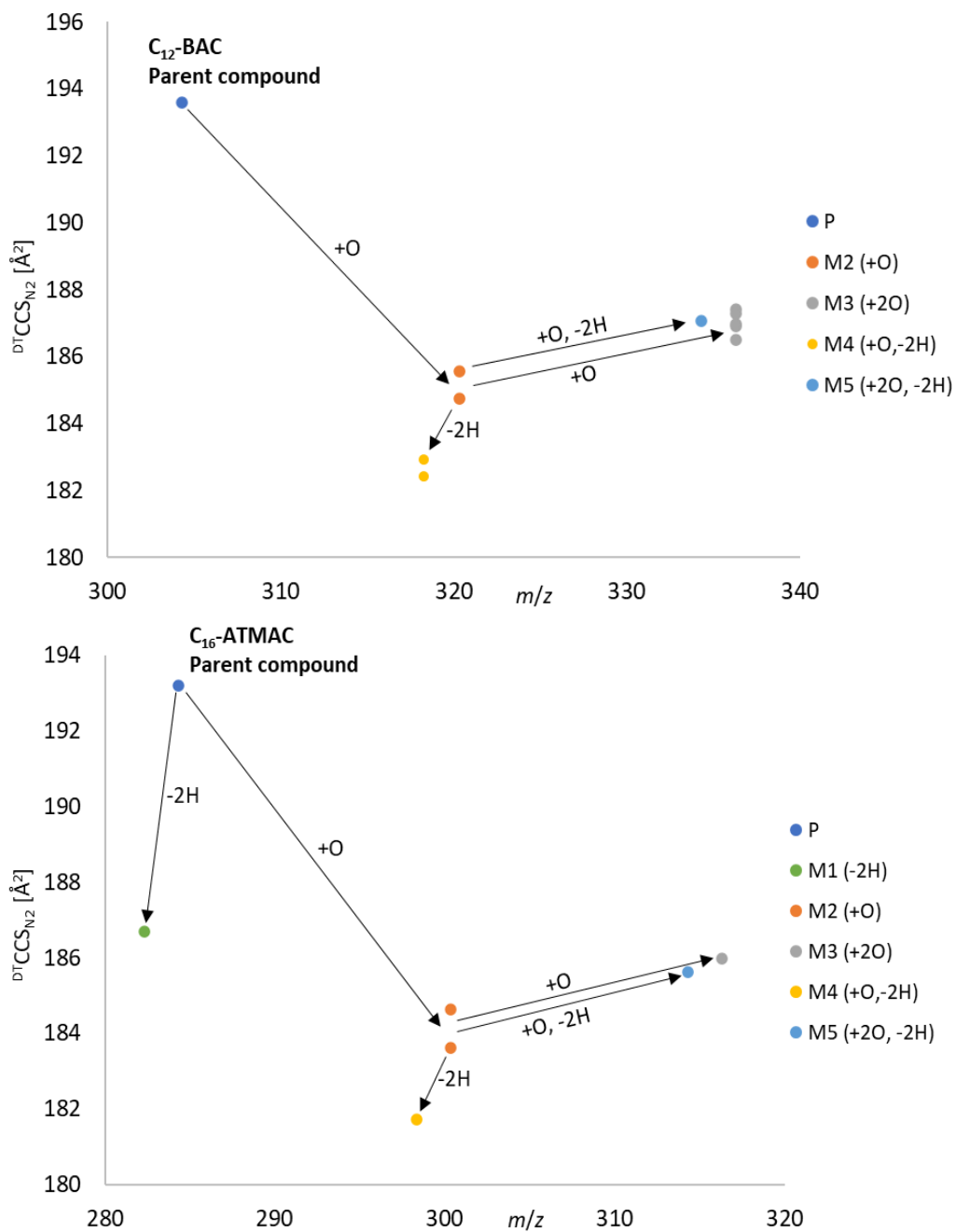


**Figure SI-6.11:**  $DTCCS_{N_2}$  obtained for metabolites of C<sub>12</sub>-BAC (above) and C<sub>16</sub>-ATMAC (below) as a function of the corresponding  $m/z$  ratios. The detailed data of each metabolite is summarized in **Tables SI-6.4** and **SI-6.5**, respectively. Black arrows indicate metabolization reactions leading to observed trends in  $DTCCS_{N_2}$  values.

**Table SI-6.10:** Summary of C<sub>12</sub>-BAC metabolites detected in human urine samples. Data are given per participant for each of which four urine samples were analyzed. The average mass error and peak area (Peak area<sub>metab.</sub>) are given for the number of samples in which the corresponding metabolite was detected. Latter is indicated in the column with detection frequency (DF). For comparison, the average peak area (Peak area<sub>IS</sub>) obtained for the internal standard (D<sub>7</sub>-C<sub>12</sub>-BAC) in the urine samples is indicated.

Compound	Proposed metabolite	Formula	RT <sub>HLM</sub> [min]	Participant C (n = 4)				
				$\bar{x}$ mass error [ppm]	CL	Peak area <sub>metab.</sub> [cps] (± SD)	Peak area <sub>IS</sub> [cps] (± SD)	DF
C <sub>12</sub> -BAC-M2.1	(+O)	[C <sub>21</sub> H <sub>38</sub> NO] <sup>+</sup>	7.12	0.66	3	3.01E+04 ± 1.56E+04	4.32E+05 ± 9.72E+04	100% (4/4)
C <sub>12</sub> -BAC-M2.2	(+O)	[C <sub>21</sub> H <sub>38</sub> NO] <sup>+</sup>	6.88	0.51	3	2.39E+04 ± 1.15E+04	4.32E+05 ± 9.72E+04	75% (3/4)
C <sub>12</sub> -BAC-M4.1	(+O, -2H)	[C <sub>21</sub> H <sub>36</sub> NO] <sup>+</sup>	7.39	1.78	3	1.91E+04 ± 8.05E+03	4.32E+05 ± 9.72E+04	100% (4/4)
C <sub>12</sub> -BAC-M5.1	(+2O, -2H)	[C <sub>21</sub> H <sub>36</sub> NO <sub>2</sub> ] <sup>+</sup>	6.81	1.38	3	7.36E+04 ± 3.03E+04	4.32E+05 ± 9.72E+04	100% (4/4)

**Table SI-6.11:** Summary of C<sub>10</sub>-DDAC metabolites detected in human urine samples. Data are given per participant for each of which four urine samples were analyzed. The average mass error and peak area (PA.M) are given for the number of samples in which the corresponding metabolite was detected. Latter is indicated in the column with detection frequency (DF). For comparison, the average peak area (PA.IS) obtained for the internal standard (D<sub>7</sub>-C<sub>12</sub>-BAC) in the urine samples is indicated. \*The +4O,-4H metabolite was detected in two samples of participant D with highly varying peak areas. Therefore, for this metabolite not the average peak area but the two individual values obtained in the two positive samples are given.

Compound	Participant C (n = 4)					Participant D (n = 4)					Participant E (n = 4)				
	$\bar{x}$ mass error [ppm]	CL	PA.M [cps] ( $\pm$ SD)	PA.IS [cps] ( $\pm$ SD)	DF	$\bar{x}$ mass error [ppm]	CL	PA.M [cps]*	PA.IS [cps] ( $\pm$ SD)	DF	$\bar{x}$ mass error [ppm]	CL	PA.M [cps] ( $\pm$ SD)	PA.IS [cps] ( $\pm$ SD)	DF
C <sub>10</sub> -DDAC-M6.1 (+3O, -2H)	2.07	4	1.49E+04 $\pm$ 1.41E+03	4.32E+05 $\pm$ 9.72E+04	75% (3/4)	n.d.					n.d.				
C <sub>10</sub> -DDAC-M6.2 (+3O, -2H)	0.74	4	2.72E+04 $\pm$ 2.31E+03	4.32E+05 $\pm$ 9.72E+04	75% (3/4)	n.d.					n.d.				
C <sub>10</sub> -DDAC-M7 (+3O, -4H)	0.75	4	6.69E+03 $\pm$ 5.60E+02	4.32E+05 $\pm$ 9.72E+04	75% (3/4)	n.d.					n.d.				
C <sub>10</sub> -DDAC-M8 (+4O, -4H)	0.73	3	1.20E+04 $\pm$ 4.69E+03	4.32E+05 $\pm$ 9.72E+04	100% (4/4)	1.04	3	1.30E+05 / 1.97E+04	4.53E+05 $\pm$ 1.06E+05	50% (2/4)	0.78	3	1.76E+04 $\pm$ 1.65E+03	3.52E+05 $\pm$ 8.71E+04	50% (2/4)

**Table SI-6.12:** <sup>DT</sup>CCS<sub>N2</sub> values obtained for C<sub>12</sub>-BAC and C<sub>10</sub>-DDAC metabolites in human urine samples. For mobility measurements, four urine samples of each participant were pooled and the <sup>DT</sup>CCS<sub>N2</sub> value and mass error obtained in the pooled sample is given. <sup>DT</sup>CCS<sub>N2</sub> values obtained in urine were compared with <sup>DT</sup>CCS<sub>N2</sub> values obtained in the 1h HLM incubations (see Tables S7 and S9 for C<sub>12</sub>-BAC and C<sub>10</sub>-DDAC, respectively).

Compound	Proposed metabolite	Ref. <sup>DT</sup> CCS <sub>N2</sub> [Å <sup>2</sup> ]	Participant C (n = 4)			Participant D (n = 4)			Participant E (n = 4)		
			mass error [ppm]	<sup>DT</sup> CCS <sub>N2</sub> [Å <sup>2</sup> ]	ΔCCS [%]	mass error [ppm]	<sup>DT</sup> CCS <sub>N2</sub> [Å <sup>2</sup> ]	ΔCCS	mass error [ppm]	<sup>DT</sup> CCS <sub>N2</sub> [Å <sup>2</sup> ]	ΔCCS
C <sub>12</sub> -BAC-M2.1	(+O)	185.56	0.03	185.10	-0.25	n.d.			n.d.		
C <sub>12</sub> -BAC-M2.2	(+O)	184.73	-0.31	184.31	-0.23	n.d.			n.d.		
C <sub>12</sub> -BAC-M4.1	(+O, -2H)	182.93	-0.63	182.98	0.03	n.d.			n.d.		
C <sub>12</sub> -BAC-M5.1	(+2O, -2H)	187.08	0.60	186.61	-0.25	n.d.			n.d.		
C <sub>10</sub> -DDAC-M6.1	(+3O, -2H)	196.70	1.07	197.30	0.31	n.d.			n.d.		
C <sub>10</sub> -DDAC-M6.2	(+3O, -2H)	196.66	3.49	196.85	0.10	n.d.			n.d.		
C <sub>10</sub> -DDAC-M7	(+3O, -4H)	196.39	n.d.			n.d.			n.d.		
C <sub>10</sub> -DDAC-M8	(+4O, -4H)	198.71	0.52	198.82	0.06	0.78	198.87	0.08	0.26	198.93	0.11



# Chapter 7:

## General discussion and future perspectives



## 7.1 General discussion

The increasing pollution of the environment with industrial chemicals is a key challenge of our time and poses a major risk to human health. This is reflected in an increasing occurrence of contaminants of emerging concern (CECs) in various environmental matrices. Still, most studies investigating known contaminants and CECs apply a targeted approach focusing on a limited number of *a priori* selected analytes. While these studies provide indispensable quantitative data crucial for the assessment of contaminant concentration in human and environmental samples, they overlook all CECs not included in the selection of analytes.

To bridge this gap, suspect and non-target screening analyses (SSA/NTS) are gaining increasing attention. These methods can contribute to the identification of CECs by vastly increasing the coverage of analytical methodologies. Nevertheless, the high complexity of sample matrices and occurring CECs requires a constant development of SSA/NTS platforms and introduction of new mass-spectrometric approaches. One emerging technique is ion-mobility mass spectrometry (IM-MS) providing an additional separation dimension for screening studies. Furthermore, IM-MS allows the calculation of collision cross section (CCS) values which can serve as an additional identification parameter for compound annotation.

This thesis focused on the application of SSA and NTS for the identification of CECs and their metabolites and covered several matrices relevant for the assessment of human exposure to CECs. Firstly, indoor dust samples were analyzed applying a suspect screening approach (**chapter 4**). Numerous previous studies have characterized indoor dust as a relevant matrix for human exposure assessment since it can be viewed as representative for numerous contributing sources (electronics, furniture, solid air pollution) and since humans spend most of their time indoors (Christia et al., 2021b; Zheng et al., 2020). Secondly, human urine samples originating from the Flemish Environment and Health Study (FLEHS IV) were screened (**chapter 5**) aiming to identify CEC metabolites which are overlooked by targeted biomonitoring methods commonly applied within FLEHS. Lastly, *in vitro* biotransformation products of quaternary ammonium compounds (QACs), a class prioritized within the analyses of indoor dust samples, were characterized using human liver microsomes (HLMs) as *in vitro* model (**chapter 6**). This aimed at facilitating future biomonitoring studies of this emerging class of contaminants.

The second main aim of this thesis was the implementation of IM-MS in all described steps of CECs' identification and assessment of human exposure. First, a database containing experimental reference CCS values of more than 140 CECs and their metabolites was built, compiled and compared with data acquired on other instrumental

IM-MS set-ups (**chapter 3**). Next, the reference data derived from database compilation was implemented in all studies described above aiming to assess its added value for compound annotation (**chapters 4 and 6**).

In summary, the presented thesis aimed to answer the following research questions:

- What are the reference  $^{DT}CCS_{N_2}$  values of most relevant CEC classes? How can  $^{DT}CCS_{N_2}$  databases for environmental contaminants and their metabolites be built and compiled in a reproducible manner? (**Chapter 3**)
- Are  $CCS_{N_2}$  reproducible between different instrumental set-ups and prediction models? Which factors contribute to  $CCS_{N_2}$  biases between experimental and predicted values? (**Chapter 3**)
- How can SSA and NTS facilitate the annotation of emerging contaminant classes in indoor dust samples? Can identified CECs be prioritized based on semi-quantified concentrations and can these values be used for estimations of human exposure and potential health risks? (**Chapter 4**)
- Can IM-MS derived reference  $^{DT}CCS_{N_2}$  values improve the identification confidence for CECs in indoor dust samples? (**Chapter 4**)
- How can SSA methods be employed to identify metabolites of CECs in human urine which are overlooked in current biomonitoring campaigns? (**Chapter 5**)
- What are the *in vitro* biotransformation products of prioritized CECs? Which influence do biotransformation reactions have on  $^{DT}CCS_{N_2}$  values of the metabolites and how can this information be used for compound identification? (**Chapter 6**)

#### **$^{DT}CCS_{N_2}$ database compilation and comparability with different IM-MS setups and prediction models**

The added value of the extra separation dimension provided by IM-MS has been described in detail previously (Celma et al., 2021; Crowell et al., 2013; Menger et al., 2022). However, given the fact that IM-MS derived CCS values are no chemical constant (such as, e.g., a compound's *m/z* value), but calculated empirical values, their utilization for compound annotations relies on the availability of reference CCS databases with which experimental data can be compared. Such reference data was lacking for several classes of CECs and their metabolites. Therefore, in **chapter 3.1**, a reference  $^{DT}CCS_{N_2}$  database was compiled reporting a total of 311  $^{DT}CCS_{N_2}$  values for 113 CECs and their metabolites. To the best of our knowledge, for 105 compounds,  $^{DT}CCS_{N_2}$  values were reported for the first time. Drift-tube ion-mobility spectrometry (DTIM) used for database

compilation here, is the only IM-MS instrument from which ion mobilities (and consequently,  $^{DT}CCS_{N_2}$  values) can be retrieved using a primary method (referred to as 'stepped field calibration') and is therefore considered the 'gold standard' IM technique (Reardon et al., 2024). Also, for  $^{DT}CCS_{N_2}$  values calculated based on the single-field method, good interlaboratory reproducibility has been shown. Stow et al. reported average interlaboratory RSDs  $0.38 \pm 0.19\%$  for a set of  $> 100$   $^{DT}CCS_{N_2}$  values of 65 endogenous compounds (amino and fatty acids, proteins) acquired in three laboratories. Here, individual RSDs did not exceed 1% for any of the single charged ions. These findings proved the reliability of DTIM for  $CCS_{N_2}$  database compilations. High interlaboratory reproducibility was also confirmed through the observation of an average RSD of 0.05% for the reference  $^{DT}CCS_{N_2}$  values reported in **chapter 3.1**, which were based on five injections.

From the compiled database,  $CCS$ - $m/z$  trendlines could be described for the major CEC classes included. This allowed to distinguish between different classes based on their clustering within the  $CCS$ - $m/z$  plot. For example, the trendline calculated for reference values of per- and polyfluoroalkyl substances (PFAS) showed a clearly smaller slope compared to other CEC classes allowing a clear distinguishment. The presence of a high number of  $CF_2$ -moieties leads to increasing masses and thereof decreased  $^{DT}CCS_{N_2}$  values in relation to the  $m/z$  ratios. Generally, an increase in  $^{DT}CCS_{N_2}$  value with increasing  $m/z$  ratio was observed resulting in higher  $^{DT}CCS_{N_2}$  values for sodium adducts compared to proton adducts of the same compound. This trend, however, was not reproduced by phthalates with longer side chains ( $>C_9$ ) for which similar  $^{DT}CCS_{N_2}$  values for both adducts were observed. This characteristic trend was of high relevance for phthalate annotations in later studies (**chapter 4.2**).

Despite the described good interlaboratory reproducibility of DTIM measurements, these findings cannot be directly extrapolated to the comparison of  $CCS_{N_2}$  acquired using other IM-MS set-ups (TWIMS and TIMS). Therefore, in **chapters 3.2** and **3.3**, based on a sub-selection of CECs, reference  $^{DT}CCS_{N_2}$  values (**chapter 3.1**) were compared with data acquired on TWIMS and TIMS systems, respectively, whereby for TWIMS measurements two instrumental set-ups (Synapt-G2 and VION) were available. For the comparison of TWIMS and DTIM data (with latter set as reference) absolute percent errors (APEs)  $< 2\%$  were observed for 83% and 82% percent of the datapoints for VION ( $n = 94$ ) and Synapt ( $n = 97$ ) systems, respectively. When considering only protonated ions, these percentages decrease to 64% (VION,  $n = 22$ ) and 57% (Synapt,  $n = 23$ ). Interestingly, an association between observed APEs and investigated CEC class was observed, as most datapoints showing the highest APEs derived from the class of (mostly halogenated) OPFRs. Here, an influence of the applied calibration approach was assumed

as only the calibrants applied for DTIM measurements incorporated halogens allowing to account for the above-described different positioning of halogenated in CCS-*m/z* plot.

When comparing  $^{TIMS}CCS_{N_2}$  and  $^{DT}CCS_{N_2}$  values (latter set as reference), 91 % (n = 80) of the datapoints showed APEs < 2%. Interestingly, compounds showing highest APEs overlapped between TWIMS and TIMS comparisons (**chapters 3.2/3.3**) even though for the latter,  $^{TIMS}CCS_{N_2}$  calculations were based on the same set of calibrants as DTIM measurements. Additionally, TIMS measurement achieved mobility resolution > 110 through slight adjustments of the applied instrumental settings. For DTIM measurements, an additional post-acquisition data processing step is needed to achieve comparable instrument performance.

Lastly, for 56 CECs, CCS values predicted using two different prediction models (based on artificial neural networks (ANN) and multivariate adaptive regression splines (MARS) and trained with TWIMS derived data) were compared with corresponding experimental  $^{DT}CCS_{N_2}$  values. It could be shown that 95<sup>th</sup> percentile of observed APEs ranged between 5.7% and 11.1%, whereby the highest APEs were calculated for sodium adducts.

The findings described in **chapters 3.2** and **3.3** are of special interest when selecting a cut-off value for CCS database matching within environmental screening studies. The increasing use of IM-MS in such studies was accompanied by the implementation of CCS values in the well-established scheme of  $^{DT}CCS_{N_2}$  values (Celma et al., 2020; Schymanski et al., 2014). A cut-off value of 2% was proposed for the comparison of experimental IM data with database CCS values. Nevertheless, the deviations reported here indicate that this cut-off value should not be applied without assessment of potential bias introduced by the investigated compound class and applied calibration approach.

To achieve better inter-platform  $CCS_{N_2}$  reproducibility and method transparency, two factors are crucial. On the one hand, the implementation of suitable QC measures in  $CCS_{N_2}$  database compilations can facilitate assessment of inter-platform  $CCS_{N_2}$  reproducibility. In **chapter 3.1**, comprehensive QC guidelines proposed in the scope of the compilation of a large-scale harmonized  $^{DT}CCS_{N_2}$  database, were implemented (Picache et al., 2019). For the used QC compounds, reference  $^{DT}CCS_{N_2}$  values acquired on a reference DTIM system with well-characterized measurement uncertainty were available (Stow et al., 2017). The applied QC approaches also allowed the implementation of the  $^{DT}CCS_{N_2}$  values reported in **chapter 3.1** into the PubChem entities of the corresponding compound making them freely available for the scientific community (Kim et al., 2023). A harmonized implementation of similar QC measures for future  $CCS_{N_2}$  databases acquired on other instrumental set-ups could ease the assessment of possible biases and the selection of suitable cut-off values for screening studies.

On the other hand, the choice of  $\text{CCS}_{\text{N}_2}$  calibrants was identified as a major contributor to  $\text{CCS}_{\text{N}_2}$  deviations. For example, the TWIMS VION measurements conducted within **chapter 3.2**, were performed applying a calibration approach proposed by the instrument's manufacturer, whereby the calibrants' reference  $\text{CCS}_{\text{N}_2}$  values were implemented in the data processing software. Shortly after these experiments were performed, Feuerstein et al. proposed a new set of DTIM derived reference  $^{\text{DT}}\text{CCS}_{\text{N}_2}$  values for the established TWIMS calibrants. These showed to decrease the bias between DTIM and TWIMS datasets (Feuerstein et al., 2022b). A harmonized implementation of the same sets of calibrants and reference values could therefore vastly increase inter-platform reproducibility.

Similarly, for  $\text{CCS}_{\text{N}_2}$  prediction models, as discussed in **chapter 3.2**, a transparent communication of the datasets used for model training and the validation results observed during model development are crucial. Generally, predicted values must be used with caution, since the observed bias do not allow to unequivocally distinguish between candidate compounds for which small CCS differences are expected, e.g., isomers or compounds from the same compound class with minor structural differences. In those cases, extrapolation of experimentally derived  $\text{CCS}-m/z$  trendlines can be more reliable, as shown in **chapters 4.1** and **4.2**.

### **Suspect screening of CECs in indoor dust samples**

The indoor environment has a major contribution to human exposure to various environmental contaminants. In this context the ingestion and inhalation of or the dermal contact with indoor dust represent main exposure routes which are especially relevant for toddlers due to crawling behavior and frequent hand-to-mouth contact (Wilson et al., 2013). Several studies have identified various contaminant classes in dust such as alternative plasticizers, flame retardants, UV filters, antioxidants and others (Ao et al., 2018; Christia et al., 2021b; Liu and Mabury, 2020; Mullin et al., 2020). These characterizations were facilitated by the application of SSA and NTS approaches. However, SSA and NTS studies often prioritize the reporting of high numbers of compounds (up to several hundreds) over reporting small numbers of CECs with higher confidence and estimated quantitative data which would ease CEC prioritization for further targeted studies.

Therefore, **chapters 4.1** and **4.2** focused on the application of SSA approaches for the identification of CECs in indoor dust samples with as high identification confidence as possible. The implementation of semi-quantification and IM-MS allowed to increase confidence in compound assignment and provide estimated analyte concentration for exposure assessment and further CEC prioritization.

In **chapter 4.1**, the screening focused on QACs. For this class, 21 reference standards were available for targeted screening covering the three major QAC classes and allowing their semi-quantification (BACs, ATMAC and DDACs). All targeted QACs were detected in indoor dust samples with DFs between 4.2 and 100%. 15 targeted QACs were showed DFs above 90%. Suspect screening allowed the identification of 17 additional QACs. Suspect QACs mainly included homologues from the three mentioned classes whereby (combinations of) different hydrocarbon chain lengths were observed. Since possible branching of side chain could not be excluded resulting in more than one possible structure, CL3 was assigned to most suspects. This increased the need for additional molecular identifiers. Therefore,  $^{DT}CCS_{N_2}$  values were acquired for all suspect QACs. These were compared with  $CCS-m/z$  trendlines described for the reference DTIM data of the targeted QACs. For all suspect QACs assigned to one of the three classes,  $^{DT}CCS_{N_2}$  values clustered well on the trendline of the corresponding class confirming QAC annotations.

For all suspect QACs, semi-quantified concentrations were estimated using reference standards of structurally similar QACs as calibrants. Concentrations of individual targeted QACs showed a maximum of 32.23  $\mu\text{g/g}$  with a median  $\Sigma$ QAC concentration of 13.05  $\mu\text{g/g}$ . For one DDAC with mixed chain lengths (C16:C18), characterized as a major QAC homologue through SSA, a maximum concentration of 24.90  $\mu\text{g/g}$  was semi-quantified. This indicates similar concentrations for targeted and suspect QACs, again confirming the potential of the applied approach in characterizing homologues with relevant environmental concentrations. Overall, observed concentrations were lower than reported for indoor dust collected in the USA, where maximum concentrations up to 530  $\mu\text{g/g}$  were reported (Zheng et al., 2020). Besides the study of Zheng et al., there is no other data on QACs in indoor dust with which the presented findings could be compared. Semi-quantified concentrations were then used to estimate daily intakes (EDI), based on a dust ingestion exposure pathway, and hazard quotients (HQ), latter of which were based on the ratio between available ADIs for QACs (EFSA, 2014b) and the calculated EDIs. All obtained HQs were  $< 1$ , indicating no potential health risks. However, this approach does not consider other exposure routes and an exposure to mixtures latter of which is further discussed below.

In **chapter 4.2**, the same set of indoor dust samples was screened for a wide variety of CEC classes. This allowed the annotation of a total of 55 compounds. Besides numerous known contaminants such as DEHP, DEHA or TBOEP which were reported with detection frequencies (DFs)  $> 90\%$ , several novel CECs were annotated. These included phthalates with differing side chains, such as decyl nonyl and decyl undecyl phthalate with DFs  $>80\%$  and identified through the observation of characteristic neutral losses. Additionally, two novel organophosphate flame retardants not previously described in

indoor dust were identified. Again, EDIs and resulting HQs were calculated based on semi-quantified concentrations. Even though none of the HQs indicated potential adverse health effects, some of the novel phthalate homologues showed similar concentrations as legacy PHs, confirming their presence at relevant concentrations.

To increase identification confidence for the novel phthalate homologues, their  $^{DT}CCS_{N_2}$  values were compared with reference data obtained for known PHs. A clear trend was observed for all PHs showing increasing  $^{DT}CCS_{N_2}$  values with increasing length of hydrocarbon substituents. Also, the characteristic trend of similar  $^{DT}CCS_{N_2}$  values observed for proton and sodium adducts, which was described for reference PHs in **chapter 3.1**, was reproduced here by all suspect PHs.

Given the partially high bias described for predicted  $CCS_{N_2}$  values (**chapter 3.2**), the utilization of  $CCS-m/z$  trendlines could be preferred over the use of prediction models, especially if the first were derived from the same instrumental set-up. As shown here, the observed good fit of  $^{DT}CCS_{N_2}$  values of suspect compounds with trendlines described for database values can have great potential to increase confidence in compound assignments. It can even be used for non-targeted approaches further extrapolating the described trendlines prioritizing features clustering close to the extrapolated lines. Even though similar  $CCS-m/z$  trends have been characterized for other CEC classes (Dodds et al., 2020; Song et al., 2022), their utilization for the characterization of homologue series is still limited.

Both in **chapter 4.1** and **4.2**, newly identified CECs could be grouped in homologue series differing in the lengths and combinations of hydrocarbon side chains, e.g. phthalates carrying  $C_9-C_{10}$ ,  $C_{10}-C_{10}$ ,  $C_{10}-C_{11}$ , etc. side chains (**chapter 4.2**). This is assumed to result from varying compositions of reagents used during industrial processing. For example, phthalates are synthesized through esterification of phthalate anhydride with primary alcohols (Bajracharya et al., 2021). In an industrial setting, the latter are commonly composed of mixtures of different hydrocarbon chains leading to the homologue series described here. The findings presented in **chapter 4.2** show that these mixed side chain 'impurities' can reach similar concentrations as the known phthalates making them relevant for human exposure assessment. The same applies for the mixed chain DDAC homologues described in **chapter 4.1**. These observations suggest that in these cases exposure risk assessment should be based on groups of chemicals rather than single compounds, since an exposure to homologue mixtures is expected. The EFSA recently proposed guidelines on criteria to be applied for grouping of chemicals for human risk assessment (EFSA et al., 2021). However, these approaches largely rely on quantitative data on external or internal concentrations to be available. Here, this data gap was addressed by the application of a semi-quantification approach.

However, as discussed in **chapter 4.1**, this approach has several limitations such as differences in structure between calibrant and quantified (suspect) analyte, unavailability of labeled IS for all suspects, etc. Generally, semi-quantification approaches are still at an early development stage within the exposomics field. In 2021, a first set of guidelines for their implementation has been published (Malm et al., 2021). Nevertheless, the assessment of most suitable approaches is still ongoing. Recently, a first inter-laboratory comparison study, in which we have participated, was conducted aiming to compare semi-quantification results obtained in different laboratories with a predefined set of approaches. The results are expected to increase the reliability of these approaches ultimately aiming at the use of semi-quantified data for a holistic risk assessment of CECs.

To address the rising issue of chemical pollution on a regulatory level, the ultimate goal of the characterization of CECs through SSA and NTS and, if possible, assessment of their exposure should be the communication of the results to policy makers. The dust samples collected for **chapters 4.1** and **4.2** were part of a project focusing on the characterization of hazardous chemicals in indoor environments. The project was funded by the Flemish Ministry of Environment and conducted by our research group in collaboration with the Flemish Institute for Technological Research (VITO). The results described here were also communicated to the Flemish Ministry of Environment.

However, for a broader communication of SSA and NTS results to policy makers and risk assessors and their implementation in chemical pollution prevention guidelines, more harmonization in SSA and NTS methodologies is needed. This especially applies to the implementation of harmonized QA/QC measures to allow comparability of different study results and assessment of their reliability. Early in the development of in-house approaches, we have therefore proposed harmonized criteria QA/QC in SSA and NTS studies (Caballero-Casero et al., 2021a). Additionally, an active involvement in the NORMAN network (Network of reference laboratories, research centers and related organizations for monitoring of emerging environmental substances) played a central role in the comparison and harmonization of SSA and NTS approaches at European level. NORMAN has established a well-recognized platform for suspect list exchange (to which also the database generated in **chapter 3.1** was submitted) facilitating the implementation of comparable sets of suspects within SSA studies (Taha et al., 2022). Recently, a general set of guidelines for SSA and NTS, covering the whole analytical workflow from sample collection to data interpretation and reporting, has been published as a collaborative effort of numerous NORMAN members (Hollender et al., 2023).

The assessment of strengths and limitations of SSA/NTS and their harmonization is also a major focus within the European Partnership for the Assessment of Risks from Chemicals (PARC) project. For example, work package 4.3, in which we are actively involved, investigates the chemical coverage of SSA and NTS approaches for the assessment of occupational exposure to CECs. A collaborative approach is applied including the analysis of a defined set of human samples by different laboratories thereby expanding on the work conducted within the NORMAN network. All these actions underline the current focus of the exposomics field on SSA and NTS techniques and the ongoing efforts in their implementation in future policy making decisions. The results of this thesis will make an important contribution to this overarching goal.

### **Suspect screening of CECs in human urine samples**

Currently, biomonitoring studies conducted in the scope of the Flemish Environment and Health Study (FLEHS IV) focus solely on the application of targeted methods quantified *a priori* selected set of analytes. While these methods are crucial for a reliable exposure and risk assessment of known contaminants, they do not allow to investigate the exposure to suspect or unknown CECs.

To assess the presence of urine CEC metabolites currently not reflected in the targeted biomonitoring studies, 83 urine samples of Flemish adolescents (47 males, 36 females) collected in the frame of the 4<sup>th</sup> FLEHS cycle were analyzed (**chapter 5**) using a previously developed method involving a suspect screening approach to annotate CECs and their metabolites. Samples were selected with the aim to include a low and high exposure group based on concentrations measured for known contaminants in the targeted studies conducted in the scope of FLEHS IV. The applied suspect list contained >12,500 CECs and their known and predicted metabolites resulting from several metabolization reactions, such as hydroxylation, glucuronidation and methylation. In total, 63 compounds were annotated at a confidence level of 3 or better, with most of the detected compounds not included in current biomonitoring programs. The largest group of assigned CEC metabolites derived (42%) personal care products (PCPs), followed by food related compounds (21%) and (alternative) plasticizers (11%).

When comparing the number of assigned CEC metabolites between low and high exposure groups, significantly higher number ( $p < 0.05$ ) were observed in the latter of the two group. This suggests that a high exposure to known CECs is associated with an increased exposure to suspect CECs.

Despite the high added value of SSA approaches for metabolite applications, the number of similar studies investigating the presence of CEC metabolites in other cohorts is scarce. A study published shortly after the results discussed here identified 74 biomarkers of exposure in urine from 200 Slovenian children (Tkalec et al., 2022). Several

results showed an overlap with the findings discussed in **chapter 5**. For example, PCPs were a major contaminant class in both studies with partially overlapping reported compounds, including, e.g., parabens and benzophenones. As can be expected from targeted studies, the report of phthalate and alternative plasticizer metabolites was included in both studies. On the contrary, Tkalec et al. reported a substantial number of pharmaceuticals and pesticides which were not reported within our study. This can be attributed to absence of exposure to these compounds in our study cohort, but also to differences in the applied suspect lists or sample preparation approaches.

Generally, based on the results presented in **chapter 5**, several challenges and critical points of screening studies can be discussed which should be considered when interpreting results from these sorts of studies. Firstly, we faced a limitation in the well-established confidence level scheme proposed by Schymanski et al. (Schymanski et al., 2014). For the identification of targeted compounds at CL1, this scheme requires the match of all mass-spectrometric identifiers (i.e.,  $m/z$  ratio, RT, isotopic pattern and fragmentation spectrum) between a reference standard and experimental data. However, high-quality fragmentation spectra cannot always be obtained due to low abundances of the compound or strong matrix effect. This, strictly speaking, would result in the assignment of CL4 since one important identifier is missing. However, in this case, an assignment of CL4 does not reflect that all other identifiers are matched with a reference standard thereby vastly underestimating the identification confidence. Therefore, we proposed the addition of a third sub-division of CL2, referred to as CL 2C, which is assigned if all identifiers, except for fragmentation data, are matched with a reference standard. Other studies have proposed alternative approaches to expand the existing scheme and allow a more detailed communication of available identifiers. For example, Alygizakis et al. proposed an identification point (IP) system scoring from 0 to 1 whereby the IP score is composed of different parameters/evidence available (Alygizakis et al., 2023). This ever-new expansion introduced to the existing scoring system raises the need for a more harmonized approach which, on the one hand, allows a concise communication of identification confidence and, on the other hand, provides enough room for a detailed reporting of data supporting the chosen levels of identification confidence.

Secondly, the results discussed in **chapter 5** reveal the presence of numerous glucuronide metabolites. No enzymatic deconjugation step was applied aiming to access the influence of the potential presence of glucuronide metabolites on metabolite assignment and identification confidence. Indeed, the assignment of CLs for the annotation of glucuronidated metabolites was challenging in some cases. For most of these compounds, obtained fragmentation spectra mainly showed fragments derived from the neutral loss of the glucuronide moiety and subsequent further fragmentation of the latter. This provided little structural information for the parent compound decreasing identification confidence. Such challenges can be addressed by the

implementation of a deconjugation step through which, however, information on phase II metabolism and ultimately on potential excretion pathways is lost. Alternatively, a previous study introduced a data analysis tool allowing *in silico* deconjugation thereby filtering out glucuronide derived fragments and facilitating library matching of fragments originating from the parent compound (Huber et al., 2022a). It is advised that one of the mentioned measures are considered when expecting glucuronidated metabolites within SSA studies.

The observed significant differences in numbers of CEC metabolites between high and low exposure group indicate cumulative exposure to complex mixtures of compounds. This was further supported by the fact that a parallel study, conducted on the same set of samples, identified nine persistent and mobile (PMs) chemicals (Kim et al., 2022). This emphasizes the need for the implementation of screening approaches in human biomonitoring studies allowing to account for fast changing compositions of CECs present in the environment and ultimately entering the human body.

### Human biotransformation of QACs

The assessment of human exposure to novel CECs identified at relevant concentrations in environmental samples (**chapter 4.1 and 4.2**) is often hampered by the unavailability of data on biotransformation products. As shown for numerous environmental contaminants, upon exposure latter are biotransformed by human Phase I and II metabolism (Van den Eede et al., 2013; Völkel et al., 2002). These include oxidation reactions (Phase I) and subsequent conjugation reactions (e.g., glucuronidation, sulfation; Phase II). For some contaminants, these reactions lead to detoxification. For example, in contrast to the parent compound bisphenol A (BPA), the BPA-glucuronide shows no endocrine disrupting activity (Matthews et al., 2001). On the contrary, biotransformation can also lead to the formation of metabolites showing higher toxicity than their parent compounds as was described, e.g., for phthalate monoesters (Koch and Calafat, 2009).

For QACs, identified as an abundant emerging group of contaminants in **chapter 4.1**, very limited data on their biotransformation reactions was available. Only two studies assessed *in vitro* formation of Phase I metabolites (Nguyen et al., 2024; Seguin et al., 2019). Thus, no data was available on time trends of *in vitro* metabolization reactions. Also, only one study had confirmed oxidized Phase I metabolites in human urine thereby covering only one QAC class (BACs) (Li et al., 2023).

To fill the described data gaps, in **chapter 6**, the *in vitro* Phase I and II metabolism of three QACs (including one homologue from each of the three classes which showed the highest semi-quantified concentrations in **chapter 4.1**) was investigated. These included C<sub>12</sub>-BAC, C<sub>16</sub>-ATMAC and C<sub>10</sub>-DDAC. Experiments were based on an in-house

developed metabolization assay applying human liver microsomes (HLMs) and two incubation times (1h and 3h) (Gys et al., 2018; Mortelé et al., 2018). These contain the cytochrome P450 (CYP 450) and UDP-glucuronosyltransferase (UGT) enzymes which are the two major enzymatic systems involved in the metabolism of exogenous compounds. Additionally, human liver cytosol (HLCYT) was employed allowing sulfotransferase (SULT) reactions.

In total, 31 Phase I metabolites were identified originating from nineteen biotransformation reactions. For C<sub>12</sub>-BAC and C<sub>16</sub>-ATMAC, eleven and six Phase I metabolites were identified, respectively, originating from five metabolization reactions in both cases. For both compounds, a stepwise oxidation and desaturation of the hydrocarbon side chain was observed leading up to a +2O,-2H-metabolite. For C<sub>12</sub>-BAC, this metabolite (+2O, -2H) showed the highest relative abundance in the 3h time points. In contrast, for C<sub>16</sub>-ATMAC, monohydroxy (+O) metabolites were most abundant in 3h time points. This might be attributed to the longer hydrocarbon chain length of C<sub>16</sub>-ATMAC since decreasing metabolization rates (and thus lower oxidation states) with increasing hydrocarbon chain length have been reported for HLM *in vitro* metabolization of lipids (Adas et al., 1999).

For C<sub>10</sub>-DDAC, fourteen metabolites covering nine metabolization reactions were reported. Their assignment was based on the observation of characteristic neutral losses in the fragmentation spectra allowing to assess that the oxidations occur in parallel on separate hydrocarbon side chains.

For all three QACs, identified metabolites were in line with data described by Nguyen et al. who had used a similar *in vitro* approach (Nguyen et al., 2024). Additionally, four (higher oxidized) metabolites of C<sub>10</sub>-DDAC are described here for the first time as they were not reported in the above-mentioned study.

For all identified metabolites, <sup>DT</sup>CCS<sub>N2</sub> values were calculated to increase identification confidence and to assess changes in CCS-*m/z* trends introduced by metabolization reactions. Previous studies have addressed such trends for other groups of compounds. For example, Lanshoeft et al. characterized shifts in <sup>TW</sup>CCS<sub>N2</sub> observed between parent drugs and their metabolites. Based on this, average changes in <sup>TW</sup>CCS<sub>N2</sub> values following certain metabolization reactions were proposed. For example, hydroxylation lead to an increase in <sup>TW</sup>CCS<sub>N2</sub> by  $+ 3.8 \pm 1.4 \text{ \AA}^2$  (Lanshoeft et al., 2024). However, in our study, the contrary was observed: For all QACs, the introduction of a hydroxy group lead to a clear decrease in <sup>DT</sup>CCS<sub>N2</sub> value. For C<sub>10</sub>-DDAC, the same trend was also observed after the addition of another hydroxy group on the other hydrocarbon side chain. These effects were assumed to be caused by ion-dipole interactions between the positively charged nitrogen and the added oxygen (Nguyen et al., 2024). In contrast to the proposal of Lanshoeft et al. which suggested the use of CCS<sub>N2</sub> shifts to propose

underlying metabolization reactions for identified metabolites, the presented data show that such trends can differ between compound classes and depend not only on the net addition/elimination of functional groups but also on potential changes in gaseous ion confirmation induced by the latter.

Within the interpretation of the results obtained through applied *in vitro* assay some limitations have to be considered. Even though good simulations of the CYP/UGT/SULF metabolic reactions have been reported for this set-up, these findings cannot be directly extrapolated to *in vivo* settings. Within the applied *in vitro* model, subcellular fractions are used in which enzymes are highly enriched. This can lead to overestimation of metabolization rates hampering the unequivocal characterization of the main metabolization pathways (Brandon et al., 2003).

Nevertheless, eight metabolites, including four metabolites of both C<sub>12</sub>-BAC and C<sub>10</sub>-DDAC, were confirmed in human urine samples showing high oxidation states through introduction of up to four oxygen atoms. To the best of our knowledge, this is the first report of higher oxidized C<sub>10</sub>-DDAC metabolites in human urine samples, while oxidized C<sub>12</sub>-BAC have been measured in urine before (Li et al., 2023). Generally, the data on toxicokinetics of QACs is scarce. Only one study has compared QAC excretion through urine and feces (Li and Kannan, 2024). In urine, no parent QACs were detected and hydroxylated and carboxylated BAC metabolites were quantified at a median concentration (summer of all eight targeted BAC metabolites) of 0.49 ng/mL. Other metabolites were not targeted showing that the C<sub>10</sub>-DDAC metabolites confirmed in urine (**chapter 6**) can be of great added value for biomarker selection in future biomonitoring studies. Lastly, it has to be noted that parent QAC levels detected in feces were two orders of magnitude higher than the levels quantified in urine, with median summed QAC concentrations ranging from 170 to 8270 ng/g, suggesting a primarily fecal excretion (Li and Kannan, 2024).

## 7.2 Future perspectives

The occurrence of CECs in both environmental and human samples is ubiquitous. This presence poses a major risk for human health given the potential, in many cases yet uncharacterized, toxic effects resulting from the exposure to complex mixtures of CECs. SSA and NTS approaches have evolved in recent years allowing simultaneous identification of a high number of compounds. As shown in this thesis, these techniques can be applied throughout the whole analysis cycle of CECs, ranging from the screening of environmental samples to the identification of biotransformation products of prioritized contaminants. As a consequence, IM-MS can be of great added value providing an extra separation dimension and the possibility of CCS value calculations, serving as an

additional identification parameter. This thesis aimed at providing a strong contribution to the development of SSA and NTS techniques and to the implementation of IM-MS for CEC identifications. However, several research gaps remain which should be addressed in future research.

**Chapters 3.2** and **3.3** revealed that the reproducibility of  $CCS_{N_2}$  values on different instrumental set-ups has its limitations as for some CEC classes deviations exceeding the proposed cut-off value of  $\pm 2\%$  (Celma et al., 2020) were observed. Future comparison studies covering high numbers of CEC classes are needed to further characterize potential dependencies of CCS deviations on the investigated compound groups or other factors. Currently, an inter-laboratory trial, in which we are participating, on the reproducibility of  $CCS_{N_2}$  values is ongoing within the NORMAN network. In the future,  $CCS_{N_2}$  values of a harmonized set of environmental contaminants will be acquired in different laboratories implementing different instrumental set-ups aiming to further characterize the strengths and limitations of database transfer.

Such inter-laboratory comparisons will remain relevant given the constant development of IM-MS instrumentation. Currently, two new IM systems are gaining popularity: A cyclic TWIMS system launched in 2019 (Giles et al., 2019) and structures for lossless ion manipulation (SLIM) technology (Ibrahim et al., 2017), for which the first commercially available instrument was introduced in 2021 (Newswire, 2021). For these techniques, interlaboratory CCS deviations are not well studied, yet requiring further research. Lastly, as discussed in **chapter 3.2** and other studies (Feuerstein et al., 2022b), further efforts on the harmonization of  $CCS_{N_2}$  calibrations are of high relevance to increase  $CCS_{N_2}$  reproducibility.

In **chapters 4.1** and **4.2**, a high number of CECs was identified in indoor dust samples. New phthalate and DDAC homologues were identified as major classes which, in contrast to legacy homologues, carried different chain lengths. Based on semi-quantified concentrations, it could be shown that some of these homologues showed similar concentrations as observed for the known PHs and QACs, underlying their relevance for human exposure. However, they are currently not measured within targeted methods on PHs or QACs in environmental samples, suggesting a potential underestimation of human exposure to these chemical classes. Therefore, the expansion of targeted methods should be a focus of future research to allow to account for these major 'impurities'.

Semi-quantification approaches have shown great added value for compound prioritization in **chapters 4.1** and **4.2**. Currently, this field is vastly developing and is expected to evolve to a research area of great interest and potential (Malm et al., 2021). Nevertheless, large efforts are still needed to assess the reliability of different semi-quantification approaches. It is yet unclear whether data from these methods, which are

not validated in the classical sense and are aiming to quantify compounds for which no reference standards are available, will ever be of acceptable quality to support or lead to policy decision. Nevertheless, these approaches are expected to have great potential for compound prioritization vastly streamlining possible custom syntheses of reference standards and the development of targeted methods.

The results of chapters 4 and 5 were also communicated to Flemish policy makers (Flemish Environmental Planning Agency). Within the submitted report, only compounds annotated with CL3 or better were included since CL4 and CL5 were not considered sufficient for a reliable reporting. A communication of tentatively annotated chemicals required detailed explanations of the underlying scheme of identification confidence to the policy makers to clarify the limitations of the presented results. Additionally, it is debatable whether the communication of CL3 (i.e., a tentative candidate for which no library reference data is available) is acceptable in such cases. These questions underline the need for a discussion of communication strategies between research and policy makers to allow to exploit the maximum potential of SSA and NTS results while avoiding precipitate policy decision made based on tentative data.

Generally, SSA and NTS approaches are gaining increasing interest in the scope of large European collaborations. For example, the ongoing PARC project includes several tasks assessing the current status of these techniques. One aim is the development of a harmonized Early Warning System (EWS) providing guidelines for the identification and prioritization of CECs ultimately aiming to propose policy actions for contamination prevention. Such large-scale screening studies are also expected to benefit from current developments in the fields of machine learning approaches and artificial intelligence. These bioinformatic tools can vastly improve data processing algorithms easing compound annotation.

Lastly, *in vitro* biotransformation studies conducted in **chapter 6** provided insights into the metabolization of QACs. Similar approaches applied for other abundant CECs identified in **chapters 4.1** and **4.2** could facilitate the implementation of these compounds in future biomonitoring studies. Given the high structural similarities within homologue series of QACs characterized in **chapter 4.1**, it can also be hypothesized that metabolites identified for legacy QACs (**chapter 6**) can be extrapolated to newly identified QACs. An extensive screening study on QACs in human urine should be conducted to confirm this hypotheses. Thereby, the data provided on  $^{DT}CCS_{N2}$  values of QAC metabolites can be used to facilitate metabolite annotations. Necessary tools needed for the design of such a study are provided in this thesis.



## Summary

The occurrence of industrial chemicals in the environment is ubiquitous. Alongside well-studied legacy contaminants, humans can be exposed to numerous unknown or less characterized contaminants. For these compounds, the collective term 'contaminants of emerging concern' (CECs) is used indicating that data on the occurrence, toxicity and biotransformation of these chemicals is scarce.

The occurrence of contaminants in environmental and human samples is commonly accessed by the application of so-called targeted methods. These provide an unequivocal identification and quantitative data for a set of *a priori* selected compounds for which reference standards are available. While such data is crucial for profound biomonitoring and exposure assessment, targeted methods cannot measure the presence of CECs since all compounds not included in the list of targets remain undetected. To fill this gap, SSA and NTS approaches gained increasing attention in recent years. These methods, commonly based on high-resolution mass spectrometry, allow the simultaneous detection and identification of a high number of compounds. To cope with the high complexity of matrices present in environmental and human samples, sophisticated instrumental techniques can be of added value for CECs analyses. In recent years, the implementation of IM-MS in environmental analyses has gained increasing attention. IM-MS allows the separation of analyte ions based on their mobility through a buffer gas under the influence of an electric field. Besides the filtering of potentially interfering matrix components, leading to cleaner mass spectra, this allows the calculation of CCS values which can be used as an additional identification parameter in CEC annotations thereby improving identification confidence.

The presented thesis aimed at applying SSA, and partially NTS, for a holistic assessment of the presence of CECs in the indoor environment and in human urine as well as the investigation of their biotransformation.

The utilization of CCS values as an additional identification parameter relies on the availability of reference data to be matched against experimental data obtained for samples of interest. However, the coverage of CECs by existing CCS databases was poor. Therefore, in **chapter 3.1**, a  $^{DT}CCS_{N_2}$  database was introduced containing 311  $^{DT}CCS_{N_2}$  values of more than 140 CECs and their metabolites. When plotting  $^{DT}CCS_{N_2}$  values as a function of  $m/z$  ratios, different classes of CECs clustered in different areas of the CCS- $m/z$  plot and could be described by separate trendlines.  $^{DT}CCS_{N_2}$  values of a sub selection of AP and OPFR metabolites acquired in spiked urine samples showed good reproducibility of reference data ( $\Delta CCS < 1\%$ ) indicating that  $^{DT}CCS_{N_2}$  value calculations are independent of the investigated matrix.

The inter-laboratory implementation of the  $^{DT}CCS_{N_2}$  database (**chapter 3.1**) in other environmental studies required the investigation of the reproducibility of  $CCS_{N_2}$  calculations using other IM-MS set-ups. Therefore, for sub-selections of CECs,  $CCS_{N_2}$  values were acquired on TWIMS and TIMS systems (**chapters 3.2** and **3.3**, respectively). For TWIMS measurement, two datasets originating from Synapt-G2 and VION systems were available. Additionally, CCS values were predicted using two prediction models both of which were trained with TWIMS derived data. This aimed at assessing whether these models were suitable for  $^{DT}CCS_{N_2}$  predictions.

The comparison of  $^{TWIMS}CCS_{N_2}$  and  $^{DT}CCS_{N_2}$  values (latter set as reference) revealed APEs < 2% for 83% and 82% of the datapoints for VION (n = 94) and Synapt (n = 97) systems, respectively. Here, an influence of the investigated compound class was assumed as most compounds showing the highest APEs belonged to the class of (mostly halogenated) OPFRs. Observed difference were assumed to derive from the different calibrants used in DTIM and TWIMS measurements.

For the comparison of  $^{TIMS}CCS_{N_2}$  and  $^{DT}CCS_{N_2}$  values (**chapter 3.3**), 91% of the datapoints (n = 80) showed APEs < 2%. This suggest a slight better reproducibility of  $^{DT}CCS_{N_2}$  values by the TIMS system which can be attributed to the fact that the same set of calibrants is used in both approaches. Within the interpretation of these results, a limited sample size and no full overlap in compound selections between TIMS and TWIMS comparisons must be taken into account.

To assess the presence of CECs in the indoor environment, 46 dust samples collected in Flanders were screened. Indoor dust has been identified as an important matrix for human exposure to CECs previously. The screening focused on QACs and a general suspect list covering various CEC classes (**chapters 4.1** and **4.2**, respectively). QACs gained increased interest in recent years due to their ubiquitous use as disinfectants during the COVID-19 pandemic. For 21 QACs from the three main classes (BACs, ATMACs and DDACs) reference standards were available allowing their targeted screening. All 21 QACs were detected in indoor dust samples with DFs ranging between 4.2% and 100% with 15 QACs showing DFs > 90%. Semi-quantified concentrations of individual QACs showed a maximum of 32.23  $\mu\text{g/g}$  with a median  $\sum$ QAC concentration of 13.05  $\mu\text{g/g}$  and allowed the calculation of EDIs for adults and toddlers. These did not indicate any potential negative health effects. Suspect screening led to the identification of 17 additional QACs. A dialkyl dimethyl ammonium compound with mixed chain lengths (C16:C18) was characterized as a major QAC homologue with a maximum semi-quantified concentration of 24.90  $\mu\text{g/g}$ . The high detection frequencies and structural variabilities observed call for more European studies on potential human exposure to these compounds. For all assigned QACs,  $^{DT}CCS_{N_2}$  values were acquired.  $^{DT}CCS_{N_2}$  values of suspect QACs were compared with the  $CCS-m/z$  trendlines derived from reference

$^{DT}CCS_{N_2}$  values acquired for QAC standards. The good alignment between the two datasets served as an additional confirmation of the assigned suspect QACs.

In **chapter 4.2**, a generic screening of indoor dust samples allowed the detection of a total of 55 CECs, 34 and 21 of which were identified with confidence level (CL) 1/2 or CL 3, respectively. Besides numerous known contaminants such as DEHP, DEHA or TBOEP which were reported with DFs > 90%, several novel CECs were annotated. These included phthalates with differing side chains, such as decyl nonyl and decyl undecyl phthalate detected with DFs > 80% and identified through the observation of characteristic neutral losses. Additionally, two novel organophosphate flame retardants not previously described in indoor dust, i.e. didecyl butoxyethoxyethyl phosphate (DDeBEEP) and bis(butoxyethyl) butyl phosphate (BBEBP), were identified. Similar to **chapter 4.1**, all suspect compounds were semi-quantified implementing structurally similar calibrants. Semi-quantified concentrations obtained for novel phthalates were in the same order of magnitude as the concentrations observed for legacy phthalates indicating their high relevance for human exposure. From the semi-quantitative data, estimated daily intakes and resulting hazard quotients (HQs) were calculated to estimate the exposure and potential health effects. Neither of the obtained HQ values exceeded the risk threshold, indicating no expected adverse health effects.

**Chapter 5** addressed the application of SSA for the screening of CEC metabolites in human urine samples. From a cohort of Flemish adolescents, whose urine had been collected in the scope of the fourth cycle of the Flemish Environment and Health Study (FLEHS), a total of 83 urine samples were collected. Sample selection aimed at including a low and high exposure dose group based on the concentrations of legacy contaminants measured in the targeted biomonitoring of the FLEHS study. In total, 63 compounds were annotated at a confidence level of 3 or better, with most of the detected compounds not included in current biomonitoring programs. Five out of the 63 compounds were assigned with CL 2. Five compounds could unequivocally be identified (CL 1) through the comparison with reference standards. Personal care products were the main detected compound class (42% of detected compounds). Lastly, in the urine samples, a significantly higher number ( $p < 0.05$ ) of compounds was detected in the high exposure group as opposed to the low exposure group. This difference could only be observed between high and low exposure load samples of female participants ( $p < 0.01$ ).

Further investigation of CECs in human samples require the availability of data on their biotransformation products. For QACs, identified at high semi-quantified concentration in **chapter 4.1**, this data was scarce. Therefore, **chapter 6** investigated the *in vitro* biotransformation of three QACs, including the most abundant homologue from each class characterized in **chapter 4.1**. The applied *in vitro* model implemented human liver microsomes and cytosol mimicking Phase I and II reactions. Thirty-one Phase I

metabolites were identified originating from nineteen biotransformation reactions. Four metabolites of C<sub>10</sub>-DDAC were described for the first time. A detailed assessment of experimental fragmentation spectra allowed to characterize potential oxidation sites. For each identified metabolite, <sup>DT</sup>CCS<sub>N2</sub> values were reported, serving as an additional identification parameter and allowing the characterization of changes in <sup>DT</sup>CCS<sub>N2</sub> values following metabolization. Lastly, eight metabolites, including four metabolites of both C<sub>12</sub>-BAC and C<sub>10</sub>-DDAC, were confirmed in human urine samples showing high oxidation states through introduction of up to four oxygen atoms. This was the first report of higher oxidized C<sub>10</sub>-DDAC metabolites in human urine samples. These findings can facilitate future biomonitoring studies on QACs aiming at a comprehensive assessment of human exposure to these compounds.

Finally, **chapter 7** includes a discussion of the presented results and their positioning in a broader research context. Perspectives for future studies are also suggested identifying remaining research gaps.

## Samenvatting

Industriële chemicaliën komen overal in het milieu voor. Naast bekende en goed bestudeerde verontreinigingen kan de mens blootgesteld worden aan talrijke onbekende of minder goed gekarakteriseerde verontreinigingen. Voor deze verbindingen wordt de verzamelnaam 'verontreinigingen van toenemende zorg' (contaminants of emerging concern; CEC's) gebruikt omdat data over het voorkomen, de toxiciteit en de biotransformatie van deze chemische stoffen schaars is.

Het voorkomen van verontreinigingen milieu- en menselijke monsters wordt meestal geanalyseerd door de toepassing van zogenaamde doelgerichte kwantitatieve methoden. Deze leveren een eenduidige identificatie en kwantitatieve gegevens op voor een reeks a priori geselecteerde verbindingen waarvoor referentiestandaarden beschikbaar zijn. Hoewel dergelijke gegevens cruciaal zijn voor een grondige biomonitoring en blootstellingsbeoordeling, kunnen deze methoden de aanwezigheid van CEC's niet meten, aangezien alle verbindingen die niet in de lijst van analyten zijn opgenomen onopgemerkt blijven. Om deze leemte op te vullen hebben verdachte screening benaderingen de afgelopen jaren steeds meer aandacht gekregen. Deze methoden, meestal gebaseerd op hoge-resolutie massaspectrometrie, maken de gelijktijdige detectie en identificatie van een groot aantal verbindingen mogelijk. Om de hoge complexiteit van matrices in milieu- en menselijke monsters te kunnen analyseren, kunnen geavanceerde instrumentele technieken van toegevoegde waarde zijn voor CECs-analyses. De afgelopen jaren heeft de toepassing van ionmobiliteit spectrometrie (IMS) in milieuanalyses steeds meer aandacht gekregen. IMS maakt de scheiding van analytioneen mogelijk op basis van hun mobiliteit door een buffergas onder invloed van een elektrisch veld. Naast het filteren van mogelijk storende matrixcomponenten, wat leidt tot zuivere massaspectra, maakt dit de berekening van 'collision cross section' (CCS) waarden mogelijk die kunnen worden gebruikt als een extra identificatieparameter in CEC-annotaties, waardoor de betrouwbaarheid van de identificatie toeneemt.

Het doel van dit proefschrift was om verdachte screening toe te passen voor een holistische beoordeling van de aanwezigheid van CEC's in het binnenmilieu en in menselijke urine, en om hun biotransformatie te onderzoeken.

Het gebruik van CCS-waarden als een extra identificatieparameter is afhankelijk van de beschikbaarheid van referentiegegevens die vergeleken kunnen worden met experimentele data. De dekking van CEC's door bestaande CCS-databases was echter slecht. Daarom werd in **hoofdstuk 3.1** een  $^{DT}CCS_{N_2}$ -database geïntroduceerd met 311  $^{DT}CCS_{N_2}$ -waarden van meer dan 140 CEC's en hun metabolieten. Bij het plotten van  $^{DT}CCS_{N_2}$ -waarden als functie van  $m/z$ -verhoudingen, clusteren verschillende klassen van

CEC's in verschillende delen van de CCS-m/z-plot en kunnen ze worden beschreven door afzonderlijke trendlijnen.  $^{DT}CCS_{N_2}$ -waarden van een subselectie van metaboliëten van alternatieve weekmakers en vlamvertragers verkregen in gespikete urinemonsters vertoonden een goede reproduceerbaarheid van referentiegegevens ( $\Delta CCS < 1\%$ ), wat aangeeft dat  $^{DT}CCS_{N_2}$ -waardeberekeningen onafhankelijk zijn van de onderzochte matrix.

De interlaboratorium implementatie van de  $^{DT}CCS_{N_2}$ -databank (**hoofdstuk 3.1**) in andere milieustudies vereiste onderzoek naar de reproduceerbaarheid van  $CCS_{N_2}$ -berekeningen met andere IMS-toestellen. Daarom werden voor subselecties van CEC's  $CCS_{N_2}$ -waarden verkregen met 'lopende golf IMS' (TWIMS) en 'trapped IMS' (TIMS) systemen (respectievelijk **hoofdstuk 3.2** en **3.3**). Voor TWIMS-metingen waren twee datasets beschikbaar die afkomstig waren van Synapt-G2- en VION-systemen. Daarnaast werden CCS-waarden voorspeld met behulp van twee voorspellingsmodellen die beide waren getraind met van TWIMS afgeleide gegevens. Het doel hiervan was om te beoordelen of deze modellen geschikt waren voor  $^{DT}CCS_{N_2}$ -voorspellingen.

De vergelijking van  $^{TWIMS}CCS_{N_2}$ - en  $^{DT}CCS_{N_2}$ -waarden (de laatste gebruikt als referentie) onthulde absolute procentuele fouten (APF)  $< 2\%$  voor respectievelijk 83% en 82% van de datapunten voor VION (n = 94) en Synapt (n = 97) systemen. Hier werd een invloed van de onderzochte verbindingenklasse verondersteld, aangezien de meeste verbindingen met de hoogste APF's tot de klasse van (meestal gehalogeneerde) fosfaat vlamvertragers behoorden. Het werd aangenomen dat de verschillen het gevolg waren van de verschillende kalibratiemiddelen die bij de DTIM- en TWIMS-metingen werden gebruikt.

Voor de vergelijking van  $^{TIMS}CCS_{N_2}$ - en  $^{DT}CCS_{N_2}$ -waarden (**hoofdstuk 3.3**) vertoonden 91% van de datapunten (n = 80) APF's  $< 2\%$ . Dit duidt op een iets betere reproduceerbaarheid van  $^{DT}CCS_{N_2}$ -waarden door het TIMS-systeem, wat kan worden toegeschreven aan het feit dat in beide systemen dezelfde set kalibratiemiddelen wordt gebruikt. Bij de interpretatie van deze resultaten moet rekening worden gehouden met een beperkte steekproefomvang en geen volledige overlap in de samenstellingsselecties tussen TIMS- en TWIMS-vergelijkingen.

Om de aanwezigheid van CEC's in het binnenmilieu te beoordelen, werden 46 stofmonsters die in Vlaanderen verzameld werden, gescreend. Stof binnenshuis is al eerder geïdentificeerd als een belangrijke matrix voor blootstelling van de mens aan CECs. De screening was gericht op quaternaire ammoniumverbindingen (QAV's) en een algemene lijst die verschillende CEC-klassen omvat (respectievelijk **hoofdstuk 4.1** en **4.2**). QAV's kregen de afgelopen jaren meer aandacht door hun alomtegenwoordig gebruik als desinfectiemiddel tijdens de COVID-19 pandemie. Voor 21 QAV's uit de drie hoofdklassen (benzylalkyl dimethylammoniumverbindingen, BAC's; alkyl trimethylammoniumverbindingen, ATMAC's; dialkyldimethylammoniumverbindingen DDAC's) waren referentiestandaarden beschikbaar die een gerichte screening mogelijk maakten. Alle 21 QAV's werden

gedetecteerd in binnenstofmonsters met detectiefrequenties (DF's) variërend tussen 4,2% en 100%, waarbij 15 QAV's DF's > 90% vertoonden. Semi-gekwantificeerde concentraties van individuele QAV's toonden een maximum van 32,23 µg/g met een mediaan  $\Sigma$ QAV-concentratie van 13,05 µg/g en maakten de berekening van een geschatte dagelijkse inname voor volwassenen en peuters mogelijk. Deze wezen niet op mogelijke negatieve gezondheidseffecten. Screening leidde tot de identificatie van 17 extra QAV's. Een dialkyl-dimethylammoniumverbinding met gemengde ketenlengtes (C16:C18) werd gekarakteriseerd als een belangrijke QAV-homoloog met een maximale semi-gekwantificeerde concentratie van 24,90 µg/g. De hoge detectiefrequenties en structurele variabiliteit die werden vastgesteld, vragen om meer Europese studies naar mogelijke blootstelling van de mens aan deze verbindingen. Voor alle QAV's werden  $^{DT}CCS_{N_2}$ -waarden verkregen.  $^{DT}CCS_{N_2}$  waarden van tentatief geïdentificeerde QAV's werden vergeleken met de CCS-m/z trendlijnen die waren afgeleid van referentie- $^{DT}CCS_{N_2}$ -waarden die waren verkregen voor QAC-standaards. De goede afstemming tussen de twee datasets diende als extra confirmatie van de geïdentificeerde QAC's.

In **hoofdstuk 4.2** liet een generieke screening van binnenstofmonsters de detectie toe van in totaal 55 CEC's, waarvan er 34 en 21 werden geïdentificeerd met respectievelijk betrouwbaarheidsniveau (CL) 1/2 of CL 3. Naast talrijke bekende contaminanten zoals DEHP, DEHA of TBOEP die werden gerapporteerd met DF's > 90%, werden verscheidene nieuwe CEC's geannoteerd. Deze omvatten ftalaten met verschillende zijketens, zoals decylnonyl- en decylondecylftalaat die werden gedetecteerd met DF's > 80% en werden geïdentificeerd door de detectie van karakteristieke fragmentatie spectra. Daarnaast werden twee nieuwe organofosfaat vlamvertragers geïdentificeerd die nog niet eerder waren beschreven in binnenshuis stof, namelijk didecyl butoxyethoxyethylfosfaat (DDeBEEP) en bis(butoxyethyl)butylfosfaat (BBEBP). Net als in **hoofdstuk 4.1** werden alle verbindingen semikwantitatief onderzocht met behulp van structureel vergelijkbare kalibratiemiddelen. De semikwantitatieve concentraties die verkregen werden voor nieuwe ftalaten lagen in dezelfde grootteorde als de concentraties die berekend werden voor bekende ftalaten, wat wijst op hun hoge relevantie voor menselijke blootstelling. Op basis van de semi-kwantitatieve gegevens werden geschatte dagelijkse innames en daaruit voortvloeiende gevarenquotiënten (HQ's) berekend om de blootstelling en mogelijke gezondheidseffecten in te schatten. Geen van de verkregen HQ-waarden overschreed de risicodrempel, wat erop wijst dat er geen nadelige gezondheidseffecten worden verwacht.

**Hoofdstuk 5** behandelde de toepassing van verdachte screening voor de identificatie van CEC-metabolieten in menselijke urinemonsters. Van een cohort Vlaamse adolescenten, van wie de urine werd verzameld in het kader van de vierde cyclus van de Vlaamse Milieu- en Gezondheidstudie (FLEHS), werden in totaal 83 urinemonsters geselecteerd. De selectie van de monsters was gericht op het opnemen van een lage en hoge blootstellingsdosisgroep op basis van de concentraties van verontreinigende

stoffen die gemeten werden in de gerichte biomonitoring van de FLEHS-studie. In totaal werden 63 verbindingen geannoteerd met een betrouwbaarheidsniveau van 3 of beter, waarbij de meest gedetecteerde verbindingen niet in de huidige biomonitoringprogramma's waren opgenomen. Aan vijf van de 63 verbindingen werd CL 2 toegekend. Vijf verbindingen konden ondubbelzinnig worden geïdentificeerd (CL 1) door vergelijking met referentiestandaarden. Producten voor persoonlijke verzorging vormden de belangrijkste klasse gedetecteerde verbindingen (42% van de gedetecteerde verbindingen). Tot slot werd in de urinemonsters een significant hoger aantal ( $p < 0,05$ ) verbindingen gedetecteerd in de groep met een hoge blootstelling dan in de groep met een lage blootstelling. Dit verschil kon alleen worden waargenomen tussen vrouwelijke deelnemers met een hoge en een lage blootstelling ( $p < 0,01$ ).

Verder onderzoek naar CEC's in menselijke monsters vereist de beschikbaarheid van gegevens over hun biotransformatieproducten. Voor QAV's, geïdentificeerd in hoge semi-gekwantificeerde concentraties in **hoofdstuk 4.1**, waren deze gegevens schaars. Daarom werd in **hoofdstuk 6** de *in vitro* biotransformatie van drie QAC's onderzocht, waaronder de meest voorkomende homolog uit elke klasse die in **hoofdstuk 4.1** werd gekarakteriseerd. Het toegepaste *in vitro* model bestond uit menselijke levermicrosomen en cytosol die fase I- en fase II-reacties nabootsten. Er werden eenendertig fase I-metabolieten geïdentificeerd die afkomstig waren van negentien biotransformatiereacties. Vier metabolieten van C<sub>10</sub>-DDAC werden voor het eerst beschreven. Een gedetailleerde beoordeling van experimentele fragmentatiespectra maakte het mogelijk om potentiële oxidatiesites te karakteriseren. Voor elke geïdentificeerde metaboliet werden <sup>DT</sup>CCS<sub>N2</sub>-waarden gerapporteerd, die dienen als een extra identificatieparameter en waarmee veranderingen in <sup>DT</sup>CCS<sub>N2</sub>-waarden na metabolisering kunnen worden gekarakteriseerd. Tot slot werden acht metabolieten, waaronder vier metabolieten van zowel C<sub>12</sub>-BAC als C<sub>10</sub>-DDAC, die een hoge oxidatietoestand vertoonden door de introductie van maximaal vier zuurstofatomen bevestigd in menselijke urinemonsters. Dit was het eerste rapport van hoger geoxideerde C<sub>10</sub>-DDAC-metabolieten in menselijke urinemonsters. Deze resultaten kunnen toekomstige biomonitoringstudies naar QAC's, gericht op een uitgebreide beoordeling van de menselijke blootstelling aan deze verbindingen, ondersteunen.

Ten slotte, bevat **hoofdstuk 7** een discussie over de gepresenteerde resultaten en hun positionering binnen een bredere onderzoekscontext. Er worden ook perspectieven voor toekomstig onderzoek gesuggereerd, waarbij resterende onderzoeksuitdagingen worden geïdentificeerd.





## References

### A

- Aalizadeh, R., Nika, M.-C., Thomaidis, N.S. Development and application of retention time prediction models in the suspect and non-target screening of emerging contaminants. *Journal of Hazardous Materials*. **2019**. 363: 277-285.
- Abdelhamid, L., Cabana-Puig, X., Mu, Q., Moarefian, M., Swartwout, B., Eden, K., Das, P., Seguin, R.P., Xu, L., Lowen, S., Lavani, M., Hrubes, T. C., Jones, C. N., Luo, X. M. Quaternary ammonium compound disinfectants reduce lupus-associated splenomegaly by targeting neutrophil migration and t-cell fate. **2020**. *Frontiers in Immunology*. 11: 2738.
- Adas, F., Salaün, J., Berthou, F., Picart, D., Simon, B., Amet, Y. Requirement for  $\omega$  and ( $\omega$ -1)-hydroxylations of fatty acids by human cytochromes P450 2E1 and 4A11. **1999**. *Journal of Lipid Research*. 40: 1990-1997.
- Ahmed, E., Mohibul Kabir, K.M., Wang, H., Xiao, D., Fletcher, J., Donald, W.A. Rapid separation of isomeric perfluoroalkyl substances by high-resolution differential ion mobility mass spectrometry. **2019**. *Analytica Chimica Acta*. 1058: 127-135.
- Ali, N., Dirtu, A.C., Van den Eede, N., Goosey, E., Harrad, S., Neels, H., Coakley, J., Douwes, J., Covaci, A. Occurrence of alternative flame retardants in indoor dust from New Zealand: indoor sources and human exposure assessment. **2012**. *Chemosphere*. 88: 1276-1282.
- Alygizakis, N., Galani, A., Rousis, N.I., Aalizadeh, R., Dimopoulos, M.-A., Thomaidis, N.S. Change in the chemical content of untreated wastewater of Athens, Greece under COVID-19 pandemic. **2021**. *Science of The Total Environment*. 799: 149230.
- Alygizakis, N., Lestremau, F., Gago-Ferrero, P., Gil-Solsona, R., Arturi, K., Hollender, J., Schymanski, E.L., Dulio, V., Slobodnik, J., Thomaidis, N.S. Towards a harmonized identification scoring system in LC-HRMS/MS based non-target screening (NTS) of emerging contaminants. **2023**. *Trends in Analytical Chemistry*. 159: 116944.
- Anderson, S. E., Shane, H., Long, C., Lukomska, E., Meade, B. J., Marshall, N. B. Evaluation of the irritancy and hypersensitivity potential following topical application of didecyldimethylammonium chloride. **2016**. *Journal of Immunotoxicol*. 13: 557-566.
- Ao, J., Yuan, T., Gu, J., Ma, Y., Shen, Z., Tian, Y., Shi, R., Zhou, W., Zhang, J. Organic UV filters in indoor dust and human urine: A study of characteristics, sources, associations and human exposure. **2018**. *Science of the Total Environment*. 640: 1157-1164.
- Arnold, W.A., Blum, A., Branyan, J., Bruton, T.A., Carignan, C.C., Cortopassi, G., Datta, S., DeWitt, J., Doherty, A.-C., Halden, R.U. Quaternary ammonium compounds: a chemical class of emerging concern. **2023**. *Environmental Science & Technology*. 57: 7645-7665.
- Arp, H.P.H., Aurich, D., Schymanski, E.L., Sims, K., Hale, S.E. Avoiding the next silent spring: our chemical past, present, and future. **2023**. *Environmental Science & Technology*. 57: 6355-6359.

## B

- Baduel, C., Mueller, J. F., Tsai, H., Gomez Ramos, M. J. Development of sample extraction and clean-up strategies for target and non-target analysis of environmental contaminants in biological matrices. **2015**. *Journal of Chromatography A*. 1426: 33-47.
- Bajracharya, G.B., Koju, R., Ojha, S., Nayak, S., Subedi, S., Sasai, H. Plasticizers: Synthesis of phthalate esters via FeCl<sub>3</sub>-catalyzed nucleophilic addition of alcohols to phthalic anhydride. **2021**. *Results in Chemistry*. 3: 100190.
- Ballesteros-Gómez, A., Erratico, C.A., Van den Eede, N., Ionas, A.C., Leonards, P.E., Covaci, A. In vitro metabolism of 2-ethylhexyldiphenyl phosphate (EHDPHP) by human liver microsomes. **2015**. *Toxicology Letters*. 232: 203-212.
- Bastiaensen, M., Ait Bamai, Y., Araki, A., Van den Eede, N., Kawai, T., Tsuboi, T., Kishi, R., Covaci, A. Biomonitoring of organophosphate flame retardants and plasticizers in children: Associations with house dust and housing characteristics in Japan. **2019**. *Environmental Research*. 172: 543-551.
- Bastiaensen, M., Gys, C., Colles, A., Malarvannan, G., Verheyen, V., Koppen, G., Govarts, E., Bruckers, L., Morrens, B., Franken, C. Biomarkers of phthalates and alternative plasticizers in the Flemish Environment and Health Study (FLEHS IV): Time trends and exposure assessment. **2021a**. *Environmental Pollution*. 276: 116724.
- Bastiaensen, M., Gys, C., Colles, A., Verheyen, V., Koppen, G., Govarts, E., Bruckers, L., Morrens, B., Loots, I., De Decker, A. Exposure levels, determinants and risk assessment of organophosphate flame retardants and plasticizers in adolescents (14–15 years) from the Flemish Environment and Health Study. **2021b**. *Environment International*. 147: 106368.
- Bastiaensen, M., Gys, C., Malarvannan, G., Fotache, M., Bombeke, J., Bamai, Y.A., Araki, A., Covaci, A. Short-term temporal variability of urinary biomarkers of organophosphate flame retardants and plasticizers. **2021c**. *Environment International*. 146: 106147.
- Bastiaensen, M., Xu, F., Been, F., Van den Eede, N., Covaci, A. Simultaneous determination of 14 urinary biomarkers of exposure to organophosphate flame retardants and plasticizers by LC-MS/MS. **2018**. *Analytical and Bioanalytical Chemistry*. 410: 7871-7880.
- Been, F., Malarvannan, G., Bastiaensen, M., Yin, S., van Nuis, A. L. N., Covaci, A. Development and validation of a bioanalytical assay based on liquid chromatography-tandem mass spectrometry for measuring biomarkers of exposure of alternative plasticizers in human urine and serum. **2019**. *Talanta*. 198: 230-236.
- Béranger, R., Billoir, E., Nuckols, J.R., Blain, J., Millet, M., Bayle, M.-L., Combourieu, B., Philip, T., Schüz, J., Fervers, B. Agricultural and domestic pesticides in house dust from different agricultural areas in France. **2019**. *Environmental Science and Pollution Research*. 26: 19632-19645.
- Bertuzzi, T., Pietri, A. Determination of Benzalkonium Homologues and Didecyldimethylammonium in Powdered and Liquid Milk for Infants by Hydrophilic

- Interaction Liquid Chromatography–Mass Spectrometry. **2014**. *Food Analytical Methods*. 7: 1278-1284.
- Bieber, S., Letzel, T., Krueve, A. Electrospray Ionization Efficiency Predictions and Analytical Standard Free Quantification for SFC/ESI/HRMS. **2023**. *Journal of the American Society for Mass Spectrometry*. 34: 1511-1518.
- Biel-Maeso, M., Corada-Fernández, C., Lara-Martín, P.A. Removal of personal care products (PCPs) in wastewater and sludge treatment and their occurrence in receiving soils. **2019**. *Water Research*. 150: 129-139.
- Bijlsma, L., Bade, R., Celma, A., Mullin, L., Cleland, G., Stead, S., Hernandez, F., Sancho, J.V. Prediction of Collision Cross-Section Values for Small Molecules: Application to Pesticide Residue Analysis. **2017**. *Analytical Chemistry*. 89: 6583-6589.
- Bijlsma, L., Berntssen, M.H., Merel, S. A refined nontarget workflow for the investigation of metabolites through the prioritization by in silico prediction tools. **2019**. *Analytical Chemistry*. 91: 6321-6328.
- Bletsou, A.A., Jeon, J., Hollender, J., Archontaki, E., Thomaidis, N.S. Targeted and non-targeted liquid chromatography-mass spectrometric workflows for identification of transformation products of emerging pollutants in the aquatic environment. **2015**. *Trends in Analytical Chemistry*. 66: 32-44.
- Bonvallot, N., Jamin, E.L., Regnaut, L., Chevrier, C., Martin, J.-F., Mercier, F., Cordier, S., Cravedi, J.-P., Debrauwer, L., Le Bot, B. Suspect screening and targeted analyses: Two complementary approaches to characterize human exposure to pesticides. **2021**. *Science of the Total Environment*. 786: 147499.
- Bořík, A., Nováková, P., Stroski, K.M. Rapid target screening and quantitative analysis of various environmental pollutants. **2023**. *Rapid Communications in Mass Spectrometry*. e9517.
- Brandon, E.F., Raap, C.D., Meijerman, I., Beijnen, J.H., Schellens, J.H. An update on in vitro test methods in human hepatic drug biotransformation research: pros and cons. **2003**. *Toxicology and Applied Pharmacology*. 189: 233-246.
- Bu, S., Wang, Y., Wang, H., Wang, F., Tan, Y. Analysis of global commonly-used phthalates and non-dietary exposure assessment in indoor environment. **2020**. *Building and Environment*. 177: 106853.
- Buekers, J., Verheyen, V., Remy, S., Covaci, A., Colles, A., Koppen, G., Govarts, E., Bruckers, L., Leermakers, M., St-Amand, A. Combined chemical exposure using exposure loads on human biomonitoring data of the 4th Flemish Environment and Health Study (FLEHS-4). **2021**. *International Journal of Hygiene and Environmental Health*. 238: 113849.
- Bui, T.T., Giovanoulis, G., Cousins, A.P., Magnér, J., Cousins, I.T., de Wit, C.A. Human exposure, hazard and risk of alternative plasticizers to phthalate esters. **2016**. *Science of the Total Environment*. 541: 451-467.
- Burnett, C. L., Heldreth, B., Bergfeld, W. F., Belsito, D. V., Hill, R. A., Klaassen, C. D., Liebler, D. C., Marks Jr, J. G., Shank, R. C., Slaga, T. J. Safety assessment of 6-hydroxyindole as used in cosmetics. **2014**. *International Journal of Toxicology*. 33: 24S-35S.

- Bush, M.F., Campuzano, I.D., Robinson, C.V. Ion mobility mass spectrometry of peptide ions: effects of drift gas and calibration strategies. **2012**. *Analytical Chemistry*. 84: 7124-7130.
- Bush, M.F., Hall, Z., Giles, K., Hoyes, J., Robinson, C.V., Ruotolo, B.T. Collision cross sections of proteins and their complexes: a calibration framework and database for gas-phase structural biology. 2010. *Analytical Chemistry*. 82: 9557-9565.

## C

- Caballero-Casero, N., Belova, L., Vervliet, P., Antignac, J.-P., Castano, A., Debrauwer, L., López, M.E., Huber, C., Klanova, J., Krauss, M. Towards harmonised criteria in quality assurance and quality control of suspect and non-target LC-HRMS analytical workflows for screening of emerging contaminants in human biomonitoring. **2021a**. *Trends in Analytical Chemistry*. 136: 116201.
- Caballero-Casero, N., Castro, G., Bastiaensen, M., Gys, C., van Larebeke, N., Schoeters, G., Covaci, A. Identification of chemicals of emerging concern in urine of Flemish adolescents using a new suspect screening workflow for LC-QTOF-MS. **2021b**. *Chemosphere*. 280: 130683-130692.
- Campuzano, I., Bush, M.F., Robinson, C.V., Beaumont, C., Richardson, K., Kim, H., Kim, H.I. Structural characterization of drug-like compounds by ion mobility mass spectrometry: comparison of theoretical and experimentally derived nitrogen collision cross sections. **2012**. *Analytical Chemistry*. 84: 1026-1033.
- Carpinteiro, I., Abuin, B., Rodriguez, I., Ramil, M., Cela, R. Pressurized solvent extraction followed by gas chromatography tandem mass spectrometry for the determination of benzotriazole light stabilizers in indoor dust. **2010**. *Journal of Chromatography A*. 1217: 3729-3735.
- Carson, R. Silent Spring. **1962**. Houghton Mifflin Harcourt.
- Causon, T.J., Hann, S. Uncertainty Estimations for Collision Cross Section Determination via Uniform Field Drift Tube-Ion Mobility-Mass Spectrometry. **2020**. *Journal of the American Society for Mass Spectrometry*. 31: 2102-2110.
- Causon, T.J., Ivanova-Petropulos, V., Petrusheva, D., Bogeve, E., Hann, S. Fingerprinting of traditionally produced red wines using liquid chromatography combined with drift tube ion mobility-mass spectrometry. **2019a**. *Analytica Chimica Acta*. 1052, 179-189.
- Causon, T.J., Si-Hung, L., Newton, K., Kurulugama, R.T., Fjeldsted, J., Hann, S. Fundamental study of ion trapping and multiplexing using drift tube-ion mobility time-of-flight mass spectrometry for non-targeted metabolomics. **2019b**. *Analytical Bioanalytical Chemistry*. 411: 6265-6274.
- Celma, A., Ahrens, L., Gago-Ferrero, P., Hernandez, F., Lopez, F., Lundqvist, J., Pitarch, E., Sancho, J.V., Wiberg, K., Bijlsma, L. The relevant role of ion mobility separation in LC-HRMS based screening strategies for contaminants of emerging concern in the aquatic environment. **2021**. *Chemosphere*. 280: 130799.
- Celma, A., Bade, R., Sancho, J.V., Hernandez, F., Humphries, M., Bijlsma, L. Prediction of retention time and collision cross section (CCSH+, CCSH-, and CCSNa+) of emerging

- contaminants using multiple adaptive regression splines. **2022**. *Journal of Chemical Information and Modeling*. 62: 5425-5434.
- Celma, A., Sancho, J.V., Schymanski, E.L., Fabregat-Safont, D., Ibanez, M., Goshawk, J., Barkowitz, G., Hernandez, F., Bijlsma, L. Improving Target and Suspect Screening High-Resolution Mass Spectrometry Workflows in Environmental Analysis by Ion Mobility Separation. **2020**. *Environmental Science & Technology*. 54: 15120-15131.
- Cequier, E., Ionas, A. C., Covaci, A., Marce, R. M., Becher, G., Thomsen, C. Occurrence of a broad range of legacy and emerging flame retardants in indoor environments in Norway. 2014. *Environmental Science & Technology*. 48: 6827-35.
- Chai, M., Young, M.N., Liu, F.C., Bleiholder, C. A transferable, sample-independent calibration procedure for trapped ion mobility spectrometry (TIMS). **2018**. *Analytical Chemistry*. 90: 9040-9047.
- Chao, A., Al-Ghoul, H., McEachran, A.D., Balabin, I., Transue, T., Cathey, T., Grossman, J.N., Singh, R.R., Ulrich, E.M., Williams, A.J. In silico MS/MS spectra for identifying unknowns: a critical examination using CFM-ID algorithms and ENTACT mixture samples. **2020**. *Analytical and Bioanalytical Chemistry*. 412: 1303-1315.
- Chiellini, F., Ferri, M., Morelli, A., Dipaola, L., Latini, G. Perspectives on alternatives to phthalate plasticized poly (vinyl chloride) in medical devices applications. **2013**. *Progress in Polymer Science*. 38: 1067-1088.
- Chouinard, C.D., Cruzeiro, V.W.D., Roitberg, A.E., Yost, R.A. Experimental and Theoretical Investigation of Sodiated Multimers of Steroid Epimers with Ion Mobility-Mass Spectrometry. **2017**. *Journal of the American Society for Mass Spectrometry*. 28: 323-331.
- Christia, C., Poma, G., Basis, A., Samara, C., Covaci, A. Legacy and emerging organophosphomicrocrystalline flame retardants in car dust from Greece: Implications for human exposure. **2018**. *Chemosphere*. 196: 231-239.
- Christia, C., Poma, G., Caballero-Casero, N., Covaci, A. From suspect screening to target analysis: Occurrence of six newly identified compounds in indoor dust from Belgium. **2021a**. *Environmental Research*. 197: 111193.
- Christia, C., Poma, G., Caballero-Casero, N., Covaci, A. Suspect screening analysis in house dust from Belgium using high resolution mass spectrometry; prioritization list and newly identified chemicals. **2021b**. *Chemosphere*. 263: 127817.
- Christia, C., Poma, G., Harrad, S., De Wit, C.A., Sjoström, Y., Leonards, P., Lamoree, M., Covaci, A. Occurrence of legacy and alternative plasticizers in indoor dust from various EU countries and implications for human exposure via dust ingestion and dermal absorption. **2019**. *Environmental Research*. 171: 204-212.
- Commission Regulation (EC) 1107/2009, Regulation (EC) No 1107/2009 of the European Parliament and of the Council of 21 October 2009 concerning the placing of plant protection products on the market and repealing Council Directives 79/117/EEC and 91/414/EEC. Online: <https://eur-lex.europa.eu/legal-content/EN/ALL/?uri=CELEX%3A32009R1107> (Accessed on 10/02/2022).
- Commission Regulation (EC) 1333/2008, Regulation (EC) No 1333/2008 of the European Parliament and of the Council of 16 December 2008 on food additives. Online:

<https://eur-lex.europa.eu/legal-content/EN/TXT/?uri=celex%3A32008R1333>

(Accessed on 10/02/2022).

- Cohen, M.J., Karasek, F. Plasma chromatography™—a new dimension for gas chromatography and mass spectrometry. **1970**. *Journal of Chromatographic Science*. 8: 330-337.
- Colby, S.M., Thomas, D.G., Nunez, J.R., Baxter, D.J., Glaesemann, K.R., Brown, J.M., Pirrung, M.A., Govind, N., Teeguarden, J.G., Metz, T.O., Renslow, R.S. ISiCLE: A Quantum Chemistry Pipeline for Establishing in Silico Collision Cross Section Libraries. **2019**. *Analytical Chemistry*. 91: 4346-4356.
- Crowell, K.L., Baker, E.S., Payne, S.H., Ibrahim, Y.M., Monroe, M.E., Slysz, G.W., LaMarche, B.L., Petyuk, V.A., Piehowski, P.D., Danielson, W.F., 3rd, Anderson, G.A., Smith, R.D. Increasing Confidence of LC-MS Identifications by Utilizing Ion Mobility Spectrometry. **2013**. *International Journal of Mass Spectrometry*. 354-355: 312-317.
- Cui, D., Cox, J., Mejias, E., Ng, B., Gardinali, P., Bagner, D.M., Quinete, N. Evaluating non-targeted analysis methods for chemical characterization of organic contaminants in different matrices to estimate children's exposure. **2023**. *Journal of Exposure Science & Environmental Epidemiology*. 33: 589-601.

## D

- del Mar Gómez-Ramos, M., Pérez-Parada, A., García-Reyes, J.F., Fernández-Alba, A.R., Agüera, A. Use of an accurate-mass database for the systematic identification of transformation products of organic contaminants in wastewater effluents. **2011**. *Journal of Chromatography A*. 1218: 8002-8012.
- den Ouden, F., Estévez-Danta, A., Belova, L., Gys, C., Klimowska, A., Roggeman, M., Van Wichelen, N., Quintana, J.B., Rodil, R., Poma, G. Investigation of in vitro biotransformation of tris (1-chloro-2-propyl) phosphate and confirmation in human urine. **2024**. *Current Research in Toxicology*. 6: 100164.
- Deventer, K., Pozo, O.J., Verstraete, A.G., Van Eenoo, P. Dilute-and-shoot-liquid chromatography-mass spectrometry for urine analysis in doping control and analytical toxicology. **2014**. *Trends in Analytical Chemistry*. 55: 1-13.
- Ding, J., Xu, Z., Huang, W., Feng, L., Yang, F. Organophosphate ester flame retardants and plasticizers in human placenta in Eastern China. **2016**. *Science of the Total Environment*. 554-555: 211-217.
- Dionisio, K. L., Phillips, K., Price, P. S., Grulke, C. M., Williams, A., Biryol, D., Hong, T., Isaacs, K. K. The Chemical and Products Database, a resource for exposure-relevant data on chemicals in consumer products. **2018**. *Scientific Data*. 5: 1-9.
- Djombou-Feunang, Y., Pon, A., Karu, N., Zheng, J., Li, C., Arndt, D., Gautam, M., Allen, F., Wishart, D.S. CFM-ID 3.0: significantly improved ESI-MS/MS prediction and compound identification. **2019**. *Metabolites*. 9: 72.
- Dodds, J.N., Hopkins, Z.R., Knappe, D.R.U., Baker, E.S. Rapid Characterization of Per- and Polyfluoroalkyl Substances (PFAS) by Ion Mobility Spectrometry-Mass Spectrometry (IMS-MS). **2020**. *Analytical Chemistry*. 92: 4427-4435.

- Dolios, G., Patel, D., Arora, M., Andra, S.S. Mass defect filtering for suspect screening of halogenated environmental chemicals: a case study of chlorinated organophosphate flame retardants. **2019**. *Rapid Communications in Mass Spectrometry*. 33: 503-519.
- Dou, M., Wang, L. A review on organophosphate esters: physicochemical properties, applications, and toxicities as well as occurrence and human exposure in dust environment. **2023**. *Journal of Environmental Management*. 325: 116601.
- Du, B., He, Y., Liang, B., Li, J., Luo, D., Chen, H., Liu, L.-Y., Guo, Y., Zeng, L. Identification of triazine UV filters as an emerging class of abundant, ubiquitous pollutants in indoor dust and air from South China: call for more concerns on their occurrence and human exposure. *Environmental Science & Technology*. **2022**. 56: 4210-4220.
- Dubocq, F., Kärrman, A., Gustavsson, J., Wang, T. Comprehensive chemical characterization of indoor dust by target, suspect screening and nontarget analysis using LC-HRMS and GC-HRMS. **2021**. *Environmental Pollution*. 276: 116701.
- Dvorščak, M., Jakovljević, I., Jagić, K., Tariba Lovaković, B., Klinčić, D. Polybrominated diphenyl ethers and polycyclic aromatic hydrocarbons in dust from different indoor environments in Zagreb, Croatia: Levels and human exposure assessment. **2022**. *Indoor Air*. 32: e13145.

## E

- Ebert, K. E., Belov, V. N., Weiss, T., Brüning, T., Hayen, H., Koch, H. M., Bury, D. Determination of urinary metabolites of the UV filter homosalate by online-SPE-LC-MS/MS. **2021**. *Analytica Chimica Acta*. 1176: 338754.
- EFSA. Opinion of the Scientific Panel on food additives, flavourings, processing aids and materials in contact with food (AFC) related to Di-isodecylphthalate (DIDP) for use in food contact materials. **2005a**. *EFSA Journal*. 3: 245.
- EFSA. Opinion of the Scientific Panel on food additives, flavourings, processing aids and materials in contact with food (AFC) related to Di-isononylphthalate (DINP) for use in food contact materials. **2005b**. *EFSA Journal*. 3: 244.
- EFSA. European Food Safety Authority. Reasoned opinion on the dietary risk assessment for proposed temporary maximum residue levels (MRLs) of didecyltrimethylammonium chloride (DDAC) and benzalkonium chloride (BAC). **2014a**. *EFSA Journal*. 12: 3675.
- EFSA. Reasoned opinion on the dietary risk assessment for proposed temporary maximum residue levels (MRLs) of didecyltrimethylammonium chloride (DDAC) and benzalkonium chloride (BAC). **2014b**. *EFSA Journal*. 12: 3675.
- EFSA Scientific Committee, More, S.J., Bampidis, V., Benford, D., Bragard, C., Hernandez-Jerez, A., Bennekou, S.H., Halldorsson, T.I., Koutsoumanis, K.P., Lambré, C. Guidance Document on Scientific criteria for grouping chemicals into assessment groups for human risk assessment of combined exposure to multiple chemicals. **2021**. *EFSA Journal*. 19: e07033.
- Eggen, T., Moeder, M., Arukwe, A. Municipal landfill leachates: a significant source for new and emerging pollutants. **2010**. *Science of the Total Environment*. 408: 5147-5157.

- EPA, U.S. Environmental Protection Agency. Health And Environmental Effects Profile for Quinoline. EPA/600/X-85/355 (NTIS PB88183124). Online: <https://cfpub.epa.gov/ncea/risk/hhra/recordisplay.cfm?deid=48746> (accessed on 14 February 2022). 1985.
- EPA, U.S. Environmental Protection Agency. Priority Pollutant List. Online: <https://www.epa.gov/sites/default/files/2015-09/documents/priority-pollutant-list-epa.pdf> (accessed 15 February 2022). **2014**.
- EPA, U.S. Environmental Protection Agency. United States Environmental Protection Agency: IRIS Assessments. **1992**. ([https://cfpub.epa.gov/ncea/iris2/chemicalLanding.cfm?substance\\_nmbr=420](https://cfpub.epa.gov/ncea/iris2/chemicalLanding.cfm?substance_nmbr=420); accessed on 27/10/2023).
- EPA, U.S. Environmental Protection Agency. Exposure Factors Handbook Chapter 5 (Update): Soil and Dust Ingestion. U.S. EPA Office of Research and Development, Washington, DC, EPA/600/R-17/384F, **2017a**.
- EPA, U.S. Environmental Protection Agency. Safer Chemical Ingredients List. Online: <https://www.epa.gov/saferchoice/safer-ingredients#scil> (accessed on 17 February 2022). **2017b**.
- EPA, U.S. Environmental Protection Agency. United States Environmental Protection Agency: List N Advanced Search Page: Disinfectants for Coronavirus (COVID-19). **2020**. (<https://www.epa.gov/coronavirus/about-list-n-disinfectants-coronavirus-covid-19-0>; accessed on 15/02/2023).
- EPA, U.S. Environmental Protection Agency. United States Environmental Protection Agency: Regional Screening Levels (RSLs) - Generic Tables. **2024**. (<https://www.epa.gov/risk/regional-screening-levels-rsls-generic-tables>; accessed on 25/04/2023).
- Esplugas, R., Rovira, J., Mari, M., Fernández-Arribas, J., Eljarrat, E., Domingo, J.L., Schuhmacher, M. Emerging and legacy flame retardants in indoor air and dust samples of Tarragona Province (Catalonia, Spain). **2022**. *Science of the Total Environment*. 806: 150494.
- Esquenazi, E., Daly, M., Bahrainwala, T., Gerwick, W.H., Dorrestein, P.C. Ion mobility mass spectrometry enables the efficient detection and identification of halogenated natural products from cyanobacteria with minimal sample preparation. **2011**. *Bioorganic & Medicinal Chemistry*. 19: 6639-6644.
- Eurostat. Chemicals production and consumption statistics. 2023. [https://ec.europa.eu/eurostat/statistics-explained/index.php?title=Chemicals\\_production\\_and\\_consumption\\_statistics#Total\\_production\\_of\\_chemicals](https://ec.europa.eu/eurostat/statistics-explained/index.php?title=Chemicals_production_and_consumption_statistics#Total_production_of_chemicals) (accessed on 19/06/2024).
- Ewing, M.A., Glover, M.S., Clemmer, D.E. Hybrid ion mobility and mass spectrometry as a separation tool. *Journal of Chromatography A*. **2016**. 1439: 3-25.

## F

- Fabregat-Safont, D., Ibáñez, M., Bijlsma, L., Hernández, F., Waichman, A.V., de Oliveira, R., Rico, A. Wide-scope screening of pharmaceuticals, illicit drugs and their metabolites in the Amazon River. **2021**. *Water Research*. 200: 117251.
- Feuerstein, M.L., Hernández-Mesa, M., Kiehne, A., Le Bizec, B., Hann, S., Dervilly, G., Causon, T. Comparability of steroid collision cross sections using three different IM-HRMS technologies: an interplatform study. **2022a**. *Journal of the American Society for Mass Spectrometry*. 33: 1951-1959.
- Feuerstein, M.L., Hernández-Mesa, M., Valadbeigi, Y., Le Bizec, B., Hann, S., Dervilly, G., Causon, T. Critical evaluation of the role of external calibration strategies for IM-MS. **2022b**. *Analytical and Bioanalytical Chemistry*. 414: 7483-7493.
- Fisher, M.B., Campanale, K., Ackermann, B.L., VandenBranden, M., Wrighton, S.A. In vitro glucuronidation using human liver microsomes and the pore-forming peptide alamethicin. **2000**. *Drug Metabolism and Disposition*. 28: 560-566.
- Fitzgerald, C.C., Hedman, R., Uduwela, D.R., Paszerbovics, B., Carroll, A.J., Neeman, T., Cawley, A., Brooker, L., McLeod, M.D. Profiling urinary sulfate metabolites with mass spectrometry. **2022**. *Frontiers in Molecular Biosciences*. 9: 829511.

## G

- Gabelica, V., Shvartsburg, A.A., Afonso, C., Barran, P., Benesch, J.L.P., Bleiholder, C., Bowers, M.T., Bilbao, A., Bush, M.F., Campbell, J.L., Campuzano, I.D.G., Causon, T., Clowers, B.H., Creaser, C.S., De Pauw, E., Far, J., Fernandez-Lima, F., Fjeldsted, J.C., Giles, K., Groessl, M., Hogan, C.J., Jr., Hann, S., Kim, H.I., Kurulugama, R.T., May, J.C., McLean, J.A., Pagel, K., Richardson, K., Ridgeway, M.E., Rosu, F., Sobott, F., Thalassinos, K., Valentine, S.J., Wyttenbach, T. Recommendations for reporting ion mobility Mass Spectrometry measurements. **2019**. *Mass Spectrometry Reviews*. 38: 291-320.
- Gakidou, E., Afshin, A., et al. Global, regional, and national comparative risk assessment of 84 behavioural, environmental and occupational, and metabolic risks or clusters of risks, 1990–2016: a systematic analysis for the Global Burden of Disease Study 2016. **2017**. *The Lancet*. 390: 1345-1422.
- Gelb, A.S., Jarratt, R.E., Huang, Y., Dodds, E.D. A study of calibrant selection in measurement of carbohydrate and peptide ion-neutral collision cross sections by traveling wave ion mobility spectrometry. 2014. *Analytical Chemistry*. 86: 11396-11402.
- George, A.D., Gay, M.C.L., Wlodek, M.E., Trengove, R.D., Murray, K., Geddes, D.T. Untargeted lipidomics using liquid chromatography-ion mobility-mass spectrometry reveals novel triacylglycerides in human milk. **2020**. *Scientific Reports*. 10: 9255.
- Gerona, R. R., Schwartz, J. M., Pan, J., Friesen, M. M., Lin, T., Woodruff, T. J. Suspect screening of maternal serum to identify new environmental chemical biomonitoring targets using liquid chromatography-quadrupole time-of-flight mass spectrometry. **2018**. *Journal of Exposure Science & Environmental Epidemiology*. 28: 101-108.

- Gerona, R.R., Schwartz, J.M., Pan, J., Friesen, M.M., Lin, T., Woodruff, T.J. Suspect screening of maternal serum to identify new environmental chemical biomonitoring targets using liquid chromatography-quadrupole time-of-flight mass spectrometry. **2018**. *Journal of Exposure Science & Environmental Epidemiology*. 28: 101-108.
- Gilbert, P., Moore, L. Cationic antiseptics: diversity of action under a common epithet. **2005**. *Journal of Applied Microbiology*. 99: 703-715.
- Giles, K., Ujma, J., Wildgoose, J., Pringle, S., Richardson, K., Langridge, D., Green, M. A cyclic ion mobility-mass spectrometry system. **2019**. *Analytical Chemistry*. 91: 8564-8573.
- Giles, K., Williams, J.P., Campuzano, I. Enhancements in travelling wave ion mobility resolution. **2011**. *Rapid Communications in Mass Spectrometry*. 25: 1559-1566.
- Godfrey, A.R., Dunscombe, J., Gravell, A., Hunter, A., Barrow, M.P., van Keulen, G., Desbrow, C., Townsend, R. Use of QuEChERS as a manual and automated high-throughput protocol for investigating environmental matrices. **2022**. *Chemosphere*. 308: 136313.
- Gong, S., Ren, K., Ye, L., Deng, Y., Su, G. Suspect and nontarget screening of known and unknown organophosphate esters (OPEs) in soil samples. **2022**. *Journal of Hazardous Materials*. 436: 129273.
- González-Gaya, B., Lopez-Herguedas, N., Bilbao, D., Mijangos, L., Iker, A., Etxebarria, N., Irazola, M., Prieto, A., Olivares, M., Zuloaga, O. Suspect and non-target screening: the last frontier in environmental analysis. **2021**. *Analytical Methods*. 13: 1876-1904.
- Gonzalez, M., Jégu, J., Kopferschmitt, M.C., Donnay, C., Hedelin, G., Matzinger, F., Velten, M., Guilloux, L., Cantineau, A., de Blay, F. Asthma among workers in healthcare settings: role of disinfection with quaternary ammonium compounds. **2014**. *Clinical & Experimental Allergy*. 44: 393-406.
- Govarts, E., Portengen, L., Lambrechts, N., Bruckers, L., Den Hond, E., Covaci, A., Nelen, V., Nawrot, T.S., Loots, I., Sioen, I. Early-life exposure to multiple persistent organic pollutants and metals and birth weight: Pooled analysis in four Flemish birth cohorts. **2020**. *Environment International*. 145: 106149.
- Gray, C., Thomas, B., Upton, R., Migas, L., Eysers, C., Barran, P., Flitsch, S. Applications of ion mobility mass spectrometry for high throughput, high resolution glycan analysis. **2016**. *Biochimica et Biophysica Acta (BBA)-General Subjects*. 1860: 1688-1709.
- Groh, K.J., Backhaus, T., Carney-Almroth, B., Geueke, B., Inostroza, P.A., Lennquist, A., Leslie, H.A., Maffini, M., Slunge, D., Trasande, L. Overview of known plastic packaging-associated chemicals and their hazards. **2019**. *Science of the Total Environment*. 651: 3253-3268.
- Guo, Z., Huang, S., Wang, J., Feng, Y.L. Recent advances in non-targeted screening analysis using liquid chromatography - high resolution mass spectrometry to explore new biomarkers for human exposure. **2020**. *Talanta*. 219: 121339.
- Gys, C., Bastiaensen, M., Bruckers, L., Colles, A., Govarts, E., Martin, L.R., Verheyen, V., Koppen, G., Morrens, B., Den Hond, E., 2021a. Determinants of exposure levels of bisphenols in Flemish adolescents. **2021a**. *Environmental Research*. 193: 110567.

- Gys, C., Bastiaensen, M., Malarvannan, G., Bamai, Y.A., Araki, A., Covaci, A. Short-term variability of bisphenols in spot, morning void and 24-hour urine samples. **2021b**. *Environmental Pollution*. 268: 115747.
- Gys, C., Kovačič, A., Huber, C., Lai, F.Y., Heath, E., Covaci, A. Suspect and untargeted screening of bisphenol S metabolites produced by in vitro human liver metabolism. **2018**. *Toxicology Letters*. 295: 115-123.

## H

- Hammel, S.C., Levasseur, J.L., Hoffman, K., Phillips, A.L., Lorenzo, A.M., Calafat, A.M., Webster, T.F., Stapleton, H.M. Children's exposure to phthalates and non-phthalate plasticizers in the home: the TESIIE study. **2019**. *Environment International*. 132: 105061.
- Harrad, S., Ibarra, C., Diamond, M., Melymuk, L., Robson, M., Douwes, J., Roosens, L., Dirtu, A.C., Covaci, A. Polybrominated diphenyl ethers in domestic indoor dust from Canada, New Zealand, United Kingdom and United States. **2008**. *Environment International*. 34: 232-238.
- Harris, M. O., Corcoran, J. Toxicological profile for dinitrophenols. 1995. *Environmental Science*.
- HBM4EU, Second list of HBM4EU priority substances and Chemical Substance Group Leaders for 2019-2021 Deliverable Report D 4.5 WP 4-Prioritisation and input to the Annual Work Plan. **2018**.
- He, L., Lin, Y., Day, D., Teng, Y., Wang, X., Liu, X. L., Yan, E., Gong, J., Qin, J., Wang, X. Nitrated polycyclic aromatic hydrocarbons and arachidonic acid metabolisms relevant to cardiovascular pathophysiology: findings from a panel study in healthy adults. **2021**. *Environmental Science and Technology*. 55: 3867-3875.
- Heffernan, A.L., Thompson, K., Eaglesham, G., Vijayasarathy, S., Mueller, J., Sly, P., Gomez, M. Rapid, automated online SPE-LC-QTRAP-MS/MS method for the simultaneous analysis of 14 phthalate metabolites and 5 bisphenol analogues in human urine. **2016**. *Talanta*. 151: 224-233.
- Hermabessiere, L., Receveur, J., Himber, C., Mazurais, D., Huvet, A., Lagarde, F., Lambert, C., Paul-Pont, I., Dehaut, A., Jezequel, R., Soudant, P., Duflos, G. An Irgafos(R) 168 story: When the ubiquity of an additive prevents studying its leaching from plastics. **2020**. *Science of the Total Environment*. 749: 141651.
- Hernandez-Mesa, M., Le Bizec, B., Monteau, F., Garcia-Campana, A.M., Dervilly-Pinel, G. Collision Cross Section (CCS) Database: An Additional Measure to Characterize Steroids. **2018**. *Analytical Chemistry*. 90: 4616-4625.
- Herron, J., Reese, R.C., Tallman, K.A., Narayanaswamy, R., Porter, N.A., Xu, L. Identification of environmental quaternary ammonium compounds as direct inhibitors of cholesterol biosynthesis. **2016**. *Toxicological Sciences*. 151: 261-270.
- Hines, K.M., Herron, J., Xu, L. Assessment of altered lipid homeostasis by HILIC-ion mobility-mass spectrometry-based lipidomics. **2017a**. *Journal of Lipid Research*. 58: 809-819.

- Hines, K.M., May, J.C., McLean, J.A., Xu, L. Evaluation of Collision Cross Section Calibrants for Structural Analysis of Lipids by Traveling Wave Ion Mobility-Mass Spectrometry. **2016**. *Analytical Chemistry*. 88: 7329-7336.
- Hines, K.M., Ross, D.H., Davidson, K.L., Bush, M.F., Xu, L. Large-Scale Structural Characterization of Drug and Drug-Like Compounds by High-Throughput Ion Mobility-Mass Spectrometry. **2017b**. *Analytical Chemistry*. 89: 9023-9030.
- Hinnenkamp, V., Klein, J., Meckelmann, S.W., Balsaa, P., Schmidt, T.C., Schmitz, O.J. Comparison of CCS Values Determined by Traveling Wave Ion Mobility Mass Spectrometry and Drift Tube Ion Mobility Mass Spectrometry. **2018**. *Analytical Chemistry*. 90: 12042-12050.
- Hinson, J.A. Reactive metabolites of phenacetin and acetaminophen: a review. **1983**. *Environmental Health Perspectives*. 49: 71-79.
- Hoang, M.T.T., Le, G.T., Kiwao, K., Duong, H.T., Nguyen, T.Q., Phan, T.Q., Bui, M.Q., Truong, D.A., Trinh, H.T. Occurrence and risk of human exposure to organophosphate flame retardants in indoor air and dust in Hanoi, Vietnam. **2023**. *Chemosphere*. 328: 138597.
- Hollender, J., Schymanski, E.L., Ahrens, L., Alygizakis, N., Béen, F., Bijlsma, L., Brunner, A.M., Celma, A., Fildier, A., Fu, Q. NORMAN guidance on suspect and non-target screening in environmental monitoring. **2023**. *Environmental Sciences Europe*. 35: 75.
- Hora, P.I., Pati, S.G., McNamara, P.J., Arnold, W.A. Increased use of quaternary ammonium compounds during the SARS-CoV-2 pandemic and beyond: consideration of environmental implications. *B. Environmental Science & Technology Letters*. 7: 622-631.
- Horai, H., Arita, M., Kanaya, S., Nihei, Y., Ikeda, T., Suwa, K., Ojima, Y., Tanaka, K., Tanaka, S., Aoshima, K. MassBank: a public repository for sharing mass spectral data for life sciences. **2010**. *Journal of Mass Spectrometry*. 45: 703-714.
- Hou, R., Xu, Y., Wang, Z. Review of OPFRs in animals and humans: Absorption, bioaccumulation, metabolism, and internal exposure research. **2016**. *Chemosphere*. 153, 78-90.
- Hrubec, T.C., Melin, V.E., Shea, C.S., Ferguson, E.E., Garofola, C., Repine, C.M., Chapman, T.W., Patel, H.R., Razvi, R.M., Sugrue, J.E. Ambient and dosed exposure to quaternary ammonium disinfectants causes neural tube defects in rodents. **2017**. *Birth Defects Research*. 109: 1166-1178.
- Hrubec, T.C., Seguin, R.P., Xu, L., Cortopassi, G.A., Datta, S., Hanlon, A.L., Lozano, A.J., McDonald, V.A., Healy, C.A., Anderson, T.C. Altered toxicological endpoints in humans from common quaternary ammonium compound disinfectant exposure. **2021**. *Toxicology Reports*. 8: 646-656.
- Hu, S., Zhao, M., Mao, Q., Fang, C., Chen, D., Yan, P. Rapid one-step cleanup method to minimize matrix effects for residue analysis of alkaline pesticides in tea using liquid chromatography–high resolution mass spectrometry. **2019**. *Food Chemistry*. 299: 125146.

- Huang, W., Shi, Y., Huang, J., Deng, C., Tang, S., Liu, X., Chen, D. Occurrence of substituted p-phenylenediamine antioxidants in dusts. **2021**. *Environmental Science & Technology Letters*. 8: 381-385.
- Huber, C., Krauss, M., Reinstadler, V., Denicolò, S., Mayer, G., Schulze, T., Brack, W., Oberacher, H. In silico deconjugation of glucuronide conjugates enhances tandem mass spectra library annotation of human samples. **2022a**. *Analytical and Bioanalytical Chemistry*. 414: 2629-2640.
- Huber, C., Nijssen, R., Mol, H., Antignac, J.P., Krauss, M., Brack, W., Wagner, K., Debrauwer, L., Vitale, C.M., Price, E.J. A large scale multi-laboratory suspect screening of pesticide metabolites in human biomonitoring: from tentative annotations to verified occurrences. **2022b**. *Environment International*. 168: 107452.
- Huntscha, S., Hofstetter, T.B., Schymanski, E.L., Spahr, S., Hollender, J. Biotransformation of benzotriazoles: insights from transformation product identification and compound-specific isotope analysis. **2014**. *Environmental Science & Technology*. 48: 4435-4443.

## I

- IARC, Agents classified by the IARC Monographs, Sup 7, 32, 88, 100F. Online: <https://monographs.iarc.who.int/list-of-classifications> (accessed 15 February 2022). 2012.
- IARC, Agents classified by the IARC Monographs, Volume 29, Sup 7, 100F, 120. Online: <https://monographs.iarc.who.int/list-of-classifications> (accessed 15 February 2022). 2018.
- Ibrahim, Y.M., Hamid, A.M., Deng, L., Garimella, S.V., Webb, I.K., Baker, E.S., Smith, R.D. New frontiers for mass spectrometry based upon structures for lossless ion manipulations. **2017**. *Analyst*. 142: 1010-1021.
- International Agency for Research on Cancer [IARC], Agents classified by the IARC Monographs, Volume 15, Sup 7, 71. Online: <https://monographs.iarc.who.int/list-of-classifications> (accessed 15 February 2022). 1999.

## J

- Jeilani, Y.A., Cardelino, B.H., Ibeanusi, V.M. Density functional theory and mass spectrometry of phthalate fragmentations mechanisms: modeling hyperconjugated carbocation and radical cation complexes with neutral molecules. **2011**. *Journal of the American Society for Mass Spectrometry*. 22.
- Ji, X., Li, N., Ma, M., Rao, K., Yang, R., Wang, Z. Tricresyl phosphate isomers exert estrogenic effects via G protein-coupled estrogen receptor-mediated pathways. **2020**. *Environmental Pollution*. 264: 114747.
- Johnson Jr, W., Bergfeld, W. F., Belsito, D. V., Hill, R. A., Klaassen, C. D., Liebler, D., Marks Jr, J. G., Shank, R. C., Slaga, T. J., Snyder, P. W. Safety assessment of 1, 2-glycols as used in cosmetics. **2012**. *International Journal of Toxicology*. 31: 147S-168S.

## K

- Kim, D.-H., Jeong, Y., Belova, L., Roggeman, M., Fernández, S.F., Poma, G., Remy, S., Verheyen, V.J., Schoeters, G., van Nuijs, A.L., 2022. Comprehensive investigation of persistent and mobile chemicals and per-and polyfluoroalkyl substances in urine of Flemish adolescents using a suspect screening approach. *Environmental Pollution* 312, 119972.
- Kim, S., Chen, J., Cheng, T., Gindulyte, A., He, J., He, S., Li, Q., Shoemaker, B. A., Thiessen, P. A., Yu, B. PubChem in 2021: new data content and improved web interfaces. **2021**. *Nucleic acids research*. 49: D1388-D1395.
- Kim, S., Chen, J., Cheng, T., Gindulyte, A., He, J., He, S., Li, Q., Shoemaker, B.A., Thiessen, P.A., Yu, B. PubChem 2023 update. **2023**. *Nucleic Acids Research*. 51: D1373-D1380.
- Kind, T., Tsugawa, H., Cajka, T., Ma, Y., Lai, Z., Mehta, S.S., Wohlgemuth, G., Barupal, D.K., Showalter, M.R., Arita, M. Identification of small molecules using accurate mass MS/MS search. **2018**. *Mass Spectrometry Reviews*. 37: 513-532.
- Kirkwood-Donelson, K.I., Dodds, J.N., Schnetzer, A., Hall, N., Baker, E.S. Uncovering per- and polyfluoroalkyl substances (PFAS) with nontargeted ion mobility spectrometry–mass spectrometry analyses. **2023**. *Science Advances*. 9: eadj7048.
- Klepeis, N.E., Nelson, W.C., Ott, W.R., Robinson, J.P., Tsang, A.M., Switzer, P., Behar, J.V., Hern, S.C., Engelmann, W.H. The National Human Activity Pattern Survey (NHAPS): a resource for assessing exposure to environmental pollutants. 2001. *Journal of Exposure Science & Environmental Epidemiology*. 11: 231-252.
- Koch, H.M., Calafat, A.M. Human body burdens of chemicals used in plastic manufacture. **2009**. *Philosophical Transactions of the Royal Society B: Biological Sciences*. 364: 2063-2078.
- Koelmel, J. P., Kroeger, N. M., Gill, E. L., Ulmer, C. Z., Bowden, J. A., Patterson, R. E., Yost, R. A., Garrett, T. J. Expanding Lipidome Coverage Using LC-MS/MS Data-Dependent Acquisition with Automated Exclusion List Generation. **2017**. *Journal of the American Society for Mass Spectrometry*. 28: 908-917.
- Köppe, T., Jewell, K.S., Ehlig, B., Wick, A., Koschorreck, J., Ternes, T.A. Identification and trend analysis of organic cationic contaminants via non-target screening in suspended particulate matter of the German rivers Rhine and Saar. **2023**. *Water Research*. 229: 119304.

## L

- Lacalle-Bergeron, L., Portoles, T., Lopez, F.J., Sancho, J.V., Ortega-Azorin, C., Asensio, E.M., Coltell, O., Corella, D. Ultra-Performance Liquid Chromatography-Ion Mobility Separation-Quadrupole Time-of-Flight MS (UHPLC-IMS-QTOF MS) Metabolomics for Short-Term Biomarker Discovery of Orange Intake: A Randomized, Controlled Crossover Study. **2020**. *Nutrients*. 12.
- LaKind, J. S., Goodman, M. Methodological evaluation of human research on asthmagenicity and occupational cleaning: a case study of quaternary ammonium compounds (“quats”). **2019**. *Allergy, Asthma & Clinical Immunology*. 15: 69.

- Landrigan, P., Fuller, R., Haines, A., Watts, N., McCarthy, G. Pollution prevention and climate change mitigation: measuring the health benefits of comprehensive interventions. **2018**. *The Lancet Planetary Health*. 2: e515-e516.
- Lanshoeft, C., Schütz, R., Lozac'h, F., Schlotterbeck, G., Walles, M. Potential of measured relative shifts in collision cross section values for biotransformation studies. **2024**. *Analytical and Bioanalytical Chemistry*. 416: 559-568.
- Larsen, S.T., Verder, H., Nielsen, G.D. Airway effects of inhaled quaternary ammonium compounds in mice. **2012**. *Basic & Clinical Pharmacology & Toxicology*. 110: 537-543.
- Lee, H.K., Kang, H., Lee, S., Kim, S., Choi, K., Moon, H.B. Human exposure to legacy and emerging flame retardants in indoor dust: A multiple-exposure assessment of PBDEs. **2020**. *Science of the Total Environment*. 719: 137386.
- Lennon, S., Chaker, J., Price, E.J., Hollender, J., Huber, C., Schulze, T., Ahrens, L., Béen, F., Creusot, N., Debrauwer, L. Harmonized quality assurance/quality control provisions to assess completeness and robustness of MS1 data preprocessing for LC-HRMS-based suspect screening and non-targeted analysis. **2024**. *Trends in Analytical Chemistry*. 174: 117674.
- Léon, A., Cariou, R., Hutinet, S.b., Hurel, J., Guitton, Y., Tixier, C.I., Munsch, C., Antignac, J.-P., Dervilly-Pinel, G., Le Bizec, B. HaloSeeker 1.0: a user-friendly software to highlight halogenated chemicals in nontargeted high-resolution mass spectrometry data sets. **2019**. *Analytical Chemistry*. 91: 3500-3507.
- Li, D., Sangion, A., Li, L. Evaluating consumer exposure to disinfecting chemicals against coronavirus disease 2019 (COVID-19) and associated health risks. **2020**. *Environment International*. 145: 106108.
- Li, X., Brownawell, B.J. Analysis of quaternary ammonium compounds in estuarine sediments by LC-TOF-MS: very high positive mass defects of alkylamine ions as powerful diagnostic tools for identification and structural elucidation. **2009**. *Analytical Chemistry*. 81: 7926-7935.
- Li, Z.-M., Kannan, K. Occurrence of 1, 3-diphenylguanidine, 1, 3-di-o-tolylguanidine, and 1, 2, 3-triphenylguanidine in indoor dust from 11 countries: implications for human exposure. **2023**. *Environmental Science & Technology*. 57: 6129-6138.
- Li, Z.-M., Kannan, K. Quaternary Ammonium Compounds in Paired Human Urine and Feces: Relative Significance of Biliary Elimination. **2024**. *Environmental Science & Technology Letters*. 11: 533-538.
- Li, Z.-M., Lakuleswaran, M., Kannan, K. LC-MS/MS methods for the determination of 30 quaternary ammonium compounds including benzalkonium and paraquat in human serum and urine. **2023**. *Journal of Chromatography B*. 1214: 123562.
- Li, Z., Mao, W., Yao, L., Zhao, N., Zhang, Y., Zhao, M., Jin, H. First report on occurrence of bisphenol A isomers in human serum and whole blood. **2022**. *Journal of Hazardous Materials*. 424: 127549.
- Lietz, C.B., Yu, Q., Li, L. Large-scale collision cross-section profiling on a traveling wave ion mobility mass spectrometer. 2014. *Journal of the American Society for Mass Spectrometry*. 25: 2009-2019.

- Liigand, J., Wang, T., Kellogg, J., Smedsgaard, J., Cech, N., Krueve, A. Quantification for non-targeted LC/MS screening without standard substances. **2020**. *Scientific Reports*. 10: 5808.
- Liu, R., Mabury, S.A. Organophosphite antioxidants in indoor dust represent an indirect source of organophosphate esters. **2019**. *Environmental Science & Technology*. 53: 1805-1811.
- Liu, R., Mabury, S.A. Novel high molecular weight synthetic phenolic antioxidants in indoor dust in Toronto, Canada. **2020**. *Environmental Science & Technology Letters*. 7: 14-19.
- López, A., Dualde, P., Yusà, V., Coscollà, C. Retrospective analysis of pesticide metabolites in urine using liquid chromatography coupled to high-resolution mass spectrometry. **2016**. *Talanta*. 160: 547-555.
- López-García, M., Romero-González, R., Frenich, A.G. Monitoring of organophosphate and pyrethroid metabolites in human urine samples by an automated method (TurboFlow™) coupled to ultra-high performance liquid chromatography-Orbitrap mass spectrometry. **2019**. *Journal of Pharmaceutical and Biomedical Analysis*. 173: 31-39.
- Luo, M.-D., Zhou, Z.-W., Zhu, Z.-J. The Application of Ion Mobility-Mass Spectrometry in Untargeted Metabolomics: from Separation to Identification. **2020**. *Journal of Analysis and Testing*. 4: 163-174.
- Lyche, J.L., Rosseland, C., Berge, G., Polder, A. Human health risk associated with brominated flame-retardants (BFRs). **2015**. *Environment international*. 74: 170-180.

## M

- Malm, L., Palm, E., Souihi, A., Plassmann, M., Liigand, J., Krueve, A. Guide to semi-quantitative non-targeted screening using LC/ESI/HRMS. **2021**. *Molecules*. 26: 3524.
- Manier, M.L., Cornett, D.S., Hachey, D.L., Caprioli, R.M. Identification of dimethyldioctadecylammonium ion (m/z 550.6) and related species (m/z 522.6, 494.6) as a source of contamination in mass spectrometry. **2008**. *Journal of the American Society for Mass Spectrometry*. 19: 666-670.
- Mao, J.F., Li, W., Ong, C.N., He, Y., Jong, M.-C., Gin, K.Y.-H. Assessment of human exposure to benzophenone-type UV filters: a review. **2022**. *Environment International*. 167: 107405.
- Mason, E.A., Schamp Jr, H.W. Mobility of gaseous ions in weak electric fields. **1958**. *Annals of Physics*. 4: 233-270.
- Matthews, J.B., Twomey, K., Zacharewski, T.R. In vitro and in vivo interactions of bisphenol A and its metabolite, bisphenol A glucuronide, with estrogen receptors  $\alpha$  and  $\beta$ . **2001**. *Chemical Research in Toxicology*. 14: 149-157.
- May, J.C., Goodwin, C.R., Lareau, N.M., Leaptrot, K.L., Morris, C.B., Kurulugama, R.T., Mordehai, A., Klein, C., Barry, W., Darland, E., Overney, G., Imatani, K., Stafford, G.C., Fjeldsted, J.C., McLean, J.A. Conformational ordering of biomolecules in the gas phase: nitrogen collision cross sections measured on a prototype high resolution

- drift tube ion mobility-mass spectrometer. **2014**. *Analytical Chemistry*. 86: 2107-2116.
- May, J.C., Knochenmuss, R., Fjeldsted, J.C., McLean, J.A. Resolution of Isomeric Mixtures in Ion Mobility Using a Combined Demultiplexing and Peak Deconvolution Technique. **2020**. *Analytical Chemistry*. 92: 9482-9492.
- May, J.C., McLean, J.A. Ion mobility-mass spectrometry: time-dispersive instrumentation. **2015**. *Analytical Chemistry*. 87:, 1422-1436.
- McGrath, T.J., Christia, C., Poma, G., Covaci, A. Seasonal variation of short-, medium-and long-chain chlorinated paraffin distribution in Belgian indoor dust. **2022**. *Environment International*. 170: 107616.
- Meeker, J. D., Stapleton, H. M. House dust concentrations of organophosphate flame retardants in relation to hormone levels and semen quality parameters. **2010**. *Environmental Health Perspectives*. 118: 318-23.
- Meijer, J., Lamoree, M., Hamers, T., Antignac, J.-P., Hutinet, S., Debrauwer, L., Covaci, A., Huber, C., Krauss, M., Walker, D.I. An annotation database for chemicals of emerging concern in exposome research. **2021**. *Environment International*. 152: 106511.
- Melin, V.E., Potineni, H., Hunt, P., Griswold, J., Siems, B., Werre, S.R., Hrubec, T.C. Exposure to common quaternary ammonium disinfectants decreases fertility in mice. **2014**. *Reproductive Toxicology*. 50: 163-170.
- Menger, F., Celma, A., Schymanski, E.L., Lai, F.Y., Bijlsma, L., Wiberg, K., Hernández, F., Sancho, J.V., Ahrens, L. Enhancing spectral quality in complex environmental matrices: Supporting suspect and non-target screening in zebra mussels with ion mobility. **2022**. *Environment International*. 170: 107585.
- Michelmann, K., Silveira, J.A., Ridgeway, M.E., Park, M.A. Fundamentals of trapped ion mobility spectrometry. **2014**. *Journal of the American Society for Mass Spectrometry*. 26: 14-24.
- Mollerup, C.B., Mardal, M., Dalsgaard, P.W., Linnet, K., Barron, L.P. Prediction of collision cross section and retention time for broad scope screening in gradient reversed-phase liquid chromatography-ion mobility-high resolution accurate mass spectrometry. **2018**. *Journal of Chromatography A*. 1542: 82-88.
- Mordehai, A., Kurulugama, R.T., Darland, E., Stafford, G., Fjeldsted, J.C. Single Field Direct Drift Time to CCS Calibration for a Linear Drift Tube Ion Mobility Mass Spectrometer. **2015**. ASMS, Agilent Technologies, 1-4.
- Mortelé, O., Vervliet, P., Gys, C., Degreef, M., Cuykx, M., Maudens, K., Covaci, A., van Nuijs, A.L., Lai, F.Y. In vitro Phase I and Phase II metabolism of the new designer benzodiazepine cloniprazepam using liquid chromatography coupled to quadrupole time-of-flight mass spectrometry. **2018**. *Journal of Pharmaceutical and Biomedical Analysis*. 153: 158-167.
- Müller, E., Huber, C.E., Brack, W., Krauss, M., Schulze, T. Symbolic aggregate approximation improves gap filling in high-resolution mass spectrometry data processing. **2020**. *Analytical Chemistry*. 92: 10425-10432.
- Mullin, L., Jobst, K., DiLorenzo, R.A., Plumb, R., Reiner, E.J., Yeung, L.W.Y., Jogsten, I.E. Liquid chromatography-ion mobility-high resolution mass spectrometry for analysis

of pollutants in indoor dust: Identification and predictive capabilities. **2020**. *Analytica Chimica Acta*. 1125: 29-40.

## N

- Nair, B. Final report on the safety assessment of Benzyl Alcohol, Benzoic Acid, and Sodium Benzoate. **2001**. *International Journal of Toxicology*. 20: 23-50.
- National Institute for Health and Care Excellence [NICE], Asthma: diagnosis, monitoring and chronic asthma management. [NICE guideline No. 80] **2017**. Online: <https://www.nice.org.uk/guidance/ng80> (accessed February 12 2022).
- National Institute for Health and Care Excellence [NICE], Chronic obstructive pulmonary disease in over 16s: diagnosis and management. [NICE guideline No. 115] 2018. Online: <https://www.nice.org.uk/guidance/ng115> (accessed February 12 2022).
- National Library of Medicine USA, Hazardous Substances Data Bank (HSDB). **2019**. Online: <https://toxnet.nlm.nih.gov/newtoxnet/hsdb.htm> (accessed February 10 2022).
- Net, S., Sempéré, R., Delmont, A., Paluselli, A., Ouddane, B. Occurrence, fate, behavior and ecotoxicological state of phthalates in different environmental matrices. **2015**. *Environmental Science & Technology*. 49: 4019-4035.
- Newswire, P., **2021**. <https://www.prnewswire.com/news-releases/mobilion-systems-launches-mobie-the-first-slim-based-high-resolution-ion-mobility-hrim-product-to-accelerate-biotherapeutic-drug-development-and-multiomic-biomarker-discovery-301312609.html> (Last accessed on 02/07/2024).
- Nguyen, M.-K., Lin, C., Nguyen, H.-L., Hung, N.T.Q., La, D.D., Nguyen, X.H., Chang, S.W., Chung, W.J., Nguyen, D.D. Occurrence, fate, and potential risk of pharmaceutical pollutants in agriculture: Challenges and environmentally friendly solutions. **2023**. *Science of the Total Environment*. 899: 165323.
- Nguyen, R., Seguin, R.P., Ross, D.H., Chen, P., Richardson, S., Liem, J., Lin, Y.S., Xu, L. Development and Application of a Multidimensional Database for the Detection of Quaternary Ammonium Compounds and Their Phase I Hepatic Metabolites in Humans. **2024**. *Environmental Science & Technology*. 58: 6236-6249.
- Nichols, C.M., Dodds, J.N., Rose, B.S., Picache, J.A., Morris, C.B., Codreanu, S.G., May, J.C., Sherrod, S.D., McLean, J.A. Untargeted Molecular Discovery in Primary Metabolism: Collision Cross Section as a Molecular Descriptor in Ion Mobility-Mass Spectrometry. **2018**. *Analytical Chemistry*. 90: 14484-14492.
- Niu, J., Zhao, X., Jin, Y., Yang, G., Li, Z., Wang, J., Zhao, R., Li, Z. Determination of aromatic amines in the urine of smokers using a porous organic framework (JUC-Z2)-coated solid-phase microextraction fiber. **2018**. *Journal of Chromatography A*. 1555: 37-44.
- Nowak, K., Ratajczak-Wrona, W., Górska, M., Jabłońska, E. Parabens and their effects on the endocrine system. **2018**. *Molecular and Cellular Endocrinology*. 474: 238-251.
- Nys, G., Nix, C., Cibraiville, G., Servais, A.C., Fillet, M. Enhancing protein discoverability by data independent acquisition assisted by ion mobility mass spectrometry. **2020**. *Talanta*. 213: 120812.

## O

- Oberacher, H., Sasse, M., Antignac, J.-P., Guitton, Y., Debrauwer, L., Jamin, E.L., Schulze, T., Krauss, M., Covaci, A., Caballero-Casero, N., Rousseau, K., Damont, A., Fenaille, F., Lamoree, M., Schymanski, E.L. A European proposal for quality control and quality assurance of tandem mass spectral libraries. **2020**. *Environmental Sciences Europe*. 32: 43.
- Ong, C.-N., Lee, B.-L. Determination of benzene and its metabolites: application in biological monitoring of environmental and occupational exposure to benzene. **1994**. *Journal of Chromatography B*. 660: 1-22.
- Oropeza, A.R., Friis, U.F., Johansen, J.D. Occupational contact urticaria caused by didecyl dimethyl ammonium chloride. **2011**. *Contact Dermatitis*. 64: 297-298.
- Östman, M., Lindberg, R.H., Fick, J., Björn, E., Tysklind, M. Screening of biocides, metals and antibiotics in Swedish sewage sludge and wastewater. **2017**. *Water Research*. 115: 318-328.
- Ouyang, X., Weiss, J.M., de Boer, J., Lamoree, M.H., Leonards, P.E. Non-target analysis of household dust and laundry dryer lint using comprehensive two-dimensional liquid chromatography coupled with time-of-flight mass spectrometry. **2017**. *Chemosphere*. 166: 431-437.

## P

- Panagopoulos Abrahamsson, D., Park, J.-S., Singh, R.R., Sirota, M., Woodruff, T.J. Applications of machine learning to in silico quantification of chemicals without analytical standards. **2020**. *Journal of Chemical Information and Modeling*. 60: 2718-2727.
- Parida, V.K., Saidulu, D., Majumder, A., Srivastava, A., Gupta, B., Gupta, A.K. Emerging contaminants in wastewater: A critical review on occurrence, existing legislations, risk assessment, and sustainable treatment alternatives. **2021**. *Journal of Environmental Chemical Engineering*. 9: 105966.
- Pati, S.G., Arnold, W.A. Comprehensive screening of quaternary ammonium surfactants and ionic liquids in wastewater effluents and lake sediments. **2020**. *Environmental Science: Processes & Impacts*. 22: 430-441.
- Peyneau, M., De Chaisemartin, L., Gigant, N., Chollet-Martin, S., Kerdine-Römer, S. Quaternary ammonium compounds in hypersensitivity reactions. **2022**. *Frontiers in Toxicology*. 4.
- Picache, J.A., Rose, B.S., Balinski, A., Leaptrot, K.L., Sherrod, S.D., May, J.C., McLean, J.A. Collision cross section compendium to annotate and predict multi-omic compound identities. **2019**. *Chemical Science*. 10: 983-993.
- Picardo, M., Núñez, O., Farré, M. A data independent acquisition all ion fragmentation mode tool for the suspect screening of natural toxins in surface water. **2021**. *MethodsX*. 8: 101286.
- Pieke, E.N., Granby, K., Trier, X., Smedsgaard, J. A framework to estimate concentrations of potentially unknown substances by semi-quantification in liquid chromatography

- electrospray ionization mass spectrometry. **2017**. *Analytica Chimica Acta*. 975: 30-41.
- Pintado-Herrera, M.G., Wang, C., Lu, J., Chang, Y.-P., Chen, W., Li, X., Lara-Martín, P.A. Distribution, mass inventories, and ecological risk assessment of legacy and emerging contaminants in sediments from the Pearl River Estuary in China. **2017**. *Journal of Hazardous Materials*. 323: 128-138.
- Plante, P.L., Francovic-Fontaine, E., May, J.C., McLean, J.A., Baker, E.S., Laviolette, F., Marchand, M., Corbeil, J., Predicting Ion Mobility Collision Cross-Sections Using a Deep Neural Network: DeepCCS. **2019**. *Analytical Chemistry*. 91: 5191-5199.
- Plassmann, M.M., Brack, W., Krauss, M. Extending analysis of environmental pollutants in human urine towards screening for suspected compounds. **2015**. *Journal of Chromatography A*. 1394: 18-25.
- Pluym, N., Petreanu, W., Weber, T., Scherer, G., Scherer, M., Kolossa-Gehring, M. Biomonitoring data on young adults from the Environmental Specimen Bank suggest a decrease in the exposure to the fragrance chemical 7-hydroxycitronellal in Germany from 2000 to 2018. **2020**. *International Journal of Hygiene and Environmental Health*. 227: 113508.
- Poma, G., Glynn, A., Malarvannan, G., Covaci, A., Darnerud, P. O. Dietary intake of phosphorus flame retardants (PFRs) using Swedish food market basket estimations. **2017**. *Food and Chemical Toxicology*. 100: 1-7.
- Poma, G., McGrath, T.J., Christia, C., Malarvannan, G., Covaci, A. Emerging halogenated flame retardants in the indoor environment. **2020**. *Comprehensive Analytical Chemistry*. 88: 107-140.
- Poma, G., Sales, C., Bruyland, B., Christia, C., Gosciny, S., Van Loco, J., Covaci, A. Occurrence of organophosphorus flame retardants and plasticizers (PFRs) in Belgian foodstuffs and estimation of the dietary exposure of the adult population. **2018**. *Environmental Science & Technology*. 52: 2331-2338.
- Pourchet, M., Debrauwer, L., Klanova, J., Price, E.J., Covaci, A., Caballero-Casero, N., Oberacher, H., Lamoree, M., Damont, A., Fenaille, F., Vlaanderen, J., Meijer, J., Krauss, M., Sarigiannis, D., Barouki, R., Le Bizec, B., Antignac, J.P. Suspect and non-targeted screening of chemicals of emerging concern for human biomonitoring, environmental health studies and support to risk assessment: From promises to challenges and harmonisation issues. **2020**. *Environment International*. 139: 105545.
- Pringle, S.D., Giles, K., Wildgoose, J.L., Williams, J.P., Slade, S.E., Thalassinos, K., Bateman, R.H., Bowers, M.T., Scrivens, J.H. An investigation of the mobility separation of some peptide and protein ions using a new hybrid quadrupole/travelling wave IMS/oa-ToF instrument. **2007**. *International Journal of Mass Spectrometry*. 261: 1-12.
- Prost, S.A., Crowell, K.L., Baker, E.S., Ibrahim, Y.M., Clowers, B.H., Monroe, M.E., Anderson, G.A., Smith, R.D., Payne, S.H. Detecting and removing data artifacts in Hadamard transform ion mobility-mass spectrometry measurements. **2014**. *Journal of the American Society for Mass Spectrometry*. 25: 2020-2027.

Purohit, A., Kopferschmitt-Kubler, M.-C., Moreau, C., Popin, E., Blaumeiser, M., Pauli, G. Quaternary ammonium compounds and occupational asthma. **2000**. *International Archives of Occupational and Environmental Health*. 73: 423-427.

## Q

Qadeer, A., Anis, M., Warner, G.R., Potts, C., Giovanoulis, G., Nasr, S., Archundia, D., Zhang, Q., Ajmal, Z., Tweedale, A.C. Global environmental and toxicological data of emerging plasticizers: current knowledge, regrettable substitution dilemma, green solution and future perspectives. **2024**. *Green Chemistry*. 26: 5635-5683.

Qu, J., Xia, W., Qian, X., Wu, Y., Li, J., Wen, S., Xu, S. Geographic distribution and time trend of human exposure of Di (2-ethylhexyl) phthalate among different age groups based on global biomonitoring data. **2022**. *Chemosphere*. 287: 132115.

## R

Raposo, F., Barceló, D. Challenges and strategies of matrix effects using chromatography-mass spectrometry: An overview from research versus regulatory viewpoints. **2021**. *Trends in Analytical Chemistry*. 134: 116068.

REACH, **2020**. Entry 51 of Annex XVII to REACH Regulation (EC) No 1907/2006.

Reardon, A.R., May, J.C., Leaprot, K.L., McLean, J.A. High-resolution ion mobility based on traveling wave structures for lossless ion manipulation resolves hidden lipid features. **2024**. *Analytical and Bioanalytical Chemistry*.

Regueiro, J., Negreira, N., Hannisdal, R., Berntssen, M.H.G. Targeted approach for qualitative screening of pesticides in salmon feed by liquid chromatography coupled to traveling-wave ion mobility/quadrupole time-of-flight mass spectrometry. **2017**. *Food Control*. 78: 116-125.

Reid, A. M., Brougham, C. A., Fogarty, A. M., Roche, J. J. An investigation into possible sources of phthalate contamination in the environmental analytical laboratory. **2007**. *International Journal of Environmental Analytical Chemistry*. 87: 125-133.

Renaud, J.B., Sabourin, L., Topp, E., Sumarah, M.W. Spectral counting approach to measure selectivity of high-resolution LC-MS methods for environmental analysis. **2017**. *Analytical Chemistry*. 89: 2747-2754.

Revercomb, H., Mason, E.A. Theory of plasma chromatography/gaseous electrophoresis. Review. **1975**. *Analytical Chemistry*. 47: 970-983.

Ridgeway, M.E., Lubeck, M., Jordens, J., Mann, M., Park, M.A. Trapped ion mobility spectrometry: A short review. **2018**. *International Journal of Mass Spectrometry*. 425: 22-35.

Righetti, L., Dreolin, N., Celma, A., McCullagh, M., Barknowitz, G., Sancho, J.V., Dall'Asta, C. Travelling Wave Ion Mobility-Derived Collision Cross Section for Mycotoxins: Investigating Interlaboratory and Interplatform Reproducibility. **2020**. *Journal of Agricultural and Food Chemistry*. 68: 10937-10943.

Ross, D.H., Cho, J.H., Xu, L. Breaking down structural diversity for comprehensive prediction of ion-neutral collision cross sections. **2020**. *Analytical Chemistry*. 92: 4548-4557.

- Rostkowski, P., Haglund, P., Aalizadeh, R., Alygizakis, N., Thomaidis, N., Arandes, J.B., Nizzetto, P.B., Booij, P., Budzinski, H., Brunswick, P. The strength in numbers: comprehensive characterization of house dust using complementary mass spectrometric techniques. **2019**. *Analytical and Bioanalytical Chemistry*. 411: 1957-1977.
- Ruan, T., Song, S., Wang, T., Liu, R., Lin, Y., Jiang, G. Identification and composition of emerging quaternary ammonium compounds in municipal sewage sludge in China. **2014**. *Environmental Science & Technology*. 48: 4289-4297.
- Ruotolo, B.T., Benesch, J.L., Sandercock, A.M., Hyung, S.-J., Robinson, C.V. Ion mobility–mass spectrometry analysis of large protein complexes. **2008**. *Nature Protocols*. 3: 1139-1152.
- Ruttkies, C., Schymanski, E.L., Wolf, S., Hollender, J., Neumann, S. MetFrag relaunched: incorporating strategies beyond in silico fragmentation. **2016**. *Journal of Cheminformatics*. 8: 1-16.

## S

- Sauve, S., Desrosiers, M. A review of what is an emerging contaminant. **2014**. *Chemistry Central Journal*. 8: 15.
- Schoeters, G., Govarts, E., Bruckers, L., Den Hond, E., Nelen, V., De Henauw, S., Sioen, I., Nawrot, T.S., Plusquin, M., Vriens, A. Three cycles of human biomonitoring in Flanders– Time trends observed in the Flemish Environment and Health Study. **2017**. *International Journal of Hygiene and Environmental Health*. 220: 36-45.
- Schrank, C.L., Minbiole, K.P., Wuest, W.M. Are quaternary ammonium compounds, the workhorse disinfectants, effective against severe acute respiratory syndrome-coronavirus-2? **2020**. *ACS Infectious Diseases*. 6: 1553-1557.
- Schymanski, E.L., Jeon, J., Gulde, R., Fenner, K., Ruff, M., Singer, H.P., Hollender, J. Identifying small molecules via high resolution mass spectrometry: communicating confidence. 2014. *Environmental Science & Technology*. 48: 2097-2098.
- Schymanski, E.L., Singer, H.P., Slobodnik, J., Ipolyi, I.M., Oswald, P., Krauss, M., Schulze, T., Haglund, P., Letzel, T., Grosse, S. Non-target screening with high-resolution mass spectrometry: critical review using a collaborative trial on water analysis. **2015**. *Analytical and Bioanalytical Chemistry*. 407: 6237-6255.
- Seguin, R.P., Herron, J.M., Lopez, V.A., Dempsey, J.L., Xu, L. Metabolism of benzalkonium chlorides by human hepatic cytochromes P450. **2019**. *Chemical Research in Toxicology*. 32: 2466-2478.
- Sharkey, M., Harrad, S., Abdallah, M.A.-E., Drage, D.S., Berresheim, H. Phasing-out of legacy brominated flame retardants: The UNEP Stockholm Convention and other legislative action worldwide. **2020**. *Environment International*. 144: 106041.
- Shi, Y., Liu, X., Xie, Q., Pan, X.-F., Mei, Z. Plastic additives and personal care products in south China house dust and exposure in child-mother pairs. **2021**. *Environmental Pollution*. 281: 116347.

- Silveira, J.A., Ridgeway, M.E., Laukien, F.H., Mann, M., Park, M.A. Parallel accumulation for 100% duty cycle trapped ion mobility-mass spectrometry. **2017**. *International Journal of Mass Spectrometry*. 413: 168-175.
- Silveira, J.A., Ridgeway, M.E., Park, M.A. High resolution trapped ion mobility spectrometry of peptides. **2014**. *Analytical Chemistry*. 86: 5624-5627.
- Slimani, K., Féret, A., Pirotais, Y., Maris, P., Abjean, J.-P., Hurtaud-Pessel, D. Liquid chromatography-tandem mass spectrometry multiresidue method for the analysis of quaternary ammonium compounds in cheese and milk products: Development and validation using the total error approach. **2017**. *Journal of Chromatography A*. 1517: 86-96.
- Smolders, R., Schramm, K.-W., Stenius, U., Grellier, J., Kahn, A., Trnovec, T., Sram, R., Schoeters, G. A review on the practical application of human biomonitoring in integrated environmental health impact assessment. **2009**. *Journal of Toxicology and Environmental Health. Part B*. 12: 107-123.
- Song, X.-C., Canellas, E., Dreolin, N., Goshawk, J., Nerin, C. A Collision Cross Section Database for Extractables and Leachables from Food Contact Materials. **2022**. *Journal of Agricultural and Food Chemistry*. 70: 4457-4466.
- Sreevidya, V.S., Lenz, K.A., Svoboda, K.R., Ma, H. Benzalkonium chloride, benzethonium chloride, and chloroxylenol-Three replacement antimicrobials are more toxic than triclosan and triclocarban in two model organisms. **2018**. *Environmental Pollution*. 235: 814-824.
- Stein, S. Mass spectral reference libraries: an ever-expanding resource for chemical identification. **2012**. *Analytical Chemistry*. 84: 7274-7282.
- Stoekelhuber, M., Krnac, D., Pluym, N., Scherer, M., Peschel, O., Leibold, E., Scherer, G. Human metabolism and excretion kinetics of the fragrance 7-hydroxycitronellal after a single oral or dermal dosage. **2018**. *International Journal of Hygiene and Environmental Health*. 221: 239-245.
- Stow, S.M., Causon, T.J., Zheng, X., Kurulugama, R.T., Mairinger, T., May, J.C., Rennie, E.E., Baker, E.S., Smith, R.D., McLean, J.A., Hann, S., Fjeldsted, J.C. An Interlaboratory Evaluation of Drift Tube Ion Mobility-Mass Spectrometry Collision Cross Section Measurements. **2017**. *Analytical Chemistry*. 89: 9048-9055.
- Struwe, W.B., Pagel, K., Benesch, J.L., Harvey, D.J., Campbell, M.P. GlycoMob: an ion mobility-mass spectrometry collision cross section database for glycomics. **2016**. *Glycoconjugate Journal*. 33: 399-404.
- Subedi, B., Sullivan, K.D., Dhungana, B. Phthalate and non-phthalate plasticizers in indoor dust from childcare facilities, salons, and homes across the USA. **2017**. *Environmental Pollution*. 230: 701-708.
- Sushko, I., Novotarskyi, S., Körner, R., Pandey, A.K., Rupp, M., Teetz, W., Brandmaier, S., Abdelaziz, A., Prokopenko, V.V., Tanchuk, V.Y. Online chemical modeling environment (OCHEM): web platform for data storage, model development and publishing of chemical information. **2011**. *Journal of Computer-Aided Molecular Design*. 25: 533-554.

Swan, S.H. Environmental phthalate exposure in relation to reproductive outcomes and other health endpoints in humans. **2008**. *Environmental Research*. 108: 177-184.

## T

Taha, M.H., Aalizadeh, R., Alygizakis, N., Antignac, J.-P., Arp, H.P.H., Bade, R., Baker, N., Belova, L., Bijlsma, L., Bolton, E.E. The NORMAN Suspect List Exchange (NORMAN-SLE): facilitating European and worldwide collaboration on suspect screening in high resolution mass spectrometry. **2022**. *Environmental Sciences Europe*. 34: 104.

Tang, B., Christia, C., Malarvannan, G., Liu, Y.E., Luo, X.J., Covaci, A., Mai, B.X., Poma, G. Legacy and emerging organophosphorus flame retardants and plasticizers in indoor microenvironments from Guangzhou, South China. **2020**. *Environment International*. 143: 105972.

Tang, C., Tan, J., Fan, R., Zhao, B., Tang, C., Ou, W., Jin, J., Peng, X. Quasi-targeted analysis of hydroxylation-related metabolites of polycyclic aromatic hydrocarbons in human urine by liquid chromatography–mass spectrometry. **2016**. *Journal of Chromatography A*. 1461: 59-69.

Tao, L., McLean, J.R., McLean, J.A., Russell, D.H. A collision cross-section database of singly-charged peptide ions. **2007**. *Journal of the American Society for Mass Spectrometry*. 18: 1232-1238.

Tejada-Casado, C., Hernandez-Mesa, M., Monteau, F., Lara, F.J., Olmo-Iruela, M.D., Garcia-Campana, A.M., Le Bizec, B., Dervilly-Pinel, G. Collision cross section (CCS) as a complementary parameter to characterize human and veterinary drugs. **2018**. *Analytica Chimica Acta*. 1043: 52-63.

Testa, B., Krämer, S.D. The biochemistry of drug metabolism—an introduction: part 1. principles and overview. **2006**. *Chemistry & Biodiversity*. 3: 1053-1101.

Testa, B., Kramer, S. The Biochemistry of Drug Metabolism. Volume 1: Principles, Redox Reactions, Hydrolyses and Volume 2: Conjugations, Consequences of Metabolism, Influencing Factors. **2005**. Wiley-VCH: New York, New York.

Thompson, J. Further experiments on positive rays. **1912**. *Philosophical Magazine*. 24: 209-253.

Tkalec, Ž., Codling, G., Tratnik, J.S., Mazej, D., Klánová, J., Horvat, M., Kosjek, T. Suspect and non-targeted screening-based human biomonitoring identified 74 biomarkers of exposure in urine of Slovenian children. **2022**. *Environmental Pollution*. 313: 120091.

Tran, C. D., Dodder, N. G., Quintana, P. J. E., Watanabe, K., Kim, J. H., Hovell, M. F., Chambers, C. D., Hoh, E. Organic contaminants in human breast milk identified by non-targeted analysis. **2020**. *Chemosphere*. 238: 124677.

## U

U.S. Food & Drug Administration, Reporting Harmful and Potentially Harmful Constituents in Tobacco Products and Tobacco Smoke Under Section 904(a)(3) of the Federal Food, Drug, and Cosmetic Act. Draft Guidance for Industry. **2012**. Online: <https://www.fda.gov/regulatory-information/search-fda-guidance->

[documents/reporting-harmful-and-potentially-harmful-constituents-tobacco-products-and-tobacco-smoke-under](#) (accessed 11 February 2022).

## V

- Van den Eede, N., Ballesteros-Gomez, A., Neels, H., Covaci, A. Does Biotransformation of Aryl Phosphate Flame Retardants in Blood Cast a New Perspective on Their Debated Biomarkers? **2016**. *Environmental Science & Technology*. 50: 12439-12445.
- Van den Eede, N., Dirtu, A.C., Ali, N., Neels, H., Covaci, A. Multi-residue method for the determination of brominated and organophosphate flame retardants in indoor dust. **2012**. *Talanta*. 89: 292-300.
- Van den Eede, N., Maho, W., Erratico, C., Neels, H., Covaci, A. First insights in the metabolism of phosphate flame retardants and plasticizers using human liver fractions. **2013**. *Toxicology Letters*. 223: 9-15.
- Van der Veen, I., de Boer, J. Phosphorus flame retardants: properties, production, environmental occurrence, toxicity and analysis. **2012**. *Chemosphere*. 88: 1119-1153.
- Vereshchagin, A.N., Frolov, N.A., Egorova, K.S., Seitkalieva, M.M., Ananikov, V.P. Quaternary ammonium compounds (QACs) and ionic liquids (ILs) as biocides: From simple antiseptics to tunable antimicrobials. **2021**. *International Journal of Molecular Sciences*. 22: 6793.
- Verheyen, V.J., Remy, S., Govarts, E., Colles, A., Rodriguez Martin, L., Koppen, G., Voorspoels, S., Bruckers, L., Bijmens, E.M., Vos, S. Urinary polycyclic aromatic hydrocarbon metabolites are associated with biomarkers of chronic endocrine stress, oxidative stress, and inflammation in adolescents: FLEHS-4 (2016–2020). **2021**. *Toxics*. 9: 245.
- Völkel, W., Colnot, T., Csanády, G.A., Filser, J.G., Dekant, W. Metabolism and kinetics of bisphenol A in humans at low doses following oral administration. **2002**. *Chemical Research in Toxicology*. 15: 1281-1287.

## W

- Wang, F., Xiang, L., Leung, K.S.-Y., Elsner, M., Zhang, Y., Guo, Y., Pan, B., Sun, H., An, T., Ying, G. Emerging contaminants: a One Health perspective. **2024**. *The Innovation*. 5: 100612.
- Wang, F., Liigand, J., Tian, S., Arndt, D., Greiner, R., Wishart, D.S. CFM-ID 4.0: more accurate ESI-MS/MS spectral prediction and compound identification. **2021**. *Analytical Chemistry*. 93: 11692-11700.
- Wang, H., Xi, H., Xu, L., Jin, M., Zhao, W., Liu, H. Ecotoxicological effects, environmental fate and risks of pharmaceutical and personal care products in the water environment: A review. **2021**. *Science of the Total Environment*. 788: 147819.
- Wang, L., Jia, Y., Hu, J. Nine alkyl organophosphate triesters newly identified in house dust. **2022**. *Environment International*. 165 107333.

- Wang, L., Jia, Y., Kang, Q., Song, W., Hu, J.,. Nontarget discovery of 11 aryl organophosphate triesters in house dust using high-resolution mass spectrometry. **2020a**. *Environmental Science & Technology*. 54: 11376-11385.
- Wang, Y., de B. Harrington, P., Chang, T., Wu, X., Chen, P. Analysis of cranberry proanthocyanidins using UPLC-ion mobility-high-resolution mass spectrometry. **2020b**. *Analytical Bioanalytical Chemistry*. 412: 3653-3662.
- Waters Corporation. **2013**. QUANTOF - High-resolution, accurate mass, quantitative time-of-flight MS technology: <https://www.waters.com/webassets/cms/library/docs/720004545en.pdf> (last accessed on 29/06/2024).
- Wegh, R.S., Berendsen, B.J., Driessen-Van Lankveld, W.D., Pikkemaat, M.G., Zuidema, T., Van Ginkel, L.A. Non-targeted workflow for identification of antimicrobial compounds in animal feed using bioassay-directed screening in combination with liquid chromatography-high resolution mass spectrometry. **2017**. *Food Additives & Contaminants: Part A*. 34: 1935-1947.
- Wieck, S., Olsson, O., Kümmerer, K. Not only biocidal products: Washing and cleaning agents and personal care products can act as further sources of biocidal active substances in wastewater. **2018**. *Environment International*. 115: 247-256.
- Wild, C.P. Complementing the genome with an “exposome”: the outstanding challenge of environmental exposure measurement in molecular epidemiology. **2005**. *Cancer Epidemiology Biomarkers & Prevention*. 14: 1847-1850.
- Wilkinson, J., Hooda, P.S., Barker, J., Barton, S., Swinden, J. Occurrence, fate and transformation of emerging contaminants in water: An overarching review of the field. **2017**. *Environmental Pollution*. 231: 954-970.
- Williams, A., Grulke, C., Edwards, J., McEachran, A., Mansouri, K., Baker, N., Patlewicz, G., Shah, I., Wambaugh, J., Judson, R. The CompTox chemistry dashboard: a community data resource for environmental chemistry. **2017**. *Journal of Cheminformatics*. 9: 61.
- Wilson, R., Jones-Otazo, H., Petrovic, S., Mitchell, I., Bonvalot, Y., Williams, D., Richardson, G.M. Revisiting dust and soil ingestion rates based on hand-to-mouth transfer. **2013**. *Human and Ecological Risk Assessment: An International Journal*. 19: 158-188.
- Wishart, D. S., Guo, A., Oler, E., Wang, F., Anjum, A., Peters, H., Dizon, R., Sayeeda, Z., Tian, S., Lee, B. L. HMDB 5.0: the Human Metabolome Database for 2022. **2022**. *Nucleic Acids Research*. 50: D622-D631.
- Wu, C., Siems, W.F., Asbury, G.R., Hill, H.H. Electrospray ionization high-resolution ion mobility spectrometry– mass spectrometry. **1998**. *Analytical Chemistry*. 70: 4929-4938.

## X

- Xian, Y., Dong, H., Wu, Y., Guo, X., Hou, X., Wang, B. QuEChERS-based purification method coupled to ultrahigh performance liquid chromatography–tandem mass spectrometry (UPLC–MS/MS) to determine six quaternary ammonium compounds (QACs) in dairy products. **2016**. *Food Chemistry*. 212: 96-103.

- Xu, F., Garcia-Bermejo, A., Malarvannan, G., Gomara, B., Neels, H., Covaci, A. Multi-contaminant analysis of organophosphate and halogenated flame retardants in food matrices using ultrasonication and vacuum assisted extraction, multi-stage cleanup and gas chromatography-mass spectrometry. **2015**. *Journal of Chromatography A*. 1401: 33-41.
- Xu, F., Giovanoulis, G., Van Waes, S., Padilla-Sanchez, J.A., Papadopoulou, E., Magnér, J., Haug, L.S., Neels, H., Covaci, A. Comprehensive study of human external exposure to organophosphate flame retardants via air, dust, and hand wipes: the importance of sampling and assessment strategy. **2016**. *Environmental Science & Technology*. 50: 7752-7760.
- Xu, S., Li, C. Phthalates in house and dormitory dust: occurrence, human exposure and risk assessment. **2021**. *Bulletin of Environmental Contamination and Toxicology*. 106: 393-398.

## Y

- Yan, Z., Caldwell, G.W., Jones, W.J., Masucci, J.A. Cone voltage induced in-source dissociation of glucuronides in electrospray and implications in biological analyses. **2003**. *Rapid Communications in Mass Spectrometry*. 17: 1433-1442.
- Younes, M., Aquilina, G., Castle, L., Engel, K.-H., Fowler, P., Fürst, P., Gürtler, R., Gundert-Remy, U., Husøy, T., Mennes, W., Moldeus, P., Oskarsson, A., Shah, R., Waalkens-Berendsen, I., Wölfle, D., Boon, P., Crebelli, R., Di Domenico, A., Filipič, M., Mortensen, A., Van Loveren, H., Woutersen, R., Gergelova, P., Giarola, A., Lodi, F., Fernandez, M. J. F. Re-evaluation of benzyl alcohol (E 1519) as food additive. **2019**. *EFSA Journal*. 17: 5876.
- Yu, J., Wang, B., Cai, J., Yan, Q., Wang, S., Zhao, G., Zhao, J., Pan, L., Liu, S. Selective extraction and determination of aromatic amine metabolites in urine samples by using magnetic covalent framework nanocomposites and HPLC-MS/MS. **2020**. *RSC Advances*. 10: 28437-28446.
- Yukioka, S., Tanaka, S., Suzuki, Y., Fujii, S., Echigo, S. A new method to search for per- and polyfluoroalkyl substances (PFASs) by linking fragmentation flags with their molecular ions by drift time using ion mobility spectrometry. **2020**. *Chemosphere*. 239: 124644.

## Z

- Zedda, M., Zwiener, C. Is nontarget screening of emerging contaminants by LC-HRMS successful? A plea for compound libraries and computer tools. **2012**. *Analytical and Bioanalytical Chemistry*. 403: 2493-2502.
- Zeleny, J. Mobilities of the ions in gases at low pressures. **1898**. *Philosophical Magazine*. 46: 120-154.
- Zhang, H., Luo, M., Wang, H., Ren, F., Yin, Y., Zhu, Z.-J. AllCCS2: Curation of ion mobility collision cross-section atlas for small molecules using comprehensive molecular representations. **2023**. *Analytical Chemistry*. 95: 13913-13921.

- Zhang, Y., Li, J., Su, G. Identifying citric acid esters, a class of phthalate substitute plasticizers, in indoor dust via an integrated target, suspect, and characteristic fragment-dependent screening strategy. **2021**. *Environmental Science & Technology*. 55: 13961-13970.
- Zheng, G., Filippelli, G.M., Salamova, A. Increased indoor exposure to commonly used disinfectants during the COVID-19 pandemic. **2020**. *Environmental Science & Technology Letters*. 7: 760-765.
- Zheng, G., Schreder, E., Sathyanarayana, S., Salamova, A. The first detection of quaternary ammonium compounds in breast milk: Implications for early-life exposure. **2022**. *Journal of Exposure Science & Environmental Epidemiology*. 32: 682-688.
- Zheng, G., Webster, T.F., Salamova, A. Quaternary Ammonium Compounds: Bioaccumulation Potentials in Humans and Levels in Blood before and during the Covid-19 Pandemic. **2021**. *Environmental Science & Technology*. 55: 14689-14698.
- Zheng, X., Aly, N.A., Zhou, Y., Dupuis, K.T., Bilbao, A., Paurus, V.L., Orton, D.J., Wilson, R., Payne, S.H., Smith, R.D., Baker, E.S. A structural examination and collision cross section database for over 500 metabolites and xenobiotics using drift tube ion mobility spectrometry. **2017**. *Chemical Science*. 8: 7724-7736.
- Zheng, X., Dupuis, K.T., Aly, N.A., Zhou, Y., Smith, F.B., Tang, K., Smith, R.D., Baker, E.S. Utilizing ion mobility spectrometry and mass spectrometry for the analysis of polycyclic aromatic hydrocarbons, polychlorinated biphenyls, polybrominated diphenyl ethers and their metabolites. **2018**. *Analytica Chimica Acta*. 1037: 265-273.
- Zhou, L., Hiltcher, M., Püttmann, W. Occurrence and human exposure assessment of organophosphate flame retardants in indoor dust from various microenvironments of the Rhine/Main region, Germany. **2017a**. *Indoor Air*. 27: 1113-1127.
- Zhou, Z., Shen, X., Tu, J., Zhu, Z.J. Large-Scale Prediction of Collision Cross-Section Values for Metabolites in Ion Mobility-Mass Spectrometry. **2016**. *Analytical Chemistry*. 88: 11084-11091.
- Zhou, Z., Tu, J., Xiong, X., Shen, X., Zhu, Z.J. LipidCCS: Prediction of Collision Cross-Section Values for Lipids with High Precision To Support Ion Mobility-Mass Spectrometry-Based Lipidomics. **2017b**. *Analytical Chemistry*. 89: 9559-9566.
- Zhou, Z., Xiong, X., Zhu, Z.-J. MetCCS predictor: a web server for predicting collision cross-section values of metabolites in ion mobility-mass spectrometry based metabolomics. **2017c**. *Bioinformatics*. 33: 2235-2237.
- Zhu, L., Hajeb, P., Fauser, P., Vorkamp, K. Endocrine disrupting chemicals in indoor dust: A review of temporal and spatial trends, and human exposure. **2023**. *Science of the Total Environment*. 874: 162374.
- Zweigle, J., Bugsel, B., Zwiener, C. FindPFAS: non-target screening for PFAS-comprehensive data mining for MS2 fragment mass differences. **2022**. *Analytical Chemistry*. 94: 10788-10796.





# Curriculum Vitae

## Personalia

---

Name Lidia Belova  
Date of birth 14<sup>th</sup> January 1995  
Place of birth Ludwigshafen am Rhein, Germany

## Education

---

07/2019 - 11/2024 **PhD candidate in Pharmaceutical Sciences**  
Toxicological Centre, University of Antwerp  
Promotors: Prof. Dr. Adrian Covaci, Prof. Dr. Alexander L. N. van Nuijs

10/2016 - 03/2019 **Master of Science in Food Chemistry**  
University of Münster, Germany  
Thesis title: Implementation of sphinganine-1-P/sphingosine-1-P analysis in a dried blood spot multi-mycotoxin method  
Promotors: Prof. Dr. Hans-Ulrich Humpf, Dr. Jessica Schmidt

10/2013 - 09-2016 **Bachelor of Science in Food Chemistry**  
University of Münster, Germany  
Thesis title: Interaction of storage containers and filter materials with mycotoxins during storage and sample preparation  
Promotors: Prof. Dr. Hans-Ulrich Humpf, Dr. Florian Hübner

## Academic Experience

---

11/2023 Visiting researcher at the Institute of Chemistry for Energy and the Environment, University of Córdoba, Spain  
Supervisors: Prof. Dr. Ana Ballesteros, Dr. Noelia Caballero-Casero  
Topic: Trapped ion-mobility spectrometry for the analysis of environmental contaminants

04/2019 - 07/2019	<p>Visiting research at the Centre of Excellence in Mycotoxicology and Public Health, Ghent University, Belgium</p> <p><u>Supervisors:</u> Prof. Dr. Sarah De Saeger, Dr. Arnau Vidal</p> <p><u>Topic:</u> Volumetric absorptive microsampling as an alternative tool for multi-mycotoxin analysis in blood</p>
10/2019 - 03/2019	<p>Student Associate (responsible for tutorials, supervision of laboratory internships)</p> <p>University of Münster, Germany; Department of Chemistry</p>

## Scientific Awards

---

05/2022	<p>Best poster award (1st place; 500 EUR price money). 17th International Symposium on Hyphenated Techniques in Chromatography and Separation Technology, 18/05-20/05/2022, Ghent, Belgium.</p> <p><u>Title:</u> Identification of novel halogenated naturally-occurring compounds in sea sponge by high-resolution mass spectrometry and combined screening approaches.</p>
10/2023	<p>Best poster award (1st place; 200 EUR book voucher (Springer)). International Conference on Non-Target Screening, 16/10-19/10/2023, Erding, Germany.</p> <p><u>Title:</u> Identification and semi-quantification of known and novel contaminants in indoor dust by ion-mobility high-resolution mass spectrometry and estimation of risks for human exposure.</p>

## List of publications

---

Total number of citations: 282 (h-index: 8)

Total number of publications: 22 (8 as first author)

### List of manuscripts published in peer-reviewed journals (\* joined first author)

Malm, L., Liigand, J., Aalizadeh, R., Alygizakis, N., Ng, K., Frøkjær, E., Nanusha, M., Hansen, M., Plassmann, M., Bieber, S., Letzel, T., Balest, L., Abis, P. P., Mazzetti, M.,

Kasprzyk-Hordern, B., Ceolotto, N., Kumari, S., Hann, S., Kochmann, S., Mairinger, T., Soulier, C., Mascolo, G., Murgolo, S., Garcia-Vara, M., López de Alda, M., Hollender, J., Arturi, K., Coppola, G., Peruzzo, M., Joerss, H., Ieke, E., Ferrero, P., Gil-Solsona, R., Licul-Kucera, V., Roscioli, C., Valsecchi, S., Luckute, A., Christensen, J., Tisler, S., Vughs, D., Meekel, N., Talavera Andújar, B., Aurich, D., Schymanski, E. L., Frigerio, G., Macherius, A., Kunkel, U., Bader, T., Rostowski, P., Gundersen, H., Valdecanas, B., Davis, W., Schulze, B., Kaserzon, S., Pijnappels, M., Esperanza, M., Fildier, A., Vulliet, E., Wiest, L., Covaci, A., Macan Schönleben, A., **Belova, L.**, Celma-Tirado, A., Bijlsma, L., Caupos, E., Mebold, E., Le Roux, J., Troia, E., de Rijke, E., Helmus, R., Leroy, G., Haelewyck, N., Chrastina, D., Verwoert, M., Thomaidis, N., Krueve, A. Evaluation of Quantitative Approaches in Non-Target LC/ESI/HRMS Analysis. *Analytical Chemistry*. **2024**. 96(41): 16215-16226.

**Belova, L.**, Musatadi, M., Gys, C., Roggeman, M., den Ouden, F., Olivares, M., van Nuijs, A. L. N., Poma, G., Covaci, A. In vitro metabolism of quaternary ammonium compounds and confirmation in human urine by liquid chromatography ion-mobility high-resolution mass spectrometry. In press in *Environmental Science & Technology*. **2024**.

**Belova, L.**, Caballero-Casero, N., Ballesteros, A., Poma, G., van Nuijs, A. L. N., Covaci, A. Trapped and drift-tube ion-mobility spectrometry for the analysis of environmental contaminants: Comparability of collision cross section values and resolving power. *Rapid Communications in Mass Spectrometry*. **2024**. 38(21): e9901.

Celma, A., Alygizakis, N., **Belova, L.**, Bijlsma, L., Fabregat-Safont, D., Menger, F., Gil-Solsona, R. Ion Mobility Separation coupled to High-Resolution Mass Spectrometry in Environmental Analysis - Current state and Future potential. *Trends in Environmental Analytical Chemistry*. **2024**. 43: e00239.

Van Wichelen, N., Estévez-Danta, A., **Belova, L.**, den Ouden, F., Verougstraete, N., Roggeman, M., Boogaerts, T., Quireyns, M., Robeyns, R., De Brabanter, N., Benito Quintana, J., Rodil, R., van Nuijs, A. L. N., Covaci, A., Gys, C. In vitro biotransformation of 3-methylmethcathinone (3-MMC) through incubation with human liver microsomes and cytosol and application to in vivo samples. *Journal of Pharmaceutical and Biomedical Analysis*. **2024**. 248: 116335.

Tkalec, Ž., Antignac, J.-P., Bandow, N., Béen, F. M., **Belova, L.**, Bessems, J., Le Bizec, B., Brack, W., Cano-Sancho, G., Chaker, J., Covaci, A., Creusot, N., David, A., Debrauwer, L., Dervilly, G., Duca, R. D., Fessard, V., Grimalt, J. O., Guérin, T., Habchi, B., Hecht, H., Hollender, J., Jamin, E. L., Klánová, J., Kosjek, T., Krauss, M., Lamoree, M., Lavison-Bompard, G., Meijer, J., Moeller, R., Mol, H., Mompelat, S., Van Nieuwenhuysse, A., Oberacher, H., Parinet, J., Van Poucke, C., Roškar, R., Togola, A., Trontelj, J., Price E. J. Innovative analytical methodologies for characterizing chemical exposure with a view to next-generation risk assessment. *Environment International*. **2024**. 186: 108585.

Macan Schönleben, A., Yin, S., Strak, E., Johnson, A., **Belova, L.**, Ait Bamai, Y., van Nuijs, A. L. N., Poma, G., Covaci, A. Stable isotope ratios and current-use pesticide levels in edible insects: Implications on chemical food safety. *Food Research International*. **2024**. 179: 114020.

**Belova, L.**, Roggeman, M., den Ouden, F., Cleys, P., Ait Bamai, Y., Yin, S., Zhao, L., Bombeke, J., Peters, J., Berghmans, P., Gys, C., van Nuijs, A. L. N., Poma, G., Covaci, A. Identification, semi-quantification and risk assessment of contaminants of emerging concern in Flemish indoor dust through high-resolution mass spectrometry. *Environmental Pollution*. **2024**. 345: 123475.

den Ouden, F., Estévez-Danta, A., **Belova, L.**, Gys, C., Klimowska, A., Roggeman, M., Van Wichelen, N., Benito Quintana, J., Rodil, R., Poma, G., Covaci, A. Investigation of in vitro biotransformation of tris (1-chloro-2-propyl) phosphate and confirmation in human urine. *Current Research in Toxicology*. **2024**. 6: 100164.

Lievens, S., Yin, S., **Belova, L.**, Fujii, Y., Bombeke, J., De Smet, J., Van Der Borght, M., Covaci, A., Poma, G. Bioaccumulation and biotransformation of plasticisers diisononyl phthalate and di(2-ethylhexyl) terephthalate in black soldier fly larvae reared on (micro)plastic-contaminated food waste. *Journal of Environmental Exposure Assessment*. **2024**. 3(1): 1-15.

Altamirano, J. C., Yin, S., **Belova, L.**, Poma, G., Covaci, A. Exploring the hidden chemical landscape: Non-target and suspect screening analysis for investigating solid waste-associated environments. *Environmental Research*. **2024**. 245: 118006.

Dürig, W., Lindblad, S., Golovko, O., Gkotsis, G., Aalizadeh, R., Nika, M.-C., Thomaidis, N., Alygizakis, N. A., Plassmann, M., Haglund, P., Fu, Q., Hollender, J., Chaker, J., David, A., Kunkel, U., Macherius, A., **Belova, L.**, Poma, G., Preud'Homme, H., Munsch, C., Aminot, Y., Jaeger, C., Lisec, J., Hansen, M., Vorkamp, K., Zhu, L., Cappelli, F., Roscioli, C., Valsecchi, S., Bagnati, R., González, B., Prieto, A., Zuloaga, O., Gil-Solsona, R., Gago-Ferrero, P., Rodriguez-Mozaz, S., Budzinski, H., Devier, M.-H., Dierkes, G., Boulard, L., Jacobs, G., Voorspoels, S., Rüdell, H., Ahrens, L. What is in the fish? Collaborative trial in suspect and non-target screening of organic micropollutants using LC-and GC-HRMS. *Environment International*. **2023**. 181: 108288.

Kim, D.-H., Ait Bamai, Y., **Belova, L.**, Bessems, J., Poma, G., Covaci, A. Human exposure to persistent and mobile chemicals: A review of sources, internal levels and health implications. *Science of The Total Environment*. **2023**. 893: 164764.

**Belova, L.**, Poma, G., Roggeman, M., Jeong, Y., Kim, D.-H., Berghmans, P., Peters, J., Salamova, A., van Nuijs, A. L. N., Covaci, A. Identification and characterization of quaternary ammonium compounds in Flemish indoor dust by ion-mobility high-resolution mass spectrometry. *Environment International*. **2023**. 177: 108021.

Taha, H. M., Aalizadeh, R., Alygizakis, N., Antignac, J.-P., Arp, H. P. H., Bade, R., Baker, N., **Belova, L.**, Bijlsma, L., Bolton, E. E., Brack, W., Celma, A., Chen, W.-L., Cheng, T., Chirsir, P., Čirka, L., D'agostino, L. A., Djoumbou Feunang, Y., Dulio, V., Fischer, S., Gago-Ferrero, P., Galani, A., Geueke, B., Głowacka, N., Glüge, J., Groh, K., Grosse, S., Haglund, P., Hakkinen, P. J., Hale, S. E., Hernandez, F., Janssen, E. M.-L., Jonkers, T., Kiefer, K., Kirchner, M., Koschorreck, J., Krauss, M., Krier, J., Lamoree, M., Letzel, M., Letzel, T., Li, Q., Little, J., Liu, Y., Lunderberg, D. M., Martin, J. W., McEachran, A. D., McLean, J. A., Meier, C., Meijer, J., Menger, F., Merino, C., Muncke, J., Muschket, M., Neumann, M., Neveu, V., Ng, K., Oberacher, H., O'Brien, J., Oswald, P., Oswaldova, M., Picache, J. A., Postigo, C., Ramirez, N., Reemtsma, T., Renaud, J., Rostkowski, P., Rüdell, H., Salek, R. M., Samanipour, S., Scheringer, M., Schliebner, I., Schulz, W., Schulze, T., Sengl, M., Shoemaker, B. A., Sims, K., Singer, H., Singh, R. R., Sumarah, M., Thiessen, P. A., Thomas, K. V., Torres, S., Trier, X., Van Wezel, A. P., Vermeulen, R., Vlaanderen, J. J., von Der Ohe, P. C., Wang, Z., Williams, A. G., Willighagen, E. L., Wishart, D. S., Zhang, D., Thomaidis, N. S., Hollender, J., Slobodnik, J., Schymanski, E. L. The NORMAN Suspect List Exchange (NORMAN-SLE): facilitating European and worldwide collaboration on suspect screening in high resolution mass spectrometry. *Environmental Sciences Europe*. **2022**. 1(34): 1-26.

Kim, D.-H., Jeong, Y., **Belova, L.**, Roggeman, M., Fernández, S. F., Poma, G., Remy, S., Verheyen, V. J., Schoeters, G., van Nuijs, A. L. N., Covaci, A. Comprehensive investigation of persistent and mobile chemicals and per-and polyfluoroalkyl substances in urine of Flemish adolescents using a suspect screening approach. *Environmental Pollution*. **2022**. 312: 119972.

Roggeman, M.\* **Belova, L.\***, Fernández, S. F., Kim, D.-H., Jeong, Y., Poma, G., Remy, S., Verheyen, V. J., Schoeters, G., van Nuijs, A. L. N., Covaci, A. Comprehensive suspect screening for the identification of contaminants of emerging concern in urine of Flemish adolescents by liquid chromatography high-resolution mass spectrometry. *Environmental Research*. **2022**. 214: 114105.

**Belova, L.**, Celma, A., Van Haesendonck, G., Lemièrre, F., Sancho, J. V., Covaci, A., van Nuijs, A. L. N., Bijlsma, L. Revealing the differences in collision cross section values of small organic molecules acquired by different instrumental designs and prediction models. *Analytica Chimica Acta*. **2022**. 1229: 340361.

**Belova, L.**, Fujii, Y., Cleys, P., Śmiełowska, M., Haraguchi, K., Covaci, A. Identification of novel halogenated naturally occurring compounds in marine biota by high-resolution mass spectrometry and combined screening approaches. *Environmental Pollution*. **2021**. 289: 117933.

Vidal, A., **Belova, L.**, Stove, C., De Boevre, M., De Saeger, S. Volumetric absorptive microsampling as an alternative tool for biomonitoring of multi-mycotoxin exposure in resource-limited areas. *Toxins*. **2021**. 13(5): 345.

**Belova, L.**, Caballero-Casero, N., van Nuijs, A. L. N., Covaci, A. Ion mobility-high-resolution mass spectrometry (IM-HRMS) for the analysis of contaminants of emerging concern (CECs): Database compilation and application to urine samples. *Analytical Chemistry*. **2021**. 93(16): 6428-6436.

Caballero-Casero, N., **Belova, L.**, Vervliet, P., Antignac, J.-P., Castano, A., Debrauwer, L., Esteban López, M., Huber, C., Klanova, J., Krauss, M., Lommen, A., Mol, H. G. J., Oberacher, H., Pardo, O., Price, E. J., Reinstadler, V., Vitale, C. M., Van Nuijs, A. L. N., Covaci, A. Towards harmonised criteria in quality assurance and quality control of suspect and non-target LC-HRMS analytical workflows for screening of emerging contaminants in human biomonitoring. *Trends in Analytical Chemistry*. **2021**. 136: 116201.

## **Participation to scientific conferences and seminars**

---

### **Oral presentations (n = 5)**

Ion Mobility-High Resolution Mass Spectrometry for Screening of Contaminants of Emerging Concern (CECs) - Database Compilation and Application to Plastics Samples. International Conference on Non-Target Screening, 4<sup>th</sup> to 7<sup>th</sup> October 2021, Erding, Germany. **Belova, L.**, Caballero-Casero, N., van Nuijs A. L. N., Covaci, A. (presenter)

Identification of novel halogenated naturally occurring compounds in sea sponge by high-resolution mass spectrometry and combined screening approaches. 41<sup>st</sup> International Symposium on Halogenated Persistent Organic Pollutants, 8<sup>th</sup> to 11<sup>th</sup> November 2021, Tianjin, China (attended online). **Belova, L.**, Fujii, Y., Cleys, P., Haraguchi, K., Covaci, A. (presenter)

Semi-quantitative identification of known and novel contaminants in indoor dust by ion-mobility high-resolution mass spectrometry and estimation of risks for human exposure. Dioxin2023 Symposium, 10<sup>th</sup> to 14<sup>th</sup> September 2023, Maastricht, Netherlands. **Belova, L.**, Roggeman, M., Poma, G., Ait Bamai, Y., Gys, C., den Ouden, F., Berghmans, P., Peters, J., van Nuijs, A. L. N., Covaci, A. (presenter)

Implementation of ion-mobility spectrometry derived CCS-*m/z* trendlines in the identification of quaternary ammonium compounds (QACs). International Conference on Non-Target Screening, 16<sup>th</sup> to 19<sup>th</sup> October 2023, Erding, Germany. **Belova, L.**, Poma, G., Roggeman, M., Jeong, Y., Kim, D.-H., Salamova, A., van Nuijs, A. L. N., Covaci, A. (presenter)

Ion-mobility high-resolution mass spectrometry for the annotation of novel emerging contaminants and their metabolites in indoor dust and *in vitro* biotransformation samples. 18<sup>th</sup> International Symposium on Hyphenated Techniques in Chromatography and Separation Technology, 28<sup>th</sup> to 31<sup>st</sup> May 2024, Leuven, Belgium. **Belova, L.**,

Roggeman, M., Poma, G., Ait Bamai, Y, Gys, C., Cleys, P., den Ouden, F., Berghmans, P., Peters, J., van Nuijs, A. L. N., Covaci, A. (presenter)

### Poster presentations (n = 13)

Inter-comparison of CCS databases built using different ion-mobility MS set-ups and prediction models. International Conference on Non-Target Screening, 4<sup>th</sup> to 7<sup>th</sup> October 2021, Erding, Germany. **Belova, L.**, Celma, A., Sterckx, J., Sancho, J. V., Lemière, F., Bijlsma, L., van Nuijs A. L. N., Covaci, A. (presenter)

Biotransformation of tris (1-chloro-2-propyl) phosphate (TCIPP) and tris (p-tert-butylphenyl) phosphate (TTBPP) in human liver microsomes. 10<sup>th</sup> International Symposium on Flame Retardants BFR, 3<sup>rd</sup> to 6<sup>th</sup> April 2022, Athens, Greece. den Ouden, F., Estevez Danta, A., **Belova, L.**, Gys, C., Roggeman, M., Van Wichelen, N., Poma, G., Covaci, A. (co-author)

Development of a comprehensive suspect screening approach for the identification of contaminants of emerging concern in urine of Flemish adolescents through LC-QTOF-MS. 17<sup>th</sup> International Symposium on Hyphenated Techniques in Chromatography and Separation Technology, 18<sup>th</sup> to 20<sup>th</sup> May 2022, Ghent, Belgium. **Belova, L.**, Roggeman, M., Jeong, Y., Kim, D., Fernández, S. F., van Nuijs A. L. N., Covaci A. (co-author)

Ion Mobility Spectrometry as an Additional Separation Dimension for the Screening of Contaminants of Emerging Concern (CECs) - Database Compilation and Application to Plastics Samples. 17<sup>th</sup> International Symposium on Hyphenated Techniques in Chromatography and Separation Technology, 18<sup>th</sup> to 20<sup>th</sup> May 2022, Ghent, Belgium. **Belova, L.**, Caballero-Casero, N., Celma, A., Sterckx, J., Sancho, J. V., Lemière, F., Bijlsma, L., van Nuijs A. L. N., Covaci, A. (presenter)

Implementation of CCS-m/z trendlines in the identification process of quaternary ammonium compounds (QACs) in indoor dust samples through drift tube ion-mobility quadrupole time-of-flight mass spectrometry. 24<sup>th</sup> International Mass Spectrometry Conference, 27<sup>th</sup> August to 2<sup>nd</sup> September 2022, Maastricht, Netherlands. **Belova, L.**, Poma, G., van Nuijs A. L. N., Covaci, A. (presenter)

Ion Mobility Separation Coupled to High Resolution Mass Spectrometry for the Analysis of Organic Micropollutants in Aquatic Samples. SETAC Europe 33<sup>rd</sup> Annual Meeting, 30<sup>th</sup> April to 4<sup>th</sup> May 2022, Dublin, Ireland. Celma, A., Ahrens, L., **Belova, L.**, Covaci, A., Hernández, F., Yin Lai, F., Menger, F., Sancho, J. V., Schymanski, E. L., van Nuijs, A. L. N., Wiberg, K., Bijlsma, L. (co-author)

Pesticide Occurrence in Edible Insects from Asia, Europe and Africa Using Liquid Chromatography Coupled to High-Resolution or Tandem Mass Spectrometry. 18<sup>th</sup> International Conference on Chemistry and the Environment, 11<sup>th</sup> to 15<sup>th</sup> June 2023,

Venice, Italy. Schönleben, A. M., Yin, S., **Belova, L.**, Ait Bamai, Y., van Nuijs, A. L. N., Poma, G., Covaci, A. (co-author)

A Review of the Occurrence of Persistent and Mobile Chemicals in Environmental Samples Relevant for Human Exposure. 18<sup>th</sup> International Conference on Chemistry and the Environment, 11<sup>th</sup> to 15<sup>th</sup> June 2023, Venice, Italy. Kim, D.-H., Ait Bamai, Y., **Belova, L.**, Bessems, J., Poma, G., Covaci, A. (co-author)

Comparison of collision cross section (CCS)-*m/z* trendlines of perfluoroalkyl carboxylic acid dimers between Trapped, Traveling Wave and Drift Tube ion mobility spectrometry strategies to suggest their structure. 32<sup>nd</sup> International Conference on Ion Mobility Spectrometry, 19<sup>th</sup> to 25<sup>th</sup> August 2023, Maastricht, Netherlands. Schneiders, A., Far, J., De Pauw, E., **Belova, L.**, Covaci, A., Eppe, G. (co-author)

In vitro biotransformation of 3-methylmethcathinone (3-MMC) in human liver microsomes and correlation with the in vivo situation. The International Association of Forensic Toxicologists Annual Meeting, 27<sup>th</sup> to 31<sup>st</sup> August 2023, Rome, Italy. Van Wichelen, N., Estévez-Danta, A., den Ouden, F., Verougstraete, N., **Belova, L.**, Roggeman, M., Boogaerts, T., Quireyns, M., Benito Quintana, J., Rodil, R., van Nuijs, A. L. N., Covaci, A., Gys, C. (co-author)

A review of the human exposure to persistent and mobile chemicals and their potential health risk assessments. Dioxin2023 Symposium, 10<sup>th</sup> to 14<sup>th</sup> September 2023, Maastricht, Netherlands. Kim, D.-H., Ait Bamai, Y., **Belova, L.**, Bessems, J., Poma, G., Covaci, A. (co-author)

Identification and characterisation of quaternary ammonium compounds in Flemish indoor dust by ion-mobility high-resolution mass spectrometry. Dioxin2023 Symposium, 10<sup>th</sup> to 14<sup>th</sup> September 2023, Maastricht, Netherlands. **Belova, L.**, Poma, G., Roggeman, M., Jeong, Y., Kim, D.-H., Berghmans, P., Peters, J., van Nuijs, A. L. N., Covaci, A. (presenter)

Identification and semi-quantification of known and novel contaminants in indoor dust by ion-mobility high-resolution mass spectrometry and estimation of risks for human exposure. International Conference on Non-Target Screening, 16<sup>th</sup> to 19<sup>th</sup> October 2023, Erding, Germany. **Belova, L.**, Roggeman, M., Poma, G., Ait Bamai, Y., Gys, C., Cleys, P., den Ouden, F., Berghmans, P., Peters, J., van Nuijs, A. L. N., Covaci, A. (co-author)

## **Supervised dissertations**

---

Identification of phenolic natural halogenated compounds in seaweed and marine organisms using LC/ESI-HRMS. Cleys, P. Master thesis Pharmaceutical Sciences (January 2021)

Identification of plastic-related chemicals in food contact materials using LC-QTOF-MS: Targeted and suspect screening. Danilina, O. Master thesis Pharmaceutical Sciences (June 2022)

## **Scientific contributions**

---

### **Scientific reports**

Verheyen, V., Govarts, E., Loots, I., Nelen, V., Den Hond, E., Baeyens, W., Belova, L., et al., Final report of the 'Environment and Health Project 2021' funded by the Flemish Environmental Planning Agency in the scope of the 4th Flemish Biomonitoring Cycle.

Belova, L., Roggeman, M., Jeong, Y., Kim, D.-H., McGrath, T., Cseresznye, A., Cleys, P., den Ouden, F., Bombeke, J., Yin, S., Zhao, L., Ait Bamai, Y., Gys, C., Poma, G., Covaci, A., Peters, J., Berghmans, P., Collens, A., Brabers, R., Poelmans, D., Research for the prevention of unhealthy substances in the indoor environment by non-targeted screening of dust samples. Final report of a project funded by the Flemish Environmental Planning Agency focusing on the screening of indoor dust samples aiming to identify contaminants potentially harmful for human health.

### **Invited seminars**

Belova, L., et al. Drift-tube ion-mobility for screening and identification of small molecules: Applications for exposomics and metabolomics. Agilent International User Meeting 2023. Vienna, Austria, 25<sup>th</sup> to 26<sup>th</sup> September 2023.

### **Reviewing activities**

Active reviewer for *Analytica Chimica Acta*, *Environment International*, *Environmental Pollution*, *Environmental Science & Technology*, *Journal of Proteome Research*, *Journal of the American Society for Mass Spectrometry*, *Science of the Total Environment*.



## Acknowledgments

My first heartfelt thank you is for Prof. Adrian Covaci who gave me the possibility to start on a journey which ultimately led to this thesis. From a very early stage you trusted in my capabilities (sometimes maybe even more than I did myself) knowing very well when to push me towards new goals and when to give me freedom in my research. For both aspects I am tremendously grateful. Thank you for providing not only the infrastructural framework but constant moral support through your sincere interest and involvement in my work which were, literally, available at all times. I have learned a lot from your passion for and understanding of science and the 'scientific world' (with its pitfalls and challenges which are sometimes unavoidable). Thank you for seeing the potential, the bigger picture when I first visited the lab, when there was no project and (at least for me) no clear idea - look where it has broad us.

I thank Prof. Alexander van Nuijs for your support, encouragement and constant interest in scientific and non-scientific updates. Your ability to efficiently and openly narrow down challenges and soft spots in my research to very particular questions, helped me to improve many aspects of this thesis and research.

I want to express my gratitude towards my internal jury members, Prof. Nina Hermans and Prof. Karolien De Wael for their close evaluation of my thesis and valuable feedback during the internal defense. A heartfelt thank you to my external jury members Prof. Gauthier Eppe and Prof. Tim Causon. Your powerful research in the field of ion-mobility and environmental screening has been an example and inspiration to me throughout my whole thesis.

A heartfelt thank you to Noelia Caballero-Casero. I had the privilege to work with you in the early stages of my PhD and learned so much from your scientific expertise and passion. I thank you and Ana Ballesteros for welcoming to Cordoba, guiding me and giving me the opportunity to explore your TIMS instrument.

I thank Prof. Lubertus Bijlsma, Prof. Juan Vincente Sancho and Dr. Alberto Celma for sharing their expertise with me and giving me the opportunity for our great collaboration.

Celine, thank you for being a dear colleague and dear friend. Your open, warm and kind way towards everyone is unique and I was and am so grateful to have it around me. In and outside the lab, you are one of the most determined people I met, at the same time never losing track of the people around you (which, let's be honest, are the most important thing).

A big thank you to Giulia, your warmth and enthusiasm set the tone in our group. I have learned endless things from you - from project writing, to study design, exposure assessment, desirable salt content in our lunches and just being a kind and supporting colleague. Thank you for that.

Maarten R., thank you for being there and sharing all the side-project hassles, weekend lab sessions, skiing trip discussions, training desperations and scheduling puzzles. Thanks for pacing me in and outside the lab and your unbreakable enthusiasm.

Steven, thank you for keeping the lab running. Early on in my PhD you once told me: 'Don't be scared to take things apart to fix the problem' - I have learned a lot from this principle, from following your expertise and enjoyed every mass-spec-opening-session. I also thank Stijn and Jasper for their continuous help in the every-day lab challenges.

Thank you to Tim - quickly sharing everything you learn with the people around you was an example to me. Thanks a lot to the 'exile office team', Natan, Rani, Maria del Mar, Alicia, Adam, ... for a warm working atmosphere and for lifting each other up when we need it. A special thanks to Fatima and Paulien for their data analysis help during the most stressful times and their unique humor in every situation which I enjoyed very much. I thank the past and current metabolomics team - Annemieke, Rani, Maria del Mar, Elias, Manuela - I have learned a lot from your expertise.

The whole ToxLab team has been a wonderful group of colleagues each of which adds his/her unique contribution to create a warm and fun atmosphere - thank you for that to Adam, Alicia, Allen, Annemieke, Ardiana, Catalina, Celine, Fabian, Fatima, Francesca, Leen, Maarten Q, Maarten R, Maosen, Maria del Mar, Marta, Natan, Oliver, Paulien, Tim. A big thank you to Yu for all the scientific input, your kindness and all the gym sessions we got to do together. I also thank all the other great researches who were part of our group throughout my PhD and whom I had the privilege to meet - Shanshan, Yukiko, Yunsun, Da-Hye, Christina, Tom, Siebe, Philippe, Michiel, Olivier, Ting, Lu, Jorgelina, Andrea, Begona. I am sure that I am unintentionally forgetting someone and I am very sorry for that.

I thank the visiting students, Sandra F. Fernández and Mikel Musatadi, with whom I got the opportunity to work together closely leading to exciting publications. A heartfelt thank you to Prof. Hugo Neels for his interest in my work and sharing his scientific passion.

I thank my dear friends who have always supported me from near and far - Kathi, Jana, Matze, Lydia, Nils, Philipp G., Magnus, Kim, Gordon, Britta, Lukas, Laura, Philipp H., Leonie, Esther, Andi, Katja, Flo, JP, ... Thank you for all the trips and cozy weekends we got to spend together. I thank my Belgian badminton-family which welcomed me dearly and made sure that I get to share the best sport with the best people: Emma, Joke, Silke, Daria, Astrid, Ben, Sarah, Ine, Sanne, Aurelie, Saskia, Robin, Dave, Michiel and many others.

A warm thank you to Micheline, Jean-Marie, David, Karen, Ana, Matthias for all your support, for welcoming me into your family and for giving me a home-away-from-home.

Finally, I thank my parents for their constant love and support. Thank you for giving me a passion for science, creating all the opportunities and opening all the doors to pursue it.

Without you this would have not been possible. Nadja, thank you for being there at all times, sharing the hassles and bustles of the academic world. You are a role model to me in so many ways and I am so grateful to have you as a big sister and a best friend. Lastly, I thank Kris for being there throughout all of this and beyond. Thank you for all the things you share with me - your love, calmness, kindness, interest in all aspects of my and our life, passion for the mountains, your Ghent accent and so much more. Thank you for always being my place of rest.